PUMP HANDBOOK

EDITED BY

Igor J. Karassik
Joseph P. Messina
Paul Cooper
Charles C. Heald

FOURTH EDITION



New York Chicago San Francisco Lisbon London Madrid
Mexico City Milan New Delhi San Juan Seoul
Singapore Sydney Toronto

LIBERTY EXHIBIT 1017, Page 1

The McGraw-Hill Companies

Cataloging-in-Publication Data is on file with the Library of Congress.

McGraw-Hill books are available at special quantity discounts to use as premiums and sales promotions, or for use in corporate training programs. For more information, please write to the Director of Special Sales, Professional Publishing, McGraw-Hill, Two Penn Plaza, New York, NY 10121-2298. Or contact your local bookstore.

Pump Handbook, Fourth Edition

Copyright © 2008, 2001, 1986, 1976 by The McGraw-Hill Companies, Inc. All rights reserved. Printed in the United States of America. Except as permitted under the United States Copyright Act of 1976, no part of this publication may be reproduced or distributed in any form or by any means, or stored in a data base or retrieval system, without the prior written permission of the publisher.

1 2 3 4 5 6 7 8 9 0 DOC/DOC 0 1 2 1 0 9 8 7

ISBN 978-0-07-146044-6
MHID 0-07-146044-6

This book is printed on acid-free paper.

Sponsoring Editor
Larry S. Hager

Acquisitions Coordinator
Alexis Richard

Editorial Supervisor
David E. Fogarty

Project Manager
Vastavikta Sharma, International Typesetting and Composition

Copy Editor
Surendra Nath Shivam

Proofreader
Shruti Pande

Indexer
Paul Cooper and Charles C. Heald

Production Supervisor
Richard C. Ruzycka

Composition
International Typesetting and Composition

Art Director, Cover
Jeff Weeks

Cover illustration credits: Pump station—Courtesy, Alyeska Pipeline Service Company; Impeller CFD mesh—*Proceedings of the 11th International Pump Users Symposium,* sponsored by Texas A&M University.

Information contained in this work has been obtained by The McGraw-Hill Companies, Inc. ("McGraw-Hill") from sources believed to be reliable. However, neither McGraw-Hill nor its authors guarantee the accuracy or completeness of any information published herein, and neither McGraw-Hill nor its authors shall be responsible for any errors, omissions, or damages arising out of use of this information. This work is published with the understanding that McGraw-Hill and its authors are supplying information but are not attempting to render engineering or other professional services. If such services are required, the assistance of an appropriate professional should be sought.

In memory of our good friends and colleagues
William C. Krutzsch
Warren H. Fraser
Igor J. Karassik

ABOUT THE EDITORS

IGOR KARASSIK, now deceased, was an original editor of this book. Many of his extensive contributions to the earlier editions remain in this edition. A major figure in the pump industry for the greater part of the past century, he also authored six books in this field. Beginning in 1936, he wrote more than 600 articles on centrifugal pumps and related subjects, which appeared in over 1500 publications worldwide. For the greater part of his career, he held senior engineering and marketing positions within the Worthington Pump & Machinery Company, which after a number of permutations became part of the Flowserve Corporation. Igor Karassik received his B.S. and M.S. degrees in Mechanical Engineering from Carnegie Mellon University. He was a Life Fellow of the American Society of Mechanical Engineers and recipient of the first ASME *Henry R. Worthington Medal* (1980).

JOSEPH P. MESSINA, also one of the original editors, has spent his entire career in the pump industry, and his past contributions on pump and systems engineering continue to be presented in their entirety in this edition. He served as Manager of Applications Engineering at the Worthington Pump Company. He became a Pump Specialist at the Public Service Electric and Gas Company in New Jersey, serving as a committee member of the Electric Power Research Institute to improve the performance of boiler feed pumps. He assisted in updating the Hydraulic Institute Standards and taught centrifugal pump courses. He also taught Fluid and Solid Mechanics at the New Jersey Institute of Technology and holds a B.S. in Mechanical Engineering and an M.S. in Civil Engineering from the same institution. He has been a contributor to the technical journals and holds pump-related patents.

PAUL COOPER has been involved in the pump industry for nearly 50 years. He began by specializing in the hydraulic design of centrifugal pumps and inducers for aerospace applications at TRW Inc. This was followed by a career in research and development on pump hydraulics and cavitation at the Ingersoll-Dresser Pump Company, now part of the Flowserve Corporation, where he served as the director of R&D for the company. A Life Fellow of the ASME, he received that society's *Fluid Machinery Design Award* (1991), *Henry R. Worthington Medal* (1993), and *Fluids Engineering Award* (2002). He received his B.S. (Drexel University) and M.S. (Massachusetts Institute of Technology) degrees in Mechanical Engineering and a Ph.D. in Engineering from Case Western Reserve University. He is the author of many technical papers and holds several patents on pumps.

CHARLES C. HEALD has spent his entire career in the pump industry. He conducted the hydraulic and mechanical design of several complete lines of single and multistage pumps for the Cameron Pump Division of Ingersoll-Rand, which became part of the Ingersoll-Dresser Pump Company. He served as Chief Engineer and Manager of Engineering and became an Engineering Fellow in the company. He continues as the editor of the company's *Cameron Hydraulic Data Book*. The petroleum industry has always been the focus of his efforts, and he has served for over 40 years as a member of the API 610 specification task force, receiving a resolution of appreciation from API in 1995. A Life Member of the ASME, he obtained the B.S. degree in Mechanical Engineering from the University of Maine, and he is the author of several technical articles and the holder of patents pertaining to pumps.

LIST OF CONTRIBUTORS*

°**Able, Stephen D.,** B.S. (M.E.), MBA, M.S. (Eng), P.E. SECTION 3.6 DIAPHRAGM PUMPS
Late Principal Engineer, Ingersoll-Rand Fluid Products, Bryan, OH

Addie, Graeme, B.S. (M.E.) SECTION 4.2 APPLICATION AND CONSTRUCTION OF CENTRIFUGAL SOLIDS HANDLING PUMPS
Vice President, Engineering and R&D, GIW Industries, Inc., Grovetown, GA

Arnold, Conrad L., B.S. (E.E.) SECTION 9.2.3 VARIABLE SPEED FLUID DRIVES
Director of Engineering, American Standard Industrial Division, Detroit, MI

Ashton, Robert D., B.S. (E.T.M.E.) SECTION 5.3 CENTRIFUGAL PUMP INJECTION-TYPE SHAFT SEALS
Manager, Proposal Applications, Byron Jackson Pump Division, Borg-Warner Industrial Products, Inc., Long Beach, CA

Bean, Robert, B.A. (Physics), M.S. (M.E.) SECTION 3.6 DIAPHRAGM PUMPS
Engineering Manager, Milton Roy Company, Flow Control Division, Ivyland, PA

Beck, Wesley W., B.S. (C.E.), P.E. CHAPTER 16 PUMP TESTING
Hydraulic Consulting Engineer, Denver, CO. Formerly with the Chief Engineers Office of the U.S. Bureau of Reclamation

Beckman, K. O., B.S. (M.E.) SECTION 9.2.4 GEARS
Chief Engineer, Lufkin Industries, Power Transmission Division, Lufkin, TX

*Note: Positions and affiliations of the contributors generally are those held at the time the respective contributions were made.

°Deceased

LIBERTY EXHIBIT 1017, Page 5

Behnke, Paul W., B.S. (M.E.), MBA, P.E. SECTION 12.5 STEAM POWER PLANTS
Senior Principal Engineer, Mechanical Engineering Staff, Bechtel Power Corporation, Frederick, MD

Benjes, H. H., Sr., B.S. (C.E.), P.E. SECTION 12.2 SEWAGE TREATMENT
Retired Partner, Black & Veatch, Engineers-Architects, Kansas City, MO

Bergeron, Wallace L., B.S. (E.E.) SECTION 9.1.2 STEAM TURBINES
Senior Market Engineer, Elliott Company, Jeannette, PA

Bird, Jim, B.M.E. SECTION 12.1 WATER SUPPLY; SECTION 12.3 DRAINAGE AND IRRIGATION
Principal Engineer, Pump Division, Flowserve Corporation, Taneytown, MD

Boyadjis, Paul A., B.S. (M.E.), M.S. (M.E.) SECTION 2.1.4 CENTRIFUGAL PUMP MECHANICAL BEHAVIOR AND VIBRATION
Engineer, Mechanical Solutions, Inc., Whippany, NJ

Brennan, James R., B.S. (M.I.E.) SECTION 3.7 SCREW PUMPS
Manager of Engineering, Imo Pump, a member of the Colfax Pump Group, Monroe, NC

Buse, Frederic W., B.S. (Marine Engrg.) SECTION 2.2.2 CENTRIFUGAL PUMP PRIMING, SECTION 2.2.3.1 SEALLESS PUMPS: MAGNETIC DRIVE PUMPS; SECTION 3.1 POWER PUMP THEORY; SECTION 3.2 POWER PUMP DESIGN AND CONSTRUCTION; SECTION 8.2 MATERIALS OF CONSTRUCTION FOR NONMETALLIC (COMPOSITE) PUMPS
Retired Senior Engineering Consultant, Flowserve Corporation, Phillipsburg, NJ

Cappellino, C. A., B.S. (M.E./I.E.), M.S. (Product Dev't.), P.E. SECTION 12.9 PULP AND PAPER MILLS
Director of Engineering and Product Development, ITT Corporation, Industrial and Biopharm Group, Seneca Falls, NY

Chaplis, William K., B.S. (M.E.), MBA SECTION 3.1 POWER PUMP THEORY; SECTION 3.2 POWER PUMP DESIGN AND CONSTRUCTION
Product Engineering Manager, Flowserve Corporation, Phillipsburg, NJ

Chu, Y. J., B.S. (Agricultural Machinery) M.S. (M.E.), P.E. SECTION 12.18.1 AIRCRAFT FUEL PUMPS
Business Development Team Leader, Nichols Airborne Division, Parker Hannifin Corporation, Elyria, OH

Clasby, Gary C., B.S. (M.E.), P.E. SECTION 12.7 CHEMICAL INDUSTRY
Principal Engineer, Pump Division, Flowserve Corporation, Dayton, OH

Cooper, Paul, B.S. (M.E.). M.S. (M.E.), Ph.D. (Engrg.), P.E. SI UNITS—A COMMENTARY; CHAPTER 1 INTRODUCTION: CLASSIFICATION AND SELECTION OF PUMPS; SECTION 2.1.1 CENTRIFUGAL PUMP THEORY; SECTION 2.1.2 CFD ANALYSIS OF FLOW AND PERFORMANCE; SECTION 2.1.3 CENTRIFUGAL PUMPS: HYDRAULIC PERFORMANCE AND BEHAVIOR; SECTION 6.3 CENTRIFUGAL PUMP MAGNETIC BEARINGS; SECTION 12.18.2 LIQUID ROCKET PROPELLANT PUMPS
Retired Director, Advanced Technology, Ingersoll-Dresser Pumps, now Flowserve Corporation, Phillipsburg, NJ

Costigan, James L., B.S. (Chem.) SECTION 12.10 FOOD AND BEVERAGE PUMPING
Sales Manager, Tri-Clover Division, Ladish Company, Kenosha, WI

Cronin, Richard J., B.S. (M.E.), M.S. (M.E.), P.E. SECTION 2.1.4 CENTRIFUGAL PUMP MECHANICAL BEHAVIOR AND VIBRATION
Senior Staff Engineer, Mechanical Solutions, Inc., Whippany, NJ

Cunningham, Richard G., B.S. (M.E.), M.S. (M.E.), Ph.D. (M.E.) SECTION 7.1 JET PUMP THEORY
Vice President Emeritus for Research and Graduate Studies and Professor Emeritus of Mechanical Engineering, Pennsylvania State University, University Park, PA

Cutler, Donald B., B.S. (M.E.) SECTION 9.3 PUMP COUPLINGS
Technical Services Manager, Rexnord Corporation, Warren, PA

Cygnor, John E., B.S. (M.E.) SECTION 12.18.1 AIRCRAFT FUEL PUMPS
Retired Manager, Advanced Fluid Systems, Hamilton Sundstrand, Rockford, IL

Czarnecki, G. J., B.Sc., M.Sc. (Tech.) SECTION 3.7 SCREW PUMPS
Chief Engineer (Retired), Imo Pump, a member of the Colfax Pump Group, Monroe, NC

Dahl, Trygve, B.S. (M.E.), M.S. (Mfg. Systems Engrg.), Ph.D. (M.E.), P.E. CHAPTER 14 SELECTING AND PURCHASING PUMPS
VP Technology, Intelliquip, LLC, Bethlehem, PA.

Day, Michael W., B.S. (Ch.E.), SECTION 12.9 PULP AND PAPER MILLS
Product Manager, ITT Corporation, Industrial and Biopharm Group, Seneca Falls, NY

Denault, Gregory, M., B.S. (M. E.) SECTION 2.2.3.1 MAGNETIC DRIVE PUMPS
Senior Engineer, Flowserve Corporation, Pump Division, Dayton, OH

Dijkers, Ronald J. H., B.S. (M.E.), SECTION 13.1 INTAKES, SUCTION PIPING, AND STRAINERS
Senior Hydraulic Engineer, Flowserve Corporation, Hengelo, Netherlands

DiMasi, Mario, B.S. (M.E.), M.B.A. SECTION 12.4 FIRE PUMPS
District Manager, Peerless Pump, Union, NJ

Divona, A. A., B.S. (M.E.) SECTION 9.1.1 ELECTRIC MOTORS AND MOTOR CONTROLS
Account Executive, Industrial Sales, Westinghouse Electric Corporation, Hillside, NJ

Dolan, A. J., B.S. (E.E.), M.S. (E.E.), P.E. SECTION 9.1.1 ELECTRIC MOTORS AND MOTOR CONTROLS
Fellow District Engineer, Westinghouse Electric Corporation, Hillside, NJ

Dornaus, Wilson L., B.S. (C.E.), P.E. SECTION 13.1 INTAKES, SUCTION PIPING, AND STRAINERS
Pump Consultant, Lafayette, CA

Drane, John, C.Eng., M.I. (Ch.E) SECTION 12.10 FOOD AND BEVERAGE PUMPING
Technical Support Engineer, Mono Pumps Limited, Manchester, England, UK

°Elvitsky, A. W., B.S. (M.E.), M.S. (M.E.), P.E. SECTION 12.8 PETROLEUM INDUSTRY
Late Vice President and Chief Engineer, United Centrifugal Pumps, San Jose, CA

°Foster, W. E., B.S. (C.E.), P.E. SECTION 12.2 SEWAGE TREATMENT
Partner, Black & Veatch, Engineers-Architects, Kansas City, MO

°Fraser, Warren H., B.M.E. SECTION 2.1.3 CENTRIFUGAL PUMPS: HYDRAULIC PERFORMANCE AND BEHAVIOR
Late Chief Design Engineer, Worthington Pump Group, McGraw-Edison Company, Harrison, NJ

Freeborough, Robert M., B.S. (Min.E.) SECTION 3.3 STEAM PUMPS
Manager, Parts Marketing, Worthington Corporation, Timonium, MD

Furst, Raymond B. SECTION 12.18.2 LIQUID ROCKET PROPELLANT PUMPS
Retired Manager of Hydrodynamics, Rocketdyne, now The Boeing Company, Canoga Park, CA

°Deceased

LIBERTY EXHIBIT 1017, Page 7

Gaydon, Matthew A., B.S. (M.E.), M.S. (M.E.) SECTION 2.1.4 CENTRIFUGAL PUMP MECHANICAL BEHAVIOR AND VIBRATION
Senior Engineer, Bechtel Power Corporation, Baltimore, MD

Giberson, Melbourne F., B.S. (M.E.), M.S. (Applied Mechanics), Ph.D. (Applied Mechanics), P.E. SECTION 9.2.3 VARIABLE SPEED FLUID DRIVES
President and Sr. Technical Officer, TRI Transmission & Bearing Corp. / Turbo Research, Inc., Lionville, PA

Giddings, J. F., Diploma, Mechanical, Electrical, and Civil Engineering SECTION 12.9 PULP AND PAPER MILLS
Development Manager, Parsons & Whittemore, Lyddon, Ltd., Croydon, England

Glanville, Robert H., M.E. SECTION 12.15 METERING
Vice President Engineering, BIF, A Unit of General Signal, Providence, RI

Goodman, W. G., B.S. (M.E.T) SECTION 6.1 CENTRIFUGAL PUMP BEARINGS
Engineering Manager, ITT Goulds Pumps, Seneca Falls, NY

Guinzburg, Adiel, B.Sc. (Aero. E.), M.S. (Aero.), Ph.D. (M.E.) SECTION 12.18.2 LIQUID ROCKET PROPELLANT PUMPS
Deputy, Development Process Excellence, The Boeing Company, Seattle, WA

°**Gunther, F. J.,** B.S. (M.E.), M.S. (M.E.) SECTION 9.1.3 ENGINES
Late Sales Engineer, Waukesha Motor Company, Waukesha, WI

Haentjens, W. D., B.M.E., M.S. (M.E.), P.E. SECTION 12.11 MINING
Manager, Special Pumps and Engineering Services, Hazleton Pumps, Inc., Hazleton, PA

Halverson, Loern A., B.S. (M.E.), M.S. (M.E.), P.E. SECTION 9.2.1 PERMANENT-MAGNET ADJUSTABLE-SPEED DRIVES
Engineering Manager, MagnaDrive Corporation, Bellevue, WA

Hawkins, Larry, B.S. (M.E.), M.S. (M.E.) SECTION 6.3 CENTRIFUGAL PUMP MAGNETIC BEARINGS
Principal, Calnetix, Torrance, CA

Heald, Charles C., B.S. (M.E.) SECTION 2.2.1 CENTRIFUGAL PUMPS: MAJOR COMPONENTS; SECTION 6.1 CENTRIFUGAL PUMP BEARINGS; SECTION 12.8 PETROLEUM INDUSTRY; SECTION 13.1 INTAKES, SUCTION PIPING, AND STRAINERS; CHAPTER 15 INSTALLATION, OPERATION, AND MAINTENANCE
Retired Chief Engineer / Engineering Fellow, Ingersoll-Dresser Pump Company, now Flowserve Corporation, Phillipsburg, NJ

Hendershot, J. R., B.S. (Physics) SECTION 9.1.1 ELECTRIC MOTORS AND MOTOR CONTROLS; SECTION 9.2.2 SINGLE-UNIT ADJUSTABLE-SPEED ELECTRIC DRIVES
President, Motorsoft, Inc., Lebanon, OH

Highfill, Greg. S., B.S. (E.T.), P.E. SECTION 9.2.1 PERMANENT-MAGNET ADJUSTABLE-SPEED DRIVES
Director of Engineering, MagnaDrive Corporation, Bellevue, WA

Hosangadi, Ashvin, B.S., M.S. Ph.D. SECTION 2.1.2 CFD ANALYSIS OF FLOW AND PERFORMANCE
Principal Engineer, Combustion Research and Flow Technology, Inc., Pipersville, PA

House, D. A., B.S. (M.E.) SECTION 12.2 SEWAGE TREATMENT
Principal Engineer, Pump Division, Flowserve Corporation, Taneytown, MD

°Deceased

Huebner, Michael B., B.S. (Engrg. Technology) SECTION 5.2 CENTRIFUGAL PUMP MECHANICAL SEALS
Principal Engineer, Flowserve Corporation, Deer Park, TX

Jaskiewicz, Stephen A., B.A. (Chemistry) SECTION 2.2.3.2 SEALLESS PUMPS: CANNED MOTOR PUMPS
Product Manager, Chempump (Division of Crane Pumps & Systems, Inc.), Warrington, PA

Jones, Graham, B.S. (M.E.), M.B.A. SECTION 6.3 CENTRIFUGAL PUMP MAGNETIC BEARINGS
Former Project Manager for Magnetic Bearings, Technology Insights, San Diego, CA

Jones, R. L., B.S. (M.E.), M.S. (M.E.), P.E. SECTION 12.8 PETROLEUM INDUSTRY
Rotating Equipment Consultant, Retired from Shell Global Solutions, Houston, TX

Jumpeter, Alex M., B.S. (Ch.E.) SECTION 7.2 JET PUMP APPLICATIONS
Engineering Manager, Process Equipment, Schutte and Koerting Company, Cornwells Heights, PA

Kalix, David A., B.S. (Ch.E.) SECTION 11.4 MINIMUM FLOW CONTROL SYSTEMS
Senior Product Development Engineer, Yarway Corporation, Blue Bell, PA

°**Karassik, Igor J.,** B.S. (M.E.), M.S. (M.E.), P.E. SECTION 2.2.1 CENTRIFUGAL PUMPS: MAJOR COMPONENTS; SECTION 2.2.2 CENTRIFUGAL PUMP PRIMING; SECTION 12.5 STEAM POWER PLANTS; CHAPTER 15 INSTALLATION, OPERATION, AND MAINTENANCE
Chief Consulting Engineer, Worthington Group, McGraw-Edison Company, Basking Ridge, NJ

Kawohl, Rudolph, Dipl. Ing. SECTION 12.4 FIRE PUMPS
Retired Engineering Manager, Ingersoll-Dresser Pumps, now Flowserve Corporation, Arnage, France

Kelly, William J., B.S. (M.E.), M.S. (M.E.), P.E. SECTION 2.1.4 CENTRIFUGAL PUMP MECHANICAL BEHAVIOR AND VIBRATION
Principal Engineer, Mechanical Solutions, Inc., Whippany, NJ

°**Kittredge, C. P.,** B.S. (C.E.), Doctor of Technical Science (M.E.) SECTION 2.1.3 CENTRIFUGAL PUMPS: HYDRAULIC PERFORMANCE AND BEHAVIOR
Consulting Engineer, Princeton, NJ

°**Koch, Richard P.,** B.S. (M.E.) SECTION 12.5 STEAM POWER PLANTS
Late Manager of Engineering, Pump Services Group, Flowserve Corporation, Phillipsburg, NJ

Kron, H. O., B.S. (M.E.), P.E. SECTION 9.2.4 GEARS
Executive Vice President, Philadelphia Gear Corporation, King of Prussia, PA

°**Krutzsch, W. C.,** B.S. (M.E.), P.E. SI UNITS—A COMMENTARY; CHAPTER 1 INTRODUCTION: CLASSIFICATION AND SELECTION OF PUMPS
Late Director, Research and Development, Engineered Products, Worthington Pump Group, McGraw-Edison Company, Harrison, NJ

Landon, Fred K., B.S. (Aero. E.), P.E. SECTION 9.3 PUMP COUPLINGS
Manager, Engineering, Rexnord, Inc., Houston, TX

Larsen, Johannes, B.S. (C.E.), M.S. (M.E.) SECTION 13.2 INTAKE MODELING
Retired Vice President, Alden Research Laboratory, Inc., Holden, MA

Lee, Jinkook, B.S. (M.E.), M.S. (M.E.), Ph.D. SECTION 12.16 CRYOGENIC PUMPS FOR LIQUEFIED GAS SERVICE
Chief Engineer, Aerospace Division, Eaton Corporation, Cleveland, OH

°Deceased

LIBERTY EXHIBIT 1017, Page 9

Link, Ellen E., B.S., M.S., (Materials Science and Engineering) SECTION 8.1 METALLIC MATERIALS AND DAMAGE MECHANISMS
Materials Engineer, Ingersoll-Rand Company, Huntersville, NC

Lippincott, J. K., B.S. (M.E.) SECTION 3.7 SCREW PUMPS
Vice President, General Manager (Retired), Imo Pump, a member of the Colfax Pump Group, Monroe, NC

Little, C.W., Jr., B.E. (E.E.), D. Eng. SECTION 3.8 VANE, GEAR, AND LOBE PUMPS
Former Vice President, General Manager, Manufactured Products Division, Waukesha Foundry Company, Waukesha, WI

Mahan, James W., B.S. (M. E.), MBA SECTION 9.3 PUMP COUPLINGS
Director of Engineering, Lovejoy Inc., Downers Grove, TX

Marscher, William D., B.S. (M.E.), M.S. (M.E.), P.E., Fellow STLE SECTION 2.1.4 CENTRIFUGAL PUMP MECHANICAL BEHAVIOR AND VIBRATION
President and Technical Director, Mechanical Solutions, Inc., Whippany, NJ

Martin, C. Samuel, B.S. (C.E.), M.S. (C.E.), Ph.D. (C.E.), P.E. SECTION 11.3 WATERHAMMER; SECTION 12.14 PUMPED STORAGE
Emeritus Professor, Georgia Institute of Technology

Maxwell, Horace J., B.S. (M.E.) SECTION 11.4 MINIMUM FLOW CONTROL SYSTEMS
Director of Engineering, Yarway Corporation, Blue Bell, PA

Mayo, Howard A., Jr., B.S. (M.E.), P.E. SECTION 9.1.4 HYDRAULIC TURBINES
Consulting Engineer, Hydrodynamics Ltd., York, PA

McCaul, Colin O., B.S., M.S. (Metallurgical Engrg.), P.E. SECTION 8.1 METALLIC MATERIALS AND DAMAGE MECHANISMS
Pump Division Metallurgist, Flowserve Corporation, Phillipsburg, NJ

McGuire, J. T., B.S. (M.E.) SECTION 12.8 PETROLEUM INDUSTRY
Director, Applied Technology, Flowserve Corporation, Vernon, CA

Messina, Joseph P., B.S. (M.E.), M.S. (C.E.), P.E. SECTION 11.1 GENERAL CHARACTERISTICS OF PUMPING SYSTEMS AND SYSTEM-HEAD CURVES; SECTION 11.2 BRANCH-LINE PUMPING SYSTEMS
Consultant

Miller, Alan C., B.S. (M.E.) CHAPTER 16 PUMP TESTING
Senior Upgrades Engineer, Pump Division, Flowserve Corporation, Taneytown, MD

Miller, Ronald S., B.Sc. (M.E.), B.Sc. (Metallurgical Engrg.) SECTION 8.1 METALLIC MATERIALS AND DAMAGE MECHANISMS
Manager, Advanced Materials Engineering, Ingersoll-Rand Company

Nardone, Richard A., B.S. (M.E.) SECTION 12.9 PULP AND PAPER MILLS
Product Manager, ITT Corporation, Industrial and Biopharm Group, Seneca Falls, NY

Nelik, Lev, B.S., M.S., Ph.D., P.E. SECTION 3.8 VANE, GEAR, AND LOBE PUMPS
President and Technical Director, Pumping Machinery, LLC, Atlanta GA

Netzel, James P., B.S. (M.E.) SECTION 5.1 CENTRIFUGAL PUMP PACKING
Chief Engineer, John Crane, Inc., Morton Grove, IL

Nolte, P. A., B.S. (M.E.) SECTION 12.17 PORTABLE TRANSFER OF HAZARDOUS LIQUIDS
Director of Agricultural Business, Flowserve Corporation, Memphis, TN

Nuta, D., B.S. (C.E.), M.S. (Applied Mathematics and Computer Science), P.E. SECTION 12.6.2 NUCLEAR PUMP SEISMIC QUALIFICATIONS
Associate Consulting Engineer, Ebasco Services, Inc., New York, NY

LIBERTY EXHIBIT 1017, Page 10

Olson, Eric J., B.S. (M.E.) SECTION 2.1.4 CENTRIFUGAL PUMP MECHANICAL BEHAVIOR AND VIBRATION
Principal Engineer, Mechanical Solutions, Inc., Whippany, NJ

°Olson, Richard G., M.E. M.S., P.E. SECTION 9.1.5 GAS TURBINES
Late Marketing Supervisor, International Turbine Systems, Turbodyne Corporation, Minneapolis, MN

Onari, Maki M., B.S. (M.E.) SECTION 2.1.4 CENTRIFUGAL PUMP MECHANICAL BEHAVIOR AND VIBRATION
Senior Staff Engineer, Mechanical Solutions, Inc., Whippany, NJ

Padmanabhan, Mahadevan, B.S. (C.E.), M.S. (C.E.), Ph.D., P.E. SECTION 13.2 INTAKE MODELING
Vice President, Alden Research Laboratory, Inc. Holden, MA

Parry, W. W., Jr., B.S. (M.E.), P.E. SECTION 12.6.1 NUCLEAR ELECTRIC GENERATION; SECTION 12.6.2 NUCLEAR PUMP SEISMIC QUALIFICATIONS
Senior Mechanical Engineer, Fybroc Division, Met-Pro Corporation, Telford, PA

Palombo, D. SECTION 12.18.1 AIRCRAFT FUEL PUMPS
President and C.E.O., Aveox, Inc., Simi Valley, CA

Patel, Vinod P., B.S. (M.E.), M.S. (Metallurgical Engrg.), P.E. CHAPTER 14 SELECTING AND PURCHASING PUMPS
Senior Principal Engineer, Machinery Technology, Kellogg Brown & Root, Inc., Houston, TX

Platt, Robert A., B.E., M.E., P.E. SECTION 3.8 VANE, GEAR, AND LOBE PUMPS
General Manager, Sales and Marketing, Carver Pump Company, Muscatine, IA

Potthoff, E. O., B.S. (E.E.), P.E. SECTION 9.2.2 SINGLE-UNIT ADJUSTABLE-SPEED ELECTRIC DRIVES
Industrial Engineer (retired), Industrial Sales Division, General Electric Company, Schenectady, NY

Prang, A. J. SECTION 3.7 SCREW PUMPS
Engineering Consultant, Flowserve Corporation, Brantford, Ontario, Canada

Robertson, John S., B.S. (C.E.), P.E. SECTION 12.3 DRAINAGE AND IRRIGATION
Chief, Electrical and Mechanical Branch, Engineering and Construction, Headquarters, U.S. Army Corps of Engineers

Rishel, Burt, B.S. (M.E.) SECTION 12.13 HEATING AND AIR CONDITIONING
Consultant, Pumping Solutions, LLC, Dublin, Ohio

Roll, Daniel R., B.S. (M.E.), P.E. SECTION 12.9 PULP AND PAPER MILLS
Vice President, Engineering & Development, Finish Thompson Inc, Erie, PA

Rupp, Warren E. SECTION 3.6 DIAPHRAGM PUMPS
President, The Warren Rupp Company, Mansfield, OH

Sellgren, Anders, M.S. (C.E.), Ph.D. (Hydraulics) SECTION 4.1 HYDRAULIC TRANSPORT OF SOLIDS; SECTION 4.2 APPLICATION AND CONSTRUCTION OF CENTRIFUGAL SOLIDS HANDLING PUMPS
Professor, Division of Water Resources Engineering, Lulea University of Technology, Lulea, Sweden

Sembler, William J., B.S. (Marine Engrg.), M.S. (M.E.) SECTION 12.12 MARINE PUMPS
Tenured Associate Professor, United States Merchant Marine Academy, Kings Point, NY

°Deceased

LIBERTY EXHIBIT 1017, Page 11

Shapiro, Wilbur, B.S., M.S. SECTION 6.2 OIL FILM JOURNAL BEARINGS
Consultant, Machinery Components, Niskayuna, NY

Sloteman, Donald P., B.S. (M. E.), M.S. (Executive Engrg.) CHAPTER 10 PUMP NOISE
Director, Advanced Technology, Engineered Pump Division, Curtiss-Wright Corporation, Phillipsburg, NJ

°**Smith, Will,** B.S. (M.E.), M.S. (M.E.), P.E. SECTION 3.5 DISPLACEMENT PUMP FLOW CONTROL; SECTION 4.3 CONSTRUCTION OF SOLIDS-HANDLING DISPLACEMENT PUMPS
Engineering Product Manager, Custom Pump Operations, Worthington Division, McGraw-Edison Company, Harrison, NJ

Sparks, Cecil R., B.S. (M.E.), M.S. (M.E.), P.E. CHAPTER 10 PUMP NOISE
Director of Engineering Physics, Southwest Research Institute, San Antonio, TX

Spence, Thomas C., B.S. (Met. Eng.), MBA SECTION 12.7 CHEMICAL INDUSTRY
NACE Senior Corrosion Technologist, Director Materials Engineering, *Flowserve Corporation, Dayton, OH*

Szenasi, Fred R., B.S. (M.E.), M.S. (M.E.), P.E. SECTION 3.4 DISPLACEMENT PUMP PERFORMANCE, INSTRUMENTATION, AND DIAGNOSTICS; CHAPTER 10 PUMP NOISE
Senior Project Engineer, Engineering Dynamics Inc., San Antonio, TX

Taylor, Ken W., MIProdE. CEng. SECTION 12.15 METERING
Vice President, Global Business Development, Wayne Division, Dresser Equipment Group, a Halliburton Company

°**Tullo, C. J.,** P.E. SECTION 2.2.2 CENTRIFUGAL PUMP PRIMING
Chief Engineer (retired), Centrifugal Pump Engineering, Worthington Pump, Inc., Harrison, NJ

van der Sluijs, Kees, B.S. (M.E.T.) SECTION 8.2 MATERIALS FOR NONMETALLIC (COMPOSITE) PUMPS
Senior Engineer, Flowserve Corporation, Dayton, OH

Van Laningham, F. L., SECTION 9.2.4 GEARS
Consultant, Rotating and Turbomachinery Consultants

Wachel, J. C., B.S. (M.E.), M.S. (M.E.) SECTION 3.4 DISPLACEMENT PUMP PERFORMANCE, INSTRUMENTATION, AND DIAGNOSTICS; CHAPTER 10 PUMP NOISE
Manager of Engineering, Engineering Dynamics, Inc., San Antonio, TX

Webb, Donald R., B.S. (M.E.), M.S. (Engrg. Administration) SECTION 9.1.4 HYDRAULIC TURBINES
Manager, Hydraulic Applications, Voith Siemens, York, PA

Wepfer, W. M., B.S. (M.E.), P.E. SECTION 12.6.1 NUCLEAR ELECTRIC GENERATION
Consulting Engineer, formerly Manager, Pump Design, Westinghouse Electric Corporation, Pittsburgh, PA

Whippen, Warren G., B.S. (M.E.), P.E. SECTION 9.1.4 HYDRAULIC TURBINES
Retired Manager of Hydraulic Engineering, Voith Siemens Hydro, York, PA

Wilson, Kenneth C., B.A.Sc. (C.E.), M.Sc.(Hydraulics), Ph.D. SECTION 4.1 HYDRAULIC TRANSPORT OF SOLIDS
Professor Emeritus, Dept. of Civil Engineering, Queen's University, Kingston, Ontario, Canada

Wotring, Timothy L., B.S. (M.E.), P.E. SECTION 5.3 CENTRIFUGAL PUMP INJECTION-TYPE SHAFT SEALS
Vice President, Engineering and Technology, Flowserve Corporation, Phillipsburg, NJ

°Deceased

LIBERTY EXHIBIT 1017, Page 12

SI UNITS— A COMMENTARY

W.C. KRUTZSCH
P. COOPER

Since the publication of the first edition of this handbook in 1976, the involvement of the world in general, and of the United States in particular, with the SI system of units has become common. Accordingly, throughout this book, SI units have been provided as a supplement to the United States customary system of units (USCS).

The designation SI is the official abbreviation, in any language, of the French title "Le Système International d'Unités," given by the 11th General Conference on Weights and Measures (sponsored by the International Bureau of Weights and Measures) in 1960 to a coherent system of units selected from metric systems. This system of units has since been adopted by the International Organization for Standardization (ISO) as an international standard.

The SI system consists of seven basic units, two supplementary units, a series of derived units, and a series of approved prefixes for multiples and submultiples of the foregoing. The names and definitions of the basic and supplementary units are contained in Tables 1A and 1B of the Appendix. Table 2 lists the units and Table 3 the prefixes. Table 10 provides conversions of USCS to SI units. Conversions can also be found in NIST Special Publication 811 "Guide for the Use of the International System of Units" available at http://www.nist.gov/metric.

As with the earlier editions, the decision has been made to accept variations in the expression of SI units that are widely encountered in practice. The quantities mainly affected are pressure and flow rate, the situation with each being explained as follows.

The standard SI unit of pressure, the pascal, equal to one newton* per square meter,† is a minuscule value relative to the pound per square inch (1 lb/in^2 or 1 psi = 6,894.757 Pa) or to the old, established metric unit of pressure the kilogram per square centimeter

*The newton (symbol N) is the SI unit of force, equal to that which, when applied to a body having a mass of 1 kg, gives it an acceleration of 1 m/s^2.

†In countries using the SI system exclusively, the correct spelling is *metre*. This book uses the spelling *meter* in deference to prevailing U.S. practice.

LIBERTY EXHIBIT 1017, Page 13

(1 kgf/cm^2 = 98,066.50 Pa). In order to eliminate the necessity for dealing with significant multiples of these already large numbers when describing the pressure ratings of modern pumps, different sponsoring groups have settled on two competing proposals. One group supports selection of the kilopascal, a unit which does provide a numerically reasonable value (1 lb/in^2 = 6.894757 kPa) and is a rational multiple of a true SI unit. The other group, equally vocal, supports the bar (1 bar = 10^5 Pa). This support is based heavily on the fact that the value of this special derived unit is close to one atmosphere. It is important, however, to be aware that it is not exactly equal to a standard atmosphere (101,325.0 Pa) or to the so-called metric atmosphere (1 kgf/cm^2 = 98,066.50 Pa), but is close enough to be confused with both.

As yet, there is no consensus about which of these units should be used as the standard. Accordingly, both are used, often in the same metric country. Because the world cannot agree and because we must all live with the world as it is, the editors concluded that restricting usage to one or the other would be arbitrary, grossly artificial, and not in the best interests of the reader. We therefore have permitted individual authors to use what they are most accustomed to, and both units will be encountered in the text.

Units of pressure are utilized to define both the performance and the mechanical integrity of displacement pumps. For dynamic pumps, however, which are by far the most significant industrial pumps, pressure is used only to describe rated and hydrostatic values, or mechanical integrity. Performance is generally measured in terms of total head, expressed as feet in USCS units and as meters in SI units. This sounds straightforward enough until a definition of head, including consistent units, is attempted. Then we encounter the dilemma of mass versus force, or weight.

The total head developed by a dynamic pump, or the head contained in a vertical column of liquid, is actually a measure of the internal energy added to or contained in the liquid. The units used to define it could be energy per unit volume, or energy per unit mass, or energy per unit weight. If we select the last, we arrive conveniently, in USCS units, as foot-pounds per pound, or simply feet. In SI units, the terms would be newton-meters per newton, or simply meters. In fact, however, metric countries weigh objects in kilograms, not newtons, and so the SI term for head may be defined at places in this volume in terms of kilogram-meters per kilogram, even though this does not conform strictly to SI rules.

Similar ambiguity is observed with the units of flow rate, except here there may be even more variations. The standard SI unit of flow rate is the cubic meter per second, which is indeed a very large value (1 m^3/s = 15,850.32 U.S. gal/min = 15,850.32 gpm) and is therefore really only suitable for very large pumps. Some industry groups have suggested that a suitable alternative might be the liter per second (1 l/s = 10^{-3} m^3/s = 15.85032 U.S. gal/min), while others have maintained strong support for the traditional metric unit of flow rate, the cubic meter per hour (1 m^3/h = 4.402867 U.S. gal/mm). All of these units will be encountered in the text.

These variations have led to several forms of the specific speed, which is the fundamentally dimensionless combination of head, flow rate, and rotative speed that characterizes the geometry of kinetic pumps. These forms are all related to a truly unitless formulation called "universal specific speed," which gives the same numerical value for any consistent system of units. Although not yet widely used, this concept has been appearing in basic texts and other literature, because it applies consistently to all forms of turbomachinery. Equivalencies of the universal specific speed to the common forms of specific speed in use worldwide are therefore provided in this book. This is done with a view to eventual standardization of the currently disparate usage in a world that is experiencing globalization of pump activity.

The value for the unit of horsepower (hp) used throughout this book and in the United States is the equivalent of 550 foot pounds (force) per second, or 0.74569987 kilowatts (kW). The horsepower used herein is approximately 1.014 times greater than the metric horsepower, which is the equivalent of 75 kgf · m/s or 0.735499 kW. Whenever the rating of an electric motor is given in this book in horsepower, it is the output rating. The equivalent output power in kilowatts is shown in parentheses.

Variations in SI units have arisen because of differing requirements in various user industry groups. Practices in the usage of units will continue to change, and the reader will have to remain alert to further variations of national and international practices in this area.

LIBERTY EXHIBIT 1017, Page 14

PREFACE

As this comprehensive work on pumps takes on a renewed existence in the fourth edition, it is the hope of the present editors that the original purpose of the work is still being served. When the first edition appeared in 1976—and the second edition in 1985—the editors Igor J. Karassik, William C. Krutzsch, Warren H. Fraser, and Joseph P. Messina had two objectives:

- First, to present sufficient information on the theory of design and operation of both rotodynamic (or simply "dynamic") and positive displacement (both reciprocating and rotary) pumps to assist engineers in designing, analyzing, testing, and troubleshooting all sizes and configurations of these machines.
- Second, to review a representative array of application areas and systems, describing to users, buyers, and operators how pumps are specified, purchased, selected, deployed, started, operated, and maintained to meet the requirements of several environments from water supply, marine, and mining services to chemical plants, petroleum production, electric power generation, aerospace systems, and many others.

The rapid pace of recent industrial and technological developments has made it necessary to update the third edition, which appeared in 2000, in order that the *Pump Handbook* can continue to serve the global pump community in keeping with these two major objectives. The volume of material that could be included to do this is greater than a manageable size; yet it has been found possible to add new material while retaining most of the subject areas, each of which has been treated exclusively in one of the many dedicated sections contained in the chapters of the earlier editions. In this fourth edition, these sections have been regrouped to satisfy present needs, additional chapters having been established for solids pumping, sealing, bearings, and noise. The resulting 16 chapters together with the appendix contain 71 sections, most of which have been updated and some of which are new or are completely new replacements of the earlier sections.

The new sections include Centrifugal Pump Mechanical Behavior and Vibration, including a comprehensive troubleshooting list; CFD Analysis of Flow and Performance,

LIBERTY EXHIBIT 1017, Page 15

providing an overview of this increasingly useful analytical tool; Centrifugal Pump Bearings, including a new treatment of rolling element bearings; Water Supply, illustrating current water distribution systems; Cryogenic Pumps for Liquefied Gas Service, detailing the role of pumps in the emerging LNG infrastructure; Pumped Storage, presenting the new machinery and plants in this time-honored energy management area; and Waterhammer, including a new and clear presentation of the transient behavior involved. In regard to transients, these latter two sections, as well as the updated and renamed earlier section, Centrifugal Pumps: Hydraulic Performance and Behavior, present the "complete characteristics," "four-quadrant," or "abnormal" behavior of pumps—both theory and test data—in the context of the particular subject area being addressed.

In updating existing sections from the earlier editions, significant new material has been included in Aircraft Fuel Pumps, which also details the emerging brushless dc electric motor technology for driving these pumps in new airframes; Screw Pumps; Vane, Gear, and Lobe Pumps; Electric Motors and Motor Controls; Permanent Magnet Adjustable Speed Drives; Variable Speed Fluid Drives; Gears; Pump Couplings; Centrifugal Pump Mechanical Seals; Drainage and Irrigation; Metallic Materials and Damage Mechanisms; Pulp and Paper Mills; Heating and Air-Conditioning; Selecting and Purchasing Pumps; and Pump Testing.

Not requiring significant updating are some of the sections that were new for the third edition, including Hydraulic Transport of Solids, an elegant, classical presentation of the flow regimes and losses in slurry pipelines; Application and Construction of Centrifugal Solids Handling Pumps, a companion to the preceding section that clearly presents the slurry pumps used for such transport; and Jet Pump Theory, another classic that treats both single- and two-phase jet pumping.

As the reader will see in the heading of each section, many contributors have prepared or assisted in the preparation of these sections for the *Pump Handbook*, and the editors take this opportunity to thank and honor these experts, who have been willing to share their knowledge and to make the effort required to present it clearly.

As in prior editions, the quantities involved are expressed in both the SI and the U.S. system of units. In each section of the book, either one of these systems is treated as primary, according to the style of the contributor. In all cases, the conversions to the other system are shown, are evident, or are not required in view of global understanding and convention.

In conclusion, the guiding principle of the editors has been to build on the previous editions while at the same time producing a work that is up to date. We recognize that new developments in the world of pumping are going on apace and that more could have been done. Nevertheless we offer this fourth edition of the *Pump Handbook* as a practical tool for the present day, and we hope that readers will benefit from this effort.

PAUL COOPER
CHARLES C. HEALD
JOSEPH P. MESSINA

LIBERTY EXHIBIT 1017, Page 16

CONTENTS

List of Contributors / *ix*
Preface / *xvii*
SI Units—A Commentary / *xix*

Chapter 1 Introduction: Classification and Selection of Pumps 1.1

Chapter 2 Centrifugal Pumps 2.1

2.1 Centrifugal Pump Theory, Analysis, and Performance / 2.3
- 2.1.1 Centrifugal Pump Theory / 2.3
- 2.1.2 CFD Analysis of Flow and Performance / 2.97
- 2.1.3 Centrifugal Pumps: Hydraulic Performance and Behavior / 2.121
- 2.1.4 Centrifugal Pump Mechanical Behavior and Vibration / 2.191

2.2 Centrifugal Pump Construction / 2.249
- 2.2.1 Centrifugal Pumps: Major Components / 2.249
- 2.2.2 Centrifugal Pump Priming / 2.317
- 2.2.3 Sealless Pumps / 2.329
  - 2.2.3.1 Magnetic Drive Pumps / 2.331
  - 2.2.3.2 Canned Motor Pumps / 2.349

LIBERTY EXHIBIT 1017, Page 17

Chapter 3 Displacement Pumps 3.1

3.1 Power Pump Theory / 3.3
3.2 Power Pump Design and Construction / 3.21
3.3 Steam Pumps / 3.37
3.4 Displacement Pump Performance, Instrumentation, and Diagnostics / 3.63
3.5 Displacement Pump Flow Control / 3.75
3.6 Diaphragm Pumps / 3.85
3.7 Screw Pumps / 3.99
3.8 Vane, Gear, and Lobe Pumps / 3.123

Chapter 4 Solids Pumping 4.1

4.1 Hydraulic Transport of Solids / 4.3
4.2 Application and Construction of Centrifugal Solids Handling Pumps / 4.33
4.3 Construction of Solids-Handling Displacement Pumps / 4.49

Chapter 5 Pump Sealing 5.1

5.1 Centrifugal Pump Packing / 5.3
5.2 Centrifugal Pump Mechanical Seals / 5.17
5.3 Centrifugal Pump Injection-Type Shaft Seals / 5.63

Chapter 6 Pump Bearings 6.1

6.1 Centrifugal Pump Bearings / 6.3
6.2 Oil Film Journal Bearings / 6.13
6.3 Centrifugal Pump Magnetic Bearings / 6.43

Chapter 7 Jet Pumps 7.1

7.1 Jet Pump Theory / 7.3
7.2 Jet Pump Applications / 7.23

Chapter 8 Materials of Construction 8.1

8.1 Metallic Materials and Damage Mechanisms / 8.3
8.2 Materials of Construction for Nonmetallic (Composite) Pumps / 8.51

Chapter 9 Pump Drivers and Power Transmission 9.1

9.1 Pump Drivers / 9.3
9.1.1 Electric Motors and Motor Controls / 9.3
9.1.2 Steam Turbines / 9.37

LIBERTY EXHIBIT 1017, Page 18

9.1.3 Engines / 9.55
9.1.4 Hydraulic Turbines / 9.75
9.1.5 Gas Turbines / 9.87
9.2 Speed-Varying Devices / 9.97
9.2.1 Permanent Magnet Adjustable Speed Drives / 9.97
9.2.2 Single-Unit Adjustable-Speed Electric Drives / 9.111
9.2.3 Variable Speed Fluid Drives / 9.129
9.2.4 Gears / 9.147
9.3 Pump Couplings / 9.169

Chapter 10 Pump Noise 10.1

Chapter 11 Pump Systems 11.1

11.1 General Characteristics of Pumping Systems and System-Head Curves / 11.3
11.2 Branch-Line Pumping Systems / 11.83
11.3 Waterhammer / 11.91
11.4 Minimum Flow Control Systems / 11.123

Chapter 12 Pump Services 12.1

12.1 Water Supply / 12.3
12.2 Sewage Treatment / 12.29
12.3 Drainage and Irrigation / 12.47
12.4 Fire Pumps / 12.63
12.5 Steam Power Plants / 12.79
12.6 Nuclear / 12.117
12.6.1 Nuclear Electric Generation / 12.117
12.6.2 Nuclear Pump Seismic Qualifications / 12.139
12.7 Chemical Industry / 12.151
12.8 Petroleum Industry / 12.169
12.9 Pulp and Paper Mills / 12.191
12.10 Food and Beverage Pumping / 12.233
12.11 Mining / 12.243
12.12 Marine Pumps / 12.261
12.13 Heating and Air Conditioning / 12.299
12.14 Pumped Storage / 12.309
12.15 Metering / 12.327
12.16 Cryogenic Pumps for Liquefied Gas Service / 12.335
12.17 Portable Transfer of Hazardous Liquids / 12.361
12.18 Aerospace / 12.367
12.18.1 Aircraft Fuel Pumps / 12.367
12.18.2 Liquid Rocket Propellant Pumps / 12.397

Chapter 13 Intakes and Suction Piping 13.1

13.1 Intakes, Suction Piping, and Strainers / 13.3
13.2 Intake Modeling / 13.37

Chapter 14 Selecting and Purchasing Pumps 14.1

Chapter 15 Installation, Operation, and Maintenance 15.1

Chapter 16 Pump Testing 16.1

Appendix Technical Data A.1

Index I.1

LIBERTY EXHIBIT 1017, Page 20

C • H • A • P • T • E • R • 1

INTRODUCTION: CLASSIFICATION AND SELECTION OF PUMPS

W. C. Krutzsch

Paul Cooper

INTRODUCTION

Only the sail can contend with the pump for the title of the earliest invention for the conversion of natural energy to useful work, and it is doubtful that the sail takes precedence. Because the sail cannot, in any event, be classified as a machine, the pump stands essentially unchallenged as the earliest form of machine for substituting natural energy for human physical effort.

The earliest pumps we know of are variously known, depending on which culture recorded their description, as *Persian wheels*, *waterwheels*, or *norias*. These devices were all undershot waterwheels containing buckets that filled with water when they were submerged in a stream and that automatically emptied into a collecting trough as they were carried to their highest point by the rotating wheel. Similar waterwheels have continued in existence in parts of the Orient even into the present century.

The best-known of the early pumps, the Archimedean screw, also persists into modern times. It is still being manufactured for low-head applications where the liquid is frequently laden with trash or other solids.

Perhaps most interesting, however, is the fact that with all the technological development that has occurred since ancient times, including the transformation from water power through other forms of energy all the way to nuclear fission, the pump remains probably the second most common machine in use, exceeded in numbers only by the electric motor.

Because pumps have existed for so long and are so widely used, it is hardly surprising that they are produced in a seemingly endless variety of sizes and types and are applied to an apparently equally endless variety of services. Although this variety has contributed to an extensive body of periodical literature, it has also tended to preclude the publication of comprehensive works. With the preparation of this handbook, an effort has been made to create just such a comprehensive source.

Even here, however, it has been necessary to impose a limitation on subject matter. It has been necessary to exclude material uniquely pertinent to certain types of auxiliary pumps that lose their identity to the basic machine they serve and where the user controls neither the specification, purchase, nor operation of the pump. Examples of such pumps would be those incorporated into automobiles or domestic appliances. Nevertheless, these pumps do fall within classifications and types covered in the handbook, and basic information on them may therefore be obtained herein after the type of pump has been identified. Only specific details of these highly proprietary applications are omitted.

Such extensive coverage has required the establishment of a systematic method of classifying pumps. Although some rare types may have been overlooked in spite of all precautions, and obsolete types that are no longer of practical importance have been deliberately omitted, principal classifications and subordinate types are covered in the following section.

CLASSIFICATION OF PUMPS

Pumps may be classified on the basis of the applications they serve, the materials from which they are constructed, the liquids they handle, and even their orientation in space. All such classifications, however, are limited in scope and tend to substantially overlap each other. A more basic system of classification, the one used in this handbook, first defines the principle by which energy is added to the fluid, goes on to identify the means by which this principle is implemented, and finally delineates specific geometries commonly employed. This system is therefore related to the pump itself and is unrelated to any consideration external to the pump or even to the materials from which it may be constructed.

Under this system, all pumps may be divided into two major categories: (1) *dynamic*, in which energy is continuously added to increase the fluid velocities within the machine

LIBERTY EXHIBIT 1017, Page 22

to values greater than those occurring at the discharge such that subsequent velocity reduction within or beyond the pump produces a pressure increase, and (2) *displacement*, in which energy is periodically added by application of force to one or more movable boundaries of any desired number of enclosed, fluid-containing volumes, resulting in a direct increase in pressure up to the value required to move the fluid through valves or ports into the discharge line.

Dynamic pumps may be further subdivided into several varieties of centrifugal and other special-effect pumps. Figure 1 presents in outline form a summary of the significant classifications and subclassifications within this category.

Displacement pumps are essentially divided into reciprocating and rotary types, depending on the nature of movement of the pressure-producing members. Each of these major classifications may be further subdivided into several specific types of commercial importance, as indicated in Figure 2.

Definitions of the terms employed in Figures 1 and 2, where they are not self-evident, and illustrations and further information on classifications shown are contained in the appropriate sections of this book.

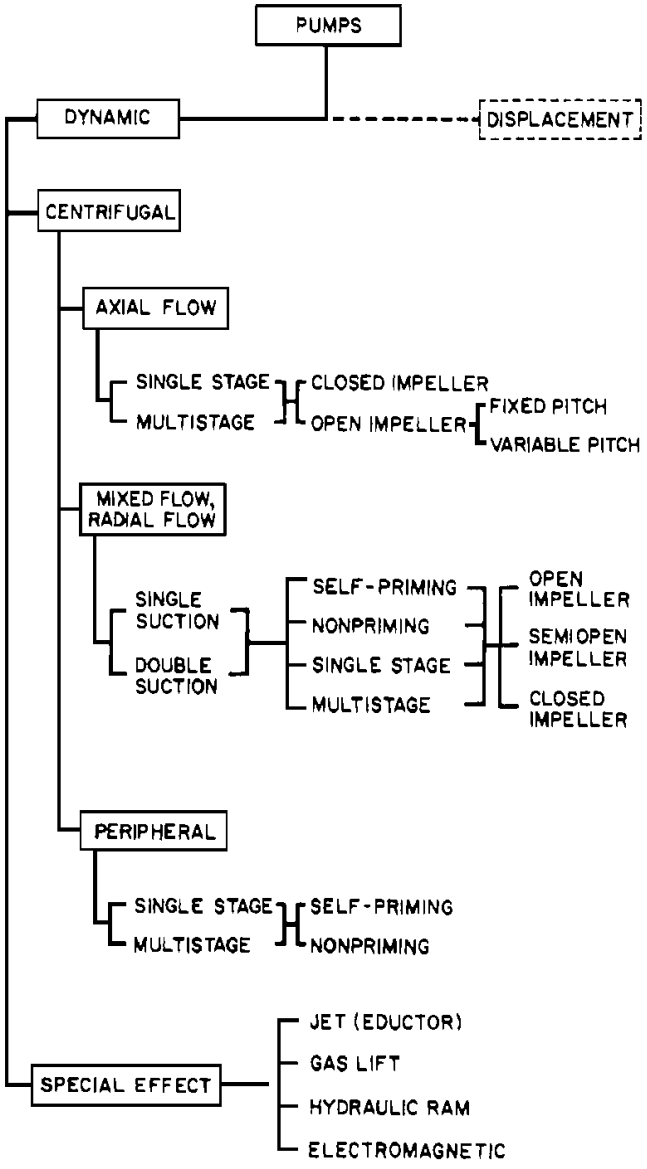


FIGURE 1 Classification of dynamic pumps

LIBERTY EXHIBIT 1017, Page 23

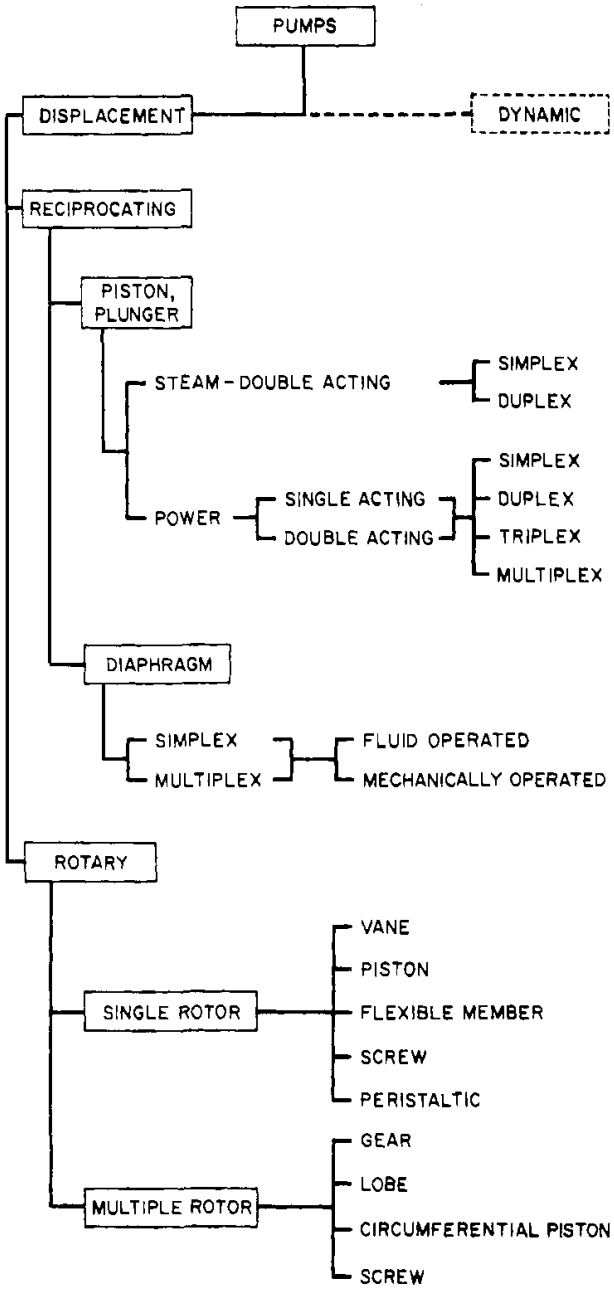


FIGURE 2 Classification of displacement pumps

OPTIMUM GEOMETRY VERSUS SPECIFIC SPEED

Fundamental to any system of classifying pumps is the rotor geometry that is optimum for each type, as illustrated in Figure 3 in terms of the specific speed N_S or Ω_S. Here Q is the volume flow rate or capacity, N is the rotative speed, Ω is the angular speed, and ΔH (or just H) is the pump head—all at the best efficiency point (BEP). Derived in Section 2.1.1 for dynamic pumps, this theoretically dimensionless quantity can also be applied to displacement pumps, at least for selection purposes. For low viscosity, Ω_S emerges as the major influence on rotor geometry. In this case, the pump performance in terms of the head coefficient $\psi = g\Delta H/(\Omega^2 r^2)$ is influenced only by the flow coefficient or "specific flow" $Q_S = Q/(\Omega r^3)$. Now, if one divides $Q_S{}^{1/2}$ by $\psi^{3/4}$, the rotor radius r (= $D_2/2$) drops out (which is convenient because we don't usually know it ahead of time), and we get the universal specific speed Ω_S as the major dependent variable—in terms of which the hydraulic design is optimized for maximum efficiency, as shown in Figure 3.

LIBERTY EXHIBIT 1017, Page 24

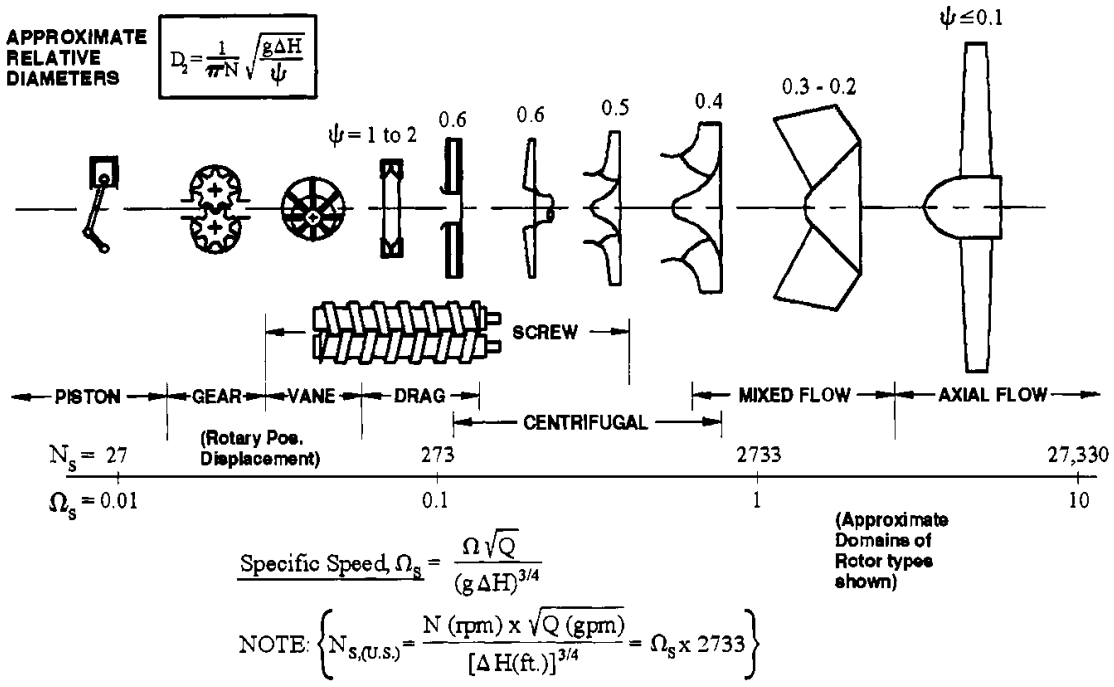


FIGURE 3 Optimum geometry as a function of BEP specific speed (for single stage rotors)

This optimum geometry carries with it an associated unique value of the head coefficient ψ, thereby effectively sizing the rotor. For dynamic, "rotodynamic" or impeller pumps, imagining speed N and head ΔH to be constant over the N_S-range shown yields increasing optimum impeller diameter as shown. This size progression shows that the optimum head coefficient ψ decreases with increasing specific speed.

Outside the N_S range shown in Figure 3 for each type of rotor, the efficiency becomes unsatisfactory in comparison to that achievable with the configuration shown for this N_S. Rotary positive displacement machines such as vane pumps, gear pumps, and a variety of screw pump configurations (all commonly called "rotary pumps") are more appropriate for the lower values of N_S, the lowest N_S-values requiring reciprocating (piston or plunger) positive displacement pumps.

Single-suction rotors are shown in Figure 3; however, if there are two inlets to the rotor (double suction), the usual practice is that the total discharge flow rate is used for Q in the specific speed expression. An exception to this is found in some places, notably in Europe, wherein the flow rate through one of the two inlets, namely half of the discharge flow rate, is used instead. In terms of the optimum geometry of centrifugal pumps, the latter practice would appear logical for impellers, because a double-suction rotor can be viewed simplistically as two back-to-back single-suction rotors. However in terms of performance (efficiency and head coefficient), the discharge portion of a double-suction impeller and the surrounding volute usually tend to play the dominant role, and these are designed for the discharge flow rate. On the other hand, the design and performance of the inlet regions of the impeller are based on the flow rate through one eye. Nevertheless, unless specifically stated to the contrary, the usage in this book is that the value of Q in the expression for specific speed represents the total discharge flow rate.

Regarding units for these relationships, the rotative speed N is in revolutions per second (rps) unless stated to be in rpm because the quantity $g\Delta H$ usually has the units of length squared per second squared. The diameter D_2 has the same length unit as the head; for example, in the rotor size equation, head in feet would imply diameter in feet. The universal specific speed Ω_S has the same value for any combination of consistent units, and similarly shaped turbine and compressor wheels have similar values of Ω_S—making it truly "universal." Note that for the unit of time being seconds, Ω is given as radians per second [= N(rpm) $\times$ $\pi/30$], where radians are unitless.

LIBERTY EXHIBIT 1017, Page 25

SELECTION OF PUMPS

Given the variety of pumps that is evident from the foregoing system of classification, it is conceivable that an inexperienced person might well become somewhat bewildered in trying to determine the particular type to use in meeting most effectively the requirements for a given installation. Recognizing this, the editors have incorporated in Chap. 14, "Selecting and Purchasing Pumps," a guide that provides the reader with reasonable familiarity regarding the details that must be established by or on behalf of the user in order to assure an adequate match between system and pump.

Supplementing the information contained in Chap. 14, the sections on centrifugal, rotary, and reciprocating pumps also provide valuable insights into the capabilities and limitations of each of these classes. None of these, however, provide a concise comparison between the various types, except for Figure 3. Moving on from that figure by assuming for these pump types their typical ranges of rotative speed N, liquid density, number of stages, and so on, makes it possible to compare them in terms of the respective ranges of the dimensional quantities of pressure (more precisely, pressure rise) and capacity (or flow rate) to which they are commonly applied. Figure 4 has been included here to do just that.

The lines plotted in Figure 4 for each of the three pump classes represent the upper limits of pressure and capacity currently available commercially throughout the world. At or close to the limits shown, only a few sources may be available, and pumps may well be specially engineered to meet performance requirements. At lower values of pressure and capacity, well within the envelopes of coverage, pumps may be available from dozens of sources as pre-engineered, or standard, products. Note also that reciprocating pumps run off the pressure scale, whereas centrifugals run off the capacity scale. For the former, some highly specialized units are obtainable at least up to 150,000 lb/in^2 (10,350 bar)[1] and perhaps slightly

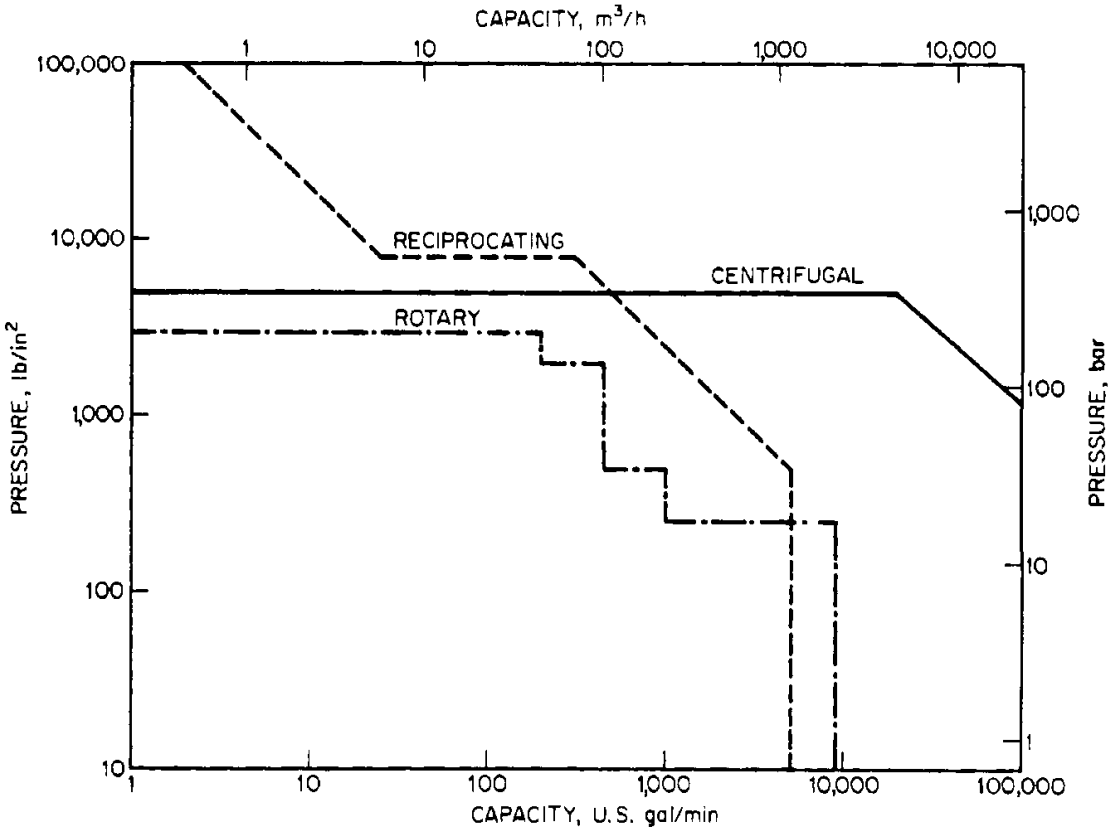


FIGURE 4 Approximate upper limit of pressure and capacity by pump class

[1] 1 bar = 10^5 Pa. For a discussion of bar, see "SI Units—A Commentary" in the front matter.

LIBERTY EXHIBIT 1017, Page 26

higher. For the latter, custom-engineered pumps would probably be available up to about 3,000,000 U.S. gal/min (680,000 m^3/h), at least for pressures below 10 lb/in^2 (0.69 bar).

Given that the liquid can be handled by any of the three basic types and given conditions within the coverage areas of all three, the most economic order of consideration for a given set of conditions would generally be centrifugal, rotary, and reciprocating, in that order. In many cases, however, either the liquid may not be suitable for all three or other considerations—such as self-priming or air-handling capabilities, abrasion resistance, control requirements, or variations in flow—may preclude the use of certain pumps and limit freedom of choice. Nevertheless, it is hoped that the information in Figure 4 will be a useful adjunct to that contained elsewhere in this volume.

C • H • A • P • T • E • R • 2

CENTRIFUGAL PUMPS

SECTION 2.1
CENTRIFUGAL PUMP THEORY, ANALYSIS, AND PERFORMANCE

2.1.1
CENTRIFUGAL PUMP THEORY

PAUL COOPER

INTRODUCTION

A centrifugal pump is a rotating machine in which flow and pressure are generated dynamically. The inlet is not walled off from the outlet as is the case with positive displacement pumps, whether they are reciprocating or rotary in configuration. Rather, a centrifugal pump delivers useful energy to the fluid or "pumpage" largely through velocity changes that occur as this fluid flows through the impeller and the associated fixed passageways of the pump; that is, it is a "rotodynamic" pump. All impeller pumps are rotodynamic, including those with radial-flow, mixed-flow, and axial-flow impellers: the term "centrifugal pump" tends to encompass all rotodynamic pumps.

Although the actual flow patterns within a centrifugal pump are three-dimensional and unsteady in varying degrees, it is fairly easy, on a one-dimensional, steady-flow basis, to make the connection between the basic energy transfer and performance relationships and the geometry or what is commonly termed the "hydraulic design" (more properly the "fluid dynamical design") of impellers and stators or stationary passageways of these machines.

In fact, disciplined one-dimensional thinking and analysis enables one to deduce pump operational characteristics (for example, power and head versus flow rate) at both the optimum or design conditions and off-design conditions. This enables the designer and the user to judge whether a pump and the fluid system in which it is installed will operate smoothly or with instabilities. The user should then be able to understand the offerings of a pump manufacturer, and the designer should be able to provide a machine that optimally fits the user's requirements.

LIBERTY EXHIBIT 1017, Page 29

The complexities of the flow in a centrifugal pump command attention when the energy level or power input for a given size becomes relatively large. Fluid phenomena such as recirculation, cavitation, and pressure pulsations become important; "hydraulic" and mechanical interactions—involving stress, vibration, rotor dynamics, and the associated design approaches, as well as the materials used—become critical; and operational limits must be understood and respected.

NOMENCLATURE

NOTE: The units for each quantity defined are as stated in this nomenclature, unless otherwise specifically stated in the text, equations, figures, or tables.

A = area, ft^2 (m^2).

a = constant of the diffuser or volute configuration in Pfleiderer's slip relation.

a = radius of impeller disk, ft (m), = $r_{t,2}$.

A_p = area of flow passage normal to the flow direction, ft^2 (m^2).

b = width of an impeller or other bladed passage in the meridional plane, ft (m).

NOTE: When dealing with radial thrust, b_2 includes also the thickness of the shrouds.

C_p = specific heat of liquid being pumped, Btu/(lbm-degF); [kcal/(kg-degC)].

c or V = absolute velocity, ft/sec (m/s).

D = diameter; unless otherwise subscripted = impeller exit diameter, ft (m).

d = diameter, ft (m).

D_h = hydraulic diameter of flow passage (= $4A_p/\wp$), ft (m).

F = thrust force, lbf (N).

g = acceleration due to gravity, = 32.174 ft/sec^2 (9.80665 m/s^2) at earth sea level.

g_o = constant in Newton's Second Law, = 32.174 (lbm-ft)/(lbf-sec^2). (There is no SI equivalent; use the dimensionless constant 1 in place of g_o in SI computations.)

$\{g_p\}$ = set of fluid properties associated with gas-handling phenomena.

H = head of liquid column, ft (m) (Eq. 3); can also have the same meaning as the change in head ΔH (that is, the same meaning as "pump head").

ΔH = change in head across pump or pump stage, also called the "pump head" or "total dynamic head" ft (m).

ΔH = the small reduction in pump head (usually 3%) in testing for NPSHR, ft (m).

H_e = $H_{i,\infty}$ = the ideal head for an infinite number of blades that produce no blockage.

H_i = ideal head [= $H + \Sigma(H_L)$], ft (m) (Eq. 15b); sometimes called the "input head."

H_L = head loss, ft (m).

ΣH_L = all losses in the main flow passages from pump inlet to pump outlet, ft (m).

h = static enthalpy in Btu/lbm times $g_o J$, ft^2/sec^2; (or in kcal/kg times J, $m^2/s^2 = J$/kg).

h_{sv} or NPSH = net positive suction head, ft (m).

ID = inner diameter.

J = the mechanical equivalent of heat, 778 ft-lbf/Btu (4184 N-m/kcal).

ℓ = blade, vane, or passage arc length, ft (m).

M or T = torque, lbf-ft (N-m).

m = distance in streamwise direction in meridional plane (Figure 14), in or ft (m).

$\dot{m}$ = mass flow rate, lbf-sec/ft (kg/s), = ρQ.

$MCSF$ or Q_{min} = minimum continuous stable flow, ft³/sec (m³/s).

N or n = rotative speed of the impeller, rpm.

NPSH or h_{sv} = net positive suction head, ft (m).

$NPSHA$ or $NPSH_A$ = available NPSH.

$NPSHR$ or $NPSH_R$ = required NPSH to prevent significant loss (> 3%) of pump Δp or to protect the pump against cavitation damage, whichever is greater.

$NPSH3\%$ or $NPSH_{3\%}$ = required NPSH to prevent significant loss (> 3%) of pump Δp; this is the "performance NPSH" defined in Section 2.1.3.

n_b or Z_i = number of impeller blades.

n_q = specific speed in rpm, m³/s, m units (Eq. 38b) = N_s/51.64 (Eq. 39c).

n_v or Z_d = number of vanes in diffuser or stator.

N_s or $N_{s(US)}$ or n_s = specific speed in rpm, gpm, ft units (Eq. 38a).

N_{ss} or S = suction specific speed in rpm, gpm, ft units (Eq. 42).

OD = outer diameter.

P = total pressure, lbf/ft² (Pa).

p = pressure, lbf/ft² [Pa (=N/m²)] (= "static pressure").

Δp = pressure rise, lbf/ft² (Pa).

p_L = pressure loss, lbf/ft² (Pa).

$p_{L,i}$ = impeller pressure loss from its inlet to the point of interest, lbf/ft² (Pa).

$p_{L,i+IL}$ = pressure loss $p_{L,i}$ in impeller plus pressure loss in inlet passage, lbf/ft² (Pa).

Σp_L = all losses in the main flow passages from pump inlet to pump outlet, lbf/ft² (Pa).

p_v or p_{vp} = vapor pressure of liquid being pumped, lbf/ft² (Pa).

P_I = power delivered to all fluid flowing through the impeller, ft-lbf/sec (kW).

P_S = shaft power, ft-lbf/sec (kW).

$\wp$ = perimeter of flow passage cross section normal to the flow direction, ft (m).

Q = volume flow rate or, more conveniently, "flow rate" or "capacity," ft³/sec (m³/s).

Q_{DR} = flow rate below which discharge recirculation exists, ft³/sec (m³/s).

Q_L = leakage from impeller exit to inlet, ft³/sec (m³/s).

Q_{min} or $MCSF$ = minimum continuous stable flow rate, ft³/sec (m³/s).

Q_R = flow rate below which recirculation exists, ft³/sec (m³/s).

LIBERTY EXHIBIT 1017, Page 31

Q_{SR} = flow rate below which suction recirculation exists, ft³/sec (m³/s).

Q3D (quasi-3D) = quasi-three dimensional.

R = radius of curvature of meridional streamline, ft (m) (Figures 13, 14, and 25).

r = radial distance from axis of rotation, ft (m).

r_b = radial distance from axis of rotation to center of circle defining impeller passage width, ft (m) (Figures 13 and 25).

r_e = maximum value of r within the "eye plane." (Figures 13 and 25.)

s = width of gap between impeller disk and adjacent casing wall, ft (m).

S = N_{ss}, suction specific speed in rpm, gpm, ft units (Eq. 42).

sp. gr. = specific gravity, namely, the ratio of liquid density to that of water at 60°F (15.6°C).

$\{S\}$ = set of flow properties associated with solids in the pumpage

T = axial thrust, lbf (N).

T or $\mathbf{T}$ or M = torque, lbf-ft (N-m).

T = temperature, °F or °R (°C or °K).

ΔT_c = temperature rise due to compression, °F (°C).

t = time, sec (s).

t = blade or vane thickness, ft (m).

u = internal energy in Btu/lbm multiplied by $g_o J$, ft²/sec²; (or in kcal/kg times J, m²/s²).

U = tangential speed Ωr of the point on the impeller at radius r, ft/sec (m/s).

U_e = the value of U at the maximum radial location r_e within the "eye plane."

$\mathbf{V}$ = volume, ft³ (m³).

V or c = absolute velocity of fluid, ft/sec (m/s).

V_e = the average value of the meridional velocity component V_m in the eye (= Q/A_e), ft/sec (m/s).

V_s = slip velocity (Figure 15), ft/sec (m/s).

W or w = velocity of fluid relative to rotating impeller, ft/sec (m/s).

W_g = the one-dimensional value of W that would exist if there were no slip.

w_1 = throat width (Figure 21), ft (m).

y = transformed distance along blade from trailing edge (Figure 19), in or ft (m).

z = axial distance in polar coordinate system, ft (m).

Z or Z_e = elevation coordinate, ft (m).

Z_d or n_v = number of vanes in diffuser or stator.

Z_i or n_b = number of impeller blades.

α = angle of the absolute velocity vector from the circumferential direction.

β = angle of the relative velocity vector or impeller blade in the plane of the velocity diagram (as seen, for example, in Figure 3) from the circumferential (tangential) direction.

γ = fluid weight density, lbf/ft^3 (N/m^3) = ρg. (1N = 1 kg-m/s^2).

δ = clearance, ft (m).

δ^* = displacement thickness of the boundary layer, ft (m).

δ_0^* = displacement thickness of the zero-pressure-gradient boundary layer, ft (m), ($\approx 0.002 \times \ell$ for turbulent boundary layers at $\nu = 1$ cs in typical centrifugal pumps).

ε = absolute roughness height, ft (m).

ε_2 = fraction of impeller discharge meridional area (that is, the area normal to the velocity component $V_{m,2}$) that is *not* blocked by the thickness of the blades and the boundary layer displacement thickness on blades and on hub and shroud surfaces.

$\varepsilon_{2,b}$ = fraction of the circumference at the exit of the impeller that is *not* blocked by the thickness of the blades and boundary layer displacement thickness on blades. (See computation in Table 10.)

η = η_p = pump efficiency; or a component efficiency (different subscript, Eqs. 8–11).

θ = rotational polar coordinate or central angle about the impeller axis, radians.

NOTE: In a polar-coordinate description of impeller blades or stationary vanes, θ becomes the construction angle and is usually regarded as positive in the direction of the blade development from inlet to exit of the impeller or other blade row.

μ = slip factor = V_s/U_2 (=1 − h_0, where h_0 is the slip factor as defined by Busemann[18]).

μ = absolute viscosity, lbf-sec/ft^2 (Pa-s or N-s/m^2); often quoted in centipoises, abbreviated to "cp" (1 cp = 0.001 Pa-s). [(μ in cp) = sp. gr. × (ν in cs).]

ν = kinematic viscosity (= μ/ρ), ft^2/sec (m^2/s); often quoted in centistokes, abbreviated to "cs" (1 cs = 1 mm^2/s). [(ν in cs) = (μ in cp)/sp. gr.]

ρ = fluid mass density, lbf-sec^2/ft^4 (kg/m^3),= γ/g.

σ = solidity (Eq. 53).

σ = Thoma's cavitation parameter = h_{sv}/H.

T or T or M = torque, lbf-ft (N-m).

ϕ = flow coefficient.

ϕ_e = V_e/U_e = impeller inlet or eye flow coefficient.

ϕ_i (or $\phi_{i,2}$) = impeller exit flow coefficient = $V_{m,2}/U_2$ (Figure 12).

ψ = head coefficient (Figure 12); stream function (Figure 14).

ψ_i = ideal head coefficient [= $\psi_{i,2} = V_{\theta,2}/U_2$ for zero inlet swirl ($V_{\theta,1} = 0$)].

$\psi_{i,2}$ = $V_{\theta,2}/U_2$ [= ψ_i for zero inlet swirl ($V_{\theta,1} = 0$)].

Ω = angular speed of the impeller in radians per second (1/s) = $N\pi/30$.

Ω_s = universal specific speed (unitless) (Eq. 37) = $N_s/2733$ (Eq. 38a) = $n_q/52.92$ (Eq. 38b).

Ω_{ss} = universal suction specific speed (unitless) (Eq. 41) = $N_{ss}/2733$ (Eq. 42).

{2-ph} = set of fluid properties associated with vaporization.

Subscripts

b = impeller blade.

BEP = best efficiency point.

D = drag due to disk friction, bearings, and seals.

DF = disk friction.

d = discharge flange or exit (ex) of the pump.

e = at the "eye" of the impeller. The "eye" is the throat (minimum-diameter point) at the entrance into the impeller and is the area defined by the "eye plane," which is normal to the axis of rotation. "e" can refer more specifically to the shroud or maximum-diameter point within the eye, as with r_e (Figure 13) or U_e. The inlet tips of the impeller blades are generally at or near this location.

ex = exit of diffuser or the discharge flange or port of the pump (d).

f = the direction of the flow.

h = hub.

i = inner limit of region or gap (Tables 4 and 5)

i (or ideal) = ideal.

i (or imp) = impeller.

in (or s) = pump inlet flange or port.

I/L = inlet passage; that is, the passage from the pump inlet flange or port to the impeller.

I = input to fluid.

L = losses.

m = "mechanical" (pertaining to efficiency, Eq. 9).

m = component of velocity in the meridional plane (that is, the axial-radial plane containing the axis of rotation).

mean = the 50% or rms meridional streamline.

n = normal or BEP value.

o = outer limit of region or gap (Tables 4 and 5).

out = pump outlet flange or port.

p = pressure side of blade or passage.

R = value of r at the impeller ring clearance.

S = shaft.

s (or in) = suction flange or inlet of the pump.

SE = shockless entry (that is, inlet velocity vector aligned with blade camber line).

s/o = shut-off or zero flow rate Q.

r = in the radial direction.

rms = the 50% or mean meridional streamline.

s = suction side of blade or passage; shaft.

s = same meaning as sh and t.

sh = shroud (also at the eye plane at inlet—and in general "t" at outlet).

stg = stage.

T = entry throat of volute or diffuser.

t = the tip or maximum radial position of the impeller blades at inlet or outlet (same meaning as s and sh).

t = tongue or cutwater.

u (see θ, below).

v = volumetric (pertaining to efficiency, Eq. 11).

v = volute.

z = in the axial direction.

θ or u = component of velocity in the circumferential direction (that is, the tangential direction in the polar view that is perpendicular to the axis of rotation).

1 = impeller inlet at the blade leading edge—at the mean unless further defined.

2 = impeller outlet at the blade trailing edge—at the mean unless further defined.

3 = volute base circle or entrance to diffuser.

∞ = for an infinite number of blades that also produce zero blockage of the flow.

Superscripts

$^-$ = average value

ENERGY TRANSFER

Hydraulics or fluid dynamics has the primary influence on the geometry of a rotodynamic pump stage—of all the engineering disciplines involved in the design of the machine. It is basic to the energy transfer or pumping process. Staging is also influenced by the other disciplines, especially in high-energy pumps. The basic energy transfer relationships need to be thoroughly understood to achieve a credible design and to understand the operation of these machines. Action of the mechanical input shaft power to effect an increase in the of energy of the pumpage is governed by the first law of thermodynamics. Realization of that energy in terms of pump pressure rise or head involves losses and the second law of thermodynamics.

The First Law of Thermodynamics Fluid flow, whether liquid or gas, through a centrifugal pump is essentially adiabatic, heat transfer being negligible in comparison to the other forms of energy involved in the energy transfer process. (Yet, even if the process were not adiabatic, the density of a liquid is only weakly dependent on temperature.) Further, while the delivery of energy to fluid by rotating blades is inherently unsteady (varying pressure from blade to blade as viewed in an absolute reference frame), the flow across the boundaries of a control volume surrounding the pump is essentially steady, and the first law of thermodynamics for the pump can be expressed in the form of the adiabatic steady-flow energy equation (Eq. 1) as follows:

$$P_S = \dot{m}\left[\left(h + \frac{V^2}{2} + gZ_e\right)_{\text{out}} - \left(h + \frac{V^2}{2} + gZ_e\right)_{\text{in}}\right]$$

where

$$h = u + \frac{p}{\rho} \tag{1}$$

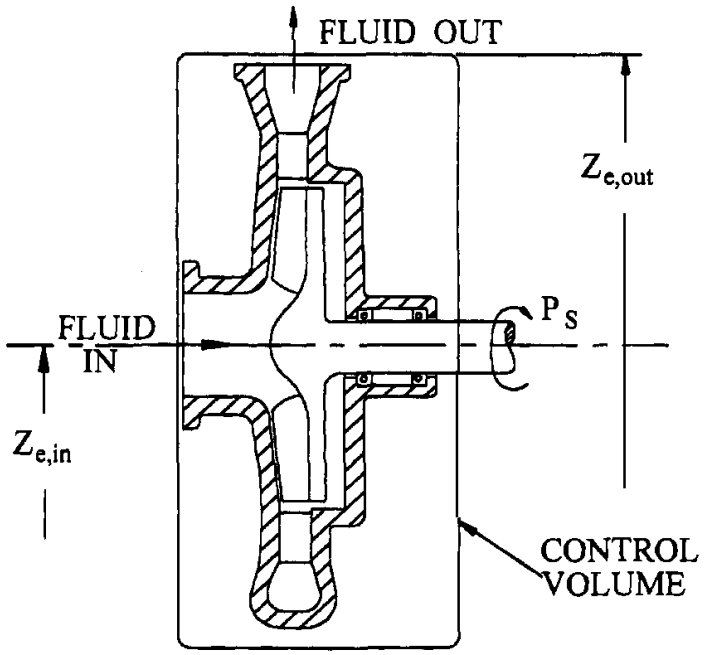


FIGURE 1 Energy transfer in a centrifugal pump

Here, shaft power P_s is transformed into fluid power, which is the mass flow rate $\dot{m}$ times the change in the total enthalpy (which includes static enthalpy, velocity energy per unit mass, and potential energy due to elevation in a gravitational field that produces acceleration at rate g) from inlet to outlet of the control volume (Figure 1).

When dealing with essentially incompressible liquids, the shaft power is commonly expressed in terms of "head" and mass flow rate, as in Eq. 2:

$$\frac{P_S}{\dot{m}} = g\Delta H + \Delta u \tag{2}$$

where

$$H = \frac{p}{\rho g} + \frac{V^2}{2g} + Z_e \tag{3}$$

The change in H is called the "head" ΔH of the pump; and, because H (Eq. 3) includes *the velocity head* $V^2/2g$ and the *elevation head* Z_e at the point of interest, ΔH is often called the "total dynamic head." ΔH is often abbreviated to simply "H" and is the increase in height of a column of liquid that the pump would create if the *static pressure head* $p/\rho g$ and the velocity head $V^2/2g$ were converted without loss into elevation head Z_e at their respective locations at the inlet to and outlet from the control volume; that is, both upstream and downstream of the pump.

The Second Law of Thermodynamics: Losses and Efficiency As can be seen from Eq. 2, not all of the mechanical input energy per unit mass (that is, the shaft power per unit of mass flow rate) ends up as useful pump output energy per unit mass $g\Delta H$. Rather, losses produce an internal energy increase Δu (accompanied by a temperature increase) in addition to that due to any heat transfer into the control volume. This fact is due to the second law of thermodynamics and is expressed for pumps in Eq 4:

$$g\Delta H < \frac{P_S}{\dot{m}} \quad \text{or} \quad \eta < 1 \tag{4}$$

where

$$\dot{m} = \rho Q$$

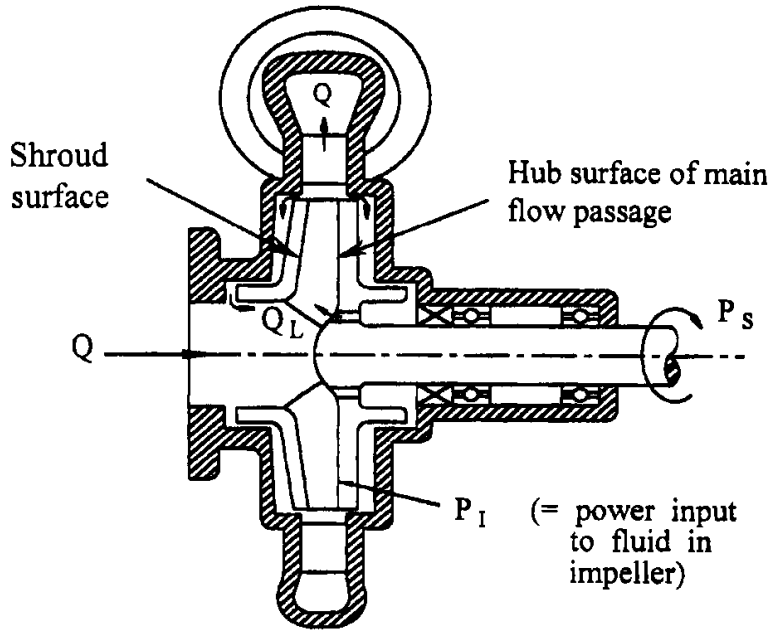


FIGURE 2 Determining component efficiencies. (This is a meridional view.)

The losses in the pump are quantified by the overall efficiency η, which must be less than unity and is expressed in Eq. 5:

$$\eta = \frac{g\Delta H\dot{m}}{P_S} = \text{Overall Pump Efficiency} \tag{5}$$

It should be pointed out here that real liquids undergo some compression—which is accompanied by a reversible increase in the temperature ΔT_c of the liquid—called the "heat of compression." This portion of the actual total temperature rise ΔT is in addition to that arising from losses and must therefore be taken into account when determining efficiency from measurements of the temperature rise of the pumpage.[1] See the discussion on this subject in Section 2.1.3.

To pinpoint the losses, it is convenient to deal with them in terms of "component efficiencies." For the typical shrouded- or closed-impeller pump shown in Figure 2, Eq. 5 can be rewritten as follows:

$$\eta = \frac{P_I}{P_S} \times \frac{g\Delta H(\dot{m} + \dot{m}_L)}{P_I} \times \frac{\dot{m}}{\dot{m} + \dot{m}_L} \tag{6}$$

Noting that

$$P_I = g\Delta H_i(\dot{m} + \dot{m}_L) \tag{7}$$

and

$$\dot{m} = \rho Q$$

$$H_i = \text{Ideal Head}$$

one may rewrite Eq. 6 as follows:

$$\eta = \frac{P_I}{P_S} \times \frac{\Delta H}{\Delta H_i} \times \frac{Q}{Q + Q_L} = \eta_m \times \eta_{HY} \times \eta_v \tag{8}$$

where

$$\left.\begin{matrix}\text{"Mechanical"}\\ \text{Efficiency}\end{matrix}\right\}\eta_m = \frac{P_I}{P_S} = \frac{P_S - P_D}{P_S} \tag{9}$$

$$\left.\begin{matrix}\text{Hydraulic}\\ \text{Efficiency}\end{matrix}\right\}\eta_{HY} = \frac{\Delta H}{\Delta H_i} = \frac{\Delta H_i - \Sigma H_L}{\Delta H_i} \tag{10}$$

$$\left.\begin{matrix}\text{Volumetric}\\ \text{Efficiency}\end{matrix}\right\}\eta_v = \frac{Q}{Q + Q_L} \tag{11}$$

Approximate formulas for the three component efficiencies of Eq. 8 will be given further on. Their product yields the overall pump efficiency as defined in Eq. 5, and reflects the following division of the pump losses:

a. External drags on the rotating element due to i) bearings, ii) seals, and iii) fluid friction on the outside surfaces of the impeller shrouds—called "disk friction"; the total being $P_D = P_S - P_I$. Generally, the major component of P_D is the disk friction, and the "mechanical efficiency" is that portion of the shaft power that is delivered to the fluid flowing through the impeller passages.

b. Hydraulic losses in the main flow passages of the pump; namely, inlet branch, impeller, diffuser or volute, return passages in multistage pumps, and outlet branch. The energy loss per unit mass is $g\Sigma H_L = g(H_i - \Delta H)$, the ratio of output head ΔH to the input head H_i being the hydraulic efficiency. This is the major focus of the designer for typical centrifugal pump geometries (which are associated with normal "specific speeds"—to be defined later). The other two component efficiencies are then quite high and of relatively little consequence.

c. External leakages totaling Q_L leaking past the impeller and back into the inlet eye. This leakage has received its share of the full amount of power $P_I = \rho g\, \Delta H_i (Q + Q_L)$ delivered to all the fluid $(Q + Q_L)$ passing through the impeller. This leakage power is $P_L = \rho g\, \Delta H_i\, Q_L$, which is lost as this fluid leaks back to the impeller inlet. The remaining fluid input power is thus $(P_I - P_L) = \rho g\, \Delta H_i\, Q$, the ratio of this power to the total (P_I) being the volumetric efficiency.

There are exceptions to this convenient model for dividing up pump losses. The main exception is that if the pump has an open impeller, that is, one without either or both shrouds, that portion of the total leakage Q_L disappears. The leakage now occurs across the blade tips and affects the main flow passage hydraulic losses. The volumetric efficiency is now higher, but the hydraulic efficiency is lower. In that case disk friction is still present, as the impeller still has to drag fluid along the adjacent stationary wall(s). Another exception—for closed impellers—is that disk friction is fundamentally an inefficient pumping action, the fluid being flung radially outward[2]; and this can result in a slight increase in pump head if the fluid on the outside of an impeller shroud or disk is pumped into the main flow downstream of the impeller.

VELOCITY DIAGRAMS AND HEAD GENERATION

The mechanism of the transfer of shaft torque (or power) to the fluid flowing within the impeller is fundamentally dynamic; that is, it is connected with changes in fluid velocity. This requires the introduction of Newton's second law, which when combined with the first law of thermodynamics, yields Euler's Pump Equation. Fluid velocities at inlet and exit of the impeller are fundamental to this development. Fluid flowing along the blades of an impeller rotating at angular velocity Ω and viewed in the rotating reference frame of that

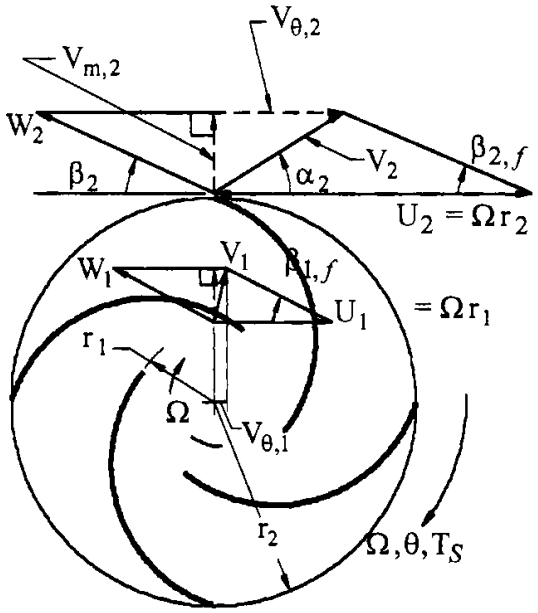


FIGURE 3 Impeller velocity diagrams (1 = inlet; 2 = outlet)

impeller has relative velocity W. Vectorially adding W to impeller blade speed $U = \Omega r$ yields the absolute velocity V, as shown in the velocity diagrams of Figure 3.

Newton's Second Law for Moments of Forces and Euler's Pump Equation Relating impeller torque $\mathbf{T}$ to fluid angular momentum per unit mass rV_θ is the convenient way of applying Newton's second law to centrifugal pumps. This is stated as follows for the control volume $\mathbf{V}$ that contains the pump impeller:

$$\Sigma \mathbf{T} = \int_{\mathbf{V}} [\partial(\rho r V_\theta)/\partial t]\, d\mathbf{V} + \int_{\mathbf{S}} \rho r V_\theta\, dQ \tag{12}$$

where $\Sigma \mathbf{T} = \mathbf{T}_S - \mathbf{T}_D$ is the summation of torques acting on the impeller; namely, the net torque $\mathbf{T}_I$ acting on the fluid flowing through it. The volume integral (first term on the right side) of Eq. 12 is the unsteady term, which is zero for steady operation. It comes into play during changing or transient conditions, such as start-up and shutdown; that is, when the angular momentum per unit volume $\rho r V_\theta$ is changing with time within the impeller control volume $\mathbf{V}$.

The surface integral (second term on the right hand side) of Eq. 12 is the one that pump designers and users are mainly concerned with. Its integration over the exterior surface $\mathbf{S}$ of the control volume $\mathbf{V}$ is effectively accomplished for most impellers by combining one-dimensional results from inlet to outlet on each of several stream surfaces—imagined to be nested surfaces of revolution bounded by the hub and shroud stream surfaces (indicated in Figure 2). Insight into the significance of this term can be gained by taking the mean value of the integrand in terms of the velocities on a representative stream surface; that is, essentially the surface of revolution lying at an appropriate mean location between hub and shroud. Each of the two velocity diagrams of Figure 3 lies in a plane tangent to this mean stream surface. For flow through an impeller, the torque delivered to the fluid is therefore given by the following relationship involving these average quantities:

$$\mathbf{T}_I = (\dot{m} + \dot{m}_L) \times (r_2 V_{\theta,2} - r_1 V_{\theta,1}) \tag{13}$$

or $\times\, \Omega$:

$$P_I = (\dot{m} + \dot{m}_L) \times (U_2 V_{\theta,2} - U_1 V_{\theta,1}) \tag{14}$$

LIBERTY EXHIBIT 1017, Page 39

Eq. 13 says that the torque is equal to the mass flow rate times the change of angular momentum per unit mass $\Delta(rV_\theta)$. This becomes the "power" statement of Eq. 14 when both sides are multiplied by Ω. Following the statement of the second law of thermodynamics in Eq. 4, we now can similarly say that $g\Delta H$ must be less than the power input to the fluid per unit of mass flow rate, namely $\Delta(UV_\theta)$ from Eq. 14. So, we now arrive at Euler's Pump Equation—expressed three different ways as follows:

$$g\Delta H < \Delta(UV_\theta) \tag{15a}$$

$$g\Delta H_i = \Delta(UV_\theta) \tag{15b}$$

or

$$g\Delta H = \eta_{HY}\Delta(UV_\theta) \tag{15c}$$

The inequality (Eq. 15a) is quantified by Eq. 15b, which follows in view of Eq. 7. Eq. 15c then follows from the definition of hydraulic efficiency (Eq. 10). Euler's Pump Equation makes one of the most profound statements in the field of engineering, because it determines the major geometrical features of the design of a rotodynamic machine. By reversing the inequality in Eq. 15a, the same principle applies to turbines; hence, the more encompassing title, "Euler's Pump and Turbine Equation."

So, to design or analyze a pump, one needs to a) obtain the velocity diagrams that will produce the ideal head at the design flow rate and b) determine how the shape of these diagrams affects the hydraulic efficiency η_{HY}, so as to obtain the desired pump stage head. Step (a) for a given pump is a simple one-dimensional exercise that utilizes the principles of continuity and kinematics (Eqs. 16 and 17) to construct the velocity diagrams for a given total impeller volume flow rate Q and pump rotative speed (Ω or N):

Continuity: $$Q = 2\pi rbV_m \tag{16}$$

where $W = V_m/\sin\beta_f$

Kinematics: $$V_\theta = U - W\cos\beta_f \tag{17}$$

Step (b) is in essence the evaluation of the hydraulic losses ΣH_L in Eq. 10, which depend mainly on the relative and absolute velocities, the associated flow passage dimensions, and incidence angles. Eq. 15c then gives the head that the pump stage will generate. Performing steps (a) and (b) at several other flow rates at the same speed enables one to develop the pump performance characteristics.

STATIC PRESSURE GENERATION

The Extended Bernoulli Equation To estimate the losses, it is convenient first to investigate the static pressure and velocity head portions of the total head. Eq. 15c can be written in terms of the total pressure P, which equals $\rho gH - \rho gZ_e$. Similarly, we may speak of hydraulic losses as losses of static pressure Σp_L, which equals $\rho g\Sigma H_L$; so

$$P = P_{in} + \rho(UV_\theta - U_1V_{\theta,1}) - \Sigma p_L - \Delta(\rho gZ_e) \tag{18}$$

where, from Eq. 3, the static (pressure) and dynamic (velocity) components of the total pressure are brought into evidence:

$$P = p + \frac{1}{2}\rho V^2 = \rho gH - \rho gZ_e \tag{19}$$

LIBERTY EXHIBIT 1017, Page 40

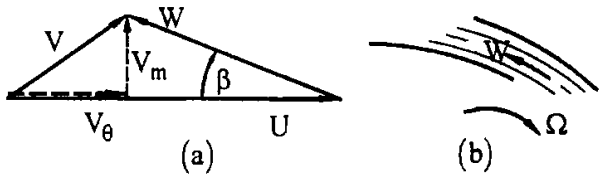


FIGURE 4 Velocity triangle and flow within impeller passageway

Eq. 18 is the turbomachine form of the "extended Bernoulli equation," which states that along a streamline the total pressure P—in the absence of significant changes of potential energy (elevation)—is a) decreased by losses and b) increased by energy addition that occurs along the streamline.

Centrifugal and Diffusion Effects in Impellers Changes in potential energy across a pump stage are small; so the static pressure rise is found essentially from subtracting the dynamic (velocity) pressure change from the total pressure change. Within the impeller, the static pressure in turn arises from a) centrifugal and b) passage diffusion effects.

Fluid in the impeller passage of Figure 4b flows from low to high radius r or blade speed U, often also experiencing a decrease in passage relative velocity W. The geometry of the velocity diagram (Figure 4a) leads to the following combination of Eqs. 18 and 19 applied across the impeller:

$$\Delta\left(p + \frac{1}{2}\rho V_m^2 + \frac{1}{2}\rho V_\theta^2\right) = \Delta[\rho U \times (U - W\cos\beta)] - p_{L,i} - \Delta(\rho g Z_e) \tag{20}$$

and, because $V_m = W_m$, this simplifies to the following form of the extended Bernoulli equation, which applies along a streamline from the inlet of the impeller:

$$\underbrace{p - p_1}_{\text{Static Pressure Change}} = \frac{1}{2}\rho\underbrace{(U^2 - U_1^2}_{\text{Centrifugal Effect}} + \underbrace{W_1^2 - W^2)}_{\text{Passage Diffusion}} - \underbrace{p_{L,i}}_{\text{Losses:}} - \rho g(Z_e - Z_{e,1}) \tag{21}$$

Losses: Incidence, Friction, Secondary Flow, Tip Leakage, Mixing $\}(\rho\Delta u)$

Here, the U-increase corresponds to the centrifugal contribution to the static pressure rise, and the W-decrease to the diffusion contribution. There is no U-change along an axial streamline in an axial-flow impeller or propeller; so, static pressure rise is due only to diffusion. Radial-flow impellers, on the other hand, often have little or no net W-change, the centrifugal effect being paramount. [A study of the velocity diagrams of Figure 3 suggests that such impellers possess a high "degree of reaction." The degree of reaction is defined as that fraction of the total energy addition within the impeller (Eq. 15b) that does *not* include the change in absolute velocity energy, $\Delta(V^2/2)$. This fraction is, therefore, the sum of the static pressure energy change, that due to elevation change, and the energy losses in the impeller, as can be seen from Eqs. 18 and 19.]

Collector Static Pressure Rise, Inlet Nozzle Drop A similar form of Eq. 21 applies in the stationary flow elements, where W is also the absolute velocity V and blade speed U is

LIBERTY EXHIBIT 1017, Page 41

zero. (This would be a more recognizable form of the extended Bernoulli equation, which differs from the classical Bernoulli equation only by the presence of the loss term.[3]) A further static pressure increase occurs in the stationary collection system downstream of the impeller (with the attendant losses); namely, in the stationary volute or diffuser. This static rise is generally about a third of that in the impeller, and it is due only to diffusion, that is, the decrease in velocity in that passage. To complete the picture, there is often an increase in the comparatively small velocity in the approach passageway or nozzle or suction branch from the pump inlet port or flange to the impeller eye or blade leading edge. This is accompanied by an attendant small pressure drop.

Internal Static Pressure Distribution If the fluid enters the pump from a stagnant pool, the total pressure at the impeller eye P_1 will be very nearly the static pressure of the upstream pool (plus the pressure equivalent of the elevation of the pool above the eye). This is one reason why the local static pressure p within the pump is often referenced to P_1, as indicated in the following form of Eq. 21:

$$p - P_1 \approx \frac{1}{2}\rho(U^2 - W^2) - p_{L,i} - \rho g(Z_e - Z_{e,1}) - \rho U_1 V_{\theta,1} \tag{22}$$

where

$$P = p_1 + \rho\frac{V^2}{2} \tag{23}$$

Figure 5 is an illustration of the internal static pressure development. The difference between P_1 and p_1 is due to the impeller inlet absolute velocity head or dynamic pressure $\rho V_1^2/2$, a much larger difference existing at the impeller exit, namely $\rho V_2^2/2$. Losses in the collector result in the pump or stage outlet total pressure P_{out} being less than P_2, the rise in total pressure ΔP_{pump} from port to port being $P_{out} - P_{in}$. In the figure, P_{in} is very nearly the same as P_1, the inlet passage loss being comparatively small for most pumps.

NET POSITIVE SUCTION HEAD

Local reduction of the static pressure p to the vapor pressure p_v of the liquid causes vaporization of the liquid and cavitation. Internal pressure drops are due to a) impeller inlet velocity head and inlet passage loss and b) blade loading and loss within the impeller. In order to prevent a substantial decrease of impeller pressure rise, the sum of these pressure drops should not exceed the difference between P_{in} and p_v, the head equivalent of which is called "net positive suction head" or NPSH:

$$\frac{P_{in} - p_v}{\rho g} \equiv NPSH \Rightarrow P_{in} = \rho g NPSH + p_v \tag{24}$$

Insufficient NPSH leads to cavitation and loss of pump pressure rise. That is because the impeller can become filled with vapor, in which case the density ρ of the fluid within the impeller is then reduced by orders of magnitude. This in turn, as can be seen in Eqs. 18–22, results in essentially zero pump pressure rise; that is, total loss of pump performance.

Eq. 24 substituted into Eq. 22 yields the local static pressure above vapor pressure in terms of the NPSH:

$$p - p_v = \rho g NPSH + \rho(U^2 - W^2) \tag{25}$$

$$- p_{L,i+I/L} - \rho g(Z_e - Z_{e,1}) - \rho U_1 V_{\theta,1}$$

LIBERTY EXHIBIT 1017, Page 42

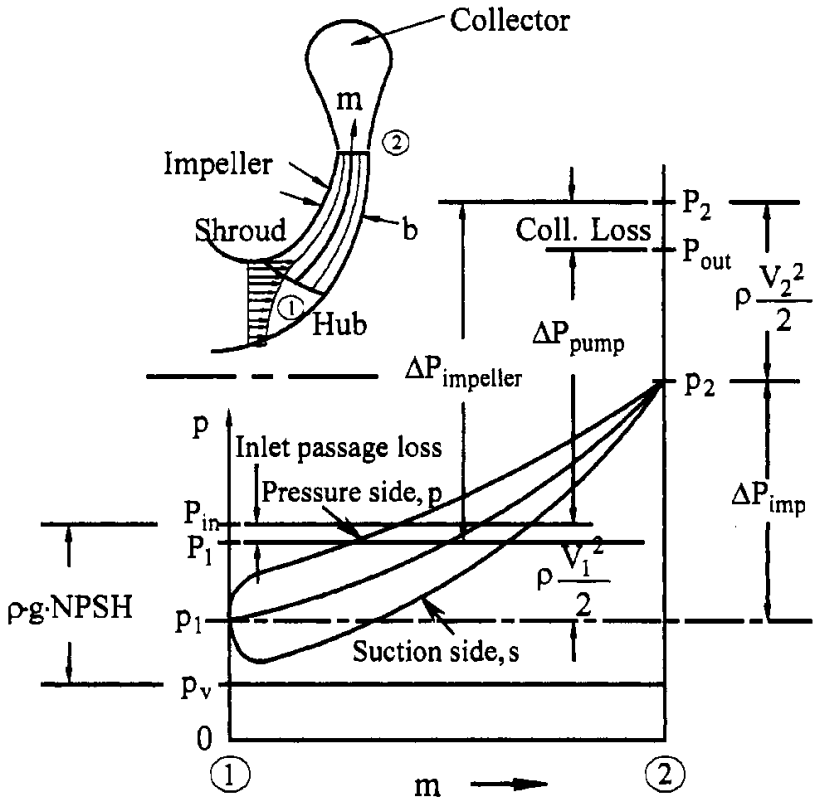
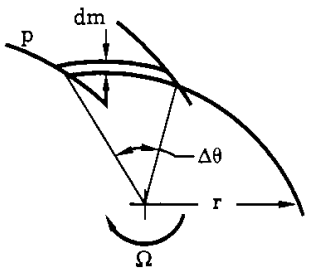


FIGURE 5 Pump stage internal pressure development. Total pressure rise $\Delta P = \rho g \Delta H$

This, together with the foregoing pressure drops, which occur in the inlet region of the pump, is illustrated in Figure 5. The figure contains three plots of p along the representative streamline from 1 to 2, m being distance along this line in the meridional plane. These plots are for the suction side or trailing face of an impeller blade, the pressure side or driving face, and the average or mid-passage position. The middle or average pressure plot is readily described by Eq. 25 in terms of the local average W-distribution. The local blade-to-blade static pressure difference $p_p - p_s$ arises from the torque exerted on a strip of fluid between the blades and approximated here via blade-to-blade average velocity components in Newton's Second Law for Moments of Forces:



$$r(p_p - p_s)b\,dm = \rho V_m b r \cdot \Delta\theta \cdot d(rV_\theta) \tag{26}$$

$$p_p - p_s = \frac{2\pi}{n_b} \frac{\rho V_m}{\Omega} \frac{d(UV_\theta)}{dm}$$

where, for ease of illustration, the blade-to-blade polar angle difference $\Delta\theta$ is taken equal to $2\pi/n_b$, the actual value of $\Delta\theta$ being slightly less than this due to the thickness of the blades. Thus, for example, too small a number of blades n_b results in a larger value of $p_p - p_s$ and a lower minimum static pressure in the inlet region of the impeller.

CFD codes have been developed that simulate the density reduction in a cavitating impeller and can accurately predict the resulting effect on pump performance.[4] More rapid and convenient approximations to CFD predictions are available to engineers and

LIBERTY EXHIBIT 1017, Page 43

designers in the form of empirical relationships for acceptable levels of NPSH. These will be presented further on, as guidelines for design and performance prediction are developed.

PERFORMANCE CHARACTERISTIC CURVES

Velocity diagrams and ideal head-rise vary with flow rate Q as illustrated in Figure 6 for the typical case of constant rotative speed N or angular speed Ω. Flow patterns in Figure 6b correspond to points on the characteristic curves of Figure 6a. The inlet velocity diagrams (just upstream of the impeller) are shown there for high and low flow rate—with zero swirl being delivered by the inlet passageway to the impeller; that is, $V_{\theta,1} = 0$. The outlet velocity diagrams on Figure 6a are found one-dimensionally, the magnitude of the exit relative velocity vector W_2 varying directly with Q and its direction being nearly tangent to the impeller blade. From these diagrams are found the absolute velocity vector V_2 and its circumferential component $V_{\theta,2}$. Because blade speed U_2 is constant, the resulting plot of the ideal head $\Delta H_i = U_2 V_{\theta,2}/g$ (from Eq. 15b) is a straight line, rising to the point U_2^2/g at zero-Q or "shut-off head." This is twice the impeller OD tip speed head $U_2^2/2g$. The right-most velocity diagram in Figure 6a has zero $V_{\theta,2}$; however, the maximum or "runout" flow rate happens at lower Q than this. That is because the actual head H is less than ΔH_i due to losses (as seen in Eq. 10), and $\Delta H = 0$ at runout—where overall pump efficiency (Eq. 8) is also zero.

This one-dimensional analysis works well in the vicinity of the best efficiency point (b.e.p. or BEP) and at higher Q because the fluid flows smoothly through the impeller passages as illustrated in Figure 6b for "high Q." However, it fails at "low Q," where recirculating flow develops—indicated by a substantial one-dimensional deceleration or reduction in the fluid velocity relative to those passages—that is, $W_2 \ll W_1$. This is analogous to a diffuser with side walls that diverge too much: the main fluid stream separates from one or both walls and flows along in a narrow portion of the passage in a jet—the rest of the passage being occupied with eddying fluid that can recirculate out of the impeller inlet and exit. Consequently, the real outlet velocity diagram at low Q is the one with the dashed lines and the smaller value of $V_{\theta,2}$, rather than the solid-lined, one-dimensional diagram superimposed on it. This in turn reduces the ideal head at the low-Q point of the curves.

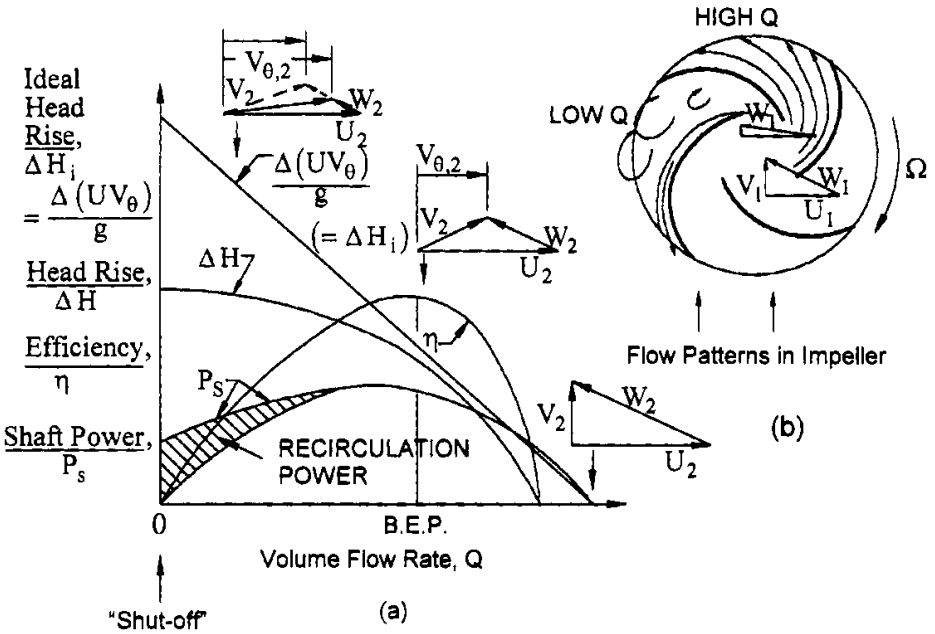


FIGURE 6A and B Characteristic performance curves of a pump stage, related to velocity diagrams

LIBERTY EXHIBIT 1017, Page 44

To complicate matters further at low Q, one-dimensional application of this "corrected" outlet velocity diagram via Eq. 14 would produce a pump power consumption curve that passes through the origin of Figure 6a. Such a result (assuming negligible external drag power P_D), is known not to occur in a real pump. Rather, superimposed on the jet flow pattern just described is recirculating fluid that leaves the impeller, gives up its angular momentum to its surroundings, and re-enters the impeller to be re-energized.

In other words, the one-dimensional simplifications mentioned after Eq. 12 do not hold at low Q; rather, there is an added "recirculation power," which is the UV_θ-change experienced by the recirculating fluid integrated over each element of re-entering mass flow rate[5]. The complexity of this recirculation destroys one's ability to interpret pump performance under such conditions by means of velocity diagrams. Instead, a transition is made from empirical correlations for head and power at "shutoff" or zero net flow rate to the high-Q, one-dimensional analysis, enabling one to arrive at the complete set of characteristic curves for efficiency, power, and head illustrated in Figure 6a. In fact, impeller pressure-rise at shutoff is very nearly what would be expected due to the centrifugal effect of the fluid rotating as a solid body, namely $\rho U_2^2/2$. The recirculating flow patterns seem to be merely superimposed with little effect on impeller pressure-rise. This recirculation, on the other hand, does produce some additional shutoff pressure rise in the collecting and diffusing passages downstream of the impeller.

SCALING AND SIMILITUDE

When a set of characteristic curves for a given pump stage is known, that machine can be used as a model to satisfy similar conditions of service at higher speed and a different size. Scaling a given geometry to a new size means multiplying every linear dimension of the model by the scale factor, including all clearances and surface roughness elements. The performance of the model is then scaled to correspond to the scaled-up model by requiring similar velocity diagrams (often called "velocity triangles") and assuming that the influences of fluid viscosity and vaporization are negligible. The proportions associated with Eqs. 27, 29, and 32 illustrate this. The blade velocity U (Eq. 30) varies directly with rotative speed N or angular speed Ω—and directly with size, as expressed by the radius r. For the velocity V (or W) to be in proportion to U, the flow rate Q must therefore vary as Ωr^3; hence, the "specific flow" Q_s must be constant (Eq. 28). Further, as the head is the product of two velocities, it must vary as $\Omega^2 r^2$; hence, the head coefficient ψ must be constant (Eq. 31). Finally, as power is the product of pressure-rise and flow rate, shaft power P_s must vary as $\rho\Omega^3 r^5$; hence, the power coefficient must be constant.

$$Q = AV \quad \begin{cases} A \propto r_2^2 & \propto D^2 \\ V \propto \Omega r_2 & \propto ND \end{cases}$$

$$\Rightarrow Q \propto ND^3 \quad \text{or} \quad \Omega r_2^3 \tag{27}$$

and

$$\frac{Q}{\Omega r_2^3} = \text{Constant} = Q_s \tag{28}$$

At above Q,

$$\eta = \text{Constant, and}$$

$$g\Delta H = \eta_{HY}\Delta(UV_\theta)$$

$$\Rightarrow \Delta H \propto N^2 D^2 \tag{29}$$

$$U = \Omega r \tag{30}$$

LIBERTY EXHIBIT 1017, Page 45

and
$$\psi = \frac{g\Delta H}{U_2^2} = \text{constant} \tag{31}$$

$$P_S = \frac{\rho Q g \Delta H}{\eta}$$

$$\Rightarrow P_S \propto \rho N^3 D^5 \tag{32}$$

and
$$\hat{P}_S = \frac{P_S}{\rho \Omega^3 r_2^5} = \text{constant} \tag{33}$$

Figure 7a is the result of following these similarity rules for a given pump that undergoes a change in speed from full speed to half speed without a change in size. The similar Q at half speed for a given Q at full speed is half that at full speed. At each such half-speed Q-value, the head ΔH is accordingly one-fourth of its full-speed value and the efficiency η is unchanged. One can avoid replotting the characteristic curves in this manner for every change in speed (and size) by expressing them nondimensionally in terms of Q_s, ψ, η, and $\hat{P}_s$. They then all collapse on one another as illustrated in Figure 7b. Note that a change in pump geometry or shape of the hydraulic passageways destroys this similitude and necessarily produces a new set of curves—shaped differently but similar to each other.

Similitude enables the engineer to work from a single dimensionless set of performance curves for a given pump model. This is a practical but special case of the more

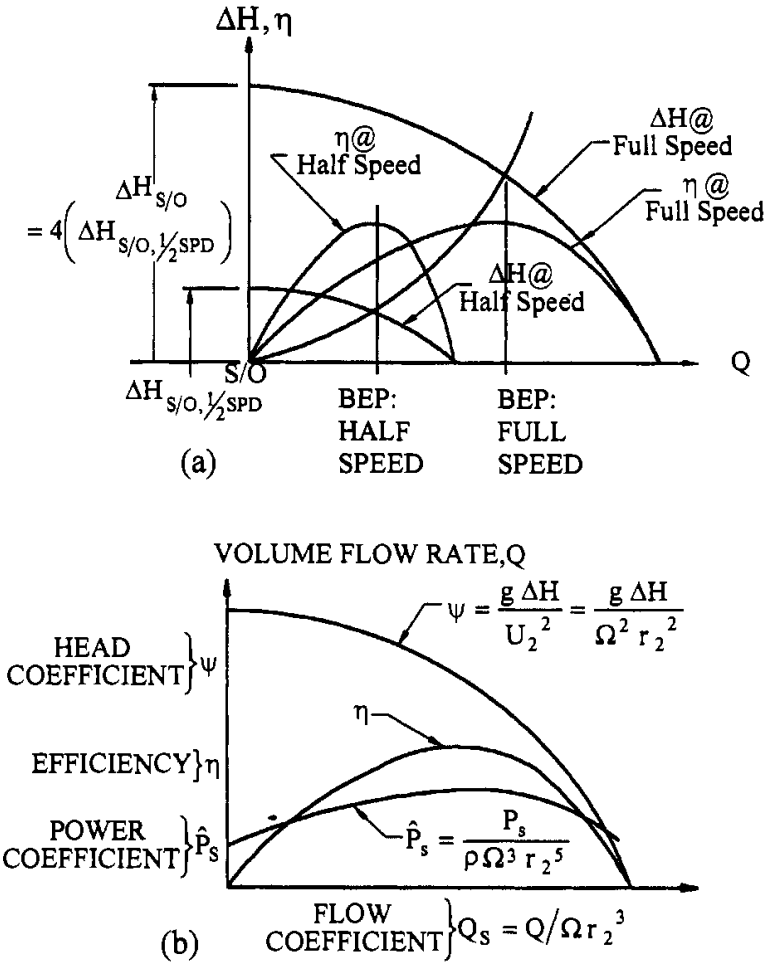


FIGURE 7 Similar performance curves: a) dimensional; b) dimensionless

LIBERTY EXHIBIT 1017, Page 46

general statement that pump performance as represented by efficiency, head, and power, is more generally expressed in terms of the complete physical equation as follows:

$$\eta,\ \Delta H,\ P_S\ = \text{fct's. } (Q,\ r_2,\ \Omega,\ \rho,\ \nu,\ NPSH,\ \{2\text{-}ph\},\ \{g_p\},\ \{S\},\{\ell_i\}) \tag{34}$$

where $\{\ell_i\}$ is the infinite set of lengths that defines the pump stage geometry. A common group of these lengths is illustrated in Figure 8. Dimensionlessly, Eq. 34 becomes

$$\eta,\ \psi,\ \hat{P}_S = \text{fct's. } (Q_s,\ R_e,\ \tau_2,\ \{2\text{-}\Phi\},\ \{\Gamma_p\},\ \{\Sigma\},\ \{G_i\}) \tag{35}$$

where the dimensionless quantities containing flow rate, viscosity and NPSH are respectively defined as follows:

where

$$Q_s = \frac{Q}{\Omega r_2^3} \qquad R_e = \frac{\Omega r_2^2}{\nu} \qquad \tau_2 = \frac{2gNPSH}{\Omega^2 r_2^2}$$

Specific Flow	Machine Reynolds Number	Cavitation Coefficient

(36)

and

- $\{G_i\} = \{\ell_i/r\}$ defines the dimensionless geometry or shape.
- $\{2\text{-}\Phi\}$ = the dimensionless quantities arising from the set of fluid, thermal, vaporization, and heat transfer properties $\{2\text{-}ph\}$ that influence the flow of two-phase vapor and liquid. These quantities come into play when the NPSH is low enough for such flow to be extensive enough to influence pump performance.
- $\{\Sigma\}$ = the dimensionless quantities arising from the set of properties $\{S\}$ associated with entrained solids and emulsifying fluids that affect the performance of slurry pumps and emulsion pumps. Similarly, $\{\Gamma_p\}$ arises from $\{g_p\}$ for entrained gases.

SPECIFIC SPEED AND OPTIMUM GEOMETRY

The hydraulic geometry or shape of a pump stage can in principle be chosen for given values of the other independent variables in Eqs. 34 or 35 so as to optimize the resulting performance; for example, to maximize the best efficiency η_{BEP} under certain conditions on the head and power. Two such conditions that are common are a) no positive slope is allowed anywhere along the ΔH-vs.-Q curve of Figure 7 (called the "no drooping nor dip" condition) and b) the maximum power consumption must occur at the BEP (often called the "non-overloading" condition). A fundamental and generally typical pumping situation involves a) negligible influence of viscosity, (that is, high Reynolds number) b) the absence of two-phase fluid effects, (that is, the existence of sufficient NPSH or τ) and c) the absence of entrained gases, solid particles and emulsion-related substances in the fluid. In this situation, Eq. 35 has one remaining significant independent variable; namely, the specific flow Q_s, which in the definitions of Eq. 36 contains the volume flow rate Q, the pump speed Ω, and the characteristic radius r_2. Most users don't know the size of the pump stage a priori; so, r_2 is eliminated by replacing Q_s in Eq. 35 with a new quantity that is the result of dividing the square root of Q_s by the $\frac{3}{4}$-power of the head coefficient ψ. Thus, from the definitions just given of Q_s and ψ, one arrives at the *specific speed* Ω_s as the independent variable in terms of which the geometry is optimized[3]:

$$\Omega_s = \frac{\Omega\sqrt{Q}}{(g\Delta H)^{3/4}} = \frac{\sqrt{Q_s}}{\psi^{3/4}} \tag{37}$$

For convenience, specific speed is usually expressed in terms of the conventional quantities N, Q, and ΔH that correspond to the factors in Eq. 37, which quantities are expressed

LIBERTY EXHIBIT 1017, Page 47

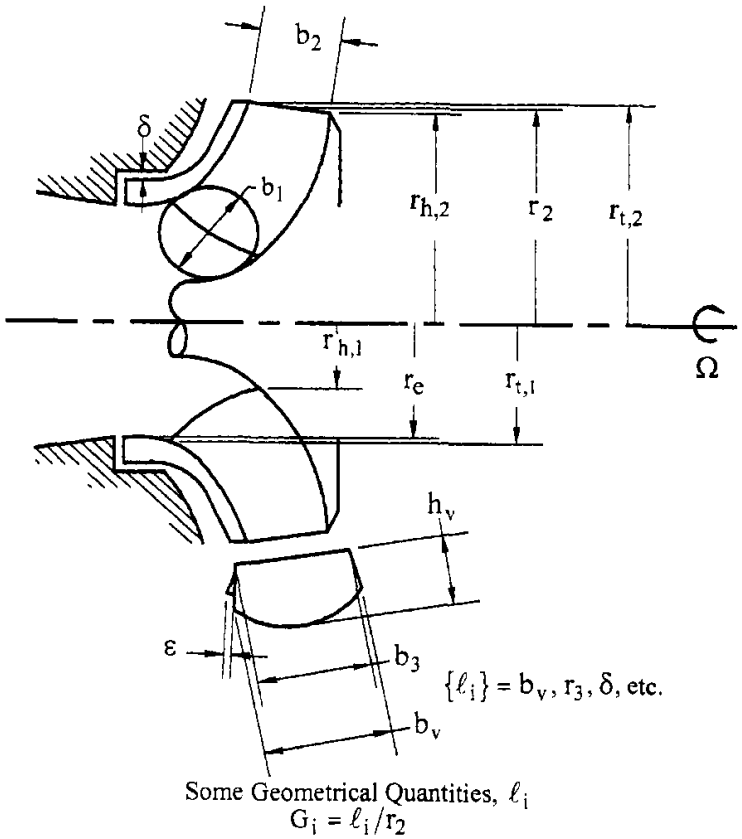


FIGURE 8 Defining the geometry of a pump stage

in the units commonly used commercially. For example, forms found in the United States and in Europe and the relationship of these to the truly unitless "universal specific speed" Ω_s defined in Eq. 37 are as follows:

$$\Omega_s = \frac{N(\text{rpm})\sqrt{Q(\text{USgpm})}/[\Delta H(\text{ft})]^{3/4}}{2733.016} = \frac{N_{s,(\text{U.S.})}}{2733.016} \tag{38a}$$

$$\Omega_s = \frac{N(\text{rpm})\sqrt{Q(\text{m}^3/\text{s})}/[\Delta H(\text{m})]^{3/4}}{52.919} = \frac{n_q}{52.919} \tag{38b}$$

Thus,

$$n_q(\text{m}^3/\text{s, m}) = N_s(\text{USgpm, ft})/51.64 \tag{38c}$$

Rotor Shape as a Function of Specific Speed Optimization of pump hydraulic geometry in terms of the BEP specific speed has taken place empirically and analytically throughout the history of pump development. An approximate illustration of the results of this process for pump rotors or impellers is shown in Figure 9. Not only does the geometry emerge from the optimization process but also the head, flow, and power coefficients for each shape as well. Approximate values for the optimum BEP head coefficient ψ are shown on the figure. The actual rotor diameter can then be deduced as noted—from the ψ-definition of Eq. 31. The relationship among the various rotors is illustrated in the figure—assuming that they all have the same speed and head; that is, as one moves along

LIBERTY EXHIBIT 1017, Page 48

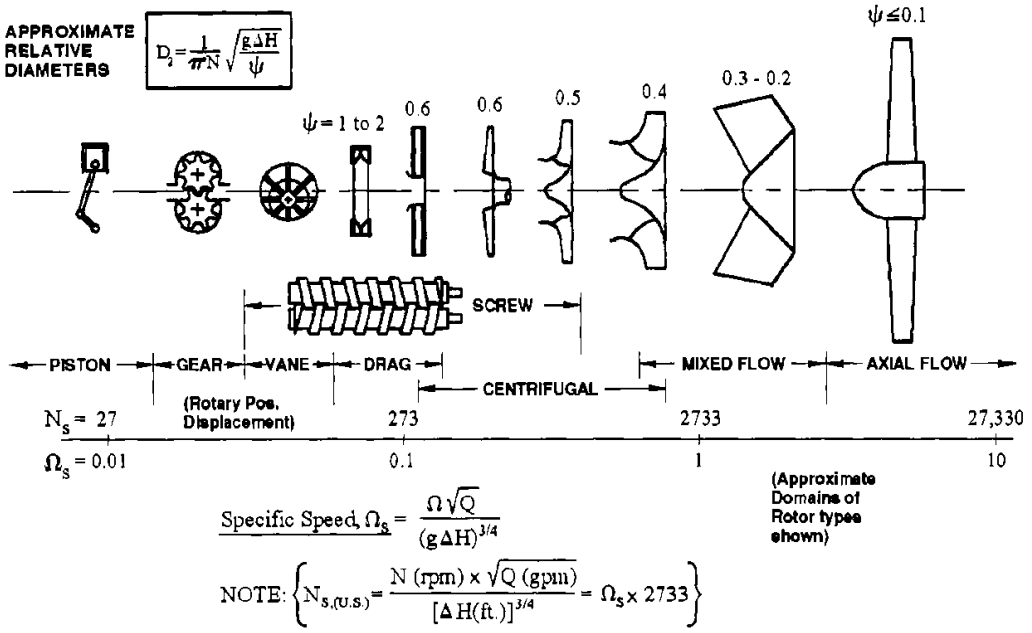


FIGURE 9 Optimum geometry as a function of BEP specific speed (for single-stage rotors)

the abscissa or specific speed axis of Figure 9, only the flow rate is changing as far as the illustrations of the rotors are concerned. As would be expected, therefore, high-specific-speed impellers need to have large passages relative to their overall diameter. Conversely, the passages become smaller as the centrifugal range is traversed toward lower specific speed, the low limit effectively being $\Omega_s = 0.2$ ($N_s \approx 500$), at which point an open impeller of the "Barske" type is illustrated as being typical for this part of the range. Yet centrifugal impellers are found at values of Ω_s as small as 0.1, at which point the impeller is sometimes simply a disk with drilled holes for passages, as illustrated.

For simplicity, the common "double-suction" arrangement, wherein two centrifugal impellers are effectively configured back-to-back, is not shown in Figure 9. Double-suction impellers commonly discharge into a single, surrounding collector designed to accommodate twice the flow rate of one side. Because this collector can be fed by an equivalent single-suction impeller, the specific speed of the whole pump stage is computed using the combined flow rate of the two sides of the double-suction impeller. While this is common practice in the United States, the practice in some other parts of the world is to compute the specific speed of such a pump stage using the flow rate of only one side of the impeller. The former approach is convenient for associating the exit geometrical features and flow behavior of the stage with the magnitude of the specific speed, while the latter favors the suction or inlet characteristics.

At the lower end of the specific speed range shown in Figure 9, rotodynamic pumps (that is, centrifugal pumps, in which category mixed- and axial-flow geometries are generally included) would be too low in efficiency to be practical. Rather, rotary positive displacement pumps take over, there being a transition through the drag pump domain. Sometimes called a regenerative or periphery pump, the drag pump is actually a rotodynamic machine, developing head peripherally around the impeller through successive passes radially through the blades on both sides until a barrier is reached at some point on the periphery, where the fluid is then discharged.[6]

The screw pump, on the other hand, is a truly positive displacement (rotary) machine. It can have two, three, or more meshing screws and can move large quantities of fluid—both single- and multiphase—against a large pressure difference Δp, giving it a specific speed range that extends well into centrifugal pump territory. Screw pump rotors are often configured back-to-back in a double-suction arrangement, as this balances the considerable axial thrust of these rotors. Not shown is the progressive cavity pump, which has a single screw surrounded by an elastomer sealing member.

LIBERTY EXHIBIT 1017, Page 49

Lower flow rates are readily accommodated by the vane pump, whereas gear pumps handle a higher range of pressure differences at such flow rates. Finally, extremely high pressures are produced by reciprocating pumps, the specific speed range of which extends off the figure on the left.

Positive displacement pumps appear in Figure 9 in order to provide perspective. The concept of specific speed is not generally applied to these machines, because a given positive displacement pump can have such a wide range of pressure-rise capability at a chosen flow rate and speed as to make it difficult to associate a given rotor geometry with a particular value of specific speed. On the other hand, a unique rotodynamic pump geometry is readily associated with the specific speed of the BEP of such a machine.

Performance of Optimum Geometries Figure 9 enables one to easily identify the pump stage types associated with required pumping tasks in terms of head, flow rate, and rotative speed. Beyond this general picture is the related performance of a real pump geometry in a real fluid. Although, for centrifugal pumps, the specific speed has the major effect on performance, the available NPSH and the viscosity of the pumpage also have an influence. These are evident in the following formal statement of the efficiency of an optimized pump (cf Eq. 35)

$$(\eta_{\max})_{\{G_i\}_{\text{opt}}} = f(\Omega_s, \Omega_{ss}, \{2\text{-}\Phi\}, \{\Gamma_p\}, \{\Sigma\}, R_{e,H,Q}) \tag{39}$$

where the radius r_2, representing the size, has been eliminated from the other variables in Eq. 35 by introducing the *suction specific speed* Ω_{ss} and the *head-flow Reynolds number* $R_{e,H,Q}$, which are defined in Eqs. 40 and 41:

$$R_{e,H,Q} = \frac{\sqrt{Q}\,(g\Delta H)^{1/4}}{\nu} = R_e\sqrt{Q_s}\,\psi^{1/4} \tag{40}$$

$$\Omega_{ss} = \frac{\Omega\sqrt{Q}}{(g\,NPSH)^{3/4}} = \frac{\sqrt{Q_s}}{(\tau_2/2)^{3/4}} \tag{41}$$

where, the common form of the suction specific speed, called N_{ss}, is given in commercial U.S. units by (Eq. 42)

$$N_{ss,\,(\text{U.S.})} = \frac{N(\text{rpm})\sqrt{Q(\text{gpm})}}{[NPSH\,(\text{ft})]^{3/4}} = \Omega_{ss} \times 2733.016 \tag{42}$$

Size Effect For sufficiently high NPSH (or sufficiently low suction specific speed) and low viscosity (or high Reynolds number), real pumps also possess a strong size effect on efficiency. This is because, in normal manufacturing processes, the clearances δ preventing internal leakage Q_L (for example, past the impeller sealing rings in Figure 2) do not scale up in proportion to the size (represented by r_2), nor do the surface roughness heights ε. Thus, a larger pump tends to be more efficient. Strictly speaking, however, the geometry of the larger pump is not the same as that of the smaller pump, and this forces one to modify Eq. 39 by reintroducing two of the length ratios G_i that were part of the set $\{G_i\}$ in Eq. 35 which characterize the hydraulic shape of the machine. Thus, Eq. 39, revised to reflect these realities, becomes

$$(\eta_{\max})_{\{G_i\}_{\text{opt.}}} = f_1\left(\Omega_s, \Omega_{ss}, R_{e,H,Q}, \{2\text{-}\Phi\}, \{\Gamma_p\}, \{\Sigma\}, \frac{\varepsilon}{r_2}, \frac{\delta}{r_2}\right) \tag{43}$$

A study of a large number of commercial centrifugal pumps by H. H. Anderson[7] has quantified Eq. 43 for such machines. These pumps were all operating in water and had

LIVE GRAPH
Click here to view

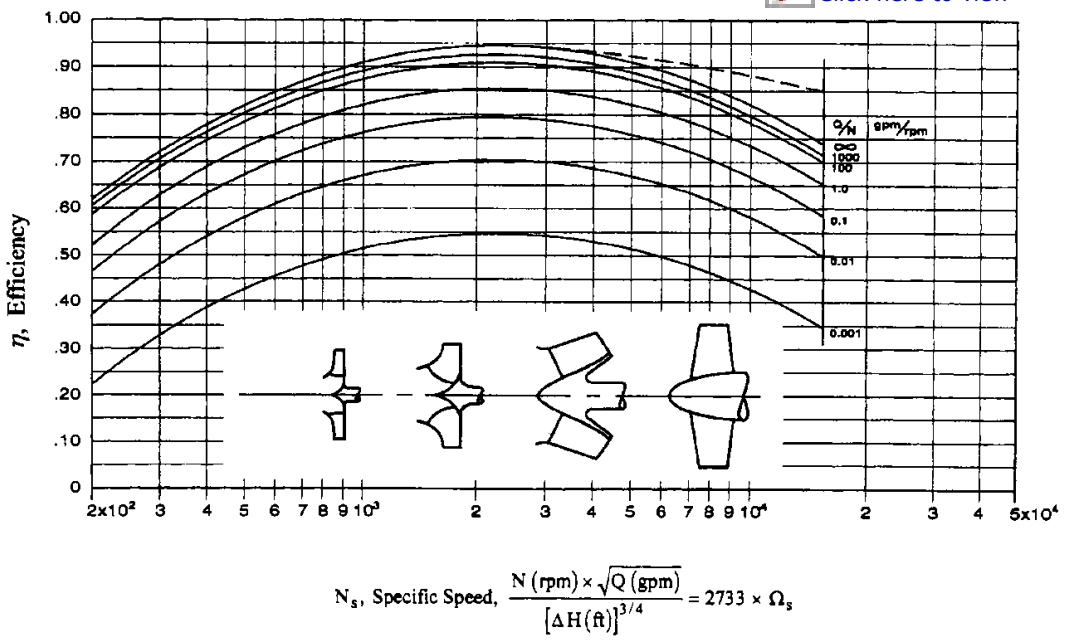


FIGURE 10 Efficiency at the BEP of centrifugal pumps versus specific speed, size, and shape–adapted from Anderson[7] for X = 1

Note: Actual experience for $Ns > 2286$ shows higher efficiency, as indicated by the dashed line. $m^3/h = 0.227 \times gpm$.

sufficient NPSH for performance not to be influenced by Ω_{ss}. The results are given by Eq. 44, which is plotted in Figure 10 for the quantity X = 1:

$$\eta = 0.94 - 0.08955 \times \left[\frac{Q(\text{gpm})}{N(\text{rpm})} \times X\right]^{-0.21333} - 0.29 \times \left[\log_{10}\left(\frac{2286}{N_s}\right)\right]^2 \qquad (44)$$

where

$$X = \left[\frac{140}{\varepsilon(\mu\text{-in.})}\right]^2 = \left[\frac{3.56}{\varepsilon(\mu\text{m})}\right]^2$$

Eq. 44 is a combination of separate relationships developed by Anderson for efficiency and speed as functions of flow rate[7]. Included is a correction for specific speed that is too conservative for $N_{s\,(US.)} > 2286$ or Ω_s greater than about unity. With this qualification, Figure 10 is a useful representation for centrifugal pumps and is often as far as many users go in determining the performance of these machines.

Viscosity Effects Centrifugal pump geometries have not generally been optimized versus Reynolds number—often because the effect on hydraulic shape is not very great except for the highest viscosities of the pumpage, and a given application can sometimes experience a substantial range of viscosity. Studies of conventional centrifugal pumps over a range of Reynolds number have been combined in nomographic charts in the Hydraulic Institute Standards, which yield correction factors to the head, efficiency, and flow rate of the BEP of a water (low viscosity) pump in order to obtain the BEP of that pump when operating at higher viscosity[8]. Figure 11 is a presentation of these correction factors in terms of the head-flow Reynolds number. Values of the head correction factor C_H are also given for flow rates other than that of the BEP, enabling one to produce a completely corrected curve of head vs. flow rate. Strictly speaking, in view of Eq. 43, each pump geometry has a unique set of such correction factors, yet the data presented in Figure 11 have been widely utilized as reasonably representative of conventional centrifugal pumps.

NPSH Effects In many cases, the available NPSH is low enough, or the suction-specific speed Ω_{ss} at which the pump stage must operate is high enough for significant two-phase activity to exist within the impeller. This is to be expected in centrifugal impellers of water

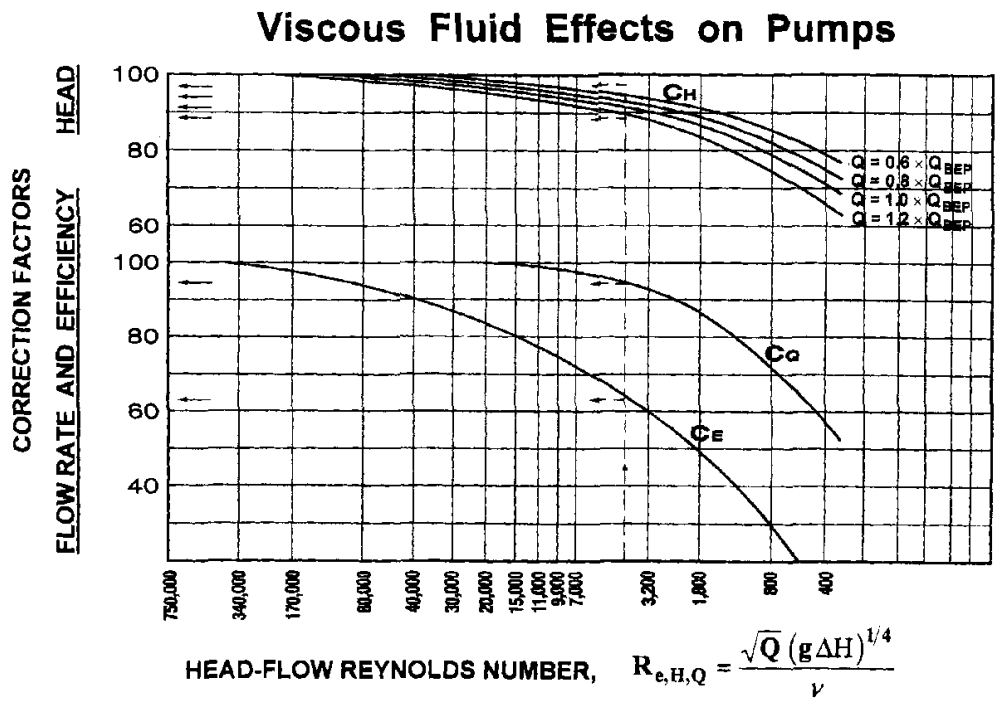


FIGURE 11 Viscous fluid effects on centrifugal pumps—adapted from Hydraulic Institute ANSI/HI 2000 Edition Pump Standards, Reference 8. Values of the correction factors C_Q, C_E, and C_H are each shown as the percent of the water flow rate, efficiency, and head, respectively, that is realized for operation of the same pump in a high-viscosity fluid (low Reynolds number). Except as noted for the C_H curves, these are BEP quantities. The BEP values of Q and H in water operation, together with the higher viscosity of interest, are used in forming the Reynolds number.

pumps if the available Ω_{ss} is greater than about 3 to 4 (or $N_{ss,(U.S.)} = 8{,}000$ to 11,000). In such a case, Ω_{ss} and the vaporization quantities $\{2\text{-}\Phi\}$ in Eq. 35 dictate a profound change in the impeller geometry into that of an inducer. The inducer has an entering or "eye" diameter that is significantly enlarged—together with tightly wrapped helical blading. Often the inducer is a separate stage that pressurizes the two-phase fluid as needed to provide a sufficiently low value of Ω_{ss} at the entrance of the more typical impeller blading that is immediately downstream of the inducer. If the two-phase fluid is near its thermodynamic critical point, the $\{2\text{-}\Phi\}$ operate to greatly reduce the amount of two-phase activity within the pump. (At the critical point, the liquid and gas phases are identical, and therefore both have the same specific volume.) An example is the pumping of liquid hydrogen, for which an inducer is unnecessary until much higher values of Ω_{ss} are reached. Moreover, inducers—typically limited to Ω_{ss}-values of about 10 ($N_{ss,(U.S.)} = 27{,}000$) in water—can, at sufficiently low tip speed, operate at zero NPSH, which corresponds to an infinite value of Ω_{ss}[9].

Pumping Entrained Gas In addition to the liquid's own vapor (which is the gas involved in the NPSH-effects discussion), many pumping applications deal with a different gas; that is, a different substance from the liquid being pumped. The effects of this gas on performance arise from a) the volume flow rate of the gas at the inlet, b) the pressure ratio of the pump, which determines how far into the impeller this gas volume persists; that is, how much it gets compressed, and c) how much of the gas dissolves in the liquid as the pressure increases within the pump, which depends on both the solubility and the degree of agitation of the fluid produced by the pump. The set of fluid properties associated with these gas-handling phenomena are represented by $\{g_p\}$ in Eq. 34, the dimensionless form (Eqs. 35 and 43) of this set being $\{\Gamma_p\}$. Generally, for typical commercial centrifugal pumps, the performance under such conditions usually manifests itself as a loss of pressure rise, which is reasonably stable up to an inlet volume flow rate fraction of gas to liquid of 0.04 to 0.07[10]. Inducers can handle larger inlet volume fractions of gas, and, under Dalton's law for partial pressures, the liquid's own vapor also occupies the volume of the gas bubbles.

LIBERTY EXHIBIT 1017, Page 52

Single and multistage centrifugal pumps have been built that handle far greater gas volume than these single-stage values[11,12]; moreover, multiphase rotary positive displacement screw pumps can handle gas volume fractions up to 1 (100% gas)[12].

Effects of Slurries and Emulsions Finally there is the influence of the dimensionless quantities $\{\Sigma\}$ in Eq. 43. Impeller and casing design are altered so as to reduce wear-producing velocities if the pumpage is a slurry of solids contained in a carrier liquid. (Slurry pumps are usually single-stage machines with a collector or volute casing surrounding the impeller.) This usually means a smaller impeller eye diameter (which, as can be seen in Figure 6, reduces the inlet relative velocity W_1,) and a larger radial distance from the impeller to the surrounding volute because the circumferential velocity component V_θ of the fluid emerging from the impeller (also seen in Figure 6) slows down with increasing radial position and is then lower in the volute passageway[13]. Performance also is altered, depending on the composition and concentration of the slurry. These are complicated non-Newtonian flows and are covered in detail elsewhere in this book in conjunction with a thorough treatment on solids-handling pumps. Emulsions are another example of such flows, many of which are destroyed by excessive local shear in the fluid. For this reason, screw pumps are sometimes utilized for emulsions rather than oversized, slow-running centrifugal pumps. Except for thin layers of the fluid at the clearances, most of the flow in a screw pump experiences very little shear in comparison to the flow through a centrifugal pump.

Electromagnetic Effects Not appearing in Eq. 43 are quantities associated with electromagnetic phenomena. For example, electric current flowing radially outward through fluid contained in an axially directed magnetic field is capable of producing a rotating flow. Called a hydromagnetic pump, this device is therefore "centrifugal," yet it has no moving parts. Such pumps have been used for liquid metals and could be made reasonably efficient for any pumpage with high conductivity.

DESIGN PROCEDURES

Establishing the Pump Configuration The first step in designing a pump is to determine the type and number of stages that are needed to meet the given set of operating conditions, usually Q, p_1, p_2, available NPSH (= *NPSHA*) and specific gravity of the fluid. If the pump must meet several such sets of operating conditions, one set has to be chosen for the BEP or design point so all the others are satisfied, if possible. Making the proper choice of this BEP may require some iteration: first making a trial choice, doing a preliminary design, and determining the corresponding pump performance characteristic curves, and then repeating these steps if necessary.

Pump rotative speed N (rpm) must be chosen in order to proceed. Selection of the highest practical rpm is desirable because it yields the smallest size and therefore usually the lowest cost and easiest containment of system pressure. If, for the chosen number of stages, the stage specific speed is too low, Figure 10 indicates that efficiency is generally improved with greater speed. The maximum possible rpm is that which yields a value for the suction specific speed Ω_{ss} (Eq. 41) or N_{ss} (Eq. 42) that the first stage of the pump can accommodate, where NPSH is found respectively from Eq. 41 or Eq. 42 as follows:

$$NPSH = \frac{1}{g}\left(\frac{\Omega}{\Omega_{ss}}\right)^{4/3} Q^{2/3} \quad or \quad NPSH(ft) = \left(\frac{N(rpm)}{N_{ss,(U.S.)}}\right)^{4/3} [Q(gpm)]^{2/3} \tag{45}$$

Typically, the Ω_{ss}-capability of an impeller does not exceed a value that is somewhere in the range 3 to 4.5 (N_{ss} = 8,200 to 12,300), depending on minimum (off-design) flow rate requirements, and it is typically 10 (27,000) or less for inducers. Generally, the supplier furnishes a pump that has a value of NPSH-capability (or "*NPSHR*") smaller than the stated *NPSHA*. This difference or "NPSH-margin" is desirable if there is any uncertainty as to the true value of *NPSHA*. It is essential for high values of Δp_{stg}; (see discussion of

LIBERTY EXHIBIT 1017, Page 53

"high-energy pumps" further on in this section). Often a higher speed can be employed if a double-suction impeller (entry of fluid from both sides) can be used, as then only half of the given Q enters each side of this impeller, and only that half can be used in the Ω_{ss}-equation applying to that fluid and impeller type.

The double-suction configuration is popular for large, single-stage pumps because the axial thrust is nominally zero. It is also found as the first stage in some multistage pumps, in which case the arrangement of the remaining impellers can be "back-to-back" (half of them facing in one direction and half opposite) to achieve axial thrust balance. On the other hand, the interstage flow passages are simpler if these impellers are all facing in the same direction—in which case the thrust is opposed by a balancing drum or disk as described in Section 2.2.1. Forming the specific speed from N, Q, and ΔH (from Eq. 3) and referring to Figure 9 for the kind of impeller (which then gives one an idea of the other hydraulic components (inlet passage, diffuser and collector, and so on) and Figure 10 for the expected efficiency, one can decide whether the pump would perform better and still meet any installation and size restrictions with more than the one stage implied by this first N_s-calculation.

If the user requires the performance characteristics of a positive displacement pump—such as a wide range of pressure-rise at a nearly constant flow rate Q—selecting such a pump may be possible if the specific speed is not too high. (See Figure 9.) The choice of speed for positive displacement pumps is sometimes determined by mechanical considerations rather than suction capability.

Sizing the Pump The next step is to determine the approximate size of a pump or pump installation. Beginning with the impeller, the agent of the energy transfer to the fluid in a pump, one utilizes the results of the pump hydraulic geometry optimization process. This also yields the proportions of the velocity diagrams that correspond to the geometry associated with the desired value of specific speed. These in turn lead to two major sizing factors for an impeller, which are plotted for typical commercial pumps in Figure 12; namely the head coefficient ψ (originally defined in Eq. 31) and the outlet flow

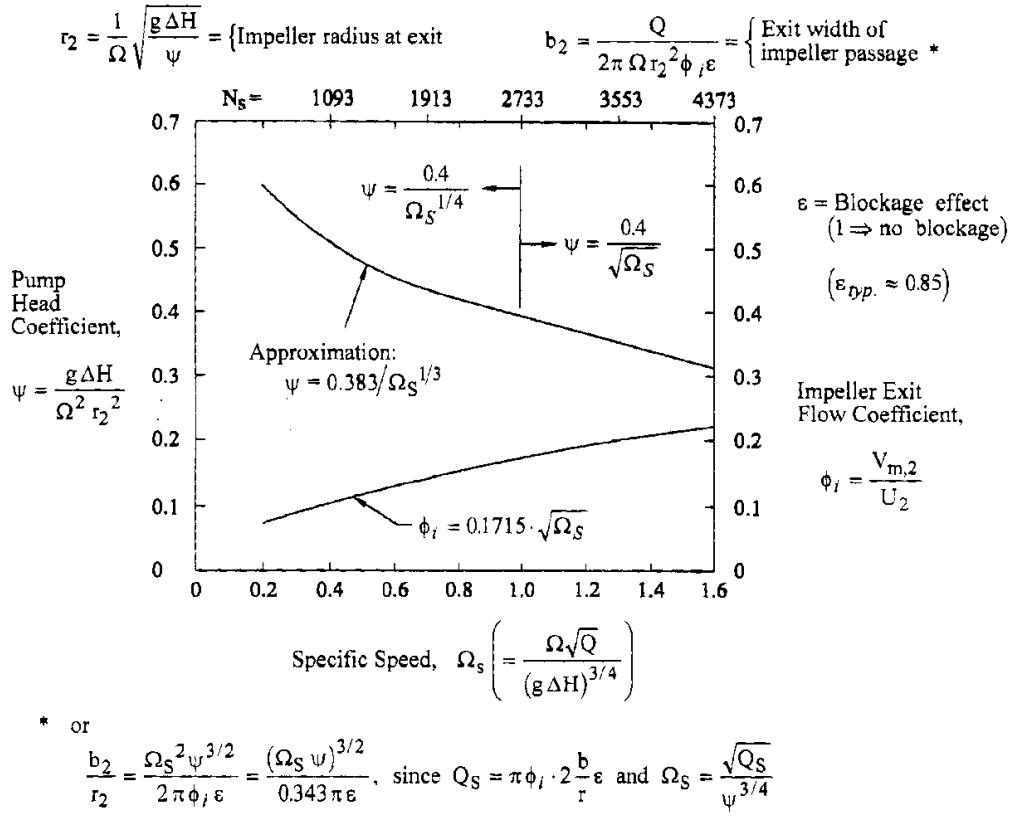


FIGURE 12 Sizing factors for the diameter and width of typical impellers—adapted from Stepanoff[5]

LIBERTY EXHIBIT 1017, Page 54

coefficient ϕ_i defined on this figure[5]. Equations in the figure show how these factors are used to determine the exit radius r_2 (or diameter D_2) and the width b_2 (Figure 8) respectively. The flow coefficient ϕ_i is obviously a velocity component ratio. For the head coefficient of a pump with zero inlet prewhirl to the impeller (that is, $V_{\theta,1} = 0$), the relevant velocity ratio (see Figure 3) is $V_{\theta,2}/U_2$, which in view of Eqs. 15b and 31 is equal to the ideal head coefficient ψ_i, as this corresponds to the ideal head H_i. Referring to Eq. 15c, it is obvious that the actual head coefficient $\psi = \eta_{HY} \times \psi_i$, or, in the (common) case of zero prewhirl, $\psi_i = V_{\theta,2}/U_2$.

Overall pump dimensions are conveniently viewed in terms of factors times the impeller diameter. The overall diameter exceeds that of the impeller due to the surrounding casing. For single stage pumps, this casing will include a volute and perhaps a set of diffuser vanes immediately surrounding the impeller; so, the casing diameter can be 50% greater than D_2 or more. On multistage pumps (many with radial-outflow diffusers and return vanes), this excess is often less than 50%.

Single-stage pump axial length includes provision for inlet passageways and bearing housings and is therefore approximately the same as the overall pump diameter. On the other hand, the axial length of a stage in a multistage pump is often less than half of the impeller diameter. Minimizing this "stage length" (and diameter) is a goal of competitive pump designers in the quest to create a machine of light weight and low cost. But too small a stage length is accompanied by inferior hydraulic performance because not enough room is provided for the passages around and within the impeller to turn the fluid with minimum loss. Further, the bearing housings and the suction and discharge "heads" or end pieces must be considered in arriving at the overall length of a multistage pump.

This sizing discussion so far has focused on pumps with a radial-outflow geometry. For the axial-flow geometries of higher specific speeds, the situation is simpler. The diameters of the propeller (Figure 9) and any stationary vanes downstream (or upstream) are essentially the same. The approach and discharge piping is of about the same size. A simple guideline for the maximum radius of the propeller is found from the following approximate extrapolation of the ψ-curve of Figure 12:

$$\psi_t = \frac{0.53}{\Omega_s} \tag{46}$$

where the outer radius of the propeller $r_{t,2}$ should be substituted for the mean exit radius r_2 in the ψ-definition. Thus the ψ-curve is in reality a ψ_t-curve for non-radial-flow pumps. For small departures from radial flow, as illustrated in Figure 8, the ψ-curve of Figure 12 can be used either way.

These guidelines are often all that pump users or fluid system designers need to plan their installations. To get beyond this overview, one must pursue the hydraulic design in detail—as afforded by the following development and examples.

Designing the Impeller Determination of the geometrical features of the impeller is generally accomplished in the following order: a) the "eye" radius r_e, b) the exit radius r_2 or $r_{t,2}$, and c) the exit width b_2 or, in the case of mixed- and axial-flow impellers, the hub exit radius $r_{h,2}$—all of which form the starting point for d) shaping the hub and shroud profiles (Figure 13); and, finally, e) construction of the blades.

a) The eye. The inlet radius of the impeller eye r_e (Figure 13) is nearly the same as $r_{t,1}$, which is the diameter of the tips of the impeller blades at the inlet. This emerges after the eye flow coefficient $\phi_e = V_e/U_e$ [the ratio of the one-dimensional axial velocity entering the eye (Figure 8) to the tangential speed of the impeller eye $U_e = \Omega r_e$] is known:

$$\phi_e = \frac{Q/A_e}{\Omega r_e} = \frac{\overline{V_e}}{U_e} \tag{47}$$

$$A_e = \pi(r_e^2 - r_s^2) \tag{48}$$

LIBERTY EXHIBIT 1017, Page 55

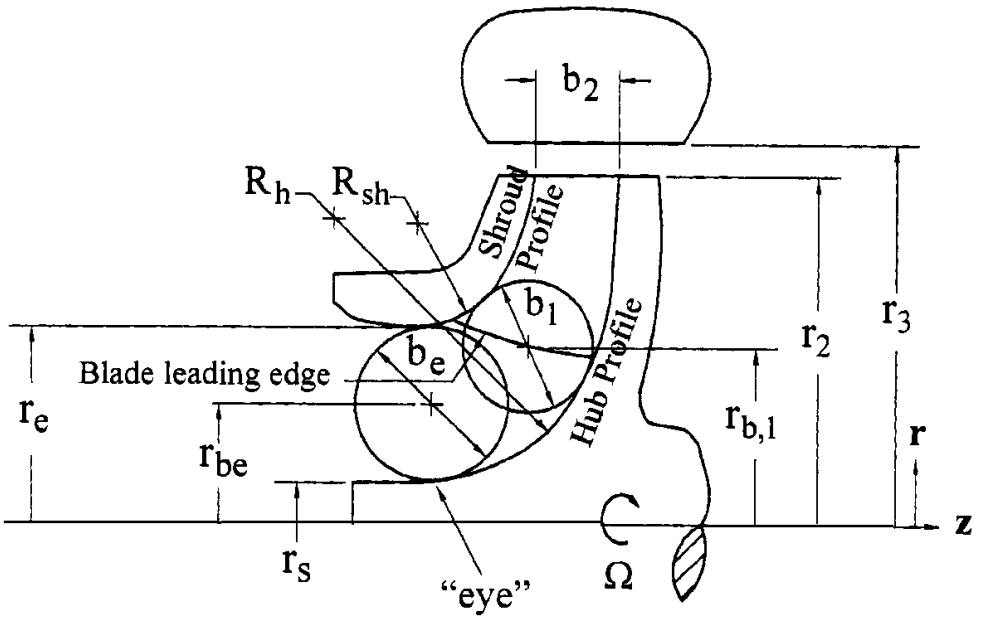


FIGURE 13 Hub and shroud profiles of centrifugal pump impeller

Thus, r_e can be found from the following combination of Eqs. 47 and 48:

$$r_e = \left[\frac{Q}{\pi \Omega \phi_e \left(1 - \dfrac{r_s^2}{r_e^2} \right)} \right]^{1/3} \tag{49}$$

where the shaft-to-eye ratio r_s/r_e can be estimated at first. Typical values for ϕ_e vary from 0.2 to 0.3 for impellers and down to 0.1 or less for inducers, depending on suction conditions, as can be seen from its relationship to suction-specific speed:

$$\Omega_{ss} = \frac{\Omega \sqrt{Q}}{(g\,NPSH)^{3/4}} = \sqrt{\pi \phi_e \left(1 - \frac{r_s^2}{r_e^2} \right)} \Big/ (\tau/2)^{3/4} \tag{50}$$

where the cavitation coefficient τ (cf. τ_2 in Eq. 36) is defined in terms of the eye speed $U_e = \Omega r_e$ (Table 1). τ is related to ϕ_e through empirical correlations, such as those given in Table 1. (Gongwer's[14] values for the correlation factors k_1 and k_2 apply to large pumps. The larger "typical" values shown for 3% breakdown apply to the more common smaller sizes. The inducer correlation is a curve fit to the data of Stripling and Acosta[15] for the breakdown value of τ.) Thus one can solve for ϕ_e from a given suction-specific speed and, through Eq. 49, obtain the eye size. However, the value of ϕ_e at the BEP or design point rarely exceeds 0.3, regardless of how much NPSH is available. This ϕ_e-limit therefore applies to impellers that follow and are in series with the first stage in a multistage pump. These are variously referred to as "series" or "intermediate" stages. (Slurry pump impellers are an exception to this guideline, for then the relative velocity is minimized to avoid excessive wear. In this case ϕ_e can be as high as 0.4 and *NPSHA* is generally more than adequate for these slow-running machines.)

b) The exit radius r_2 (or diameter D_2). This is found from head-coefficient ψ by means of the equation for r_2 in Figure 12. The curve for ψ can be used unless detailed performance analysis or a desired performance characteristic curve indicates otherwise. Eq. 46 can be used for specific speeds Ω_s greater than 1.6 ($N_s > 4373$), where the maximum radius $r_{t,2}$ is computed per the previous discussion accompanying that equation. At this point, it can be seen that the equation in Figure 12 for exit radius r_2 and Eq. 49 for the

LIBERTY EXHIBIT 1017, Page 56

TABLE 1 NPSH correlations for breakdown of pressure rise due to two-phase activity in pump

$$\tau = \frac{NPSH}{\frac{U_e^2}{2g}} \qquad \Omega_{ss} = \frac{\sqrt{\pi\phi_e\left(1 - \frac{r_s^2}{r_e^2}\right)}}{\left(\frac{\tau}{2}\right)^{3/4}}$$

a) Impellers (Gongwer[14])

$$NPSH_{3\%} = k_1\frac{V_e^2}{2g} + k_2\frac{W_{1,sh}^2}{2g} = \left(\frac{V_{1,sh}}{V_e}\right)^n\frac{V_e^2}{2g} + k_2\frac{W_{1,sh}^2}{2g}$$

For $V_{\theta,1} = 0$: $\boxed{\tau_{3\%} = \dfrac{NPSH_{3\%}}{\frac{U_e^2}{2g}} = (k_1 + k_2)\phi_e^2 + k_2}$

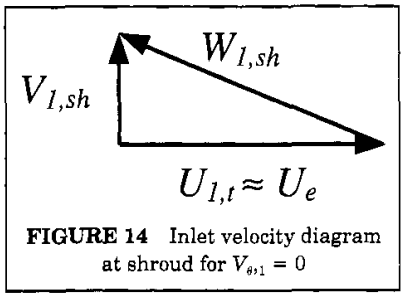


FIGURE 14 Inlet velocity diagram at shroud for $V_{\theta,1} = 0$

where,
for large pumps (Gongwer[14]), $k_1 = 1.4$, and $k_2 = 0.085$
and, for typical pumps, $k_1 \approx 1.69$, and $k_2 \approx 0.102$

b) Inducers (curve fit to the data of Stripling and Acosta[15])

$$\boxed{\tau = 0.02 + 0.02\left[\log_{10}\left(\frac{\phi_e \sin\beta_{b,1,sh}}{1 + \cos\beta_{b,1,sh}}\right) + 3\right]^{3.5}}$$

eye radius r_e can be combined to yield the ratio of eye size to that of the OD for centrifugal impellers; viz.:

$$\frac{r_e}{r_2} = \frac{D_e}{D_2} = \frac{\Omega_s^{2/3}\sqrt{\psi}}{\left[\pi\phi_e\left(1 - \frac{r_s^2}{r_e^2}\right)\right]^{1/3}} \tag{51}$$

Except for inducers, which have very low values of ϕ_e, this ratio is affected mainly by specific speed as illustrated in Figure 9.

c) The exit width b_2. The equation for exit passage width b_2 in Figure 12 can be used for radial-outflow and mixed-flow impellers, r_2 being located halfway across the passage. This involves the exit flow coefficient or meridional velocity ratio $\phi_i = V_{m,2}/U_2$, the lower curve of Figure 12 being for typical values of this quantity. The "openness" factor ε allows for blockage due to blade thickness and to the buildup of boundary layers on the surfaces of the passageways (blades and hub and shroud). The value of ε is generally between 0.8 and 0.9, the higher figure applying to larger machines. For axial-flow impellers or propellers and inducers, a choice of the hub-to-tip radius ratio at the exit defines the passage width instead. This ratio decreases with specific speed from about $\frac{2}{3}$ at the right end of Figure 12 to $\frac{1}{3}$ or less at the highest specific speeds.

d) Hub and shroud profiles. With the eye and the outlet sizing established, the two are connected by specifying the hub and shroud profiles. Some texts illustrate the variation

LIBERTY EXHIBIT 1017, Page 57

of hub and shroud profiles with specific speed[16]. Although these are excellent guidelines coming from experience, what follows is the approach one would take to synthesize these shapes on the basis of fundamental fluid dynamical considerations, at the same time taking experience into account. Referring to Figure 13, an acceptable geometry can be achieved by following these guidelines:

i. Maintaining the meridional flow area $2\pi r_{b,1} b_1$ at the blade leading edge at about the same as it is at the eye, namely $\pi(r_e^2 - r_s^2)$, or slightly larger to compensate for blade blockage; but then gradually increasing it versus meridional distance to the generally larger value already established at the exit, namely $2\pi r_2 b_2$.

ii. Choosing the minimum radius of curvature R_{sh} of the shroud to be about half the radial opening at the eye. This avoids excessive local velocity $V_{1,sh}$ at the blade leading edge, (Figure 14 in Table 1.) This has two consequences. Shaping the impeller blades to match a widely varying meridional approach velocity can complicate the construction of these blades. Also, on first-stage impellers, if $V_{1,sh}$ is too great, the local pressure at that location will be closer to the vapor pressure, increasing the required NPSH (or $NPSH_{3\%}$). This is due to a larger resulting value of the empirical factor k_1, presented in Table 1 as the n^{th} power of the velocity ratio $V_{1,sh}/V_e$. $n = 2$ is expected from Bernoulli considerations, and if $V_{1,sh}/V_e = 1.3$, the value of 1.69 emerges for k_1 as shown in Table 1. $V_{1,sh}/V_e = 1.25$ is a typical choice of designers for setting the impeller blades at inlet. A CFD solution of the combined inlet passage and impeller blading would show the actual resulting value of this velocity ratio, which might then lead to a change in the impeller blading or radius of curvature R_{sh}. The powerful effect on this velocity ratio of the sharpness of the turn that the flow negotiates in coming into the impeller eye and turning toward the radial direction can be seen from the following finite-difference form of the differential equation governing axisymmetric inviscid flow in the impeller eye region:

$$\frac{\Delta V_m}{V_e} = \frac{b_e}{R}$$

where R is the average radius of curvature of the flow in the meridional plane of Figure 13, ΔV_m is the difference in V_m from hub to shroud over a distance b_e perpendicular to the direction of flow that moves at an average meridional velocity V_e. Thus a sharp turn with its small value of R produces a large value of $\Delta V_m/V_e$, which in turn corresponds to a large value of the velocity ratio $V_{1,sh}/V_e$.

iii. Shaping the hub profile compatibly with the guidelines as stated earlier. This is best done after making an initial estimate of the shroud profile as outlined previously. The distribution of meridional flow area from the eye to the exit should then be specified. From this, a hub profile will emerge. As seen in Figure 13, the hub of a radial-outflow impeller becomes essentially radial over the outer portion of its extent. If this does not result from this procedure, appropriate adjustments can be made to the shroud profile and the process repeated.

iv. For a high-specific-speed, axial-flow impeller, or inducer, the hub profile is often a cone or a reverse curve between a smaller radial location at inlet to a larger one at outlet, the latter radius decreasing with increasing specific speed as mentioned earlier. A cone or cylinder for the shroud profile is often found in such machines.

e) Construction of the blades. The blades are designed by i) selecting the locus of the leading and trailing edges in the meridional plane, ii) establishing the surfaces of revolution (streamwise lines in the meridional plane) from inlet to outlet along which the construction proceeds, iii) selecting the inlet angles, iv) selecting the outlet angles, v) establishing the number of blades, and vi) obtaining the blade coordinates from inlet to outlet:

i. *Leading and trailing edge loci.* If every point along the leading and trailing edges is revolved about the axis of rotation so as to lie in one meridional plane, the loci of these

LIBERTY EXHIBIT 1017, Page 58

edges appear as shown in Figure 13. The outer or shroud end of the blade leading edge is positioned at or near the minimum radial location; that is, at or near the eye plane, whereas the inner or hub end is typically well back and largely around the corner along the hub profile. These locations are desirable; first, at the shroud, because the absolute velocity V (typically = V_m) approaching the blade begins to decelerate beyond the eye plane, so starting the blade ahead of this decelerating region tends to prevent separation of the fluid from the shroud surface due to the pumping action in the blade channels[17]; and secondly, being far enough along the hub in the streamwise direction to avoid impractical blade shapes (excessive twist, rake, and so on) that would make both the construction and the flow inefficient. The locus of the blade trailing edges is normally straight in the meridional plane and is axial in orientation for most centrifugal pumps. At the higher specific speeds, this locus becomes more and more slanted until it takes on the nearly radial orientation it has for a propeller (Figure 9).

ii. *Surfaces of revolution for blade construction.* Developing the coordinates of the blades along three streamwise surfaces of revolution—the hub, mean, and shroud, whose intersections with the meridional plane appear as streamwise lines in that plane—usually provides a sufficient framework for shaping the blades of an impeller. However, for high specific-speed impellers, where the passage width in the meridional plane b (Figure 13) is large (about equal to or greater that the meridional distance from leading to trailing edge), definition along two intermediate surfaces of revolution is also needed to achieve a satisfactory design.

The "mean" line is one that is representative of the flow from a one-dimensional standpoint as well as for the construction of the blades. Precisely, this is the mass-averaged or "50%" streamline (that is, the streamline for $\psi = 0.5$ in Figure 14)—which evenly divides the mass flow[17]. This line is reasonably and conveniently approximated by the "rms streamline;" that is, the line that would result in a uniform meridional velocity distribution from hub to shroud and therefore equal areas $2\pi r\Delta n$ normal to the meridional velocity component V_m. In this case, Δn (= Δb) is the spacing between the rms streamline and the hub or shroud line. This would put each point on the mean line at the root mean square radial position along a true normal to the meridional streamlines; hence, the "rms" terminology.

iii. *Inlet blade angles.* The blade angles are set to match the inlet flow field. This is done where each of the previously chosen surfaces of revolution (that intersect the meridional plane in the streamwise lines just described) crosses the chosen locus of the blade leading edges in the meridional plane. At each such crossing point, an inlet velocity diagram of the type shown in Figure 3 is plotted in a plane tangent to the surface of revolution at that point. (Figure 3, representing a purely radial-flow configuration, is a view of such a plane, as the surfaces of revolution are then simply disks.) Each such velocity diagram or triangle contains a specific value of the angle $\beta_{f,1}$ between the relative velocity vector W_1 and the local blade speed vector $U_1 = \Omega r_1$.

The corresponding blade angle $\beta_{b,1}$ between the mean camber line of the blade and the circumferential direction is set equal to $\beta_{f,1}$ or slightly higher than this to allow for the higher $V_{m,1}$ caused by non-zero blade thickness at the leading edge and to allow for higher flow rates that may be called for at off-design conditions. To construct the triangle, one first plots U_1 and then $V_{m,1}$, which is taken from a CFD or other analysis of the meridional velocity variation across the inlet eye as discussed above under *d) Hub and shroud profiles* or is chosen as the mean value $Q/2\pi r_{b,1}b_1$ (Figure 13) at the rms streamline. It is adjusted from experience at the shroud and hub. Likewise, if any prewhirl $V_{\theta,1}$ is delivered to the impeller, it must be taken into account as illustrated in Figure 3.

iv. *Outlet blade angles.* Whereas the inlet velocity diagrams enable the designer to correctly set the blades to receive the incoming fluid with minimum loss, the outlet velocity diagram displays the evidence—through the magnitude of the circumferential velocity component $V_{\theta,2}$ that the intended head will be delivered by the pump in accordance with Eq. 15c. As shown in Figure 3, $V_{\theta,2}$ is determined—for the given impeller tip speed U_2—by the exit relative flow angle $\beta_{f,2}$ in conjunction with the exit meridional

LIBERTY EXHIBIT 1017, Page 59

velocity component $V_{m,2}$. This value of V_m is somewhat larger than that given by Eq. 16 because of a) blockage due to blade thickness and boundary layer displacement thickness and b) the presence of any leakage flow Q_L (Figure 2 and Eq. 11) that may also be flowing through the impeller exit plane or Station 2.

Well inward of the exit plane, the direction of the one-dimensional relative velocity vector W can be assumed to be parallel to the blade surface; however, in the last third of the passage, the blade-to-blade distribution of the local relative velocity changes due to the unloading of the blades at the exit. This produces a deviation of the direction of W_2 from that of the blade. This deviation, called "slip" in centrifugal pumps, results in less energy being delivered to the fluid by the impeller than would be the case if there were "perfect guidance" such as would occur with an infinite number of blades. Accordingly, in the outlet velocity diagram of Figure 15, the relative flow angle β_f is less than the blade angle β_b. This deviation is quantified by the "slip velocity" V_s. The magnitude of V_s depends on the distribution of loading along the blades from inlet to exit and therefore on the geometry of the flow passages and the number of blades. (Without slip, W_2 is the same as the "geometric" relative velocity $W_{g,2}$ shown in the figure.) The slip factor $\mu = V_s/U_2$—typically between 0.1 and 0.2—was determined theoretically by Busemann for frictionless flow through impellers with zero-thickness, logarithmic-spiral blades (constant-β from inlet to exit) and a two-dimensional, radial-flow geometry with parallel hub and shroud[18]. Applicability of this theory to typical impellers, despite the differences in geometry and the real fluid effects, was found to be good by Wiesner, who represented Busemann's results by the following convenient approximation[19]:

$$\left.\begin{aligned} \mu \equiv \frac{V_s}{U_2} &= \frac{\sqrt{\sin\beta_2}}{\bar{n}_b^{0.7}} \quad if \frac{r_1}{r_2} < \varepsilon_{limit}, \quad where\ \varepsilon_{limit} = \frac{1}{e^{\left(\frac{8.16\sin\beta_2}{\bar{n}_b}\right)}} \\ \mu \equiv \frac{V_s}{U_2} &= 1 - \left\{ \left(1 - \frac{\sqrt{\sin\beta_2}}{\bar{n}_b^{0.7}}\right) \times \left[1 - \left(\frac{\frac{r_1}{r_2} - \varepsilon_{limit}}{1 - \varepsilon_{limit}} \right)^3 \right] \right\} \quad if \frac{r_1}{r_2} > \varepsilon_{limit} \end{aligned}\right\} \quad (52)$$

A broader, empirical slip correlation for pumps was developed by Pfleiderer, taking into account impeller geometry and blade loading, as well as the influence of the downstream collecting system (volute or diffuser)[20]. Pfleiderer computes the slip velocity as the product of a slip factor p and the impeller exit tangential velocity $V_{\theta,2}$, where p is computed as shown in Table 2. This table also contains a simple example; namely, a

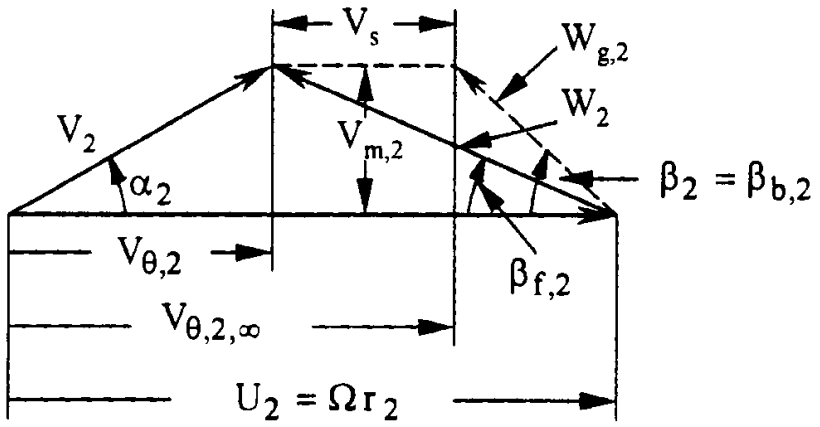


FIGURE 15 Impeller outlet velocity diagram

LIBERTY EXHIBIT 1017, Page 60

TABLE 2 Pfleiderer's slip formula

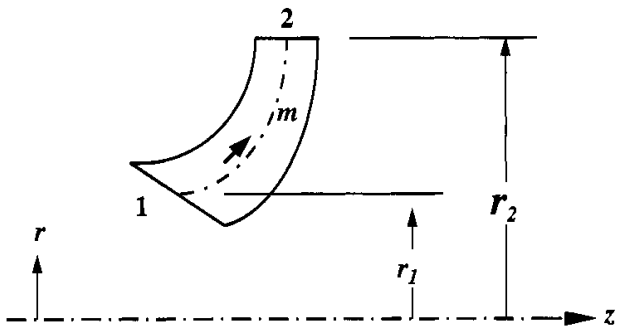
Slip velocity, $V_S = pV_{\theta,2}$

Thus, $\dfrac{V_{\theta,\infty,2}}{V_{\theta,2}} = 1 + p$

where $p = \dfrac{\psi' r_2^2}{\int_1^2 n_b r dm}$

and where $\psi' = a \times (1 + \sin \beta_{b,2})$

and $a = \begin{Bmatrix} 0.6 & \text{for vaned diffuser;} \\ 0.65 & \text{to 0.85, volute;} \\ 0.85 & \text{to 1.0, vaneless diffuser.} \end{Bmatrix}$



Example: $r_2 = 1$; $r_1 = 0.4$; $V_{\theta,2} = \dfrac{U_2}{2}$; $n_b = 7$; $\beta_{b,2} = 20$ degrees; $a = 0.8$ (volute)

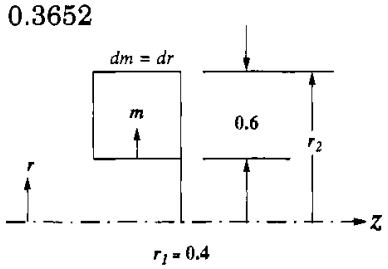
Results:

$$\psi' = 0.8 \times (1 + 0.342)$$

$$\int_1^2 n_b r dm = n_b \times \frac{1}{2} \times (r_2^2 - r_1^2) = n_b \times \frac{r_2 + r_1}{2} \times (r_2 - r_1)$$

$$p = \frac{V_S}{V_{\theta,2}} = \frac{\psi' r_2^2}{\int_1^2 n_b r dm} = \frac{0.8 \times (1 + 0.342) \times 1^2}{7 \times \dfrac{1 + 0.4}{2} \times 0.6} = 0.3652$$

$$\mu = \frac{V_S}{U_2} = p \times \frac{V_{\theta,2}}{U_2} = 0.3652 \times \frac{1}{2} = 0.1826$$



radial flow impeller of a volute pump, for which the resulting value of μ is 0.1826—versus 0.1498 via Eq. 52; however, in this case the latter result is low by about 15%. A study of the Busemann plots in Wiesner's paper yields $\mu = 0.18$. Yet, if this had been a vaned-diffuser pump, Pfleiderer would have predicted $\mu = 0.1468$ for the same impeller, as it would have delivered more $V_{\theta,2}$ for the same $\beta_{b,2}$, $W_{g,2}$, and, therefore, $V_{\theta,2,\infty}$, (Figure 15). This stems from the factor "a" in Table 2 having the value 0.6 (for a vaned diffuser) instead of 0.8 (for a volute). So by this combination of circumstances—and in this example—Eq. 52 describes the slip of a diffuser pump impeller. But, despite the simplicity of Eq. 52, Pfleiderer's method (Table 2) would appear to be a more rational, comprehensive, and satisfying method for estimating slip in real pumps.

So, to find the outlet blade angle, the designer begins by deciding upon the required value of $V_{\theta,2}$; finds the exit flow angle and other elements of the diagram assuming the existence of slip. Next, the designer computes the slip and then obtains the value of

LIBERTY EXHIBIT 1017, Page 61

the outlet blade angle $\beta_{b,2}$. The process is iterative because the forementioned blockage depends on the blade angle as well as the thickness.

v. *Number of blades.* The choice of the number of impeller blades is influenced by a) interaction of the flow and pressure fields of the impeller and adjacent vaned structures such as the volute tongues or diffuser vanes and b) the need to maintain smooth, attached—and therefore efficient—fluid flow within the impeller passages. The effect of the number of blades on the interaction phenomenon is addressed in the latter part of this section under the topic of high-energy pumps, where this issue becomes critical. Smooth, attached flow is assured if the product of the number of blades and their total arc length ℓ along a given meridional streamline, as illustrated in Figure 16, is of sufficient magnitude. Divided by a representative circumference on that streamline, usually that of the impeller outer diameter (OD), this product is called the solidity σ:

$$\sigma = \frac{n_b \times \ell}{2\pi r_2} \tag{53}$$

If splitter blades are used, the value of n_b changes from impeller inlet to outlet (1 to 2). In that case, the numerator of Eq. 53 is replaced by the implied sum of the arc lengths of all the blades in the impeller.

In practice, solidity varies from about 1.8 at low specific speed ($\Omega_s < 0.4$ or $N_s < 1093$) to slightly less than unity at $\Omega_s = 3$ ($N_s = 8199$). For example, Dicmas' curve[21] is useful for $\Omega_s > 1$ ($N_s > 2733$). This limits the relative velocity reduction that occurs on the blade surfaces. Illustrated in Figure 17, this reduction or diffusion arises from the loading on the blades expressed in terms of the blade-to-blade relative velocity difference ΔW_b:

$$W_s - W_p (= \Delta W_b) = \frac{2\pi}{\Omega n_b} \times \frac{V_{m,o}}{\overline{W}} \frac{d(UV_\theta)}{dm} \tag{54}$$

$V_{m,o}$ is the local meridional velocity component neglecting blockage. (One-dimensionally, $V_{m,o}$ is the value of V_m found from Eq. 16, where the radius r is that from the axis of rotation to the center of the circle of diameter b in Figure 8, which in turn lies on an

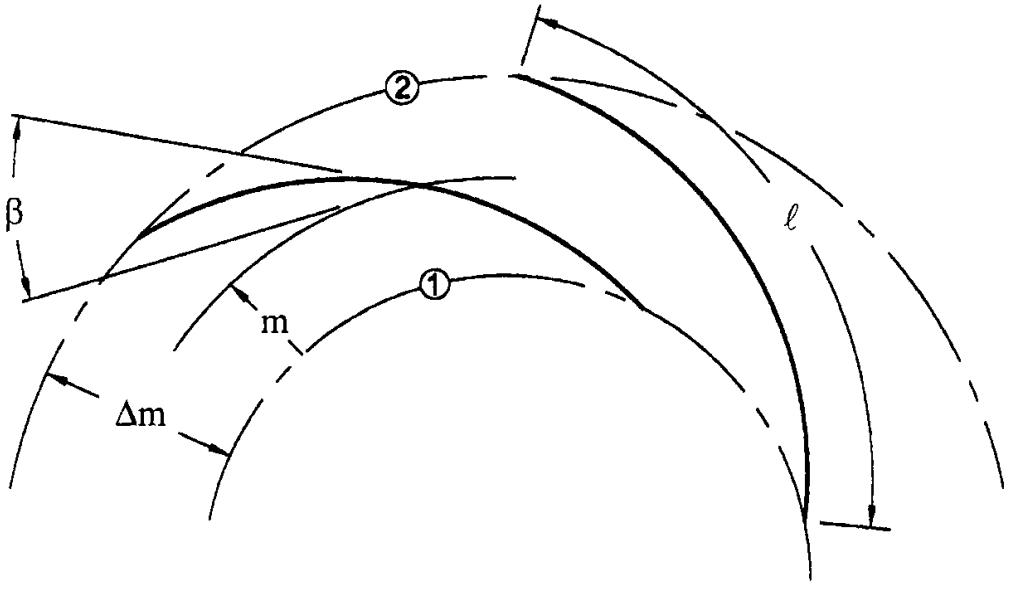


FIGURE 16 Intersection of impeller blades with mean surface of revolution

LIBERTY EXHIBIT 1017, Page 62

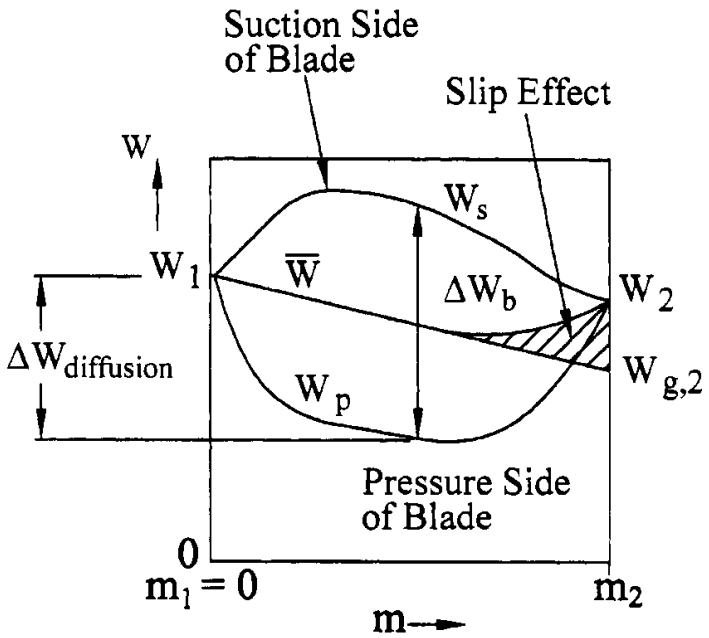


FIGURE 17 Relative velocity distributions

imaginary line in Figure 8 that is normal to the hub, shroud, and intermediate stream surfaces.) Here, ΔW_b emerges by applying Bernoulli equation [Eq. 21 with no change in radius (that is, no change in U) or loss as one traverses from pressure side to suction side of the passage] to the static pressure difference $p_p - p_s$ arising from the delivery of angular momentum to the fluid (Eq. 26). This in turn results from the application of the shaft torque to the blades. It is also assumed in the derivation of Eq. 54 that the *blade-to-blade average relative velocity W lies halfway between the surface velocities W_s and W_p* (which would exist just outside the boundary layers on the blades,) as illustrated in Figure 17. This is a good assumption for efficient flow well within a bladed channel[22]. ΔW_b is inversely proportional to the solidity because, on the average, from inlet to outlet, Eq. 54 becomes

$$\overline{W_s - W_p} = \overline{\Delta W_b} \approx \left(\frac{2\pi r_2 \overline{\sin\beta}}{n_b \Delta m}\right)\Delta\left(\frac{r}{r_2}\, V_\theta\right) \tag{55}$$

where it can be seen from Figure 16 and Eq. 53 that the fraction involving the number of blades n_b is the reciprocal of the solidity σ because

$$\ell = \Delta m/\overline{\sin\beta} \tag{56}$$

If splitter blades are used, an appropriate average number of blades is substituted for n_b in Eq. 53.

For unconventional impeller geometries, the foregoing solidity guidelines may be inadequate to assure efficient flow. For any geometry, though, the concept of a diffusion factor D, utilized by NACA researchers[23] to assess stationary cascades of airfoils can be employed. In view of Eqs. 53–56, their equation for D takes the following form for both axial- and non-axial-flow geometries, rotating or not:

$$D = 1 - \frac{W_2}{W_1} + \frac{\Delta\left(\frac{r}{r_2}\, V_\theta\right)}{2\sigma W_1} \tag{57}$$

LIBERTY EXHIBIT 1017, Page 63

This can be deduced from Figure 17 as follows:

$$D = \frac{W_1 - W_2}{W_1} + \frac{\overline{\Delta W_b}}{2W_1} \left(\approx \frac{\Delta W_{\text{diffusion}}}{W_1} \right) \tag{58}$$

Then, Eq. 57 is obtained through the definitions of the average value of ΔW_b (Eq. 55 with Eq. 56) and σ (Eq. 53). NACA researchers found that losses increase rapidly if $D > 0.6$. However, many centrifugal pump impellers have virtually the same value of relative velocity W at inlet and at outlet—along the rms streamline (Figure 17), so D from Eq. 57 is less than 0.6 on the rms streamline and even negative along the hub streamline. This situation was encountered in accelerating (turbine) cascades and led to the use of local diffusion factors, one for each side of the blade, namely D_p and D_s. Here, inspection of Figure 17 and Eq. 58 leads to

$$D_p = 1 - \frac{W_{p,\min}}{W_1} \quad ; \quad D_s = 1 - \frac{W_2}{W_{s,\max}} \tag{59a and b}$$

where the 0.6 limit applies individually to D_p and D_s. Eqs. 59a and 59b, therefore, constitute a more useful form of the diffusion factor concept for assessing the blade loading and the choice of the number of blades in centrifugal pump impellers[24].

Finally, the total blade length or number of blades, should not exceed that necessary to limit the diffusion as just described, as this adds unnecessary skin friction drag, which causes a reduction in efficiency. Thus the solidity values given in conjunction with Eq. 53 should not be appreciably exceeded, unless blade load needs to be reduced to lower levels, as with inducers to limit cavitation[9] or impellers for pumps that must produce lower levels of pressure pulsations.

vi. *Development of the blade shape.* Blades are developed by defining the intersection of the mean blade surface (really an imaginary surface) or camber line on one or more nested surfaces of revolution. Two such surfaces are formed by the hub and shroud profiles. If the blade shape is two-dimensional (that is, the same shape at all axial positions z), the mean blade surface is completely defined by constructing it on only one such surface of revolution. Generally, however, the shape is three-dimensional and is a fit to the shapes constructed on two or more of these surfaces of revolution; namely, the hub and shroud and usually at least one surface between them. After this final shape is known, half of the blade thickness is added to each side. (Sometimes the full blade thickness is added to one side only, meaning that the constructed surface just mentioned ends up—usually—as the pressure side of the finished blade rather than the mean or "camber" surface. The effective blade angles are then slightly different from those of the pressure side used in the construction process.) The construction along a mean surface of revolution is illustrated in Figure 18. The distribution of the local blade angle β (or more precisely, β_b) is found first by either the *"point-by-point"* method or the *conformal transformation* method—both of which yield the polar coordinates of the blade, r, θ, and z. These coordinates also depend on the chosen shapes of the intersections of the surfaces of revolution with the meridional plane; that is, the hub, shroud, and mean meridional "streamline" or rms line, as in Figure 18c, and the fact that, on the surface of revolution Figure 18a, $\tan \beta = \text{arc } bc/\text{arc } ac = dm/dy$. The elemental tangential length dy (= arc ac) is the same on both the surface of revolution (Figure 18a) and in the polar view (Figure 18b). From Figure 18b, it is seen that $dy = rd\theta$, so the "wrap" angle θ is found from

$$\tan \beta_b = \frac{dm}{rd\theta} \tag{60}$$

and r and z are found from the fact that the coordinate m along each of the construction surfaces is a function of r and z (Figure 18c).

LIBERTY EXHIBIT 1017, Page 64

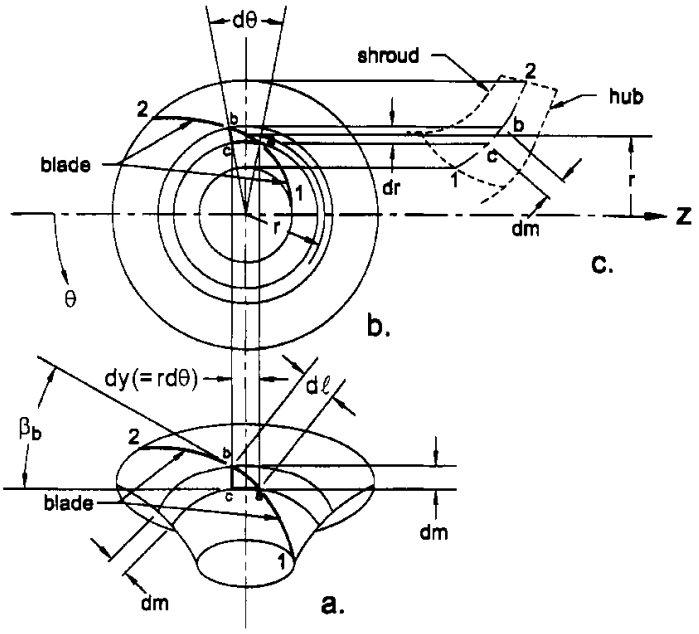


FIGURE 18 Blade construction: a) view of construction surface of revolution; b) polar view; c) meridional view

If the blade is two-dimensional, its mean surface consists of a series of straight-line axial elements, each having a unique r and θ at all z. Such a blade is typical of low-specific-speed, radial-flow impellers, and can be easily constructed by the *"point-by-point"* method. Here, one specifies the distribution of W_g—often linear as in Figure 17—after determining the hub and shroud profiles and the corresponding distribution of V_m[16]. In effect, one obtains the distribution of the blade angle β_b by constructing a velocity diagram like the one in Figure 15 at every m-location from inlet (1) to outlet (2) in Figure 18c, dealing only with the "geometric" or nondeviated velocities, in order to get a smooth variation of the blade angle β_b vs m. Allowance is made for blockage due to the thickness of the blades and the displacement thickness of the boundary layers in the passage. The resulting wrap angle θ for each m-point—as well as the corresponding r and z—is then found from Eq. 60. (For convenience in designing the blades, the construction angle θ is often taken as positive as one advances from impeller inlet to exit. For most impellers, this turns out to be opposite to the direction of rotation; and θ is taken in the direction of rotation for most other purposes of pump design and analysis.) As discussed previously in Paragraph iv and illustrated in Figure 17, the actual flow will deviate from the resulting blade via the "slip" phenomenon.

The point-by-point method allows the designer to exercise control over the relative velocity distributions on the blade surfaces (Eq. 54 and Figure 17) via specification of the distribution of W_g or other velocity component in Figure 15; for example, V_{θ_1}. This becomes more important if an unconventional impeller geometry is being developed[17].

The point-by-point method can also be used for three-dimensional blades. A simple approach in this respect would be to use this method to determine the blade shape along the rms- or 50%-streamline (that is, on the mean surface of revolution depicted in Figure 18). The shapes on the other streamlines, generally the hub and the shroud, can also be found by this method. The resulting overall blade shape, however, is subject to the condition that the resulting wrap $\theta_2 - \theta_1$ cannot greatly differ on all streamlines without the blade taking on a shape that is difficult to manufacture and which may turn out to be structurally unsound or create additional flow losses. This is because the final blade shape is the result of stacking the shapes that have been established on the nested stream surfaces defined by these meridional streamlines. Blade forces due to twists arising from this stacking could modify the expected flow and cause unexpected diffusion losses.

LIBERTY EXHIBIT 1017, Page 65

One way to generate blade shapes along the hub and shroud that have the same (or nearly the same) wrap as that obtained from point-by-point construction of the blade on the mean surface of revolution is to establish the desired inlet and outlet blade angles β_b on each such surface and then mathematically fit a smooth shape $y(m)$ to these end and wrap conditions, where y is the tangential coordinate seen in Figure 18 and defined in Figure 19. A conformal representation of the shapes of the blades resulting from such a procedure on each of the three surfaces is seen in Figure 19. These shapes are sometimes called "grid-lines" or simply "grids"—from the description of the graphical procedure that relates these shapes in the conformal representation to those on the actual, physical surfaces[5]. In such a representation, the blade angles are the same as they are on the physical surface of revolution because $\tan \beta = dm/dy$ and $dy = rd\theta$, also yielding Eq. 60.

If the associated distributions of W_g and V_m are smooth, one can expect to have a satisfactory result if these conformal representations are also smooth. Thus, many skilled designers bypass the computations just described for the point-by-point method and use the *conformal transformation* method of blade design. Here, one simply establishes the grid-line shapes by eye in the conformal plane of Figure 19, specifying the blade angles β at inlet and outlet by the previous procedures as the starting point for drawing each grid-line. This conformal blade shape is then transformed onto the physical surface, the differential tangential distance dy becoming $rd\theta$ on the physical surface (Figure 18) and the differential meridional distance dm being identical in both the conformal and physical representations. If the resulting blade shape appears to be unsatisfactory, the designer repeats this process, possibly first altering the hub and shroud profiles or the blade leading and trailing edge locations on these profiles and recomputing the βs.

Designing the Collector The fluid emerging from the impeller is conducted to the pump discharge port or entry to another stage by the collecting configuration, which can employ one or more of the following elements in combination: a) *volutes*, which can be used for designs of all specific speeds, b) *diffuser or stator vanes*, which are often more economical of space in high-specific-speed single-stage pumps and in multistage pumps, and for the latter, c) *return or crossover passages*, which bring the fluid from the volute or diffuser to the eye of the next-stage impeller. Generally, the most efficient impeller has

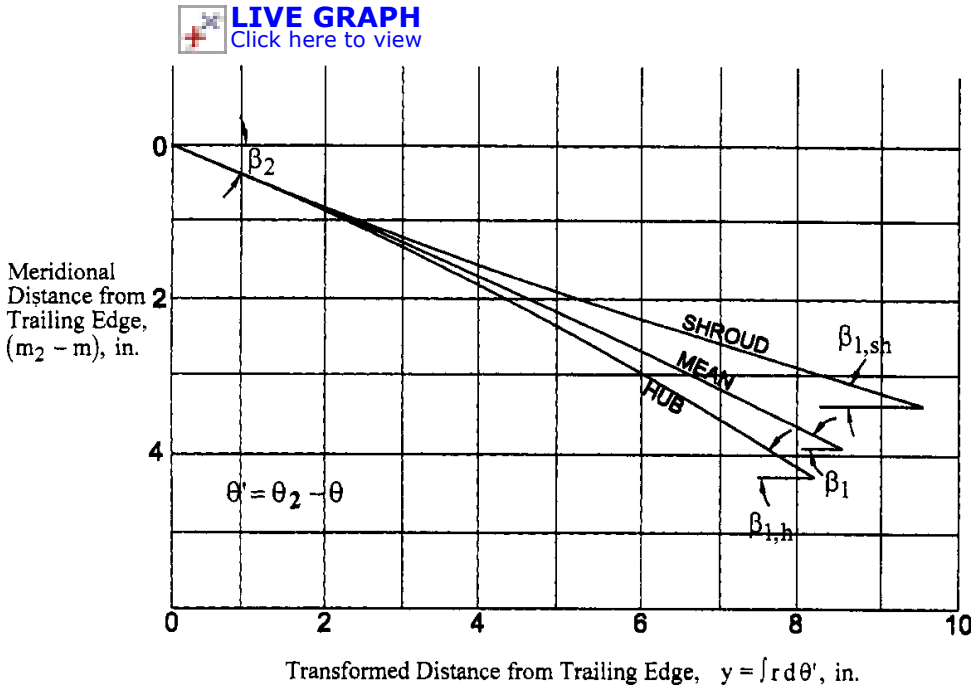


FIGURE 19 Conformal transformation of blade shape: "grid-lines"

LIBERTY EXHIBIT 1017, Page 66

a steady internal relative flow field as it rotates in proximity to these configurations. This is assured by all of these elements because they are designed to maintain uniform static pressure around the impeller periphery—at least at the design point or BEP. An exception to this rule is the concentric, "doughnut"-type, "circular-volute" collector, which is used on small pumps or in special instances where the uniform pressure condition is desired at zero flow rate.

The proximity of stationary vanes in these collecting configurations to the impeller must be considered in their design. Called "Gap B," the meridional clearance between the exit of the impeller blades and adjacent vanes ranges from 4 to 15% of the impeller radius, volutes having higher values in this range than diffusers, and pumps of higher energy level requiring the larger values. If these gaps are too small, the interactions of the pressure fields of the adjacent blade and vane rows passing each other can cause vibration and structural failure of impeller blades, diffuser vanes, and volute tongues.

a) Volutes. A volute is built by distributing its cross-sectional area on a "base circle" that touches the tongue or "cutwater" and is meridionally removed from the impeller exit by Gap B. (For radial-discharge impellers, as in Figure 20, this is a radial gap, and the base circle has radius r_3.) Beginning at the tongue, the cross-sectional area A_v of the volute passage is zero, but it increases with angle θ in the direction of rotation, ending up at area A_T in the "throat" T, as depicted in Figure 20. Worster demonstrated that the desired peripheral uniformity of static pressure can be achieved if the product rV_θ is constant everywhere in the volute[25]. One-dimensionally, this means that $r_T V_{\theta,T} = r_2 V_{\theta,2}$; and, if the velocity V_T is essentially tangential (in the θ-direction), $r_T V_T \cong r_2 V_{\theta,2}$. The diffusion or reduction of the velocity V from the impeller periphery at r_2 to the larger r_T of the throat produces a static pressure increase above that at the impeller exit; however, friction losses in the volute would cause a reduction in static pressure around the impeller at r_2 from tongue to throat unless the throat area $A_T = Q/V_T$ is slightly enlarged, creating a little more diffusion to compensate for this loss. Thus, in practice, at the BEP,

$$r_T V_T \cong (0.9 \text{ to } 0.95) \times r_2 V_{\theta,2} \tag{61}$$

At off-BEP conditions, the volute will be either too large or too small and Eq. 61 will not be satisfied. When the flow coefficient (or Q/N) drops below the BEP value, there will be excessive diffusion and an increase of static pressure around the volute from the zero area point around to the maximum area point at the throat. Proceeding around further, past the throat, a sudden drop in pressure occurs across the tongue to bring the pressure back to what it was at the starting point[25]. The opposite situation occurs above BEP.

Each of these off-BEP circumferential static pressure distributions is properly viewed as the consequence of a mismatch between the head-versus-flow characteristics of the impeller and volute[26]. For the impeller, there is the falling, straight, H_i-versus-Q line or "impeller line" of Figure 6, whereas the volute characteristic or "casing line" would be a straight line starting at the origin of Figure 6 and crossing the impeller line at the match point, which is generally at or close to the BEP flow rate. This casing line is straight because the throat velocity V_T varies directly with flow rate Q and, through Eq. 61, directly with the ideal head H_i—because $\Omega \times r_2 V_{\theta,2} = H_i$ (Eq. 15b for $V_{\theta,1} = 0$). In other words, the same volute could be optimum at a different value of Q if it were paired with another impeller whose H_i-versus-Q line crossed this same casing line at that different Q.

To essentially eliminate the consequent radial thrust on the impellers of large pumps at off-BEP conditions, a double volute is used; that is, there are two throats, 180° apart, there being either two discharge ports or a connecting "back channel" to carry the fluid from one of the throats around to join the flow emerging from the other—to form a single discharge port.

The value of the volute cross-sectional area A_v at a given polar position θ_v can be found for the portion of the total pump flow rate Q being carried in the volute at that θ_v-position together with the condition rV_θ = constant versus radius. This will produce a distribution $A_v(\theta)$ that is slightly below a straight-line variation versus θ_v from zero to A_T. Often, the practice is to use the latter straight-line design because this produces larger values of A_v

LIBERTY EXHIBIT 1017, Page 67

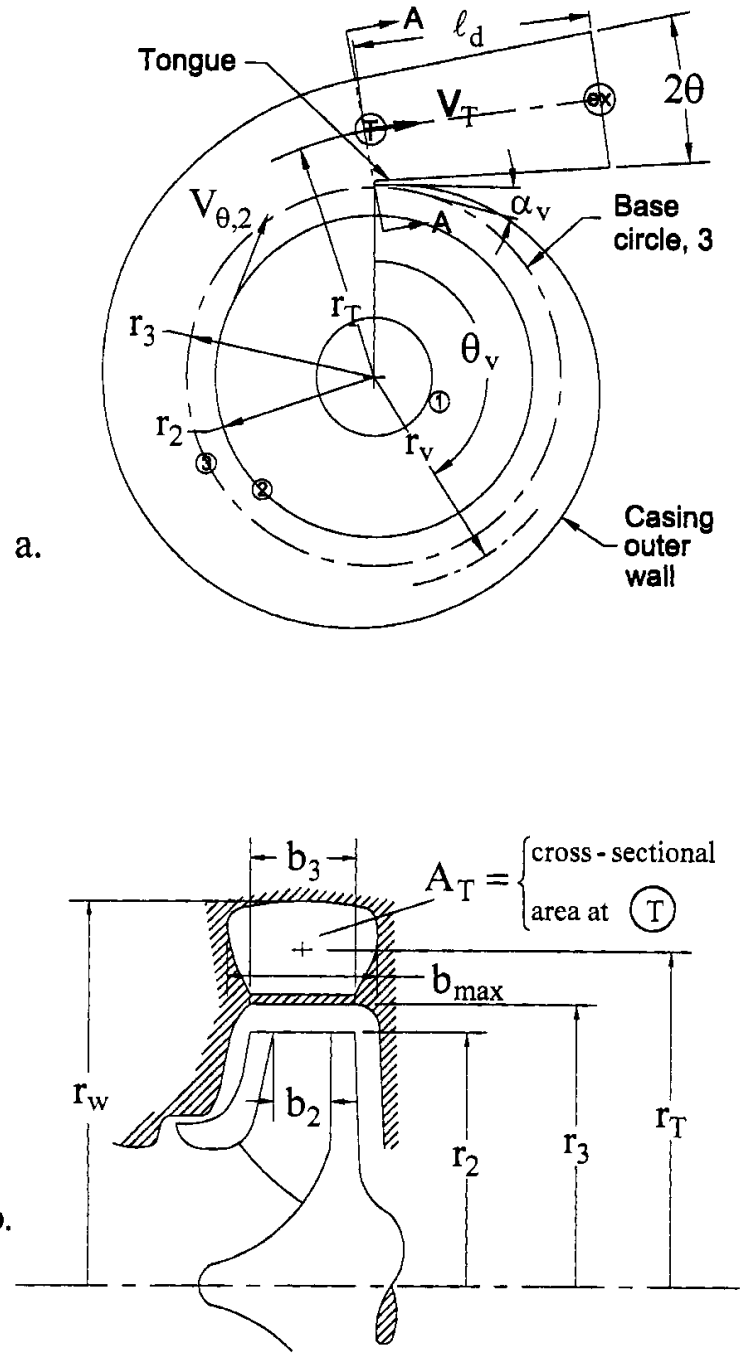


FIGURE 20 Volute casing: a) polar view; b) meridional view including Section A-A of throat T

where the hydraulic radius of the volute is small, thus compensating for the greater friction loss in that region through lower velocity—particularly for the smaller pump sizes. The cross-sectional shape of the volute is dictated by the need to make a minimum-loss transition from a small area at the beginning of the volute where the height (as can be deduced from Figure 20b) is much smaller than the width b_3 to the throat, for which the height (to the outer casing wall at r_w) and the width b_{max} are more nearly equal. Too small an aspect ratio (height/width) decreases the hydraulic diameter too much and increases the loss. There is another transition from the throat through an essentially conical diffuser (which may negotiate a turn) to a larger, circular exit port. This diffuser can be designed with the help of charts of flow elements and will normally have a 7° angle of divergence and a discharge area up to twice that of the throat A_T[27]. Thus, there is a substantial diffusion from

LIBERTY EXHIBIT 1017, Page 68

Next Page

the impeller periphery to the pump or stage exit port. This generally produces a static pressure rise in the collection system that is 20 to 25% of that of the whole stage.

b) Vaned diffusers. A vaned diffuser is rotationally symmetric and, if properly applied, produces minimal radial thrust over the whole flow rate range of a pump. Although diffusion can be accomplished in a radial outflow configuration without vanes due to the essential constancy of the angular momentum per unit mass rV_θ, one rarely finds a pump with a vaneless diffuser, partly because so much radial distance is needed to effect the reduction of tangential velocity required, as well as the still larger volute needed on single-stage pumps to collect the fluid at the exit of such a diffuser. Also, the absolute flow angle α_2 (Figure 15) of the fluid leaving the impeller is usually too small to satisfy the conditions for stall-free flow in a vaneless diffuser[28]. A vaned diffuser, on the other hand, can accomplish the reduction of velocity in a shorter radial distance. Also it can diffuse axially and, to a degree, even with radially inward flow.

Vaned diffusers are similar to multiple volutes in concept, except they are subject to off-design flow instabilities if not shaped correctly. Width b_3 is usually slightly greater than b_2 in order to accommodate discrepancies in the axial positions of impellers that feed them. With reference to Figure 21, "Gap B" ($= r_3 - r_2$) is in effect a short vaneless diffuser, and by the time the fluid has reached the throat (the dashed line at Station 4), it has gained a substantial portion of the static pressure recovery that takes place via diffusion from Station 2 to Station "ex." This "prediffusion" is enhanced by the fact that the throat area at Station 4 ($= b_3 w_1$ per passage for parallel-walled radial-flow diffusers) is larger than it is for volutes, the following relation applying to diffusers[29]:

$$r_T V_T \cong 0.8 r_2 V_{\theta,2} \tag{62}$$

Therefore, more diffusion than would result from applying Eq. 61 occurs in a vaned diffuser, the skin friction loss due to an otherwise higher velocity at the throat being offset by an efficient reduction of the velocity up to that point and a lower velocity onward.

The fully vaned portion from throat to exit (Figure 21), which performs most of the rest of the diffusion and associated static pressure recovery of the stage, is designed to perform efficiently and maintain stable flow. For typical radial-flow geometries with parallel walls, the vanes can be of constant thickness and comparatively thin or can thicken up to form "islands." The latter approach usually produces a channel that is two-dimensional with straight sides diverging at an included angle, length-to-entrance width ℓ/w_1, and area ratio A_{ex}/A_T in a combination that avoids appreciable stall[30]. A typical combination is an included angle of $11\frac{1}{2}$ degrees, $\ell/w_1 = 4$, and $A_{ex}/A_T = 1.8$, which also applies for vanes of constant thickness, as illustrated in Figure 21. Constant thickness vanes have curvature. This modifies the performance somewhat[31,32], but it allows a smaller overall radius ratio of the diffuser, r_{ex}/r_3.

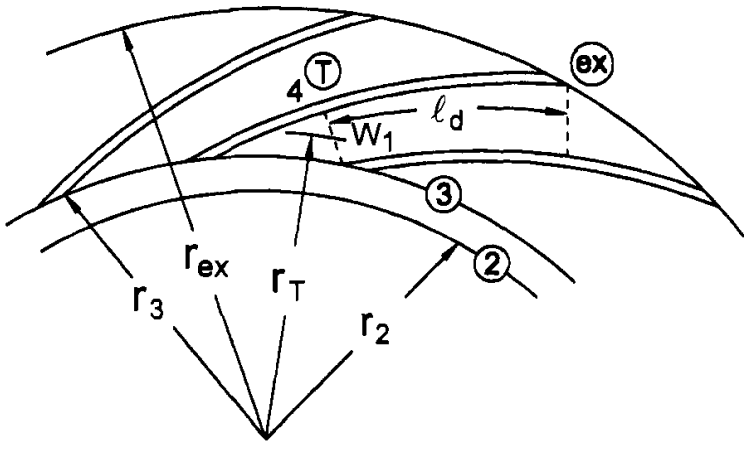


FIGURE 21 Vaned diffuser

LIBERTY EXHIBIT 1017, Page 69

Previous Page

Also, this ratio r_{ex}/r_3 will be smaller as the *number of vanes* n_v increases. The best experience seems to be with diffusers that have only a few more vanes than the number of impeller blades n_b (n_b rarely exceeds 7 in traditional commercial pumps). For pumps of higher energy levels (or high head per stage, as discussed further on in connection with high-energy pumps), it is important that n_v be chosen so as to avoid a difference of 0 or 1 between n_b and n_v or their multiples—up to at least the third multiple or "order" of each. A difference of 2 should also be avoided for at least the lower orders[33].

At off-design flow-coefficients (or off-design flow rate at a constant speed), the angle α of the absolute velocity vector V (Figure 15) approaching the diffuser will vary; yet, for typical stages, a wide range of flow coefficient is possible without damaging instabilities, even at high energy levels. This is likely the case because α is rather small at the design point or BEP (except for designs having high specific speed), so variations of the angle that occur with flow changes are within the unstalled performance range of the diffuser vane system.

c) Return passages. Conducting the relatively low-velocity fluid from the diffuser to the eye of the next impeller in a multistage pump is accomplished with return vanes or passages that also deswirl the fluid wholly or partially. Except for development of stall in the diffuser, these passages will not see a changing angle of the approaching velocity vector because the diffuser feeding them is also a stationary element. In radial-flow pumps, there is a sharp turn in the meridional plane in order to redirect the fluid radially inward. The fluid, still possessing a circumferential component of velocity that is greater than the meridional component, actually sees a much gentler turn. However, downstream of this point, a sharp turn of the blades is invariably a feature of a return passage; and this, together with the need to ensure undistorted flow into the following impeller, often dictates that the vane system accelerate the fluid as it approaches the eye. Although losses in the return passages—being related to the low velocity within them—have a minor effect on the overall stage efficiency, the design of such passages must ensure unstalled flow into the impeller in order to avoid the negative impact of a distorted inlet flow on the efficiency and to promote pulsation-free operation of the impeller.

A variety of return-passage geometries exist, some of which are presented in the literature [29,34]. The continuous-vane type is integral with the upstream diffuser, thereby eliminating the entry losses into yet another vane system after the diffuser[5,34]. Improvements in manufacturing technology have made this potentially more efficient approach more viable for radial machinery. The continuous-vane concept is standard practice in the design of mixed-flow "bowl"-type pumps[21]. The diffusing stator vane row that receives the fluid from the impeller of an axial-flow pump—being an axial-flow element itself—possesses the return feature already. Diffusion in axial-flow stators is typically accomplished by a reduction in velocity of about 30 to 40%. The actual value is governed by an acceptable level of the diffusion factor, Eq. 57. (A similar reduction in relative velocity is needed for an axial-flow impeller to generate static pressure, as can be seen from Eq. 21. By comparison, centrifugal impellers, on the rms streamline, usually have W_2 about equal to W_1—as seen in Figure 17.)

Axial-Flow Pumps The preceding development, though general, is applicable mainly to centrifugal and mixed-flow pumps. In that procedure, the impellers have appreciable solidity, and original blade shapes are constructed from the viewpoint of one- or two-dimensional channel flow. The collectors are often volutes or non-axial-flow vane systems. Performance is not known a priori and so must be estimated, as outlined further on. On the other hand, the extensive two-dimensional, experimental, axial-flow cascade data amassed by NACA researchers[23] and others enables the designer to adopt existing airfoil blade shapes and so predict the performance with greater confidence. The procedure for utilizing these shapes and the corresponding experimental results has long been the basis for designing axial-flow compressors for gas-turbine engines and is clearly described by Hill and Peterson[35]. This approach is widely used, especially for high-specific-speed, low-solidity axial-flow propeller pumps—in designing both rotating and stationary blade rows. Insights for propeller pump design and performance characteristics can be found in Stepanoff.[6]

An exception to this axial-flow pump design approach is the case of inducers. Although they are axial-flow pumps, they have high solidity and are usually designed as channel-flow machines. The design philosophy outlined in the preceding paragraphs is applicable,

LIBERTY EXHIBIT 1017, Page 70

except that the blades usually approximate constant- or variable-pitch helices. Performance prediction is generally accomplished via one-dimensional calculations and the correlations described in the following paragraphs and, increasingly, via CFD analysis.

PREDICTING THE PERFORMANCE CURVES

The choices made in the foregoing design procedures can and should be verified analytically, the objectives being first to generate the performance characteristic curves for head and power at constant speed and second to ensure stable behavior of the various systems in which the pump is to be applied. For the first objective, the solution involves analytical or empirical approaches: a) at non-recirculating flow conditions; that is, from flow rates Q somewhat below Q_{BEP} out to the maximum "runout" flow rate, b) at shut-off ($Q = 0$) and low flow, or c) the complete set of curves for a given pump predicted by means of computational fluid dynamics (CFD).

Generating Performance Curves The fluid dynamical limitation on the deceleration of the relative velocity W determines the shape of the head-versus-flow curves. This is inherent in the choice made for the head coefficient ψ in Figure 12, which sizes the impeller and is illustrated in Figure 22. The typical situation of zero (or nearly so) inlet whirl $V_{\theta,1} = 0$ means that the ideal head coefficient ψ_i equals the most significant ratio of the outlet velocity diagram because from Eqs. 15 and 31 (with $V_{\theta,1} = 0$):

$$\psi_{\text{ideal}} = \frac{\mathcal{U}_2^2 \, (V_{\theta,2}/U_2)}{\mathcal{U}_2^2} \tag{63}$$

$$\psi = \eta_{HY} \, \psi_{\text{ideal}} = \eta_{HY} \, \frac{V_{\theta,2}}{U_2} \tag{64}$$

Figure 22 illustrates how specific speed Ω_s affects the BEP value of ψ_i and therefore ψ. Overall, only a small reduction of W occurs in most impellers. So, at low Ω_s, the low value of W_1 associated with the small eye relative to the maximum diameter (Figure 9) enables the outlet velocity diagram (Figure 22a) to have a high value of $V_{\theta,2}/U_2$. On the other hand, this ratio drops as Ω_s increases and the eye grows to be as large as the maximum diameter of the wheel. Figure 22b is the result because the value of ψ at shut-off (about $\frac{1}{2}$) is not based on the one-dimensional concept of velocity diagrams but primarily on the pressure generated by solid body rotation of stalled (though recirculating) fluid contained within the impeller. The BEP values of ψ in Figure 22b are consistent with Figure 12 and illustrate why a high-specific-speed impeller has such a substantial "rise to shut-off" of the head curve. This is dramatically illustrated in Figures 8–10 of Section 2.1.3 in which the head curves are normalized to that of the BEP[36].

a) Non-recirculating flows. The BEP efficiency and head can be determined from correlations for typical pumps or from computation of the losses. Fluid dynamic procedures described in this section can be used to determine the shapes of the head and power curves at all flow rates to runout, using the BEP as an anchor point for such computations. For pumps designed conventionally, beginning with Figure 12, Anderson's overall (BEP) efficiency correlation (Eq. 44) as modified in Figure 10 is useful. Other similar charts, especially Figure 6 in Section 2.1.3, are in widespread use. The breakdown of the losses involved, as expressed by Eqs. 8–11, is quantified through the development of the three component efficiencies η_{HY}, η_m, and η_v in Table 3. All three decrease with decreasing specific speed—as might be expected from the charts just mentioned.

This can be seen in the η_{HY}-expression (a) of Table 3 because ψ_i is greater at low Ω_s as discussed relative to Figure 22. Jekat's η_{HY}-expression (b) of the table works surprisingly well, largely because of the flow effect in Figure 10 (explained there as the "size effect" of

LIBERTY EXHIBIT 1017, Page 71

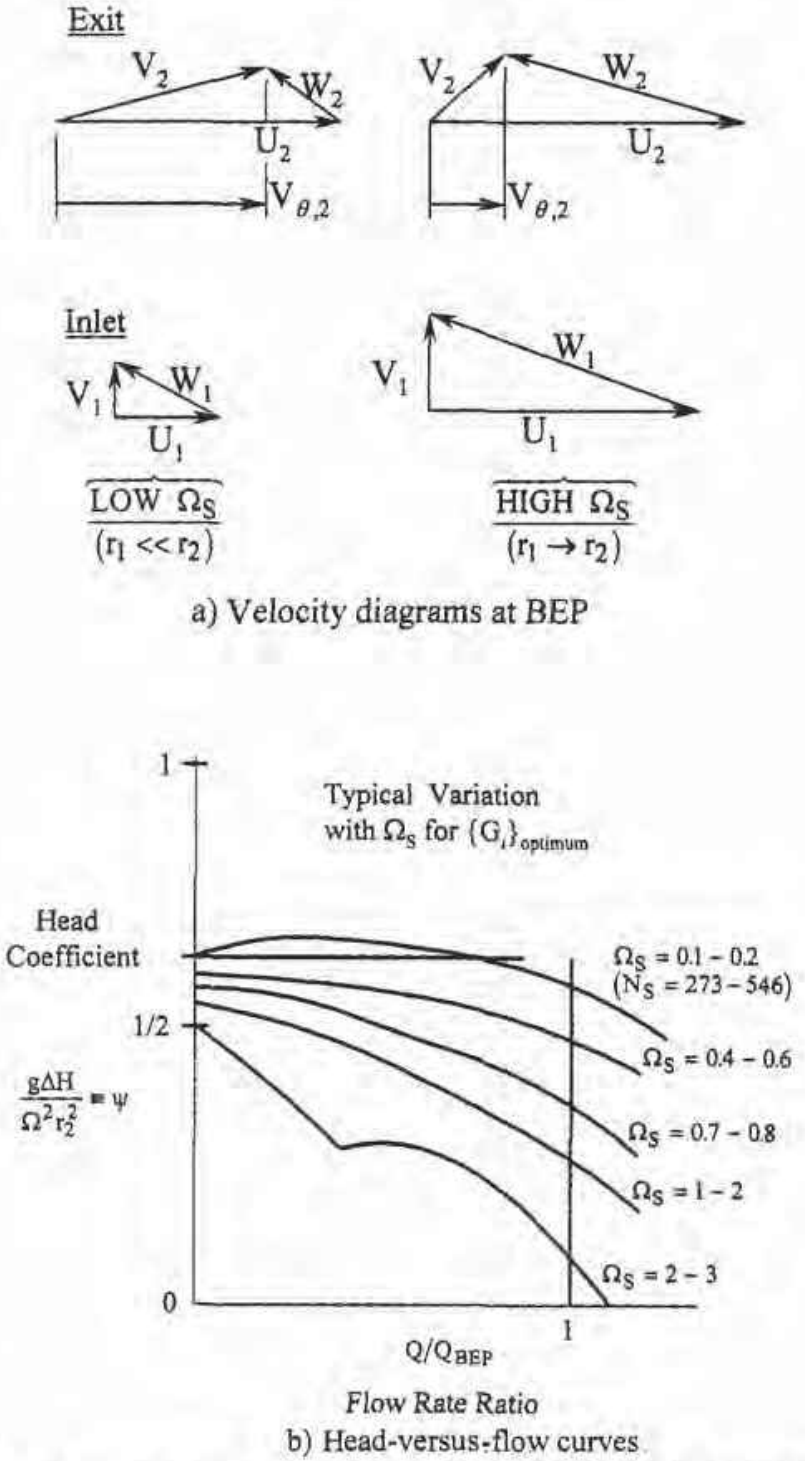


FIGURE 22 Performance versus specific speed: a) velocity diagrams at BEP; b) head-versus flow curves.

larger relative roughness and clearances in smaller pumps) and because low Ω_s tends to go hand-in-hand with low flow rate Q.

To compute η_{HY} at $Q \neq Q_{BEP}$ (and, if required, at $Q = Q_{BEP}$ as well), it is necessary to go deeper into the prediction of η_{HY} by developing *expressions for the losses* noted in Eq. 21, which are basically expansions of the expression for the collector loss coefficient ζ_c[26] and for the impeller loss expression (c) of Table 3[87]. In this expression, the incidence loss coefficient k can be obtained from cascade data or developed as a combination of a turning

LIBERTY EXHIBIT 1017, Page 72

and a sudden expansion loss[5,9,27]. The "pipe-type friction factor" f can be increased to include secondary flow and diffusion losses due to blade loading (or turning[38] of the absolute velocity vector V). The resulting f-value can thus be twice the usual pipe value associated with the skin friction losses in the passage. (The pipe value of f is found from the well-known pipe friction chart—Figure 31 in Section 11.1—by substituting a

TABLE 3 Component efficiency expressions developed

A) Hydraulic Efficiency

Breaking up the main flow losses into impeller (including inlet)

and collector losses $\sum_i L_i = L_{imp} + L_c$ and defining $L_c = \zeta_c \frac{V_2^2}{2}$, where ζ_c

is the collector loss coefficient or fraction of $V_2^2/2$ not converted into static pressure rise in the collector, we have (Eq. 10)

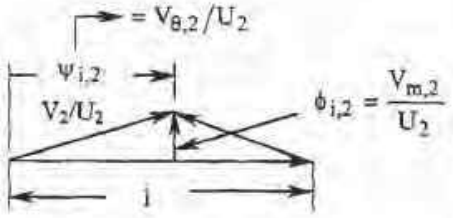
$$\eta_{HY} = 1 - \frac{\sum L_i}{\Delta(UV_\theta)} = \underbrace{1 - \frac{L_{imp}}{\Delta(UV_\theta)}}_{\eta_I} - \underbrace{\frac{\zeta_c V_2^2/2}{\Delta(UV_\theta)}}_{\zeta_c\left(\frac{\psi_{i,2}}{2} + \frac{\phi_{i,2}^2}{2\psi_{i,2}}\right)}$$

or, for no inlet whirl ($V_{\theta,1}=0$) $\psi_i = \psi_{i,2}$:1231

$$\eta_{HY} = \eta_I - \zeta_c\left(\frac{\psi_i}{2} + \frac{\phi_i^2}{2\psi_i}\right) \qquad (a)$$

Impeller hydraulic efficiency: $(\eta_I \approx 0.90 - 095)$

Collector loss: ($\psi_i/2$ predominates) $(\zeta_c \approx 0.2 - 0.3)$



Practical experience (roughness ε constant for all sizes) yields the formula by W.K. Jekat:

$$\eta_{HY} \approx 1 - 0.8/[Q\,(\text{gpm})]^{0.25} \qquad (b)$$

or $$\eta_{HY} \approx 1 - 0.071/\left[Q\left(m^3/s\right)\right]^{0.25}$$

at all specific speeds.

However a deeper analysis treats losses L_{imp} as follows:

$$L_{imp} = k\frac{W_1^2}{2} + f\frac{\overline{W^2}}{2}\frac{\ell}{D_h} \qquad (c)$$

where D_h = passage hydraulic diameter,
ℓ = passage length
f = pipe-type friction factor
k = incidence loss coefficient
$\overline{W^2}$ = the average square of the relative velocity within the passage along the rms or mean meridional streamline
W_1 = relative velocity just upstream of the impeller blades on the rms streamline

LIBERTY EXHIBIT 1017, Page 73

TABLE 3 Component efficiency expressions developed (*Continued*)

B) Mechanical Efficiency
From Eq. 9,

$$\eta_m = \frac{P_s - (P_{DF} + P_{B\&S})}{P_s} = 1 - \frac{P_{DF} + P_{B\&S}}{P_s} \qquad \text{(d)}$$

(Bearing & Seals)

$$P_{DF} = \frac{C_m}{2} \rho \Omega^3 r_2^5 \qquad \text{(e)}$$

Disk Friction

Where (for two sides of disk) $C_m \approx 0.085 \Big/ \left(\frac{\Omega r_{t,2}^2}{\nu} \right)^{0.2}$ (R_e) Typically $C_m = 0.004$ (at $R_e = 4.3 \times 10^6$) (f)

Shaft Power

$$P_s = \frac{\rho g \Delta H}{\eta_p} = \frac{\psi Q_s \rho \Omega^3 r_{t,2}^5}{\eta_p}$$

$$Q_s = \frac{Q}{\Omega r_{t,2}^5} = \Omega_s^2 \psi^{3/2} \Rightarrow P_s = \frac{\Omega_s^2 \psi^{5/2}}{\eta_p} \rho \Omega^3 r_{t,2}^5 \qquad \text{(g)}$$

Combining the usually smaller $P_{B\&S}$ with P_{DF}, Eq. (d) (with e, f and g) becomes

$$\eta_m = 1 - \frac{(C_m/2) \times \eta_p}{\Omega_s^2 \psi^{5/2}} \qquad \text{(h)}$$

C) Volumetric Efficiency
From Eq. 11,

$$\eta_v = \frac{Q}{Q + Q_L} \approx \frac{1}{1 + 5 \left[\frac{\frac{\delta}{r_R} \left(\frac{r_e}{r_2} \right)^2}{\Omega_s^2 \psi} \right]} \qquad \text{(j)}$$

The clearance ratio δ / r_R is typically 0.001 to 0.002

[Leakage back to impeller inlet across two rings (front and back) essentially doubles the leakage loss, changing the value 5 in Equation (j) to 10.]

representative average passage hydraulic diameter $D_h = 4A_p/\wp$ for the pipe diameter d.) A further increase in this f-value occurs if the impeller is missing one or both rotating shrouds; that is, it is a semi- or fully-open impeller with blade tip leakage losses appearing in the main flow stream[39]. Multiphase flows in pumps often are accompanied by greater than normal hydraulic losses; for example, increasing the concentration of solids in the carrier liquid flowing through a slurry pump increases the f-value still further[40] (see Section 4.2).

LIBERTY EXHIBIT 1017, Page 74

Quasi three-dimensional (Q3D) analysis[41] affords an assessment of the secondary flow and diffusion losses and gives results similar to inviscid three-dimensional (3D) flow analysis. Q3D analysis starts by solving the 2D meridional (hub-to-shroud) flow field. This is followed by a series of 2D blade-to-blade inviscid solutions[42] or approximations thereto[22], each on a surface of revolution generated by one of the meridional streamlines of the hub-to-shroud 2D solution and producing results like that of Figure 17. From this, one computes the diffusion factors (Eqs. 57–59) and decides whether the diffusion losses are significant—in which case a redesign is in order.

CFD Analysis finally enables one to make an accurate and complete hydraulic performance evaluation of the impeller and accompanying stationary flow elements. This can be done at all flow rates and NPSH-conditions for any fluid via a corresponding series of fully viscous, single- or multi-phase solutions of the Reynolds-averaged Navier-Stokes equations (as described in Section 2.1.2).

Mechanical efficiency η_m as stated earlier, is largely the result of impeller disk friction. If the drag of bearings and seals is added, as in Eq. (d) of Table 3, the moment coefficient C_m in the disk friction formula (e) can be increased over known disk friction values[43,44] to include these effects. (On the other hand, the drag power loss of shaft seals, though usually quite small, is generally directly proportional to speed. Such losses can therefore be significant in small pumps running at lower-than-normal speeds.) The C_m-expression given in Formula (f) reflects this adjustment and includes the drag on both sides of a smooth impeller at the usually high values of Reynolds number R_e for low-viscosity liquids and for a typical clearance ratio $s/a = 0.05$, where a is the disk radius. This works well for most impellers: The drag at the ring fits roughly compensates for the fact that the impeller eye has been cut out of the disk, and so on. (There is very little influence on C_m of the gap width s between impeller shroud and casing wall, C_m being proportional to $(s/a)^{0.1}$ in general.[43] For very small s/a, C_m instead grows as s/a decreases. See Refs. 43 and 44 for formulas that apply to the entire range of Reynolds number R_e and clearance ratio s/a.)

The value of C_m can be even larger for semi- or fully-open impellers, if the neighboring fluid is rotating faster relative to the wall—as is the case with radial-bladed open impellers. The fluid between a shrouded impeller and adjacent wall, on the other hand, rotates at half speed[43]. (In cases where the impeller surface and adjacent wall are both rough, C_m is larger than just discussed[44].) Finally, notice in Eq. (h) that very low specific speed Ω_s produces a dramatically low value of η_m. This drives ψ to the larger values of Figure 12 at low Ω_s—also dictated by the W-deceleration considerations per Figure 22. Overall there is a benefit, despite possibly lower η_{HY} [Eq. (a)] due to the consequently greater ψ_i and collector loss.

Volumetric efficiency η_v applies to leakage across impeller shroud rings or "neck rings" and balancing drums. Eq. (j) in Table 3 is an approximation for the leakage across a typical ring of a closed-impeller pump, assuming orifice-type flow at a discharge coefficient of $\frac{1}{2}$. Results can vary from this approximation of the more exact method reported by Stepanoff.[5] Referring to Figure 2, leakage Q_L occurs at $r = r_R$, (r_R being approximately 1.2 times r_e) under a pressure difference across the ring of about $\frac{2}{3}$ that of the pump stage. If the shroud is removed and the open blades are fitted closely to the adjacent wall, as with open impellers, the consequent leakage from one impeller passage to the next across the blade tips does not affect η_v, and Eq. (j) should be modified accordingly. Rather, the tip leakage causes a hydraulic efficiency loss as previously discussed. Finally, as with η_m, Eq. (j) indicates that low-Ω_s pumps have low η_v.

At flow rates Q other than Q_{BEP}, the analytical methods described previously for computing the hydraulic efficiency are utilized, together with computation of the inlet and outlet velocity diagrams, which yield the ideal head and power curves as illustrated in Figure 6. In this procedure, the slip velocity V_s (Figure 15) applies to the BEP and, at other flow rates, the exit relative flow angle β_{f2} can be assumed constant. This accords with the fact that V_s for the narrower active jet at low flow rates must be smaller. A blockage model for the thickening wakes and narrower active jets that develop as Q is decreased can be introduced to compute the one-dimensional velocity diagrams, but ignoring this at non-recirculating flow rates appears not to be serious in determining the shapes of the head and power curves.

LIBERTY EXHIBIT 1017, Page 75

b) Shut-off and low flow. The foregoing analyses apply over that portion of the flow rate range that does not involve recirculation, as illustrated in Figure 6. The complexity of recirculation had not been readily handled analytically prior to the use of CFD, and this has forced pump designers to estimate the low-flow end of the H-Q curve with the help of empirical correlations. Insightful fluid dynamical reasoning about the physics of the flow led to useful expressions for the head developed and the power consumed at shut-off. Shut-off, then, in addition to the BEP, becomes the other anchor point of the head and power curves; and this—together with the shapes established for these curves at the higher flow rates—gives the analyst an idea of the intervening shapes.

Shut-off head $H_{s/o}$ can be viewed as the sum of two effects occurring at $Q = 0$, each being represented by a term in this equation:

$$H_{s/o} = \frac{k_{imp} \times (U_{t,2}^2 - U_{h,1}^2)}{2g} + \frac{k_{ex} \times U_2^2}{2g} \tag{65}$$

or

$$\psi_{s/o} = \frac{k_{imp} \times \left(\dfrac{r_{t,2}^2}{r_2^2} - \dfrac{r_{h,1}^2}{r_2^2} \right)}{2} - \frac{k_{ex}}{2} \tag{66}$$

where the first term is the centrifugal effect of essentially solid body rotation of the fluid confined within the impeller; and the second term is the pitot effect of the recirculating fluid from the impeller that impinges against the volute or diffuser throats which in turn are connected through stagnant fluid to the exit port of the pump. While the factors k_{imp} and k_{ex} associated with these effects vary with the hydraulic configuration, the values involved can be estimated as follows: $k_{imp} \approx 1$, as the radial equation of motion[3] would indicate for fluid rotating at Ωr everywhere within the blades, i.e., for $r_{h,1} < r < r_{t,2}$ (Figure 8). Thus, as indicated by Eqs. 65 and 66, increasing the minimum radius of the blades at inlet $r_{h,1}$ tends to reduce the shut-off head. However, the presence or absence of fluid swirl in the region upstream of the impeller blades at shut-off has been found experimentally to affect the value of k_{imp} in surprising ways—sometimes increasing it above unity in such a way as to minimize the effect on shut-off head of any non-zero value of $r_{h,1}$. The value of k_{ex} depends on $(r_3 - r_2)/r_2$, or "Gap B" and other features of the impeller exit and collector geometry. It is usually in the range 0.2 ± 0.1, any change in the geometry that increases the shut-off power coefficient (see below) raising k_{ex} by driving more recirculating flow from the impeller against the volute or diffuser throats. Thus the shut-off head coefficient $\psi_{s/o}$ (Eq. 66) for typical radial-flow pumps generally exceeds $\frac{1}{2}$, the value of 0.585 being advanced by Stepanoff[5]. Estimates for $\psi_{s/o}$ are also indicated in Figure 22b.

Shut-off power consumption $P_{s/o}$ includes disk, bearing, and seal drag power P_D and that which drives the recirculation P_{recirc}. The latter is generally dominant by far. From similarity arguments (Eq. 33), the shut-off power coefficient

$$\hat{P}_{s/o} = \frac{P_{s/o}}{\rho \Omega^3 r_2^5} \tag{67}$$

is a constant for a given pump geometry. Mockridge, in a discussion attached to an ASME paper by Stepanoff, reasoned that a wider impeller (larger b_2 at the same diameter D_2) would recirculate more fluid at shut-off and therefore have a higher value of this coefficient. His correlation is shown in Figure 23 and is probably the most significant quantitative result available for predicting the performance of centrifugal pumps at shut-off conditions short of implementing a full CFD solution of the impeller and accompanying stationary flow elements[36].

The design task therefore resolves itself into an iteration between an efficient geometry-generating scheme and a rapid CFD flow and performance analysis of the geometry resulting from each iteration[45]. This is especially useful if a nontraditional geometry is

LIBERTY EXHIBIT 1017, Page 76

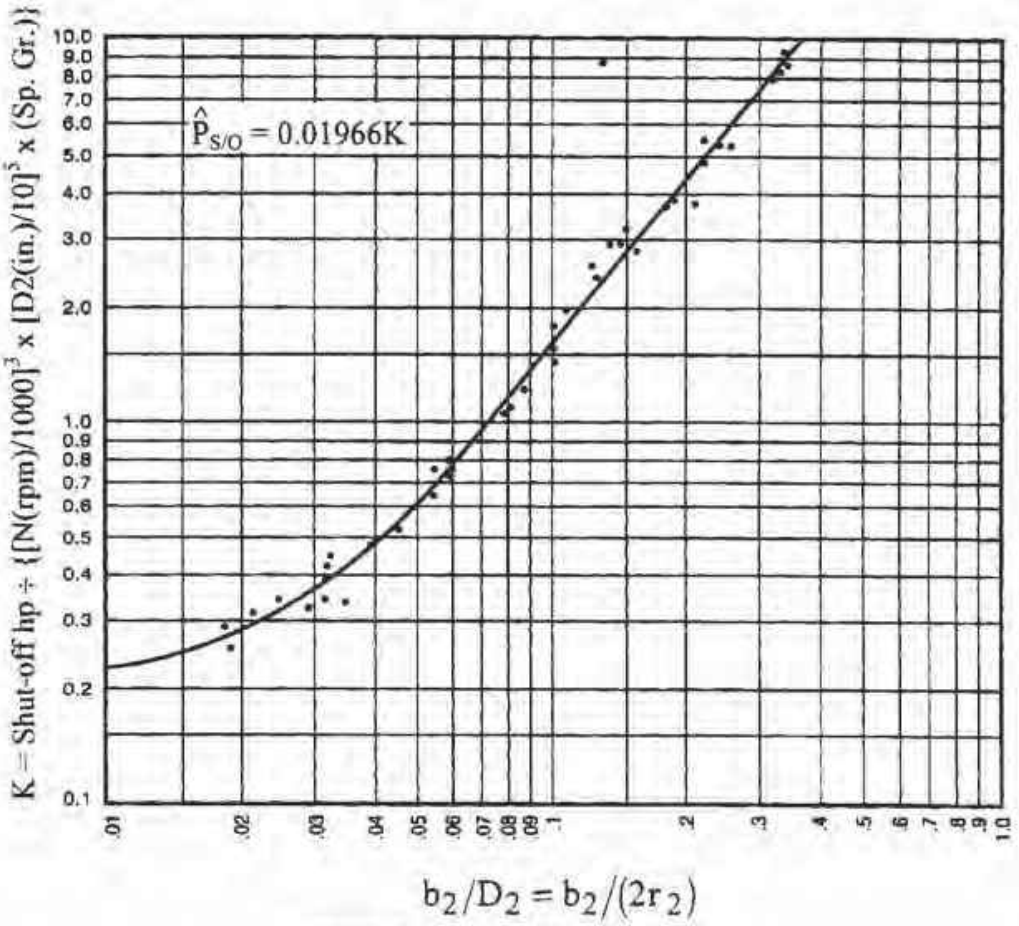


FIGURE 23 Shut-off power coefficient

involved, or if an efficient design is sought that will produce a desired performance curve shape. Nevertheless, many turbomachinery designers can make more rapid and valid judgments about their respective classes of machines through the time-honored iteration between a proprietary direct or inverse design and a convenient inviscid performance prediction scheme.[41,46] "Inverse" means that the blade shape emerges from an initial specification of certain desired fluid velocity component distributions.[17] This concept has been expanded through more formal geometry optimization employing neural networks.[47] Thus, designers have developed reliable diffusion criteria (computed, for example, from Eqs. 59a and 59b) for interpreting the acceptability of the free-stream relative velocity distributions W_s and W_p on the blade surfaces (Figure 17) produced by the Q3D blade-to-blade solutions[43]. Because CFD codes solve the actual viscous flow field, the boundary condition on the blade surface is zero relative velocity. This can be at least partly overcome by displaying the CFD-distributions of pressures on the blade surfaces, the interpretation of which would require knowledge of the corresponding criteria for these pressures[48]. Also, the velocities at the edge of the boundary layer could be extracted from the CFD solution and displayed in familiar terms. A useful design approach for the present may therefore be to a) produce the final design by the more traditional methods and b) predict the performance curves via CFD[49].

Predicting Axial Thrust The prediction of pump performance is not truly complete without the corresponding prediction of the hydrodynamic axial and radial thrust that the impeller(s) can be expected to encounter. A comprehensive treatment of radial thrust appears in Section 2.1.3, and a review of axial thrust and thrust balancing devices is covered in Section 2.2.1. However, obscure flow phenomena can profoundly affect the radial

LIBERTY EXHIBIT 1017, Page 77

distributions of pressure on the outside surfaces of a shrouded impeller that give rise to the net axial thrust. These phenomena become even more complex when discharge recirculation occurs and can cause adverse mechanical response in high-energy pumps, as will be explained further on. As a basis for tackling such problems, the fundamentals of axial thrust are presented in Table 4 for shrouded centrifugal impellers that have leaking fluid flowing in the gaps between the impeller shrouds and the adjacent casing walls. The positive direction of the thrust T is taken toward the suction or eye of the single-suction impeller shown. The incoming axial momentum $\rho Q V_{z,1}$ is generally quite small for radial impellers and has been omitted from the Table. It serves, however, to reduce T.

The centrifugal effect of the fluid spinning in the sidewall gaps causes a reduction in static pressure from the outer periphery (OD) of the impeller to the sealing ring, and this is quantified in the expressions given for the swirl velocity component V_θ. These

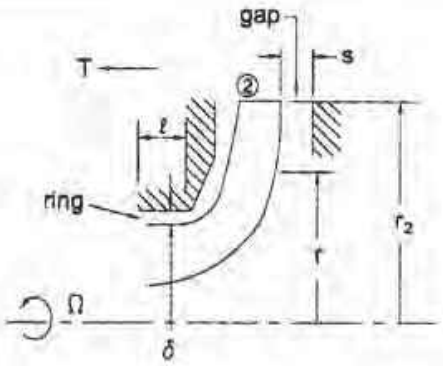
TABLE 4 Leakage effects on axial thrusts

Thrust $= (T_B - T_F)\, n_{stgs.} - T_{slv}$

where $T = \int_{r_{min}}^{r_{max}} 2\pi r p\, dr$

where $p = p_2 - \int^2 \frac{\rho}{g} \frac{V_{\theta,gap}^{\,2}}{r} dr$

and p and $V_{\theta,gap}$ are determined as follows in the absence of vanes in the gap:



A) For zero leakage flow, fluid outside impeller rotates at half speed; i.e., at $\frac{\Omega r}{2}$; namely, $V_{\theta,gap} = \frac{\Omega r}{2}$; so that

$$p_o - p_i = \int_i^o \rho \frac{V_{\theta,gap}^{\,2}}{r} dr = \frac{\rho\Omega^2}{4} \int_i^o r\, dr = \rho \frac{\Omega^2 \left(r_o^{\,2} - r_i^{\,2}\right)}{8}$$

or

$$p_o - p_i = \frac{\rho}{8} \Omega^2 r_o^{\,2} \left[1 - \left(\frac{r_i}{r_o}\right)^2\right]$$

[Note: This is 1/4 of what $(p_o - p_i)$ would be if $V_{\theta,gap} = \Omega r$ (full wheel speed - as on the front side of a semi-open impeller)

then, one gets $(p_o - p_i) = \frac{\rho}{2} \Omega^2 r_o^{\,2} \left[1 - \left(\frac{r_i}{r_o}\right)^2\right]$]

B) For non-zero leakage

1) Inflow: $V_{\theta,gap}$ averages to be > half speed

⇒ greater $(p_o - p_i)$ than at half speed (or zero leakage)

2) Outflow: $V_{\theta,gap}$ averages to be < half speed

⇒ nearly constant pressure from $(p_o - p_i)$

LIBERTY EXHIBIT 1017, Page 78

TABLE 4 Leakage effects on axial thrusts (*Continued*)

Specifically,

$$\text{where } V_{\theta,gap} = \begin{cases} \Omega r_2 \times f_{inflow}\left(\dfrac{r}{r_2}, \Phi_{lkg}\right) \times f_{width} \\ \text{or} \\ \Omega r \times f_{outflow}\left(\Phi_{lkg}\right) \times f_{width} \end{cases}$$

$$\text{where } \Phi_{lkg} = \frac{Q_{leakage}}{\Omega r_2^{\,3}} \Rightarrow \begin{cases} \text{Interaction of} \\ \text{leakage and} \\ \text{pressure at ring} \end{cases}$$

$$\text{where } Q_{leakage} = f_L\left(\ell,\ \delta,\ \Omega,\ \nu,\ \Delta p_{ring}\right)$$

$$f_{inflow} = \left(0.5 - \frac{450}{\pi}\left|\Phi_{lkg}\right|\right)\frac{r}{r_2} + \frac{450}{\pi}\left|\Phi_{lkg}\right|$$

$$f_{outflow} = 0.5 - 100\left|\Phi_{lkg}\right|$$

$$f_{width} = \frac{\sqrt{A^2 + A} - A}{0.5}$$

$$\text{where } A = 1/\left[5\, s/r_2\right]$$

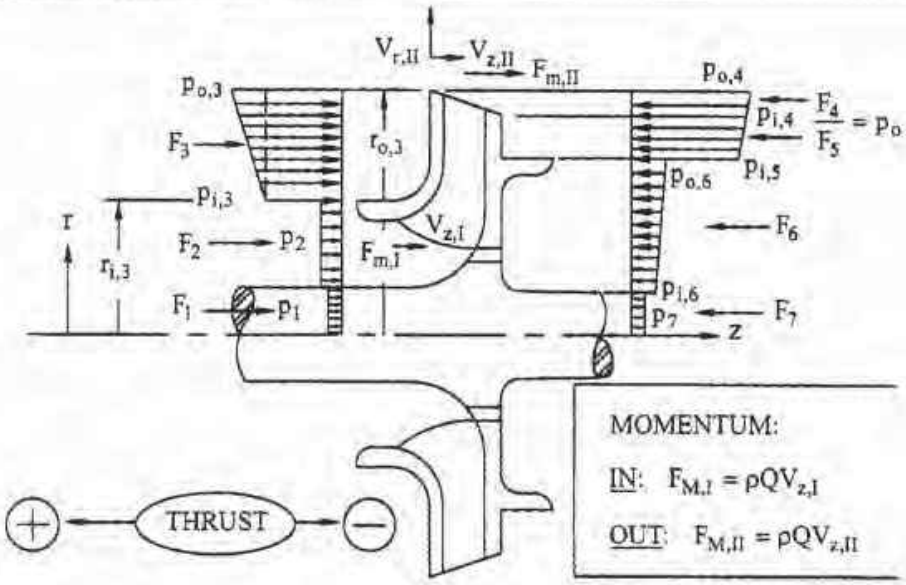
expressions are curve fits to experimental data for the leakage flowing radially inward on either or both sides of the impeller[50] and for outflowing leakage as occurs on the back side (away from the "front" or suction side) of multistage pump impellers due to the higher pressure arising from the diffusing system downstream of each impeller[51]. In the absence of leakage, the fluid in the sidewall gap rotates at about half the local impeller wheel speed; that is, $V_\theta = \Omega r/2$, and this half speed is typical of the gap flow near the impeller OD, even in the presence of leakage. The greater the inflow leakage, the lower the pressure becomes at the entrance to the ring clearance. The major effect is that of swirl or the tangential component of velocity V_θ, which varies inversely with radius; although casing wall drag tends to slow it toward half speed. More leakage flow is less influenced by this drag and so experiences a greater centrifugal effect. This in turn means more pressure drop from OD to ring. (The leakage rate, of course, is affected, the solutions for both leakage and pressure distribution being linked and usually requiring iteration.) The opposite effect happens for outflow on the back side of multistage pump impellers. Here the fluid enters the sidewall gap at a small radius (see Section 2.2.1) and so with negligible swirl. It flows outward without picking up much swirl, especially if there is substantial radial outflow leakage, which means the centrifugal effect is small, yielding a nearly constant pressure versus radius. The overall result is more net thrust toward suction than might be expected from a cursory look at the pressure-loaded surfaces.

If wear ring clearances increase during the life of the pump, the net thrust of multistage pump impellers increases. Likewise, unequal ring wear leads to uncertain changes in the thrust of a "balanced" single- or double-suction impeller with inflow to wear rings on both sides. Similarly, these theories can be applied to balancing drums and other such devices described in Section 2.2.1.

Integration of the pressure equation in Table 4 becomes a chore unless the whole theory is computerized. A quick estimate of the thrust is possible, however, if the distributions of pressure in the separable domains of the surfaces are assumed to be linear; in that case, the integration is simple and yields the closed-form results of Table 5. This table also

LIBERTY EXHIBIT 1017, Page 79

TABLE 5 Approximate axial thrust calculation



$$\underline{\text{THRUST}} = F_7 + F_6 + F_5 + F_4 - F_3 - F_2 - F_1 - F_{m,I} + F_{m,II}$$

$$\underline{\text{For Const. - p Forces}}: \quad F_j = p_j \times \pi \left(r_{j,o}^2 - r_{j,i}^2 \right) \qquad j = 1,\ldots,7$$

i = inner; o = outer

$$\underline{\text{For Linear p(r) Forces}}: \quad F_j = F_{j,\text{const}} + F_{j,\text{var}}$$

$$\text{where} \quad F_{j,\text{var}} = \tfrac{1}{3} \pi r_{j,o}^2 \left[2 - \frac{r_{j,i}}{r_{j,o}} - \left(\frac{r_{j,i}}{r_{j,o}} \right)^2 \right] \times \left(p_{j,o} - p_{j,i} \right)$$

Example:

$$F_3 = p_{i,3} \times \pi \left(r_{o,3}^2 - r_{i,3}^2 \right) + \tfrac{1}{3} \pi r_{3,o}^2 \left[2 - \frac{r_{3,i}}{r_{3,o}} - \left(\frac{r_{3,i}}{r_{3,o}} \right)^2 \right] \times \left(p_{o,3} - p_{i,3} \right)$$

indicates how to account for each element of the thrust, including the axial momentum terms, which become significant for higher-specific-speed mixed-flow impellers. In all cases, in order to proceed with the calculation, the static pressure at the impeller OD must be known, as it is from the boundary condition imposed at the OD that the rest of the pressure distribution emerges. Even for substantial leakage, the pressure drop of the fluid entering the sidewall gaps from the impeller exit is small or negligible; therefore, the impeller pressure essentially applies in the gap (at the OD) as well. The foregoing methods of predicting pump head also yield the impeller OD pressure, which is usually between 75 and 80% of the stage pressure rise above inlet.

Thrust computations can therefore be coupled with the head-curve prediction scheme being employed for the pump, thereby yielding predicted thrust curves together with the predictions of hydraulic performance.

Ensuring Stable Performance The ability for a pump to run smoothly with minimal pressure-rise and flow-rate excursions is dependent on the shape of the pump head-flow

LIBERTY EXHIBIT 1017, Page 80

performance curve and the characteristics of the system in which it operates. There are two types of pump-system instability; namely, a) static instability, which can be ascertained by studying the pump and system head curves, and b) dynamic instability, which requires more detailed knowledge of the system[52]. (In addition to these system-related instabilities, there is the unsteady behavior of the separated and recirculating flows that occur when a pump operates at a flow rate substantially below the BEP. Called hydraulic instability, this becomes important in higher-energy applications and is therefore discussed later.)

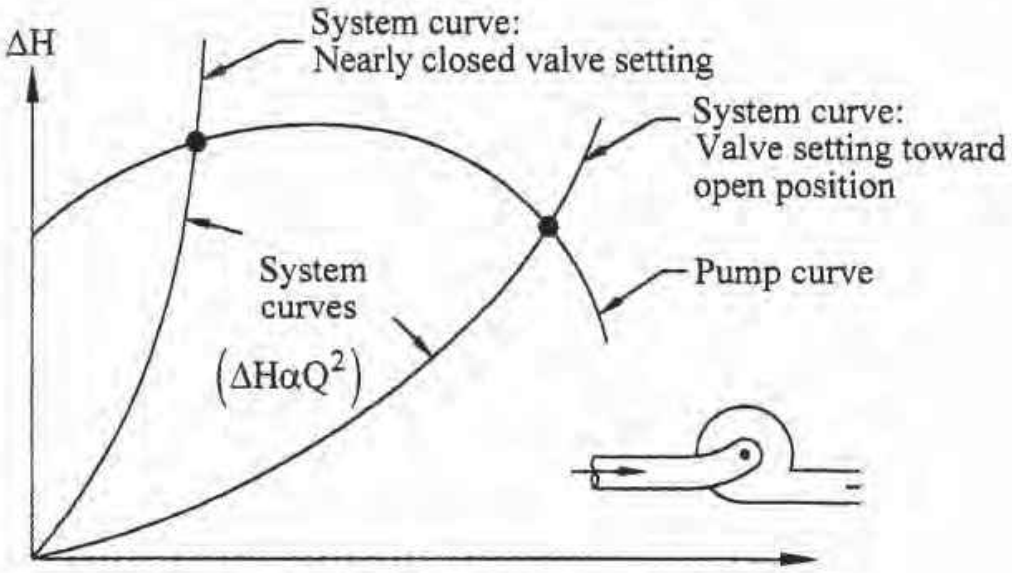
a) Static stability and instability. Figure 24 illustrates two pumping systems; namely, a) a piping system in which the flow is turbulent and largely independent of Reynolds number; so, the head drop ΔH through it is proportional to Q^2, and b) two reservoirs with a constant difference ΔH between the two liquid surfaces and comparatively negligible head loss in the pipes connecting them. In each case, the pump is designed to produce head ΔH, as required to deliver the desired flow rate Q. The influence of the pump head curve shape is immediately appreciated in Case (b): the curve "droops" as Q is reduced to shut-off, thereby producing two vastly different flow rates at the same head. In fact, however, the pump will not operate at the lower-Q intersection point of the two curves. The pump shut-off head is less than ΔH, so it will produce no positive flow rate. Instead, as discussed in Section 2.1.3, fluid will flow backwards through the pump. Further, if circumstances could allow operation at this lower-Q point, even a vanishingly small increase of Q would cause a further, divergent increase because the head of the pump exceeds the ΔH of the system. Likewise, a small decrease leads to even lesser Q because the system ΔH exceeds that of the pump. This is called "static instability." Conversely, the higher-Q point of Figure 24b is "statically stable," small departures in Q being suppressed by algebraically opposite signs of the difference between the system and pump heads. Both intersection points of Figure 24a are seen by this type of analysis to be statically stable. If the operator increases the frictional resistance by closing up a valve in the piping system, the operating point simply moves to the left on the curve and remains stable. Thus, it is concluded that if the slope of the pump H-versus-Q curve is *less* than that of the system, operation will be *statically stable*—and vice versa.

Most pumping systems are combinations of the "pure friction" type of Figure 24a and the "purely elevation" type of Figure 24b. In this case of static stability, the drooping pump head curve presents no problem. Theoretically, it is possible to have a pump head curve with a kink that could have a more positive slope than that of a system curve, which might intersect it at such a kink. The high-Ω_s curve of Figure 22b depicts a kink or dip, which is due to stalled flow within a mixed- or axial-flow impeller that is not sufficiently confined by the impeller to be maintained in solid body rotation. (It is the centrifugal effect of such rotation that maintains the pressure rise in radial-flow impellers despite the stalling.) That particular pump, if applied to a system that never intersects the pump head curve at the kink, would never experience static instability. On the other hand, the designer may want to take on the challenge of designing a machine without such a kink. The previously mentioned design procedure utilizing CFD in both the impeller and the diffuser to check whether the kink is gone would be a way of tackling this problem[53].

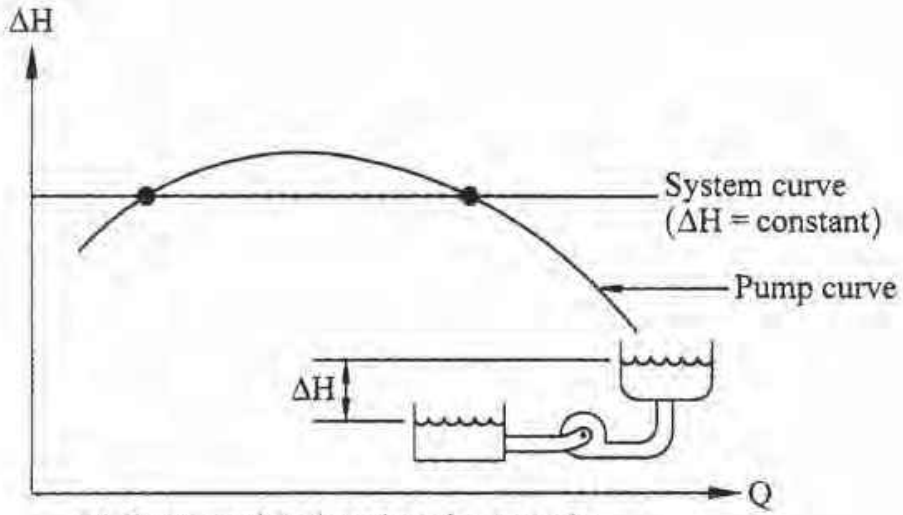
In-depth discussion of the variety of systems that can be encountered, including multiple systems and parallel operation of multiple pumps, can be found in Sections 2.1.3, 11.1, and 11.2. Purely from a static stability standpoint, most of these situations demand a substantially negative slope of the head curve throughout the range of flow rate Q—or what is commonly specified as a pump with head "continuously rising to shut-off." (This "rise in head" versus a drop in Q should not be confused with the pump developed head H, which is also properly termed the "head rise" ΔH, produced by the pump at a given value of Q.)

b) Dynamic instability. If the system has appreciable capacitance, operation may not be stable if the slope of the pump head curve is positive or even zero[54]. This is true even though the slope of the pump head curve is less than that of the system head curve as required above for static stability—as with the lower-Q intersection point of Figure 24a. Dynamic instability can be manifested as pump surge, a phenomenon wherein the flow rate oscillates and can even be alternately positive and negative through the pump[54]. This

LIBERTY EXHIBIT 1017, Page 81



a) System with frictional resistance only



b) System with elevation change only

FIGURE 24A and B Pump-system stability

is characteristic of "soft" systems that contain vessels with free surfaces and, therefore, appreciable capacitance. Two-phase flow increases the capacitance of a system and can cause dynamic instability. For example, fluctuating vapor volume within the propellant pump inducers can contribute to the dynamic instability of a rocket propulsion system[55].

On the other hand, a "hard" piping system with no capacitance is theoretically capable of accommodating a pump that has a flat or drooping head curve and that operates on that flat or drooping section of the curve. Low-specific-speed pumps can have drooping curves (Figure 22b), especially if designed with a high head coefficient ψ at the BEP. Figures 5 and 7 of Section 2.1.3 depict flat and drooping curves of low-Ω_s radial-bladed pumps, a type that is widely used in low-cost, small sizes. If properly applied, such machines will operate with stability.

However, to avoid uncertainties, a conservative approach that guarantees both static and dynamic stability for the widest range of applications is to design all pumps without

LIBERTY EXHIBIT 1017, Page 82

flat spots or droops in the head curves. In practice, this approach requires that the pump be designed to have at least 15 to 20% more head ΔH at shutoff than at BEP and, therefore, for constant-speed pumps, a value of the shutoff head coefficient $\psi_{s/o}$ which is that much greater than the BEP head coefficient ψ. Thus, it may happen that choosing ψ from Figure 12 to size the impeller conflicts with this "rise-to-shutoff" design requirement, a situation more likely to occur with low-specific-speed pumps. If so, a lower value of ψ than that of Figure 12 would need to be chosen for the BEP.

DESIGN EXAMPLE

To illustrate the application of the preceding design information, the basic hydraulic design requirements are presented in Table 6 for a single-stage centrifugal water pump with a volute collector. The chosen conditions compute to a universal specific speed Ω_s of 1 (N_s = 2733, and n_q = 52.9 from Eqs. 38a and 38b). The pump is to be designed for a suction specific speed Ω_{ss} of 4.5 ($N_{ss} \equiv S$ = 12,300 by Eqs. 41 and 42), therefore, a "performance-NPSH" (see NPSH discussion in Section 2.1.3) or $NPSH_{3\%}$ of 14 ft (4.27 m). As such, this pump is readily applicable to taking water from an atmospheric reservoir with some suction lift. Although acceptable for 1780 rpm specified for this pump, this suction-specific speed Ω_{ss} capability of 4.5 is regarded as high for pumps with more head (energy level) than this one (see the energy-level discussion later).

Impeller Design

SUCTION NOZZLE Beginning upstream, an ideal, axial-flow approach passage is assumed—this is known as an "end-suction" configuration. The suction-approach passage or suction branch (not shown) is simply a conical nozzle that increases the velocity of the fluid from the suction port to the impeller eye by about 50% in an axial distance of about half the diameter of the eye. This helps to ensure the existence of uniform flow at the eye. Too short a nozzle would mean excessive local meridional (axial in this geometry) velocity at the impeller shroud and possible separation.

IMPELLER INLET Beginning with Ω_{ss} of 4.5, computations for this example are carried out in Table 7 for the impeller eye geometry. The choice of the $NPSH_{3\%}$ correlation of Table 1

TABLE 6 Given conditions for design example (single stage, end-suction volute pump)

Speed	= 1780 RPM
Flow Rate	= 2500 gpm (0.1577 m^3/s)
Head	= 104 ft. (31.7 m) Fluid: Water $\begin{cases}\text{sp. gr.} = 1\\ \nu = 1 \text{ cs.}\end{cases}$
Specific Speed	$\Omega_s = 1; N_s = \dfrac{1780\sqrt{2500}}{(104)^{3/4}} = 2733; n_q = \dfrac{1780\sqrt{0.1577}}{(31.7)^{3/4}} = 52.9$
Suction Specific Speed	$\Omega_{ss} = 4.5 \quad (S = 12{,}300)$
	$\text{NPSH} = \left\{\dfrac{1780}{12{,}300}\right\}^{4/3}(2500)^{2/3} = 14 \text{ ft. } (4.27 \text{ m})$

LIBERTY EXHIBIT 1017, Page 83

TABLE 7 Impeller inlet (design example)

$$\Omega_{ss} = 4.5 = \frac{\sqrt{\pi \phi_e \left(1 - \frac{r_s^2}{r_e^2}\right)}}{(\tau/2)^{3/4}} \qquad \text{(from Eq. 50)}$$

For $\tau = (1.69 + 0.102)\,\phi_e^{\,2} + 0.102$

$\phi_e = 0.29$ = eye flow coefficient

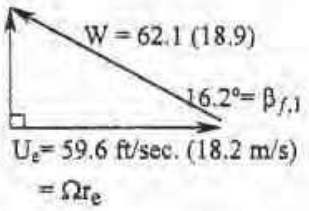
Eye dia/2 = eye radius:

$$r_e = \sqrt[3]{\frac{Q}{\Omega \pi \phi_e \left(1 - \frac{r_s^{\,2}}{r_e^{\,2}}\right)}} = \sqrt[3]{\frac{2500\text{gpm}/449\ \frac{\text{gpm}}{\text{ft}^3/\text{sec}}}{\frac{\pi}{30} \times 1780 \times \frac{\pi}{\text{sec}} \times 0.29}} \qquad \text{(from Eq. 49)}$$

$[r_s = 0$ (no shaft in eye)]

$r_e = 0.3201$ ft. (0.0976 m)

$r_e = 3.84$ in. (97.6 mm)



(See Fig. 25): $R_{sh} = \frac{r_e - r_s}{2} = 1.92$ in. (48.8 mm)

Other dimensional data shown on Fig. 25.

is used, with $k_1 = 1.69$ and $k_2 = 0.102$. The local maximum velocity at the eye $V_{1,sh}$ ($= V_{m,1,sh}$) is assumed to be 25% greater than the one-dimensional average $V_e = Q/A_e$. This is typical of this end-suction configuration. Moreover, the value of k_1 should be more than adequate for this value of $V_{1,sh}$.

The Ω_{ss} and τ-ϕ_e relationships yield the eye flow coefficient ϕ_e, which in turn sizes the eye. Had the NPSH been significantly greater than the 14 ft specified in Table 6, these relationships would have produced a value of ϕ_e that is larger than 0.3, which in the discussion following Eq. 50 was said to be the upper limit of normal design practice. In that event, ϕ_e would have been chosen independently of Ω_{ss}, and the eye radius r_e found immediately from Eq. 49. In this case, $\phi_e = 0.29$ implies a τ-value of 0.253, which is typical. However, lower ϕ_e- and τ-values are common, especially for the case of a shaft through the eye, because this tends to maintain the level of Ω_{ss} in the face of the r_e-effect in Eq. 50. The nominal velocity diagram at the eye—substantially the shroud-end or tip of the blade leading edge—shows V_e rather than $V_{1,sh}$ for the meridional component of velocity and so is not the actual velocity diagram at that location. Rather, this triangle serves to identify the geometry through the basic ratio $\phi_e = V_e/U_e$—without having to deal with the uncertain choice of $V_{1,sh}/V_e$. Moreover, ϕ_e is the tangent of the tip relative flow angle β_{f1} as it would be for a uniform axial velocity profile in the eye.

With the eye radius r_e established, the local shroud radius of curvature R_{sh} follows from the guidelines associated with Figure 13. The geometry established so far is illustrated in Figure 25. Before the full picture shown there can be established, the outlet must be sized.

LIBERTY EXHIBIT 1017, Page 84

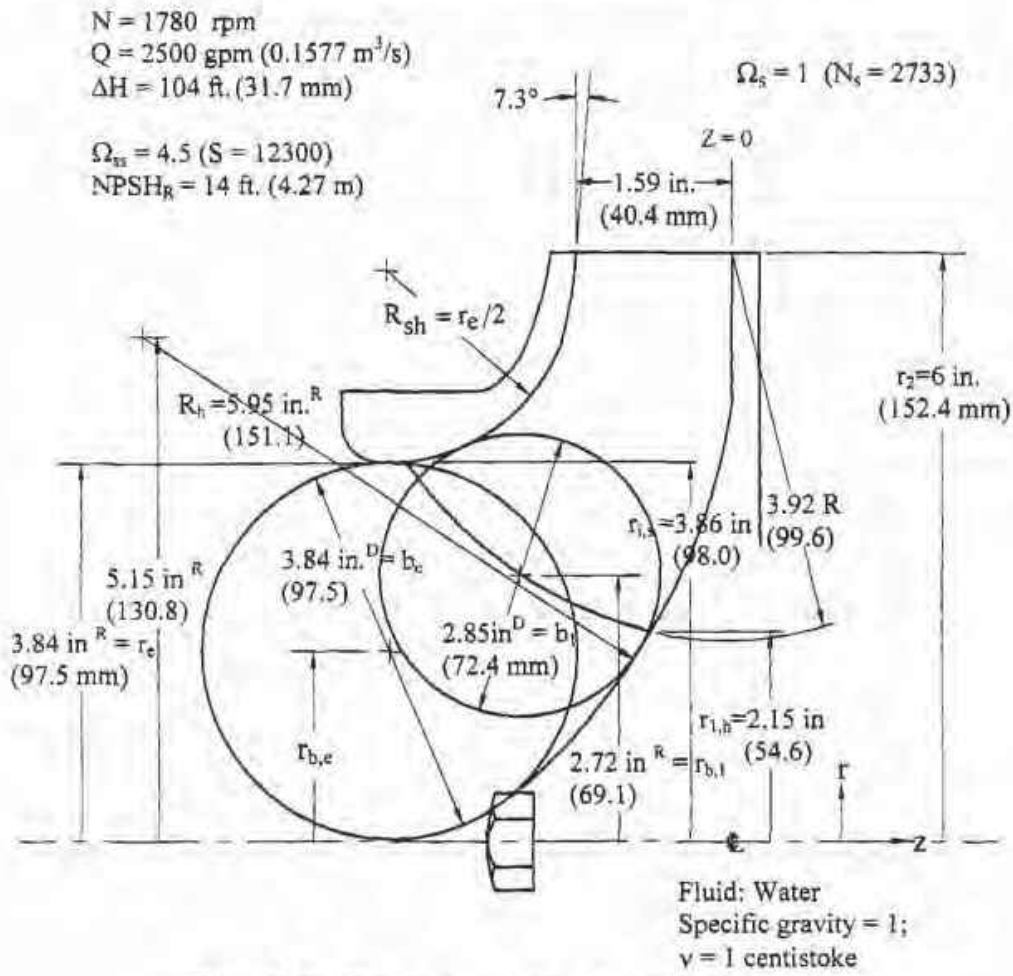


FIGURE 25 Impeller hub and shroud profiles (design example)

IMPELLER OUTLET The computations in Table 8 for the impeller exit begin with the choice of the typical value of $22\frac{1}{2}$ degrees for the outlet blade angle $\beta_{b,2}$. This enables the head coefficient ψ to be chosen under the guidance of the upper curve in Figure 12. The value 0.385 is selected, and this yields the impeller diameter of 12 in. (304.8 mm). The other curve in Figure 12 is for outlet flow coefficient $\phi_{t,2}$, which conveniently equals 0.1715 for $\Omega_s = 1$. This leads to the exit width b_2 after adding in the leakage and the blockage of blades and boundary layers per the computations of Tables 9 and 10.

However, Anderson[7] points out that what matters for centrifugal pump performance is neither the blade angle nor the exit width individually, but the impeller outlet relative area $2\pi r_2 b_2 \sin \beta_{b,2}$. Choosing a higher blade angle is possible if b_2 is correspondingly reduced (and $\phi_{t,2}$ increased) so as to maintain this area and therefore the relative velocity W. Figure 15 shows that $V_{s,2}$ is thereby essentially unchanged; this in turn preserves the impeller head.

EFFICIENCIES Anderson's overall pump efficiency correlation (Figure 10 and Eq. 44) and the component efficiency expressions of Table 3 lead to the results of Table 9. These give an indication of the relative magnitudes of the losses and are as follows:

Overall efficiency $\eta_p = 0.8550$

Mechanical efficiency $\eta_m = 0.9814$

Volumetric efficiency $\eta_v = 0.9833$ (leakage across front and back rings)

Hydraulic efficiency $\eta_{HY} = 0.8860$

LIBERTY EXHIBIT 1017, Page 85

TABLE 8 Impeller outlet (design example)

From Figure 12

$$\beta_{b,2} = 22\tfrac{1}{2}^\circ \rightarrow \phi_2 = \frac{V_{m,2}}{U_2} = 0.1715 \quad (= \phi_1)$$

$$\rightarrow \psi = \frac{g_0 \Delta H}{U_2^2} = 0.385$$

$$(U_2 = \Omega r_2) = \frac{\pi}{30} \times 1780 \times \frac{6}{12} = 93.2 \ \frac{\text{ft.}}{\text{sec.}} \ (28.4 \text{ m/s})$$

$$r_2 = \sqrt{\frac{g \Delta H}{\Omega^2 \psi}} = 12 \sqrt{\frac{32.174 \times 104}{\frac{\pi^2}{30^2} \times (1780)^2 \times 0.385}}$$

= 6 in. (152.4 mm) [12 in. (304.8 mm) dia.]

Width: $b_2 : A_2' = \pi D_2 b_2'$

$b_2 = b_2' + 2\delta_0^* +$ Leakage Effect

Solve after obtaining volumetric efficiency and getting approximate passage length (to compute δ_0^*)

η_{HY} is at this point simply deduced from the others, beginning with Anderson's correlation. Although it is confirmed by Jekat's correlation in the table, it can be found in a detailed computation of the hydraulic losses via one-dimensional methods. This will be carried out further on to obtain the performance characteristic curves. Meanwhile, this initial computation enables the determination of $V_{\theta,2}$ at the end of Table 9, which, along with $V_{m,2}$ from Table 8, is a major element of the outlet velocity diagram of Figure 26.

BLOCKAGE AND WIDTH AT IMPELLER EXIT With the leakage and exit blade angle information, Table 10 contains the computations of the blockage and the exit width b_2. This entails the choice of the number of blades, the blade thickness t (2% of the impeller diameter and typically assumed to exist at the exit and elsewhere on the blades except near the leading edges where typically half that value is chosen), and the approximate blade length ℓ (assuming the mean-streamline blade angle to be constant at $22\frac{1}{2}$ degrees). The boundary layer blockage is computed from the following approximations:

- Adverse pressure gradients on the blades lead to a boundary layer displacement thickness δ^* of twice the zero-pressure gradient value δ_0^* on each blade surface.
- Secondary flows scrub the boundary layers from the hub and shroud surfaces; so, δ^* is assumed to be equal to δ_0^* on those surfaces.
- $\delta_0^* = 0.0462\ \ell^{0.8} \nu^{0.2} / W^{0.2}$ for flat-plate, turbulent flow[56], and is approximated in this example for low viscosity by a linear growth with length along the blade.

The resulting thickness of the boundary blockage is 0.0732 in (1.86 mm) on the blades, which themselves have a thickness of 0.24 in (6.1 mm). Because these thicknesses are inclined at the $22\frac{1}{2}$-degrees outlet angle, the actual circumferential blockage is $(1 - \varepsilon_{2,b}) = (1 - 0.870)$ or 13% of $2\pi r_2$. In particular, (0.24 + 0.0732)/sin ($22\frac{1}{2}$ degrees) = 0.82 in or

LIBERTY EXHIBIT 1017, Page 86

TABLE 9 Component efficiencies (design example)

Efficiency: $\eta_p = 0.94 - 0.08955\left(\frac{2500}{1780}\right)^{-0.21333} - 0.29\left[\log_{10}\left(\frac{2286}{2733}\right)\right]^2 = 0.8550$
(Eq. 44)

Mech. Eff'y: $\eta_m = 1 - \frac{0.002 \times 0.8550}{1^2 \times (0.385)^{5/2}} = 0.9814 \quad [P_D = 1.43 \text{ hp.}(1.07 \text{ kW})]$
(from Table 3)

Volumetric Efficiency: $\eta_v = \frac{1}{1 + 5\,\frac{0.0016 \times (3.84/6)^2}{1^2 \times 0.385} \times 2} = 0.9833$
(from Table 3)

Hydraulic Efficiency: $\eta_{HY} = \frac{\eta_p}{\eta_v \eta_m} = \frac{0.8550}{0.9650} = 0.886$ vs.
(Eq. 8)

(Jekat's formula in Table 3):

$$\eta_{HY} \approx 1 - \frac{0.8}{(2500)^{0.25}} = 0.887$$

$$\Rightarrow \quad V_{\theta,2} = \frac{32.174 \times 104}{93.2 \times 0.886} = 40.5 \text{ ft/sec.}$$

$$\Rightarrow \quad \psi_i = \frac{40.5}{93.2} = 0.435$$

$(6.1 + 1.86)/\sin(22\frac{1}{2}$ degrees) = 20.8 mm per blade, which for all six blades is 0.130 times the circumference of 37.7 in (958 mm). The width b_2 is computed to maintain $V_{m,2}$ at the chosen value of $0.1715 \times U_2$, while accommodating this blockage and that of the sidewall boundary layers. Altogether, it can be computed from these data that 85% of the meridional exit area $2\pi r_2 b_2$ is estimated to remain open for the one-dimensional flow of $(Q + Q_L)$ at velocity $V_{m,2}$, the boundary layers causing $\frac{1}{3}$ of the blockage. This is quite typical. An openness of 90% is possible for larger impellers.

HUB-SHROUD PROFILES It is now possible, through the guidelines outlined in the discussion of Figure 13, to finish plotting the hub and shroud profiles in Figure 25, which are also seen in Figure 26c. At this point, the envelope of the leading edges of the blades is approximated by a circular arc—later modified somewhat in the construction of the blades. The arithmetic average radius of the meridional passage at the leading edges is found with the circle of diameter 2.85 in (72.4 mm) to be 2.72 in (69.1 mm). The resulting line passing through the center of the circle is normal to both hub and shroud and is approximated by the dashed straight-line leading-edge quasi-normal shown in the Figure 26c.

INLET VELOCITY DIAGRAMS The rms radial point on this quasi-normal line of Figure 26c crosses the leading edges of the blades at $r_{1,\text{mean}} \equiv r_{1,\text{rms}} = 2.91$ in (73.9 mm) and is slightly larger than the arithmetic average radius of 2.72 in (69.1 mm). It is this latter radius that must be used in computing the one-dimensional meridional velocity. Once obtained, it is applicable to the rms location (the location of the "mean" or "rms" inlet velocity diagram).

LIBERTY EXHIBIT 1017, Page 87

TABLE 10 Impeller blade blockage and width at exit (design example)

Blade no.: n_b: Assume = 6

$$\ell = \frac{\Delta m}{\sin\beta} \approx \frac{3.5 \text{ in.}}{\sin 22\tfrac{1}{2}^\circ} = 9.15 \text{ in.}(232.4 \text{ mm}) \quad \text{(Eq. 56)}$$

Check Solidity:

Blade thickness: $t = 0.04\, r_2 = 0.24$ in. (6.1 mm)

$$\sigma = \frac{6 \times 9.15}{\pi \times 12} = 1.46 \rightarrow \text{OK} \quad \text{(Eq. 53)}$$

$$\varepsilon_{2,b} \text{ (blades only)} = 1 - \frac{6\,(0.0732 + 0.240)}{\pi \times 12 \times \sin 22\tfrac{1}{2}^\circ} = 0.870$$

$$\delta_o^* \approx 0.002 \times \ell \approx 0.002 \times 9.15 \text{ in.}(232.4 \text{ mm})$$

$2\delta \approx 4\,\delta_o^* \approx 0.0732$ in.(1.86 mm) on blades

$2\delta \approx 2\,\delta_o^* \approx 0.0366$ in.(0.93 mm) on hub and shroud

gpm & ft/sec to inches; η_v

$$b_2 = 0.0366 + \frac{2500 \times 0.3208 / 0.9840}{\underbrace{0.1715 \times 93.2}_{V_{m,2}} \times \underbrace{0.870}_{\varepsilon_{2,b}} \times \pi \times 2 \times 6} = 1.59 \text{ in.}(40.4 \text{ mm})$$

$$\left(\text{Since } b_2 = 2\delta_o^* + \frac{Q + Q_L}{V_{m,2} \times \varepsilon_{2,b} \times \pi \times 2 \times r_2} \right)$$

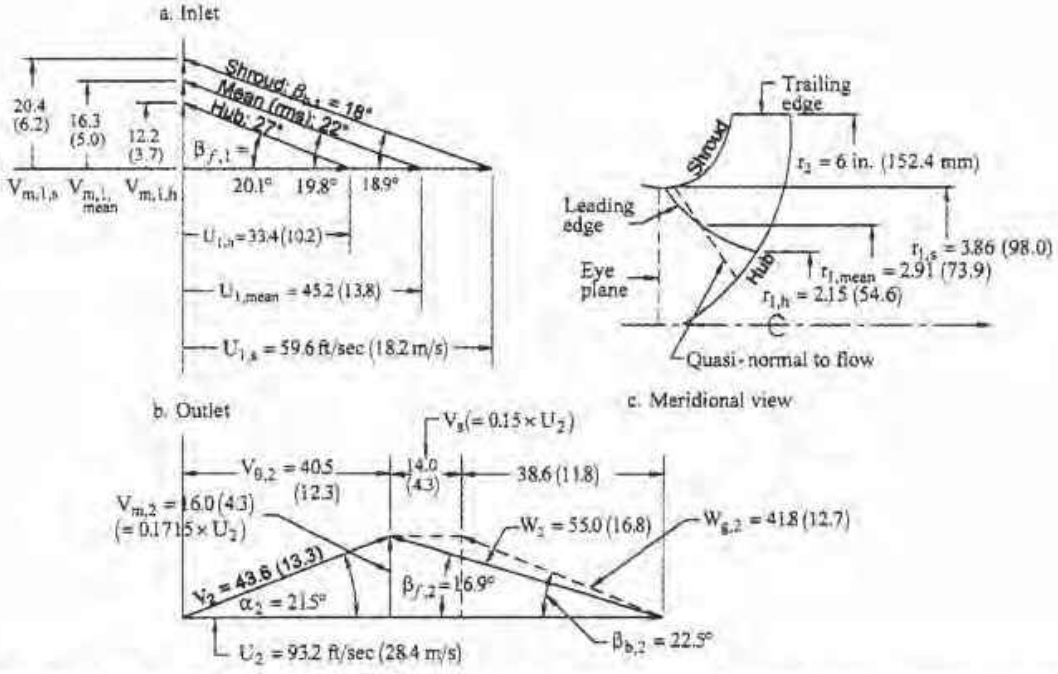


FIGURE 26A through C Impeller velocity diagrams for design example: a) inlet; b) outlet; c) meridional view

LIBERTY EXHIBIT 1017, Page 88

This diagram is one of three triangles shown for the inlet in Figure 26a, the other two being located at the hub and shroud locations of the blade leading edges. Notice that $V_{m,1}$ for the rms triangle is 16.3 ft/sec (5.0 m/s), which is slightly less than the eye velocity V_e of 17.3 (5.3). Allowing for blade blockage, this would bring the blocked meridional velocity V_m within the blading closer to V_e, the objective being to keep V_m constant in the inlet region and turn into the radial direction. The other triangles correspond to the radial locations of the blade at hub and shroud, as illustrated in Figures 26c and 27, and assume that $V_{m,1,sh}$ = 1.25 times $V_{m,1}$, and $V_{m,1,h}$ = 0.75 $V_{m,1}$. A full Q3D or CFD solution would determine these velocities more accurately; however, the design usually proceeds in this way—largely because the hub blade angle is usually a good deal larger than hub flow angle. Efforts to match the hub flow angle more closely entail special blading that is beneficial for high-energy pumps but has little effect otherwise. The blade angle at the shroud is slightly lower than the flow angle (by about 1 degree). This slightly negative incidence (to the mean camber line of the blade) is actually ideal for efficient flow and minimum cavitation. The largest values of U and W exist at the shroud, as can be seen for the shroud inlet triangle, making it important to have the best match at that point. Two or three degrees of positive incidence is quite common at the mean or rms radial location and allows for blockage by the blades that does not increase the relative velocity W as the fluid enters the impeller. (Actually a drop upon entrance to the blading in this mean W of 10% or more is often found in radial-flow impellers. Such blading tends to minimize the sum of impeller incidence and passage friction losses at the BEP flow rate and enables lower NPSH-capability at flow rates above BEP.)

OUTLET VELOCITY DIAGRAM The outlet velocity components having been found in Tables 8 and 9, the slip velocity V_s must still be found in order to obtain the complete outlet velocity diagram shown in Figure 26b. This slip is computed by Pfleiderer's method (Table 2), which utilizes the $r(m)$ shape of the mean meridional streamline illustrated in Figure 27, V_s emerging as 15% of U_2. The "a" factor for influence of the collector geometry was taken in the middle of the range for volutes at 0.75; (see Table 2). Wiesner's Eq. 52 yields 17.65%. This would mean 6% less $V_{\theta 2}$ and head. However, this discrepancy is not unexpected, and in view of the earlier discussions on slip, the Pfleiderer result is chosen as more realistic.

Nevertheless, uncertainty in the slip is the Achilles heel of the one-dimensional analysis method. For this reason, most analysts "calibrate" their codes by deducing the slip from test results and applying it to impellers of similar geometry. For Pfleiderer's method, this would be done by calibrating the "a" factor. CFD solutions are now the best approach to overcoming this difficulty.

As has been emphasized heretofore, this outlet velocity diagram contains the basic information about the performance and design of the pump. It supplies the boundary conditions for the volute design, but first the impeller blading that must produce it will be established and evaluated.

IMPELLER BLADING As indicated in Figure 26, the blade angles at both inlet and outlet have been chosen at hub, mean, and shroud (with the same $22\frac{1}{2}$ degrees all across the trailing edge being assumed, although some would specify a little variation). Fitting a reasonable blade shape between these end conditions can be done in the conformal plane (illustrated in Figure 19). These shapes, when transformed as described earlier, yield the hub, mean, and shroud blade shapes identified in the polar view of Figure 28. In actuality, the inverse "point-by-point" method was used, specifying W_g as indicated in Figure 29 and, at each of the 21 stations along the mean line of Figure 27, developing the velocity diagrams in the manner employed to arrive at Figure 26b; obtaining β_b at each station; and developing the *mean-streamline blade shape* of the polar view with Eq. 60. Involved in this procedure—which was computerized—was the calculation at each station of the blockage and of the local slip velocity, the latter being estimated as a fraction of the discharge slip velocity V_s that increases rapidly to unity as the exit is approached.

Note that the meridional area is needed at each station in order to compute V_m. As indicated in Figure 27, this is approximated here as the area of the frustum of a cone defined by the dashed lines or "quasi-normals," which are as nearly perpendicular to both hub and shroud as possible. Except for some machines with meridionally curved passages and a

LIBERTY EXHIBIT 1017, Page 89

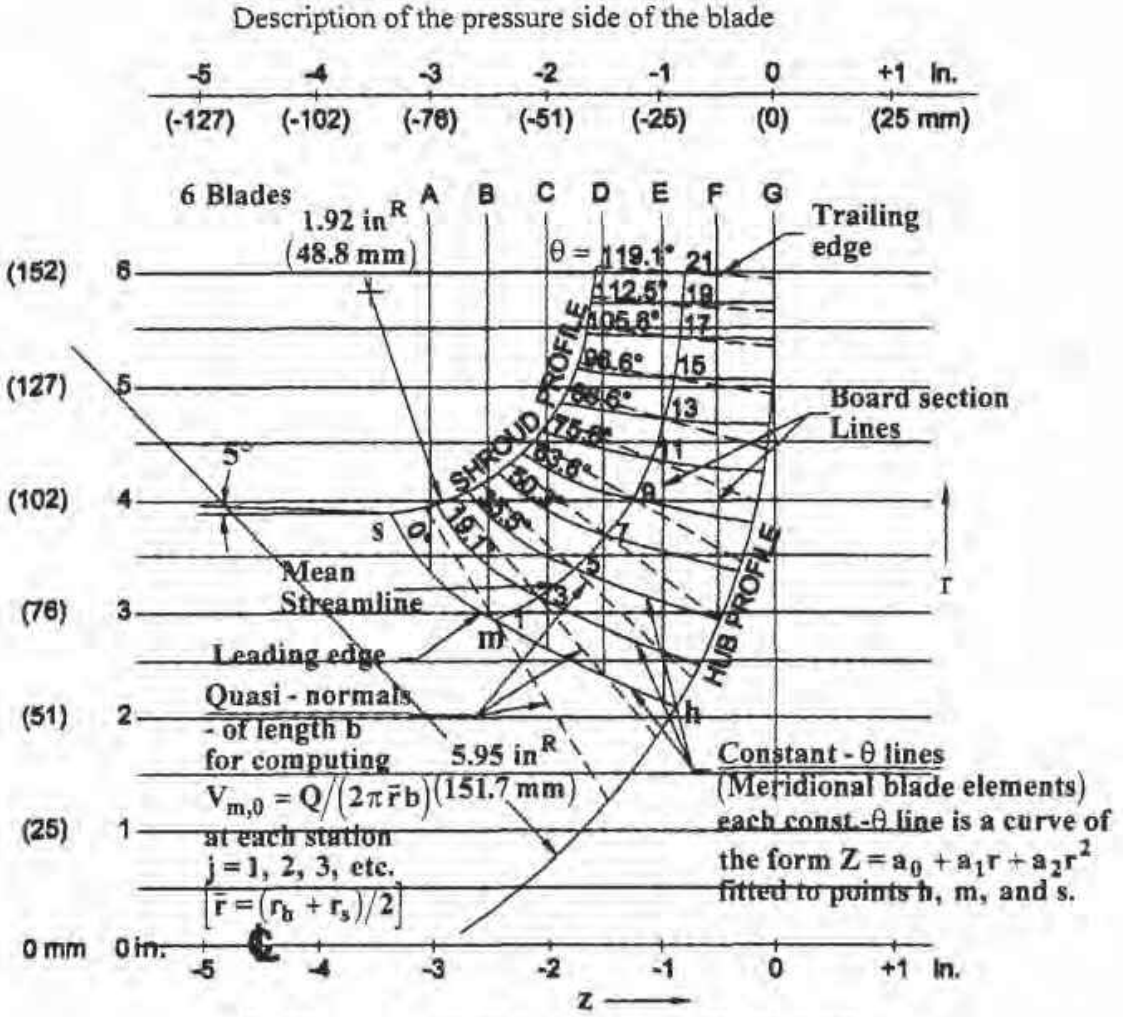


FIGURE 27 Impeller blading–meridional view (design example)

large passage width-to-length ratio causing the true normals to be strongly curved, the quasi-normal approach works well.

To establish the *blade shapes along the hub and shroud*, the corresponding "grid lines" of Figure 19 were found from polynomials satisfying the end conditions of blade angle and location, the y-position of the inlet end of the grid line being iterated until the desired blade wrap was obtained. In this way, different wrap angles $\Delta\theta$ ($= \theta_2 - \theta_1$) can be imposed, but a tolerable resulting blade shape requires that these $\Delta\theta$s be not much different from the $\Delta\theta$ (= 119.1 degrees) obtained on the mean line from the method just described. In this example, it was possible to maintain $\Delta\theta$ the same on all three construction lines. Alternatively and perhaps more consistently, the inverse approach could be applied at hub and shroud as well as on the mean line.

Regardless of which procedure is used to generate the hub, mean and shroud blade shapes—the conformal transformation method, the point-by-point method, or some combination—the *shape of the blade everywhere else* still needs to be established. To do this, the shapes of the constant-θ lines in Figure 27—called "blade elements"—must be specified. This can be done mathematically as indicated on the figure or by eye (the latter approach has been widely used). Note that each constant-θ line actually lies in a different meridional plane. Thus, Figure 27 depicts a superposition of all 21 meridional planes, each containing an intersection of the blade surface and appropriately identified as having the θ-value noted on the figure. The resulting blade shape is illustrated in the polar plots of Figure 28.

DIFFUSION ASSESSMENT Figure 29 is a presentation of the free-stream relative velocity distributions at the blade surfaces and halfway between. The rapid approximate method of

LIBERTY EXHIBIT 1017, Page 90

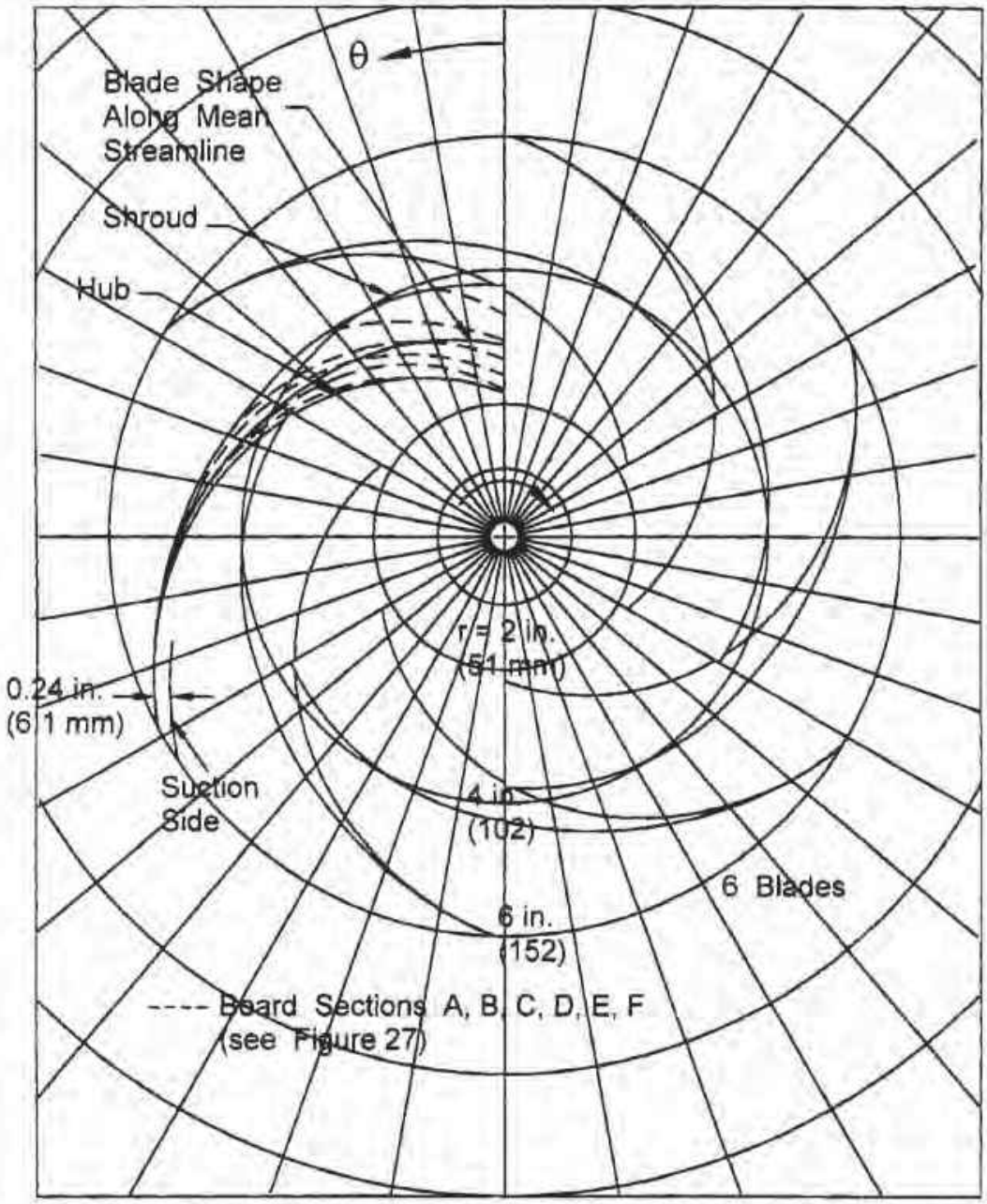


FIGURE 28 Impeller blading—polar view, showing pressure sides of the blades (design example)

Stanitz (Eq. 54) was utilized to obtain the surface W's, the mean values of W on the mean (rms) streamline coming from the local velocity diagrams developed at each station[22]. The mean W's at hub and shroud were found at the ends of the respective constant-θ lines under the assumption that the ideal head or UV_g-product is constant along each of these lines from hub to shroud. This is usually a fair approximation; however, a Q3D or CFD analysis would yield a closer estimate of these mean W-distributions[41]. Nevertheless, the diffusion factors computed from the plotted surface velocities by means of Eqs. 59 are shown on the figure—these values are well below the 0.6 limit. This would indicate that the resulting solidity of 1.48 (originally estimated at 1.46 in Table 10) is adequate, and that the correct number of blades was chosen.

Notice also on Figure 29 that the exit value of W is significantly larger than $W_{g'}$ which is consistent with the outlet velocity diagram of Figure 26b. Further, a slight jump in the mean W at the inlet above the upstream value $W_{1,mean}$ is indicated to occur one-dimensionally across the leading edge. As mentioned in the discussion following Figure 26,

LIBERTY EXHIBIT 1017, Page 91

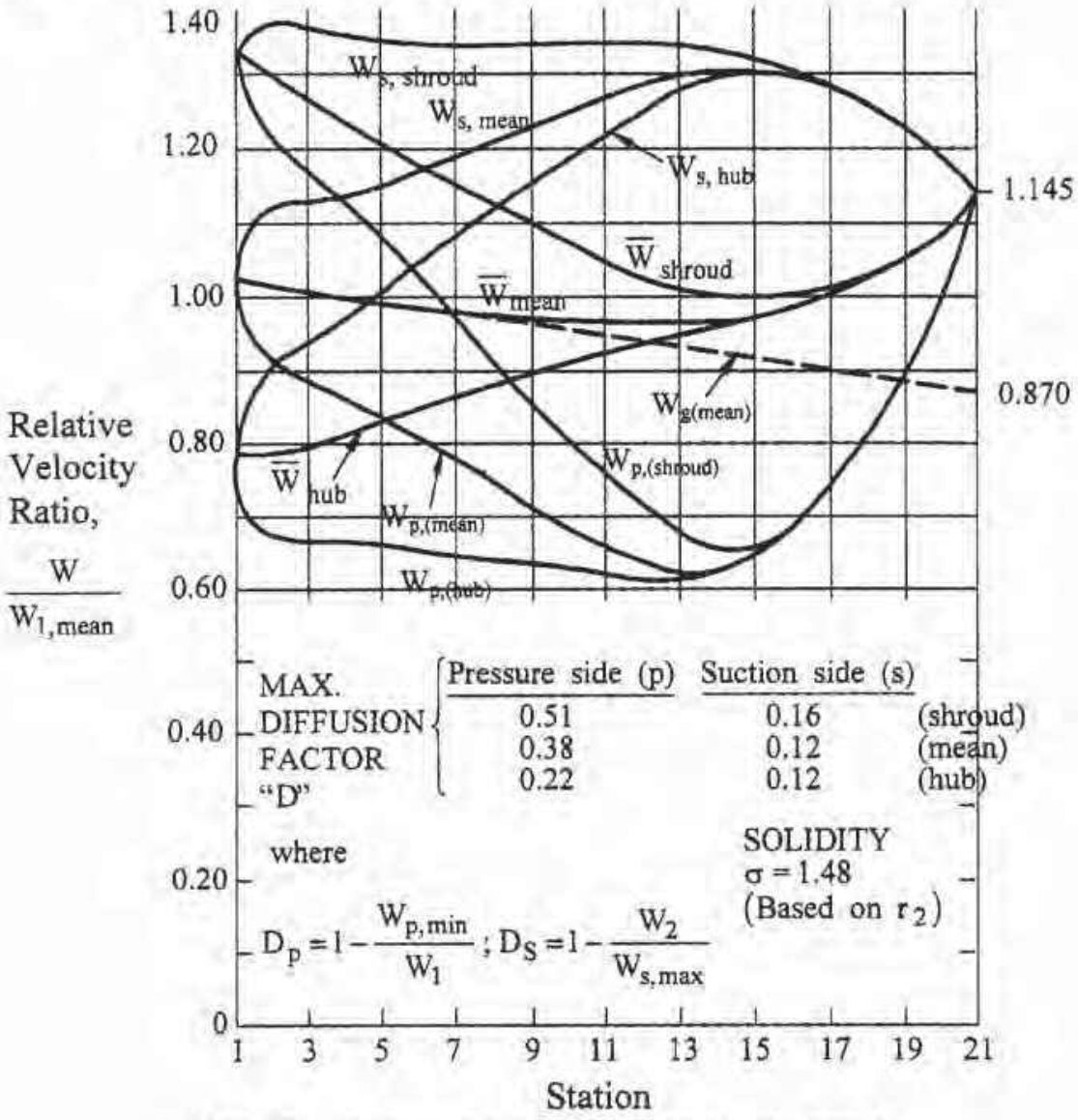


FIGURE 29 Blade surface relative velocity distributions (design example)

the actual practice of many designers is to create a drop of this mean W. However, in this example, as the higher value of W is not sustained, it is unlikely that the jump actually occurs in the 3D velocity field. Moreover, details near leading and trailing edges are not well handled by Eq. 54—a CFD or 2D blade-to-blade solution is more desirable for this type of diffusion assessment[42]. Nevertheless, the design guidelines given here were developed in the light of applicable one-dimensional velocity diagrams, computations, and experimental experience. Thus, if the flow rate for which the curves of Figure 29 were generated (namely the specified design point Q of Table 6) had been 5% lower, the same impeller would have exhibited a small drop in the value of the mean W at Station 1.

Volute Design With the exit velocity V_2 of 43.6 ft/sec (13.3 m/s) and the tangential velocity component $V_{\theta 2}$ of 40.5 ft/sec (12.3 m/s) from Figure 26b, the volute design process is started in Table 11 using Eq. 61. This entails a choice of the radial "Gap B" of 6% of the impeller radius r_2 and a tongue leading edge thickness t_t equal to 70% of the impeller blade thickness. These choices are not critical for a pump of low energy level such as this is, as the stresses imposed by the flow on structural elements are small. The *throat area* A_T is then found to be 32.60 in^2 (21,032 mm^2) and the throat velocity V_T computes to 24.60 ft/sec (7.50 m/s), which is 56% of V_2 and so represents considerable diffusion from impeller exit

LIBERTY EXHIBIT 1017, Page 92

to throat. (The throat area A_T is the fundamental feature of a volute and acts in concert with the impeller exit area, as emphasized by Anderson[7] and Worster[25] and described in the earlier part of this section on *Designing the Collector* in terms of the intersection of the casing and impeller lines[26].)

The circumferential *distribution of the volute cross-sectional area* A_v versus polar angle θ_v from the tongue (Figure 20a) is developed in the latter part of Table 11, a final listing being presented for a) linear A_v versus θ_v and b) constant one-dimensional angular momentum $r_v V_v$.

TABLE 11 Volute casing (design example)

Refer to Fig. 20

A) Throat area A_T
Simultaneously solve for A_T from

a) $r_T \dfrac{Q}{A_T} = 0.95\, r_2 V_{\theta,2}$ (Eq. 61, using 0.95) since $A_T = \dfrac{Q}{V_T}$

and

b) $r_T = r_3 + \dfrac{1}{2}\sqrt{A_T} + t_t$ (Fig. 20, assuming a square throat)

Eliminating r_T in combining (a) and (b) yields a quadratic equation in $\sqrt{A_T}$:

c) $A_T \times \left(\dfrac{0.95\, r_2 V_{\theta,2}}{Q}\right) - \dfrac{1}{2}\sqrt{A_T} - (r_3 + t_t) = 0$

Taking $r_3 = 1.06\, r_2$ (i.e., "Gap B" $= 0.06\, r_2$), $r_3 = 6.36$ in (161.5 m);
assuming $t_t = 0.7\, t_b = 0.7 \times 0.24 = 0.168$ in. (4.3 mm); and
using consistent units in (c); leads through the quadratic formula to

$A_T = 32.60$ in^2 (21,032 mm^2)

Thus $V_T = 24.60$ ft/sec (7.50 m/s)

B) Cross-sectional area

If volute cross-sectional area A_v is distributed linearly vs. θ_v, A_v and the radius r_v to the center of the cross section are as follows:

d) $A_v = A_T \dfrac{\theta_v(\text{deg})}{360} = \dfrac{32.60}{360} \times \theta_v \text{ in}^2 = \dfrac{21{,}032}{360} \times \theta_v \text{ mm}^2$

e) $r_v = r_3 + \dfrac{1}{2}\sqrt{A_v} = 6.36 + \dfrac{1}{2}\sqrt{A_T\left(\text{in}^2\right)}$ in

$= 161.5 + \dfrac{1}{2}\sqrt{A_T\left(\text{mm}^2\right)}$ mm

If A_v is found subject to constant angular momentum with $r_v V_v = 0.95\, r_2 V_{\theta,2}$,

f) $A_v = \dfrac{Q}{V_v} \times \dfrac{\theta_v(\text{deg})}{360} = \dfrac{Q\left(r_3 + \dfrac{1}{2}\sqrt{A_v}\right)}{0.95\, r_2 V_{\theta,2}} \times \dfrac{\theta_v(\text{deg})}{360}$

LIBERTY EXHIBIT 1017, Page 93

TABLE 11 Volute casing (design example) (*Continued*)

This is a quadratic equation in $\sqrt{A_v}$, which, when solved, gives the results for "constant $r_v V_v$" in the llisting below, r_v being found from Eq. (e) for both this and the linear case.

Volute cross sections (design example)

	Linear A_v vs. θ_v				Constant ($r_v \times V_v$)			
θ_v	A_v		r_v		A_v		r_v	
deg	in^2	mm^2	in	mm	in^2	mm^2	in	mm
0	0.00	0	6.36*	161.5*	0.00	0	6.36*	161.5*
45	4.08	2,629	7.37	187.2	3.15	2,031	7.25	184.1
90	8.15	5,258	7.79	197.8	6.64	4,286	7.65	194.3
135	12.23	7,887	8.11	205.9	10.39	6,701	7.97	202.5
180	16.30	10,516	8.38	212.8	14.34	9,250	8.25	209.6
225	20.38	13,145	8.62	218.9	18.48	11,922	8.51	216.1
270	24.45	15,774	8.83	224.3	22.79	14,706	8.75	222.2
315	28.53	18,403	9.03	229.4	27.27	17,596	8.97	227.9
360	32.60	21,032	9.21**	234.1**	31.91	20,588**	9.18**	233.3**

* $r_v = r_3$ at $\theta_v = 0$
** transition to $r_T = 9.38$ in (238.3 mm) and $A_T = 32.6$ in^2 (21032 mm^2) due to tongue thickness

This listing illustrates an earlier statement that the latter approach produces smaller areas upstream of the throat than does the former. Frictional effects in the smaller-A_v portion of the volute are less prominent using the linear approach. A CFD assessment at all flow rates can be made to guide the design choice here. Finally, the one-dimensional constant $r_v V_v$ method can be improved upon by integrating a constant rV_θ distribution over each cross section, and the proper design must satisfy also continuity[26].

Estimated Performance Characteristics Detailed computation of hydraulic losses, together with leakage, disk friction, and other mechanical drags was done as described previously, and the results are presented in Figure 30. The method predicts the pump efficiency to be 85.5% at the design point of 2500 gpm (0.1577 m^3/s), peaking at 86 percent at a 5% lower flow rate. In view of the preceding discussion of the behavior of the mean relative velocity W at the leading edge of the impeller blades in Figure 29, this shift of the BEP to a slightly lower flow rate than the design value comes as no surprise. Slightly larger values of the inlet blade angles than those chosen for this example (see Figure 26a) would be needed for the BEP to have the same flow rate as the design point. Peaks at the design point at 77 hp (57 kW), indicating that this is a "non-overloading" design; that is, shaft power does not increase beyond this flow rate. The empirical methods reviewed earlier for shut-off head and power were applied here and blended into the one-dimensionally computed curves at half of the BEP flow rate.

The shut-off head coefficient value of 0.596 is close to the 0.585 value of Stepanoff[5] and is admittedly open to alteration. The rise of head from design point to shut-off is from 104 up to 161 ft (31.7 up to 49.1 m) or 55%. This percentage could be smaller and still ensure stable operation in any typical system; however, the non-overloading feature could change, the power peaking at a higher flow rate. In retrospect, the design-point head coefficient ψ of 0.385 could be larger without the corresponding diffusion-factor results (Figure 29) becoming excessive. One would conclude from this exercise that the ψ-curve of Figure 12 is conservative and could be higher. Of more significance, however, is the demonstration in this design example of the utilization of easily applied fundamental fluid dynamical analyses such as the diffusion assessment illustrated in Figure 29 as the basic arbiters of design choices such as the head coefficient, number of blades, and so on. Furthermore, the shapes of the performance characteristics are revealed.

LIBERTY EXHIBIT 1017, Page 94

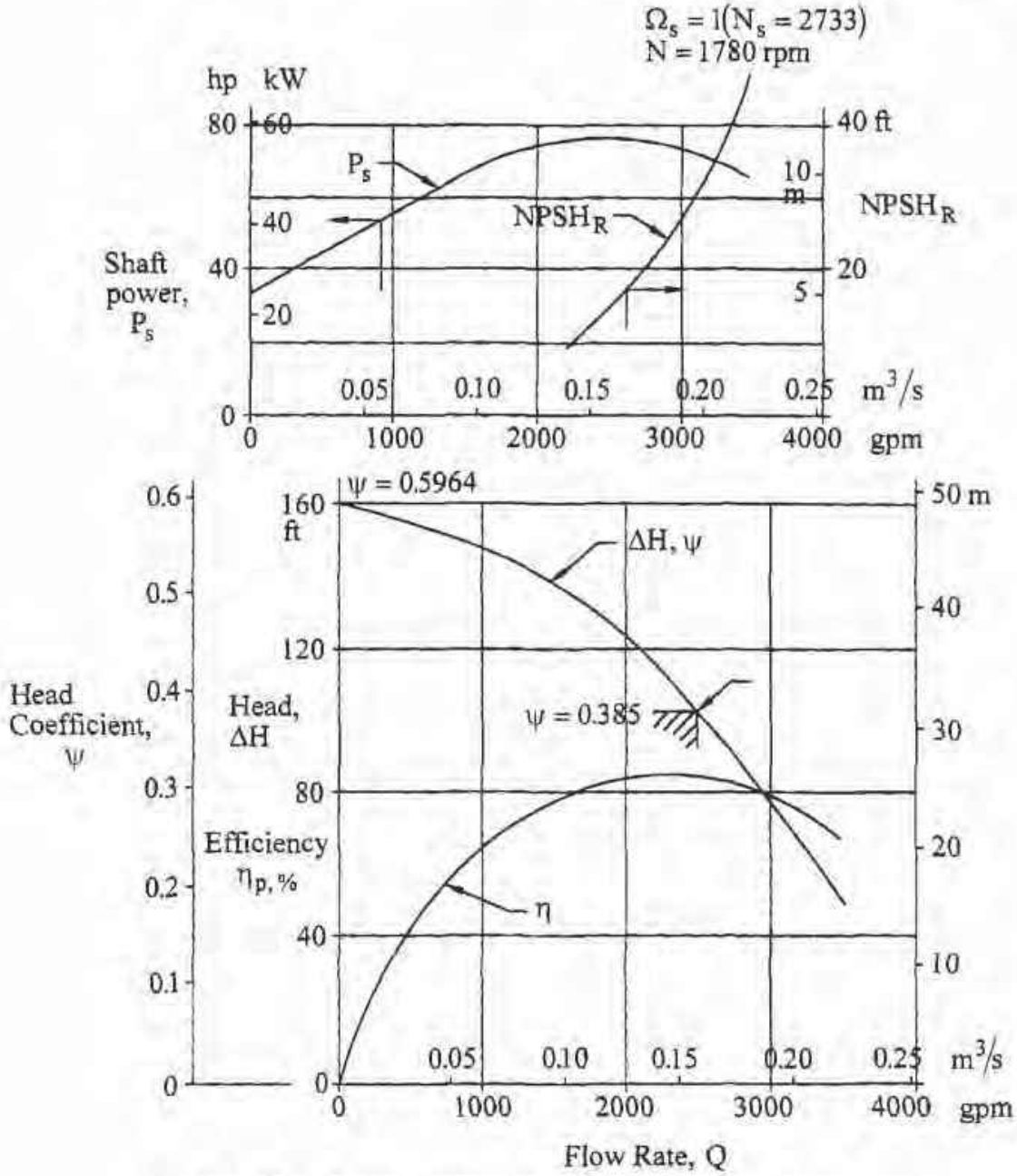


FIGURE 30 Estimated performance characteristics (design example)

The shut-off power is 34 hp (25 kW), arising from a power coefficient of 0.047 from Mockridge's correlation[36] for a b_2/D_2 of 1.59/12 (= 40.4/304.8) = 0.1325—as found from Figure 23. This is 44% of the design-point power, a typical result. As seen in Section 2.1.3, this percentage increases with specific speed, where, of course, b_2/D_2 is also larger[36].

The *NPSHR* (= $NPSH_{3\%}$ for this example) at off-design conditions was estimated empirically. At the higher, non-recirculating flow rates, *NPSHR* is related to the head required to increase the relative velocity within the blades to values higher than at the design point[15]. As stated in Section 2.1.3, operation at $NPSH_{3\%}$ involves performance in the presence of extensive internal two-phase behavior. This is complicated by recirculation at the lower flow rates. CFD codes exist that can deal with multiphase, recirculating flow and can successfully predict the entire *NPSHR* curve; which, prior to the advent of such capability, usually had to be established experimentally.

LIBERTY EXHIBIT 1017, Page 95

HIGH-ENERGY PUMPS

Over the past few decades, there has been a trend toward pumping machinery that concentrates more power within a given volume. This trend is driven by cost and technology improvements. The basic energy transfer relationships show that smaller size demands higher rotative speed. Thus, over the same time period, speeds of high-power pumps have been increasing. Moreover, the number of stages in multistage pumps has been decreasing. There have been spikes in these trends; the resulting pumps suffering from excessive vibration, rotor and hydraulic instabilities, component failure, and cavitation damage[57]. The term "high energy" has been applied to these machines, and this label can be quantified in terms of the stresses arising in critical pump components and the likelihood of an adverse mechanical response that such stress levels imply. Research has led to technical solutions for effectively controlling rotordynamic behavior and reducing unsteady hydraulic thrust and surge as well as cavitation erosion[53,58,59]. The resulting pump reliability improvements and life extension should enable the previous trends to continue. Being aware of the energy level enables the pump user to assess whether operation and maintenance difficulties are likely to occur after the pump is installed and running, and it enables the designer to take the appropriate measures to ensure the technical integrity of the product.

Pressure Pulsations Measured at the inlet or outlet port, the amplitude of the pressure pulsations can be a significant fraction of the pressure rise of the pump—especially at flow rates well below that of the BEP for the speed involved. Sources are a) the interaction of the pressure fields of the impeller and diffuser or volute, b) unsteady separated and reversed flows at impeller inlet and discharge and in the diffuser, c) cavitating flows, and d) combinations of these phenomena. Pressure pulsations presumed to exist at the impeller OD from the interaction of impeller blade-to-blade and diffuser vane-to-vane variations of pressure have been calculated by inviscid flow analysis to have a peak-to-peak amplitude that is of the same order as the static pressure rise of the impeller[60]. Moreover, the viscous, thicker wakes existing at lower-than-BEP flow rates (here called "low flows") and separated recirculating fluid from both impeller and diffuser that participate in these interactions can be expected to increase the pressure pulsation amplitude at such conditions.

Figure 31 confirms these ideas, showing a bronze impeller that operated extensively at low flow. Cavitation pitting can be observed near the OD of the impeller, which means that the rarefactions of the pressure waves were below the vapor pressure of the liquid—these pressure minima therefore being below the inlet pressure to the impeller. Moreover, the bulged-out shrouds can be assumed to be the result of the repeated occurrence of the associated pressure spikes (that is, the maxima of the pressure waves) within the radial gap ("Gap B") between the impeller blades and the diffuser vanes, the sidewall pressures on the outsides of the shrouds remaining comparatively constant. At greater values of design pressure rise than was the case for this impeller, this phenomenon creates correspondingly greater forces that have led to actual breakage of the impeller shrouds and diffuser vanes[61]. The cavitation seen in Figure 31, can also be observed on the leading edges of diffuser vanes, as in Figure 21 of Section 12.5, and this raises the possibility of diffuser vane breakage.

Energy Level: Stage Pressure Rise Even in the absence of the weakening effect of cavitation erosion, the leading edge of a diffuser vane or volute tongue is a representative, highly stressed zone within a pump that is subject to failure if the magnitude of the pressure pulsations arising from the impeller-diffuser interactions just described is sufficiently large. Thus, the fluid dynamically induced stresses in these vanes can be the basis for quantifying the energy level of a pump stage. In Table 12, this concept is developed into an expression for the stress in terms of the fluctuating pressure magnitude δp that is assumed to act across the vane leading edge as illustrated in the table. The width b of the vane is close enough to b_2 of the impeller exit to utilize the relationships for ψ and ϕ_l of Figure 12 to relate b/D to specific speed in Eq. (c) of the table. For similar velocity fields, the pressure pulsation magnitude δp is a constant multiplied by the stage pressure rise ΔP_{stg}. Thus, for a limiting value of stress, the concept of a limiting stage pressure rise

LIBERTY EXHIBIT 1017, Page 96

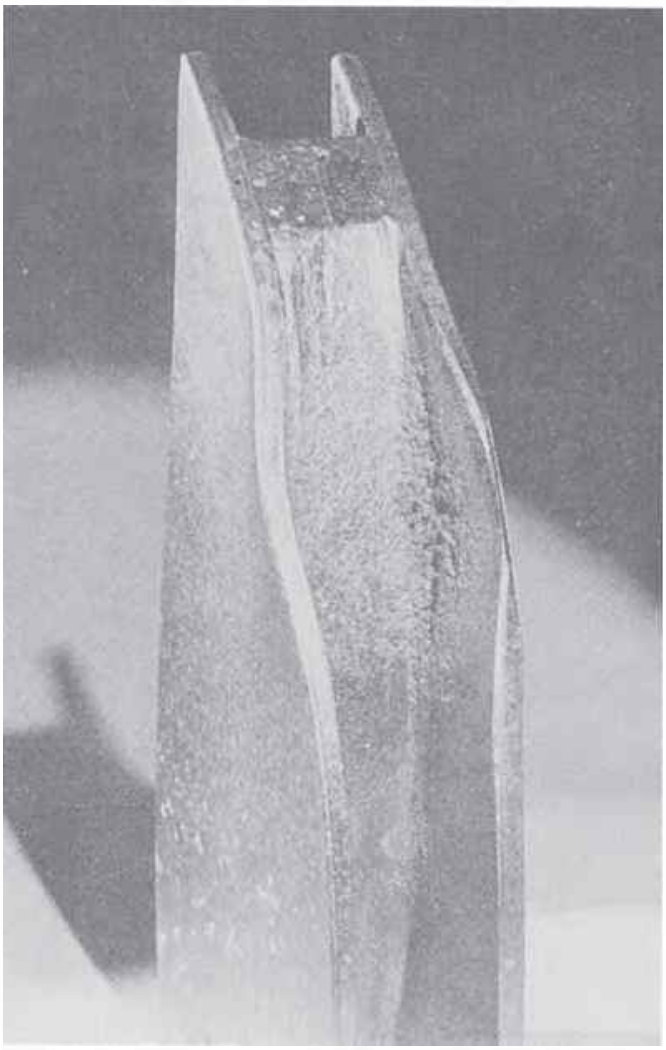


FIGURE 31 Damage to impeller from low-flow operation (Source: E. Makay in *Power*)

emerges in Eq. (e). The constant K is chosen from experience, which leads to the resulting Eq. (f). This relationship is plotted in Figure 32. [It will be observed that this choice for K corresponds to a limiting stress s from Eq. (d) of 6600 psi (45.5 MPa) that would exist if δp were equal to ΔP_{stg}—with $t/D = 0.01$ and $\varepsilon = 0.85$ as in the example.] The inverse variation with specific speed is a consequence of the greater b/D of higher-Ω_s pumps (as developed in Table 12), the wider vane introducing more stress at the juncture with the sidewalls for the same pressure loading and so imposing a lower stage pressure-rise limit. Conversely, lower-Ω_s pumps should have higher limits for ΔP_{stg}.

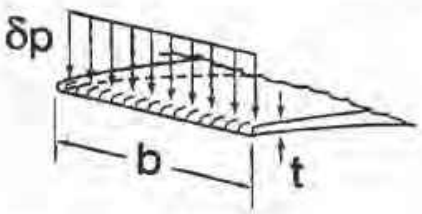
Figure 32, therefore, illustrates this concept of a *limiting stage pressure rise* as a measure of the energy level of centrifugal pumps, the basis being a limiting stress level in a critical component of the pump. Starting with stress at other locations in the pump leads to similar results. To provide perspective, specific examples of pumps that by this definition are in the *high-energy domain* are plotted on the figure. These data points are taken from Table 13, which contains information for several well-known liquid rocket engine turbo pumps[62,63,64] and for some representative high-energy electric utility boiler feed pumps[53,57].

The last column in Table 13 is another, more general way of comparing the energy level of these machines; namely, the *torque per unit volume*, which also has the dimensions of stress. For fixed ratios of stage width, casing OD, and other dimensions to impeller radius $r\ (= r_2)$, torque per unit volume differs from the listed values of torque/r^3 by a factor. The actual torque per unit volume therefore ranges from one-half to one-sixth of the tabulated

LIBERTY EXHIBIT 1017, Page 97

TABLE 12 Hydraulically induced stress levels

- Stress at juncture of diffuser vane leading edge with sidewall:



$$s = \frac{\delta p\, b^2}{2t^2} = \frac{(\delta p/2)(b/D)^2}{(t/D)^2} \qquad (a)$$

- From Fig. 12 and Eq. 36:

$$\frac{b}{D} = \frac{Q}{V_{m,2}\, 2\pi r_2 \varepsilon D} = \frac{Q}{\Omega r_2 \dfrac{V_{m,2}}{\Omega r_2} 4\pi r_2^2 \varepsilon} = \frac{Q_s}{\phi_i 4\pi \varepsilon} \qquad (b)$$

- From Eq. 50:

$$\frac{b}{D} = \Omega_s^2 \psi^{3/2} / (4\pi \phi_i \varepsilon) \qquad (c)$$

- With $\psi \approx 0.383/\Omega_s^{1/3}$ and $\phi_i \approx 0.1715\sqrt{\Omega_s}$

the stress Eq. (a) becomes, with Eq. (c)

$$s = \frac{\delta p \times \Omega_s^2}{165 \times (t/D)^2 \varepsilon^2} \qquad (d)$$

- Example for t/D=0.01, ε=0.85, Ω_s=0.6 and δp=1000 psi (6.895 MPa):

$$s = \frac{1000 \times (0.6)^2}{165 \times (0.01)^2 \times (0.85)^2} = 30{,}198 \text{ psi } (208.2 \text{ MPa})$$

- For δp being proportional to ΔP_{stg}, and for a fixed geometry and a given limiting value of stress, Eq. (d) becomes

$$\Delta P_{stg} = K/\Omega_s^2 \qquad (e)$$

- Experience leads to a choice of K such that

$$\Delta P_{stg} = \frac{78.72}{\Omega_s^2} \text{ psi} = \frac{0.5427}{\Omega_s^2} \text{ MPa} \qquad (f)$$

torque/r^5, depending on the casing or barrel thickness, and so on. However, as has been demonstrated, the critical stresses are more closely associated with the impeller OD, which makes comparison of the tabulated values more relevant. Thus, a pump with high torque/r^3 can be expected to have correspondingly high local internal stresses. The maximum values listed, namely for the high-pressure propellant pumps on the RD-170 (Russian) and SSME (U.S. Space Shuttle) engines, tend to explain the high level of research and development that was necessary to successfully deploy these machines. Illustrations of some of these rocket engine pumps can be found in Section 12.18.2. Similarly, Section 12.5

LIBERTY EXHIBIT 1017, Page 98

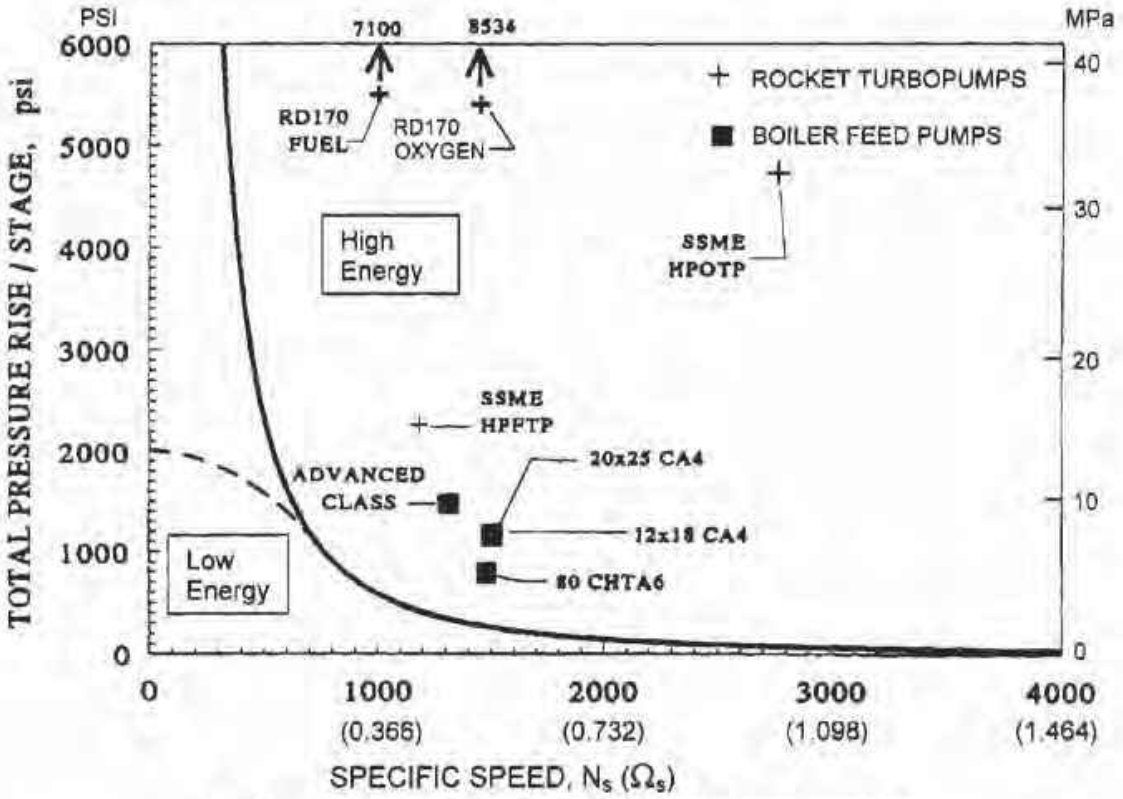


FIGURE 32 Pump energy level defined in terms of stage pressure rise

provides examples of high-energy boiler feed pumps: the massive, barrel-type construction of these machines is illustrated in Figure 18. Specifically, the first boiler feed pump listed in Table 13 is the sole feed pump supplying the steam generator of a super-critical 1300 MW electric generating unit and consumes nearly 50 MW of shaft power. It can be seen in Figures 7 and 20 of Section 12.5.

For pumps in the *low-energy domain* of Figure 32, normal design and manufacturing practices result in a more benign mechanical response to the abnormal fluid phenomena discussed here. However, for locations other than the diffuser entrance, which was the basis for the development of the figure, limiting stresses could be reached at considerably lower values of stage pressure rise. For this reason, the dashed line is offered as the upper limit of the low-energy domain; however, a thorough analysis of the stresses in any given application is the ultimate determinant of all the limits suggested in Figure 32 and of the acceptability of the design. It can now be seen that the design example treated earlier in this section is of the low-energy variety; therefore, the special design problems treated here and further on are of relatively little concern in such pumps. On the other hand, if the curve in Figure 32 were extended to much *higher specific speeds*, it would be found that many existing, large, high-Ω_s, low-head pumps are high-energy machines by this stress-related definition. It is therefore not surprising that such pumps generally require full stress and modal analyses to identify possible destructive resonances and stresses.

Fluid/Structure Interactions With the dimensions of pump energy level identified, the next step is to continue the examination of the problems mentioned previously and the methods that have become available for solving them. Attention is focused on fluid dynamical phenomena because, as the previous discussion of pressure pulsations implies, most of the adverse mechanical behavior exhibited by pumps originates from the behavior of the internal flow field. Excessive measured vibrations, material erosion, and component failures are often the external symptoms of fluid/structure interaction phenomena that are fundamentally explained from a fluid dynamics perspective. In addition to the fluid dynamically induced stresses in the pump structure that culminated in the domain

LIBERTY EXHIBIT 1017, Page 99

TABLE 13 Data on high-energy pumps*

Pump	No. of stages	Speed rpm	Flow rate gpm (m^3/s)	Head/stg ft (m)	ΔP/stg psi (MPa)	Specific Spd N_s (Ω_s)	Torque/r^3 psi (MPa)
Liquid Rocket Propellant Turbopumps							
Saturn V Booster – F1 Engine: Oxygen	1	5,490	25,080 (1.582)	3,100 (945)	1,530 (10.5)	2,095 (0.767)	371 (2.6)
Saturn V Booster – F1 Eng: Fuel (RP1)	1	5,490	15,640 (0.986)	5,100 (1,555)	1,810 (12.5)	1,130 (0.413)	172 (1.2)
Space Shuttle Main Engine: Oxygen (= SSME HPOTP)	1	31,100	7,240 (0.457)	9,700 (2,957)	4,800 (33.1)	2,700 (0.988)	1,431 (9.9)
Space Shuttle Main Engine: Fuel (H_2) (= SSME HPFTP)	3	37,400	16,300 (1.028)	66,700 (20,330)	2,280 (15.7)	1,150 (0.421)	200 (1.4)
RD-170 – Oxygen	1	13,850	25,008 (1.578)	17,300 (5,273)	8,534 (58.8)	1,448 (0.530)	1,521 (10.5)
RD-170 – Fuel (= RP1)	1	13,850	14,485 (0.914)	20,000 (6,096)	7,100 (49.0)	992 (0.363)	698 (4.8)
Boiler Feed Pumps							
20x25 CA-4 (IDP)	4	4,160	21,620 (1.364)	3,000 (914)	1,169 (8.1)	1,509 (0.552)	128 (0.9)
12x18 CA-4 (IDP)	4	5,800	11,000 (0.694)	3,000 (914)	1,169 (8.1)	1,500 (0.549)	130 (0.9)
80CHTA-6 (IDP)	6	5,800	6,250 (0.394)	2,100 (640)	820 (5.7)	1,479 (0.541)	87 (0.6)
Advanced Class (Sulzer)	2	6,500	9,510 (0.600)	3,800 (1158)	1,480 (10.2)	1,312 (0.480)	136 (0.9)

**Notes to this table:* Flow rates apply to the pump inlet. RD-170 pump data derived from Sutton[62] and Advanced Class boiler feed pump data from Ref. 57. Remaining data derived from Table 1 of Section 12.18.2, NASA reports[63,64] and from information supplied by Flowserve Corporation.[53]

definition of Figure 32, these phenomena encompass a) blade-vane interactions, b) recirculation, c) anomalous axial thrust behavior, and d) cavitation.

In order to illustrate the methods for dealing with the problems created by these fluid/structure interactions, a sample suction stage of a high-energy multistage pump is utilized as the quantifying focus in each case. Table 14 contains the conditions and essential features of this machine, a meridional view of which is shown in Figure 33. As with the earlier design example, this stage has been designed in accordance with the procedures outlined for that example. This includes the velocity diagrams shown in the figure, as well as the design of the eye, the hub and shroud profiles, and the blading. A preliminary design

LIBERTY EXHIBIT 1017, Page 100

TABLE 14 Data for high-energy pump suction stage

A. Design Inputs

Fluid: Boiler feed water at 350°F (177°C) ⇒ sp. gr. = 0.89, ν = 0.17 cs.

Flow rate, Q, gpm (m^3/s)	20,000 (1.262)
Head rise, ΔH, ft (m)	3,000 (914.4)
Rotative speed, N, rpm	4,700
Outlet flow coefficient, ϕ_2 (Figure 12)	0.1328
Head coefficient, ψ (Figure 12)	0.455
Specific speed, Ω_s (N_s / n_q)	0.6 (1640/32)
Inlet flow coefficient, ϕ_e	0.3 (=tan 16.7 deg.)
Number of Impeller blades, n_b	7
Number of Diffuser vanes, n_v	9

B. Calculated Perfomance Data

1. Efficiency
   a) BEP of 20,000 USgpm (1.2618 m^3/s)
   $\eta = \eta_p = 0.877$ (vs. η=0.8682 - from Fig 10, for X = 1)
   $\eta_{hy} = 0.900$
   $\eta_m = 0.985$
   $\eta_v = 0.989$ [216 gpm (0.0136 m^3/s) front ring leakage; rear ring leakage included in η_{hy}]

   b) At 50% Flow : η_p = 0.693 (= 0.79 of η_{BEP} ; 0.8 is typical)

2. Head Rise
   ΔH_{BEP} = 3000 ft. (914 m) ⇒ ψ = 0.455
   $\Delta H_{shutoff}$ = 3697 ft. (1127 m) ⇒ $\psi_{s/o}$ = 0.560
   ΔH-vs-Q curve stability indicator, $\Delta H_{s/o}/\Delta H_{BEP}$ = 1.23 (doubtful if less than 1.2)

3. Power
   $P_{s,BEP}$ = 15,376 hp (11,466 kW) ~ $\hat{P}$ = 0.0571

   $P_{s,SHUTOFF}$ = 6,144 hp (4,583 kW) ~ $\hat{P}_{s/o}$ = 0.0228 (= 0.01966 × 1.16 from Fig. 23)
   ↑
   = K for $\frac{b_2}{D_2}$ = 0.0779

was also made of the vaned diffuser and return vanes, following the guidelines presented in the foregoing *Design Procedures* section. The result is a representative machine to which the following paragraphs continually refer.

Blade-Vane Combinations Certain numerical combinations of impeller blades and diffuser vanes (or inlet guide vanes, where they are employed) have been shown to have acoustic consequences that can exacerbate the pressure pulsations arising from the interaction of impeller and diffuser flow fields. Bolleter reviewed the types of interactions that can occur and the consequences with regard to pressure pulsations and resonance[33]. These types are associated with the integer difference m between the multiples of the number of impeller blades and the number of diffuser vanes, as explained in Table 15. To check

LIBERTY EXHIBIT 1017, Page 101

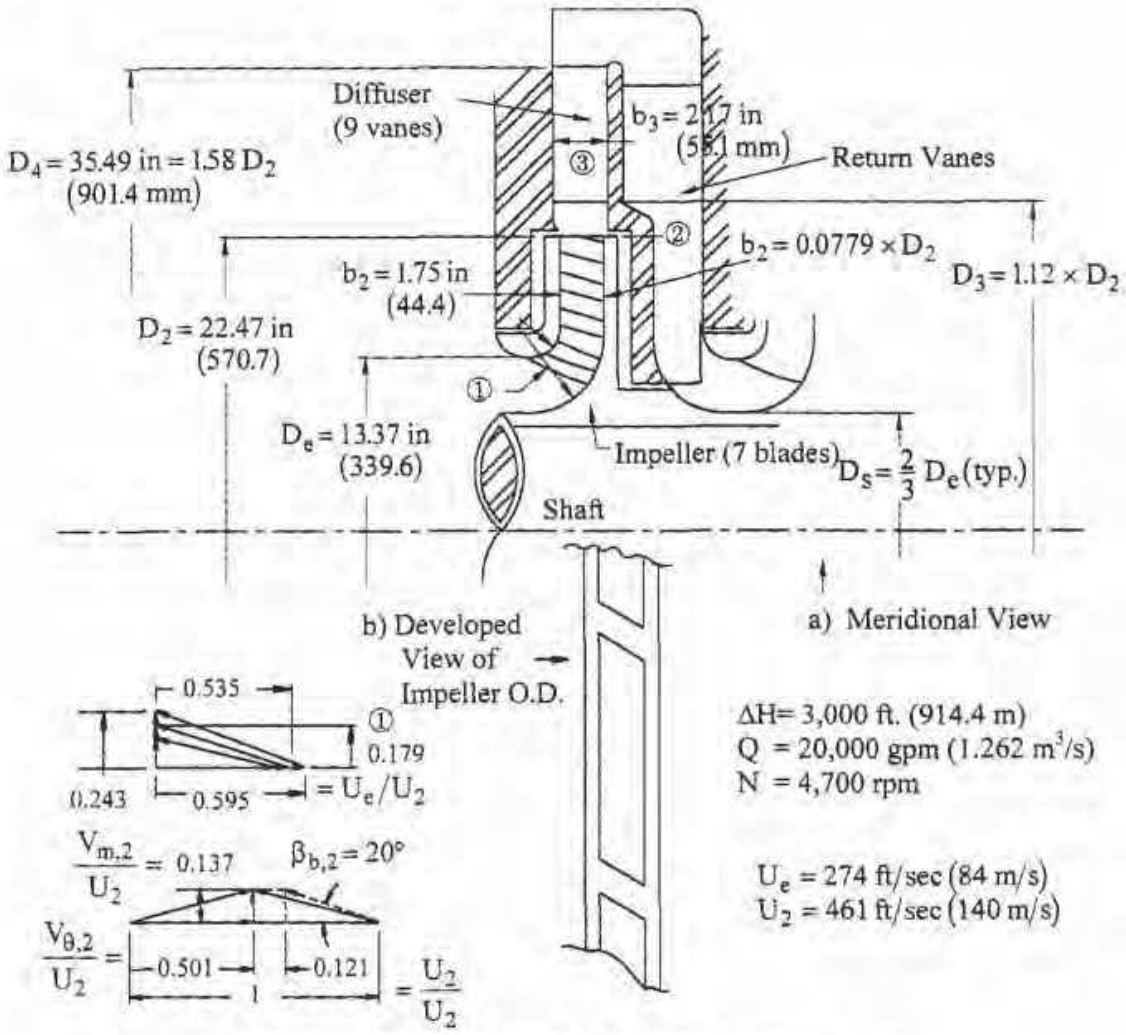


FIGURE 33 Sample suction stage of high-energy multistage pump

the blade-vane combination, one simply forms a matrix of the multiples as shown and lists the difference in each cell.

To illustrate the method, rather than use the pump of Table 14, a different example is chosen in order to dispel the notion that one can always use two different prime numbers for blade-vane combinations. This is an existing case of a 60,000 hp (45 MW) single-stage pump of $\Omega_s = 0.6$ ($N_s = 1640$) and $\Delta p = 357$ psi (2.46 MPa), which has 7 impeller blades and 13 diffuser vanes[65]. Notice that $m = 1$ in the second order of impeller blade number, which means there should be pressure pulsations at $2 \times 7 \times$ rpm/60 Hz. In fact, this pump has exactly this vibration and pressure pulsation frequency in the field, not least because the pump is operating at just the right speed for the acoustic waves emanating from successive interaction points to reinforce each other in producing unacceptable pressure pulsations.

Even with this simple method, the final choice of the blade-vane combination is usually a compromise. For example, the method shows that all double-volute pumps have $m = 0$ or 1 in the first order of impeller blade number, depending on whether this number is even or odd. $m = 0$ means that the all the blades or vanes are interacting at the same instant, a consequence of which is torque ripple. High-energy volute pumps exist for both even and odd cases, and quite large gaps between blades and vanes (= "Gap B") are employed to mitigate these effects.

The reader who checks the pump of Table 14 by this method will find that $m = 2$ in the first order of both blades (7) and vanes (9) but that $m \neq 0$ everywhere else in the matrix. $m = 1$ occurs only in the highest orders of both and should therefore be of little consequence. Checking whether 10 or 11 vanes would be better yields $m = 1$ in the third order

LIBERTY EXHIBIT 1017, Page 102

TABLE 15 Choosing vane combinations to minimize pressure pulsations[33]

1. Z_i is the number of impeller blades.
2. Z_d is the number of diffuser vanes.
3. Each vane combination produces interacting pressure fields between the blade rows.
4. These fields rotate about one or more "nodal diameters," "m" producing unsteady loads.
5. The value of "m" determines the nature and severity of these loads.
6. "m" is the difference between $(p \times Z_i)$ and $(q \times Z_d)$, where p and q are integers.
7. To find "m", one sets up a matrix of diffuser vanes and their multiples vs. impeller blades and their multiples or "orders." A minimum of the first three orders should be used. This is illustrated as follows for an impeller with 7 blades ($Z_i = 7$) and a diffuser with 13 vanes ($Z_d = 13$):

		Impeller blades and their multiples:			
		p = 1 7(= Z_i)	p = 1 14	p = 1 21	p = 1 28
Diffuser vanes and their multiples:		Differences "m" between $(p \times Z_i)$ and $(q \times Z_d)$ are given below:			
q = 1	13(= Z_d)	6	1	8	15
q = 2	26	19	12	5	2
q = 3	39	33	25	18	11

The significant values of "m" are 0, 1, and 2. The lower the order of either the impeller blades or the diffuser vanes, the stronger is the interaction. The responses that occur for these "m" values are as follows:

- m = 0 - strong pressure pulsations and fluctuating axial loads and torsional forces.
- m = 1 - pressure pulsations and fluctuating radial loads.
- m = 2 - small pressure pulsations and a chance of resonance of the impeller about the two nodal diameters—at a frequency equal to the value of $q \times Z_d$ times the rotational frequency (rpm or rps).

In this example, m = 1 in the second order of the impeller blades (i.e., p = 2); thus, the frequency of the resulting disturbances will be twice that of blade passing frequency $p \times Z_i \times$ rpm or $2 \times 7 \times$ rpm cycles per minute or $2 \times 7 \times$ rpm/60 Hz. This is therefore a poor vane combination and should be avoided—especially for such low orders of vane number; i.e., for such small values of p and q, (Here, p = 2 and q = 1.) In general, m = 0 and 1 should be avoided altogether, and m = 2 should be avoided in the lower orders.

of impeller blades and second order of diffuser vanes, which is probably less desirable than $m = 2$ in the first orders. Therefore, Figure 33 shows a value of "Gap B" that is 12% of the impeller radius, which by thus distancing the interacting flow fields of the impeller blades and diffuser vanes from one another should provide adequate protection from pressure pulsations and excitations of resonance. (The gaps at the impeller OD will be discussed further on.)

Recirculation Separation and stall of the fluid flowing in the passages of impellers and diffusers occurs at low flow because of the incidence and large reduction in the one-dimensional velocity relative to the passages that happen at low flow. This and the consequent

LIBERTY EXHIBIT 1017, Page 103

recirculation patterns in the impeller were discussed and illustrated in Figure 6. Fischer and Thoma[66] visually observed and recorded the flow patterns, finding that as flow rate is reduced, wakes on the suction side of all blades thicken until they occupy half the passage width at half the BEP flow rate. At lesser flow rates, the wakes continue to thicken but become irregular, stalling in one passage and not the others—the stall pattern moving into and out of adjacent passages and so rotating relative to the impeller. As shut-off is approached, this rotating pattern is accompanied by reversed flow emerging from the inlet of the stalled passage. Fraser, working with typical impeller geometries, formulated rules for computing the flow Q_{SR} at which this reversal occurs as Q is reduced at constant speed[67]. His expressions, found further on, include the effect of impeller eye size on Q_{SR}. As one might expect, a pump with an eye diameter approaching that of the impeller OD will have Q_{SR} approaching Q_{BEP}. At $Q < Q_{SR}$, the impeller flow patterns are highly unsteady—as is usually the case with massively separated flows—creating nonsynchronous, low-frequency or random pressure pulsations, the resulting shear layers between the reverse-flowing and in-flowing fluid having vortices with locally low pressures so that cavitation can also exist. Fraser also quantified the flow rate Q_{DR} below which impeller discharge recirculation exists. Forces from such motion can cause fatigue failure of the impeller blades, diffuser vanes or volute tongue, cavitation erosion also playing a part as in Figure 31. In Section 2.1.3, Fraser describes the identification and consequences of recirculation in detail, the more general designation Q_R referring to either Q_{SR} or Q_{DR}, depending on whether Q is between or below both.

The ability for pumps to operate with any form of separation; stall; or, worse, flow reversal (recirculation) depends on the energy level. This can be approximately quantified, as outlined under the subject of *Minimum Flow Limits* further on, which include consideration of accompanying cavitation activity.

Axial Thrust Response to Recirculation Discharge recirculation usually involves backflow from the diffuser, itself containing oscillating flow patterns and rotating stall. Fluid emerging from the diffuser will be spinning opposite to the direction of rotation, such fluid having a major effect on the sidewall gap flows as it joins the leakage flows described under *Predicting Axial Thrust*. As this fluid invades the sidewall gaps, it can slow or virtually cancel the usual positive swirling of the gap fluid. Iino, Sato, and Miyashiro experimentally observed and recorded this behavior, which was exaggerated by shifting the impeller axially and by changing the ring clearances[68].

An added, not unexpected effect is that as Q is reduced below Q_{DR}, the invading flow from the diffuser can favor the front or back side of the impeller and then *switch sides* upon further reduction of Q. This effect is clearly seen in the experimental thrust-versus-Q plots of Figure 34, the impellers having been shifted as just described. Depicted there is the resulting net load on the axial thrust bearing of an eight-stage, 3600-rpm diffuser pump (all impellers facing in the same direction) that had a cylindrical balancing drum (not a self-compensating balancing disk). The drum was sized so as not to completely eliminate the thrust—in order to avoid thrust reversals. The solid lines are the predicted net thrust according to the methods outlined in Table 4 for three axial positions of the impeller. The large excursions in net thrust were eliminated by restricting the entry of the invading diffuser backflow into the sidewall gaps—through a tightening of the gap between the shrouds of impeller and diffuser (Gap "A") in Figure 35. Gap "A" is not effective unless the "overlap" of the two mating shrouds is from four to six times the gap dimension[61]. Moreover, if Gap "A" is minimized, this can exaggerate the blade-vane interactions, making it necessary to open up Gap "B" more than would be necessary were Gap "A" not minimized[69].

A further possibility that has been observed in a single-stage double-suction pump is the *unsteadiness* of impeller discharge recirculation and, most likely, of the diffuser or volute backflow. The side-to-side switching just mentioned appears in Figure 36 to be happening as a function of time as well as of flow rate Q, as evidenced by the axial motion, which is accompanied by discharge pressure pulsations. The "fix" mentioned in the figure was, again, mainly minimizing Gap "A."

Closing Gap "A" and opening Gap "B" are procedures that have been widely and successfully applied in high-energy pumps, which usually work well at BEP but run into

LIBERTY EXHIBIT 1017, Page 104

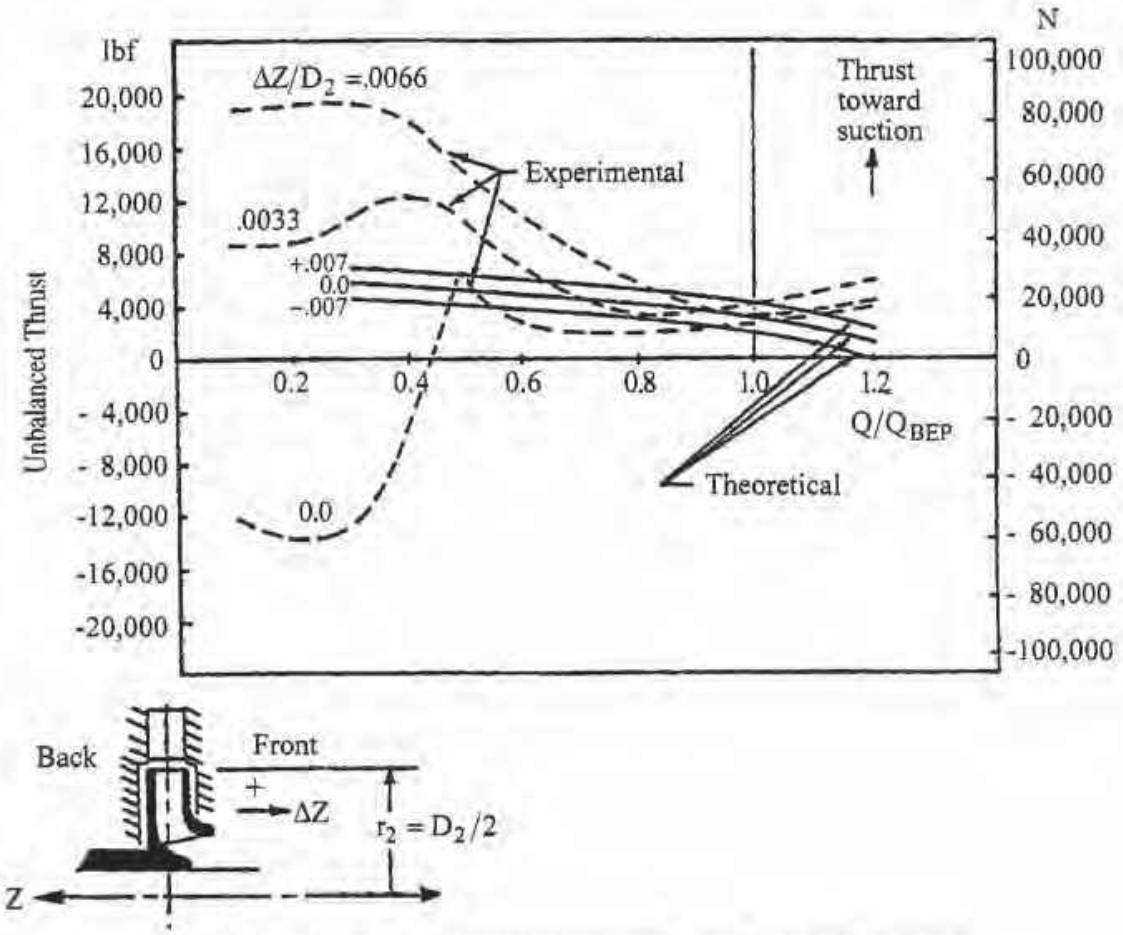


FIGURE 34 Axial thrust response to recirculation (Source: Flowserve Corporation)

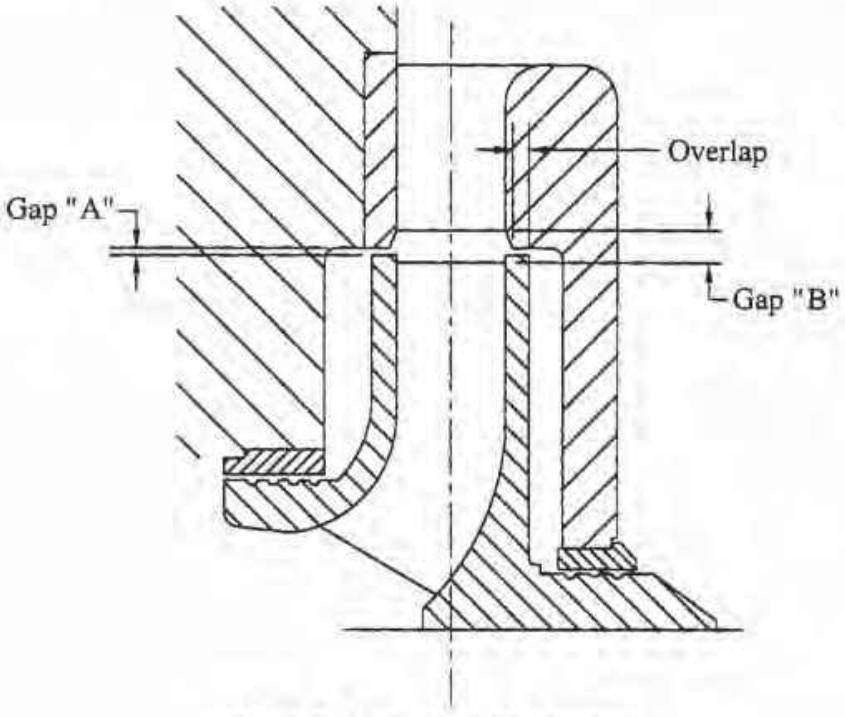


FIGURE 35 Gaps at impeller periphery[51]

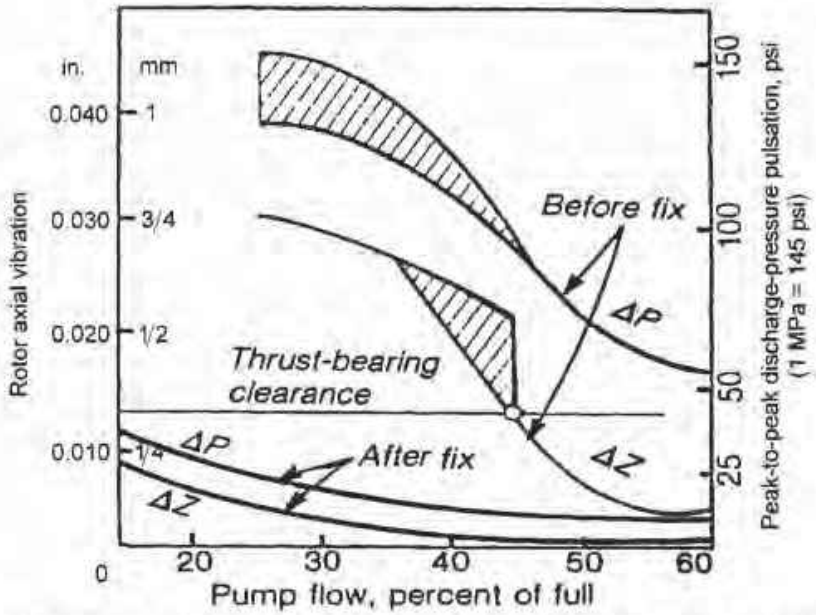


FIGURE 36 Eliminating unsteady thrust and pressure pulsations (Source: E. Makay in *Power.*)

difficulties at low flow[69]. These procedures have proven to cure the thrust and pressure pulsation behavior just described and also improve the low-flow performance curve shape[65]. The results are high-energy pumps that can operate smoothly over a wider range of flow rate than—in many cases—was originally expected or specified. Nevertheless, the higher the energy level, the more intolerable is any unsteadiness and pressure pulsation activity.

Minimum Flow Limits Because the intensity of pressure pulsations and the accompanying vibrations can increase beyond acceptable limits as flow rate is reduced at constant speed below the BEP flow, or more specifically, below Q_R, expressions for how low Q/Q_{BEP} can be without exceeding these limits have been developed. Manufacturer and user groups such as the Hydraulic Institute (HI), the International Organization for Standardization (ISO), and the American Petroleum Institute (API) have specified vibration limits that must be met at what is usually called at the minimum continuous stable flow (*MCSF*) or simply Q_{min}. In an attempt to answer the question of how far into the recirculation zone (where $Q < Q_R$) an operator can take a pump before reaching the *MCSF*, Gopalakrishnan proposed a general rationale for computing Q_{min} that takes the energy level into account—through the flow rate and rotative speed of the machine[70]. These two quantities imply the blade tip speed at the inlet of the impeller. (Through typical ratios of impeller OD to eye diameter, this also implies the OD tip speed and therefore the head, the energy level having been defined in Figure 32 in terms of stage pressure rise ΔP_{stg}.) The theory for this method is defined in Part A of Table 16, in which Q_{min} is computed as the product of a series of K-factors multiplying the value of Q_R, which is computed according to Fraser's earlier development[67]. Conceptually, the product of these factors approaches unity in the maximum-energy case, where the instabilities accompanying any recirculation at all are significant. Conceivably, this product could exceed unity at the highest energy levels, as separation and stall and the attendant unsteadiness must occur—as Q is reduced—before reaching the backflows that characterize Q_R, which was observed by Fraser as the value of flow rate for the onset of recirculation (see Section 2.1.3).

K_1 and K_3 are given in Table 16 as equations that have been curve-fitted to speed/flow rate- and NPSH-effect charts that appeared in Gopalakrishnan's presentation[70]. This includes the ability to enter any speed (rpm) into the computation for K_1, only 3600 and 1800 rpm having explicitly appeared in the charts. NPSH plays a role in the determination of Q_{min}—through the factor K_3—because of the exacerbation of the unsteadiness and pressure pulsations due to dilation of the cavities in the two-phase internal flows that

LIBERTY EXHIBIT 1017, Page 106

TABLE 16 General method for computing minimum flow: quantifying the energy-level effect on Q_{min} relative to Q_R[70]

A) Theory

$Q_{min} = Q_R \; K_1 \; K_2 \; K_3 \; K_4 \; K_5$, or Q_R, whichever is smaller (i.e., product of K's $\leq$ 1)

$$Q_R = \begin{cases} Q_{SR} \text{ if } D_e \geq 0.5\, D_2 \\ Q_{DR} \text{ if } D_e \leq 0.5\, D_2 \end{cases}$$

$$Q_{DR} = \pi D_2^{\,2}\; b_2\; \frac{\Omega}{2}\; \overline{C_{DR}}$$

$$\overline{C_{DR}} = -0.01 + \beta_{f,2}°/\,218.75$$

$$Q_{SR} = \pi \Omega r_e^3 \left(1 - \frac{D_s^2}{D_e^2}\right) \cdot \overline{C_{SR}}$$

$$\overline{C_{SR}} = \tan\beta_1 \cdot \left\{1 - 0.2091 \cdot (\beta_1° - 9.5)^{0.4}\right\}$$

$$K_1 = \left[0.06862 \times \left(\frac{N - 1800}{1700}\right)\right] + Y + 0.3843 \log_{10} Q_{BEP}$$

$$Y = \begin{cases} -0.4529 \text{ for } Q_{BEP} \text{ in gpm} \\ +1.1612 \text{ for } Q_{BEP} \text{ in } m^3/s \end{cases}$$

K_2 = Specific gravity

$$K_3 = \left\{ \begin{array}{l} 0.6 + 0.4 \times \left[\frac{1}{3}\left(\frac{4}{R} - 1\right)\right]^{1.1} \quad \text{Pump with shaft through eye} \\ 0.7 + 0.3 \times \left[\frac{1}{3}\left(\frac{4}{R} - 1\right)\right]^{1.1} \quad \text{End - suction pump} \end{array} \right\} \quad R = \frac{NPSH_A}{NPSH_{3\%}}$$

$$K_4 = \begin{cases} 1 & \text{Continuous operation at minimum flow} \\ 0.7 & \text{Operation at minimum flow less than 25\% of total operating time} \end{cases}$$

$K_5 = 1$ No specific mechanical design margins

B) Results for Sample High-Energy Pump Suction Stage (See Fig. 33)

$Q_R = Q_{SR}$, since $D_e \geq 0.5\, D_2$

$$Q_{SR} = \pi\, \Omega\, r_e^{\,3} \left(1 - \frac{D_s^{\,2}}{D_e^{\,2}}\right) \cdot \overline{C_{SR}} = \pi \times 4700\; \frac{\pi}{30} \times \left(\frac{6.6855}{12}\right)^3 \cdot \left(1 - \frac{2^2}{3^2}\right) \times \overline{C_{SR}}\; \frac{ft^3}{sec.}$$

and $\overline{C_{SR}} = 0.3 \cdot \left\{1 - 0.2091 \cdot (16.7 - 9.5)^{0.4}\right\} = 0.1618$

Q_{SR} = 24.03 ft³/sec = 10,785 gpm (0.6804 m³/s) = 0.540 × Q_{BEP}

$K_1 = 1.317$; $K_2 = 0.89$; $K_3 = 0.768$; $K_4 = 1$; $K_5 = 1$

$Q_{min} = 10{,}785 \times 0.9002 = \underline{9{,}709 \text{ gpm } (0.613 \text{ m}^3/\text{s}) = 0.485\; Q_{BEP}}$

LIBERTY EXHIBIT 1017, Page 107

exist for any value of NPSH that is less than the inception $NPSH_i$. (See the ensuing cavitation discussion and the description in Section 2.1.3 that accompanies the definition of NPSH-limits.)

As an example, the minimum flow of the high-energy pump suction stage of Table 14 and Figure 33 is computed in Part B of Table 16. (The value of R for the calculation of K_3 is taken from Table 18.) This machine has the relatively high energy level of some of the boiler feed pumps shown in Figure 32 and listed in Table 13. Thus it is not surprising that the resulting value of Q_{min} is 90% of Q_R (which equals Q_{SR}, as is typical) and 48.5% of the BEP flow rate. This is indicated on Figure 37, in which the computed performance curves of this pump are displayed. (See Part B of Table 14 for the main elements of these performance predictions.) However, some of the remedies that have been discussed in this section to counter the adverse effects of high-energy pump phenomena can reduce Q_{min} to lower values than this. In fact, the method contains the flexibility to take into account such improvements through the factor K_5.

In computing Q_{SR}, the angle β_1 is called for. This is approximated by the inlet flow coefficient $\phi_s = 0.3$ from Table 14, which corresponds to a nominal inlet tip flow angle of 16.7 degrees. The actual flow angle (and blade angle) at that location is slightly larger due to the hub-to-shroud variation of the incoming meridional velocity as assumed in the development of the inlet velocity diagrams of Figure 33. This will have a small effect on the results, depending on how one interprets "β_1". In this regard, as can also be appreciated from the choices that must be made for the K's, the method of Table 16 is not precise; however, it is a useful indicator of what the user and designer can expect in determining the operating range of a pump.

The above general theory for computing minimum flow is inclusive of all types of centrifugal pumps and has found application especially for high-energy pumps, which can be difficult to evaluate precisely in the varying circumstances of installation and operation in which they are usually applied. The judgments that must be made in order to apply the

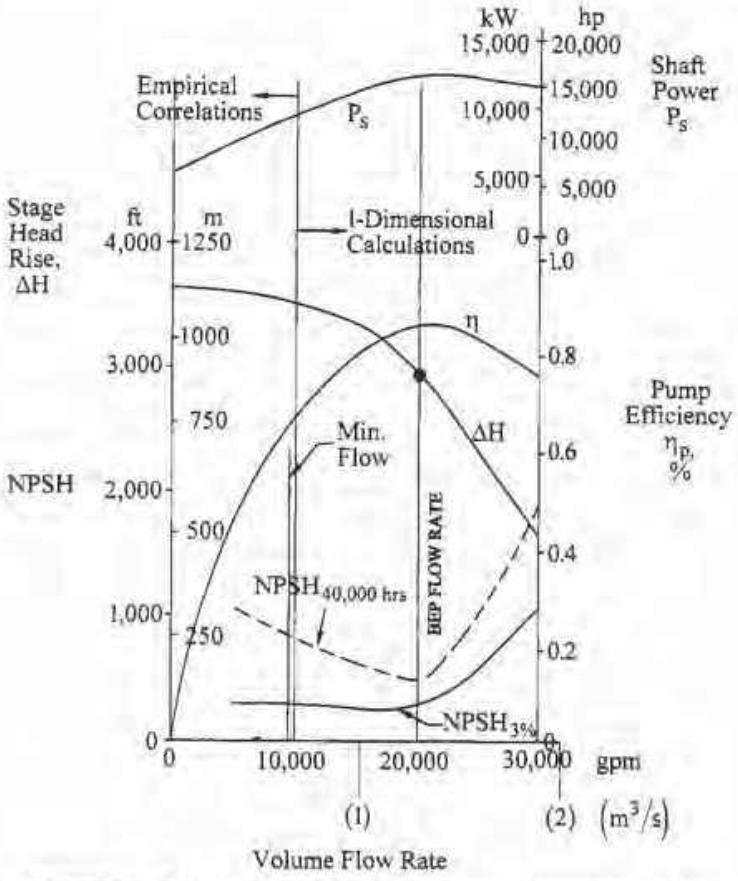


FIGURE 37 Estimated performance of high-energy pump suction stage

LIBERTY EXHIBIT 1017, Page 108

method of Table 16 can be largely avoided if actual data for Q_{min} are available. It would in fact be a monumental task to establish precise limits for all pump types and operational envelopes. Nevertheless, the effect of energy level on *MCSF* has been found experimentally for several classes of API process pumps through extensive testing. From this, Heald and Palgrave have developed a method for computing the minimum flow of these pumps as follows[71]:

$$Q_{min} = \text{MSCF} = \frac{K_7}{100} K_M \times Q_{BEP} \tag{68}$$

where

$$K_7 = K_7(\text{rpm, configuration, } N_{SS}) \tag{69}$$

and

$$K_M = K_M[(NPSH_A/NPSH_R)_{BEP}, \text{fluid}] \tag{70}$$

Obtained from Figure 38, the factor K_7 accounts for the effects of speed and configuration. As used in that chart—and in Eq. 69, the term *suction-specific speed* N_{ss} (or Ω_{ss}) does not mean that NPSH-effects are also included; rather, this expresses the fact that the impeller design is affected by the designer's choice of N_{ss} as can be seen in the case of the earlier *Design Example*, beginning in Table 6. This leads immediately in Table 7 to the inlet flow coefficient ϕ_e (through the NPSH-correlations of Table 1) and the impeller eye diameter D_e or radius r_e. Following on from the discussion of *Recirculation*, the ratio Q_{SR}/Q_{BEP} can be expected to increase with eye size or D_e/D_s. Being strictly based on experiments, the Heald and Palgrave method does not deal explicitly with Q_{SR} or Q_{DR}, but one can see from Figure 38 that this principle is operative: Higher-N_{ss} pumps require greater *MCSF*. Before this fact was clearly understood, the trend was to design for greater N_{ss}—in order to increase suction capability of these pumps. When operators ran them back to the same low flows as they had done with earlier pumps designed for lower-N_{ss} capability, failures became epidemic. This led to a call for "lower-suction specific speed

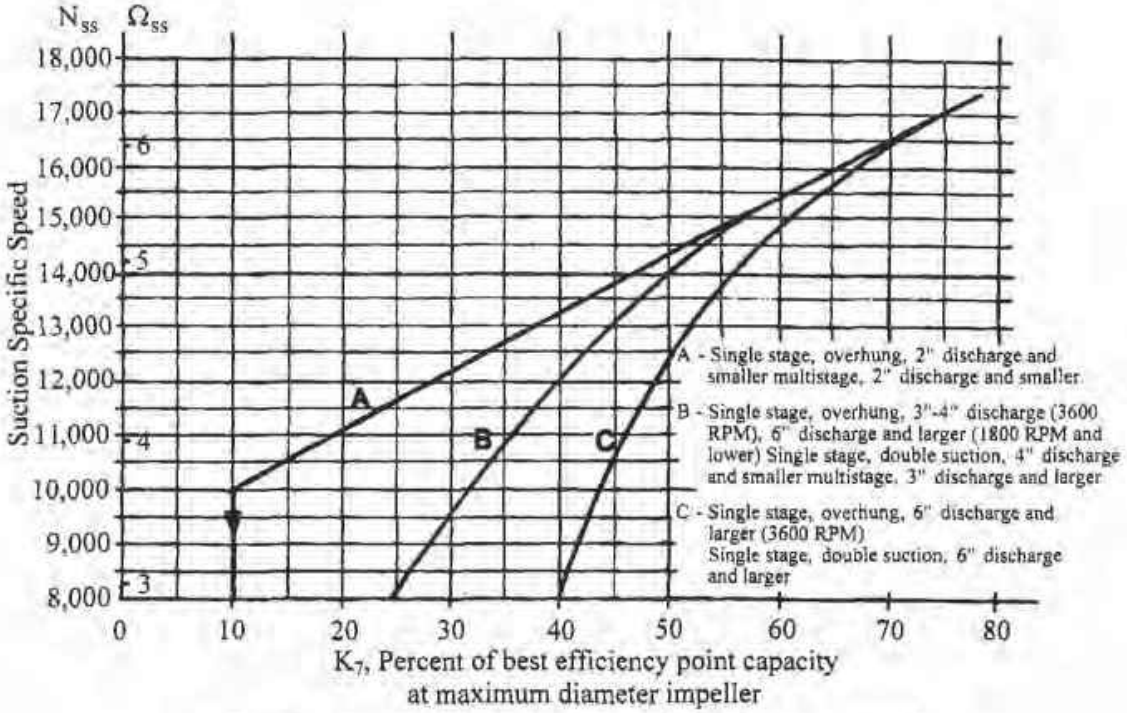


FIGURE 38 Minimum continuous stable flow (MCSF) for process pumps[71]

LIBERTY EXHIBIT 1017, Page 109

Next Page

pumps," or, more accurately, pumps designed for lower-N_{ss} capability; specifically 11,000 (Ω_{ss} = 4) or less[72].

The NPSH-effect does come into play—as with K_s in the previous general method—through the factor K_M in Figure 39a. In this case, the term $NPSH_R$ means $NPSH_{3\%}$. Here again, it is the ratio $R = NPSH_A/NPSH_R$ that is the determining factor because it is a measure of the cavitation activity that is invariably present in the first stage of a pump, and therefore in all single-stage pumps. The lower the value of R, the more violent the pressure pulsations accompanying the recirculating fluid and the consequent vibration. The situation is mitigated considerably at greater R, and K_M operates through Eq. 68 to decrease the *MCSF*. Of course, if R were great enough—often 5 or more—$NPSH_A$ would exceed $NPSH_i$ (as discussed in Section 2.1.3) and there would then finally really be no cavitation in the pump. (That high a value of *NPSHA* is rare; for, if it were supplied, there might not be a need for a pump in the first place.)

Figure 39a also brings in the effect of the liquid being pumped. When room temperature water boils (cavitates), the mass boiled off by the local drop below the vapor pressure makes considerably more cavity or bubble volume than some other liquids, namely hydrocarbons and hot water[17]. (See Section 2.1.3.) Figure 39 refers to room temperature or cold water. Figure 39b shows the value of $NPSH_{40}$; so named, because, if this amount of NPSH, which is greater than $NPSH_{3\%}$, is supplied, the impeller thereby lasts for 40,000 hours in resistance to cavitation erosion, a phenomenon which is dealt with below.

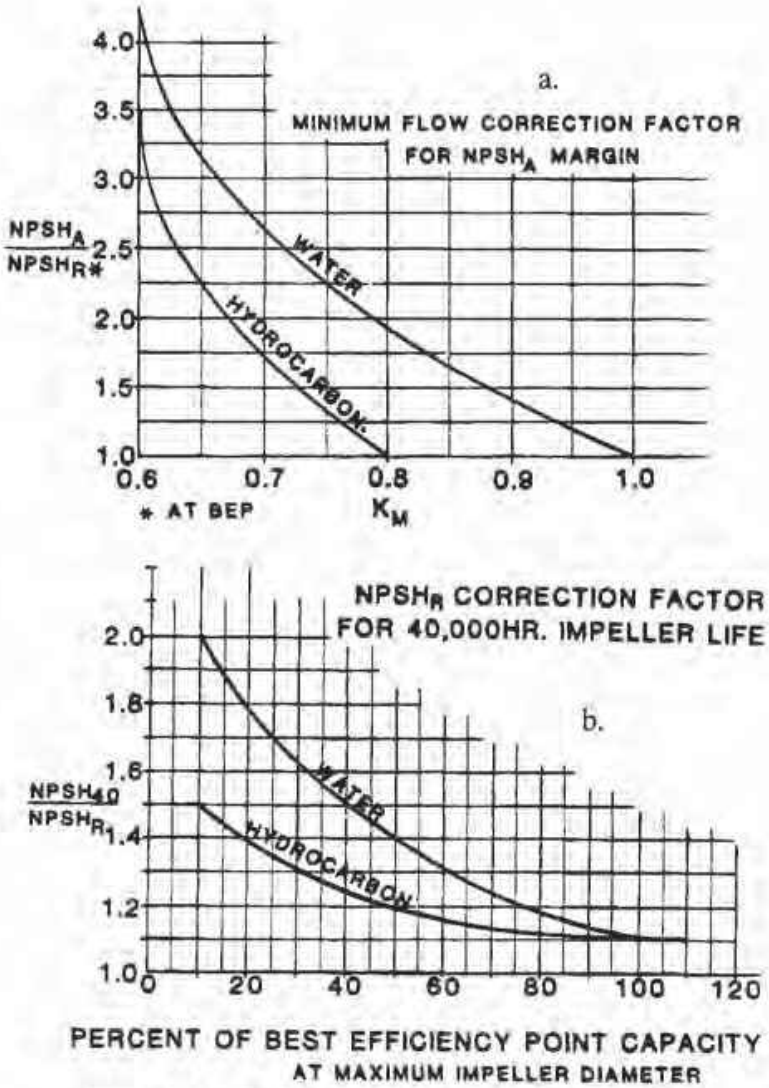


FIGURE 39 NPSH-effects on: a) MCSF and b) impeller life[71]

LIBERTY EXHIBIT 1017, Page 110

Previous Page

The relationship of the ratio R to the design value of N_{ss} has been quantified more generally in terms of the "suction energy" $SE = D_e(in.) \times N \times N_{SS} \times sp.gr.$ by Budris, wherein he calls for a greater NPSH-margin ($= NPSH_A\text{-}NPSH_R$) for pumps with high values of SE, this margin increasing as the flow rate is reduced below BEP.[73] SE and the pump energy level are connected through the ratio D_e/D_2 (Eq. 51), because the limiting stage pressure rise of Figure 32 is proportional to $sp.gr.\times\Delta H_{stg}$, the stage head being found from D_2 and N, e.g., through the equation in Figure 12.

By way of illustration, computing the minimum flow of the end-suction volute pump of the *Design Example* begins with Curve B in Figure 38 (for pumps with 6-inch discharge and larger and for 1800 rpm and lower as stated on the figure). [This pump has a discharge port of about 9 inches (229 mm) as would be the case if the velocity in this port were half of the throat velocity V_T in Part A of Table 11, as suggested previously in the paragraphs on *Volutes* under *Designing the Collector*.] N_{ss} for this pump was chosen as 12,300 ($\Omega_{ss} = 4.5$), which yields 41.5% for K_7. If it were decided to provide this cold-water pump with 16.4 ft (5 m) of $NPSH_A$, R would be 1.17, and the figure yields 0.97 for K_M. [$NPSH_{3\%}$ = 14 ft. (4.27 m) for this pump, as seen in Table 6.] Thus, from Eq. 68, this pump has an $MCSF$ of 0.415×0.97 or 40% of Q_{BEP}. Had it been designed for $N_{ss} = 11{,}000$ ($\Omega_{ss} = 4.025$), and if R still were 1.17, the $NPSH_A$ would have been 19 ft (5.8 m) and $MCFS$ would have been 0.36×0.97 or 35% of Q_{BEP}. Moreover, if it were pumping hydrocarbons at this same $NPSH_A$, $MCFS$ would have been even lower, namely 0.36×0.78 or 28% of Q_{BEP}. It would appear, though, that for many applications, the pump as designed (at $\Omega_{ss} = 4.5$) has a low enough energy level to allow for an adequate range of flow-rate capability, and that therefore, the value $N_{ss} = 12{,}300$ is in this case not excessive.

Cavitation Considerations Having alluded to and treated the subject of cavitation a number of times in this section, we should expand on the role that this ever-present phenomenon plays in the operation and durability of centrifugal pumps, particularly those having a high energy level. The manifestations of cavitation that are encountered and become issues for the operability and life of a pump are a) cavitation accompanying backflow from the impeller eye, b) cavitation-generated instabilities and pressure pulsations, and c) erosion, which involves the prediction of the $NPSH_R$-versus-flow rate characteristic curve to maintain life and, conversely (d) the prediction of life for a given $NPSH_A$. The range of NPSH over which cavitation occurs within a pump extends from the point where pump head or pressure rise undergoes an identifiable drop—usually 3% for repeatable results for the NPSH-value involved—namely the "performance-NPSH" or $NPSH_{3\%}$—upwards. As NPSH increases from this point, there is an extensive range over which no observable performance loss is detected, yet erosive damage is progressing at a sometimes excessive rate. Finally, at the upper end of the range, all two-phase activity ceases—all bubbles and cavities are suppressed—namely, at the inception-NPSH value or $NPSH_i$. As stated previously, $NPSH_i$ has been observed to be typically about five times $NPSH_{3\%}$. This is clearly described in Section 2.1.3, in which the different NPSH-limits are distinguished. The following cavitation considerations pertain to this range.

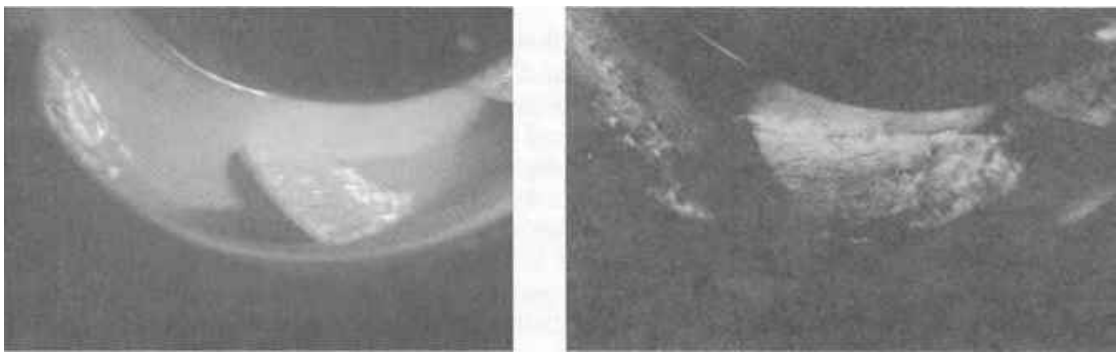
a) Cavitation and backflow. The minimum flow limits imposed by the R-value or NPSH-effect arise partly because a lower flow rate at a low NPSH—although it may be in excess of $NPSH_{3\%}$—involves a strong interaction between suction recirculation and cavitation that can be intense, especially for inducers and large-eye (large D_e/D_2) impellers. At flow rates $Q \ll Q_{SR}$, there exists upstream of the impeller an annulus of back-flowing fluid that emerges from the impeller. Drawing the velocity diagram at the impeller leading edge at the shroud for the case of reversed flow reveals that the absolute velocity component V i) is mostly circumferential and ii) is greater than the impeller tip speed $U_{t,1}$ or U_e. Thus the fluid leaving the impeller hugs the outer wall of the approach passage. If this passage is an axial pipe supplying an end-suction impeller or inducer, the pressure along the centerline can be below the vapor pressure, thus creating a vapor core that extends many diameters upstream. Obviously the energetic backflow has to be balanced by an equivalent inflow that enters the impeller from the interior of the pipe and therefore along the hub streamline of the impeller. Vapor from the core is drawn in also and tends to fill the

impeller and vapor-lock it. At this point, the pressure to drive the highly spinning liquid upstream is nonexistent and the backflow ceases. The vapor core disappears and the impeller once more begins ingesting liquid, the process just described repeating itself at a very low frequency (as low as 1 to 6 Hz) and called cavitation surge[74]. It has been found possible to passively divert the backflowing liquid outward from the inlet passage at the impeller or inducer eye into a series of vaned passages surrounding the inlet pipe, the vanes deswirling the backflowing liquid and returning it to a point or annular port upstream. Properly designed, this "backflow recirculator" has completely eliminated all cavitation instabilities in inducers—over the full range of flow rate from shut-off to run-out. It was shown to work for some high-N_{ss} impellers to which it was applied[74]. Cavitation surge, however, is rarely seen in low-N_{ss} impellers and is usually completely avoided by running the pump at flow rates greater than minimum flow Q_{min} as established by one of the previous methods or by test.

b) Cavitation-related instabilities and pressure pulsations. At flow rates greater than Q_{min}, cavitation can cause or intensify pressure pulsations. Such instabilities are connected with the variety of cavity and bubble configurations that can exist over the range of flow rates and NPSH- or R-values. The nature and extent of cavitating flow within a pump has been studied extensively by visual observation. Figures 40 and 41 are laboratory photographs[61] of a sector of a boiler feed pump impeller eye, in which the suction sides of some of the blades are visible. These were taken with the aid of a bright flash that lasted for 1 μs. They can also be found in Ref. 24 of Section 2.1.3. Figure 40a shows the sheet cavity that exists at BEP flow rate and at an R-value of 2. Also observed at BEP—but at $R = 1$ (that is, NPSH = $NPSH_{3\%}$)—is the thick, extensive cavity of Figure 40b. This cavity extends from the blade leading edge to the throat formed by the leading edge of the following blade, and this same pattern exists on every blade. Most observers note that when this suction-side cavity reaches the next throat, the pressure rise or liquid head starts breaking down—which is what is recorded at this "3-percent-NPSH" point. Instabilities tend to be at a minimum at both of these relatively steady flow conditions.

Figure 41, on the other hand, displays highly unsteady cavity flows. Both photographs (A and B) were taken at the same half-flow condition at different instants—for $R = 2$. A similar sequence of three photographs at this condition appears in Section 12.5, and none of the three possesses a cavity pattern that resembles either of the others. The position of the somewhat smaller cloud in Figure 41b that has broken off the main cavity appears to be traveling toward the pressure-side (out of sight) of the next blade. Pressure-side cavitation erosion would be the result, and this accords with the findings in Section 2.1.3.

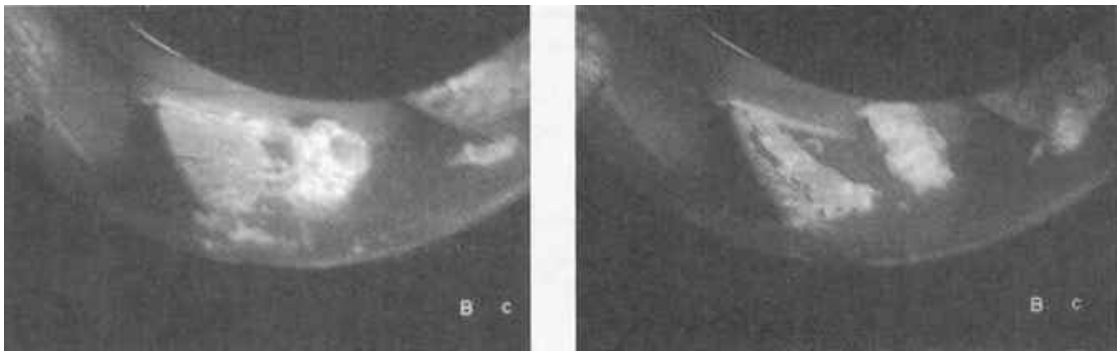
Pressure pulsations are associated with unsteady cavitation patterns, and plots of the amplitude and frequency of suction pressure pulsations show increasing frequency as R is increased—as would be expected as bubble size is reduced. The amplitude peaks at R



a. b.

FIGURE 40 Cavities on impeller blades at BEP flow rate: a) NPSH = 2 × $NPSH_{3\%}$; b) NPSH = $NPSH_{3\%}$ (Source: Flowserve Corporation)[61]

LIBERTY EXHIBIT 1017, Page 112



a. b.

FIGURE 41A and B Cavities on impeller blades at half the BEP flow rate: NPSH = 2 × $NPSH_{3\%}$ (Source: Flowserve Corporation)[61]

greater than 1—usually closer to 2. Elimination of these instabilities is best done by avoiding cavitation. This can be done by increasing *NPSHA* and optimizing the blade shape for minimum cavity activity[75]. To avoid the excessive pump and system oscillations that can occur, some users specify that a cavitation-flow visualization test be conducted and require that minimal or no cavities shall be observed.

c) Erosion due to cavitation and the prediction of the Life-NPSH. In the majority of cases cavitation is unavoidable, and the issue becomes the life of the component (usually the impeller) in resistance to attack by collapsing bubbles and larger cavities as they are swept out of the low-pressure regions near the blade leading edges. The pressure created at the point and instant of collapse is immense. Photographs of the erosive damage resulting from this activity can be found in Sections 2.1.3 and 12.5. The surface failure mechanism is one of fatigue due to repeated collapse of bubbles adjacent to the blade. This happens at a large number of closely spaced sites, the resulting erosion having a strongly pitted texture. The rate of erosive depth penetration into the surface of a venturi subject to bubble collapse was found by Knapp[76] to increase as the sixth power of velocity V at a constant cavitation number $k = 2(p_1 - p_v)/\rho V^2$. In other words, the erosion rate increased as the third power of $(p_1 - p_v)$ or NPSH at the inlet of the venturi, which means that the collapse pressure rises with NPSH, as is known from the Rayleigh bubble collapse theory.[77] The velocity V in Knapp's venturi corresponds in a pump to the maximum relative velocity W at inlet—which is conveniently represented by the impeller inlet tip speed $U_{t,1}$ as a criterion for damage rate—and τ corresponds to the cavitation number k. For a given impeller at constant Q/N and a constant value of τ, (or at a constant available suction specific speed,) the higher $U_{t,1}$ is, the greater the NPSH and the greater the damage rate. Also, as mentioned earlier, a higher value of $U_{t,1}$ implies a correspondingly greater U_2 and, therefore, greater pump pressure rise or head. Therefore, high-head pumps are more likely to suffer from cavitation erosion, making cavitation a "high-energy" pump phenomenon. High pressure-rise has already been shown to be a feature of high energy pumps through the definition of energy level in terms of classical stress loading (Figure 32).

Facing the reality of high-energy pump destruction due to cavitation erosion, Vlaming redefined the term "*NPSHR*" to mean $NPSH_{40,000\ \text{hrs.}}$; that is, the NPSH needed to limit the damage sufficiently so as to ensure an impeller life of 40,000 hours. He developed an empirical method for predicting the curve of this "damage-NPSH" versus flow rate for conventionally-designed impellers[78]. This method is defined in Table 17 and includes the inlet tip speed effect on the erosion rate. A value of the vaporization factor C_b that is less than unity applies to hot water and to other liquids such as hydrocarbons, which generate far less vapor volume when they cavitate than does cold water. (See the earlier discussion under NPSH *Effects* in the section on *Specific Speed and Optimum Geometry*.) (Rather than depend on theory for the API process pumps mentioned

TABLE 17 NPSH required for 40,000 hours life[77]

$$NPSH_R = NPSH_{SE} + f\left(\frac{Q}{Q_{BEP}}, \frac{Q_{BEP}}{Q_{SE}}, NPSH_{SE}\right)$$

where

$$NPSH_{SE} = C_a \cdot C_b \cdot C_c \cdot \left[(k_1 + k_2)\phi_e^2 + k_2\right] \cdot \frac{U_e^2}{2g}$$

and C_a = Specific Speed Effect (= 1 for $N_s \geq 1000$) ($\Omega_s \geq 0.366$)
C_b = Vaporization Effect [= 1 for cold water; 0.74 for 350°F (177°C) water]
C_c = Material Effect (= 1 for 12 Cr. Stainless Steels)
k_1 = 1.2

$$k_2 = 0.2334 + \begin{cases}\left[U_e\,(\text{ft/sec})/400\right]^4 \\ \left[U_e\,(\text{m/s})/128.3\right]^4\end{cases} = \begin{cases}\text{inlet tip} \\ \text{speed effect}\end{cases}$$

$$f = \begin{cases}\left[887\left(\frac{Q_{SE}}{Q_{BEP}} - \frac{Q}{Q_{BEP}}\right) + 893\left(\frac{Q_{SE}}{Q_{BEP}} - \frac{Q}{Q_{BEP}}\right)^2\right] \cdot X & \left\{\frac{Q}{Q_{SE}} \leq 1\right. \\ \left[2820\left(\frac{Q}{Q_{BEP}} - \frac{Q_{SE}}{Q_{BEP}}\right) + 6610\left(\frac{Q}{Q_{BEP}} - \frac{Q_{SE}}{Q_{BEP}}\right)^2\right] \cdot X & \left\{\frac{Q}{Q_{SE}} \geq 1\right.\end{cases}$$

and $X = \left(S^{1.105} - S\right)/1000$ where $S = \begin{cases}NPSH_{SE}\,(\text{ft}) \\ 3.2808 \times NPSH_{SE}\,(\text{m})\end{cases}$

earlier in connection with their minimum flow data, Heald and Palgrave quantified $NPSH_{40,000\ \text{hrs.}}$ in Figure 39b[71].)

Applied to the high-energy multistage pump suction stage of Figure 33 and Table 14, Vlaming's method yields the $NPSH_R$-values shown in Table 18 under the heading ϕ_e=0.3. These are plotted as the $NPSH_{40,000\ \text{hrs.}}$-curve on Figure 37. The blades of the pump are assumed to be set for zero incidence of the incoming flow to their camber lines at the BEP—called "shockless entry" and denoted by "SE." (Many designers make Q_{SE} somewhat larger than Q_{BEP} to achieve lower *NPSHR* at $Q > Q_{BEP}$. Also, Q_{SE} produces an even greater jump in the mean W at the leading edge than was shown in Figure 29 for the 2.2 degrees of mean positive incidence seen in Figure 26a. This is due to the blockage of the blade that is fully realized at this zero-incidence flow rate Q_{SE}. The impeller flow loss at this flow rate often causes Q_{BEP} to be about 10% less than Q_{SE}.) The column to the right in the table contains the results for the same method applied to the more common case for high-energy pump suction stages, namely $\phi_e = 0.25$ (and lower). For the same shaft diameter, flow rate and speed, $\phi_e = 0.25$ yields a larger eye diameter through Eq. 49; namely, 13.92 in. (353.6 mm) versus 13.37 in (339.6 mm) for the $\phi_e = 0.3$ case as shown in Figure 33. Moreover, that figure shows the inlet tip speed $U_{t,1}$ (U_e) to be 274 ft/sec (84 m/s), whereas for the larger-eye case the value is computed to be 286 ft/sec (87 m/s). As Table 18 reveals, this larger-eye impeller has a lower value of $NPSH_{3\%}$ (as computed from the correlations of Table 1), which is the reason for sizing large eyes. But Vlaming's method indicates that the smaller eye requires less "damage-NPSH" (R = 1.69) than does the larger eye (R = 2.06), even though the latter requires less "performance-NPSH" or $NPSH_{3\%}$. So, from both a minimum-flow and a cavitation damage standpoint, the advantage of a smaller eye for high energy levels is evident.

LIBERTY EXHIBIT 1017, Page 114

TABLE 18 *NPSHR* of high-energy pump suctions stages

A) NPSH Required to Maintain Head Rise: $NPSH_{3\%}$

$NPSH_{3\%}$, ft(m) (3% reduction in ΔH)	$\frac{Q}{Q_{BEP}}$	$NPSH_{3\%}$, ft(m) ϕ_e=0.3*	ϕ_e=0.25
$\tau_{3\%}$	[100]	0.2633	0.214
$k_1 = 1.69$, $k_2 = 0.102$ [Table (1)]	100	307(94)	271(83)
[Empirically Calculated]	150	1150(350)	1150(350)

B) NPSH Required to Limit Cavitation Damage: $NPSH_{40,000\ hrs.}$

$NPSH_{40,000\ hrs.}$ Life	$\frac{Q}{Q_{BEP}}$	$NPSH_R$, ft(m) ϕ_e=0.3*	ϕ_e=0.25
Vlaming's Empirical Method (for $Q_{SE} = Q_{BEP}$)	0.25	1081(329)	1174(358)
	0.50	840(256)	910(277)
	0.75	653(199)	705(215)
	0.90	566(173)	610(186)
$R = \frac{NPSH_{40,000\ hrs.}}{NPSH_{3\%}}$	1.00	519(158)	559(170)
	[1.00]	R=1.69	R=2.06
	1.10	687(209)	743(226)
	1.25	1058(322)	1148(350)
	1.50	1994(608)	2173(662)

*Values predicted for sample high-energy pump suction stage: $\phi_e = 0.3$; $\phi_e \leq 0.25$ widely typical of suction (1^{st}) stages.

d) Prediction of life for a given $NPSH_A$. The inverse of the foregoing problem is how to determine the life under cavitating conditions at a given value of available NPSH. Gülich found a connection between an observed length L_{cav} of the cavity trailing off the leading edge of the blade at BEP (Figure 40a) and the life of an impeller operating at this condition[79]. The resulting procedure is outlined in Table 19, beginning with the definition that the life is the time it takes for the erosion to penetrate through 75% of the blade (or wall) thickness. In the absence of a cavitation-visualizing test, L_{cav} can be estimated as suggested by the last two formulas in Table 19[75]. Critical to this estimate is the assumed value of the "inception-NPSH" or τ_i. For conventionally designed impeller blades, $\tau_i \approx 1$ at the BEP, whereas aerodynamically shaped blades that minimize the local reduction of static pressure have been produced with $\tau_i < 0.5$ at the BEP[75,80]. The life computations of Table 20 follow from application of the method of Table 19 to the sample suction stage of Figure 33 for $\tau_i = 1$ and 0.5. Higher values of τ_i apply for $Q \neq Q_{BEP}$—as might be expected from the shape of Vlaming's $NPSH_{40,000\ hrs.}$-curve in Figure 37 and the fact that the local pressure reduction in the leading-edge region increases with incidence.

LIBERTY EXHIBIT 1017, Page 115

TABLE 19 Prediction of life under cavitating conditions

Life = the minimum of ($Life_{s.s.}$, $Life_{p.s.}$), where s.s.= suction side of blade;

and p.s. = pressure side of blade.

And where Life = 0.75 x t/MDPR, where t = blade thickness, mm;

MDPR=mean depth of penetration rate, mm/hour.

$$MDPR = \left[C \times (L_{cav}/10)^n \times \left(\tau_A - \phi_e^2\right)^3 \times U_e^6 \times \rho_L^3 \times A \right] \Big/ \left[8 \times F_{mat} \times (TS)^2 \right] \text{ mm/h}$$

Where C = 8.28 E-06 (s.s.), 396 E-06 (p.s.); and n = 2.83 (s.s.), 2.6 (p.s.);

τ = $NPSH/\left(U_e^2/2g\right)$; dimension less

U_e is blade inlet tip speed in m/s

ϕ_e = $V_{m,1}/U_e$, where $V_{m,1}$ = average axial inlet velocity, (typically ϕ_e = 0.25);

ρ_L = 1000 × sp. gravity of the liquid; A = 1 for cold water, 0.705 for 350° F (177° C) water;

F_{mat} = 1 for martensitic: stainless steel, 1.7 for austenitic stainless steel;

TS = tensile strength in Pa [= 860,000,000 (= 125,000 psi) for 13 Cr and
= 552,000,000 (= 80,000 psi) for 18 Cr, 8 Ni.]

$$L_{cav} \approx (\pi \times D_e/n_b) \times \left\{1 - \left[(\tau_A - \tau_{3\%})/(\tau_i - \tau_{3\%})\right]^{1/3}\right\} \text{ if } \tau_A < \tau_i \text{ (mm)}$$

$L_{cav} = 0$ if $\tau_A > \tau_i$

From this and the results of Table 20, it is evident that improvements to conventional blade-design practice are essential if life is to exceed half a year. Further, this life calculation method is based on the existence of a sheet cavity like that of Figure 40a; and the disordered cavity structures of Figure 41, which happen in the presence of recirculation, are not addressed. Low-flow cavitation damage is generally more severe, and is described in Section 2.1.3. Moreover, corrosion can play a role in cavitation-related erosive activity, an effect that was also addressed in Gülich's work.[79] Nevertheless, the ability to compute erosive behavior—even at the BEP—allows one to evaluate design improvements and provides a good idea of the life that can be expected under normal operating conditions.

Obviously, if the available NPSH is greater than the inception-NPSH (that is, $\tau_A > \tau_i$), there is no bubble activity of any kind, and at Q_{BEP} the cavity length $L_{cav} = 0$. An illustration of what can be achieved in this regard is presented in Figures 24 and 25 of Section 12.5, which are the "before" and "after" photographs of the model impeller blades for the first stage of a 24,000 hp (18 MW) pipeline pump. Quasi-three dimensional analysis of the blade pressure loading led to changes in shape that eliminated the cavities[53,75]. This complete absence of cavitation is becoming the desired objective for the design and application of new and upgraded multistage high-energy pump suction stages. This approach eliminates both the erratic mechanical behavior that occurs in response to unsteady cavity patterns and the erosion due to bubble collapse; thereby substantially increasing the life and reliability of such machines[81].

LIBERTY EXHIBIT 1017, Page 116

TABLE 20 Life of high-energy pump suction stage

A) Pump data for computing life (at the B.E.P. of 20,000 gpm)

- $NPSH_{3\%}$ = 307 ft (94 m); thus, $\tau_{3\%}$ = 0.263
- NPSHA = 519 ft (158 m); thus, τ_A = 0.444
- t_{blade} = 0.42 in (10.7 m); thus, F_{mat} = 1 (13 Cr martensitic stainless steel)
- Suction-side cavitation in 350°F boiler feedwater, for which A = 0.705
- Inlet flow coefficient ϕ_e = 0.3; U_e = 274.2 ft/sec (83.57 m/s); $U_e^2/2g$ = 1168 ft (356 m)

B) Results for inception occurring at $NPSH_i$ = blade inlet tip speed head and half that $NPSH_i$.

a) τ_i = 1.0 = 3.8 × $\tau_{3\%}$	b) τ_i = 0.5 = 1.9 × $\tau_{3\%}$
$NPSH_i$ = 1168 ft (356 m)	$NPSH_i$ = 584 ft (178 m)
Lcav = 57.0 mm	13.1 mm
MDPR = 0.0014482 mm/h	0.0000226 mm/h
Life = 5541 h = 7.6 months	355,000 h = 40 years

C) Sample Life Calculation * {High Energy Pump Suction Stage

$$L_{cav} = 25.4 \times \frac{\pi \times 13.37}{7} \times \left[1 - \left(\frac{0.444 - 0.263}{1 - 0.263}\right)^{1/3}\right] = \underline{57.0 \text{ mm}}$$

$$\text{MDPR} = \frac{8.28 \times 10^{-6} \times \left(\frac{57}{10}\right)^{2.83} \times \left(0.444 - \overline{0.3}^2\right)^3 \times (83.57)^6 \times (890)^3 \times 0.705}{8 \times 1 \times \left(860 \times 10^6\right)^2}$$

$$= 0.0014482 \text{ mm/h} \left(\times 8760 \frac{\text{h}}{\text{year}} = 12.7 \text{ mm/y}\right)$$

Life = 0.75 × 10.7/0.0014482 = 5541 h

= 7.6 months

REFERENCES

1. Jennings, G. P., and Meade, L. P. "Determination of Pump Efficiencies from Fluid Temperature Rise." Presented at the 7th Annual Spring Pipeline Conference, Houston, Texas, May 14, 1956, under the auspices of the American Petroleum Institute's *Division of Transportation.* Published in the Division's Vol. 36 [5] 1956.
2. Cooper, P., and Reshotko, E. "Turbulent Flow Between a Rotating Disk and a Parallel Wall." *AIAA Journal.* Volume 13, No. 5, May 1975, pp. 573–578.
3. Sabersky, R., and Acosta, A. J. *Fluid Flow*, Macmillan, p. 76 (1966).
4. Sloteman, D. P., Robertson, D. A., and Margolin, L. "Demonstration of Cavitation Life Extension for Suction-Stage Impellers in High Energy Pumps." *Proceedings of the 21st International Pump Symposium*, Texas A&M University, Mar. 2004, pp. 103–115.
5. Stepanoff, A. J. *Centrifugal and Axial Flow Pumps.* 2nd ed. Krieger Publishing, Malabar, FL, 1957.
6. Iversen, H. W. "Performance of the Periphery Pump." *Transactions of the ASME.* Vol. 77, Jan. 1955, pp. 15–28.
7. Anderson, H. H. "Prediction of Head, Quantity and Efficiency in Pumps—The Area Ratio Principle." *Performance Prediction of Centrifugal Pumps and Compressors.* ASME, 1980, pp. 201–211.
8. American National Standard for Centrifugal Pumps for Design and Application, ANSI/HI 1.3-2000, Section 1.3.4.1.11-14, Hydraulic Institute, Parsippany, NJ, www.pumps.org.
9. Cooper, P. "Analysis of Single- and Two-Phase Flows in Turbopump Inducers." *Transactions of the ASME, Journal of Engineering for Power.* Vol. 89, Series A, Oct. 1967, pp. 577–588.
10. Turpin, J. L., Lea, J. F., and Bearden J. L. "Gas-Liquid Flow Through Centrifugal Pumps—Correlation of Data." *Proceedings of the Third International Pump Symposium*, Texas A&M University, 1986, pp. 13–20.
11. Runstadler, P. W., Jr., and Dolan, F. X. "Two-Phase Flow, Pump Data for a Scale Model NSSS Pump." *Polyphase Flow in Turbomachinery*, ASME, 1978, pp. 65–77.
12. Cooper, P., and others. "Tutorial on Multiphase Gas-Liquid Pumping." *Proceedings of the Thirteenth International Pump Users Symposium*, Texas A&M University, Mar. 1996, pp. 159–174.
13. Kasztejna, P. J., and Cooper, P. "Hydraulic Development of Centrifugal Pumps for Coal Slurry Service." *Proceedings of the Eighth International Symposium on Coal Slurry Fuels Preparation and Utilization.* U.S. Dept. of Energy, May 1986.
14. Gongwer, C. A. *Transactions of the ASME.* Vol. 63, Jan. 1941, pp. 29–40.
15. Stripling, L. B., and Acosta, A. J. "Cavitation in Turbopumps." Parts 1 and 2, *Transactions of the ASME.* Series D, 1961.
16. Lazarkiewicz, S., and Troskolanski, A. T. *Impeller Pumps.* Pergamon Press, 1965.
17. Cooper, P. "Application of Pressure and Velocity Criteria to the Design of a Centrifugal-Pump Impeller and Inlet." *Transactions of the ASME.* Series A, Apr. 1964, pp. 181–190.
18. Busemann, A. "Das Förderhohenverhaltniss Radialer Kreiselpumpen mit Logarithmischspiraligen Schaufeln." *Zeitschrift für Angewandte Mathematik und Mechanik.* Vol. 8, Oct. 1928, pp. 372–384.
19. Wiesner, F. J. "A Review of Slip Factors for Centrifugal Pumps." *Transactions of the ASME.* Series A, Oct. 1967, pp. 558–572.
20. Pfleiderer, C. *Die Kreiselpumpen für Flüssigkeiten und Gase.* 5te Auflage, Springer-Verlag, 1961.
21. Dicmas, J. L. *Vertical Turbine, Mixed Flow, and Propeller Pumps.* McGraw-Hill, 1987.

22. Stanitz, J. D., and Prian, V. D. "A Rapid Approximate Method for Determining the Velocity Distribution on Impeller Blades of Centrifugal Compressors." TN 2421, NACA, July 1951.

23. Lieblein, S. "Experimental Flow in Two-Dimensional Cascades." Chap. VI in *Aerodynamic Design of Axial-Flow Compressors*. SP-36, NASA, 1965, pp. 202–205.

24. Guinzburg, A., and others. "Emerging Sewage Pump Design Requirements." *1997 ASME Fluids Engineering Division Summer Meeting*. Paper FEDSM97-3325, June 1997.

25. Worster, R. C. "The Flow in Volutes and Its Effect on Centrifugal Pump Performance." *Proceedings of the Institution of Mechanical Engineers*. Vol. 177, No. 31, 1963.

26. Lorett, J. A., and Gopalakrishnan, S. "Interaction Between Impeller and Volute of Pumps at Off-Design Conditions." *Transactions of the ASME, Journal of Fluids Engineering*. Vol. 108, Mar. 1986, pp. 12–18.

27. Miller, D. S. *Internal Flow Systems*, BHRA Fluid Engineering, 1978.

28. Japikse, D. "A Critical Evaluation of Stall Concepts for Centrifugal Compressors and Pumps—Studies in Component Performance, Part 7." In *Stability, Stall and Surge in Compressors and Pumps*. FED—Vol. 19, ASME, Dec. 1984, pp. 1–10.

29. Kovats, A. "Diffusers of Multistage Centrifugal Pumps." In *Return Passages of Multi-Stage Turbomachinery*. FED—Vol. 3, ASME, June 1983, pp. 61–66.

30. Reneau, L. R., and others. "Performance of Straight, Two-Dimensional Diffusers." *Transactions of the ASME*. Series D, Vol. 89, 1967, pp. 141–150.

31. Fox, R. W., and Kline, S. J. "Flow Regimes in Curved, Subsonic Diffusers." *Transactions of the ASME*. Series D, Vol. 84, 1962, pp. 303–316.

32. Sagi, C. J, and Johnston, J. P. "The Design and Performance of Two-Dimensional, Curved Diffusers." *Transactions of the ASME*. Series D, Vol. 89, 1967, pp. 715–731.

33. Bolleter, U. "Blade Passage Tones of Centrifugal Pumps." *Vibrations*. Vol. 4, No. 3, Sep. 1988, pp. 8–13.

34. Nykorowytsch, P., Ed. *Return Passages of Multi-Stage Turbomachinery*. FED—Vol. 3, ASME, June 1983.

35. Hill, P. G., and Peterson, C. R. *Mechanics and Thermodynamics of Propulsion*. Addison-Wesley, 1965, pp. 238–280.

36. Stepanoff, A. J. "Centrifugal Pump Performance as a Function of Specific Speed." *Transactions of the ASME*. Aug. 1943, pp. 629–647.

37. Weissgerber, C., and Carter, A. F. "Comparison of Hydraulic Performance Predictions and Test Data for a Range of Pumps." *Performance Prediction of Centrifugal Pumps and Compressors*. ASME, Mar. 1980, pp. 219–226.

38. Streeter, V. L., ed. *Handbook of Fluid Dynamics*. McGraw-Hill, 1961, p. 3–23.

39. Wood, G. M., Welna H., and Lamers, R. P. "Tip–Clearance Effects in Centrifugal Pumps." Paper No. 64–WA/FE–17, ASME, Nov. 1964.

40. Stepanoff, A. J. "Pumping Solid–Liquid Mixtures." Paper No. 63–WA–102, ASME, Nov. 1963.

41. Katsanis, T. "Quasi-Three-Dimensional Full Analysis in Turbomachines: A Tool for Blade Design." In *Numerical Simulations in Turbomachinery*, FED—Vol. 120, ASME, 1991, pp. 57–64.

42. Katsanis, T. "Fortran Program for Calculating Transonic Velocities on a Blade–to–Blade Stream Surface of a Turbomachine." NASA TN D–5427, 1969.

43. Daily, J. W., and Nece, R. E. "Chamber Dimension Effects on Induced Flow and Frictional Resistance of Enclosed Rotating Disks." *Transactions of the ASME*, Series D, Vol. 82, Mar. 1960, pp. 217–232.

LIBERTY EXHIBIT 1017, Page 119

44. Nece, R. E., and Daily, J. W. "Roughness Effects on Frictional Resistance of Enclosed Rotating Disks." *Transactions of the ASME.* Series D, Vol. 82, Sep. 1960, pp. 553–562.

45. Japikse, D., Marscher, W. D., and Furst, R. B. *Centrifugal Pump Design and Performance.* Concepts, ETI, Inc., Wilder, Vermont, 1997.

46. Westra, R. W., Kruyt, N. P., and Hoeijmakerws, H. W. M. "An Inverse-Design Method for Centrifugal Pump Impellers." *2005 ASME Fluids Engineering Division Summer Meeting and Exhibition*, Paper FEDSM2005–77283, June 2005.

47. Demeulanaere, A., and others. "Design and Optimization of an Industrial Pump: application of Genetic Algorithms and Neural Network." *2005 ASME Fluids Engineering Division Summer Meeting and Exhibition*, Paper FEDSM2005–77487, June 2005.

48. Graf, E. "Analysis of Centrifugal Impeller BEP and Recirculating Flows: Comparison of Quasi-3D and Navier-Stokes Solutions." *Pumping Machinery—1993.* FED—Vol. 154, ASME, 1993, pp. 235–245.

49. Denus, K., and others. "A Study in Design and CFD Analysis of a Mixed Flow Pump Impeller." *1999 ASME Fluids Engineering Division Summer Meeting*, Paper FEDSM99–6858, July 1999.

50. Jimbo, H. "Investigation of the Interaction of Windage and Leakage Phenomena in a Centrifugal Compressor." Paper No. 56–A–47, ASME, Nov. 1956.

51. Keathly, W. C., Due, H. F., and Comolli, C. R. "A Study of Pressure Prediction Methods for Radial Flow Impellers." Final Report on NASA Contract NAS8–5442, PWA FR–952, Pratt & Whitney Aircraft, W. Palm Beach, Florida, April 1964.

52. Greitzer, E. M. "The Stability of Pumping Systems." *Transactions of the ASME, Journal of Fluids Engineering*, Vol. 103, June, 1981, pp. 193–242.

53. Cooper, P. "Perspective: The New Face of R&D—A Case Study of the Pump Industry." *Transactions of the ASME, Journal of Fluids Engineering*, Vol. 118, Dec. 1996, pp. 654–664.

54. Rothe, P. H., and Runstadler, P. W., Jr. "First–Order Pump Surge Behavior." Paper No. 77–WA/FE–12, ASME, Nov. 1977.

55. Brennen, C., and Acosta, A. J. "The Dynamic Transfer Function for a Cavitating Inducer." *Transactions of the ASME, Journal of Fluids Engineering.* Vol. 98, 1976, pp. 182–191.

56. Schlichting, H. *Boundary Layer Theory.* 4th ed. McGraw-Hill, 1960.

57. "Advanced Class Boiler Feed Pumps." *Proceedings of the Institution of Mechanical Engineers.* Vol. 184, Part 3N, 1970.

58. Gopalakrishnan, S. "Pump Research & Development—Past, Present, and Future: An American Perspective." *1997 ASME Fluids Engineering Division Summer Meeting.* Paper FEDSM97–3387, June 1997.

59. Bolleter, U., Frei, A., and Florjancic, D. "Predicting and Improving the Dynamic Behavior of Multistage High Performance Pumps." *Proceedings of the First International Pump Symposium.* Texas A&M University, College Station Texas, May 1984, pp. 1–8.

60. Iino, T. "Potential Interaction Between a Centrifugal Pump Impeller and a Vaned Diffuser." *Fluid/Structure Interactions in Turbomachinery.* ASME, Nov. 1981, pp. 63–69.

61. Cooper, P. "Hydraulics and Cavitation." *Symposium Proceedings: Power Plant Pumps.* M. L. Adams, ed. EPRI CS–5857, June 1988, pp. 4–109 to 4–149.

62. Sutton, G. P. *Rocket Propulsion Elements.* 6th ed., Wiley, 1992.

63. "Liquid Rocket Engine Centrifugal Flow Turbopumps." Report SP–8109 of the series entitled *NASA Space Vehicle Design Criteria (Chemical Propulsion).* NASA, 1973.

64. "Turbopump Systems for Liquid Rocket Engines." Report SP–8107 of the series entitled *NASA Space Vehicle Design Criteria (Chemical Propulsion).* NASA, 1975.

LIBERTY EXHIBIT 1017, Page 120

65. Makay, E., Cooper, P., Sloteman, D. P., and Gibson, R. "Investigation of Pressure Pulsations Arising from Impeller/Diffuser Interaction in a Large Centrifugal Pump." Proceedings: Rotating Machinery Conference and Exposition, ASME, Vol. 1, 1993.

66. Fischer, K., and Thoma, D. "Investigation of the Flow Conditions in a Centrifugal Pump." *Transactions of the ASME.* Vol. 54, 1932, pp. 143–155.

67. Fraser, W. H. "Recirculation in Centrifugal Pumps." *Materials of Construction of Fluid Machinery and Their Relationship to Design and Performance.* ASME, Nov. 1981, pp. 65–86.

68. Iino, T., Sato, H., and Miyashiro, H. "Hydraulic Axial Thrust in Multistage Centrifugal Pumps." *Transactions of the ASME, Journal of Fluids Engineering.* Vol. 102, Mar. 1980, pp. 64–69.

69. Makay, E., and Barrett, J. A. "Changes in Hydraulic Component Geometries Greatly Increased Power Plant Availability and Reduced Maintenance Cost: Case Histories." *Proceedings of the First International Pump Symposium.* Texas A&M University, College Station Texas, May 1984, pp. 85–97.

70. Gopalakrishnan, S. "A New Method for Computing Minimum Flow." *Proceedings of the Fifth International Pump Users Symposium.* Texas A&M University, College Station Texas, May 1988, pp. 41–47.

71. Heald, C. C., and Palgrave, R. "Backflow Control Improves Pump Performance." *Oil and Gas Journal.* Feb. 25, 1985, pp. 96–105.

72. Hallam, J. L. "Centrifugal Pumps: Which Suction-Specific Speeds Are Acceptable." *Hydrocarbon Processing,* Apr. 1982.

73. Bloch, H. P., and Budris, A. R. *Pump User's Handbook: Life Extension.* Marcel Dekker, 2004, pp. 93–98.

74. Sloteman, D. P., Cooper, P., and Dussourd, J. L. "Control of Backflow at the Inlets of Centrifugal Pumps and Inducers." *Proceedings of the First International Pump Symposium.* Texas A&M University, College Station Texas, May 1984, pp. 9–22.

75. Cooper, P., Sloteman, D. P., Graf, E., and Vlaming, D. J. "Elimination of Cavitation-Related Instabilities and Damage in High-Energy Pump Impellers." *Proceedings of the Eighth International Pump Users Symposium.* Texas A&M University, 1991, pp. 3–19.

76. Knapp, R. T. "Recent Investigations of the Mechanics of Cavitation and Cavitation Damage." *Transactions of the ASME,* Oct. 1955, pp. 1045–1054.

77. Rayleigh, Lord: "On the pressure developed in a liquid during the collapse of a spherical cavity." *Phil. Mag.,* Vol. 34, 1917, pp. 94–98.

78. Vlaming, D. J. "Optimum Impeller Inlet Geometry for Minimum NPSH Requirements for Centrifugal Pumps." *Pumping Machinery—1989.* ASME, July 1989, pp. 25–29.

79. Gülich, J. F. *Guidelines for Prevention of Cavitation in Centrifugal Feedpumps.* EPRI CS-6398, 1989.

80. Sloteman, D. P., Cooper, P., and Graf, E. "Design of High-Energy Pump Impellers to Avoid Cavitation Instabilities and Damage." EPRI Power Plant Pumps Symposium, Tampa FL, June 1991.

81. Sloteman, D. P., and others. "Experimental Evaluation of High-Energy Pump Improvements Including Effects of Upstream Piping." *Proceedings of the Twelfth International Pump Users Symposium.* Texas A&M University, Mar. 1995, pp. 97–110.

2.1.2
CFD ANALYSIS OF FLOW AND PERFORMANCE

PAUL COOPER
ASHVIN HOSANGADI

INTRODUCTION

Until relatively recently, prediction of flow behavior in pumps and the systems in which they operate has generally been limited to a practical combination of (a) obtaining, applying, and scaling experimental data on components and models, (b) modifying components according to rules that were developed for specific geometries but were often extrapolated to others, and (c) one- and two-dimensional computations by which designs of components were made and which could be used to predict flows and performance in a reasonable period of time. With respect to the pumps themselves, in Section 2.1.1, "Centrifugal Pump Theory," fluid dynamical analysis of the flow through the internal passages is demonstrated as the means for predicting the performance of pumps. Formulas are given for energy transfer, static pressure development, and flow losses, which can be applied one dimensionally to evaluate the effectiveness of the design of the impeller and the accompanying stationary inlet, volute, diffuser—and the crossover passages of multistage pumps. In several instances, one-dimensional (1D) analysis is found to be inadequate—as for example, in finding the distribution of velocity in the approaching fluid along the leading edge of an impeller. Here, the need for a two- or three-dimensional solution of the basic fluid dynamical equations of motion is called for, which now is more and more accurately and rapidly achieved on a digital computer or cluster(s) of computers as ever-increasing computing power has become available. Hence the term "Computational Fluid Dynamics" or "CFD" has become commonplace in the quest for understanding the flow behavior and patterns as needed to achieve optimum design and matching of flow elements. An accurate solution of the flow fields in the components from the inlet to the discharge port of the machine also yields the overall "hydraulic" performance; namely, head, power, efficiency—for both single- and multiphase flows. Moreover, as described in Chap. 13, flows in system

LIBERTY EXHIBIT 1017, Page 122

elements, especially intake sumps and suction piping, play a crucial role in the behavior of both pump and system. The design and deployment of such elements and especially the combinations of them that can include the pump as well are among the increasing list of CFD applications.

Yet, all this computational capability is not a substitute for the experienced and creative designer, who must provide the hydraulic geometries and fluid systems to be evaluated and interpret the results. For example, the traditional approach to creating and optimizing the gamut of highly developed impeller shapes versus specific speed—which often produce overall pump efficiencies in excess of 90% as seen in the chart efficiencies of this book—had been accomplished by the middle of the last century and well before digital computers came to be employed in the design and optimization process. Intuitive fluid dynamical reasoning had been exercised by these designers as they assessed both theoretical and experimental results. The former were the output of flow analyses of varying degrees of complexity from 1D to quasi-three dimensional (Q3D—combinations of two-dimensional [2D] solutions) that were needed in order to apply the diffusion limits per NACA research as in Figure 17 and Eqs. 57 to 59 in Section 2.1.1. This traditional approach enabled especially the development of highly efficient impellers, as well as imaginative solutions to new design and performance challenges.[1,2,3]

Early CFD work on pumps focused on the steady flow field within a single hydraulic component, usually the impeller; the objective being to provide recognizable flow data for judging it. Graf demonstrated that several of the known and observed flow patterns within impellers could be reproduced via CFD.[4] Used to judging impellers in terms of the Q3D-computed distributions of relative velocity W just outside the boundary layers on the blades, he presented in this same early work the equivalent static pressure loadings on the blade surfaces. Pressures were readily available to him on the actual blade surfaces; whereas $W = 0$ on these surfaces, because CFD solutions include the boundary layers or approximations for them.[4] Substantial improvements to inlets, diffusers, and multistage pump crossovers are often more readily identified than for the more highly developed impellers.[5,6] Indeed, many shortcomings of established geometries remain, despite the impressive achievements of generations of past designers. Even the best of these geometries can be and are being further improved. Interactive optimization of the design is thus a major function of CFD in the hydraulic development process.

Accurate prediction of overall performance has been less forthcoming, mainly because of limitations on treatment of the losses accompanying diffusing and separated flows that are imposed by inadequate computational power. As demonstrated by Gülich et al, the ideal or "theoretical" head H_i can be quite accurately calculated at flow rates near the best efficiency point (BEP) with minimum CFD power by present standards, because it is connected primarily with flow directions and velocities in the impeller and less with the details of the loss calculations therein.[7] The most accurate CFD prediction of overall pump developed head requires analyzing all hydraulic components and in turn correctly modeling the interfaces between rotating and stationary components. For example, the flow distortions produced by an asymmetric inlet passage produce losses in the impeller it feeds,[5] and an unsteady CFD solution of these coupled flow elements should correctly model these losses.

The computing power required for an unsteady solution of the entire pump has been the limiting factor for many users, as it generally requires multiple processors operating in parallel. Approximations to get around this limitation have been made by restricting the analysis to steady-flow computations—often in a single passage—and, at the interfaces between rotating and fixed components, by (a) using circumferential averages—but not spanwise hub-to-shroud averages—of the quantities being calculated or (b) freezing the impeller at a selected position relative to the fixed adjacent components and doing no such averaging. Neither (a) nor (b) prevents simulation of flows across the interfaces in both the forward and reverse directions as would happen at flow rates below BEP; however (b) preserves variations in all directions. In one typical case, the frozen rotor approach (b) predicted the head at shutoff and at flow rates from 80 to 120% of BEP within 5% of the measured head on test.[8] In another example, similarly accurate results for complete stages via the circumferential-averaging approach (a) were reported for flow rates in the neighborhood of the BEP only.[9]

LIBERTY EXHIBIT 1017, Page 123

With sufficient computing power, improvements in CFD-predicted performance are possible at all flow rates, together with the influence on this performance of rotating stall and cavitation and other multiphase flows. This includes the thermodynamic effects on vaporization and other gases that may be present in the liquid. Finally, the inherently unsteady flow in the meshing rotors of screw pumps and other rotary positive displacement pumps (Sections 3.7 and 3.8) has been investigated by CFD;[10] however, this section concentrates on the use of CFD for flows in rotodynamic pumps and inducers and particularly for understanding the off-design behavior of these machines. From the attendant description of the concept and methods of implementing it for pump internals, readers will readily appreciate the fact that CFD is equally applicable to all flow-related system elements, including intake sumps and suction piping configurations.

NOMENCLATURE

NOTE: See the Nomenclature for Section 2.1.1 for most of the symbols used in this section. Additional definitions are presented here for further clarity and convenience.

k = turbulent kinetic energy $= \frac{1}{2}\left(\overline{w'^2_r} + \overline{w'^2_\theta} + \overline{w'^2_z}\right)$ where each overbar represents a time average

t = time

u = generic velocity component

W = local mean value of fluid velocity relative to the rotating impeller, ft/s (m/s). For stationary components ($\Omega = 0$), substitute the absolute velocity V for W in the equations presented here.

w' = fluctuating component of the fluid relative velocity due to turbulence, ft/s (m/s). For stationary components ($\Omega = 0$), substitute the absolute velocity v' for w' in the equations presented here.

τ = cavitation coefficient for impeller or inducer ($= 2g \times NPSH/U_e^2$ or $2g \times NPSH/U_{1,t}^2$)

τ_{xy} = shear stress in the x-direction due to velocity variation in the y-direction

$\mu_l = \mu$ = the absolute viscosity as defined in Section 2.1.1. This quantity is more precisely known as the molecular or "laminar" viscosity.

$\mu_T = \mu_t$ = the turbulent or "eddy" viscosity, which has the same units as μ_l or μ

ε = turbulent energy dissipation rate

ϕ = flow coefficient $\left(= \overline{V_{m,1}}/U_e\right)$

ω = fluid vorticity

CFD BASICS

The Reynolds-Averaged Navier-Stokes Equations The basis for all CFD analyses are the Navier-Stokes equations. These are the equations of general, unsteady motion of a compressible viscous fluid, which relate pressure to the instantaneous velocity field. They are derived in fluid mechanics texts by applying Newton's second law, which relates forces and accelerations to those occurring in the three spatial dimensions within the fluid. For example, Schlichting does this by developing expressions for the normal and shear stresses on a fluid element and then invoking Stokes' hypothesis that these stresses are proportional to the rate of strain or shear, which is the case for a Newtonian fluid.[11] The simplest form of this hypothesis is the expression for shear stress τ_{xy} in the fluid in

LIBERTY EXHIBIT 1017, Page 124

the gap of width δ between two plates, one of these plates moving steadily at velocity U in the x-direction parallel to the other (fixed) plate:

$$\tau_{xy} = \mu\frac{U}{\delta} \quad \text{or, locally in the fluid, } \tau_{xy} = \mu\frac{du}{dy} \tag{1}$$

where μ is the absolute viscosity or constant of proportionality between the stress and the rate of strain du/dy, u is the local fluid velocity, and y is distance in the direction normal to the fixed plate. In this case du/dy is equal to U/δ throughout the gap. The fluid in this illustration is assumed to be laminar, and for this case the Navier-Stokes equations reduce to the following single expression:

$$\mu\frac{d^2u}{dy^2} = 0 \tag{2}$$

The solution of Eq. 2 is the expected straight-line velocity distribution:

$$u = \frac{U}{\delta}y \tag{3}$$

There are many other solutions in the literature for laminar flows. However, when the flow is turbulent, the quantities involved are fluctuating, and the flow field is best understood in terms of the averages of the velocity components, pressure, and density; where the instantaneous value of any velocity component u is represented as the sum of an time-averaged portion $\overline{u}$ and a fluctuating portion u'; namely,

$$u = \overline{u} + u' \tag{4}$$

When this expression for each of the velocity components (and similarly for the pressure and density) is substituted into the Navier-Stokes equations, one obtains what are called the *Reynolds-Averaged Navier-Stokes* equations, and so CFD specialists speak of *RANS* codes. For illustrative purposes and the general interest of pump engineers, it is convenient to specialize these *RANS* equations to the incompressible flow case and to render them in terms of the relative velocity componenets, W_r, W_θ, and W_z in the system of cylindrical coordinates r, θ, and z that are commonly used for analysis within the rotating frame of reference of an impeller. Four equations are involved here, the assumption being that the absolute viscosity μ is constant. The first three are Newton's second law or the momentum equation in each of the three coordinate directions, and the fourth is the continuity equation.

Momentum in the r-direction:

$$\rho\left(\frac{\partial W_r}{\partial t} + W_r\frac{\partial W_r}{\partial r} + \frac{W_\theta}{r}\frac{\partial W_r}{\partial \theta} - \frac{W_\theta^2}{r} + W_z\frac{\partial W_r}{\partial z}\right) = \rho\Omega^2 r + 2\rho\Omega W_\theta - \frac{\partial p}{\partial r} + \frac{1}{r}\frac{\partial}{\partial r}\left(\mu r\frac{\partial W_r}{\partial r} - \rho r\overline{w'^2_r}\right)$$
$$- \frac{1}{r}\left(\mu\frac{W_r}{r} - \rho\overline{w'^2_\theta}\right) + \frac{1}{r}\frac{\partial}{\partial \theta}\left(\frac{\mu}{r}\frac{\partial W_r}{\partial \theta} - \rho\overline{w'_r w'_\theta}\right) + \frac{\partial}{\partial z}\left(\mu\frac{\partial W_r}{\partial z} - \rho\overline{w'_r w'_z}\right) - \frac{2\mu}{r^2}\frac{\partial W_\theta}{\partial \theta} \tag{5}$$

Momentum in the θ-direction:

$$\rho\left(\frac{\partial W_\theta}{\partial t} + W_r\frac{\partial W_\theta}{\partial r} + \frac{W_\theta}{r}\frac{\partial W_\theta}{\partial \theta} - \frac{W_r W_\theta}{r} + W_z\frac{\partial W_\theta}{\partial z}\right) = -2\rho\Omega W_r - \frac{1}{r}\frac{\partial p}{\partial \theta} + \frac{1}{r}\frac{\partial}{\partial r}\left(\mu r\frac{\partial W_\theta}{\partial r} - \rho r\overline{w'_\theta w'_r}\right)$$
$$- \frac{1}{r}\left(\mu\frac{W_\theta}{r} + \rho\overline{w'_\theta w'_r}\right) + \frac{1}{r}\frac{\partial}{\partial \theta}\left(\frac{\mu}{r}\frac{\partial W_\theta}{\partial \theta} - \rho\overline{w'^2_\theta}\right) + \frac{\partial}{\partial z}\left(\mu\frac{\partial W_\theta}{\partial z} - \rho\overline{w'_\theta w'_z}\right) + \frac{2\mu}{r^2}\frac{\partial W_r}{\partial \theta} \tag{6}$$

LIBERTY EXHIBIT 1017, Page 125

Momentum in the z-direction:

$$\rho\left(\frac{\partial W_z}{\partial t} + W_r\frac{\partial W_z}{\partial r} + \frac{W_\theta}{r}\frac{\partial W_z}{\partial \theta} + W_z\frac{\partial W_z}{\partial z}\right) = -\frac{\partial p}{\partial z} + \frac{1}{r}\frac{\partial}{\partial r}\left(\mu r\frac{\partial W_z}{\partial r} - \rho r\overline{w_z' w_r'}\right) \tag{7}$$

$$+ \frac{1}{r}\frac{\partial}{\partial \theta}\left(\frac{\mu}{r}\frac{\partial W_z}{\partial \theta} - \rho\overline{w_z' w_\theta'}\right) + \frac{\partial}{\partial z}\left(\mu\frac{\partial W_z}{\partial z} - \rho\overline{w_z'^2}\right)$$

Continuity:

$$\frac{1}{r}\frac{\partial(rW_r)}{\partial r} + \frac{1}{r}\frac{\partial W_\theta}{\partial \theta} + \frac{\partial W_z}{\partial z} = 0 \tag{8}$$

On the left-hand side of Eqs. 5, 6, and 7 appear the fluid acceleration terms—including the unsteady terms (time derivatives) that are evaluated in unsteady CFD solutions of these equations. Because these equations apply to a reference frame rotating at angular speed Ω, the centrifugal and Coriolis terms $\rho\Omega^2 r$ and $2\rho\Omega W_\theta$ appear on the right-hand side of Eq. 5, and the Coriolis term $2\rho\Omega W_r$ on the right-hand side of Eq. 6. By setting Ω equal to zero and substituting the absolute velocity V for the relative velocity W, these equations can be applied to stators, such as vaned or vaneless diffusers.

For simplicity, the bar over each of the time-averaged velocity components has been omitted; however, the bar does appear over each of the six unique products of the fluctuating velocity components, indicating a time average of these quantities, which characterize turbulent flows and are called *Reynolds stresses*. The task for the developers of CFD codes is to properly represent or "model" these six terms.[12]

Turbulence Modeling Schemes Because the *RANS* equations (5 to 8) deal with the time-mean values of the velocity components, they are more practical to deal with in computing the flow field than are the Navier-Stokes equations, which deal with the instantaneous values. However, relationships for the Reynolds stresses must be supplied in order to obtain a solution to the *RANS* equations, and generating these relationships is called "turbulence modeling." These include the earlier algebraic eddy viscosity models and the later, now widely applied two-equation models. With an increasing array of complexity, advanced Reynolds stress models are possible, but they require many additional equations to be solved in order to define all the Reynolds stresses.

a. *Algebraic eddy viscosity models.* Thinking in terms of the mean velocities, it is logical to try and relate the Reynolds stresses of turbulent flow to the mean-velocity gradients, just as was done in Eq. 1 for the shear stress in a 2D laminar flow.

$$\rho\overline{u'v'} = \mu_t\frac{du}{dy} \tag{9}$$

where μ_t is called the eddy viscosity, and $\rho\overline{u'v'}$ is the relevant Reynolds stress from the *RANS* equations (as written in cartesian coordinates x, y, and z and therefore in terms of velocity components u, v, and w, respectively). Eq. 9 models the only Reynolds stress involved in the analysis of a 2D turbulent boundary layer of a flow in the x-direction parallel to a fixed wall. Boundary layers were the first area of endeavor in the numerical solution of the *RANS* equations that eventually came to be called CFD. The eddy viscosity μ_t in a turbulent boundary layer increases with distance from the wall in accordance with Prandtl's mixing length theory to very large multiples of the molecular viscosity μ. Incidentally, the flow becomes laminar very near the wall, which is the domain of the "laminar sublayer" in which μ alone is operative per Eq. 1. Cebeci and Smith, using algebraic equations for μ_t were successful in computing all the parameters of 2D turbulent boundary layers.[13] Similar success was achieved by applying this method to compute the pump disk friction, (see Table 3 of Section 2.1.1,) wherein

LIBERTY EXHIBIT 1017, Page 126

the skewed boundary layers on the impeller shrouds and adjacent casing walls required two Reynolds stresses to be modeled at each point in the flow—both in terms of the same value of μ_t at that point.[14] Later this μ_t model was modified by Baldwin and Lomax in order to give it wider application.[12]

b. *Two-equation models for eddy viscosity.* To apply CFD throughout the flow field involves all of the Reynolds stresses appearing in Eqs. 5 to 8, not just the one or two of boundary layer flows. The algebraic eddy viscosity model is inadequate to this task because the eddy viscosity really depends on the characteristics of the turbulence, primarily the length scale or size of the turbulent eddies. Near the wall, in the boundary layer, this length scale is known to increase with distance from the wall per the Prandtl mixing length theory, and this is included in the algebraic eddy viscosity model. Outside the boundary layer, where the flow behavior can range from frictionless to separated and recirculating, two equations are solved to determine the eddy viscosity. The quickest and most useful method of this kind is called the k-ε model. The Jones-Launder version of this model is described by Lakshminarayana and is briefly summarized here.[12] The eddy viscosity is modeled as

$$\mu_t = \mu C_\mu e^{\left(\frac{-2.5}{1+\frac{R_T}{50}}\right)} R_T \tag{10}$$

where R_T is the turbulence Reynolds number

$$R_T = \frac{\rho k^2}{\mu \varepsilon} \tag{11}$$

and where k is the kinetic energy of the turbulence

$$k = \frac{1}{2}\left(\overline{w_r'^2} + \overline{w_\theta'^2} + \overline{w_z'^2}\right) \tag{12}$$

and ε is the turbulent energy dissipation rate or dissipation power due to the action of viscous stresses.

k is found from a kinetic energy (KE) equation derived from the Navier-Stokes equation for each instantaneous velocity component. This KE transport equation equates the convection of the turbulent kinetic energy k to the diffusion of the turbulence due both to the fluctuations of pressure and velocity and to the dissipation.

ε is found from another equation derived from the Navier-Stokes equations. This resulting transport equation equates the convection of ε to the sum of (a) turbulence production, (b) diffusive transport of the turbulence, and (c) viscous destruction of the turbulence.

For incompressible flow, these latter two transport equations for k and ε, together with Eq. 10 for the eddy viscosity are solved simultaneously for the mean velocities, k, ε, and the Reynolds stresses. Finally, with this information, the solution of the *RANS* equations for the turbulent flow field is accomplished.

In summary, it can be seen that the two-equation model is far more involved in both concept and execution than is the algebraic eddy viscosity model. However, this method and some variants of it such as the k-ω model have been remarkably successful in predicting both the velocity fields and the performance characteristic curves of pumps, including head, efficiency and NPSH effects. Moreover its popularity has been the focus of much testing, correlation with experiment and improvement by CFD researchers.

While even more complex turbulence modeling and solution procedures have been and continue to be developed, these require more transport equations to be solved and assumptions to be made about constants and other parameters appearing in them. The "feel" that the simpler and practical models described here give the user—as illustrated by the original eddy viscosity concept—is lost to the practicing pump engineer who wishes to use CFD as a practical tool. In short, the k-ε model remains the quickest and most useful choice.

LIBERTY EXHIBIT 1017, Page 127

Solving the Equations The ways of dealing with the Reynolds stress terms in the *RANS* equations having been described, the next step is to obtain the solution of the systems of equations involved. This cannot be accomplished in closed mathematical form, except in some special cases as was illustrated in Eqs. 1 to 3 for 2D laminar gap flow. Rather, numerical methods are employed to obtain the values of the velocity components and pressure at all desired points in the flow field. The steps in obtaining such numerical solutions are as follows:

1. *Discretization of the equations.* The differential equations; namely, Eq. 5 to 8, as well as the eddy viscosity and transport equations if any, are changed into algebraic equations by expressing each derivative in finite-difference form. For example, the derivative du/dy in Eq. 1 is represented by the ratio of the difference in the velocity u between two points in the flow field to the difference in the position y between those two points, namely one at $y = \delta$ on the moving plate for which $u = U$ and the other at $y = 0$ on the fixed plate where $u = 0$

$$\frac{du}{dy} = \frac{U - 0}{\delta - 0} \tag{13}$$

   where the right-hand side of this expression is the finite-difference form of the derivative du/dy in this particular case. However, in general, finite differences are approximations for actual values of the derivatives they represent. Moreover, discretization can have different levels or orders of accuracy depending on the numerical scheme being utilized. Laksminarayana gives a description of these orders of accuracy.[12]

2. *Meshing the computational domain.* Accurate representation of a derivative by its equivalent finite-difference expression requires a closely spaced mesh or "grid" of points throughout the domain of interest, especially in the zones where the derivatives are expected to be large or rapidly varying. The impeller in Figure 1 is shown meshed with a grid of 62,000 points or nodes per passage,[5] a total that would result from about 25 points from hub to shroud and from blade to blade at each of 100 stations in the streamwise direction, including suitable extensions of the passage upstream and downstream to points where known boundary conditions can be imposed on the problem. CFD codes are available with grid generators that work with geometric design information in the form of 2D digitized drawings or three dimensional (3D) solid models to create the complete array of computational elements (bounded by the nodes or points) which are suitably shaped for optimum numerical stability during iterative computations of the solution.

   Today it is not uncommon for a CFD mesh to contain an order of magnitude more nodes than were used to analyze one passage of the impeller of Figure 1. However, many more nodes than this is still a challenge in terms of computer time and power. Yet the earlier very successful turbulent boundary layer work dealt with a mesh of 500 or more points in the y-direction (normal to each wall), although with far fewer in the streamwise x-direction. Moreover, the spacing of these y-points was decreased as the wall was approached, which is essential in order to properly model the very thin sublayer near the wall and so to deduce the correct shear stress at the wall.[13,14] Such a high density of grid points near wall boundaries together with the meshing requirements of a whole passage or the combined passages of the inlet, impeller, volute or diffuser, and crossover is still not feasible; so, CFD codes usually include known "wall functions" such as the turbulent "log law of the wall" related to Prandl's mixing length theory and suitable representations of the laminar sublayer in the near-wall regions instead.

3. *Iterative computation of the solution.* Next, the appropriate boundary conditions for velocity components and pressure are imposed at the solid boundaries and the upstream and downstream throughflow boundaries. These are specified to be consistent with the number of unknowns and what is known at boundaries; for example, the velocity of the fluid at a solid boundary is generally zero relative to that boundary. Commercial CFD codes provide directions in this and many other aspects of their use. Initial values of all the variables are assigned to the nodes, and the algebraic system

LIBERTY EXHIBIT 1017, Page 128

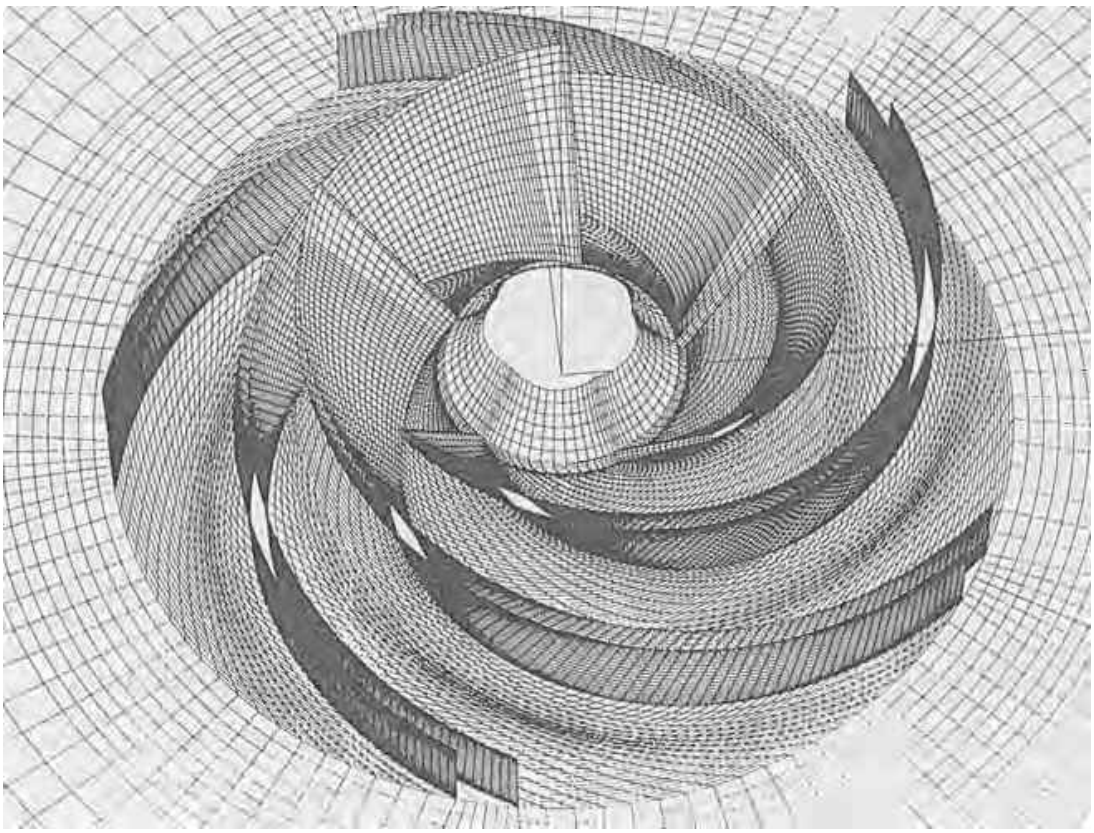


FIGURE 1 Centrifugal pump impeller of single-stage end-suction pump with a design specific speed N_s of 1500 ($\Omega_s = 0.55$), showing mesh for CFD analysis
Source: Reference 5 (International Pump Users Symposium, sponsored by Texas A&M University).

of equations is solved by iterating the values of the variables at each node until convergence on a set of values that satisfies the equations at all points is achieved within an acceptable margin of error. A variety of schemes for performing these iterations is employed such as (a) "marching" through the nodes in a prescribed order and assigning improved values at every point, such values themselves being obtained through algorithms that bring them closer to satisfying the equations; or (b) "relaxation" or making improvements first at the nodes where the errors are largest, or some combination of these and other approaches known to be suitable for the geometries and character of the expected solutions.

4. *Approximations employed in the computations.* Ideally, the CFD analysis of a pump should include all the terms of Eqs. 5 to 9 together with a level of turbulence modeling sophistication for the Reynolds stresses that is known to give results to the desired degree of accuracy. Required here is a sufficient number of nodes in both the stationary and rotating components of the entire machine from upstream of the inlet to downstream of the discharge port. This includes the unsteady terms, namely the derivatives with respect to time.
   a. *Steady flow in single components.* All of the above has indeed been done on multistage machines in research institutions. However, as mentioned in the introduction, early CFD work on pumps concentrated on steady-flow solutions (time-derivatives set to zero) for one component, especially the impeller. Moreover, such solutions were done for only one of the passages. This saved computer time and avoided the complexities of properly describing the flow across the interfaces between stationary and moving grids, and the results were surprisingly good.[5,7] For example, the total impeller head for the impeller of Figure 1 is shown in Figure 2 to be reasonably accurate over a wide range of flow rate from 25 to 100% of that at BEP.

LIBERTY EXHIBIT 1017, Page 129

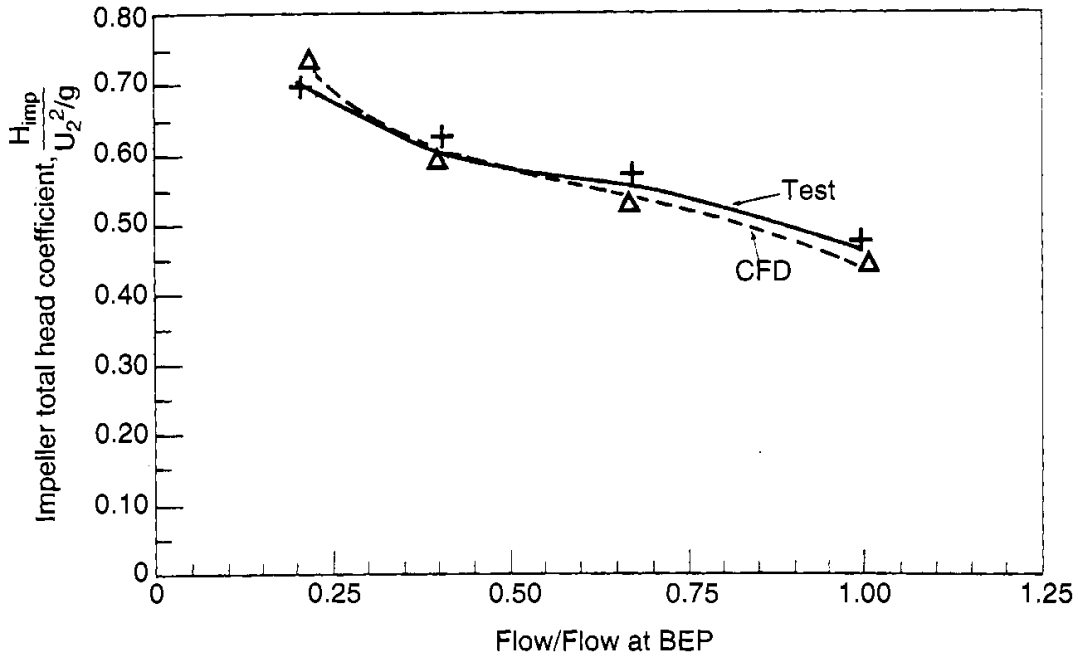


FIGURE 2 CFD prediction of total head compared to test results for the impeller of Figure 1
Source: Reference 5.

b. *Steady flow in multiple components.* The next step in complexity, while still avoiding unsteady computations, was to circumferentially average the flow variables at the interfaces between the rotating and fixed components. For example, this approach was utilized for the rotor-stator interface in the analysis of a mixed-flow diffuser pump[9] and an axial-flow water-jet pump[15] with mixed results on the accuracy of stage head and power consumption. However in another case, such averaging was avoided by freezing the impeller of a boiler feed pump stage relative to the volute and the inlet-plus-crossover passage. Moreover, all three components, including all of the impeller passages were included in the computational domain, which had a total of 276,352 nodes. This method, although for steady flow, preserved the recirculating flow patterns at the interfaces and resulted in the prediction of overall stage head at shutoff and at flow rates from 80 to 120% of BEP within 5% of the measured head on test.[8]

5. *Enhancements for greater accuracy.* Unsteady *RANS* solutions provide more accurate predictions of the flow field than the above steady-flow approximations. Yet, extensive experience with two-equation eddy viscosity models has led to advanced computational methods for further improvements of accuracy in the prediction of unsteady flow effects and losses and therefore of the overall pump performance curves. These are known as *Large Eddy Simulation* (*LES*); *Hybrid RANS-LES*, which can include the so-called *Detached Eddy Simulation* (*DES*) method; and, ultimately, *Direct Numerical Simulation* (*DNS*). Unsteady-flow computations are a feature of these enhancements, all of which require the computing power of parallel processing. Briefly these methods are described as follows.

a. *LES.* The basis of *LES* models is that fluctuations in the inertial regime, where turbulence production occurs and are characterized by a relatively large length scale, need to be resolved inherently by the numerical procedure. In contrast, turbulent eddies that have very small length scales and are primarily dissipative in nature may be modeled. Thus the grid size is chosen to be fine enough that the cell dimensions are smaller than the "large" inertial scales, while turbulent scales smaller than the cell size are modeled with so-called "sub-grid" turbulence models. For instance in wakes and other areas of turbulent mixing, especially at high Reynolds numbers, the large unsteady vortical structures as illustrated in the famous image by Brown and Roshko[16] for a mixing layer are computed as part of the unsteady

LIBERTY EXHIBIT 1017, Page 130

solution procedure while the fine-grain turbulent dissipation is modeled. The "subgrid" turbulent viscosity μ_t is low in these regions, sometimes as small as 10 to 20 times the molecular viscosity μ (also called the laminar viscosity μ_l) since it only represents the fraction of turbulent energy that is not being resolved by the calculation. In contrast, the turbulent viscosity in a *RANS* model represents the entire turbulent spectrum and may be very large (order of 3000 to 4000 times μ_l). One drawback of the LES framework is that the meshes become very large (small grid spacings), and the calculations can become very expensive particularly for very high Reynolds number flows where the dimension of the inertial length scale that needs to be resolved becomes smaller with increasing Reynolds number.

b. *Hybrid RANS-LES or DES methods.* The sheer size and computational expense of using LES methods for large scale, complex 3D applications has necessitated the development of this more practical procedure. The philosophy here is to use a fine *LES* quality grid in specific regions of the flow where unsteady effects may be expected to dominate while using a coarser *RANS* grid in other more benign regions. For example, in a mixing layer an *LES* quality grid would be used in the vicinity of the shear layer encompassing the vortical structures while a coarse *RANS* grid would be used elsewhere. Many different procedures to smoothly blend the variation of μ_t as we cross the interface from a fine cell in the *LES* region to a coarse cell in the *RANS* region have been developed. One of the more popular blending methods is the *DES* method that has been extensively used in the modeling of separated flows.

c. *DNS.* To avoid uncertainties about the scale of the turbulence as well as the exact locations of the corresponding regions of the flow field where the various scales exist, the Navier-Stokes equations can be solved directly for the unsteady velocity field. The grid for this *DNS* approach is extremely fine, and every turbulent length scale is involved. This is the ultimate way of solving a turbulent flow field; however, it is largely a theoretical concept and would command too much computer power to be practical for pump engineers. Moreover, for Reynolds numbers—based on the turbulent length scale—that are less than 1000, *DNS* is not practical.

6. *Parallel computing.* Ideally, increasing the number of processors—really individual computers networked together and sharing the computational tasks—reduces the costs, especially those of these enhanced computational methods. For example, it may take a day to generate the grid of an impeller passage and another day to run a CFD code and obtain a solution for it. In a fully unsteady computation, all the impeller passages are involved, and the number of processors should increase directly with the number of passages. Further, for multistage machines, the number of processors is found by multiplying their quantity for one stage by the number of rotor-stator combinations. More than 200 processors are required to perform unsteady flow calculations for a complete pump stage in the *Hybrid RANS-LES* mode. The computations are accomplished by transferring information for a component of the flow field, such as a rotor or rotor passage, to a waiting processor. Any disparity in the time required to compute the domain of a single component and that of another is termed "latency" because of the inaction of the waiting processors. Latency produces inefficiency in balancing the computational load across the various components. And latency, combined with inefficiencies in transferring information among the processors can lead to "saturation" or no improvement in computational speed, which in turn limits the maximum number of processors for the same grid and results in greater cost or "overhead." From this discussion it can be seen that, while solving steady problems using the coarse meshes associated with *RANS* solvers requires basic computer resources, unsteady problems of large size using the above enhanced methods and solved with parallel processing require significant investment in computer resources and system administration.

OPTIMIZING THE HYDRAULIC DESIGN

Widespread acceptance of commercial CFD codes by the fluids engineering community in the product design process is the result of the extensive development and experience

LIBERTY EXHIBIT 1017, Page 131

with this valuable tool as outlined above. CFD codes and the computers on which they run are taking the place of the traditional upfront laboratory testing phase of the pump hydraulic development process. Here, the assumptions of steady flow and circumferential averaging across interfaces between rotating and stationary members are adequate to the purpose. The resulting rapid approximate CFD solutions enable engineers to more quickly sort out ideas and to identify and focus on areas of improvement of these pump hydraulic components.

Inlet Passageways Inlet passageways or "suction approach bays" that are integral to pump casings—for example, between-bearings pumps as illustrated in Section 2.2.1—receive the incoming fluid in a plane normal to the shaft and then redirect the fluid axially into the eye of the impeller, simultaneously distributing it circumferentially. An incoming radial conduit on many multistage pumps, this passageway is essentially an elbow discharging into the first-stage impeller eye. Such asymmetric inlet passageways can create major circumferential and radial distortions of the fluid entering the impeller, producing losses, cavitation, and pump vibration. Similarly, the crossover passageways on multistage pumps can deliver poor flow to the subsequent stages of multistage pumps.[5,8] Because of its complex geometry, the suction approach bay can be one of the most challenging components for the hydraulic designer; and 3D flow analysis is essential in order to get any idea at all about the flow field approaching the impeller. This was clearly demonstrated with an early CFD-like finite-element code for the case of a low-loss double-suction pump bay. The viscous stresses were not computed; and this omission fortunately had little influence on that particular flow field, which agreed well with experimental measurements.[17]

Impellers Impellers were the first major focus of CFD-based optimization, because, as the energy transfer agent, an impeller (or inducer) has a major impact on overall pump performance. Q3D had been an effective analytical tool for judging the flow field.[2,3] The objective was to design blading that could carry the load without separating the flow and suffering the consequent mixing losses, while minimizing skin friction losses. Q3D was basically an inviscid analysis method, to which empirically based loss expressions could be added. Among the primary outputs were the distributions of the local free-stream velocity W relative to the blade surfaces, which are related to the static pressure distributions p on the blades through the Bernoulli equation in terms of W and p at successive meridional positions through the impeller from inlet to exit, as illustrated in Figures 17 and 29 and approximated by Eq. 54 of Section 2.1.1. The diffusion or "D" factors (Eqs. 57 to 59 and computed on Figure 29 of Section 2.1.1) were not supposed to exceed experiential values that were guided by the limits established by NACA for maintaining lift on airfoils by avoiding separation. However, CFD solutions compute all the losses, thereby removing the uncertainties in applying the D-factor empiricism. Nevertheless, some impeller analysts using CFD still require outputs for the equivalent static pressure distributions on the blades—as an aid to interpretation of the fluid behavior and the optimization of the impeller hydraulic design.[4,15] Moreover, in this CFD-assisted optimization process, the complexity and interrelation of the losses can reveal the need for subtle modifications in the blade shapes. In this regard, the spanwise distribution of the inlet angle and leading edge shape of the impeller blades must be optimized with respect to possible distortion of the flow entering from the inlet passageway. If needed, this is possible by coupling at least these two components in an unsteady analysis that preserves the circumferential flow distortions on the interface between the stationary inlet and rotating impeller grids. Such distortions, as stated earlier, can have a profound effect on the incidence losses of the impeller and unsteadiness arising from suction recirculation.[5]

Diffusers Substantially diffusing flows are well known to be distorted and unsteady. 1D analysis is impossible due to the unsteady blockages of boundary layers and wakes in various stages of incipient separation and stall even in the neighborhood of the BEP of the pump. Thus, in the design description of vaned diffusers in Section 2.1.1, all that can be offered by way of performance prediction are references to experimental diffuser data. As the flow rate is reduced below the design-point value, the stall patterns in vaned diffusers

LIBERTY EXHIBIT 1017, Page 132

intensify until rotating stall appears. CFD analysis of vaned diffusers, both isolated and coupled with an impeller, has reproduced these complex flow phenomena; indicated the effect of the proximity of the impeller blades to the diffuser vanes (called "Gap B" in Section 2.1.1) on the rotating stall; and provided diffuser performance predictions. These computations also illustrated the influence that recirculating flow from the diffuser into the impeller has on impeller flows at the low flow rates associated with rotating stall patterns and frequencies in both impeller and vaned diffuser.[6] Similarly, vaneless diffusers can develop stall patterns that influence impeller flow stability and so are prime candidates for unsteady CFD analysis, particularly when coupled to the impeller. An unsteady-flow study of such a pump, using k-ω turbulence modeling, revealed that this geometry produced disturbances of the jet-wake impeller flow patterns. These in turn caused periodic fluctuations of velocity and pressure that gave insight into the relation of such fluctuations to experimental acoustic measurements of the flow.[18]

Volutes The influence of the volute sizing and design on volute pump performance and the circumferential pressure distribution around the impeller is discussed in Section 2.1.1. Experimental data for the resulting radial thrust magnitude and direction on the impeller is given for a typical pump in Section 2.1.3 as a function of the flow rate relative to BEP. Thus, it is expected that the volute affects the impeller flow field and performance and vice versa, and that a meaningful CFD solution of a volute must be done with it properly coupled to the impeller. This was done in the frozen-flow computation of the previously mentioned multistage boiler feed pump, in which the crossover-and-inlet passage were also included.[8] While not truly unsteady, this solution produced the effect on the impeller and total pump performance of the circumferential pressure variation in the volute which developed at the lower flow rates that were analyzed. However, in the mid-flow range, there was some disparity between the predicted and experimental values of overall pump total head which might not occur for the predictions of a truly unsteady CFD solution.

PREDICTING PERFORMANCE

There are two main uses of CFD with regard to predicting overall pump performance, namely, (a) as part of the hydraulic design optimization process and (b) for presentation of pump characteristics of high accuracy for purchasers and users of pumps.

Predictions During the Design Process Steady-flow CFD is used to rapidly obtain reasonable approximations to the complete set of performance curves of a new pump hydraulic design. This is a step that is revisited frequently during an interactive design process. Such use is especially appreciated when designing variable geometry machines, as for example the axial flow pump of Reference 19, for which a unique set of performance curves exists for each setting of a row of inlet guide vanes. In this case the authors computed the desired range of performances by utilizing a commercial CFD code in the steady-flow mode and using circumferential averages of the velocities and pressure at the interface between the guide vanes and the impeller.[19]

Head and Efficiency versus Flow Rate As the vision for CFD usage moves beyond the optimization of hydraulic components, the degree to which such predictions approximate the actual test curves has become an increasingly visible metric for judging the effectiveness of this computational tool. Instances of steady-flow CFD solutions producing accurate results for total developed head and power—and, therefore, efficiency—of pumps in the neighborhood of the BEP have been cited in the foregoing discussions.[8,9] As will be seen below, unsteady LES and *Hybrid* RANS-LES solutions consistently achieve near-perfect duplication of test results, not only at BEP but at other flow rates as well. This includes NPSHR versus flow rate, a topic which, for clarity, has so far been omitted from this CFD presentation; however, the additions to the codes that are required for CFD to deal with cavitation will now be described.

LIBERTY EXHIBIT 1017, Page 133

CAVITATION AND TWO-PHASE FLOW

Modeling Cavitation and Two-Phase Flow In the computation of the performance of the variable-geometry pump mentioned above, the authors also computed the curve of NPSHR versus flow rate for each guide-vane setting.[19] Indeed, commercial CFD codes now possess this capability, which entails computation of the vapor cavity volumes that exist within the impeller when operating at conditions where the NPSH available is less than that of cavitation inception, $NPSH_i$ (see definition and descriptions in Sections 2.1.1 and 2.1.3.) As reviewed by Sloteman et al in Reference 20, the methods of accounting for cavitating flows in CFD codes began by establishing the domains of the vapor or gas cavities known to exist under such conditions; (see Figure 40 in Section 2.1.1 and Figure 24 in Section 12.5.) The cavities were treated as solid blockages whose extent and shape were "tracked" iteratively until their interfaces with the neighboring liquid had a uniform static pressure p that was equal to the vapor pressure p_v. The additional codes required to do this were eventually eliminated in favor of a constant-enthalpy vaporization model embedded in the RANS code, and that then evolved into a volume-of-fluid (VOF) model which combined the Rayleigh-Plesset bubble-growth equation with an accounting for the presence of noncondensable gases, such as air, in the fluid. Thermal equilibrium among the phases is assumed. This VOF model involves greater complexity in the equations but has worked well.

Cavitation Performance at the Design Point Commercial CFD codes embodying this cavitation model are now being applied in the pump industry to determine the NPSHR capability and two-phase behavior of centrifugal pumps and inducers. This had been readily accomplished at the design point, which usually does not involve backflow from the inlet.

1. *Centrifugal pump cavitation.* Applied to a boiler feed pump impeller with vapor cavities trailing off the leading edges of the blades, a commercial CFD code using a two-phase VOF model under the steady-flow approximation produced the cavity shown in Figure 3, which is seen to compare closely with the corresponding experimentally observed cavity from a laboratory flow visualization test.[20] As illustrated in Figure 4, the code was applied at each of four levels of NPSH as expressed in terms of the dimensionless

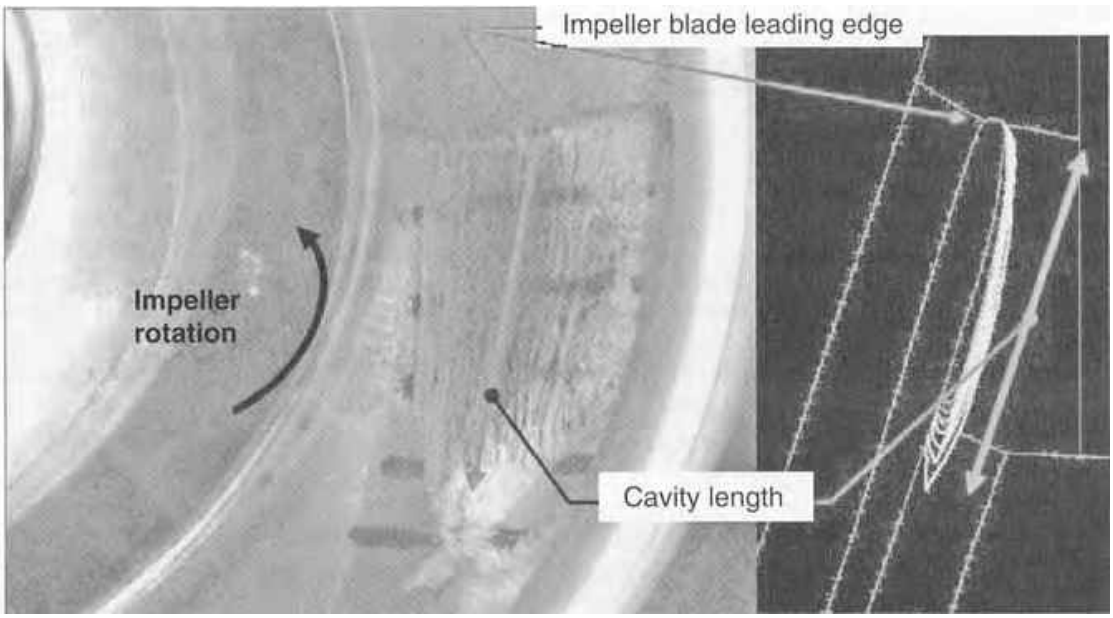


FIGURE 3 Comparison of suction surface cavity prediction with observations of the flow in a high-energy boiler-feed-pump impeller. The impeller blade on the left is operating near its design flow rate with a substantial sheet cavity. The plot at the right shows the vapor volume fraction computed with a two-phase CFD code.
Source: Reference 20 (International Pump Users Symposium, sponsored by Texas A&M University).

LIBERTY EXHIBIT 1017, Page 134

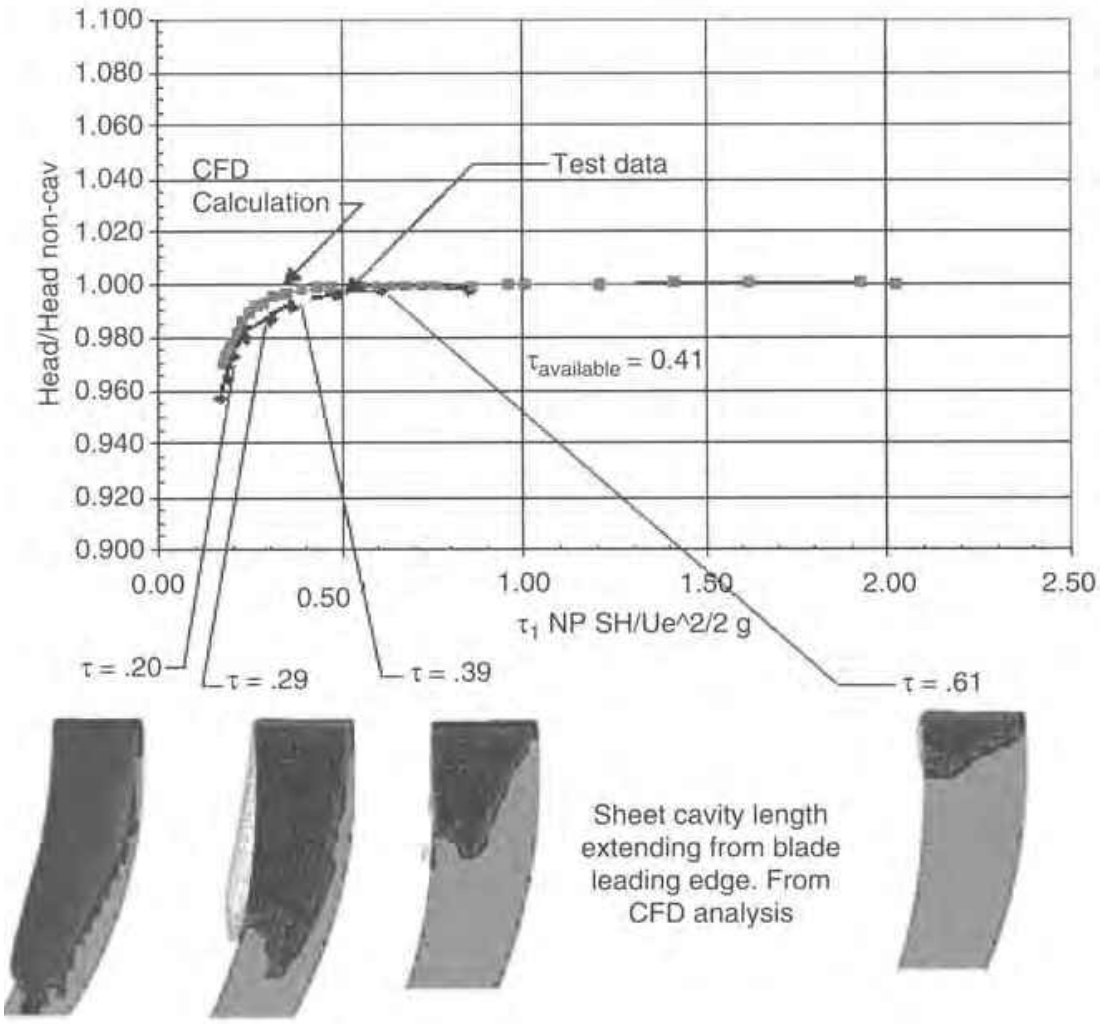


FIGURE 4 Suction performance of boiler feed pump at design flow rate compared to prediction via two-phase CFD. Illustrated at points along the curve of head versus cavitation coefficient τ (dimensionless *NPSH*) are the boundaries defined by a cavity region containing more than 10% vapor by volume. As is commonly observed, at *NPSH* 3% (i.e., for head dropping off by 3% of its noncavitating value) the cavity extends back to the throat formed by the adjacent blade.

Source: Reference 20.

quantity $\tau = 2gNPSH/U_e^2$. τ ranged from 0.65 (somewhat below visual inception at τ_i) to 0.20 at the 3% break-off point, where the pump stage liquid head had deteriorated to 97% of its noncavitating value. Comparison of computed and observed bubble lengths at each τ-point are shown. More impressive is the virtual duplication of the Head-versus-*NSPH* test curve of Figure 4 by the CFD solution. These results afford a quantitative validation of the two-phase CFD code that was used.[20]

2. *Inducer cavitation.* The axial-flow helical inducer that is used for high suction specific speed (N_{ss} or Ω_{ss}) applications such as rocket propulsion pumps (as described in Section 12.18.2) achieves its large design value of N_{ss} with extensive cavitation activity present within the internal flow field. As such, the truly meaningful hydraulic analysis of an inducer includes both single- and two-phase flows. Figure 5 shows a typical inducer meshed for CFD analysis. The head-versus-N_{ss} curve at the design point for a three-bladed inducer similar to this one was generated in the steady-flow application of a commercial CFD code with advanced cavitation modeling. The computations produced the simulated increase in blockage of the passages by vapor and the attendant progressive unloading of the inducer blades downstream of their leading

LIBERTY EXHIBIT 1017, Page 135

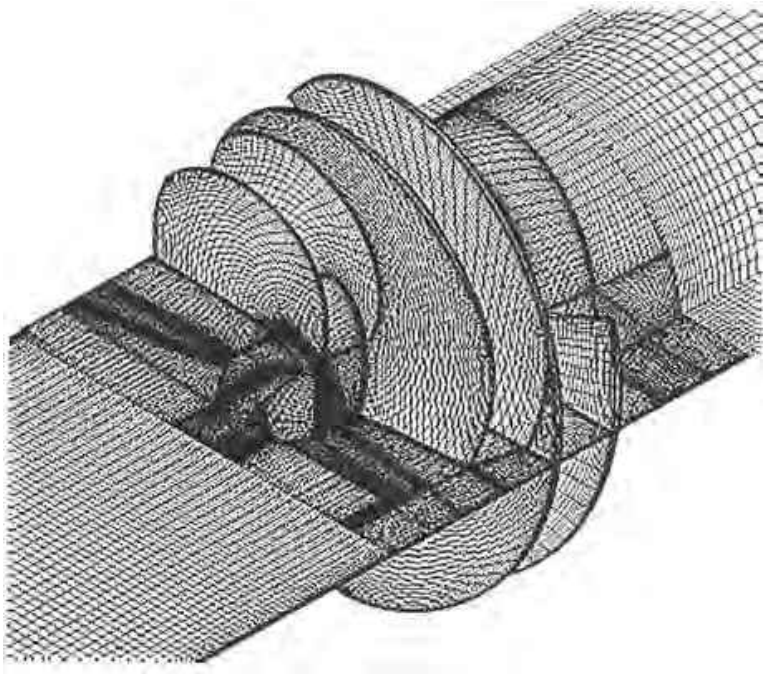


FIGURE 5 Inducer meshed for *LES*-type CFD analysis. This test inducer is similar to one used in a rocket engine liquid oxygen turbopump. It has three blades and an inlet blade angle at the tip of 7.5 degrees. Design flow inlet flow coeffient $\phi_e = 0.078$.
Source: Reference 25 (ASME).

edges as N_{ss} is increased (τ decreased), which is associated with head breakdown in these machines. Moreover, the CFD results for head versus N_{ss} agreed closely with experimental data for the whole range of NPSH to breakdown, which was a significant accomplishment in view of the large volumes of vapor involved. The cavitation modeling that was contained in this CFD code was thus validated for inducers, at least at the design point.[21] Other inducer investigations have been carried out, one of which was unsteady and revealed rotating alternate-blade cavitation in a four-bladed inducer.[22] An extensive experimental and analytical study of three inducers using the same CFD code as for the pump of Reference 20 (and in the steady-flow mode as well), produced three head-versus-NPSH curves for each inducer. Although computations were made at about 70% and 114% in addition to 100% of design flow coefficient, there was less agreement with experimental data than was realized in the pump case.[23]

Off-Design Flows In Inducers Recirculation and backflow, as discussed in Sections 2.1.1 and 2.1.3, develop at flow rates reduced below the design point or BEP of a pump. For an inducer, which typically has an inlet eye diameter equal to its exit diameter, this off-design phenomenon sets in at flow rates not far below the BEP. As cavitation is usually present in inducers, they are known to develop extensive, highly complex, unsteady, cavitating flows under such conditions.[24] (Figure 41 in Section 2.1.1 and Figure 22 in Section 12.5 visualize such off-design two-phase, recirculating flows within impellers. Note the breakup of the cavities.) Therefore inducers are a logical focus of researchers trying to achieve agreement of two-phase CFD predictions with experimental data over the whole flow range from shutoff to runout.

1. *Single-phase CFD solution for backflow.* One approach in tackling this problem was the single-phase, unsteady CFD analysis of the inducer of Figure 5, which shows the mesh used for the *LES* solution that was conducted.[25] The solution was developed over a period corresponding to 40 to 55 revolutions of the inducer. Near-perfect agreement with experiment of the predicted developed-head performance was obtained as shown in Figure 6. The design flow coefficient ϕ_d was 0.078; so, ϕ ranged from 64 to 136% of ϕ_d.

LIBERTY EXHIBIT 1017, Page 136

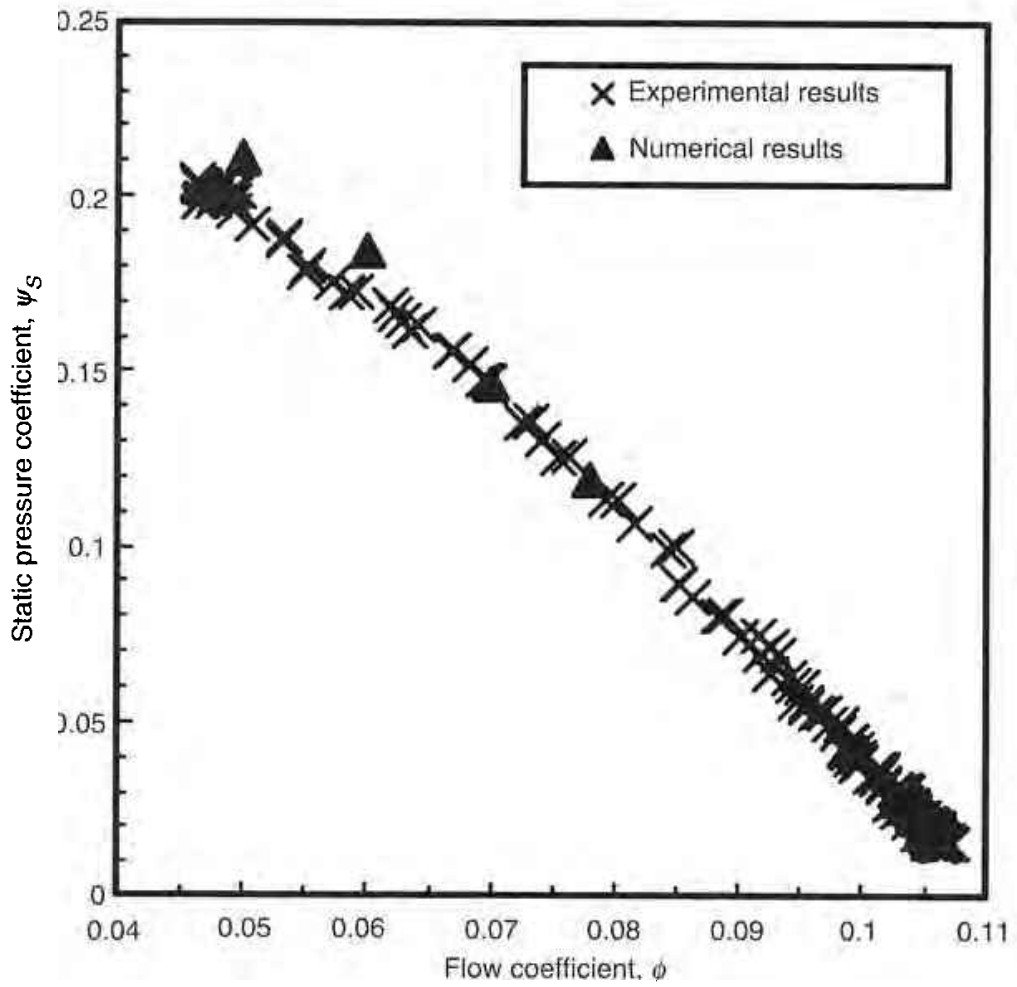


FIGURE 6 Comparison of CFD predictions of static pressure with experimental results for the test inducer of Figure 5 on water. Excellent agreement was achieved.
Source: Reference 25 (ASME).

The authors reported that backflow out of the inlet eye (left side of Figure 5) existed at 90% or ϕ = 0.070, and they computed the pattern illustrated in Figure 7 at ϕ = 0.060 (= 77% of ϕ_d). Corresponding to a high-NPSH condition, the intensity and extent of this backflow would be less at the more typical values of NPSH available to inducers, because the leading portions of the blades of an inducer tend to unload in the presence of the large volumes of vapor existing at low NPSH.[21]

2. *Single- and Two-phase CFD solutions with backflow.* As a further step in validating the unsteady *Hybrid RANS-LES* two-phase CFD code that was employed for the design-point study of Reference 21, a solution of the noncavitating backflow field was also computed for the low-pressure fuel turbopump or LPFTP on the space shuttle main engine (see Figure 3 and Table 1 of Section 12.18.2).[26] Computed at 70% of ϕ_d, the resulting upstream velocity field is presented in Figures 8 and 9. Figure 8 shows the concentration of the swirling backflow near the OD of the inlet duct, whereas the nonswirling incoming fluid is mainly at the axis of rotation. Figure 9 shows that in the region of intense interaction of these flows the turbulent viscosity μ_t is thousands of times greater than the laminar or molecular viscosity μ_l (or simply μ,) whereas μ_t vanishes outside the interaction zone. Comparison of the velocity results of Figure 8 with experimental data was made at three upstream planes, as shown in Figures 10 and 11 for the swirl and axial components, respectively. The next step was to utilize the advanced cavitation modeling feature, and this was done at 90% of ϕ_d, at which condition rotating modes of cavitation were computed. This enabled quantification of the

LIBERTY EXHIBIT 1017, Page 137

Next Page

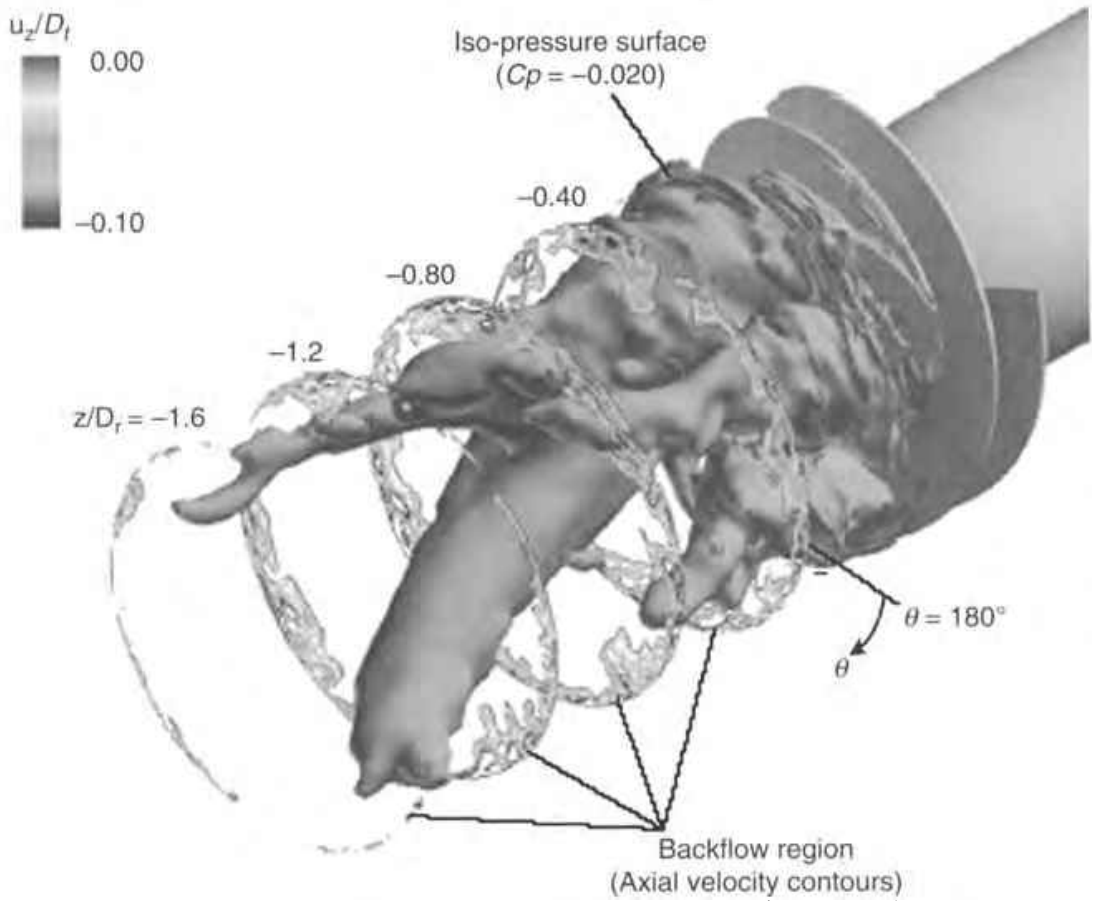


FIGURE 7 Backflow from the test inducer of Figure 5, computed at an inlet flow coefficient $\phi_e = 0.06$ after 55 revolutions. Illustrated is the backflow vortex at the shear layer between the incoming main flow and the swirling backflow.

Source: Reference 25 (ASME).

consequent radial loads that could have adverse mechanical consequences during operation at this condition. Both the computed frequency and amplitude of this instability agreed with experimental observations.

Thermodynamic Effects on Cavitation Performance Necessarily built in to the cavitation models of two-phase CFD codes is the effect of the fluid thermodynamic properties

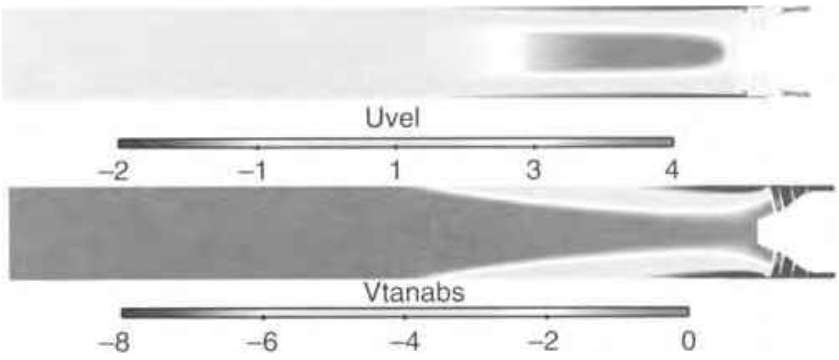


FIGURE 8 Backflow from the Space Shuttle Main Engine Low Pressure Fuel Pump (SSME LPPP) inducer, showing meridional (uvel) and swirl (vtanabs) velocity contours for 70% of design flow rate. The affected region extends well upstream of the pump, which is on the right.

Source: Reference 26 (AIAA).

LIBERTY EXHIBIT 1017, Page 138

Previous Page

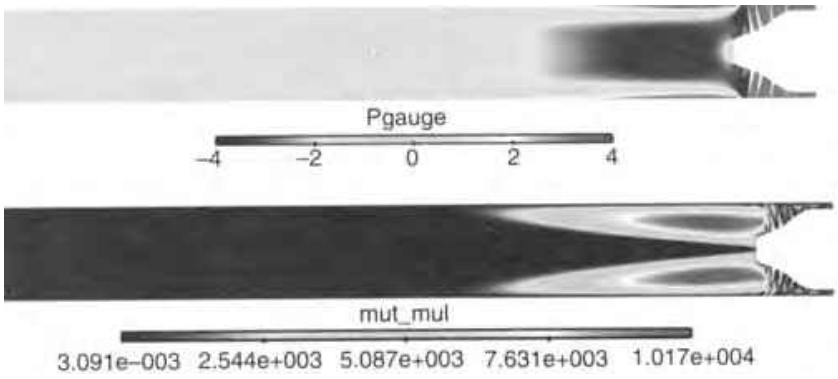


FIGURE 9 Backflow from the SSME LPPP inducer, showing static pressure p in psi (bar = psi/14.504) and turbulent viscosity μ_T contours for 70% of design flow rate. μ_T vanishes upstream of the region of interaction of the swirling backflow near the OD of the axial inlet pipe with the incoming (nonswirling) flow along the axis of rotation. μ_T is shown here as the ratio μ_T/μ_l, which is in the thousands in the highly turbulent interaction region.
Source: Reference 26 (AIAA).

involved in the vaporization process for computing the effects of cavitation. At points in the flow field where the static pressure drops below the vapor pressure, the liquid cools locally as the vapor forms, essentially by a constant-enthalpy or nearly constant-entropy process, as was alluded to in the above explanation of cavitation modeling.[20] Thus the heat of vaporization and the densities of the vapor and liquid all influence the volume of gas that appears in the flow for a given volume of liquid that is vaporized. Explained in Section 2.1.1 under NPSH *Effects*, this becomes important if the fluid is near its critical point, as are the cryogenic liquids encountered in liquid rocket propulsion systems, namely hydrogen and oxygen; (Section 12.18.2.) Inducers are generally deployed in such systems. Liquid hydrogen produces orders of magnitude less vapor volume for a given volume of liquid vaporized than does cold water. An early attempt to quantify the thermodynamic effect on the NPSH-capability of pumps was a Q3D-type inducer analysis code which contained a constant-entropy vaporization model as a point function of the pressure in the flow field.[27] That code successfully approximated this effect on breakdown NPSHR but not

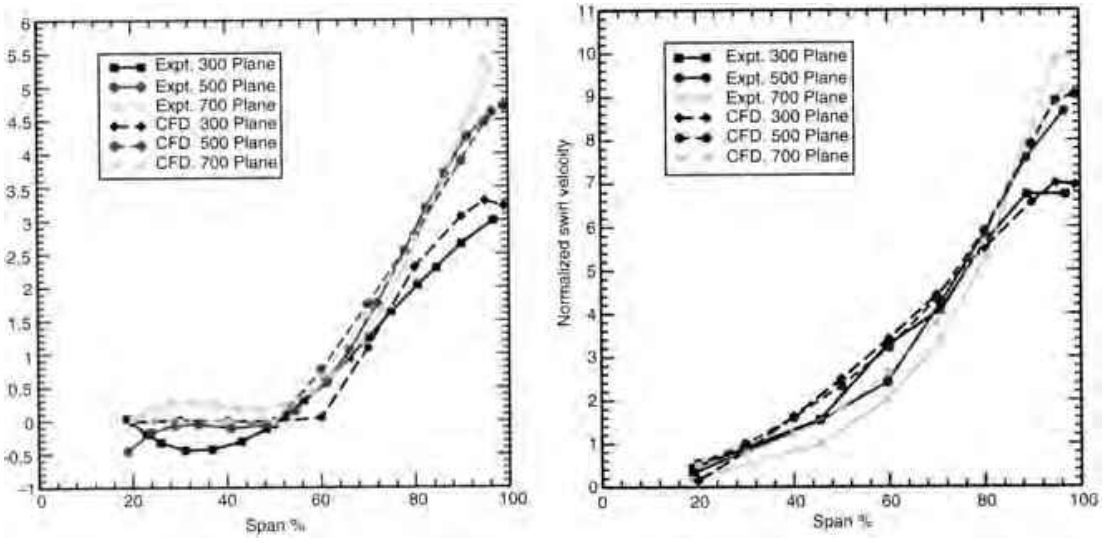


FIGURE 10 Comparisons of swirl velocity profiles with experimental data for the SSME LPPP inducer at three upstream planes, namely 0.29D (the 700 plane), 0.49D (the 500 plane), and 0.99D (the 300 plane). On the left (a) are the results for 90% of design flow rate; and, on the right (b), for 70% of design flow rate.
Source: Reference 26 (AIAA).

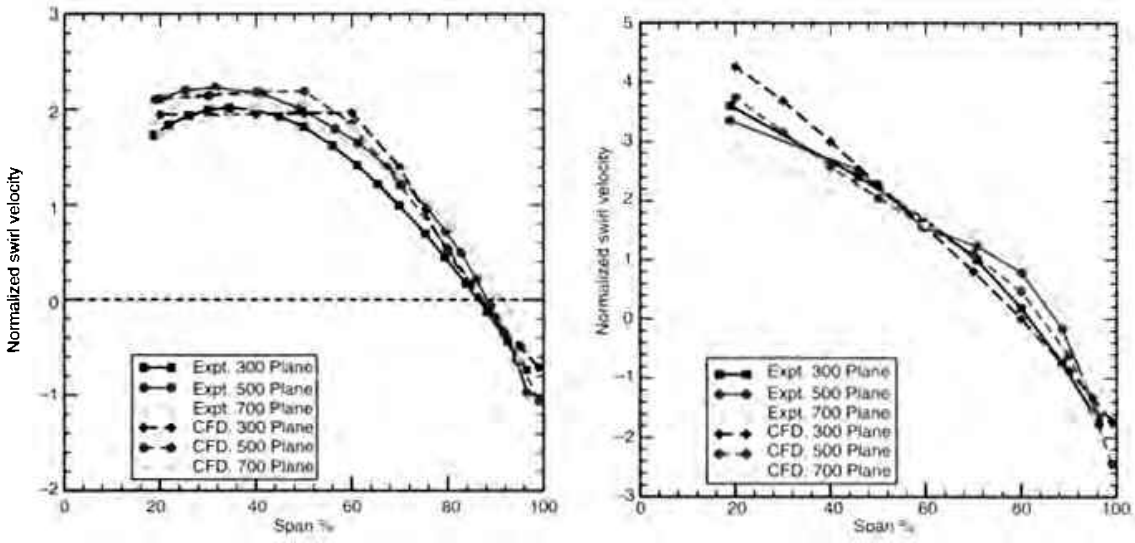


FIGURE 11 Comparisons of axial velocity profiles with experimental data for the SSME LPPP inducer at the same three upstream planes as in Figure 10. On the left (a) are the results for 90% of design flow rate; and, on the right (b), for 70% of design flow rate.

Source: Reference 26 (AIAA).

the shape of the fall-off curve of head versus NPSH. Initial efforts at validation of a current two-phase CFD code with respect to this effect consisted in successfully replicating the vapor cavity configurations and pressures observed in experiments with flows of cavitating liquid nitrogen and oxygen past bluff bodies.[28,29] Simulation of the effect on inducer head versus N_{ss} was achieved for liquid oxygen in a comparison to that of water.[29] Extensive experiments in liquid hydrogen and water by NASA on the 6 degree (inlet tip blade angle) of Figure 12 were then simulated with the same *Hybrid RANS-LES* code mentioned above in both fluids.[30] In Figure 13, results for the head breakdown in liquid hydrogen computed at the design flow coefficient $\phi_d = 0.072$ are compared with test data taken at $\phi = 0.072$, 0.074, and 0.075. Results displayed extreme sensitivity to even slight changes in liquid temperature and flow coefficient, and it is believed that uncertainties in the measurement of test temperature and flow coefficient, including variations during



FIGURE 12 NASA 6-degree flat-plate inducer, tested in water and in liquid hydrogen at various temperatures at the NASA Glenn facility between 1964 and 1970.

Source: Reference 30 (JPP).

LIBERTY EXHIBIT 1017, Page 140

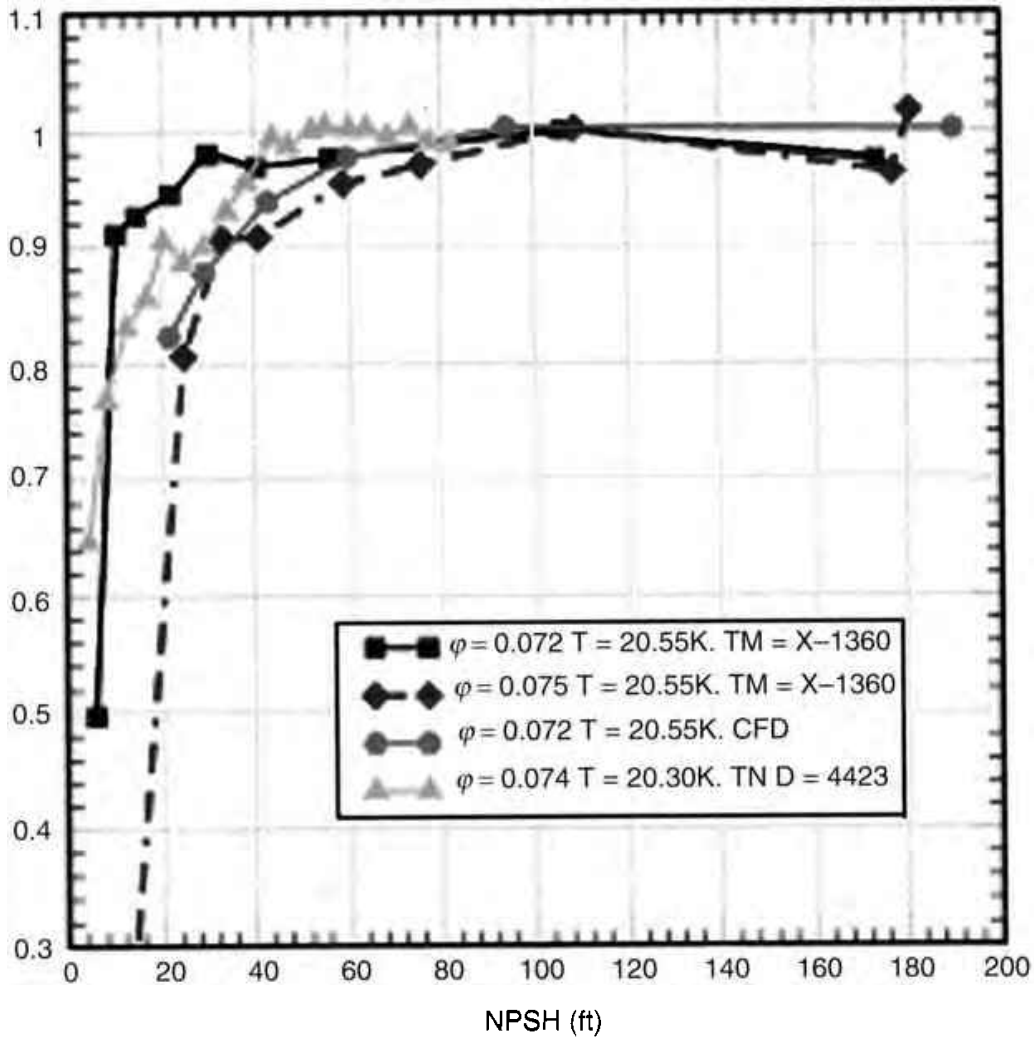


FIGURE 13 Suction performance of the NASA 6-degree inducer of Figure 12 in liquid hydrogen at 20,000 rpm and a temperature T of 20.55K (−423°F), comparing three sets of test results with computed CFD data. Flow rate at the design flow coefficient $\phi_d = 0.072$ was 1436 gpm (326 m³/h). The test flow coefficient varied slightly, the greater value of ϕ producing the expected greater value of *NPSH* at head breakdown. (m = ft × 0.3048).
Source: Reference 30 (JPP).

each test run, are of the order of the difference between CFD and experiment at $\phi = 0.072$. And the CFD curve is conservative with respect to the test curve at $\phi = 0.072$. Moreover, the slightly lower temperature for the experimental data for $\phi = 0.074$ appears to bring its results for breakdown NPSH closer to the predicted values at $\phi = 0.072$. Finally, in Figure 14, the comparison of the CFD-predicted suction specific speed (N_{ss} or Ω_{ss}) or NPSHR capability of this inducer in liquid hydrogen to that of water is dramatic but expected from the NASA tests to which the CFD results were compared.[30]

CONCLUSIONS

Computational Fluid Dynamics, or CFD, is the computerized numerical solution of the fundamental equations of motion of fluids throughout the domain of the passageways, both rotating and stationary, of a pump—either taken together or as separate components. Usually CFD involves solutions of the *Reynolds-averaged Navier-Stokes* equations (RANS equations) which contain the products of the fluctuating velocity components called Reynolds stresses. The success of CFD has depended on the relationships that represent

LIBERTY EXHIBIT 1017, Page 141

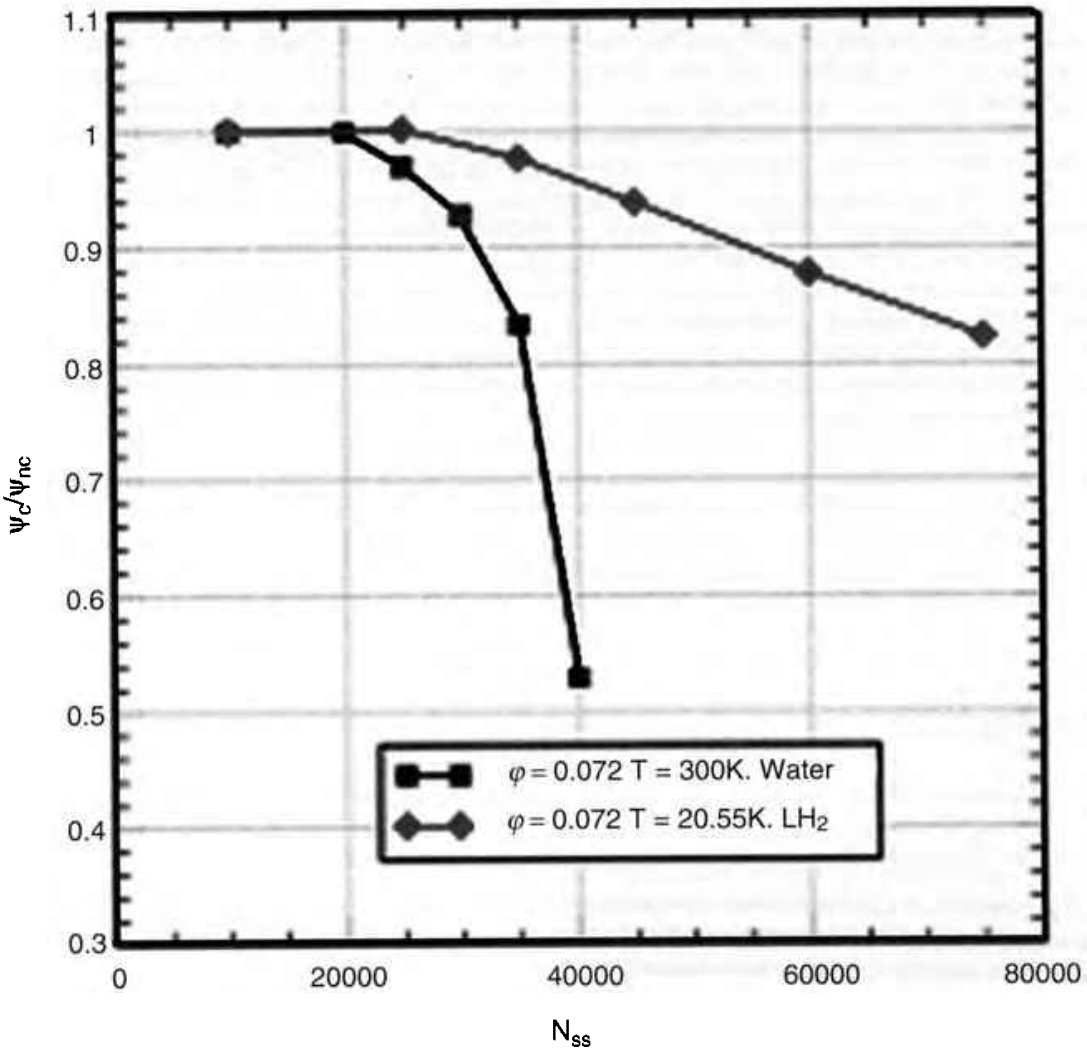


FIGURE 14 Comparison of curves of head-versus-suction specific speed N_{ss} of the NASA 6-degree inducer of Figure 12 pumping water at 300K (80°F) and liquid hydrogen at 20.55K (−423°F) as computed via CFD ($\Omega_{ss} = N_{ss}/2733$).

Source: Reference 30 (JPP).

these stresses and is called turbulence modeling. The most popular turbulence model currently in use is called the k-ε model, which expresses the eddy viscosity of the turbulence in terms of the turbulence kinetic energy k and the turbulent dissipation ε. Improvements and variations on this model to provide greater accuracy in simulation of actual flows exist and will continue to appear. To this model has been added the treatment of cavitation and two-phase flow that is needed to cover the gamut of pump flows. Methods of solution to increase accuracy in wakes and other areas of separated flows include large eddy simulation (*LES*) and *Hybrid RANS-LES*. Both steady flow and fully unsteady flow solutions can be obtained, the latter taking the most time, especially if *LES* is involved. Steady-flow CFD solutions take less time and can give useful information; however, precision and accuracy of time-varying velocities and pressures require fully unsteady computations. These are done with commercially available CFD codes running on multiple computers in a parallel processing mode.

The use of CFD in both the development and prediction of performance and the related operational features of the flow field velocities and pressures, both steady and fluctuating, has proven to be reliable and even essential for pump engineers, designers and users. Included are all flow rates from shutoff to runout, NPSH levels from inception to breakdown in liquids both close to and far from their thermodynamic critical points.

LIBERTY EXHIBIT 1017, Page 142

Head has been predicted to within experimental uncertainties at shutoff and from flow rates at least as low as 64% of BEP and at least as great at 136%. At all flow rates, predictions of both performance and flow patterns and instabilities, including domains of backflow, show the character of these phenomena with remarkable accuracy.

Inducers have been the vehicle for improving and validating both single- and two-phase CFD codes, as they have extensive zones of backflow and vapor due to cavitation. Such work has been successful and has created confidence that CFD is reliable for the more traditional and ubiquitous pumping configurations.

Applicability of CFD to any flow problem indicates that its use to define the operational behavior of systems in which pumps are installed should be as reliable as it has proven to be in turbomachinery and pumps and inducers in particular. Moreover, CFD solutions of the flow fields in system elements such as intake sumps, manifolds and the variety of suction piping configurations can function as the same aid to the system design process as has been described for pump internals.

CFD is creating a vision for the future. More computing power will lead to wider demand for and use of unsteady solutions, including *LES* and, perhaps, ultimately, direct numerical solution of the Navier-Stokes equations in terms of the instantaneous velocities and pressures. Already, development of pumps in some locations is proceeding on the basis of CFD alone—without benefit of development testing. Acceptance testing, however, will always be required.

REFERENCES

1. Sloteman, D. P., Saad, A. N., and Cooper, P. "Designing Custom Pump Hydraulics Using Traditional Methods." *Proceedings of the 2001 ASME Fluids Engineering Division Summer Meeting*, Paper FEDSM2001-18067, June 2001.
2. Katsanis, T. "Quasi-Three-Dimensional Full Analysis in Turbomachines: A Tool for Blade Design." In *Numerical Simulations in Turbomachinery,* FED—Vol. 120, ASME, 1991, pp. 57–64.
3. Katsanis, T. "Fortran Program for Calculating Transonic Velocities on a Blade-to-Blade Stream Surface of a Turbomachine." NASA TN D-5427, 1969.
4. Graf, E. "Analysis of Centrifugal Impeller BEP and Recirculating Flows: Comparison of Quasi-3D and Navier-Stokes Solutions." *Pumping Machinery—1993*. FED—Vol. 154, ASME, 1993, pp. 235–245.
5. Cooper, P., Graf, E., and Luce, T. "Computational Fluid Dynamical Analysis of Complex Internal Flows in Centrifugal Pumps." *Proceedings of the 11th International Pump Symposium*, Texas A&M University, March 1994, pp. 83–94.
6. Sano, T., Yoshida, Y., Tsujimoto, Y., Nakamura, Y., and Matsushima, T. "Numerical Study of Rotating Stall in a Pump Vaned Diffuser." *Transactions of the ASME, Journal of Fluids Engineering*, Vol. 124, June 2002, pp. 363–370.
7. Gülich, J. F. "An Assessment of Pump Impeller Performance Predictions by 3D-Navier Stokes Calculations." *Proceedings of the 1997 ASME Fluids Engineering Division Summer Meeting*, Paper FEDSM97-3341, June 1997.
8. Cugal, M., and Baché, G. " Performance Prediction from Shutoff to Runout Flows for a Complete Stage of a Boiler Feed Pump Using Computational Fluid Dynamics." *Proceedings of the 1997 ASME Fluids Engineering Division Summer Meeting*, Paper FEDSM97-3334, June 1997.
9. Goto, A. "Prediction of Diffuser Pump Performance Using 3-D Viscous Stage Calculation." *Proceedings of the 1997 ASME Fluids Engineering Division Summer Meeting*, Paper FEDSM97-3340, June 1997.
10. Vande Voorde, J. B., and Vierendeels, J. "ALE Calculations of Flow through Rotary Positive Displacement Machines." *Proceedings of the 2005 ASME Fluids Engineering Division Summer Meeting and Exhibition*, Paper FEDSM2005-77353, June 2005.

LIBERTY EXHIBIT 1017, Page 143

11. Schlichting, H. *Boundary Layer Theory*. Tr. by J. Kestin. McGraw-Hill, 4th and following editions (1960 et seq.).
12. Lakshminarayana, B. *Fluid Dynamics and Heat Transfer of Turbomachinery*. Wiley, 1996.
13. Cebeci, T., and Smith, A. M. O. *Analysis of Turbulent Boundary Layers*. Academic Press, 1974.
14. Cooper, P., and Reshotko, E. "Turbulent Flow between a Rotating Disk and a Parallel Wall." *AIAA Journal*, Vol. 13, No. 5, May 1975, pp. 573–578.
15. Gao, H., Lin, Wl, and Ye, F. "An Investigation of the Flow and Global Performance in a Water-Jet Axial Flow Pump Based on CFD and Inverse Design Method." *Proceedings of the 2005 ASME Fluids Engineering Division Summer Meeting and Exhibition*, Paper FEDSM2005-77116, June 2005.
16. Brown, G. L., and Roshko, A. "On density effects and large structure in turbulent mixing layers." *Journal of Fluid Mechanics*, Vol. 64, 1974, pp. 775–816.
17. Dhaubhadel, M. N., Akey, H. U., Singh, P. J., Spring, H., and Prescott, M. "Three-Dimensional Finite Element Analysis of Flow through a Double Suction Pump Bay." Pumping Machinery—1989, ASME, FED-Vol. 81, pp 237–245, July 1989.
18. Pavesi, G., Ardizzon, G., and Cavazzini, G. "Unsteady Flow Field and Noise Generation in a Centrifugal Pump Impeller with a Vaneless Diffuser." *Proceedings of the 2005 ASME Fluids Engineering Division Summer Meeting and Exhibition*, Paper FEDSM2005-77320, June 2005.
19. Kochevsky, A. N., Kozlov, S. N., Aye, K. M., Shelyaev, A. Y., and Konshin, V. N. "Simulation of Flow Inside an Axial-Flow Pump with Adjustable Guide Vanes." *Proceedings of the 2005 ASME Fluids Engineering Division Summer Meeting and Exhibition*, Paper FEDSM2005-77351, June 2005.
20. Sloteman, D. P., Robertson, D. A., and Margolin, L. "Demonstration of Cavitation Life Extension for Suction-Stage Impellers in High-Energy Pumps." *Proceedings of the 21st International Pump Symposium*, Texas A&M University, March 2004, pp. 103–115.
21. Hosangadi, A., Ahuja, V., and Ungewitter, R. J. "Simulations of Cavitating Flows in Turbopumps." *Jounal of Propulsion and Power*, Vol. 20, Number 4, July–August 2004, pp. 604–611.
22. Pouffary, B., Patella, R. F., and Reboud, J-L. "Numerical Analysis of Cavitation Instabilities in Inducer Blade Cascade." *Proceedings of the 2005 ASME Fluids Engineering Division Summer Meeting and Exhibition*, Paper FEDSM2005-77357, June 2005.
23. Medri, I., Bakir, F., Rey, R., and Belamri, T. "Comparison of Computational Results Obtained from a VOF Cavitation Model with Experimental Investigations of Three Inducers." *Proceedings of the 2005 ASME Fluids Engineering Division Summer Meeting and Exhibition*, Paper FEDSM2005-77084, June 2005.
24. Tsujimoto, Y., Horiguchi, H., and Qiao, X. "Backflow from Inducer and Its Dynamics." *Proceedings of the 2005 ASME Fluids Engineering Division Summer Meeting and Exhibition*, Paper FEDSM2005-77381, June 2005.
25. Yamanishi, N., Fukao, S., Qiao, X., Kato, C., and Tsujimoto, Y. "LES Simulation of Backflow Vortex Structure at the Inlet of an Inducer." *ASME Transactions, Journal of Fluids Engineering*, Vol. 129, May 2007, pp. 587–594.
26. Hosangadi, A., Ahuja, V., and Ungewitter, R.J., "Simulations of Rotational Cavitation Instabilities in the SSME LPFP Inducer." *43rd AIAA/ASME/SAE/ASEE Joint Propulsion Conference & Exhibit*, Paper AIAA-2007-5536, Cincinnati, OH, July 2007.
27. Cooper, P. "Analysis of Single- and Two-Phase Flows in Turbopump Inducers." *Transactions of the ASME, Journal of Engineering for Power*, Vol. 89, Series A, October 1967, pp. 577–588.
28. Hosangadi, A., Ahuja, V., and Ungewitter, R. J. "Simulations of Inducers at Low-Flow Off-Design Conditions." *Proceedings of the 2005 ASME Fluids Engineering Division Summer Meeting and Exhibition*, Paper FEDSM2005-77395, June 2005.

LIBERTY EXHIBIT 1017, Page 144

29. Hosangadi, A., Ahuja, V., and Ungewitter, R. J. "Simulations of Cavitating Cryogenic Inducers." *40th AIAA/ASME/SAE/ASEE Joint Propulsion Conference and Exhibit*, Paper AIAA-2004-4023, July 2004.

30. Hosangadi, A., Ahuja, V., and Ungewitter, R. J., "Numerical Study of a Flat Plate Inducer: Comparison of Performance in Liquid Hydrogen and Water." *42nd AIAA/ASME/SAE/ASEE Joint Propulsion Conference & Exhibit*, Paper AIAA-2006-5070, Sacramento, CA, July 2006.

2.1.3 CENTRIFUGAL PUMPS: HYDRAULIC PERFORMANCE AND BEHAVIOR

C. P. KITTREDGE
PAUL COOPER
WARREN H. FRASER

DEFINITIONS

Nomenclature Many of the quantities involved in this section are also dealt with in Section 2.1.1. Therefore, a single nomenclature that applies to both sections appears at the beginning of Section 2.1.1. Differences in notation exist for some of these quantities as a result of the coexistence of different traditions and pump cultures, so the nomenclature shows the equivalence in each case. An example is the use in this section of "c" and "w" to denote absolute and relative velocity respectively, whereas the NASA system of capital letters V and W is employed in Section 2.1.1.

Units The units used in this section are as defined in the nomenclature unless specifically noted in the text. In particular, the primary units for this section are those of the U.S. Customary System (USCS). A distinction in USCS usage in this section is that the pound force (lbf) is represented simply as "lb." Conversions to SI units are given throughout this section, or the actual equivalent SI values are given in parentheses.

However, the number appearing in parentheses after the USCS value of specific speed n_s is the equivalent value of the universal specific speed Ω_s. Note that the value of specific speed corresponding to the best efficiency point (BEP) operating conditions of the pump is the value of interest and is often used to identify the impeller geometry involved.

Volume Flow Rate Abbreviated to "flow rate" and known traditionally as "pump capacity" Q, this is the volume of liquid per unit time delivered by the pump. In USCS units, Q is expressed in U.S. gallons per minute or USgpm, for which the abbreviation "gpm" is used. (1 US gallon = 231 in^3)

Datum for Pump Head As defined in Eq. 3 and Figure 1 of Section 2.1.1, the total head has components of pressure, velocity, and elevation Z (or Z_e). Because pump head H (more

LIBERTY EXHIBIT 1017, Page 146

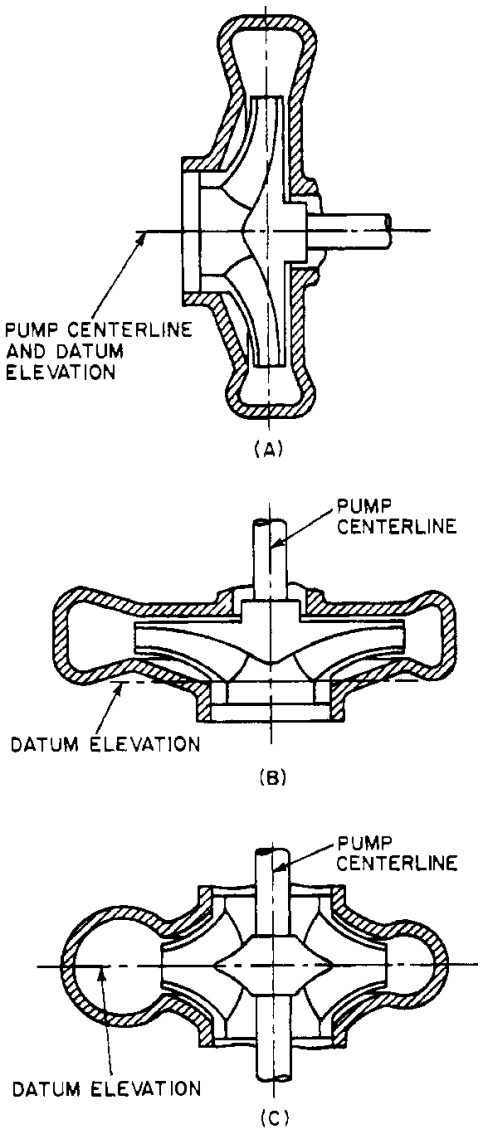


FIGURE 1A through C Elevation datum for defining pump head (Hydraulic Institute ANSI/HI 2000 Edition Pump Standards, Reference 27)

precisely ΔH) is the difference of the total heads evaluated at the discharge flange d and the suction flange s respectively, the elevation of the datum from which Z is measured cancels out. However, for purposes of identification, computing NPSH, and so on, the standard datum as shown in Figure 1 is used.

The standard datum for horizontal-shaft pumps is a horizontal plane through the centerline of the shaft (Figure la). For vertical-shaft pumps, the datum is a horizontal plane through the entrance eye of the first-stage impeller (Figure lb) if single suction or through the centerline of the first stage impeller (Figure 1c) if double suction. Because pump head is the difference between the discharge and suction heads, it is not necessary that the standard datum be used, and any convenient datum may be selected for computing the pump head.

Power In USCS, the pump output is customarily given as liquid horsepower (lhp) or as water horsepower if water is the liquid pumped. It is given by

$$lhp = \frac{QH(\text{sp. gr.})}{3960} \tag{1}$$

LIBERTY EXHIBIT 1017, Page 147

where Q is in gallons per minute, H is in feet, and sp. gr. is specific gravity. If Q is in cubic feet per second, the equation becomes

$$lhp = \frac{QH(\text{sp. gr.})}{8.82} \tag{2}$$

In SI, the power P in watts (W) is given by

$$P = 9797QH\,(\text{sp. gr.}) \tag{3}$$

where Q is in cubic meters per second and H is in meters.

When Q is in liters per second and H is in meters

$$P = 9.797QH\,(\text{sp. gr.}) \tag{4}$$

Efficiency The pump efficiency η is the liquid horsepower divided by the power input to the pump shaft. The latter usually is called the brake horsepower (bhp). The efficiency may be expressed as a decimal or multiplied by 100 and expressed as percent. In this section, the efficiency will always be the decimal value unless otherwise noted. Some pump driver-units are so constructed that the actual power input to the pump is difficult or impossible to obtain. Typical of these is the "canned" pump for volatile or dangerous liquids. In such case, only an *overall efficiency* can be obtained. If the driver is an electric motor, this is called the *wire-to-liquid efficiency* or, when water is the liquid pumped, the *wire-to-water efficiency.*

CHARACTERISTIC CURVES

Pump with Nonviscous Flow and Zero Slip The basic shapes of centrifugal pump performance characteristics arising from various geometries can be ascertained and compared without the necessity of evaluating the slip. (Illustrated in Figure 15 of Section 2.1.1, the slip phenomenon is explained in the related discussion[1].) For this purpose, one employs the artifice of nonviscous flow through an impeller with an infinite number of blades having infinitesimal thickness and that therefore produce neither structural (geometric) nor flow (boundary layer) blockage. The result is the ideal head for no slip or blockage H_e as given by Eq. 5 (cf. Eq. 15b of Section 2.1.1):

$$H_e = \frac{u_2 c_{u2}}{g} - \frac{u_1 c_{u1}}{g} \tag{5}$$

The velocity components in Eq. 5 can be seen in the velocity diagrams of Figure 2, slip being neglected. Generally the inlet swirl term is small, and Eq. 5 can be approximated by

$$H_e \cong \frac{u_2 c_{u2}}{g} \tag{6}$$

As shown in Figure 2b, the absolute velocity vector c may be resolved into the meridional, or radial, velocity c_m and the peripheral velocity c_u. From the geometry of the figure

$$c_{u2} = u_2 - \frac{c_{m2}}{\tan \beta_2} \tag{7}$$

which, substituted into Eq. 6, gives

$$H_e = \frac{u_2^2}{g} - \frac{u_2 c_{m2}}{g \tan \beta_2} \tag{8}$$

LIBERTY EXHIBIT 1017, Page 148

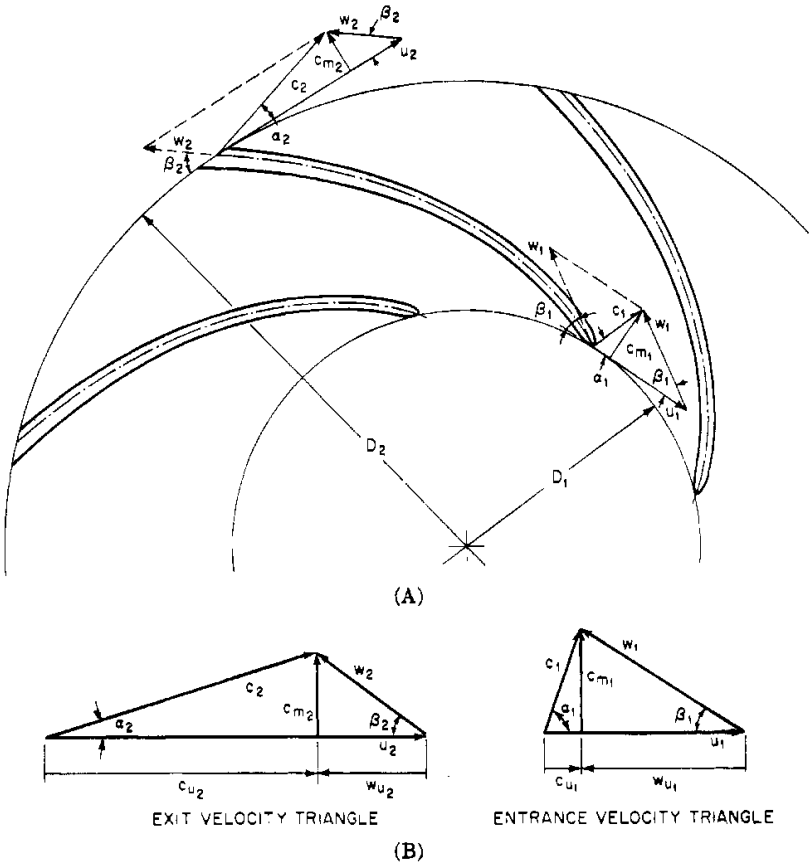


FIGURE 2A and B Velocity diagrams for radial-flow impellers, neglecting slip and blockage

Neglecting leakage flow, the meridional velocity c_m must be proportional to the flow rate Q. With the additional assumption of constant impeller speed, Eq. 8 becomes

$$H_e = k_1 - k_2 Q \tag{9}$$

in which k_1 and k_2 are constants, with the value of k_2 dependent on the value of the vane angle β_2. Figure 3 shows the H_e–*vs*–Q characteristics for the three possible conditions on the vane angle at exit β_2. The second right-hand term in Eq. 5 may be treated in like manner to the foregoing and included in Eqs. 8 and 9. The effect on Figure 3 would be to change the value of $H_e = u_2^2/g$ at $Q = 0$ and the slopes of the lines, but all head-flow rate characteristics would remain straight lines.

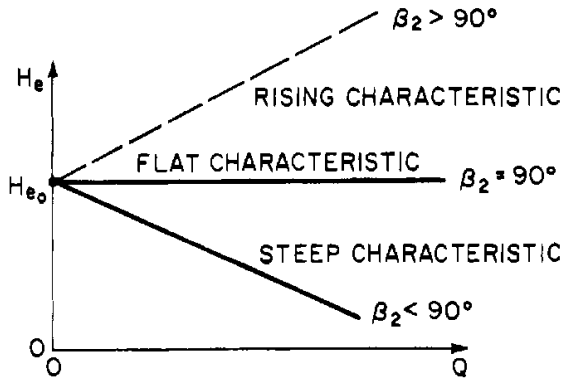


FIGURE 3 Head-versus-flow rate characteristics for nonviscous, zero-slip impeller flow

LIBERTY EXHIBIT 1017, Page 149

Viscous Flow with Slip The real flow situation involves friction losses in an impeller with a finite number of relatively widely spaced blades. Thus, slip occurs, reducing the exit flow angle $\beta_{f,2}$ below that of the blade β_2 (or, more precisely, $\beta_{b,2}$), which in turn reduces c_{u2} (cf. Figure 15 of Section 2.1.1). Therefore, the ideal head H_i drops below H_e. Moreover, losses and recirculation occur to cause additional deviation of pump head H from H_e. While CFD flow analysis can be employed to predict H with fair accuracy[2], lesser means, such as one-dimensional analysis, require experienced correlation and calibration skills to make such predictions. Therefore, many engineers commonly depend on testing and empirical modification of test results on the exact or similar geometry to make the final determination of the performance characteristics of a pump. This effort involves constant-speed plots of data as shown in the example of Figure 4.

Pumps are designed to operate at the point of best efficiency. The head, power, and flow rate at best efficiency, often called the *normal* values, are indicated in this section by H_n, P_n, and Q_n respectively. Sometimes a pump may be operated continuously at a flow rate slightly above or below Q_n. In such case, the actual operating point is called the *rated* or *guarantee* point if the manufacturer specified this flow rate in the guarantee. It is unusual to operate a pump continuously at a flow rate at which the efficiency is much below the maximum value. Apart from the unfavorable economics, the pump may be severely damaged by continued off-design operation, as described later.

Backward-Curved Blades, $\beta_2 < 90°$ Figure 4 shows the characteristics of a double-suction pump with backward-curved blades, $\beta_2 = 23°$. The impeller discharged into a single volute casing, and the specific speed was $n_s \approx 2200$ ($\Omega_s \approx 0.8$) at best efficiency. At shutoff ($Q = 0$), Eq. 8 predicts H_e to be 372 ft (113 m), whereas the pump actually developed about 210 ft (64 m), and this head remained nearly constant for the range $0 < Q < 1000$ gpm (63 l/s). For $Q > 1000$ gpm (63 l/s), the head decreased with increasing flow rate but not in the linear fashion predicted by Eq. 9. At best efficiency, where $Q_n = 3200$ gpm (202 l/s), Eq. 8 predicts $H_e = 281$ ft (86 m), whereas the pump actually developed $H_n = 164$ ft (50 m).

Radial Blades, $\beta_2 = 90°$ Large numbers of radial-blade pumps are used in many applications, from cellar drainers, cooling-water pumps for internal combustion engines, and other applications where low first cost is more important than high efficiency to highly engineered pumps designed for very high heads. The impellers are rarely more than 6 in

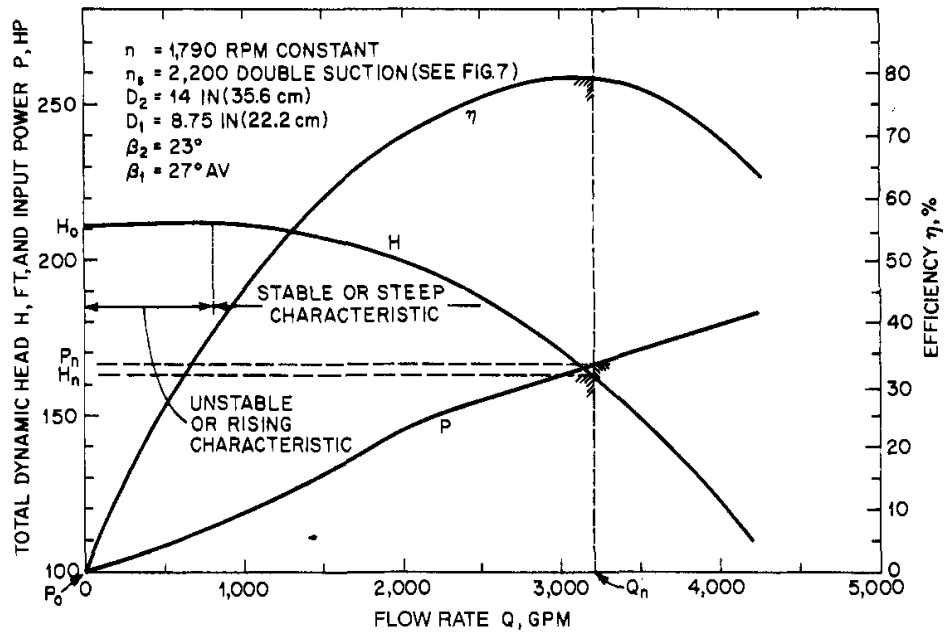


FIGURE 4 Typical pump characteristics, backward-curved blades (ft × 0.3048 = m; hp × 745.7 = W; gpm × 0.06309 = l/s)

LIBERTY EXHIBIT 1017, Page 150

(15 cm) in diameter, but the speed range may be from a few hundred to 30,000 rpm or more. The casings usually are concentric with the impellers and have one or more discharge nozzles that act as diffusers. The impellers usually are open, with three or more flat blades. The clearance between blades and casing is relatively large for easy assembly. Such pumps exhibit a flat head-capacity curve from shutoff to approximately 75% of best efficiency flow rate, and beyond this flow the head-flow curve is steep. The pumps develop a higher head, up to 8000 ft (2400 m) per stage, than pumps with backward-curved blades, but the efficiency of the former usually is lower. (See also Section 2.2.1.)

Figure 5 shows the characteristics of a pump as reported by Rupp.[3] The impeller was fully shrouded, $D = 5.25$ in (13.3 cm), and fitted with 30 blades of varying length. The best efficiency, $\eta = 55\%$, was unusually high for the specific speed $n_s = 475$ (0.174), as may be seen from Figure 6. The head-flow curve showed a rising (unstable) characteristic for $0 < Q < 25$ gpm (1.6 l/s) and a steep characteristic for $Q > 25$ gpm (1.6 l/s).

Figure 7 shows the characteristics of a pump as reported by Barske.[4] The impeller was open, $D \approx 3$ in (7.6 cm), and fitted with six radial tapered blades. The effective β_2 may have been slightly greater than 90° due to the taper. At 30,000 rpm, the best efficiency was more than 35% at $n_s = 355$ (0.130), which is much higher than for a conventional pump of this specific speed and flow rate (Figure 6). The head-flow curve showed a nearly flat characteristic over most of the usable range, as predicted by Eq. 8, but the head was always lower than H_e. The smooth concentric casing was fitted with a single diffusing discharge nozzle. When two or more nozzles were used, the head-flow curves showed irregularities at low flow rates and became steep at high flow rates.

Manson[5] has reported performance characteristics for jet engine fuel pumps having straight radial blades in enclosed impellers. The head curves showed unstable characteristics at low flow rates and steep characteristics at higher flow rates. The best efficiency reported was 54.7% for an impeller diameter of 3.300 in (8.382 cm) and speed $n =$ 28,650 rpm.

Forward-Curved Blades, $\beta_2 > 90°$ Pumps with forward-curved blades have been proposed,[6] but the research necessary to achieve an efficient design appears never to have been carried out. However, radial-flow fans with forward-curved blades are common. Tests have been made of conventional, backward-curved-blade, double-suction pumps with the impellers mounted in the reversed position but with rotation correct for the volute casing. As tested, these pumps therefore had forward-curved blades.

Table 1 shows the pertinent results for six different pumps. Both flow rate and efficiency were drastically reduced, and there was only a modest increase in head for five of the six pumps. The sixth pump showed a 38% increase in head over that obtained with the impeller correctly mounted. Published estimates[7,8] of the head-flow curves to be expected

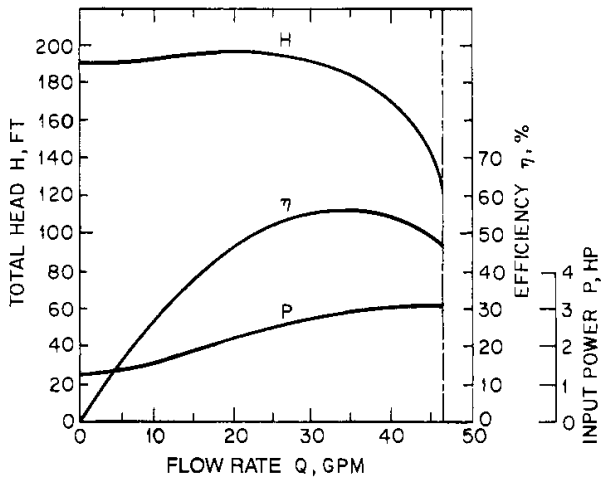


FIGURE 5 Pump characteristics, radial blades (ft × 0.3048 = m; hp × 745.7 = W; gpm × 0.06309 = l/s) (Reference 3)

LIBERTY EXHIBIT 1017, Page 151

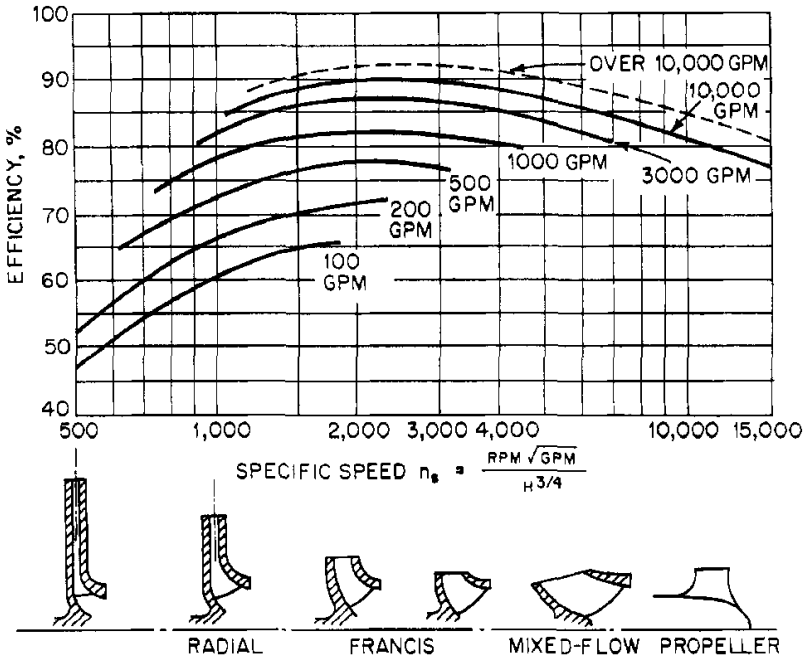


FIGURE 6 Pump efficiency versus specific speed and size. By way of comparison, Figure 10 of Section 2.1.1 (generated by Eq. 44 of that section) shows higher efficiency at low n_s and low flow rate at a constant value of surface roughness ε. However, if (in Eq. 44 of Section 2.1.1) substantially greater surface roughness is used for the small sizes, the results are similar to what is shown here. (gpm × 0.06309 = l/s, and $\Omega_s = n_s/2733$). (Flowserve Corporation)

from reversed impellers predict an unstable characteristic at the low end of the flow rate range and a steep characteristic at the high end of the range.

PERFORMANCE EFFECTS

Classification of Curve Shapes A useful method for comparing characteristics of pumps of different specific speeds is to normalize on a selected operating condition, usually best efficiency. Thus,

$$q = \frac{Q}{Q_n} \quad h = \frac{H}{H_n} \quad p = \frac{P}{P_n} \tag{10}$$

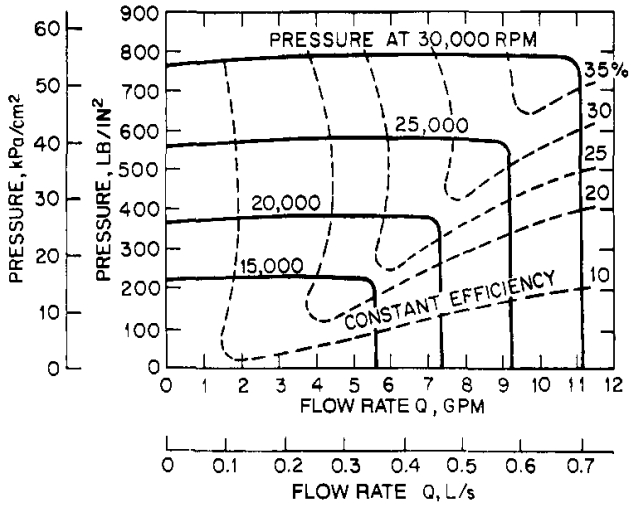


FIGURE 7 Pump characteristics, radial blades (lb/in² × 6.894 = kPa; gpm × 0.06309 = l/s) (Reference 4)

LIBERTY EXHIBIT 1017, Page 152

TABLE 1 Effects of reversed mounting of impeller

Number of stages	Specific speed per stage n_s (Ω_s)	Percent of normal shutoff head	Percent of normal values at best efficiency			
			Head	Flow Rate	Power	Efficiency
2	828 (0.303)	86	111	65	104	71
2	1024 (0.375)	82	112	88	145	68
1	1240 (0.454)	75	105	38.5	68.5	59
1	1430 (0.523)	82	106	69.7	138	53.5
1	2570 (0.940)	74.5	117	62	138	52.5
1	2740 (1.003)	77.5	138	61.5	180	47

Source: Flowserve Corporation

where the subscript n designates values for the best efficiency point. Figures 8, 9, and 10 show approximate performance curves normalized on the conditions of best efficiency and for a wide range of specific speeds as defined in Table 2. These curves are applicable to pumps of any size because absolute magnitudes have been eliminated. In Figure 8, curves 1 and 2 exhibit a *rising head* or *unstable* characteristic where the head increases with increasing flow rate over the lower part of the flow rate range. This may cause instability at heads greater than the shutoff value, particularly if two or more pumps are operated in parallel. Curve 3 exhibits an almost constant head at low flow rates and is often called a *flat* characteristic. Curves 4 to 7 are typical of a *steep* or *stable head* characteristic, in which the head always decreases with increasing flow rate. Although the shape of the head-flow curve is primarily a function of the specific speed, the designer has some control through selection of the vane angle β_2 number of impeller vanes n_b, and capacity coefficient $\phi = c_{m2}/u_2$, as described in Section 2.1.1 (see also Figure 2). For pumps having a single-suction specific speed of approximately 5000 (1.83) and higher, the power is at its maximum at shutoff and decreases with increasing flow rate. This may require an increase in the power rating of the driving motor over that required for operation at normal flow rate.

Efficiency The efficiency η is the product of three component efficiencies (defined in Section 2.1.1):

$$\eta = \eta_m \eta_v \eta_h \tag{11}$$

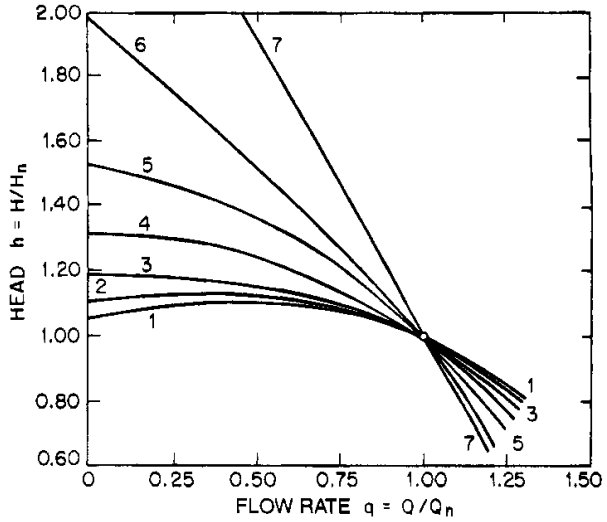


FIGURE 8 Head curves for several specific speeds, as defined in Table 2 (Reference 12)

LIBERTY EXHIBIT 1017, Page 153

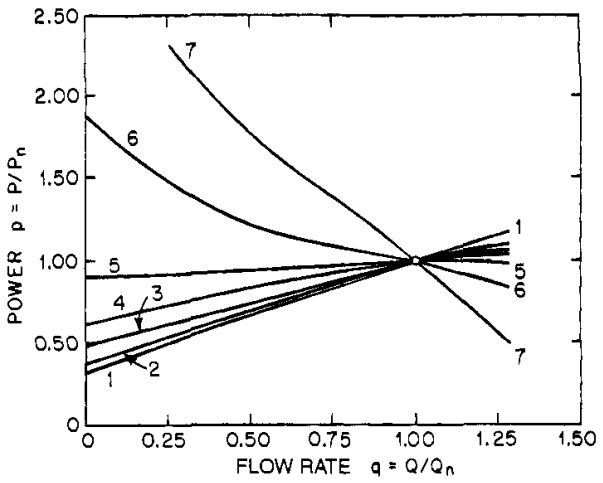


FIGURE 9 Power curves for several specific speeds, as defined in Table 2 (Reference 12)

The mechanical efficiency η_m accounts for the bearing, stuffing box, and all disk-friction losses including those in the wearing rings and balancing disks or drums if present. The volumetric efficiency η_v accounts for leakage through the wearing rings, internal labyrinths, balancing devices, and glands. The hydraulic efficiency η_h accounts for liquid friction losses in all through-flow passages, including the suction elbow or nozzle, impeller, diffusion vanes, volute casing, and the crossover passages of multistage pumps. Figure 11 shows an estimate of the losses from various sources in double-suction single-stage pumps having at least 12-in (30-cm) discharge pipe diameter. Minimum losses and hence maximum efficiencies are seen to be in the vicinity of $n_s \approx 2500$ (0.91), which agrees with Figure 6.

Effects of Pump Speed Increasing the impeller speed increases the efficiency of centrifugal pumps. Figure 7 shows a gain of about 15% for an increase in speed from 15,000 to 30,000 rpm. The increases are less dramatic at lower speeds. For example, Ippen[9] reported about 1% increase in the efficiency of a small pump, $D = 8$ in (20.3 cm) and $\eta_s = 1992$ (0.73), at best efficiency, for an increase in speed from 1240 to 1880 rpm. Within limits, the cost of the pump and driver usually decreases with increasing speed. Abrasion and wear increase with increasing speed, particularly if the liquid contains solid particles in suspension. The danger of cavitation damage usually increases with increasing speed unless certain suction requirements can be met, as described later.

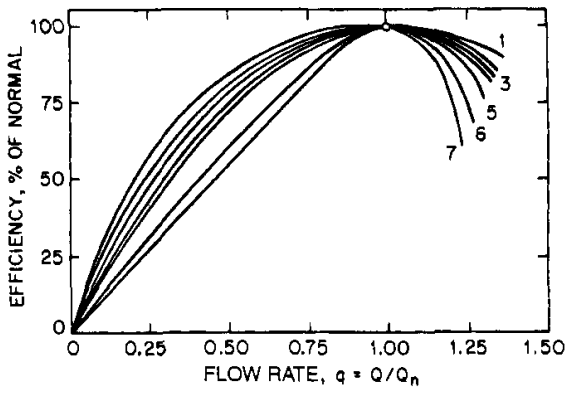


FIGURE 10 Efficiency curves for several specific speeds, as defined in Table 2 (Reference 12)

LIBERTY EXHIBIT 1017, Page 154

TABLE 2 Characteristic curves as a function of specific speed (Figures 8, 9, and 10)

Curve Number on Figures 8 , 9 , and 10	USCS Specific Speed n_s	Metric Specific Speed n_q (Eq's 38, Sect. 2.1.1)	Universal Specific Speed Ω_s	Impeller Suction Configuration
1	900	17	0.33	Double
2	1500	29	0.55	Double
3	2200	43	0.80	Double
4	3000	58	1.10	Double
5	4000	77	1.46	Double
6	5700	110	2.09	Single
7	9200	178	3.37	Single

Effects of Specific Speed Figues 6 and 11 show that maximum efficiency is obtained in the range 2000 (0.73) $< n_s <$ 3000 (1.10), but this is not the only criterion. Pumps for high heads and small flow rates occupy the range 500 (0.18) $< n_s <$ 1000 (0.37). At the other extreme, pumps for very low heads and large flow rates may have n_s = 15,000 (5.49) or higher. For given head and flow rate, the pump having the highest specific speed that will meet the requirements probably will be the smallest and least expensive. However, Figure 9 of Section 2.1 shows that it will run at the highest speed and be subject to maximum wear and cavitation damage, as previously mentioned.

Effects of Clearance

WEARING-RING CLEARANCE Details of wearing-ring construction are given in Section 2.2.1. Schematic outlines of two designs of rings are shown in Figure 12. The L-shaped construction shown in Figure 12a is very widely used with the close clearance between the cylindrical portions of the rings. Leakage losses increase and pump performance falls off as the rings wear. Table 3 shows some of the effects of increasing the clearance of rings similar to Figure 12a.

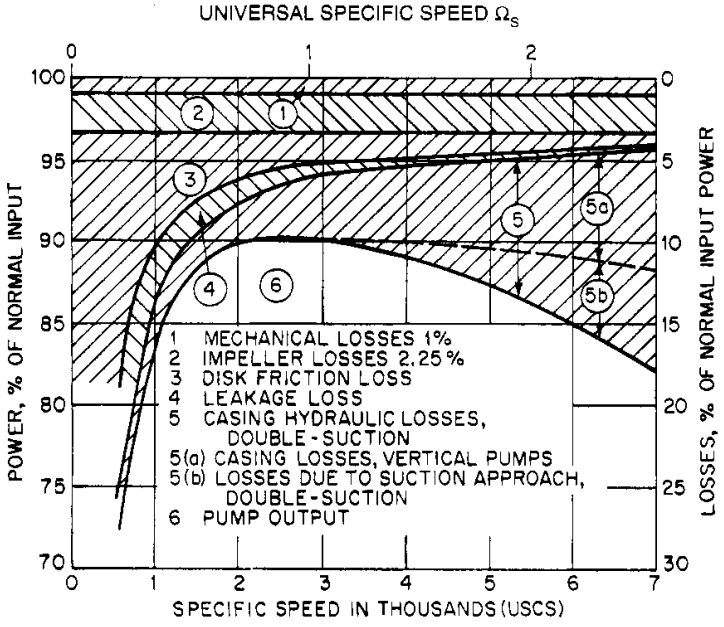


FIGURE 11 Power balance for double-suction pumps at best efficiency (Reference 12)

LIBERTY EXHIBIT 1017, Page 155

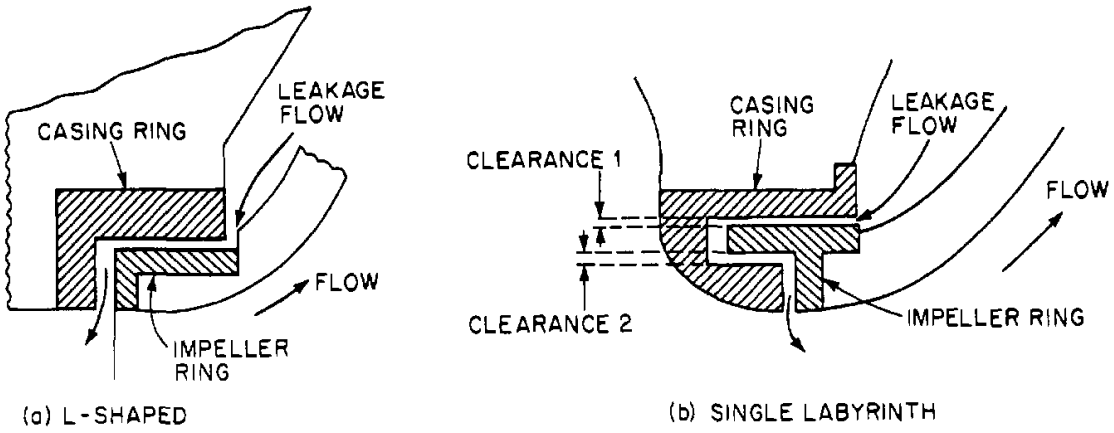


FIGURE 12A and B Typical wearing rings

The labyrinth construction shown in Figure 12b has been used to increase the leakage path without increasing the axial length of the rings. If the pressure differential across these rings is high enough, the pump shaft may take on lateral vibrations with relatively large amplitude and long period, which can cause serious damage. One remedy for these vibrations is to increase clearance 2 in Figure 12b relative to clearance 1, at the expense of an increased leakage flow. High-pressure breakdown through plain rings may cause vibration,[10] but this is not usually a serious problem. It is considered good practice to replace or repair wearing rings when the nominal clearance has doubled. The presence of abrasive solids in the liquid pumped may be expected to increase wearing-ring clearances rapidly.

BLADE-TIP CLEARANCE Many impellers are made without an outer shroud and rely on close running clearances between the blade tips and the casing to hold leakage across the blade tips to a minimum. Although this construction usually is not used with pumps having specific speeds less than about 6000 (2.20), Wood et al.[11] have reported good results with semiopen impellers at 1800 (0.66) $\leq n_s \leq$ 4100 (1.50). It appears that both head and efficiency increase with decreasing tip clearance and are quite sensitive to rather small changes in clearance. Reducing the tip clearance from about 0.060 in (1.5 mm) to about 0.010 in (0.25 mm) may increase the efficiency by as much as 10%. Abrasive solids in the liquid pumped probably will increase tip clearances rapidly.

TABLE 3 Effects of increased wearing-ring clearance on centrifugal pump performance

Specific speed n_s (Ω_s)	Design head, ft (m)	Ring clearance, % of normal value	Percent of values at shutoff with normal ring clearance			Percent of values at best efficiency with normal ring clearance		
			Q	H	P	η	H_0	P_0
2100 (0.77)	63 (19.2)	178	100	98.3	98.9	99.4	97.0	100
...	...	356	100	97.5	99.0	98.5	93.6	98.2
...	...	688	100	96.0	98.9	97.1	91.2	94.8
...	...	1375	100	94.3	97.4	96.8	88.8	92.5
3500 (1.28)	65 (19.8)	354	100	90.0	99.1	90.8	85.0	96.2
4300 (1.57)	41(12.5)	7270	62	65.5	81.7	49.8	44.3	106
4800 (1.76)	26 (7.9)	5220	96	78.8	89.2	84.8	78.2	83.3

Source: Flowserve Corporation

MODIFICATIONS TO IMPELLER AND CASING

Diameter Reduction To reduce cost, pump casings usually are designed to accommodate several different impellers. Also, a variety of operating requirements can be met by changing the outside diameter of a given radial impeller. Eq. 6 shows that the head should be proportional to $(nD)^2$ provided that the exit velocity triangles (Figure 2b) remain similar before and after cutting, with w_2 always parallel to itself as u_2 is reduced. This can be achieved if the impeller meridional exit area $A_{m,2}$ is the same before and after cutting—and if the flow angle $\beta_{f,2}$ (Figure 15, Section 2.1) also stays the same. [$\beta_{f,2}$ would stay the same if the blade angle β_2 (= $\beta_{b,2}$) does, the difference being due to slip velocity V_s that should also scale down with D.] For radial discharge impellers, area $A_{m,2}$ equals $\pi D b_2$ (minus blade and boundary layer blockage) and requires that b_2 increase as D decreases. This is typical of many impellers—as is constancy of β_2 over the cutting range—and, together with Eqs. 27–33 of Section 2.1.1, leads to the following rules for predicting performance:

$$\frac{Q_1}{Q_2} = \frac{n_1 D_1}{n_2 D_2} \tag{12a}$$

$$\frac{H_1}{H_2} = \frac{n_1^2 D_1^2}{n_2^2 D_2^2} \tag{12b}$$

$$\frac{P_1}{P_2} = \frac{n_1^3 D_1^3}{n_2^3 D_2^3} \tag{12c}$$

which apply only to a given impeller with altered D and constant efficiency but *not* to a geometrically similar series of impellers. (Eqs. 12 have been termed "affinity laws"; however, true affinity requires geometric similarity, which in turn yields the *Scaling and Similitude* relationships of Section 2.1.1.) The assumptions on which Eqs. 12 were based are rarely if ever fulfilled in practice, so exact predictions by the equations should not be expected. A common example is the low-n_s radial discharge impeller with parallel radial hub and shroud profiles over most of the path from inlet to exit (Figure 6). Here, $A_{m,2}$ decreases with cutting, and H falls more than would be predicted by Eq. 12b. [This type of impeller is often found in multistage pumps, particularly those in which the designer, driven by cost reduction goals, has minimized a) the axial length occupied by each stage and b) the number of stages, thereby pushing down the n_s of the individual stage to the point that a tolerable sacrifice in efficiency results.]

RADIAL DISCHARGE IMPELLERS Impellers of low specific speed may be cut successfully provided the following items are kept in mind:

1. The angle β_2 may change as D is reduced, but this usually can be corrected by filing the blade tips. (See the discussion on blade-tip filing that follows.)
2. Tapered blade tips will be thickened by cutting and should be filed to restore the original shape. (See the discussion below on blade-tip filing.)
3. Bearing and stuffing box friction remain constant, but disk friction should decrease with decreasing D.
4. The length of flow path in the pump casing is increased by decreasing D.
5. Because c_{m1} is smaller at the reduced flow rate, the inlet triangles no longer remain similar before and after cutting, and local flow separation may take place near the blade entrance tips.
6. The second right-hand term in Eq. 5 was neglected in arriving at Eqs. 12, but it may represent a significant decrease in head as D is reduced.
7. Some blade overlap should be maintained after cutting. Usually the initial blade overlap decreases with increasing specific speed, so the higher the specific speed, the less the allowable diameter reduction.

LIBERTY EXHIBIT 1017, Page 157

8. Diameter reductions greater than from 10 to 20% of the original full diameter of the impeller are rarely made.

Most of the losses are approximately proportional to Q^2, and hence to D^2 by Eq. 12. Because the power output decreases approximately as D^3, it is reasonable to expect the maximum efficiency to decrease as the wheel is cut, and this often is the case. By Eq. 12 and the n_s-definition (Eq. 38a of Section 2.1), the product n_sD should remain constant so the specific speed at best efficiency increases as the wheel diameter is reduced (Table 4).

The characteristics of the pump shown in Figure 13 may be used to illustrate reduction of diameter at constant speed. Starting with the best efficiency point and $D = 16\frac{5}{16}$ in (41.4 cm), let it be required to reduce the head from $H = 224.4$ to $H' = 192.9$ ft (68.4 m to 58.8 m) and to determine the wheel diameter, capacity, and power for the new conditions.

Because the speed is constant, Eqs. 12 may be written

$$H = k_H Q^2 \quad and \quad P = k_p Q^3 \tag{13}$$

where k_H and k_p may be obtained from the known operating conditions at $D = 16\frac{5}{16}$ in (41.4 cm). Plot a few points for assumed flow rates and draw the curve segments as shown by the solid lines in Figures 13*b* and 13*c*. Then, from Eqs. 12

$$D' = D\sqrt{H'/H} \qquad Q' = Q\sqrt{H'/H} \qquad P' = P(H'/H)^{3/2} \tag{14a}$$

$$D' = D(Q'/Q) \qquad H' = H(Q'/Q)^2 \qquad P' = P(Q'/Q)^3 \tag{14b}$$

from which $D = 15\frac{1}{8}$ in (38.4 cm), $Q = 3709$ gpm (234 l/s), and $P' = 215.5$ hp (160.7 kW). In Figure 13, the initial conditions were at points A and the computed conditions after cutting at points B. The test curve for $D = 15\frac{1}{8}$ in (38.4 cm) shows the best efficiency point a at a lower flow rate than predicted by Eqs. 14, but the head curve satisfies the predicted values very closely. The power prediction was not quite as good. Table 4 and Figure 13 give actual and predicted performance for three impeller diameters. The error in predicting the best efficiency point was computed by (predicted value minus test value) (100)/(test value). As the wheel diameter was reduced, the best efficiency point moved to a lower flow rate than predicted by Eq. 14 and the specific speed increased, showing that the conditions for Eqs. 12 to hold were not maintained.

Wheel cutting should be done in two or more steps with a test after each cut to avoid too large a reduction in diameter. Figure 14 shows an approximate correction, given by Stepanoff,[12] that may be applied to the ratio D'/D *as* computed by Eqs. 12 or 14. The accuracy of the correction decreases with increasing specific speed. Figure 15 shows a correction proposed by Rütschi[13] on the basis of extensive tests on low-specific-speed pumps. The corrected diameter reduction ΔD is the diameter reduction $D - D'$ given by Eqs. 14 and multiplied by k from Figure 15. The shaded area in Figure 15 indicates the range of scatter of the test points operating at or near maximum efficiency. Near shutoff the values of k were smaller and at maximum flow rate the values of k were larger than shown in Figure 15. Table 5 shows the results of applying Figures 14 and 15 to the pump of the preceding example.

There is no independent control of Q and H in impeller cutting, although Q may be increased somewhat by underfiling the blade tips as described later. The flow rate and power will automatically adjust to the values at which the pump head satisfies the system head-flow curve.

MIXED-FLOW IMPELLERS Diameter reduction of mixed-flow impellers is usually done by cutting a maximum at the outside diameter D_0 and little or nothing at the inside diameter D_i, as shown in Figure 16. Stepanoff[14] recommends that the calculations be based on the average diameter $D_{av} = (D_i + D_0)/2$ or estimated from the blade-length ratio *FK/EK* or *GK/EK* in Figure 16d. Figure 16 shows a portion of the characteristics of a mixed-flow impeller on which two cuts were made as in Figure 16b. The calculations were made by Eqs. 14 using the mean diameter

$$D_m = \sqrt{(D_o^2 + D_i^2)/2}$$

LIBERTY EXHIBIT 1017, Page 158

TABLE 4 Predicted characteristics at different impeller diameters on a radial-flow pump

	Test values					Predicted from D = $16\frac{5}{16}$ in (41.4 cm)			Predicted from D = $15\frac{1}{8}$ in (88.4 cm)		
D, in (cm)	Q, gpm (l/s)	H, ft (m)	P, hp (kW)	n_s (Ω_s)	n_sD (Ω_sD)	Q', gpm (l/s)	H', ft (m)	P', hp (kW)	Q', gpm (l/s)	H' ft (m)	P', hp (kW)
$16\frac{5}{16}$ (41.4)	4000 (252)	224.4 (68.4)	270.4 (201.6)	1953 (0.7146)	31,860 (29.54)	...	...	...	3888 (245) −2.93% error[a]	227.3 (69.3) 1.29% error[a]	272.2 (203.0) 0.68% error[a]
$15\frac{1}{8}$ (38.4)	3600 (227.1)	195.4 (59.6)	217.0 (161.8)	2055 (0.7519)	31,080 (28.87)	3709 (234) 3.02% error[a]	192.9 (58.8) −1.28% error[a]	215.5 (160.7) −0.69% error[a]	...	...	...
14 (35.6)	3200 (201.9)	163.6 (49.9)	167.2 (124.7)	2214 (0.8101)	31,000 (28.84)	3433 (217) 7.28% error[a]	165.3 (50.4) 1.03% error[a]	170.9 (127.4) 2.33% error[a]	3332 (210.2) 4.13% error[a]	167.4 (51.0) 2.33% error[a]	172.1 (128.3) 2.93% error[a]

[a]Error in predicting best efficiency point

LIBERTY EXHIBIT 1017, Page 159

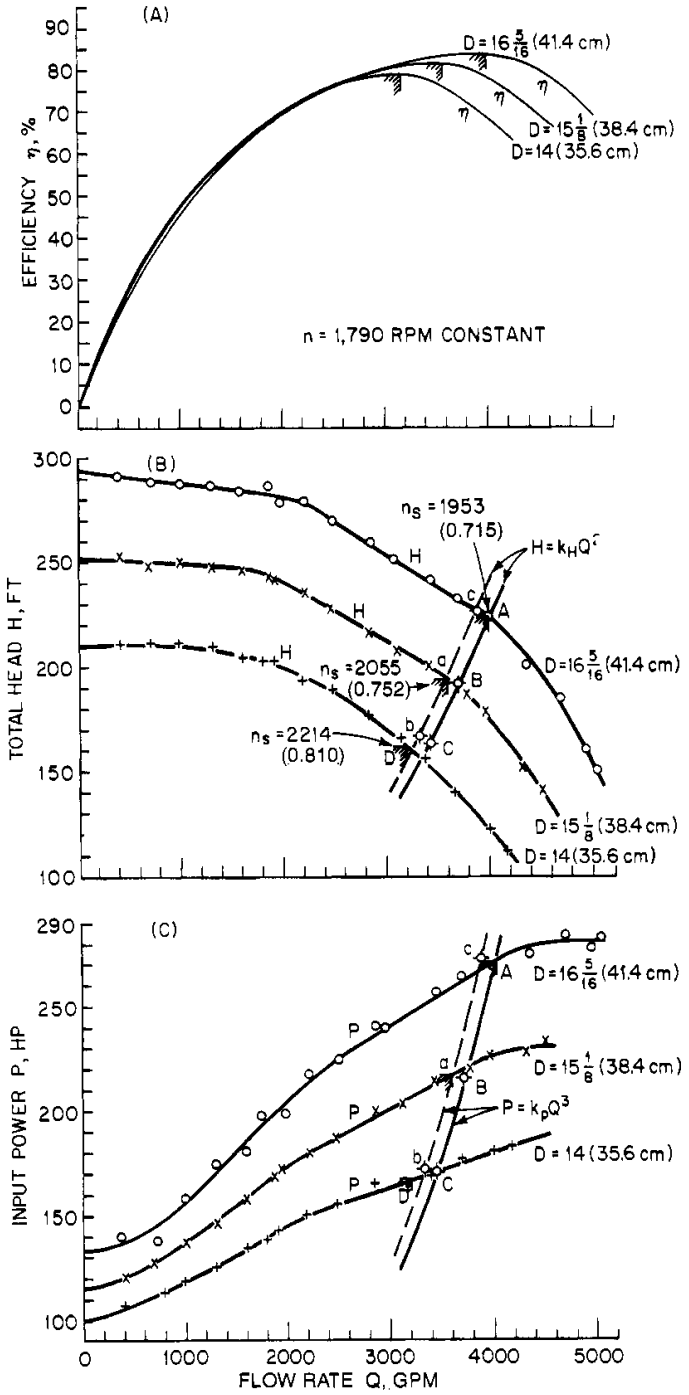


FIGURE 13A through C Diameter reduction of radial-flow impeller (gpm × 0.06309 = l/s). D is measured in inches (centimeters)

instead of the outside diameter in each case. The predictions and test results are shown in Figure 16 and Table 6. It is clear that the actual change in the characteristics far exceeded the predicted values. Except for the use of the mean diameters, the procedure was essentially the same as that described for Figure 13, and all points and curves are similarly labeled. The corrections given in Figure 14 would have made very little difference in the computed diameter reductions, and those of Figure 15 were not applicable to impellers having specific speeds greater than $n_s = 2000$ (0.73). In this case, the product $n_s D_m$ did not remain constant and the maximum efficiency increased as D_m was reduced. Although the

LIBERTY EXHIBIT 1017, Page 160

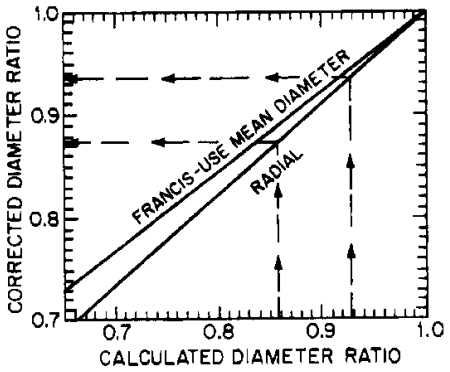


FIGURE 14 Corrections for calculated impeller diameter reductions (Reference 12)

changes in diameter were small, the area of blade removed was rather large for each cut. The second cut eliminated most of the blade overlap.

The characteristics of mixed-flow impellers can be changed by cutting, but very small cuts may produce a significant effect. The impellers of propeller pumps are not usually subject to diameter reduction.

Shaping Blade Tips If the discharge tips of the impeller blades are thick, performance usually can be improved by filing over a sufficient length of blade to produce a long, gradual taper. Chamfering, or rounding, the discharge tips may increase the losses and should never be done. Reducing the impeller diameter frequently increases the tip thickness.

OVERFILING This is shown at *B* in Figure 17, and the unfiled blade is shown at *A*. Usually there is little or no increase in the blade spacing d before and d_F after filing, so the discharge area is practically unchanged. Experience indicates that any change in the angle β_2 due to overfiling usually produces a negligible change in performance.

UNDERFILING This is shown at C in Figure 17. If properly done, underfiling will increase the blade spacing from d to d_f and hence the discharge area, which lowers the average meridional velocity c_{m2} at any given flow rate Q. The angle β_2 usually is increased slightly. Figure 18*A* and Eq. 6 show that the head and consequently the power increase at the same flow rate. The maximum efficiency usually is improved and may be moved to a higher flow rate. At the same head, Figure 18*B* shows that both c_{m2} and the flow rate will increase. The change both in the area and in C_{m2} may increase the flow rate by as much as 10%. Table 7 shows the results of tests before and after underfiling the impeller blades of nine different pumps. In general, they confirm the foregoing predictions based on changes in area and in the velocity triangles.

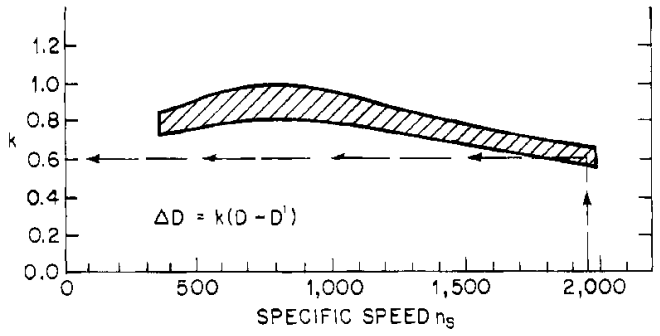


FIGURE 15 Corrections for calculated impeller diameter reductions (Reference 13). ($\Omega_s = n_s/2733$)

LIBERTY EXHIBIT 1017, Page 161

TABLE 5 Impeller diameter corrections

D before cutting	in	16.3125	16.3125
D' predicted by Eqs. (14)	in	15.125	14.000
D' corrected by Figure 14	in	15.25[a]	14.26[b]
D' corrected by Figure 15	in	15.60[c]	14.93[d]

[a] D'/D = 15.125/16.3125 = 0.927; by Figure 14, corrected D'/D = 0.935. Corrected D' = (0.935)(16.3125) = 15.25 in.

[b] D'/D = 14.000/16.3125 = 0858; by Figure 14, corrected D'/D = 0.874. Corrected D' = (0.874)(16.3125) = 14.26 in.

[c] $D - D'$ = 16.3125—15.125 = 1.1875; by Figure 15, $K \cong 0.6$ at n_s = 1,953. Corrected $D - D'$ = (0.6)(1.1875) = 0.7125 and corrected D' = 16.3125—0.7125 = 15.60 in.

[d] $D - D'$ = 16.3125—14.000 = 2.3125; by Figure 15, $K \cong 0.6$ at n_s = 1,953. Corrected $D - D'$ = (0.6)(2.3125) = 1.3875 and corrected D' = 16.3125—1.3875 = 14.93 in.

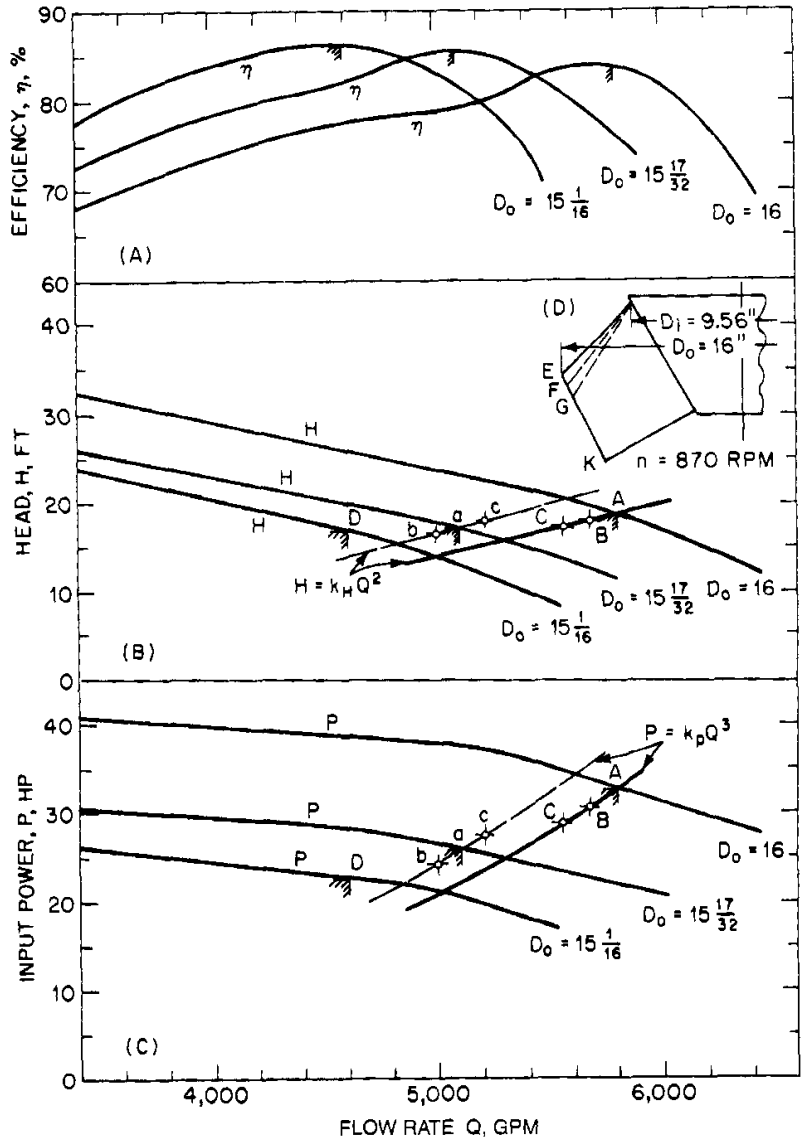


FIGURE 16A through C Diameter reduction of mixed-flow impeller (ft × 0.3048 = m; in × 2.540 = cm; gpm × 0.06309 = l/s; hp × 0.7457 = kW)

LIBERTY EXHIBIT 1017, Page 162

TABLE 6 Predicted characteristics at different impeller diameters on a mixed-flow pump

		Test values					Predicted from D = 16.00 (40.64 cm), D_m = 13.17 (33.45 cm)			Predicted from D = 15.53 (39.45 cm), D_m = 12.89 (32.74 cm)		
D, in (cm)	D_m, in (cm)	Q, gpm (l/s)	H, ft (m)	P, hp (kW)	n_s	n_sD_m	Q', gpm (l/s)	H', ft (m)	P', hp (kW)	Q', gpm (l/s)	H', ft (m)	P', bp (kW)
16 (40.64)	13.17 (33.45)	5800 (365.9)	18.6 (5.67)	32.5 (24.2)	7385 (2.702)	97,300 (90.39)	...	...	...	5210 (329) −11.3% error	17.9 (5.46) −3.91% error	27.4 (20.4) −18.6% error
$15\frac{17}{32}$ (39.45)	12.89 (32.74)	5100 (321.8)	17.1 (5.21)	25.7 (19.2)	7385 (2.702)	95,200 (88.47)	5680 (358.4) 10.2% error[a]	17.8 (5.43) 4.50% error[a]	30.4 (22.7) 15.5% error[a]			
$15\frac{1}{16}$ (38.26)	12.62 (32.05)	4600 (290.2)	16.8 (5.12)	22.6 (17.1)	7100 (2.598)	89,600 (83.26)	5560 (350.8) 17.3% error[a]	17.1 (5.21) 1.75% error[a]	28.6 (21.6) 21.0% error[a]	5000 (315.5) 8.00% error[a]	16.4 (5.00) −2.44% error[a]	24.1 (18.2) 6.22% error[a]

[a]Error in predicting best efficiency point

LIBERTY EXHIBIT 1017, Page 163

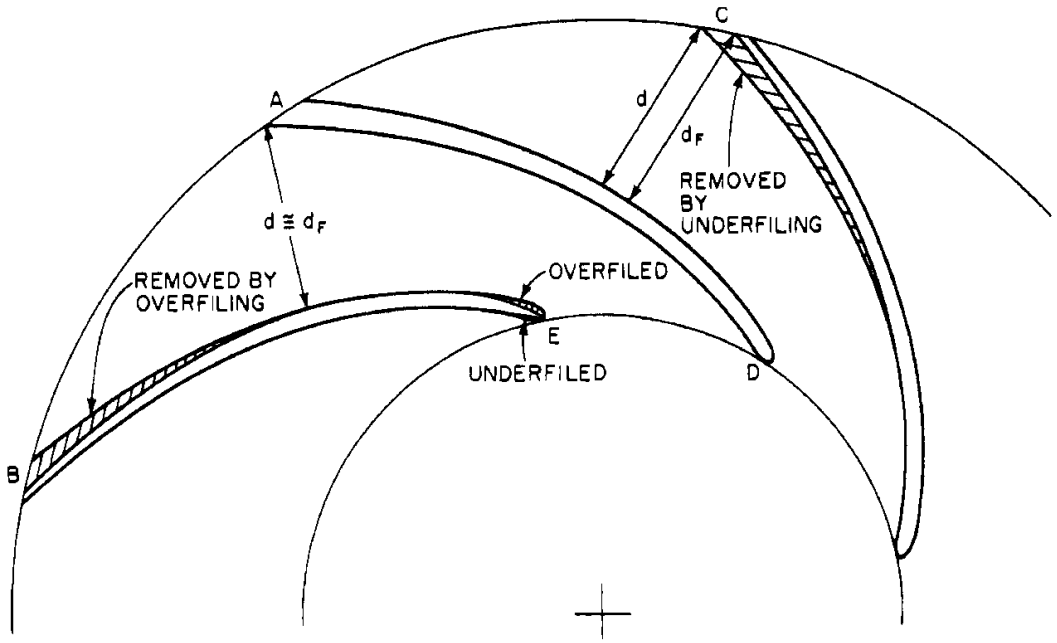


FIGURE 17 Underfiling and overfiling of blade tips

INLET BLADE TIPS If the inlet blade tips are blunt, as shown at *D* in Figure 17, the cavitation characteristics may be improved by sharpening them, as shown at *E*. In this case overfiling increases the effective flow area, which reduces c_{m1} for a given flow rate. If more area is needed, it may be advantageous to cut back part of the blade and sharpen the leading edge. Overfiling tends to increase β_1, which is incompatible with a decrease in c_{m1} (Figure 19). The increase in β_1 increases the angle of attack of the liquid approaching the blade. In Figures 2 and 19, w_1 is tangent to the centerline of the blade at entrance and w_0

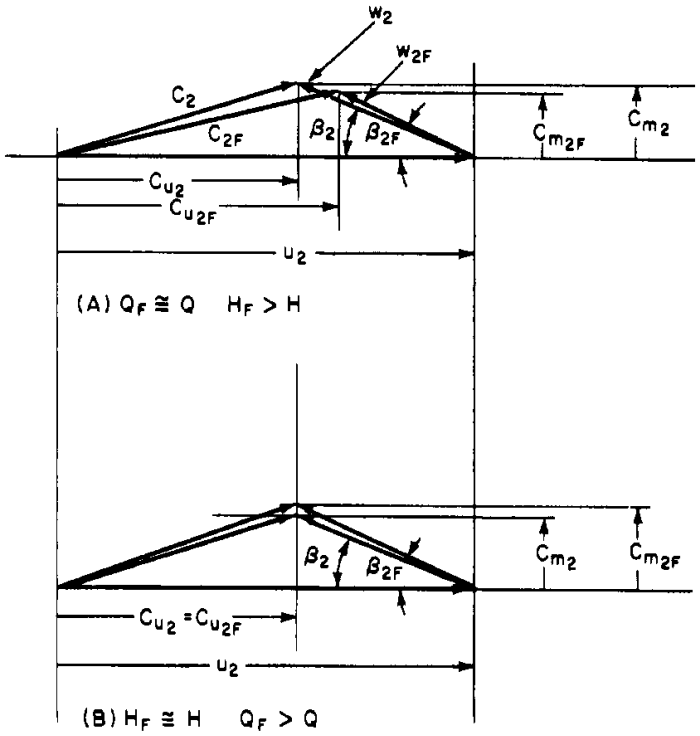


FIGURE 18 Discharge velocity triangles for underfiled blades (neglecting slip)

LIBERTY EXHIBIT 1017, Page 164

TABLE 7 Changes in performance when impeller blades are underfiled

Specific speed n_s	Specific speed Ω_s	No. of stages	Impeller diameter D_2, in	Impeller diameter D_2, (cm)	Change in blade spacing d_F/d	$\frac{H_F - H}{H}$ %[b]	Changes at best efficiency point after filing, % H_o[c]	H	Q	P	η
862	(0.3154)	1	$11\frac{1}{2}$	(29.21)	1.13	4	1.5	4	0	9	−5
945	(0.3458)	2	$8\frac{3}{8}$	(21.27)	1.05	5.5	0	3	4	−0.5	7.5[d]
1000	(0.3659)	4	$9\frac{1}{8}$	(23.18)	1.055	5.5	0	5.5	0	3	2.5
1080	(0.3952)	2	$9\frac{13}{16}$	(24.92)	1.08	10	2.5	10	0	6.8	3
1525	(0.5580)	2	$10\frac{1}{2}$	(26.67)	1.035	3.2	3	0.5	4.5	3.5	1.2
1950	(0.7135)	1	22	(55.88)	1.02	1.5	1	1.5	0	1.5	0
3300[a]	(1.2075)	1	12	(30.48)	...	7.8	2.5	7.8	0	8.5	−0.6
3450[a]	(1.2623)	1	$30\frac{1}{2}$	(77.47)	...	6.5	0.5	6.5	0	7.8	−2.2
4300	(1.5734)	1	$41\frac{1}{4}$	(104.8)	...	5		5	0	0.5	4.5[e]

[a]Double suction.
[b]H_F is head after filing.
[c]Shutoff head.
[d]Due in part to changes in pump casing.
[e]Due in part to rounding of inlet blade tips.
Source: Flowserve Corporation

is the velocity of the approaching liquid as seen by an observer moving with the blade. The angle δ between w_0 and w_1 is the angle of attack, which increases to δ_F after overfiling. Although the increase in δ tends to increase the opportunity for the liquid to separate from the low-pressure face of the blade, this disadvantage usually is outweighed by the improvement that results when c_{m1} is reduced.*

CASING TONGUE The casing tongue or cutwater forms part of the throat of the discharge nozzle of many volute casings (Figure 20a, Section 2.1.1). Frequently the throat area is small enough to act as a throttle and reduce the maximum flow rate otherwise obtainable from the impeller. Cutting back the tongue increases the throat area and increases the maximum flow rate. The head-versus-flow rate characteristic is then said to *carry out farther.* Shortening the discharge nozzle may increase the diffusion losses a little and result in a slightly lower efficiency.

CAVITATION

The formation and subsequent collapse of vapor-filled cavities in a liquid due to dynamic action are called *cavitation.* The cavities may be bubbles, vapor-filled pockets, or a combination of both. The local pressure must be at or below the vapor pressure of the liquid for cavitation to begin, and the cavities must encounter a region of pressure higher than the vapor pressure in order to collapse. Dissolved gases often are liberated shortly before vaporization begins. This may be an indication of impending cavitation, but true cavitation

*The distinction between a true velocity diagram formed just upstream of the impeller blades and the triangles shown just inside the blades in Figure 19 should be noted. w_1 in this figure is shown aligned with the blade, having undergone an adjustment in direction via incidence from that of the approaching w_0. Only by plotting the velocity diagram just upstream of this point can one determine the true value of the circumferential component c_{u1} of the absolute velocity being delivered to the impeller by the upstream piping, vanes, and so on. It is this delivered value of c_{u1} that must be used in computing input or ideal head of the impeller (Eq. 15b, Section 2.1.1 or, neglecting slip, Eq. 6 of this section). Thus w_0 is properly the true w_1 vector and should be understood as such (see Section 2.1.1).

LIBERTY EXHIBIT 1017, Page 165

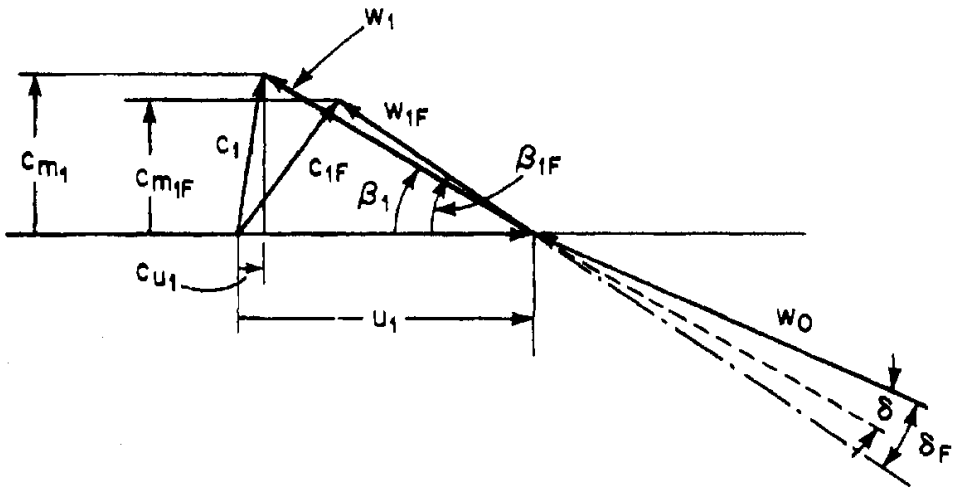


FIGURE 19 Effect of overfiling at inlet on the velocity triangle just inside the blades

requires vaporization of the liquid. Boiling accomplished by the addition of heat or the reduction of static pressure without dynamic action of the liquid is arbitrarily excluded from the definition of cavitation.

When a liquid flows over a surface having convex curvature, the pressure near the surface is lowered and the flow tends to separate from the surface. *Separation* and *cavitation* are completely different phenomena. Without cavitation, a separated region contains turbulent eddying liquid at pressures higher than the vapor pressure. When the pressure is low enough, the separated region may contain a vapor pocket that fills from the downstream end,[15] collapses, and forms again many times each second. This causes noise and, if severe enough, vibration. Vapor-filled bubbles usually are present and collapse very rapidly in any region where the pressure is above the vapor pressure. Knapp[16] found the life cycle of a bubble to be on the order of 0.003 s.

Bubbles that collapse on a solid boundary may cause severe mechanical damage. Shutler and Mesler[17] photographed bubbles that distorted into toroidal-shaped rings during collapse and produced ring-shaped indentations in a soft metal boundary. The bubbles rebounded following the initial collapse and caused pitting of the boundary. Pressures on the order of 10^4 atm have been estimated[18] during collapse of a bubble. All known materials can be damaged by exposure to bubble collapse for a sufficiently long time. This is properly called *cavitation erosion,* or *pitting.* Figure 20 shows extensive damage to the suction side of pump impeller vanes after about three months' operation with cavitation. At two locations, the pitting has penetrated deeply into the $\frac{3}{8}$-in (9.5-mm) thickness of stainless steel. The unfavorable inlet flow conditions, believed to have been the cause of the cavitation, were at least partly due to elbows in the approach piping. Modifications in the approach piping and the pump inlet passages reduced the cavitation enough to extend impeller life to several years.[19]

It has been postulated that high temperatures and chemical action may be present at bubble collapse, but any damaging effects due to them appear to be secondary to the mechanical action. It seems possible that erosion by foreign materials in the liquid and cavitation pitting may augment each other. Controlled experiments[20] with water indicated that the damage to metal depends on the liquid temperature and was a maximum at about 100 to 120°F (38 to 49°C). Cavitation pitting, as measured by weight of the boundary material removed per unit time, frequently increases with time. Cast iron and steel boundaries are particularly vulnerable. Controlled experiments have shown that cavitation pitting in metals such as aluminum, steel, and stainless steel depends strongly on the velocity of the fluid in the undisturbed flow past the boundary. On the basis of tests of short duration, Knapp[15] reported that damage to annealed aluminum increased approximately as the sixth power of the velocity of the undisturbed flow past the surface. Hammitt[21] found a more complicated relationship between velocity and damage, as shown in Figure 21. It seems clear that after cavitation begins, it will increase rapidly with increasing velocities. Frequently the rate of pitting accelerates with elapsed time. Comprehensive discussions of cavitation and erosion together with additional references are given by Preece.[22]

LIBERTY EXHIBIT 1017, Page 166

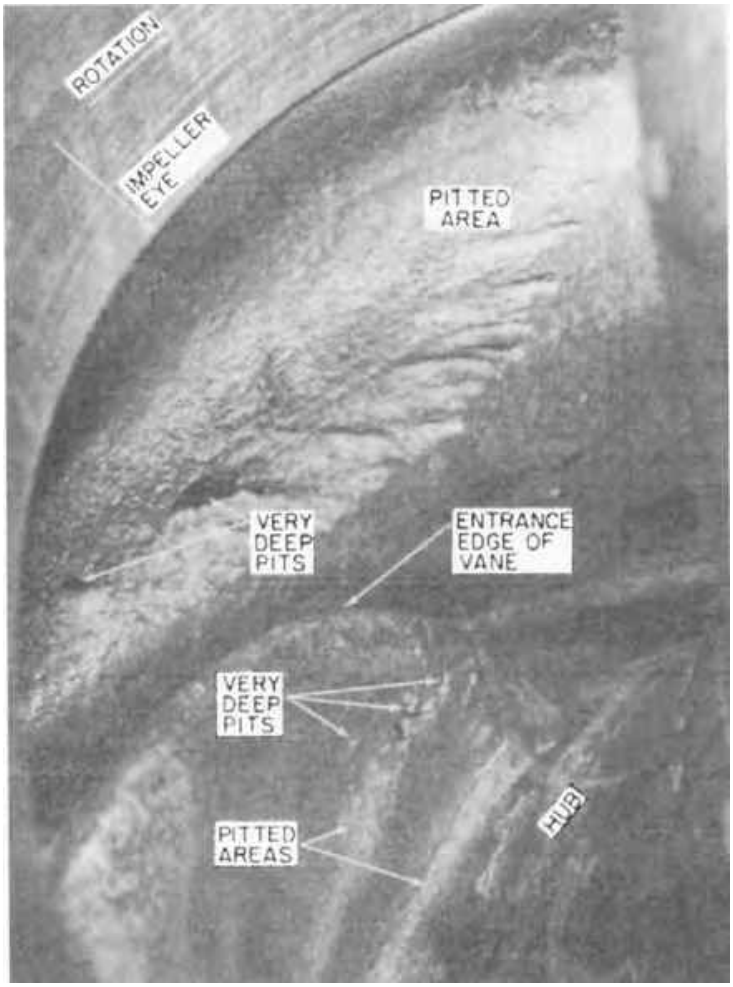


FIGURE 20 Impeller damaged by cavitation (Demag Delaval, Reference 19)

Centrifugal pumps begin to cavitate when the suction head is insufficient to maintain pressures above the vapor pressure throughout the flow passages. The most sensitive areas usually are the low-pressure sides of the impeller vanes near the inlet edge and the front shroud, where the curvature is greatest. Axial-flow and high-specific-speed impellers without front shrouds are especially sensitive to cavitation on the low-pressure sides of the blade tips and in the close tip-clearance spaces. Sensitive areas in the pump

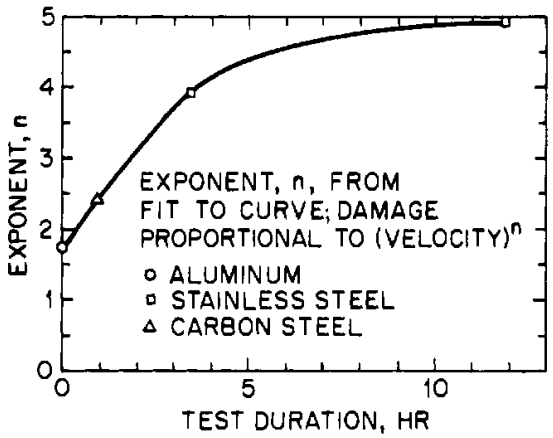


FIGURE 21 Cavitation damage exponent versus test time for several materials in water (Reference 21)

LIBERTY EXHIBIT 1017, Page 167

casing include the low-pressure side of the tongue and the low-pressure sides of diffusion vanes near the inlet edges. As the suction head is reduced, all existing areas of cavitation tend to increase and additional areas may develop. Apart from the noise and vibration, cavitation damage may render an impeller useless in as little as a few weeks of continuous operation. In multistage pumps cavitation usually is limited to the first stage, but Kovats[23] has pointed out that second and higher stages may cavitate if the flow is reduced by lowering the suction head (submergence control). Cavitation tends to lower the axial thrust of an impeller. This could impair the balancing of multistage pumps with opposed impellers. A reduction in suction pressure may cause the flow past a balancing drum or disk to cavitate where the liquid discharges from the narrow clearance space. This may produce vibration and damage resulting from contact between fixed and running surfaces.

Net Positive Suction Head (NPSH) Several criteria exist for establishing the NPSH of a pump. These are connected with a) inception of cavitation, b) loss of hydraulic performance, and c) protecting the pump against cavitation erosion or damage. These are defined and found as follows:

a. *Inception* NPSH. Cavitation can be completely prevented so long as the static pressure within the pump is everywhere greater than the vapor pressure of the liquid. This can be achieved if the NPSH (also called h_{sv}), defined in Section 2.1.1 as the total head of the pumped liquid at the pump inlet datum or suction flange above that vapor pressure, is sufficiently large. The value of NPSH that achieves this is called $NPSH_i$, namely, the "inception NPSH."

b. *Performance* NPSH. In a typical NPSH-test at constant speed n and flow rate Q, a substantial reduction of NPSH below $NPSH_i$ is usually necessary to reach the value that produces an identifiable drop in performance—usually 3% of pump stage total pressure rise or pump head. This value is called the "required NPSH," *NPSHR* or $NPSH_{3\%}$. Table 1 in Section 2.1.1 provides empirical correlations for $NPSH_{3\%}$ for common pumps and inducers. Other criteria for $NPSH_{3\%}$ will be given further on. The domains of cavitation within a pump are widespread at this condition, and experience shows that a head drop in the neighborhood of 3% must occur in order to obtain a repeatable value of *NPSHR* on test[12]. Lower percentages have been demanded by users, but they invariably give rise to a large scatter in the measured *NPSHR* for even small variations in any of the test variables.

It used to be thought throughout the pump community that there are no cavities or bubbles present at zero percent head drop due to cavitation activity within a pump. In recent decades, however, it has been proven through many observations that not only is the head drop equal to zero at inception (where NPSH = $NPSH_i$), it remains so for an enormous range of lesser NPSH-values over which extensive bubble activity is observed. In fact, $NPSH_i$ is commonly from two to five times the magnitude of the *NPSHR* that is associated with any noticeable drop in pump head. At the 3% (or lesser percentage) head drop condition, actual observations of the cavitating flow show the cavities to extend all the way from the leading edge of each blade to the throat formed by the leading edge of the next blade[24]. In the face of these learnings, it is evident that to demand a test for the NPSH required for a head drop of much less than 3% usually causes only needless misunderstandings and expenditure of time and money.

c. *Damage-Limiting* NPSH *or Life* NPSH. If it is desired to substantially reduce or eliminate cavitation activity within the pump, an acceptance test should be conducted wherein the cavitating flow can be observed visually[25]. This is indeed a serious issue if the pump energy level is high enough (and therefore the inlet pressure) for the collapsing cavities to do damage (as in Figure 20; see also Section 2.1.1). In such a case, "$NPSH_{3\%}$" has virtually no meaning; rather, the truly *required* NPSH or "*NPSHR*" is that *larger* value which satisfactorily limits the extent of this visually observed cavitation within the pump or pump model[26].

Therefore, the *available* NPSH at the installation must be at least equal to the *required* NPSH if the above consequences are to be avoided—be they significant loss of

LIBERTY EXHIBIT 1017, Page 168

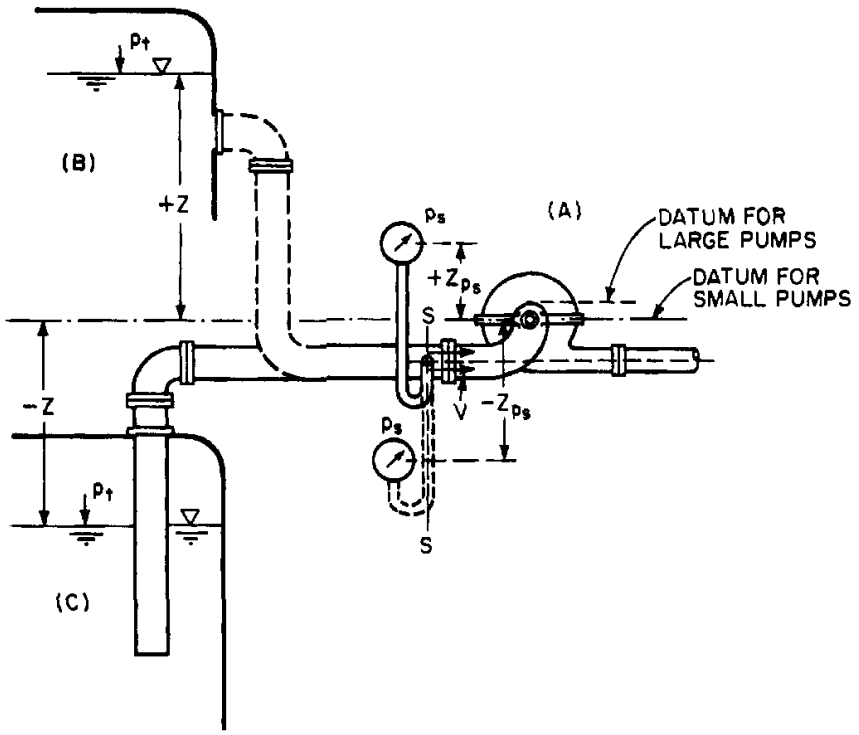


FIGURE 22 Definition sketch for computing NPSH

pump head (that is, loss of hydraulic performance) or damage due to collapsing cavities. Increasing the available NPSH above the required value provides a margin of safety against unpredictable variations of conditions, including transient behavior. Figure 22 and the following symbols will be used to compute the available NPSH:

p_a = absolute pressure in atmosphere surrounding gage, Figure 22

p_s = gage pressure indicated by gage or manometer connected to pump suction at section *s-s;* may be positive or negative

p_t = absolute pressure on free surface of liquid in closed tank connected to pump suction

p_{vp} = vapor pressure of liquid being pumped corresponding to the temperature at section *s-s* (if liquid is a mixture of hydrocarbons, p_{vp} must be measured by the *bubble point* method)

h_f = lost head due to friction in suction line between tank and section *s-s*

V = average velocity at section *s-s*

Z, Z_{ps} = vertical distances defined by Figure 22; may be positive or negative

γ = specific weight of liquid at pumping temperature

It is satisfactory to choose the datum for small pumps as shown in Figures 1 and 22, but with large pumps, the datum should be raised to the elevation where cavitation is most likely to start. For example, the datum for a large horizontal-shaft propeller pump should be taken at the highest elevation of the impeller-blade tips. The available NPSH is given by

$$h_{sv} = \frac{p_a - p_{vp}}{\gamma} + \frac{p_s}{\gamma} + Z_{ps} + \frac{V^2}{2g} \tag{15}$$

or

$$h_{sv} = \frac{p_t - p_{vp}}{\gamma} + Z - h_f \tag{16}$$

LIBERTY EXHIBIT 1017, Page 169

Consistent units must be chosen so that each term in Eqs. 15 and 16 represents feet (or meters) of the liquid pumped. Equation 15 is useful for evaluating the results of tests. Equation 16 is useful for estimating available NPSH during the design phase of an installation. In Eq. 15, the first term represents the height of a liquid barometer, h_b, containing the liquid being pumped and the sum of the remaining terms represents the suction head h_s; that is, the total head H (Eq. 3, Section 2.1.1) evaluated at the suction flange S in Figure 22. Therefore

$$h_{sv} = h_b + h_s \tag{17}$$

Usually, a positive value of h_s is called a *suction head* and a negative value of h_s is called a *suction lift.*

Many pumps draw cold water from reservoirs exposed to atmospheric pressure, so the suction lift is limited if there is to be a reasonable value of h_{sv} (= NPSH) available at the pump suction flange or port. In normal practice, rather small values of suction lift or suction head are encountered in many installations, so one can depend on the value of h_{sv} being a substantial portion of h_b—say about 60% or 20 ft (6m) of water column. Recognizing that the suction specific speed capability S of most pumps falls within a rather small range has led to charts of recommended operating speeds such as those in Section 12.11 or the speed recommendations of Figure 23 for condensate pumps for varying amounts of NPSH available. In fact, $S = 8500$ ($\Omega_{ss} = 3.11$) is recommended by the Hydraulic Institute[27]. S (= N_{ss}) and Ω_{ss} are defined in Eqs. 41 and 42 of Section 2.1.1. The relationship of suction-specific speed to other suction parameters is treated further on.

Cavitation Tests In addition to the constant-Q tests for *NPSHR* that were described in the foregoing review of the various NPSH-criteria, one can establish the curve of

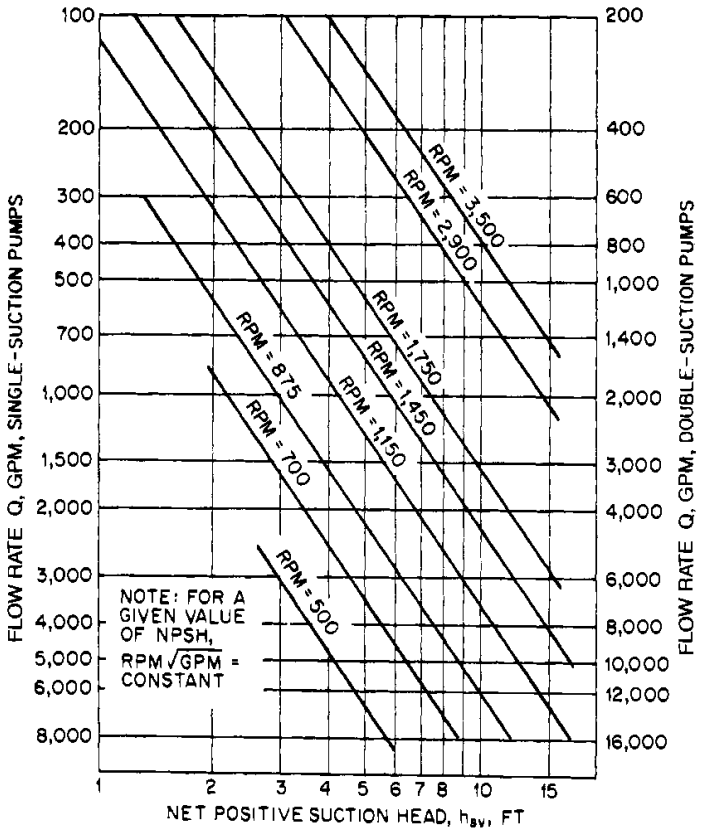


FIGURE 23 Capacity (flow rate) and speed limitations for condensate pumps with shaft through eye of impeller (ft × 0.3048 − m; gpm × 0.06309 = l/s) (adapted from Hydraulic Institute ANSI/HI 2000 Edition Pump Standards, Reference 27)

LIBERTY EXHIBIT 1017, Page 170

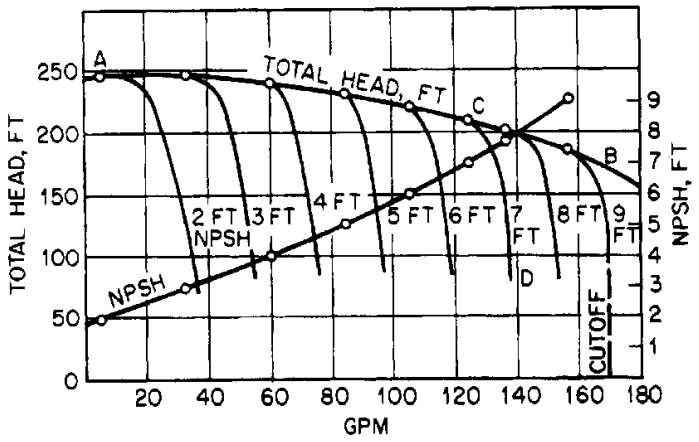


FIGURE 24 Test of a 1.5-in (3.81-cm) single-stage pump at 3470 rpm, on water, 70°F (21°C) (ft × 0.3048 = m; gpm × 0.06309 = l/s) (Reference 12)

performance NPSH versus flow rate by varying the NPSH available and seeing how much flow rate Q the pump can handle. This is illustrated in Figure 24, wherein a different head curve is found for each value of NPSH. For each such curve, as Q is increased, there is a point at which the head departs from the next one of higher NPSH. This, then, is the Q for which the given NPSH is that required to maintain head, essentially $NPSH_{3\%}$. At higher flow rate, performance is lost, each head curve possessing a "cutoff" flow rate. References 27 and 28 may be consulted for details of test procedures.

Thoma Cavitation Parameter σ All the terms in Eqs. 15 to 17 may be made dimensionless by dividing each by the pump head H. The resulting parameter

$$\sigma = \frac{h_{sv}}{H} \tag{18}$$

has proven to be useful especially for high-specific-speed pumps and turbines. The loading on the blades of a variable-pitch propeller, and therefore the minimum suction-side static pressure, is directly connected to the head developed. As this head increases with increasing blade setting angle, the loading increases, the minimum pressure drops, and the *NPSHR* goes up. Hence an identifiable limiting value of σ is found to exist for such a machine. σ-limits are presented for a range of specific speeds in Figure 25.

Performance-NPSH data are sometimes given in terms of σ; for example, Rütschi[13] presents the effect of pump hydraulic efficiency on NPSH in these terms, a consistently higher value of σ being required for pumps with lower efficiency (Figure 26).

Suction-Specific Speed For pumps in which the eye diameter of the impeller is smaller than that at exit, the pressures on the suction-sides of the blades that are associated with most of the head addition are in a region of higher pressure than in the vicinity of the eye. Thus Wislicenus[29] was able to decouple the eye from outer diameter of the pump (where most of the head is generated in a radial-flow machine) and show that only the eye geometry determines performance-NPSH and not the magnitude of the head created by the impeller. He demonstrated that for most centrifugal pumps (except the propellers just described), there is a small range of suction specific speed—from which the performance-NPSH can be determined. As in Section 2.1.1, this parameter is defined as follows:

$$S = \frac{N\sqrt{Q}}{(h_{sv})^{3/4}} \tag{19}$$

LIBERTY EXHIBIT 1017, Page 171

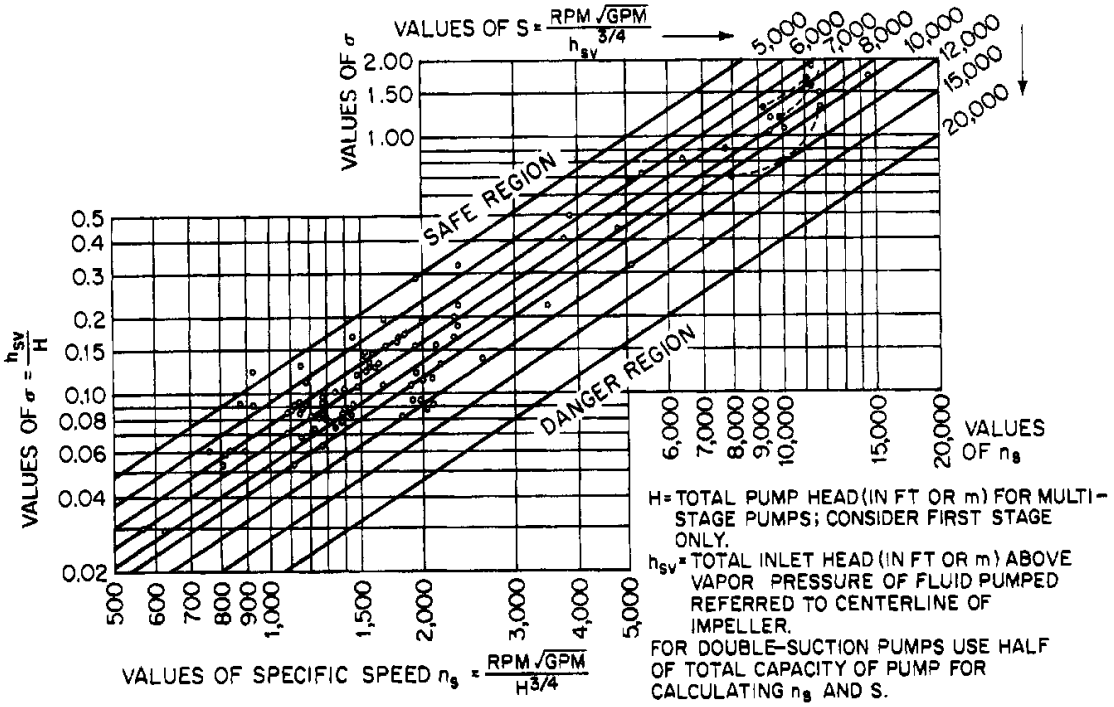


FIGURE 25 Cavitation limits of centrifugal and propeller pumps (Flowserve Corporation)

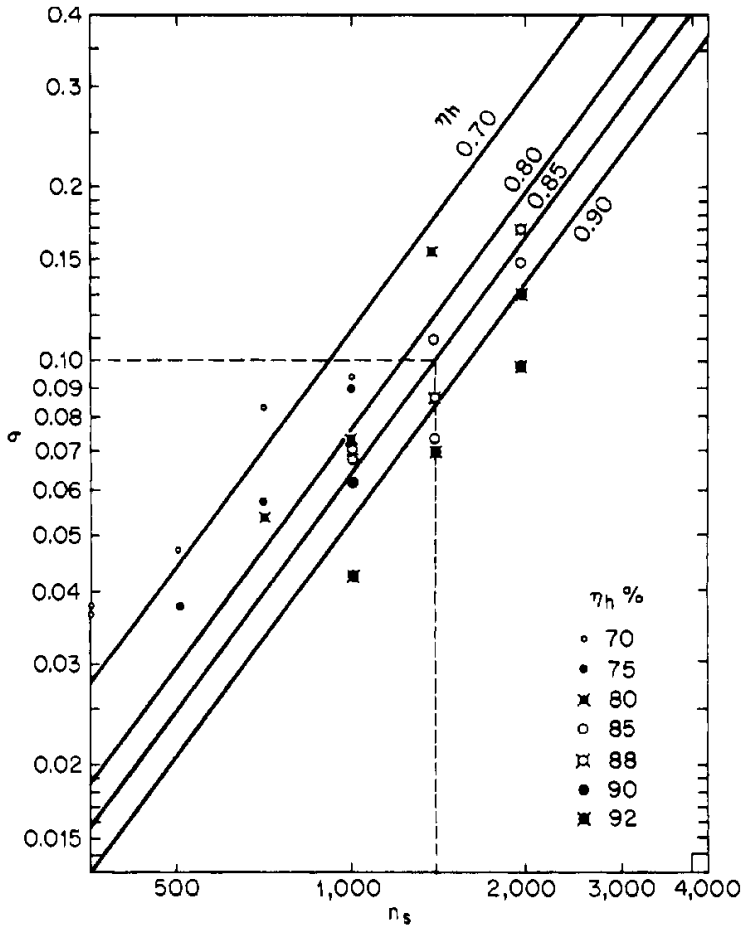


FIGURE 26 Cavitation parameter σ versus specific speed for different efficiencies ($\Omega_s = n_s/2733$) (Reference 13)

LIBERTY EXHIBIT 1017, Page 172

Note that Q = *half the discharge* of a double-suction impeller when computing S. Equations 18 and 19 and the definition of n_s may be combined to yield

$$\sigma = \left(\frac{n_s}{S}\right)^{4/3} \tag{20}$$

$$n_s = S(\sigma)^{3/4} \tag{21}$$

Figure 25 shows lines of constant S. For most pumps, $7500 < S < 11{,}000$ ($2.7 < \Omega_{SS} < 4.0$), S = 8500 (3.11) being recommended by the Hydraulic Institute ANSI/HI 2000 Pump Standards (Reference 27). Higher values may apply to special designs or service conditions, such as an inducer ahead of the first-stage impeller. For a given specific speed, the lower the value of S, the safer the pump against cavitation. Experience with large European pumped storage installations has shown that cavitation effects began at $S \approx 6000$ (2.2), and this value is recommended for large pumps. Figure 27 shows a summary of data and formulas that may be useful with commercial pumps.

German practice differs considerably from that in the United States in computing suction specific speed. Pfleiderer[1] defined a hub correction k as

$$k = 1 - \left(\frac{d_h}{D_o}\right)^2 \tag{22}$$

where d_h = the hub diameter and D_o = the diameter of the suction nozzle, in any consistent units. The suction specific speed S_G is defined as

$$S_G = \frac{(n/100)^2 Q}{k h_{sv}^{3/2}} \tag{23}$$

where n is measured in rpm, Q in cubic meters per second per impeller inlet, and h_{sv} in meters of liquid pumped. It follows that

$$S = 5164\sqrt{S_G k} \tag{24}$$

NPSH for Liquids Other Than Cold Water Field experience, together with carefully controlled laboratory experiments, has indicated that pumps handling hot water or certain

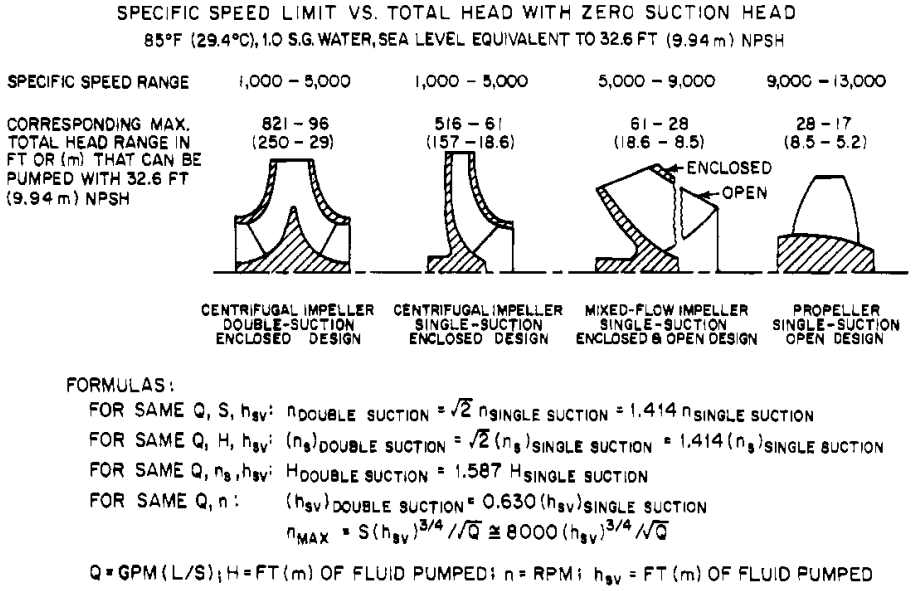


FIGURE 27 Commercial pumps applicable to zero suction head. Suction specific speed S = 8000 (Ω_{ss} = 2.93). For centrifugal impellers, n_s = 1,000-5,000 (Ω_s = 0.4-1.8); mixed-flow, 5,000-9,000 (1.8-3.3); propeller, 9,000-13,000 (1.3-4.8).

LIBERTY EXHIBIT 1017, Page 173

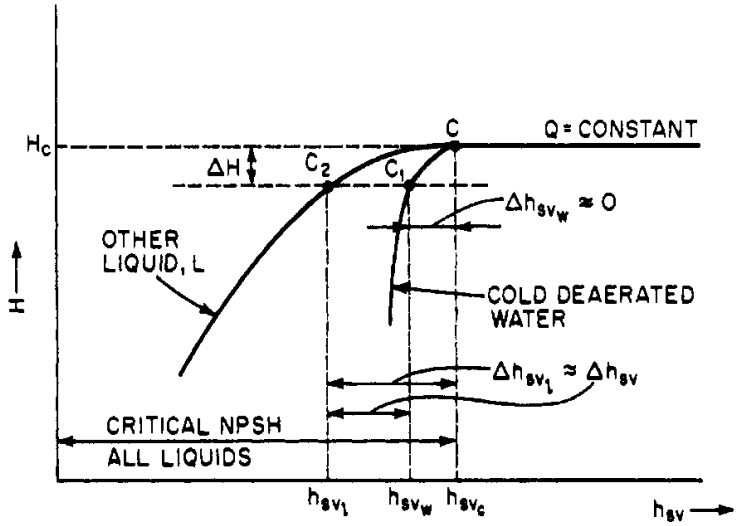


FIGURE 28 Cavitation tests with different liquids at constant speed and constant flow rate (Reference 34)

liquid hydrocarbons may be operated safely with less NPSH than would normally be required for cold water. This may lower the cost of an installation appreciably, particularly in the case of refinery pumps. A theory for this has been given by Stepanoff and others.[14,30–33] Figure 28 shows the results of cavitation tests on two liquids for constant capacity and constant pump speed. No head loss due to cavitation is present at point C or at $h_{sv} > h_{svc}$. With cold deaerated water, lowering h_{sv} slightly below h_{svc} produces limited cavitation and a decrease in pump head ΔH to point C_1, but Δh_{svw} usually is negligible. With hot water ($T \geq 100°F = 37.8°C$) or with many liquid hydrocarbons, a much larger decrease in h_{sv} will be required to produce the same drop in head ΔH that was shown by the cold water test. The NPSH *reduction,* or NPSH *adjustment,* is $\Delta H_{sv} \approx \Delta h_{svl}$. In practice, ΔH has been limited *to* $\Delta h \leq 0.03H$, for which there is a negligible sacrifice in performance. The pumps usually are made of stainless steel or other cavitation-resistant materials, and the lower NPSH results in lower collapse pressure of the vapor bubbles, reducing the damage potential.

Chart for NPSH Reductions A composite chart of NPSH *reductions* for deaerated hot water and certain gas-free liquid hydrocarbons is shown in Figure 29. The curves of vapor pressure versus temperature and the curves of constant NPSH reduction were based on laboratory tests with the liquids shown and should be used subject to the following limitations:

1. No NPSH reduction should exceed 50% of the NPSH required by the pump for cold water or 10 ft (3.0 m), whichever is smaller.
2. NPSH may have to be increased *above* the normal cold-water value to avoid unsatisfactory operation when (*a*) *entrained* air or other noncondensable gas is present in the liquid or (*b*) *dissolved* air or other noncondensable gas is present in the liquid and the absolute suction pressure is low enough to permit release of the gas from solution.
3. The vapor pressure of hydrocarbon mixtures vary significantly with temperature and so should be determined at pumping temperature (see Reference 27).
4. If the suction system may be susceptible to transient changes in absolute pressure or temperature, a suitable margin of safety in NPSH should be provided. This is particularly important with hot water and may exceed the reduction that would otherwise apply with steady-state conditions.
5. Although experience has indicated the reliability of Figure 29 for hot water and the liquid hydrocarbons shown, its use with other liquids is not recommended unless it is clearly understood that the results must be accepted on an experimental basis.

LIBERTY EXHIBIT 1017, Page 174

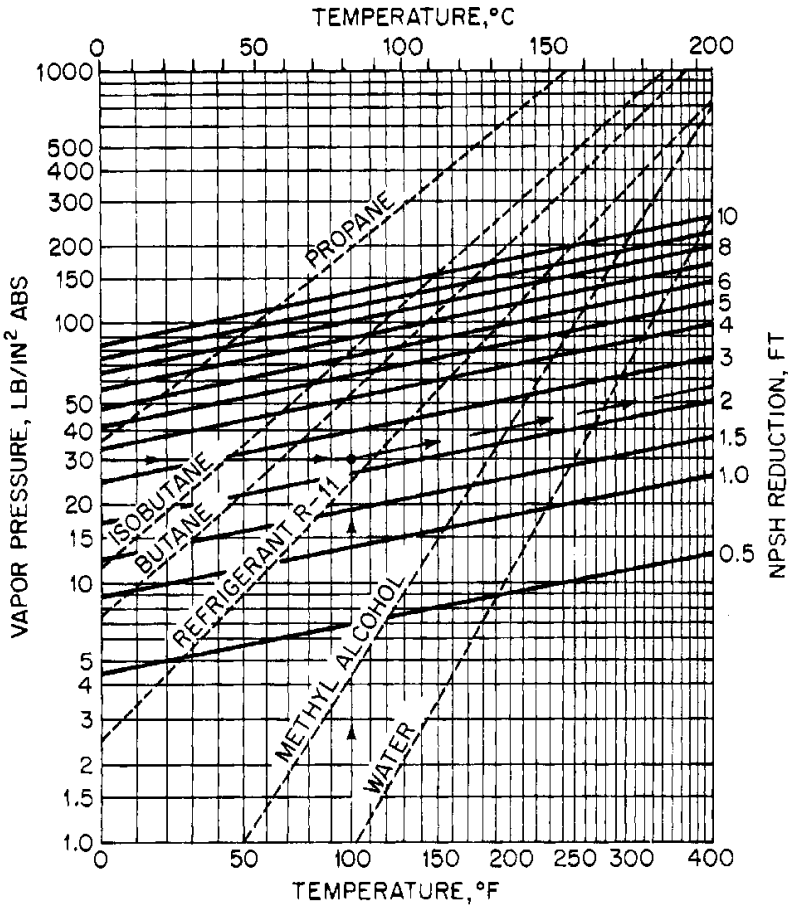


FIGURE 29 *NPSH* reductions for pumps handling liquid hydrocarbons and hot water. This chart has been constructed from test data obtained by using the liquids shown. For applicability to other liquids, refer to the text (ft × 0.3048 = m; lb/in² × 6.895 = kPa). (Hydraulic Institute ANSI/HI 2000 Edition Pump Standards, Reference 27)

USE OF FIGURE 29 Given a fluid having a vapor pressure of 30 lb/in² (210 kPa) abs at 100°F (37.8°C). Follow the arrows on the key shown on the chart and obtain an NPSH reduction of about 2.3 ft (0.70 m). Since this does not correspond to one of the liquids for which vapor pressure curves are shown on the chart, the use of this NPSH reduction should be considered a tentative value only. Given a pump requiring 16-ft (4.9-m) cold-water NPSH at the operating capacity, the pump is to handle propane at 55°F (12.8°C). Figure 29 shows the vapor pressure to be about 105 lb/in² (733 kPa) abs and the NPSH reduction to be about 9.5 ft (2.9 m). Since this exceeds 8 ft (2.44 m), which is half the cold-water NPSH, the recommended NPSH for the pump handling propane is half the cold-water NPSH, or 8 ft (2.44 m). If the temperature of the propane in the previous example is reduced to 14°F (−10°C), Figure 29 shows the vapor pressure to be 50 lb/in⁵ (349 kpa) abs and the NPSH reduction to be about 5.7 ft (1.74 m), which is less than half the coldwater NPSH. The NPSH required for pumping propane at 14°F (−10°C) is then 16 − 5.7 = 10.3 ≈ 10 ft (4.87 − 1.74 = 3.13 ≈ 3 m).

Reduction of Cavitation Damage After the pump has been built and installed*, there is little that can be done to reduce cavitation damage. As previously mentioned, sharpening the leading edges of the blades by filing may be beneficial. Stepanoff[12] has suggested cutting back part of the blades in the impeller eye together with sharpening the tips, for low-specific-speed pumps, as a means of reducing the inlet velocity c_1 and thus lowering σ. Although a small amount of prerotation or prewhirl in the direction of impeller rotation

*Sometimes it is possible to lower the pump, and this should be considered before other alterations are made.

LIBERTY EXHIBIT 1017, Page 175

may be desirable[34], excessive amounts should be avoided. This may require straightening vanes ahead of the impeller and rearranging the suction piping to avoid changes in direction or other obstructions. The cavitation damage to the impeller shown in Figure 20 was believed to have been at least partly due to bad flow conditions produced by two 90° elbows in the suction piping. The planes of the elbows were at 90° to each other, and this arrangement should be avoided.

Straightening vanes in the impeller inlet may increase the NPSH requirement at all flow rates. Three or four radial ribs equally spaced around the inlet and extending inward about one-quarter of the inlet diameter are effective against excessive prerotation and may require less NPSH than full-length vanes. This is very important with axial-flow pumps, which are apt to have unfavorable cavitation characteristics at partial flow rates. Operation near the best efficiency point usually minimizes cavitation.

The admission of a small amount of air into the pump suction tends to reduce cavitation noise.[7] This rarely is done, however, because it is difficult to inject the right amount of air under varying head and flow rate conditions and frequently there are objections to mixing air with the liquid pumped.

If a new impeller is required because of cavitation, the design should take into account the most recent advances described in the literature. Gongwer[35] has suggested (1) the use of ample fillets where the blades join the shrouds, (2) sharpened leading edges of blades, (3) reduction of β, in the immediate vicinity of the shrouds, and (4) raking the leading edges of the blades forward out of the eye. Increasing the number of blades for propeller pumps lowers σ for a given submergence. A change in the impeller material may be very beneficial, as described below.

Resistance of Materials to Cavitation Damage Table 8 shows the relative resistance of several metals to cavitation pitting produced by magnetostriction vibration. It will be seen that cast iron, the most commonly used material for impellers, has relatively little pitting resistance relative to bronze and stainless steel, which are readily cast and finished.

Damage due to cavitation erosion is commonly assessed in terms of the depth of penetration. The life of an impeller is generally considered to be the time required for cavitation erosion to reach a depth of 75% of the blade thickness at any point[36]. The life of any material in years can be expressed as the product of the mean depth of penetration rate

TABLE 8 Cavitation erosion resistance of metals

Alloy	Magnetostriction Weight Loss after 2 h, mg
Rolled stellite[a]	0.6
Welded aluminum bronze	3.2
Cast aluminum bronze	5.8
Welded stainless steel (2 layers, 17 Cr-7 Ni)	6.0
Hot rolled stainless steel (26 Cr-13 Ni)	8.0
Tempered rolled stainless steel (12 Cr)	9.0
Cast stainless steel (18 Cr-8 Ni)	13.0
Cast stainless steel (12 Cr)	20.0
Cast manganese bronze	80.0
Welded mild steel	97.0
Plate steel	98.0
Cast steel	105.0
Aluminum	124.0
Brass	156.0
Cast iron	224.0

[a]Despite the high resistance of this material to cavitation damage, it is not suitable for ordinary use because of its comparatively high cost and the difficulty encountered in machining and grinding.

Source: Reference 69.

LIBERTY EXHIBIT 1017, Page 176

(*MDPR*, in mm per year) times the thickness of the material in mm. Values of MDPR have been deduced[37] from the weight loss of test samples of known diameter in a magnetostriction test (Table 8)[38]. Unfortunately, *MDPR*-values obtained in such tests are not the same as those of actual pumps, as the mode of cavitation varies with pump operating conditions and is generally different from the laboratory results. Nevertheless, laboratory results for *MDPR* have been used to rank the ability of various materials to resist cavitation erosion in pumps. See Section 8.1 for material selection guidelines.

Cavitation-resistant coatings, either metallic or nonmetallic, have found some niche applications. Elastomeric coatings are resilient and resist cavitation through a different erosion mechanism than that of metal. As such, they can be very effective[69]. At least two considerations are involved in the use of coatings for resisting cavitation damage: 1) even if a contemplated coating demonstrates a reduced damage or erosion rate, this reduction must be enough to justify the cost of establishing a satisfactory bond between the coating and the base metal; 2) erosion of both the coating and the base material must be considered in determining the life according to the above 75%-depth criterion. Therefore, the life in this case would be equal to the *MDPR* of the coating times the coating thickness plus the *MDPR* of the base material times the allowable erosion depth of that material.

Inducers It is sometimes difficult or impossible to provide the required NPSH for an otherwise acceptable pump. Besides normal industrial situations that might produce a very low available NPSH, the need to keep the weight down in aircraft and rocket liquid-propellant pumps has led to high rotative speeds, which, for typical values of NPSH, produce extremely high suction specific speeds. The performance-NPSH required by the impeller under these circumstances can be provided by a small, axial-flow booster pump, called an inducer, placed ahead of the first-stage impeller[39]. Inducers are designed to operate with very low NPSH and to provide enough head to satisfy the NPSH required by the impeller. In fact, long stable cavities are established on the suction sides of the long, lightly-loaded blades of an inducer, which enable it to operate at about twice the suction specific speed of a conventional impeller[40,41]. At lower than normal flow rates, however, inducers readily produce swirling, destabilizing backflow at the inlet, which can cause excessive pump vibration in high-head pumps. These instabilities can be overcome by various passive design features, such as that described in Reference 39.

The inducers described in Reference 42 (Figure 30) have "constant lead" helical blades. They contribute not more than 5% of the total pump head. Although the efficiency of the inducer alone is low, the reduction in overall pump efficiency is not significant. Because this type of inducer causes prerotation, a careful match between inducer and suction impeller is required. In vertical multistage pumps, where a long shaft can be better supported, a vaned diffuser may be inserted between the inducer and the first-stage impeller. Such an arrangement is very beneficial for operation at reduced flow rate. Reference 42 shows that a suitable inducer-impeller combination can operate at about 50% of the NPSH required for the impeller alone at flow rates not exceeding the normal value. The NPSH requirement increases rapidly for flow rates above normal. Unless a variable-lead inducer is used[32,39], operation in this range should be avoided.

Entrained Air Air or other gases may enter the impeller inlet from several sources. The immediate effect usually will be a drop in pump pressure rise, flow rate, and power. This will be followed by loss of prime if more gas is present than the impeller can handle. A typical limit for commercial industrial pumps is an inlet gas-to-liquid volume fraction (GVF) of 0.03, although specialty pumps such as those used in aircraft (Section 12.18.1) can handle higher GVF. See also Reference 10, Section 2.1.1. Air may be released from solution or enter through leaks in the suction piping. Stuffing box air leakage may be prevented by lantern rings supplied with liquid from the pump discharge. If the pump takes water from a sump with a free surface, a vortex may form from the free surface to the impeller inlet. The remedy may be the introduction of one or more baffle plates or even major changes in the sump. For information on proper sump design and the prevention of air-entraining vortices, see Sections 13.1 and 13.2, pp. 457 and 460 of Reference 7, and Reference 43. It is sometimes permissible to inject a small amount of air into the pump

Previous Page

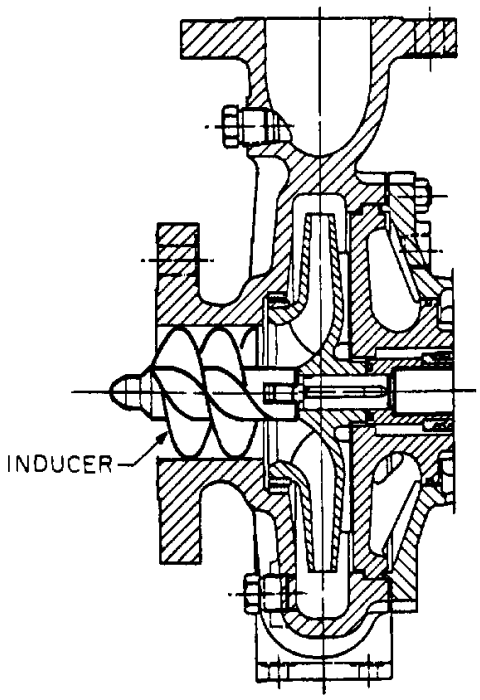


FIGURE 30 Pump fitted with inducer (Reference 42)

suction to reduce the noise and damage from cavitation caused by inadequate NPSH or recirculation in the impeller.

STARTING CENTRIFUGAL PUMPS

Priming Centrifugal pumps usually are completely filled with the liquid to be pumped *before starting*. When so filled with liquid, the pump is said to be *primed*. Pumps have been developed to start with air in the casing and then be primed.[44] This procedure is unusual with low-specific-speed pumps but is sometimes done with propeller pumps[12]. In many installations, the pump is at a lower elevation than the supply and remains primed at all times. This is customary for pumps of high specific speed and all pumps requiring a positive suction head to avoid cavitation.

Pumps operated with a suction lift may be primed in any of several ways. A relatively inexpensive method is to install a special type of check valve, called a foot *valve,* on the inlet end of the suction pipe and prime the pump by filling the system with liquid from any available source. Foot valves cause undesirable frictional loss and may leak enough to require priming before each starting of the pump. A better method is to close a valve in the discharge line and prime by evacuating air from the highest point of the pump casing. Many types of vacuum pumps are available for this service. A priming chamber is a tank that holds enough liquid to keep the pump submerged until pumping action can be initiated. Self-priming pumps usually incorporate some form of priming chamber in the pump casing. Section 2.2.2 and Reference 7 may be consulted for further details.

Torque Characteristics of Drivers Centrifugal pumps of all specific speeds usually have such low starting torques (turning moments) that an analysis of the starting phase of operation seldom is required. Steam and gas turbines have high starting torques, so no special starting procedures are necessary when they are used to drive pumps. If a pump is directly connected to an internal combustion engine, the starting motor of the engine should be made adequate to start both driver and pump. If the starter does not have enough torque to handle both units, a clutch must be provided to uncouple the pump until the driver is started.

Electric motors are the most commonly used drivers for centrifugal pumps. Direct current motors and alternating current induction motors usually have ample starting torque for all pump installations, provided the power supply is adequate. Many types of reduced voltage starters are available[7] to limit the inrush current to safe values for a given power supply. Synchronous motors are often used with large pumps because of their favorable power-factor properties. They are started as induction motors and run as such up to about 95% of synchronous speed. At this point, dc field excitation is applied and the maximum torque the motor can then develop is called the poll-in *torque,* which must be enough to accelerate the motor and connected inertia load to synchronous speed in about 0.2 s if synchronous operation is to be achieved. Centrifugal pumps usually require maximum torque at the normal operating point, and this should be considered in selecting a driver, particularly a synchronous motor, to be sure that the available pull-in torque will bring the unit to synchronous speed.

Torque Requirements of Pumps The *torque,* or turning moment, for a pump may be estimated from the power curve in USCS units by

$$M = \frac{5252P}{n} \tag{25}$$

and in SI units by

$$M = \frac{9549P}{n}$$

where M = pump torque, lb · ft (N · m)
P = power, hp (kW)
n = speed, rpm

Equation 25 makes no allowance for accelerating the rotating elements or the liquid in the pump. If a 10% allowance for accelerating torque is included, the constant should be correspondingly increased. The time Δt required to change the pump speed by an amount $\Delta n = n_2 - n_1$ is given by

$$\Delta t = \frac{I\Delta n}{k(M_m - M)} \tag{26}$$

where Δt = time, s
I = moment of inertia (flywheel effect) of all rotating elements of driver, pump, and liquid, lb · ft (kg · m^2)
Δn = change in speed, rpm
k = 307 in USCS (9.549 in SI)
M_m = driver torque, lb · ft (N · m)
M = pump torque, lb · ft (N · m) (Eq. 25)

The inertia I of the driver and pump usually can be obtained from the manufacturers of the equipment. The largest permissible Δn for accurate calculation will depend on how rapidly M_m and M vary with speed. The quantity $M_m - M$ should be nearly constant over the interval Δn if an accurate estimate of Δt is to be obtained. Torque-speed characteristics of electric motors may be obtained from the manufacturers.

Horizontal-shaft pumps fitted with plain bearings and packed glands require a *breakaway torque* of about 15% of M_n, the torque at the normal operating point, to overcome the static friction. This may be reduced to about 10% of M_n if the pump is fitted with antifriction bearings. The breakaway torque may be assumed to decrease linearly with speed to nearly zero when the speed reaches 15 to 20% of normal. Construction of torque-speed curves requires a knowledge of the pump characteristics at normal speed as well as details of the entire pumping system. Some typical examples taken from Reference 7 are given

LIBERTY EXHIBIT 1017, Page 179

below. The following forms of Eqs 12 are useful in constructing the various performance curves:

$$Q_2 = Q_1 \frac{n_2}{n_1} \tag{27}$$

$$H_2 = H_1\left(\frac{n_2}{n_1}\right)^2 = H_1\left(\frac{Q_2}{Q_1}\right)^2 \tag{28}$$

$$P_2 = P_1\left(\frac{n_2}{n_1}\right)^3 \tag{29}$$

$$M_2 = M_1\left(\frac{n_2}{n_1}\right)^2 \tag{30}$$

where Q = flow rate
n = speed
H = head
P = power
M = torque

in any consistent units of measure. After speeds n_1 and n_2 are chosen, the subscripts 1 and 2 refer to corresponding points on the characteristic curves for these speeds.

Low-Specific-Speed Pumps Figure 31 shows the constant-speed characteristics of a pump having $n_s \approx 1740$ (0.64) at best efficiency. This pump usually would be started with a valve in the discharge line closed. During the starting phase, the pump operates at shut-off with $P_1 = 25.8$ hp (19.2 kW) and $n_1 = 1770$ rpm. Then, by Eq. 25, $M_1 = 76.6$ lb · ft (103.9 $N \cdot m$). These values may be used in Eq. 30 to evaluate starting torques M_2 at as many speeds n_2 as desired and plotted in Figure 32 as curve *BCD*. Section *AB* of the starting torque curve is an estimate of the breakaway torque. If the discharge valve is now opened, the speed remains nearly constant but the torque increases as the flow rate and power increase. If the normal operating point is $Q = 1400$ gpm (88.3 l/s) and $P_n = 53.2$ hp (39.7 kW), the motor torque will be $M_n = 158$ lb · ft (214 $N \cdot m$) by Eq. 25. The vertical line DE in Figure 32 shows the change in torque produced by opening the discharge valve.

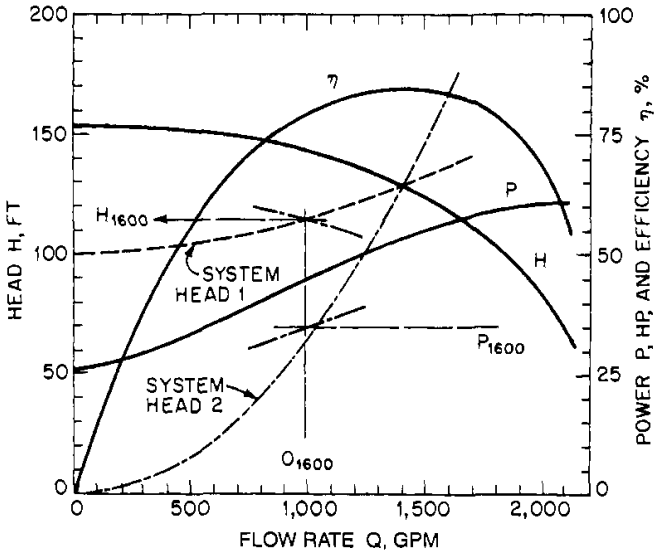


FIGURE 31 Characteristics of a 6-by-8 double-section pump at 1770 rpm (ft × 0.3048 = m; gpm × 0.06309 = l/s; hp × 0.7457 = kW) $n_s = 1{,}740$ ($\Omega_s = 0.64$) (Reference 7)

LIBERTY EXHIBIT 1017, Page 180

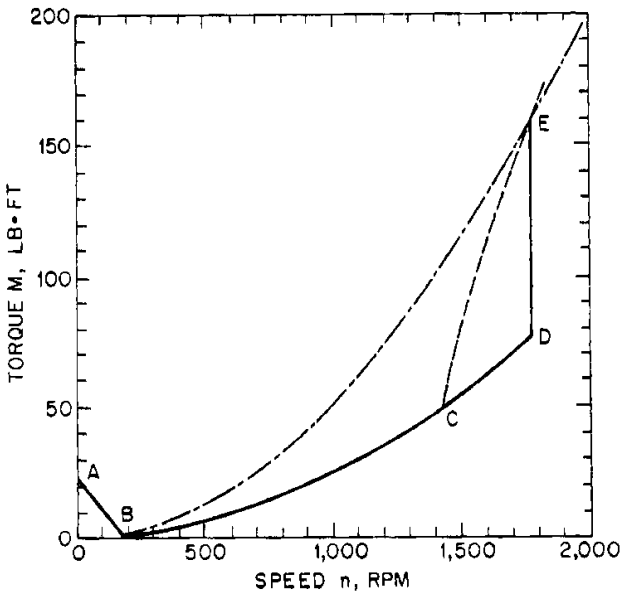


FIGURE 32 Torque characteristics of 6-by-8 pump shown in Figure 31 (lb • ft × 1.356 = N • m) (Reference 7)

Instead of starting the pump with the discharge valve closed, let the pump be started with a check valve in the discharge line held closed by a static head of 100 ft (30.5 m). The frictional head in the system may be represented by kQ^2. The value of k may be estimated from the geometry of the system or from a frictional-loss measurement at any convenient flow rate Q, preferably near the normal capacity Q_n. In this example, Q_n = 1400 gpm (88.33 l/s) and $k = 14.4/10^6$ (0.00109). The curve labeled system head 1 in Figure 31 was computed from $H = 100 + (14.4/10^6)Q^2$ ft ($H = 30.48 + 0.00109Q^2$ m) and intersects the head curve at H = 128 ft (39.01 m) and Q_n = 1400 gpm (88.33 l/s). The normal shutoff head is H_1 = 153 ft (46.6 m) at n_1 = 1770 rpm. By Eq. 28, the pump will develop a shutoff head H_2 = 100 ft (30.5 m) at n_2 = 1430 rpm. By Eq. 30, the torque at 1430 rpm will be 50 lb · ft (68 $N \cdot m$), corresponding to point C in Figure 32. The portion ABC of the starting torque curve has already been constructed. Trial-and-error methods must be used to obtain the portion ABC of the starting torque curve.

The auxiliary curves in Figure 33 are useful in constructing the CE portion of the starting torque curve. Select a value of n_2 intermediate between 1427 and 1770 rpm, say n_2 = 1600 rpm. In Figure 31, read values of Q_1, H_1, and P_1 for speed n_1 = 1770 rpm. By Eqs. 27 and 28, determine values of Q_2 and H_2 and plot as shown in Figure 31 until an intersection with the system-head 1 curve is obtained that provides Q_{1600} corresponding to n = 1600 rpm. By Eq. 29, determine value of P_2 and plot as shown in Figure 31 until an intersection is obtained with the Q_{1600} line which provides P_{1600} corresponding to n = 1600 rpm. Eq. 34 is now used to obtain M_{1600}, which is one point on the desired starting torque curve. The process is repeated for various speeds n_2 until the curve CE in Figure 32 can be drawn. The complete starting torque curve for this example is $ABCE$ in Figure 31, with steady-state operation at point E.

Assume that the pump of the preceding examples is installed in a system having zero static head but a long pipeline with friction head given by $H = (65.4/10^6)Q^2$ ft ($H = 0.00500Q^2$ m), as shown in Figure 31 by the curve labeled system head 2. The valve in the discharge line is assumed to open instantaneously when power is first applied to the pump. The procedure described to construct curve CE of the preceding example must now be used together with the system-head 2 curve of Figure 31 to obtain the curve BE of Figure 32. The complete starting torque curve for this example is ABE in Figure 32, with steady-state operation at point E.

The inertia of the fluid in the system was neglected in solving the previous examples. Some of the power must be used to accelerate the liquid, and this may be appreciable in the case of a long pipeline. Low-specific-speed pumps, which are used with long pipelines, have rising power curves with minimum power at shutoff and maximum power at normal flow

LIBERTY EXHIBIT 1017, Page 181

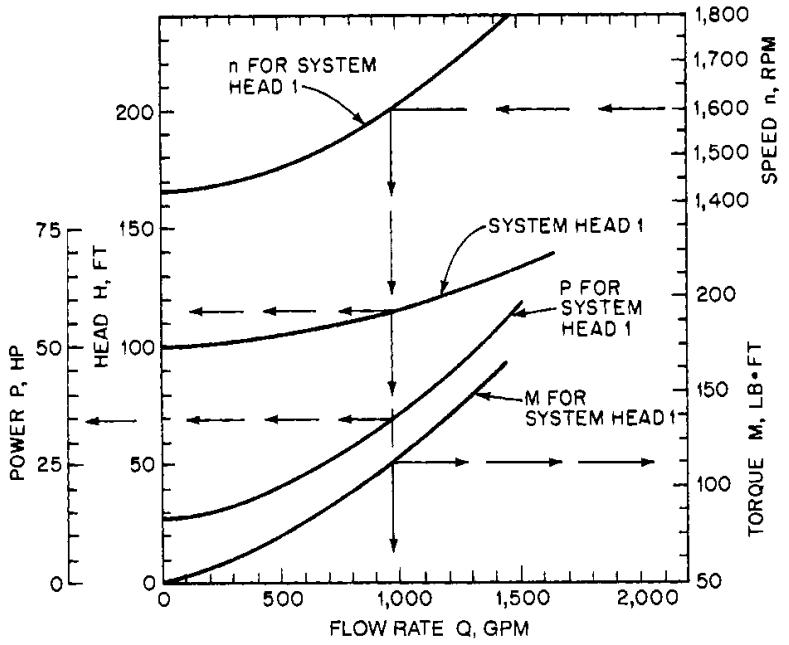


FIGURE 33 Analysis of 6-by-8 pump shown in Figure 41 (ft × 0.3048 = m; gpm × 0.06309 = l/s; lb • ft × 1.356 = N • m; hp × 0.7457 = kW) (Reference 7)

rate. Experience has shown that the starting torque-speed curves computed by neglecting the inertia of the liquid are conservative, so inertia effects need not be included. The inertia effect of the liquid does slow the starting operation. If the time required to reach any event, such as a particular speed or flow rate, is required, the inertia of the liquid should be considered, but including it greatly increases the difficulty of computation. References 45 through 48 give general methods for handling problems involving liquid transients.

High-specific-speed pumps have falling power flow rate curves with maximum power at shutoff and minimum power at normal flow rate. Neglecting the inertia of the liquid probably will result in too low a value for the computed starting torque for such pumps. If liquid inertia is to be included, consult References 44 to 47 and Section 11.1.

MEDIUM- AND HIGH-SPECIFIC-SPEED PUMPS Figure 34 shows constant-speed characteristics for a medium-specific-speed pump, $n_s = 4570$ (1.672) at best efficiency. The shutoff power

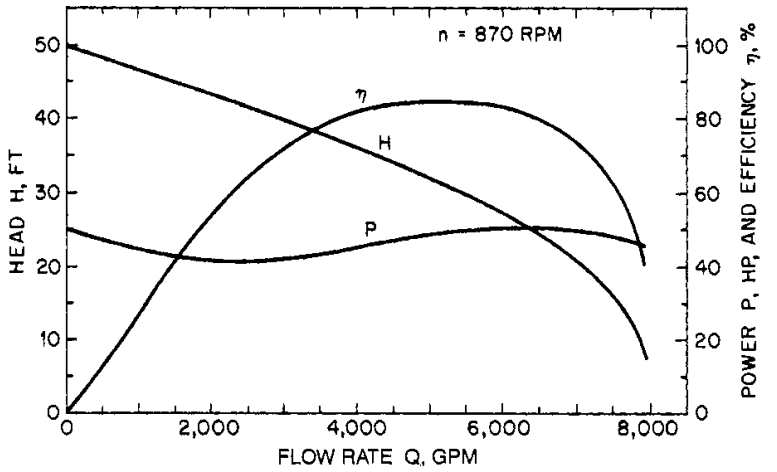


FIGURE 34 Characteristics of a 16-in (40.6cm) volute pump with mixed-flow impeller with flat power characteristic (ft × 0.3048 = m; gpm × 0.06309 = l/s; hp × 0.7457 = kW). $n_s = 4570$ ($\Omega_s = 1.672$) (Reference 7)

LIBERTY EXHIBIT 1017, Page 182

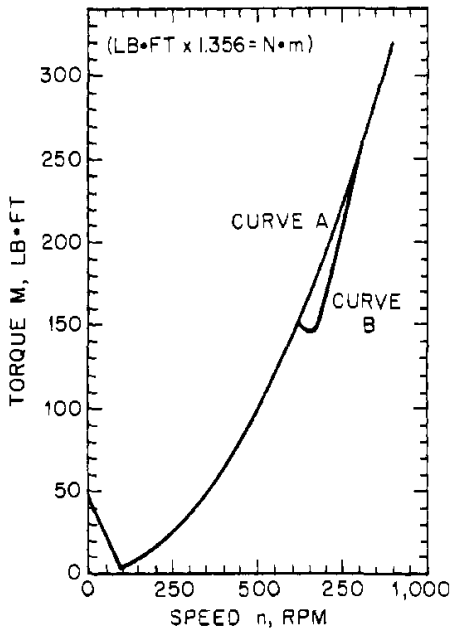


FIGURE 35 Torque characteristics of pump shown in Figure 34 (Reference 7)

is the same as the power at best efficiency, and the starting torque-speed curve is but little affected by the method of starting, as shown by Figure 35.

Figure 36 shows the constant-speed characteristics of a high-specific-speed propeller pump, $n_s \approx 12{,}000$ (4.391) at best efficiency. Figure 37 shows the starting torque-speed curve when the pump is started against a static head of 14 ft (4.3 m) and a friction head of 1 ft (0.3 m) at $Q_n = 12{,}500$ gpm (789 l/s). The system was assumed full of water with a closed check valve at the outlet end of the short discharge pipe. The methods of computation for Figures 35 and 37 were the same as for Figure 32.

Sometimes propeller pumps are started with the pump submerged but with the discharge column filled with air. In such a case, the torque-time characteristic for the driver must be known and a step-by-step calculation carried out. If the discharge column is a siphon initially filled with air, the starting torque may exceed the normal running torque during some short period of the starting operation. If the pump is driven by a synchronous

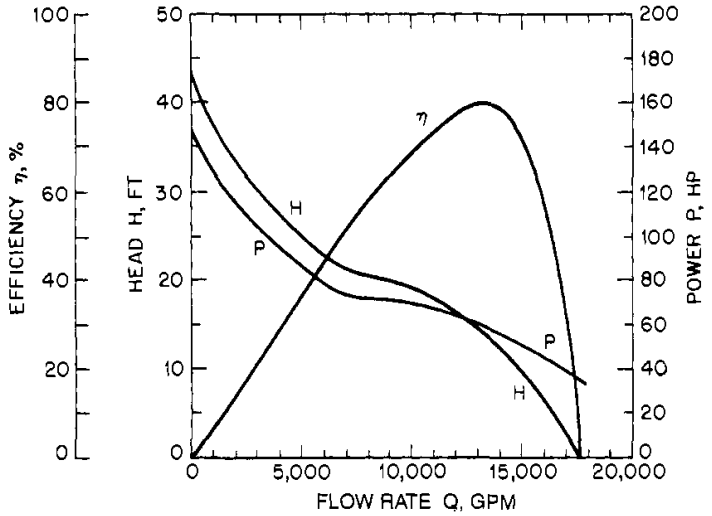


FIGURE 36 Characteristics of a 30-in (76.2-cm) discharge propeller pump at 700 rpm (ft × 0.1048 = m; gpm × 0.06309 = l/s; hp × 0.7457 = kW). $n_s = 12{,}000$ ($\Omega_s = 4.391$) (Reference 7)

LIBERTY EXHIBIT 1017, Page 183

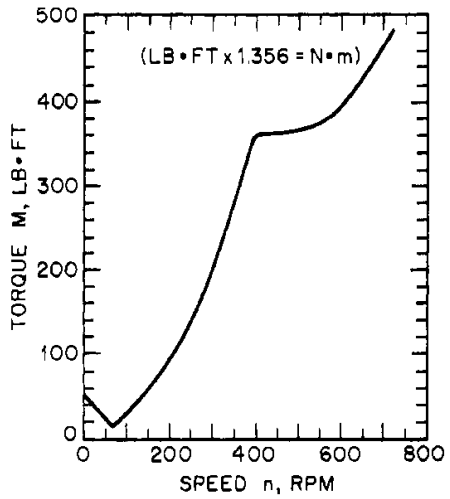


FIGURE 37 Torque characteristics of pump shown in Figure 36 (Reference 7)

motor, it is particularly important to investigate the starting torque in the range of 90 to 100% of normal speed to make sure that the pull-in torque of the motor is not exceeded. For additional information regarding starting high-specific-speed pumps discharging through long and large diameter systems, see Section 11.1.

Miscellaneous Requirements Pumps handling hot liquids should be warmed up to operating temperature before being started unless they have been especially designed for quick starting. Failure to do this may cause serious damage to wearing rings, seals, and any hydraulic balancing device that may be present. A careful check of the installation should be made before starting new pumps, pumps that have had a major overhaul, or pumps that have been standing idle for a long time. It is very important to follow the manufacturer's instructions when starting boiler-feed pumps. If these are unavailable, Reference 7 may be consulted. Ascertain that the shaft is not frozen, that the direction of rotation is correct, preferably with the coupling disengaged, and that bearing lubrication and gland cooling water meet normal requirements. Failure to do this may result in damage to the pump or driver.

A pump may run backwards at runaway speed if the discharge valve fails to close following shutdown. Any attempt to start the pump from this condition will put a prolonged overload on the motor. Figure 38 shows one example of the torque-speed transient for a pump, $n_s = 1700\ (0.622)$, started from a runaway reversed speed while normal pump head was maintained between the section and discharge flanges. In most practical cases, water hammer effects would make this transient even more unfavorable than Figure 38 indicates.

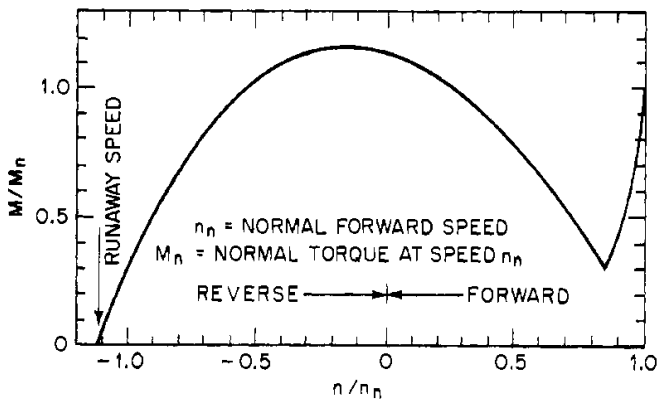


FIGURE 38 Torque characteristics of a double-suction pump, $n_s \approx 1700\ (0.64)$, from reversed runaway speed to normal forward speed (Reference 7)

LIBERTY EXHIBIT 1017, Page 184

The duration of such a transient will always be much longer than the normal starting time, and so protective devices would probably disconnect the motor from the power supply before normal operation could be achieved. Consult Section 11.1 for additional information on this subject.

REGULATION OF FLOW RATE

Flow rate variation ordinarily is accomplished by a change in pump head, speed, or both simultaneously. The flow rate and power input of pumps with specific speeds up to about 4000 (1.464) double suction increase with decreasing head, so the drivers of such pumps may be overloaded if the head falls below a safe minimum value. Increasing the head of high-specific-speed pumps decreases the flow rate but increases the power input. The drivers of these pumps should either be able to meet possible load increases or be equipped with suitable overload protection. Flow rate regulation by the various methods given below may be manual or automatic (see also References 1, 7, 12, 34 and 49).

Discharge Throttling This is the cheapest and most common method of flow rate modulation for low- and medium-specific-speed pumps. Usually its use is restricted to such pumps. Partial closure of any type of valve in the discharge line will increase the system head so the system-head curve will intersect the pump head curve at a smaller flow rate, as shown in Figure 40. Discharge throttling moves the operating point to one of lower efficiency, and power is lost at the throttle valve. This may be important in large installations, where more costly methods of modulation may be economically attractive. Throttling to the point of cutoff may cause excessive heating of the liquid in the pump. This may require a bypass to maintain the necessary minimum flow or use of different method of modulation. This is particularly important with pumps handling hot water or volatile liquids, as previously mentioned. Refer to Section 11.2 for information regarding the sizing of a pump bypass.

Suction Throttling If sufficient NPSH is available, some power can be saved by throttling in the suction line. Jet engine fuel pumps frequently are suction throttled[5] because discharge throttling may cause overheating and vaporization of the liquid. At very low flow rate, the impellers of these pumps are only partly filled with liquid, so the power input and temperature rise are about one-third the values for impellers running full with discharge throttling. The capacity of condensate pumps frequently is submergence-controlled,[7] which is equivalent to suction throttling. Special design reduces cavitation damage of these pumps to a negligible amount, the energy level (Section 2.1.1) being quite low.

Bypass Regulation All or part of the pump flow may be diverted from the discharge line to the pump suction or other suitable point through a bypass line. The bypass may contain one or more metering orifices and suitable control valves. Metered bypasses are commonly used with boiler-feed pumps for reduced-flow operation, mainly to prevent overheating. There is a considerable power saving if excess capacity of propeller pumps is bypassed instead of using discharge throttling. See Section 11.4.

Speed Regulation This can be used to minimize power requirements and eliminate overheating during flow rate modulation. Steam turbines and internal combustion engines are readily adaptable to speed regulation at small extra cost. A wide variety of variable-speed mechanical, magnetic, and hydraulic drives are available, as well as both ac and dc variable-speed motors. Usually variable-speed motors are so expensive that they can be justified only by an economic study of a particular case. Figure 39 shows a study by Richardson[50] of power requirements with various drivers wherein substantial economies in power may be obtained from variable-speed drives.

Regulation by Adjustable Vanes Adjustable guide vanes ahead of the impeller have been investigated and found effective with a pump of specific speed n_s = 5700 (2.086).

LIBERTY EXHIBIT 1017, Page 185

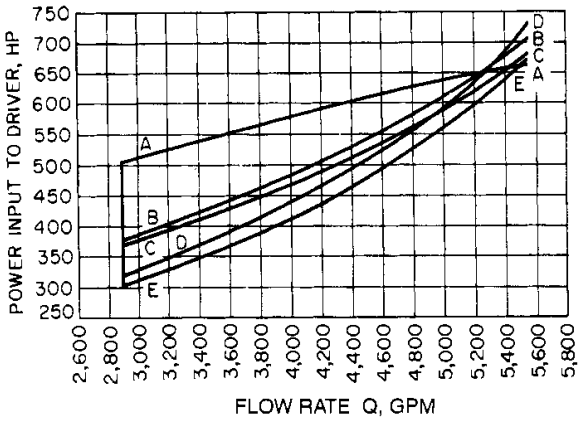


FIGURE 39 Power requirements of two double-suction pumps in series operated at constant head and variable flow rate. Total H_n = 382 ft (116 m) for both pumps at 1800 rpm (gpm × 0.06309 = l/s hp × 0.7457 = kW) (Reference 50). Curve *AA:* constant speed with discharge throttling. Curve *BB:* synchronous motor with variable-speed hydraulic coupling on each pump. Curve *CC:* variable-speed wound-rotor induction motor. Curve *DD:* dc motor with rectifier and shunt field control. Curve *EE:* synchronous motor with variable-speed constant-efficiency mechanical speed reducer

The vanes produced a positive prewhirl that reduced the head, flow rate, and efficiency. Relatively little regulation was obtained from the vanes with pumps having n_s = 3920 (1.204) and 1060 (0.39). Adjustable outlet diffusion vanes have been used with good success on several large European storage pumps for hydroelectric developments. Propeller pumps with adjustable-pitch blades have been investigated with good success. Wide flow rate variation was obtained at constant head and with relatively little loss in efficiency. These methods are so complicated and expensive that they have very limited application in practice. Reference 34 may be consulted for further discussion and bibliography.

Air Admission Admitting air into the pump suction has been demonstrated as a means of flow-rate regulation, with some savings in power over discharge throttling. Usually air in the pumped liquid is undesirable, and there is always the danger that too much air will cause the pump to lose its prime. The method has rarely been used in practice but might be applicable to isolated cases.

PARALLEL AND SERIES OPERATION

Two or more pumps may be arranged for parallel or series operation to meet a wide range of requirements in the most economical manner. If the pumps are close together, that is, in the same station, the analysis given below should be adequate to secure satisfactory operation. If the pumps are widely separated, as in the case of two or more pumps at widely spaced intervals along a pipeline, serious pressure transients may be generated by improper starting or stopping procedures. The analysis of such cases may be quite complicated, and References 46 to 48 should be consulted for methods of solution.

Parallel Operation Parallel operation of two or more pumps is a common method of meeting variable-flow-rate requirements. By starting only those pumps needed to meet the demand, operation near maximum efficiency can usually be obtained. The head-flow characteristics of the pumps need not be identical, but pumps with unstable characteristics may give trouble unless operation only on the steep portion of the characteristic can be assured. Care should be taken to see that no one pump, when combined with pumps of different characteristics, is forced to operate at flows less than the minimum required to prevent recirculation. See the discussion that follows on operation at other than normal flow rate. Multiple pumps in a station provide spares for emergency service and for the downtime needed for maintenance and repair.

LIBERTY EXHIBIT 1017, Page 186

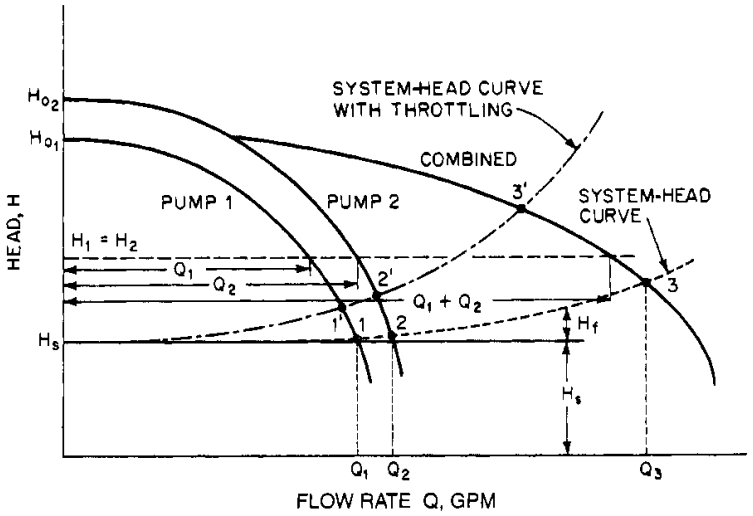


FIGURE 40 Head-flow curves of pumps operating in parallel

The possibility of driving two pumps from a single motor should always be considered, as it usually is possible to drive the smaller pumps at about 40% higher speed than a single pump of twice the capacity. The saving in cost of the higher-speed motor may largely offset the increased cost of two pumps and give additional flexibility of operation.

One of the first steps in planning for multiple-pump operation is to draw the system-head curve, as shown in Figure 40. The system head consists of the static head H_s and the sum H_f of the pipe-friction head and the head lost in the valves and fittings (see Sections 11.1 and 11.2). The head curves of the various pumps are plotted on the same diagram, and their intersections with the system-head curve show possible operating points. *Combined pump head curves* are drawn by adding the flow rates of the various combinations of pumps for as many values of the head as necessary. The intersection of any combined H-Q curve with the system-head curve is an operating point. Figure 40 shows two pump head curves and the combined curve. Points 1, 2, and 3 are possible operating conditions. Additional operating points may be obtained by changing the speed of the pumps or by increasing the system-head loss by throttling. Any number of pumps in parallel may be included on a single diagram, although separate diagrams for different combinations of pumps may be preferable.

The overall efficiency η of pumps in parallel is given by

$$\eta = \frac{H(\text{sp. gr.})}{k} \times \frac{\Sigma Q}{\Sigma P} \tag{31}$$

where H = head, ft (m)
sp. gr. = specific gravity of the liquid
k = 3960 USCS (0.1021 SI)
ΣQ = sum of the pump flow rates, gpm (l/s)
ΣP = total power supplied to all pumps, hp (W)

Series Operation Pumps are frequently operated in series to supply heads greater than those of the individual pumps. The planning procedure is similar to the case of pumps in parallel. The system-head curve and the individual head-flow curves for the pumps are plotted as shown in Figure 41. The pump heads are added as shown to obtain the combined pump head curve. In this example, Pump 2 operating alone will deliver no liquid because its shutoff head is less than the system static head.

There are two possible operating points, 1 and 2, as shown by the appropriate intersections with the system-head curve. As with parallel operation, other operating points

LIBERTY EXHIBIT 1017, Page 187

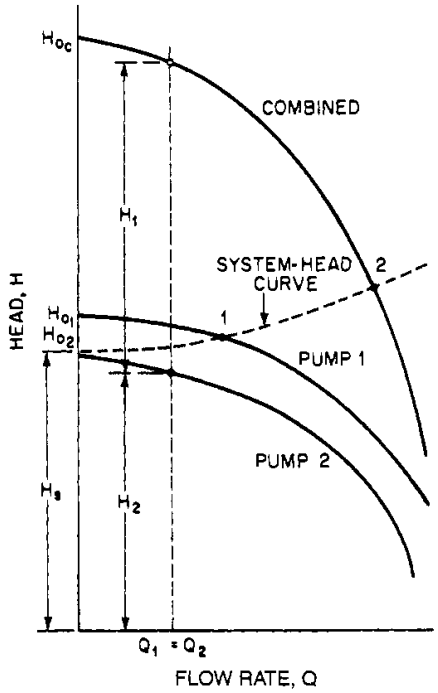


FIGURE 41 Head-flow curves of pumps operating in series

could be obtained by throttling or by changing the pump speeds. The overall efficiency of pumps in series is given by

$$\eta = \frac{Q(\text{sp. gr.})}{k} \times \frac{\Sigma H}{\Sigma P} \tag{32}$$

wherein the symbols are the same as for parallel operation. It is important to note that the stuffing box pressure of the second pump is increased by the discharge pressure of the first pump. This may require a special packing box for the second pump with leakoff to the suction of the first pump. The higher suction pressure may increase both the first cost and the maintenance costs of the second pump.

OPERATION AT OTHER THAN THE NORMAL FLOW RATE

Centrifugal pumps usually are designed to operate near the point of best efficiency, but many applications require operation over a wide range of flow rates, including shutoff, for extended periods of time. Pumps for such service are available but may require special design and construction at higher cost. Noise, vibration, and cavitation may be encountered at low flow rates. Large radial shaft forces at shutoff as well as lack of through flow to provide cooling may cause damage or breakage to such parts as shafts, bearings, seals, glands, and wearing rings of pumps not intended for such service. Some of the phenomena associated with operation at other than normal flow rate are described below.

Recirculation There is a small flow from impeller discharge to suction through the wearing rings and any hydraulic balancing device present. This takes place at all flow rates, but does not usually contribute to raising the liquid temperature very much unless operation is near shutoff.

When the flow rate has been reduced by throttling (or as a result of an increase in system head), a secondary flow called *recirculation* begins. Recirculation is a flow reversal due to separation at the suction and at the discharge tips of the impeller vanes. All impellers

LIBERTY EXHIBIT 1017, Page 188

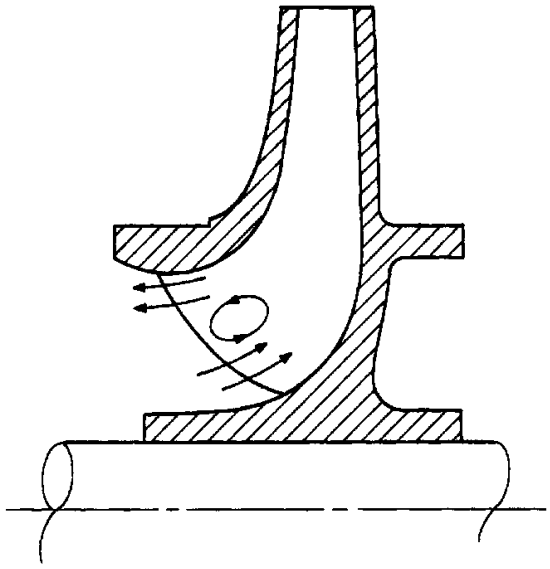


FIGURE 42 Suction recirculation

have a critical flow rate at which recirculation occurs. The flow rates at which suction and discharge recirculation begin can be controlled to some extent by design, but recirculation cannot be eliminated (see Figure 6 in Section 2.1.1).

Suction recirculation is the reversal of flow at the impeller eye. A portion of the flow is directed out of the eye at the eye diameter, as shown in Figure 42 , and travels upstream with a rotational velocity approaching the peripheral velocity of the diameter. A rotating annulus of liquid is produced upstream from the impeller inlet, and through the core of this annulus passes an axial flow corresponding to the output flow rate of the pump. In pumps equipped with long, straight suction nozzles but no suction elbow, this rotating fluid has been detected over considerable distances upstream from the impeller eye. Suction pressures measured at wall taps where this phenomenon is present are always higher than the true average static pressure across the measuring section. This means that the pump head as determined from wall taps is less than it would be if true average static pressures were measured. The high shear rate between the rotating annulus and the axial flow through the core produces vortices that form and collapse, producing noise and cavitation in the suction of the pump.

Discharge recirculation is the reversal of flow at the discharge tips of the impeller blades, as shown in Figure 43. The high shear rate between the inward and outward relative velocities produces vortices that cavitate and can attack the pressure side of the blades. This phenomenon, which tends to occur at a lower flow rate than the highest Q for suction recirculation, also involves stalled flow from the diffuser vanes or volute tongue(s). Separated reversed flow recirculates and emerges from these vane systems back into the impeller with negative swirl (that is, swirl opposite to the direction of rotation). The impeller must expend significant power to redirect the portion of this fluid (that reenters it) out again—with positive swirl. As discussed in Section 2.1.1, the portion of this backflow from the diffuser or volute that enters the spaces outside the impeller shrouds and adjacent to the casing walls has the potential to reverse the axial thrust of the impeller, and this reversal can fluctuate if the backflow is unsteady (as separated, recirculating flow normally is) and not always feeding the same side of the impeller.

DETECTING RECIRCULATION The presence of suction or discharge recirculation can be determined by monitoring the pressure pulsations in the suction and in the discharge areas of the casing. Pressure transducers, installed as close to the impeller as possible in the suction and discharge areas of the pump, can be used to detect pressure pulsations. Figure 44 is a typical plot of the amplitudes of these pulsations against flow rate—with reference to the accompanying pump head and efficiency. As the flow rate is reduced, a sudden increase in the magnitude of pressure pulsations indicates the onset of recirculation.

LIBERTY EXHIBIT 1017, Page 189

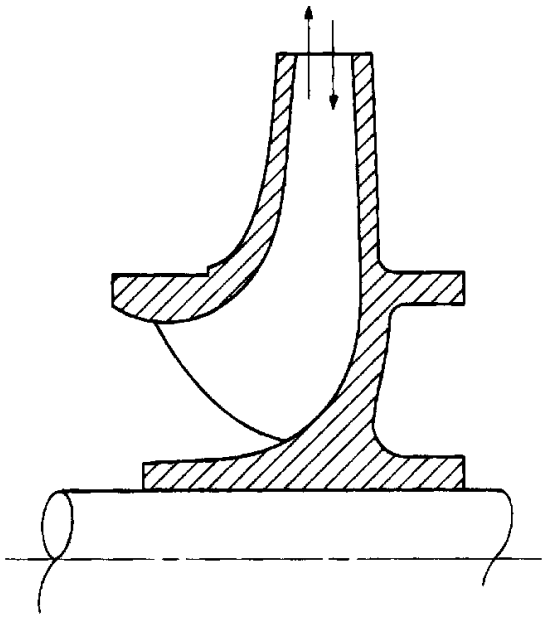


FIGURE 43 Discharge recirculation

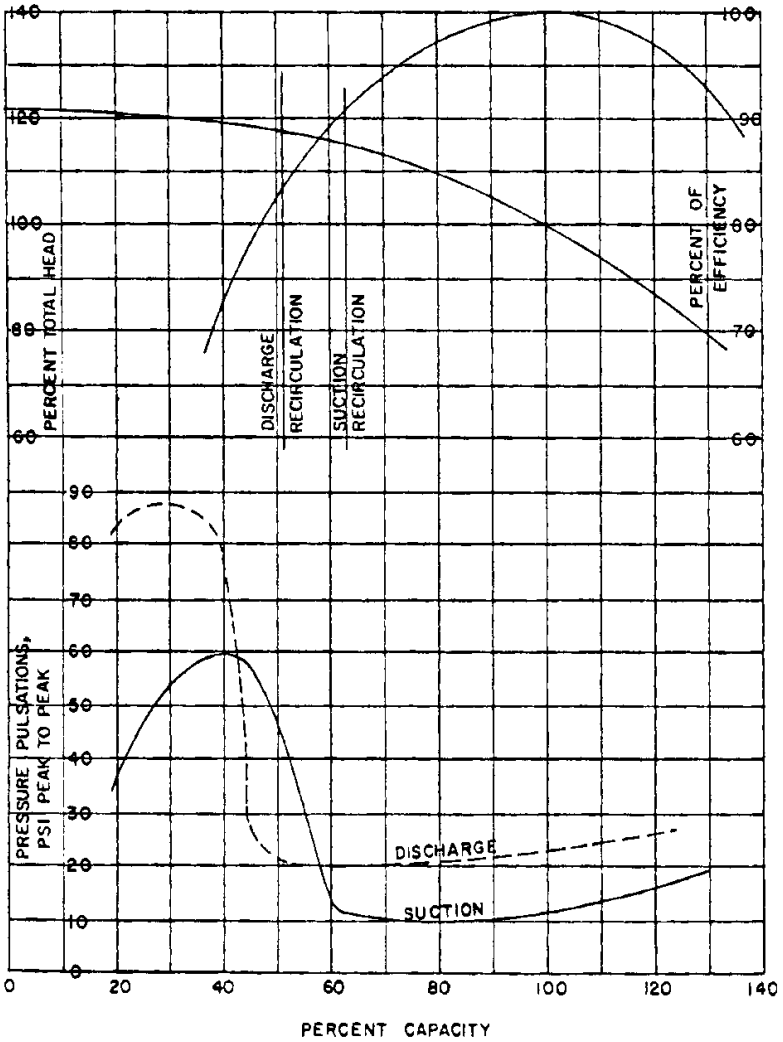


FIGURE 44 Detecting recirculation by means of pressure pulsations. As flow rate (capacity) is reduced, the initiation of recirculation is indicated by a marked increase in amplitude of the pressure pulsations.

LIBERTY EXHIBIT 1017, Page 190

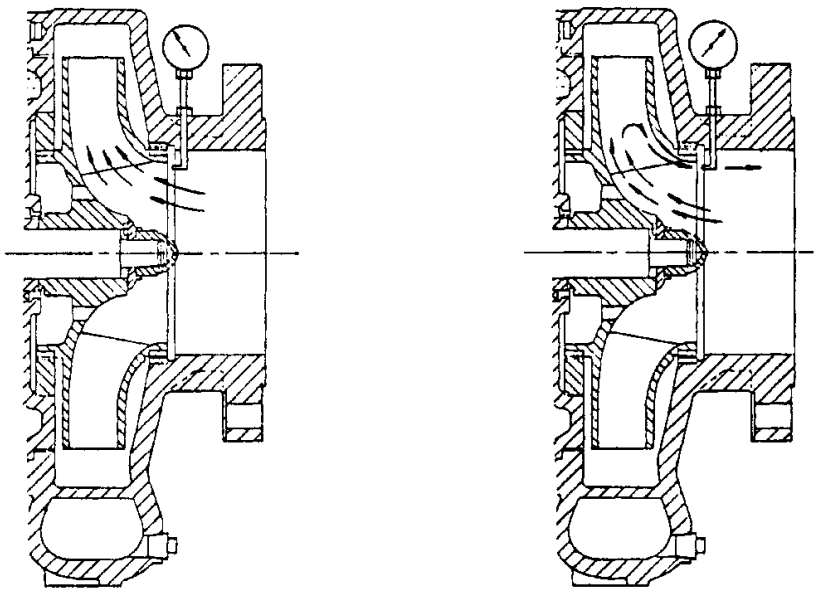


FIGURE 45 Detecting suction recirculation by means of a downstream-facing pitot tube at the impeller eye. As the flow rate is decreased, normal flow (a) gives way to recirculation (b) and the higher pressure reading due to the impact of the backflow

Also, suction recirculation can be detected by means of a pitot tube installed at the impeller eye, as shown in Figure 45. With the tube directed into the eye, the reading in the normal pumping range is the suction head minus the velocity head at the eye. At the point of recirculation, however, the flow reversal from the eye impinges on the opening of the pitot tube—with a rapid rise in the gage reading.

CORRECTIVE PROCEDURES Every impeller has specific recirculation characteristics, which usually includes the presence of cavitation bubbles and the consequent damage as they collapse on the impeller surfaces. An analysis of the symptoms associated with recirculations leads to suggested corrective procedures for avoiding damage, such as the following:

1. Increase the delivered flow rate of the pump.
2. Install a bypass between the discharge and suction of the pump. (See Section 11.4.)
3. Substitute an improved material for the impeller that is more resistant to cavitation. (See Section 8.1.)
4. Modify the impeller design. (See Section 2.1.1 and Section 12.5.)

QUANTIFYING THE ONSET OF RECIRCULATION A method for computing the flow rates Q_{SR} and Q_{DR} below which suction and discharge recirculation respectively occur is presented in Table 16 of Section 2.1.1, under the subheading "Minimum flow limits." Another method is illustrated in Figures 38 and 39 of that section. In general, these methods reveal that Q_{SR} approaches the BEP flow rate Q_{BEP} as the eye diameter of the impeller approaches that of the discharge; that is, as D_e approaches D_2. Thus, high-specific-speed (high-n_s) impellers and inducers are subject to suction recirculation over most of the flow range below BEP. However, even for lower-n_s impellers, as can be seen in the first design example of Section 2.1.1, D_e/D_2 increases with the design value of suction specific speed S, leading to the conclusion that high-S (or high-Ω_{ss}) impellers can experience the deleterious effects of recirculation at flow rates not far below BEP.

OPERATION WITH RECIRCULATION Despite the existence of suction and discharge recirculation, the mechanical response of the pump will not be serious unless the energy level is high.

LIBERTY EXHIBIT 1017, Page 191

In other words, most pumps can indeed be operated at $Q < Q_{SR}$. The minimum flow rate or simply "minimum flow" Q_{min} is quantified in Section 2.1.1. As energy level is increased, Q_{min} approaches Q_{SR} in the limit. Examples of the difference between Q_{min} and Q_{SR} are as follows: For water pumps rated at 2500 gpm (158 l/s) and 150 ft (45.7 m) total head or less, the minimum operating flows can be as low as 50% of the suction recirculation values shown for continuous operation and as low as 25% for intermittent operation. For hydrocarbons, the minimum operating flows can be as low as 60% of the suction recirculation values shown for continuous operation and as low as 25% for intermittent operation.[51, 52, 53]

Temperature Rise Under steady-state conditions, friction and the work of compression increase the temperature of the liquid as it flows from suction to discharge. A further temperature increase may arise from liquid returned to the pump suction through wearing rings, a balancing device, or a minimum-flow bypass line that protects the pump when operating at or near shutoff.

Assuming that all heat generated remains in the liquid, the temperature rise is

$$\Delta T = \frac{gH \times (1 - \eta)}{g_o C_p \eta J} + \Delta T_c \tag{33}$$

where $g/g_o = 1$ lbf/lbm; but when using SI units, g/g_o is replaced by 9.80665 m/s² (= g in the SI system). ΔT_c is due to the compression of the liquid and is not a consequence of loss or dissipation as is the term involving the pump efficiency η (see Section 2.1). As shown in Reference 1 of Section 2.1, ΔT_c is 3°F per 1000 psi (0.24°C per MPa) of pump pressure rise for hydrocarbon fuels. For boiler feedwater at 350°F (177°C), ΔT_c = 1.6°F per 1000 psi (0.129°C per MPa), but it is much smaller for cold water. By consulting tables of properties for the liquid phase of the fluid being pumped and assuming the compression process between the actual inlet and discharge pressures to be isentropic, ΔT_c can be determined. This is important if Eq. 33 is used to evaluate overall pump efficiency from temperature rise measurements. ΔT and ΔT_c are often of the same order of magnitude at BEP, and serious errors have been made by excluding ΔT_c from the efficiency computation. At very low, off-BEP flow rates, ΔT will be high in comparison to ΔT_c; so, the latter can be safely ignored in temperature rise calculations at such low-efficiency conditions.

In practice, determination of efficiency from ΔT-measurements is accomplished by the direct thermodynamic method[54], rather than by the ΔT_c-method. Both approaches are based on the definition of pump efficiency as the ratio of an isentropic rise of total enthalpy (= $g\Delta H$) to the actual rise of total enthalpy (Eq. 1 of Section 2.1.1), allowances being made for the usually small external power losses that do not appear in the pumped fluid (such as bearing drag) and the similarly small effects of heat transferred between pump and surroundings. In the direct thermodynamic method, the enthalpy rise Δh is found from the chain rule,

$$\Delta h = \int dh = \int [(\partial h/\partial p)_T dp + (\partial h/\partial T)_p dT] = a\Delta p + C_p J \Delta T$$

the coefficients a and $C_p J$ being average values of the two partial derivatives as found from tables of thermodynamic properties of the fluid. Values of these partial derivatives are conveniently tabulated for water in Reference 54.

General service pumps handling cold liquids may be able to stand a temperature rise as great as 100°F (56°C). Most modern boiler-feed pumps may safely withstand a temperature rise of 50°F (28°C). The NPSH required to avoid cavitation or to prevent flashing of hot liquid returned to the pump suction may be the controlling factor. Minimum flow may be dictated by other factors, such as recirculation and unbalanced radial and axial forces on the impeller. Axial forces can be the controlling factor with single-stage double-suction pumps.

It is especially important to protect even small pumps handling hot liquids from operation at shutoff. This is usually done by providing a bypass line fitted with a metering orifice to maintain the minimum required flow through the pump. In the case of boiler-feed pumps, the bypass flow usually is returned to one of the feed-water the water heaters. Unless especially designed for cold starting, pumps handling hot liquids should be warmed up gradually before being put into operation.

LIBERTY EXHIBIT 1017, Page 192

Radial Thrust Ideally, the circumferential pressure distribution at the impeller exit is uniform at the design condition (as explained in Section 2.1.1); however, it becomes nonuniform at off-BEP flow rates. An exception is that concentric collecting configurations will produce nonuniform pressure distributions at the BEP. Any nonuniformity leads to a radial force on the pump shaft called the radial thrust or radial reaction. The radial thrust F_r in pounds (newtons) is

$$F_r = kK_r(\text{sp. gr.})HD_2b_2 \tag{34}$$

where k = 0.433 USGS (9790 SI)
K_r = experimentally determined coefficient
sp. gr. = specific gravity of the liquid pumped (equal to unity for cold water)
H = pump head, ft (m)
D_2 = outside diameter of impeller, in (m)
b_2 = breadth of impeller at discharge, including shrouds, in (m)

Values of K_r determined by Agostinelli et al.[55] for single-volute pumps are given in Figure 46 as functions of specific speed and flow rate. The magnitude and direction of F_r on the pump shaft may be estimated from Figure 47 , but Eq. 34 probably will be more accurate for determining the magnitude of the force. The radial thrust usually is minimum near $Q = Q_n$, the flow rate at best efficiency, but rarely goes completely to zero. Near shutoff, F_r usually is maximum and may be a considerable force on the shaft in high-head pumps.

The radial thrust can be made much smaller throughout the entire flow-rate range by using a double volute (twin volute) or a concentric casing. These designs should be considered, particularly if the pump must operate at small flow rates. Figures 48 to 50 compare radial forces generated by three types of casings: a standard volute, a double volute, and a modified concentric casing. The latter casing was concentric with the impeller for 270° from the tongue and then enlarged in the manner of a single volute to form the discharge nozzle. The magnitude and direction of F_r on the pump shaft for the modified concentric casing may be estimated from Figure 51. The direction of F_r on the pump shaft with a double volute was somewhat random but in the general vicinity of the casing tongue. Radial forces on pumps fitted with diffuser vanes usually are rather small, although they may be significant near shutoff due to stall in some of the passages and not in others.

EXAMPLE Consider a single-stage centrifugal pump, n_s = 2000 (0.732) at best efficiency, handling cold water, sp. gr. = 1.0. Estimate the radial thrust on the impeller at half the normal flow rate when fitted with (a) a single volute, (b) a modified concentric casing, and (c) a double volute. Impeller dimensions are D_2 = 15.125 in (38.4 cm) and b_2 = 2.5 in (6.35 cm). The shutoff head is H = 252 ft (76.8 m), and the head at half capacity is H = 244 ft (74.4 m).

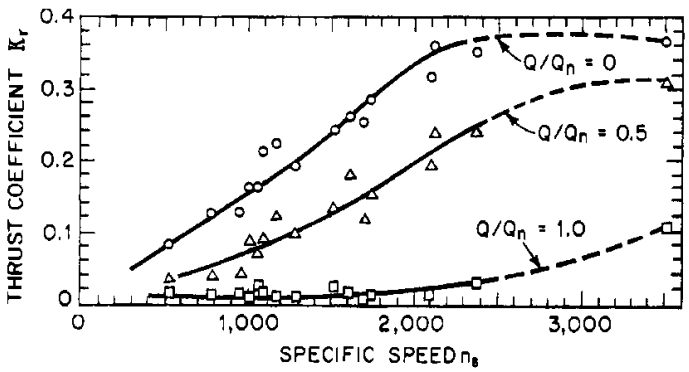


FIGURE 46 K_r as a function of specific speed and flow rate for single-volute pumps (to obtain Ω_s, divide by 2733.) (Reference 55)

LIBERTY EXHIBIT 1017, Page 193

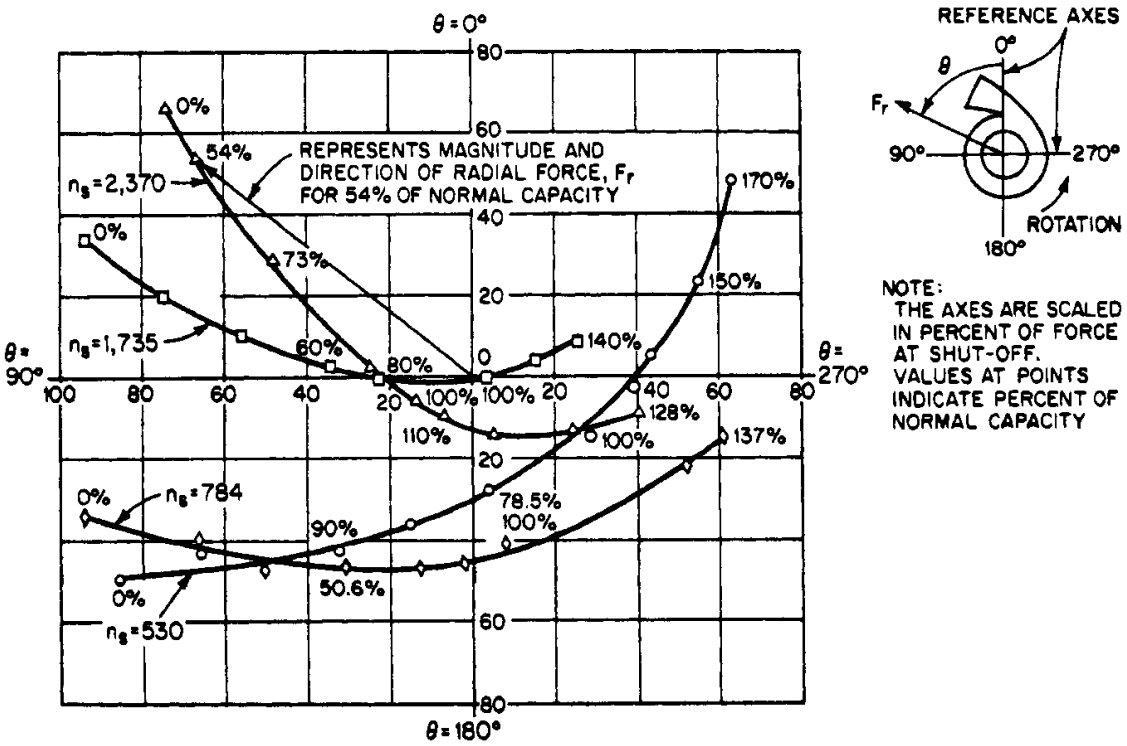


FIGURE 47 Polar plot showing direction of resultant radial forces for single-volute pumps at various flow rates ("capacities") and specific speeds. To obtain Ω_s, divide by 2733. (Reference 55)

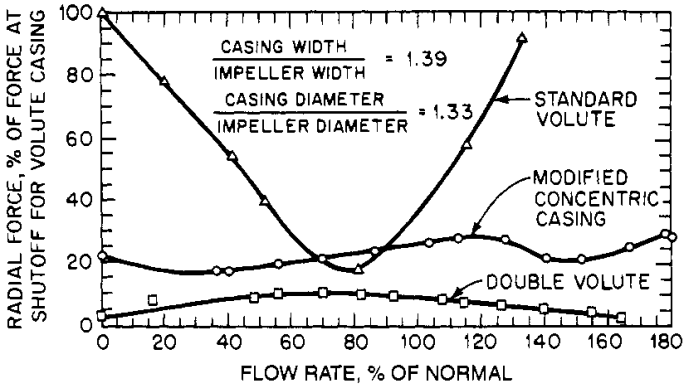


FIGURE 48 Comparison of the effect of three casing designs on radial forces for n_s = 1165 (0.426) (Reference 55)

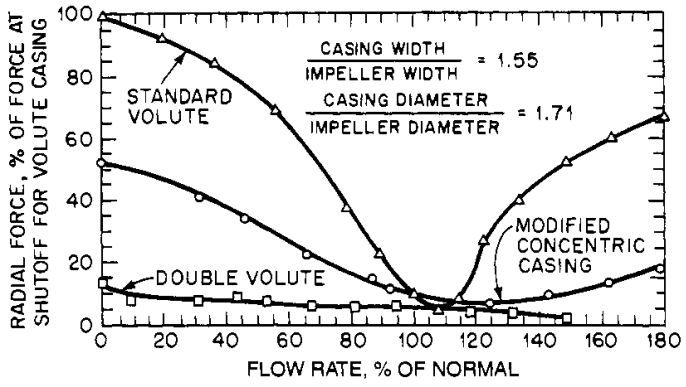


FIGURE 49 Comparison of the effect of three casing designs on radial forces for n_s = 2120 (0.776) (Reference 55)

LIBERTY EXHIBIT 1017, Page 194

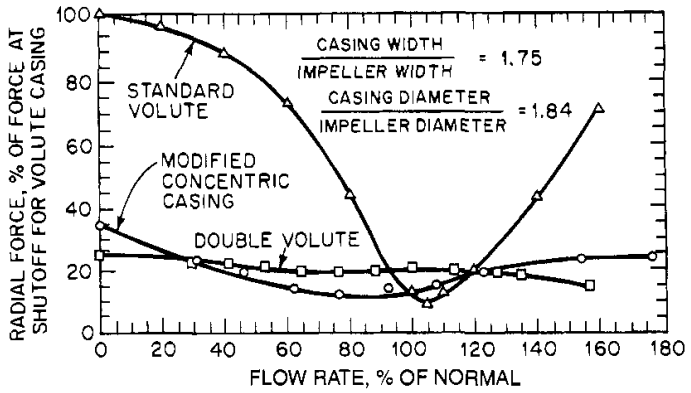


FIGURE 50 Comparison of effect of three casing designs on radial forces for n_s = 3500 (1.281) (Reference 55)

Solution

(a) $K_r = 0.2$ from Figure 46, by Eq. 34.

$$F_r = (0.433)(0.2)(1.0)(244)(15.125)(2.5) = 799 \text{ lb } (3554 \text{ N})$$

Estimating between the curves for n_S, = 2370 (0.867) and 1735 (0.635) in Figure 47, the direction of F_r on the shaft should be about 65° to 70° from the casing tongue in the direction of rotation.

(b) Use Figure 49, n_s = 2120 (0.776), which is nearest to n_s = 2000 (0.730), to find the radial force for a modified concentric casing at half flow, which is about 33%

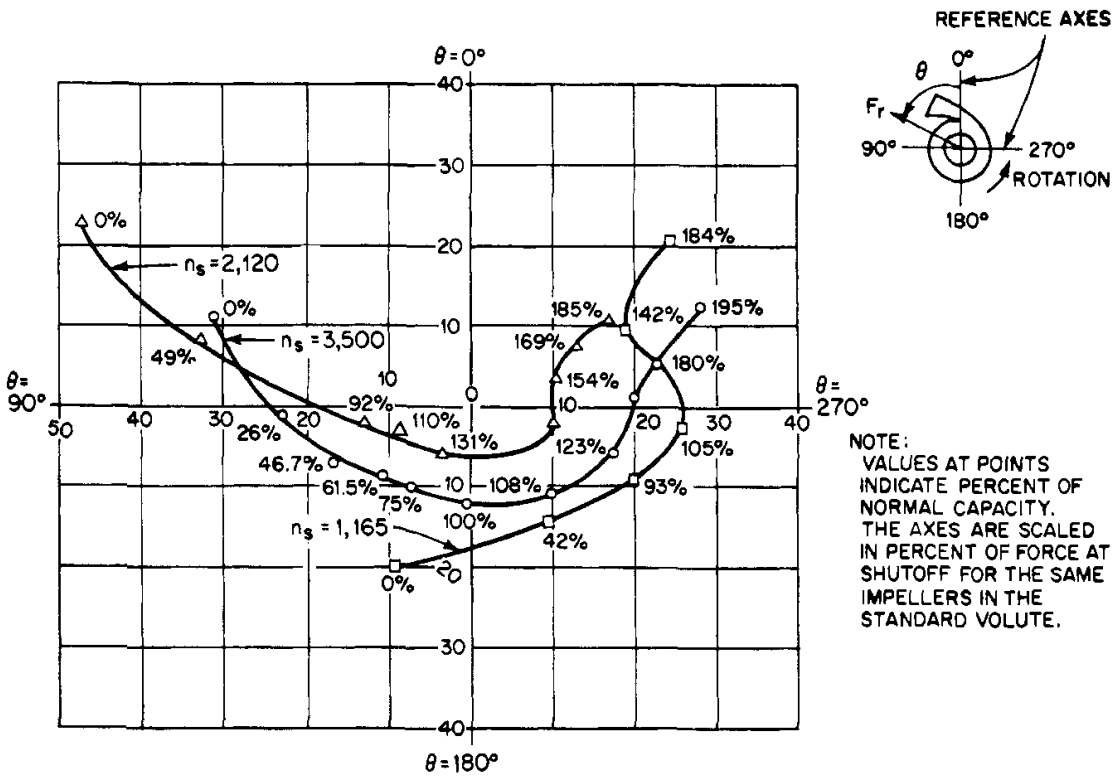


FIGURE 51 Polar plot showing direction of resultant radial forces for modified concentric casings at various flow rates and specific speeds; namely, 1,165 (0.426), 2,120 (0.776), and 3500 (1.281). The casings were concentric for 270° from the tongue. (Reference 55)

LIBERTY EXHIBIT 1017, Page 195

of shutoff value for a single-volute casing. From Figure 46, for a single-volute casing at shutoff, $K_r = 0.34$ and

$$F_r = (0.433)(0.34)(1.0)(252)(15.125)(2.5) = 1403 \text{ lb } (6241 \text{ N})$$

Then, for a modified concentric casing at half flow,

$$F_r = (0.33)(1403) = 463 \text{ lb } (2059 \text{ N})$$

From Figure 51, the direction of F_r should be about 75° to 80° from the casing tongue in the direction of rotation.

(c) From Figure 49, the radial force for a double-volute casing is about 8% of the shutoff value for the single-volute casing, and so

$$F_r = (0.08)(1403) = 112 \text{ lb } (499 \text{ N})$$

According to Agostinelli et al.,[55] the direction of the radial thrust in double-volute casings was found to be generally toward the casing tongue. Stepanoff[12] has found this direction to follow approximately that in single-volute casings (see also Biheller[56]).

Axial Thrust See Section 2.1.1 and 2.2.1.

ABNORMAL OPERATION

Complete Pump Characteristics Many types of abnormal operation involve reversed pump rotation, reversed flow direction, or both, and special tests are required to cover these modes of operation. Several methods of organizing the data have been proposed, and each has certain advantages. The Thoma diagrams shown in Figures 52 and 53[45] are easily understood and are truly *complete characteristics diagrams* because all possible modes of operation are covered (see Sections 11.3 and 12.14 and also Reference 57).

Figure 54 shows schematic cross-sections of the two pumps tested by Swanson[58] for which characteristics are given in Figure 53.

The *Karman circle diagram* (Reference 59) attempted to show the complete characteristics as a four-quadrant contour plot of surfaces representing head and torque with speed and flow rate as base coordinates. Because the head and torque tend to infinity in two zones of operation, another diagram would be required to show the complete pump characteristics. The data presented in such a diagram are, nevertheless, adequate for almost all requirements. One example of a circle diagram is given in Figures 55 and 56. Other examples may be found in References 12, 58, and 59.

Frequently, tests with negative head and torque have been omitted so that only half of the usual circle diagram could be shown. This has been called a *three-quadrant plot,* but the information necessary to predict an event, such as possible water-column separation following a power failure, is lacking.

Power Failure Transient A sudden power failure that leaves a pump and driver running free may cause serious damage to the system. Except for rare cases where a flywheel is provided, the pump and driver usually have a rather small moment of inertia, and so the pump will slow down rapidly. Unless the pipeline is very short, the inertia of the liquid will maintain a strong forward flow while the decelerating pump acts as a throttle valve. The pressure in the discharge line falls rapidly and, under some circumstances, may go below atmospheric pressure, both at the pump discharge and at any points of high elevation along the pipeline. The minimum pressure head which occurs during this phase of the motion is called the *downsurge,* and it may be low enough to cause vaporization followed by complete separation of the liquid column. Pipelines have collapsed under the external atmospheric pressure during separation. When the liquid columns rejoin, following separation, the shock pressures may be sufficient to rupture the pipe or the pump

LIBERTY EXHIBIT 1017, Page 196

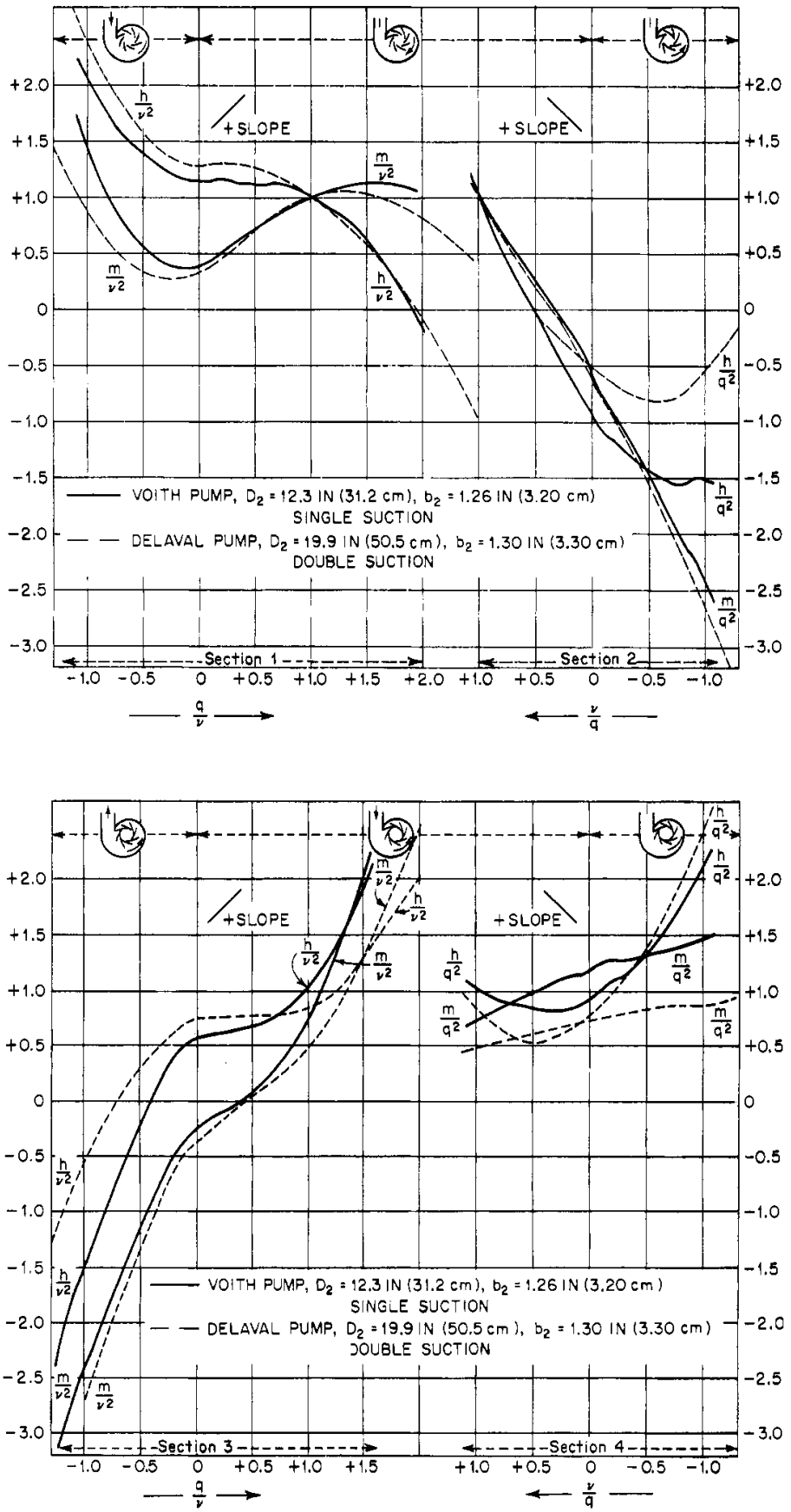


FIGURE 52 Complete pump characteristics. Specific speeds: Voith pump n_s = 1,935 (0.708); Delaval pump – n_s = 1,500 (0.549). (Reference 45)

LIBERTY EXHIBIT 1017, Page 197

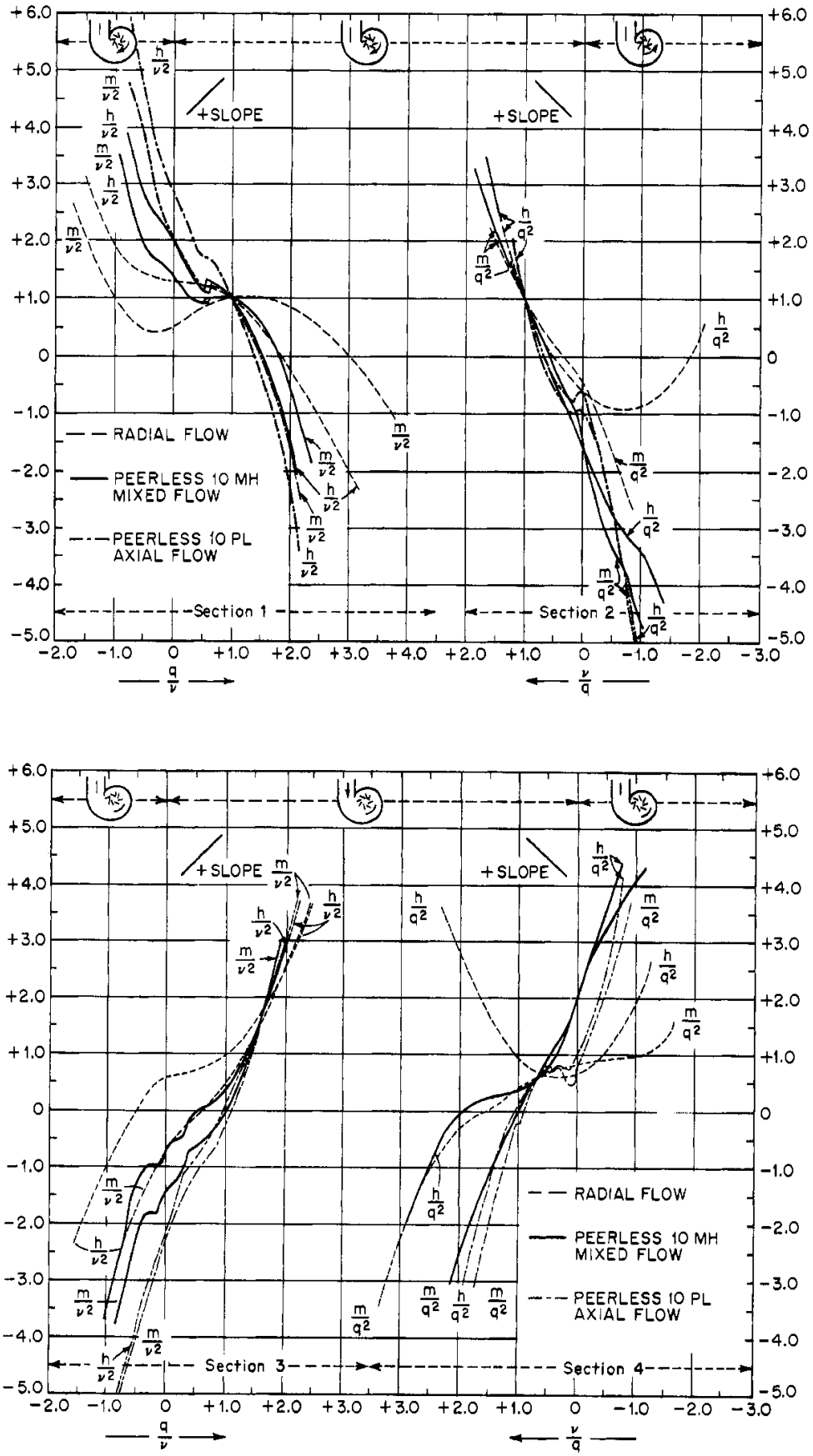


FIGURE 53 Complete pump characteristics. Specific speeds: Radial flow – n_s = 1800 (0.659); Peerless 10MH mixed flow – n_s = 7,550 (2.763); Peerless 10PL axial flow – n_s = 13,500 (4.940). (Reference 45)

LIBERTY EXHIBIT 1017, Page 198

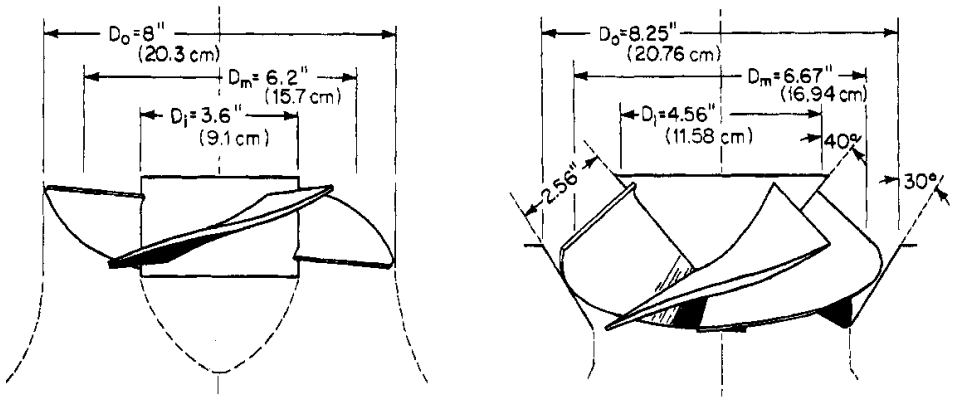


FIGURE 54 Schematic cross sections of high-specific-speed pumps. n_s = 13,500 (4.940) for axial flow pump; n_s = 7,550 (2.763) (Reference 45)

casing. Closing a valve in the discharge line will only worsen the situation, and so valves having programmed operation should be closed very little, if at all, before reverse flow begins.

Reversed flow may be controlled by valves or by arranging to have the discharge pipe empty while air is admitted at or near the outlet. If reversed flow is not checked, it will bring the pump to rest and then accelerate it with reversed rotation. Eventually the pump will run as a turbine at the runaway speed corresponding to the available static head diminished by the frictional losses in the system. However, while reversed flow is being established, the reversed speed may reach a value considerably in excess of the steady-state runaway speed. Maximum reversed speed appears to increase with increasing efficiency and increasing specific speed of the pump. Calculations indicate maximum reversed speeds more than 150% of normal speed for n_s = 1935 (0.708) and η = 84.1%[45]. This should be considered in selecting a driver, particularly if it is a large electric motor.

There will be a pressure increase, called the *upsurge,* in the discharge pipe during reversed flow. The maximum upsurge usually occurs a short time before maximum reversed speed is reached and may cause a pressure as much as 60% or more above normal at the pump discharge. A further discussion of power-failure transients is given in Section 11.3.

ANALYSIS OF TRANSIENT OPERATION The data of Figures 52 and 53 have been presented in a form suitable for general application to pumps having approximately the same specific speeds as those tested. The symbols are $h = H/H_n$, $q = Q/Q_n$, $m = M/M_n$, and $\nu = n/n_n$, wherein H, Q, M, and n represent instantaneous values of head, flow rate, torque, and speed respectively and the subscript n refers to the values at best efficiency for normal constant-speed pump operation. Any consistent system of units may be used. According to the affinity laws (Eqs. 12), q is proportional to ν, and h and m are proportional to ν^2. Thus the affinity laws are incorporated in the scales of the diagrams. Figures 52 and 53 are divided into sections for convenience in reading data from the curves. The curves of sections 1 and 3 extend to infinity as q/ν increases without limit in either the positive or negative direction. This difficulty is eliminated by sections 2 and 4, where the curves are plotted against ν/q, which is zero when q/ν becomes infinite.

Usually any case of transient operation would begin at or near the point $q/\nu = \nu/q = 1$, which appears in both sections 1 and 2 of Figures 52 and 53. The detailed analysis of transient behavior is beyond the scope of this treatise. An analytical solution by the rigid column method, in which the liquid is assumed to be a rigid body, is given in Reference 45. Friction is easily included, and the results are satisfactory for many cases. The same reference includes a semigraphical solution to allow for elastic waves in the liquid, but friction must be neglected. Graphical solutions including both elastic waves and friction are discussed in References 45 to 48. Computer solutions of a variety of transient problems are discussed in Reference 47. These offer considerable flexibility in the analysis once the necessary programs have been prepared.

LIBERTY EXHIBIT 1017, Page 199

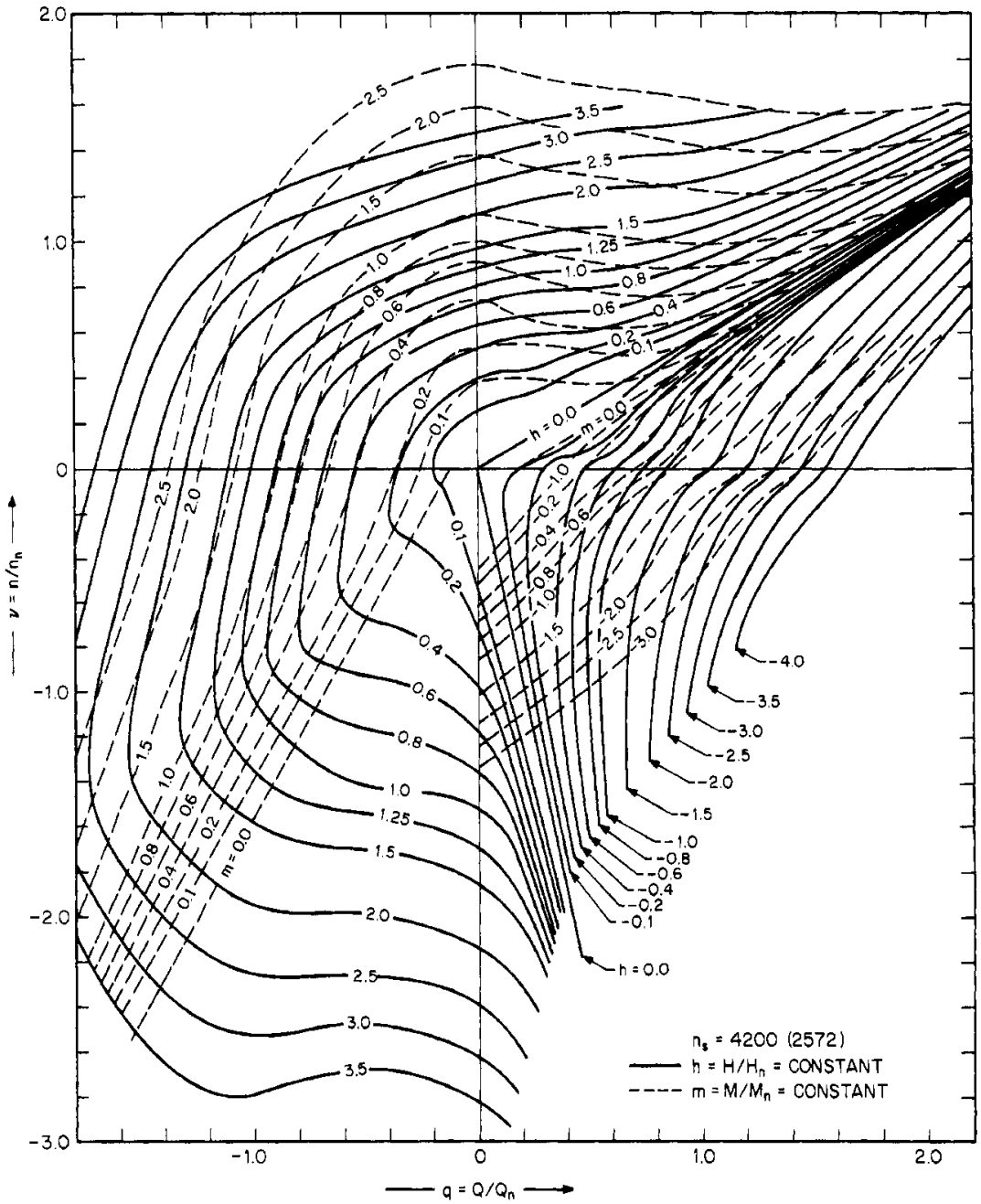


FIGURE 55 Circle diagram of pump characteristics. Specific speed n_s = 4200 (1.537). (Courtesy Combustion Engineering)

Some extreme conditions of abnormal operation can be estimated at points where the curves of Figures 52 and 53 cross the zero axes and are listed in Table 9. The data for Columns 2 to 4 of Table 9 were read from Sections 2 of Figures 52 and 53, and the data for Columns 6 and 7 were read from Sections 3. Column 8 was computed from Column 7 by assuming $h = 1$. Let the pump having $n_s = 1500$ (0.549) deliver cold water with normal head $H_n = 100$ ft (30.48 m), and let the center of the discharge flange be 4 ft (1.2 m) above the free surface in the supply sump. The discharge pressure head following power failure may be estimated by assuming the inertia of the rotating elements to be negligible relative to the inertia of the liquid in the pipeline. Then $q = 1$ and, from Column 2 of Table 9, the downsurge pressure head is (–0.22)(100) – 4 = –26 ft (–7.9 m), which is not low enough to cause separation of the water column.

LIBERTY EXHIBIT 1017, Page 200

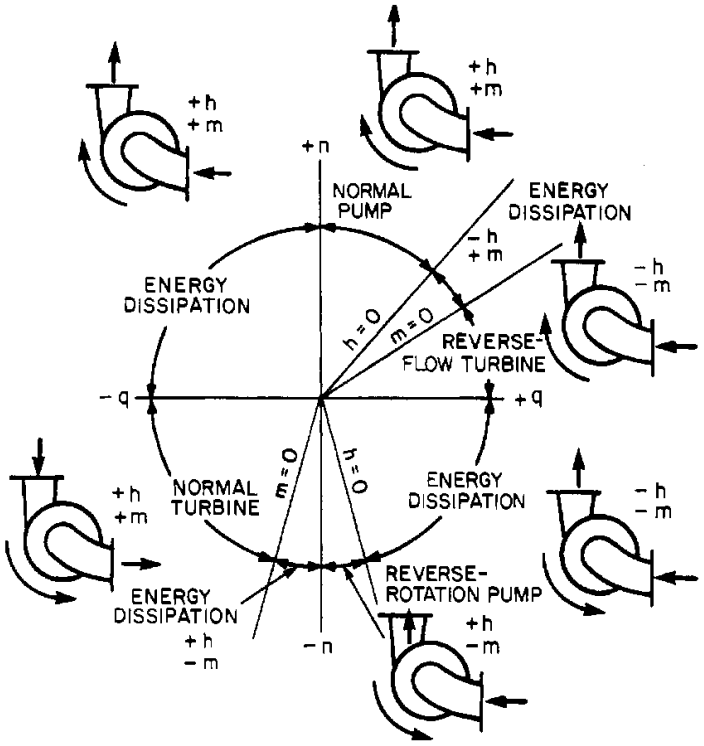


FIGURE 56 Explanatory diagram for Figure 55

Actually the downsurge would be less than this because of the effects of inertia and friction, which have been neglected. If this pump were stopped suddenly by a shaft seizure or by an obstruction fouling the impeller, Column 4 of Table 9 shows the downsurge to be (–0.55)(100) – 4 = –59 ft (–18 m), which would cause water column separation and, probably, subsequent water hammer. If, following power failure, the pump were allowed to operate as a no-load turbine under the full normal pump head, Column 8 of Table 9 shows the runaway speed would be 1.14 times the normal pump speed. The steady-state runaway speed usually would be less than this because the effective head would be decreased by friction, but higher speeds would be reached during the transient preceding steady-state operation. Column 8 shows that runaway speeds increase with increasing specific speed.

TABLE 9 Abnormal operating conditions of several pumps

Specific speed n_s (Ω_s)	Downsurge				Runaway turbine		
	Free-running $m/q^2 = 0$		Locked-rotor $\nu/q = 0$		$m/\nu^2 = 0$		$h = 1$
	h/q^2	ν/q	h/q^2	m/q^2	q/ν	h/ν^2	ν
1	2	3	4	5	6	7	8
1500 (0.549)[a]	−0.22	0.36	−0.55	−0.53	0.46	0.77	1.14
1800 (0.659)	−0.24	0.31	−0.60	−0.44	0.56	0.75	1.16
1935 (0.708)	−0.36	0.32	−0.94	−0.60	0.41	0.66	1.23
7550 (2.763)	−0.23	0.56	−1.57	−1.38	0.99	0.38	1.62
13,500 (4.940)	−0.12	0.67	−0.96	−0.60	1.08	0.33	1.73

[a]Double-suction.

LIBERTY EXHIBIT 1017, Page 201

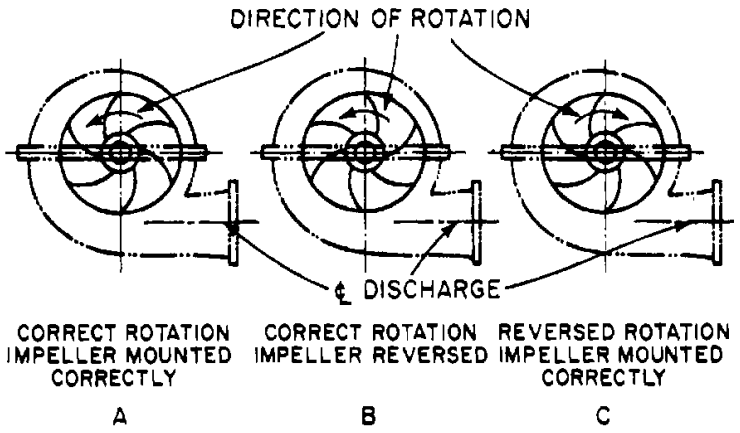


FIGURE 57A through C Pump assembly and rotation (Reference 7)

Incorrect Rotation Correct rotation of the driver should be verified before it is coupled to the pump (Figure 57). Sections 3 of Figures 52 and 53 show that reversed rotation might produce some positive head and flow rate with pumps of low specific speed, but at very low efficiency. It is unlikely that positive head would be produced by reversed rotation of a high-specific-speed pump.

Reversed Impeller Some double-suction impellers can be mounted reversed on the shaft. If the impeller is accidentally reversed, as at *B* in Figure 57, the flow rate and efficiency probably will be much reduced and the power consumption increased. Care should be taken to prevent this, as the error might go undetected in some cases until the driver was damaged by overload. Table 1 shows performance data for six pumps with reversed impellers. At least one of these would overload the driver excessively.

Further discussion of abnormal operating conditions may be found in References 7, 12, and 34.

Vibration Vibration caused by flow through wearing rings and by cavitation has been discussed in the foregoing and some remedies indicated. Vibration due to unbalance is not usually serious in horizontal units but may be of major importance in long vertical units, where the discharge column is supported at only one or two points. The structural vibrations may be quite complicated and involve both natural frequencies and higher harmonics. Vibration problems in vertical units should be anticipated during the design stage. If vibration is encountered in existing units, the following steps may help to reduce it: (1) dynamically balance all rotating elements of both pump and motor; (2) increase the rigidity of the main support and of the connection between the motor and the discharge column: (3) change the stiffness of the discharge column to raise or lower natural frequencies as required. A portable vibration analyzer may be helpful in this undertaking. Kovats[60] has discussed the analysis of this problem in some detail.

Structural vibrations can occur in most pump types. Typical sources are a) bearing housings—due to the commonly encountered cantilever construction, b) couplings, c) rotor instabilities stemming from excessive ring clearances and consequent loss of Lomakin stiffening of long-shaft multistage pumps, and d) hydraulic unbalance—due to dimensional variations in flow passages and clearances[61].

PREDICTION OF EFFICIENCY FROM MODEL TESTS

Many pumps used in pumped storage power plants and water supply projects are so large and expensive that extensive use is made of small models to determine the best design. It is often necessary to estimate the efficiency of a prototype pump, as a part of the guarantee,

LIBERTY EXHIBIT 1017, Page 202

from the performance of a geometrically similar model. A model and prototype are said to operate under dynamically similar conditions when

$$Dn/\sqrt{H} = D'n'/\sqrt{H'},$$

where D = impeller diameter
n = pump speed
H = pump head

in any consistent units of measure. Primed quantities refer to the model and unprimed quantities to the prototype. Dynamic similarity is a prerequisite to model-prototype testing so that losses that are proportional to the squares of fluid velocities, called *kinetic losses*, will scale directly with size and not change the efficiency. Surface frictional losses are boundary-layer phenomena which depend on Reynolds number

$$Re = D\sqrt{H}/\nu,$$

where ν = kinematic viscosity of the liquid pumped.

(See also Section 2.1, Eqs. 36–40.) Reynolds numbers increase with increasing size, and, within limits, surface frictional-loss coefficients decrease with increasing Reynolds number. This leads to a gain in efficiency with increasing size. Computational difficulties have forced an empirical approach to the problem. Details of the development of a number of formulas are given in Reference 62.

Moody-Staufer Formula In 1925, L. F. Moody and F. Staufer independently developed a formula that was later modified by Pantell to the form

$$\left(\frac{1-\eta_h}{1-\eta'_h}\right)\left(\frac{\eta'_h}{\eta_h}\right) = \left(\frac{D'}{D}\right)^n \tag{35}$$

where η_h = hydraulic efficiency, discussed previously, and D = impeller diameter. Primed quantities refer to the model, and n is a constant to be determined by tests. The model must be tested with the same liquid that will be used in the prototype; that is, cold water in most practical cases. The original formula contained a correction for head, which is negligible if $H' \geq 0.8H$, and this requirement is now virtually mandatory in commercial practice. The meager information available indicates $0.2 \geq n \geq 0.1$ approximately, with the higher value currently favored. Improvements in construction and testing techniques very likely will move n toward lower value in the future. The Moody-Staufer formula has been widely used since first publication. In practice, both η'_h and η_h are usually replaced by the overall efficiencies η' and η, respectively, because of the difficulty in determining proper values for the mechanical and volumetric efficiencies (see Eq. 11).

Rütschi Formulas The general form of several empirical formulas due to K. Rütschi[62] and others was originally given as

$$\eta_h = \frac{f}{f'}\eta'_h \tag{36}$$

where η_h and η'_h are the hydraulic efficiencies of the prototype and model, respectively, and f and f' are values of an empirical f function for both the prototype and the model. The f function was obtained from tests of six single-stage pumps. $n_S < 2000$ (0.732) and is shown in Figure 58 based on the *eye diameters* D_o of the pumps in *millimeters*. Thus the f function depends on actual size in addition to scale ratio. The extrapolated portion of the curve, shown dashed in Figure 58, checked well with values for a model and large prototype, shown by E' and E, respectively. One of several formulas that have been proposed to fit the curve in Figure 58 is, in SI units,

$$f = 1 - \frac{3.15}{D_o^{1.6}} \tag{37}$$

LIBERTY EXHIBIT 1017, Page 203

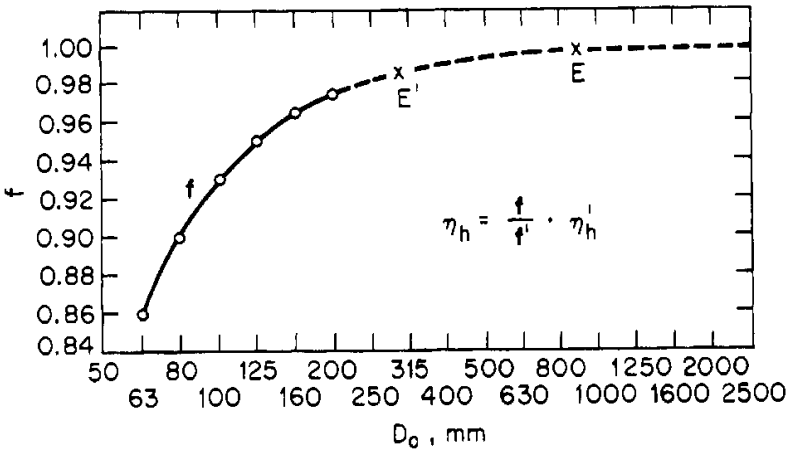


FIGURE 58 The f function for the Rütschi formula (to obtain D_o in inches, multiply by 0.03937) (References 13 and 62)

where the eye diameter D_o is in centimeters or, in USCS units,

$$f = 1 - \frac{0.0133}{D_o^{1.6}} \tag{38}$$

where D_o is in feet. Figure 59 gives a graphical solution of Eq. 38. The Society of German Engineers (VDI) has adopted a slightly modified version of the Rütschi formula as standard.

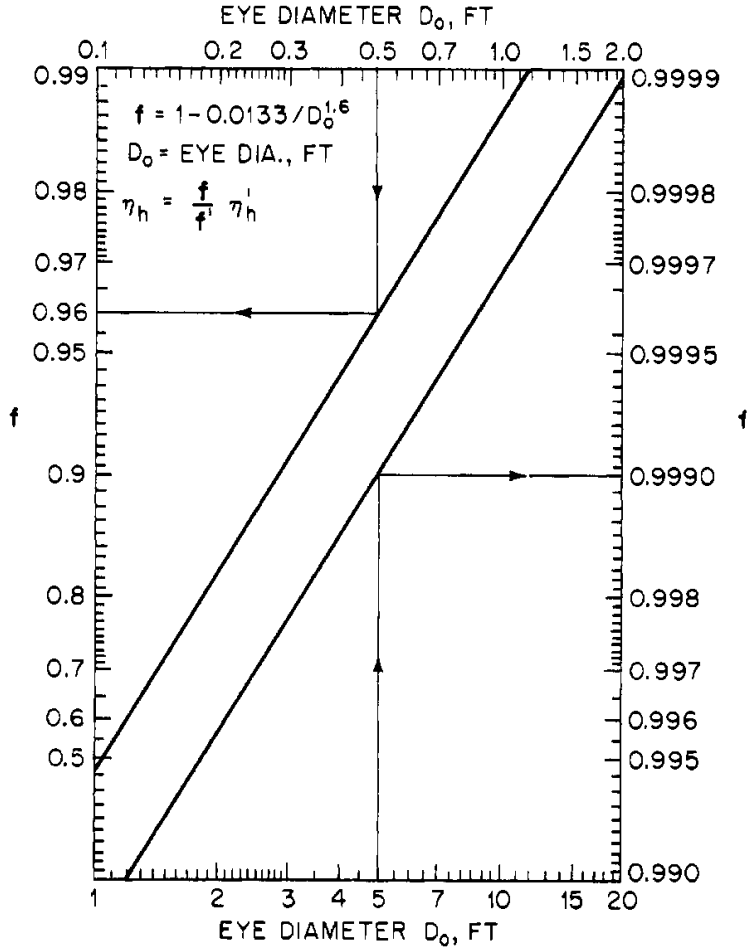


FIGURE 59 Chart for the solution of the Rütschi formula (to obtain D_o in meters, multiply by 0.3048) (Reference 62)

LIBERTY EXHIBIT 1017, Page 204

Rütschi later recommended, in discussion of Reference 62, that the internal efficiency $\eta_i = \eta/\eta_m$ be used instead of the hydraulic efficiency η_h in Eq. 45. The mechanical efficiency η_m will probably be very high for both model and prototype for most cases of interest, so good results should be obtained if the overall efficiency is used in Eq. 36.

Model-prototype geometric similarity should include surface finish and wearing ring or tip clearances, but this may be difficult or impossible to achieve. Anderson (see Section 2.1.1: Figure 10 and Reference 6) proposed a method that includes a correction for dissimilarity in surface finish.

OPERATION OF PUMPS AS TURBINES

Centrifugal pumps may be used as hydraulic turbines in some cases where low first cost is paramount. Because the pump has no speed-regulating mechanism, considerable speed variation must be expected unless the head and load remain very nearly constant. Some speed control could be obtained by throttling the discharge automatically, but this would increase the cost, and the power lost in the throttle valve would lower the overall efficiency.

Pump Selection After the head, speed, and power output of the turbine have been specified, it is necessary to select a pump that, when used as a turbine, will satisfy the requirements. Assuming that performance curves for a series of pumps are available*, a typical set of such curves should be normalized using the head, power, and flow rate of the best efficiency point as normal values. These curves will correspond to the right part of Section 1 of either Figure 52 or 53. In normalizing the power P, let $p = P/P_n$ and the curve of p/ν^3 will be identical with the curve of m/ν^2 in Figure 52 or 53. The normalized curves may be compared with the curves in Sections 1 of Figures 52 and 53 to determine which curves best represent the characteristics of the proposed pump. When a choice has been made, the approximate turbine performance can be obtained from the corresponding figure of Figures 60 to 63.

EXAMPLE Assume that the turbine specifications are $H_T = 20$ ft, $P_T = 12.75$ hp and $n = 580$ rpm, and that the characteristics of the DeLaval L1O/8 pump are representative of a series of pumps from which a selection can be made. The turbine discharge Q_T in gallons per minute after substituting the above values is

$$Q_T = \frac{3960P_T}{H_T\eta_T} = \frac{2520}{\eta_T} \tag{39}$$

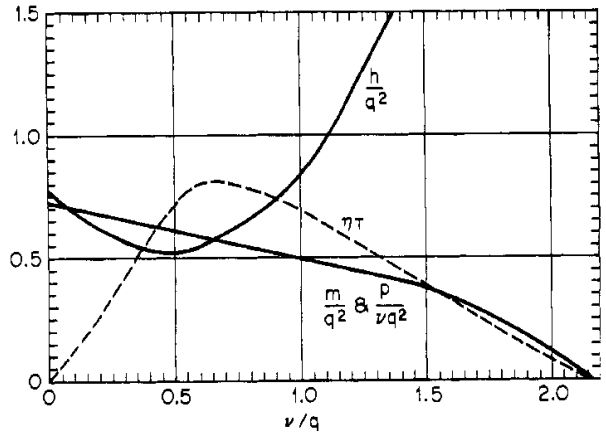


FIGURE 60 Dimensionless characteristic curves for DeLaval L 10/8 pump, constant-discharge turbine operation (Reference 63)

*It is assumed that turbine mode characteristics of the proposed pump are not available when the initial selection is made.

LIBERTY EXHIBIT 1017, Page 205

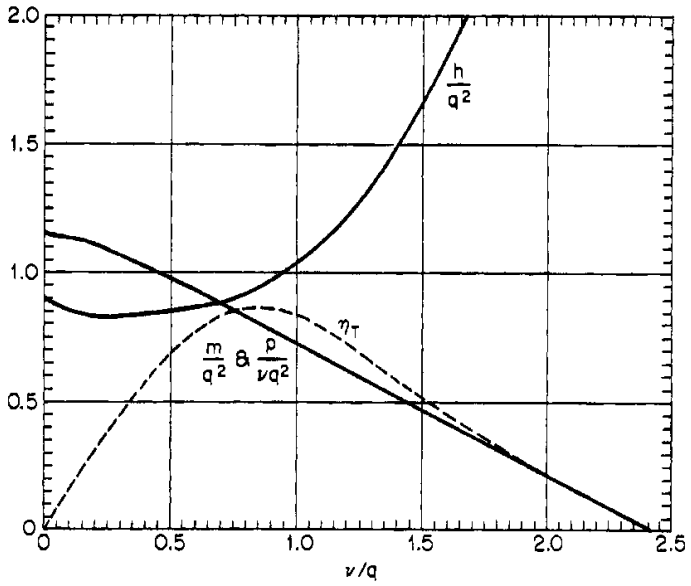


FIGURE 61 Dimensionless characteristic curves for Voith pump, constant-discharge turbine operation (Reference 63)

where η_T is turbine efficiency, shown in Figure 60. Only the normal values Q_n, H_n P_n, and so on, are common to the curves of both Figures 52 and 60, so these alone can be used in selecting the required pump. Values of ν/q, h/q^2, and η_T are read from the curves of Figure 60 and corresponding values of Q computed by Eq. 39. Values of Q_n and H_n are then given by

$$Q_n = Q(\nu/q) \tag{40}$$

$$H_n = \frac{H(\nu/q)^2}{h/q^2} = \frac{20(\nu/q)^2}{h/q^2} \tag{41}$$

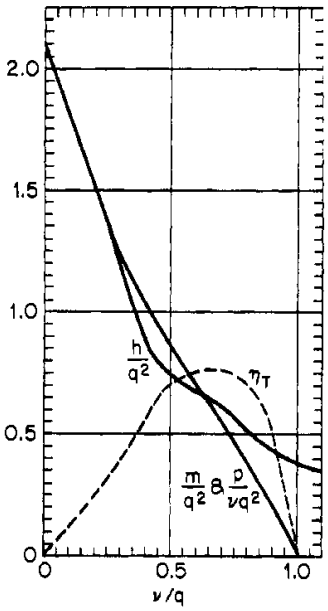


FIGURE 62 Dimensionless characteristics curves for Peerless 10MH pump, constant-discharge turbine operation (Reference 63)

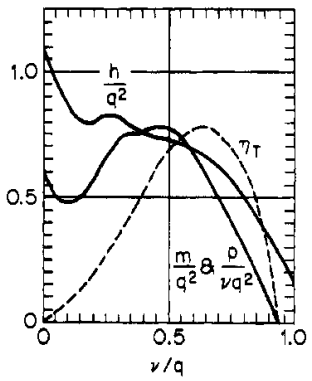


FIGURE 63 Dimensionless characteristic curves for Peerless 10PL pump, constant-discharge turbine operation (Reference 63)

LIBERTY EXHIBIT 1017, Page 206

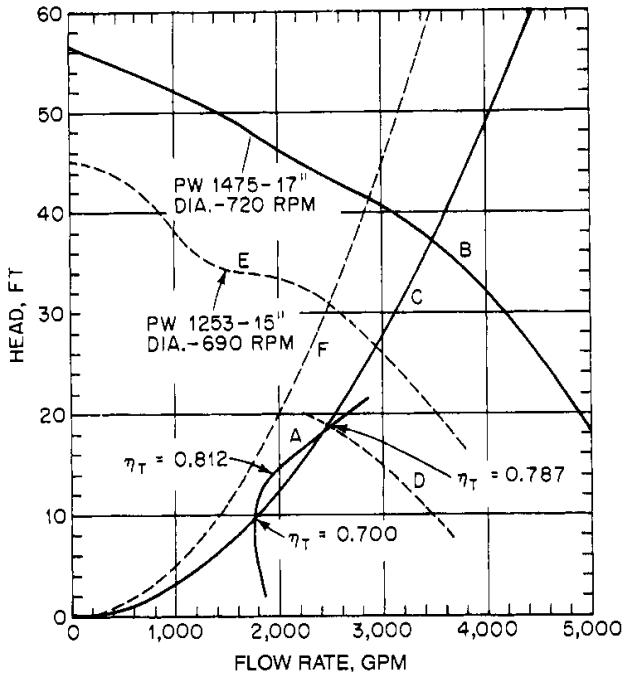


FIGURE 64 Head-flow curves of the pump selection (ft × 0.3048 = m; gpm × 0.06300 = l/s) (Reference 63)

For example, in Figure 60 at $\nu/q = 0.700$, read $h/q^2 = 0.595$ and $\eta_T = 0.805$. By Eq. 39, $Q_T = 2520/0.805 = 3130$ gpm; by Eq. 40, $Q_n = (3130)(0.700) = 2190$ gpm; and by Eq. 41, $H_n = (20)(0.700)^2/0.9595 = 16.5$ ft. In a similar manner, the locus of the best efficiency points for an infinite number of pumps, each having the same characteristics as shown in Figures 52 and 60, is obtained, and each pump would satisfy the turbine requirements. This locus of best efficiency points is plotted as curve *A* in Figure 64.

The head curve for a DeLaval L 16/14 pump having a 17-in-diameter impeller tested at 720 rpm is shown as curve *B* in Figure 64. The best efficiency point was found to be at $Q_n = 3500$ gpm and $H_n = 37.2$ ft. The locus of the best efficiency points for this pump for different speeds and impeller diameters is given by Eqs. 12 as

$$H_n = 37.2\left(\frac{Q_n}{3500}\right)^2 = \frac{3.04}{10^6}Q_n^2 \tag{42}$$

and is shown by curve *C* in Figure 64. Curve *C* intersects curve *A* at two points, showing that the L 16/14 pump satisfies the turbine requirements. Only the intersection at the higher turbine efficiency is of interest. At this point, $Q_n = 2490$ gpm and $H_n = 18.8$ ft. Because the turbine speed was specified to be 580 rpm, the required impeller diameter is given by Eqs. 12 as

$$D = \frac{(17)(2490/3500)}{580/720} = 15 \text{ in}$$

or by

$$D = \frac{17\sqrt{18.8/37.2}}{580/720} = 15 \text{ in}$$

The computed head curve for the 15-in-diameter impeller at 580 rpm is shown as curve *D* in Figure 64. The turbine discharge is 3200 gpm from Eq. 39 with $\eta_T = 0.787$.

The optimum solution would be to have Curve *C* tangent to Curve *A* at the point corresponding to maximum turbine efficiency, in this case $\eta_T = 0.812$. Because this

LIBERTY EXHIBIT 1017, Page 207

would require a smaller pump, Curve *E* in Figure 64 shows a head curve for a K 14/12 pump, which was the next smaller pump in the series. Curve *F*, the locus of the best efficiency points, does not intersect Curve *A*, showing that the smaller pump will not satisfy the turbine requirements. It is important to note that the turbine head, 20 ft, specified for this example was assumed to be the net head from the inlet to outlet flange of the pump when installed and operated as a turbine.

The procedure outlined above should lead to the selection of a pump large enough to provide the required power. However, it probably will be necessary to apply the affinity laws over such wide ranges of the variables that the usual degree of accuracy should not be expected. Considerable care should be exercised if it becomes necessary to interpolate between the curves of Figures 60 to 63. The computed performance will very likely differ from the results of subsequent tests. The curves of Figure 60 may be converted to show the constant-head characteristics of the L 16/14 pump when installed and operated as a turbine. Details of the method of computation are given in Reference 63, and the computed characteristics are shown in Figure 65.

A comprehensive study by Acres American[64,65] led to a computer program to aid in selecting a pump to meet specific requirements when operating in the turbine mode. Known pump characteristics are entered in the program according to a specified format. The computer compares them with stored characteristics of pumps for which turbine mode characteristics are known and provides estimated turbine mode characteristics for the proposed pump. Vols. I and III of Reference 64 describe the method of computation and give complete instructions for using the program.

Optimized Hydraulic Turbines A logical outgrowth of applying pumps as hydraulic turbines is the optimization of these machines as turbines. Several points of efficiency improvement have been demonstrated over that of pumps running in reverse as turbines.[66] The fluid accelerates through both the stator or nozzles and the turbine wheel or runner, whereas it decelerates through the same elements when they are acting as impeller and diffuser or volute in the pumping mode. If the fluid never has to decelerate

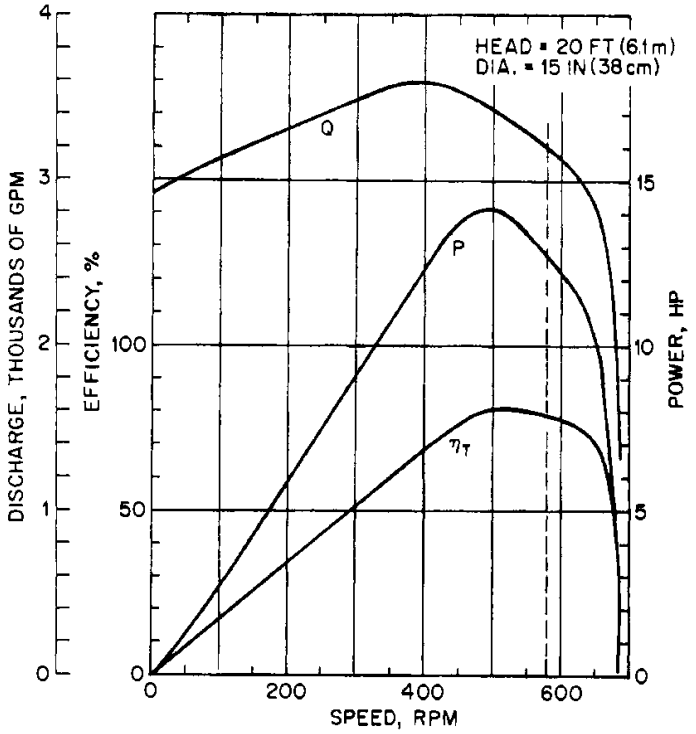


FIGURE 65 Computed constant-head turbine characteristics for DeLaval L 16/14 pump (gpm × 0.06309 = l/s; hp × 0.7457 = kW) (Reference 63)

LIBERTY EXHIBIT 1017, Page 208

because the turbine will never be used as a pump, the nozzles and runner can be designed to produce more aggressive and efficient acceleration in shorter distances than if the same machine is simply a pump being used as a turbine. If it is a radial-inflow runner, the resulting optimized turbine wheel employs a radial blade (with a blade angle $\beta = 90°$. from the tangential direction) at the outer diameter (inlet). This outer diameter is about 75% of the diameter of the impeller of the pump-as-turbine, which further improves the efficiency by reason of the reduction of the disk friction drag of the runner. Design and application of both approaches is explained and compared in Reference 67. Many of the applications of these hydraulic turbines are for power recovery in the pressure let-down processes that occur in petroleum refining. Another variable is introduced in such processes; namely, the evolution of large volumes of dissolved gas as the pressure decreases through successive stages or portions of the turbine. This phenomenon affects the performance of hydraulic turbines for such applications because somewhat more power is produced when gas evolves from the liquid than when a single-phase liquid flows through the turbine at the same pressure drop and mass flow rate.[68]

VORTEX PUMPS

A typical vortex pump is shown in Figure 66.* The ability of this type of pump to handle relatively large amounts of suspended solids as well as entrained air or gas more than offsets the relatively low efficiency. Table 10 lists performance data for four typical vortex pumps and four radial-flow centrifugal pumps of nearly the same head and flow rate. Figure 67 shows the head characteristics of a typical vortex pump with impellers of different diameters together with curves of constant efficiency and constant NPSH. Power curves for the same impellers are shown in Figure 68.

Curves for a conventional radial-flow pump have been added for comparison in Figures 67 and 68. Note that the head of the vortex pump does not decrease as rapidly with an increasing flow rate as does the head of the conventional pump. The power requirement of the vortex pump increases almost linearly with an increasing flow rate, whereas the power required by a conventional pump of about the same specific speed reaches a maximum and then decreases with the increasing flow rate.

Thus if the motor of the vortex pump has been selected to match the power required at the normal flow rate for best efficiency, it will be overloaded if the pump operates much beyond that point.

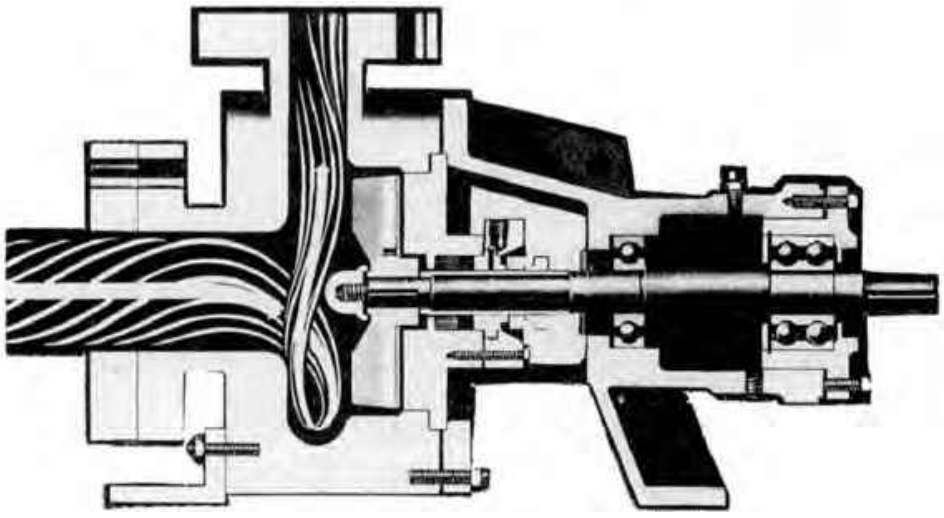


FIGURE 66 Vortex pump (courtesy Fybroc Division, METPRO)

*See also Section 12.2.

LIBERTY EXHIBIT 1017, Page 209

TABLE 10 Characteristics of typical vortex pumps and comparable radial-flow centrifugal pumps at 1750 rpm

Impeller	Flow rate, gpm	(l/s)	Total head, ft	(m)	Specific speed, n_s	(Ω_s)	Suction specific speed, S	(Ω_{ss})	Impeller diameter, in	(mm)	Sphere diameter,[a] in	(mm)	Efficiency[b] at Q = Q_n, %	Shutoff power,[b] $\%P_n$	Power[b] at $1.5Q_n$, $\%P_n$	Shutoff head,[b] $\%H_n$	Head[b] at $1.5Q_n$, $\%H_n$	NPSHR[b] at Q_n, ft	(m)	NPSHR[b] at $1.5Q_n$, ft	(m)
Vortex	100	(6.3)	24	(7.3)	1614	(0.591)	7700	(2.82)	$5\frac{7}{8}$	(149)	2	(51)	39.5	37.5	131	120	71	3	(0.9)	8	(2.4)
Radial	108	(6.8)	26	(7.9)	1580	(0.578)	6430	(2.35)	$5\frac{7}{8}$	(149)	$\frac{5}{8}$	(16)	59	50	108	144	50	4	(1.2)	7.5	(2.3)
Vortex	200	(12.6)	61	(18.6)	1134	(0.415)	7400	(2.71)	$8\frac{3}{8}$	(213)	2	(51)	45	45	129	123	82	5	(1.5)	8	(2.4)
Radial	225	(14.2)	60	(18.3)	1218	(0.446)	6450	(2.36)	$8\frac{3}{8}$	(213)	$\frac{3}{4}$	(19)	61	50	130	125	65	6.5	(2.0)	14	(3.4)
Vortex	850	(53.6)	108	(32.9)	1523	(0.557)	9820	(3.59)	$11\frac{1}{2}$	(292)	4	(102)	59	49	134	120	83	9	(2.7)	15	(4.6)
Radial	900	(56.8)	102	(31.1)	1636	(0.599)	8690	(3.18)	$11\frac{1}{2}$	(292)	$\frac{7}{8}$	(22)	76	47	113	135	44	11	(3.4)	21	(6.1)
Vortex	1050	(66.2)	150	(45.7)	1323	(0.484)	7088	(2.59)	13	(330)	$3\frac{3}{4}$	(95)	56	48	137	115	87	16	(4.9)	20	(6.1)
Radial	1250	(78.9)	154	(46.9)	1415	(0.518)			13	(330)	$1\frac{1}{32}$	(26)	83	52	123	116	45	11	(3.4)	-	(-)
Vortex average					1399	(0.512)							50	45	133	120	81				
Radial average					1462	(0.535)							70	50	119	130	51				

[a]Diameter of the largest sphere that will pass through the pump

[b]Subscript n designates values at the best efficiency point

LIBERTY EXHIBIT 1017, Page 210

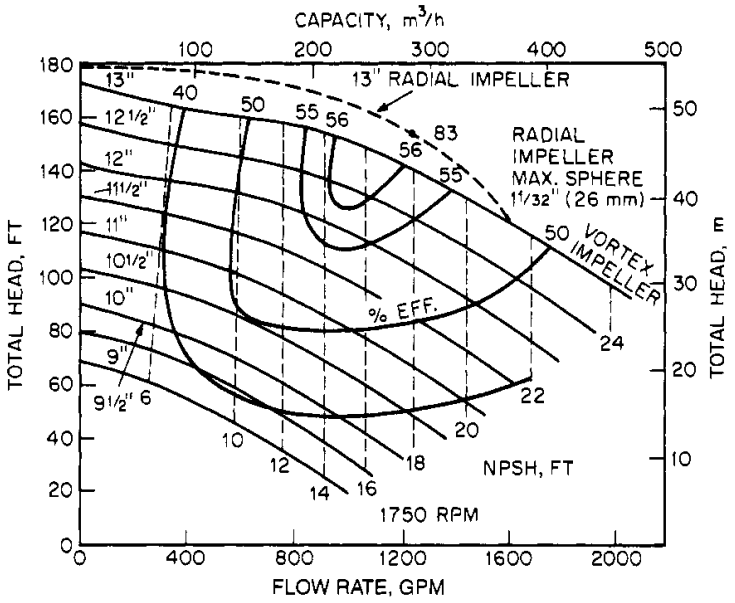


FIGURE 67 Head characteristics of a typical vortex pump. Curves show approximate characteristics when pumping clear water (in × 2.54 = cm) (Flowserve Corporation).

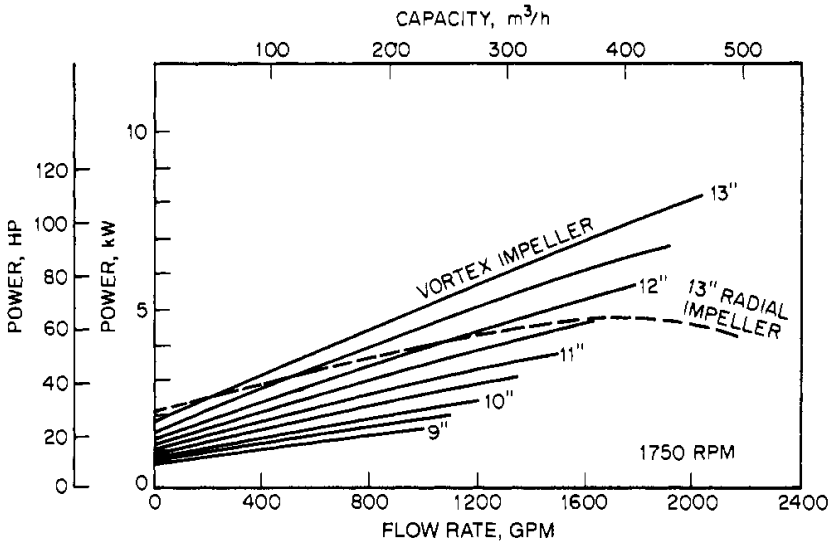


FIGURE 68 Power characteristics of a typical vortex pump. Curves show approximate characteristics when pumping clear water (in × 2.54 = cm) (Flowserve Corporation).

REFERENCES

1. Pfleiderer, C. *Die Kreiselpumpen für Flüssigkeiten und Gase.* 5te Auflage, Springer-Verlag, 1961.
2. Gülich, J., Favre, J. N., and Denus, K. "An Assessment of Pump Impeller Performance Predictions by 3D-Navier Stokes Calculations." Third International Symposium on Pumping Machinery (S239), ASME Fluids Engineering Division Summer Meeting, Paper No. FEDSM97-3341, June 1997.
3. Rupp, W. E. *High Efficiency Low Specific Speed Centrifugal Pump.* U.S. Patent No. 3,205,828, September 14, 1965.
4. Barske, U. M. "Development of Some Unconventional Centrifugal Pumps." *Proc. Inst. Mech. Eng.,* London, **174**(11):437, 1960.
5. Manson, W. W. "Experience with Inlet Throttled Centrifugal Pumps, Gas Turbine Pumps." *Cavitation in Fluid Machinery,* Symposium Publication, ASME, 1972, pp. 21–27.
6. Wislicenus, C. F. "Critical Considerations on Cavitation Limits of Centrifugal and Axial-Flow Pumps." *Trans ASME,* **78:**1707, 1956.
7. Karassik, I. J., and Carter, R. *Centrifugal Pumps: Selection, Operation and Maintenance.* McGraw-Hill, New York, 1960.
8. Holland, F. A., and Chapman, F. S. *Pumping of Liquids.* Reinhold, New York, 1966.
9. Ippen, A. T. "The Influence of Viscosity on Centrifugal Pump Performance." *Trans. ASME,* **68**(8):823, 1946.
10. Black, H. F., and Jensen, D. N. "Effects of High-Pressure Ring Seals on Pump Rotor Vibrations." ASME Paper No. 71-WA/FF-38, 1971.
11. Wood, C. M., Welna, H., and Lamers, R. P. "Tip-Clearance Effects in Centrifugal Pumps." *Trans. ASME, J. Basic Eng.,* Series D, **89:**932, 1965.
12. Stepanoff, A. J. *Centrifugal and Axial Flow Pumps,* 2nd ed., Krieger Publishing, Malabar, FL, 1957.
13. Rütschi, K. "Untersuchungen an Spiralgehäusepumpen veraschiedener Schnelläufigkeit," *Schweiz. Arch Angew, Wiss. Tech.* **17**(2):33, 1951.
14. Stepanoff, A. J. *Pumps and Blowers: Two Phase Flow.* Krieger Publishing, Malabar, FL, 1965.
15. Knapp, R. T. "Recent Investigations of the Mechanics of Cavitation and Cavitation Damage." *Trans. ASME* **77:**1045, 1955.
16. Knapp, R. T. "Cavitation Mechanics and Its Relation to the Design of Hydraulic Equipment." James Clayton, Lecture, *Proc. Inst. Mech. Eng.,* London, Sec. A, **166:**150, 1952.
17. Shutler, N. D., and Mesler, R. B. "A Photographic Study of the Dynamics and Damage Capabilities of Bubbles Collapsing Near Solid Boundaries." *Trans. ASME, J. Basic Eng.,* Series D, **87:**511, 1965.
18. Hickling, R., and Plesset, M. S. "The Collapse of a Spherical Cavity in a Compressible Liquid." Division of Engineering and Applied Sciences, Report No. 85-24, California Institute of Technology, March 1963.
19. Pilarczyk, K., and Rusak, V. "Application of Air Model Testing in the Study of Inlet Flow in Pumps." *Cavitation in Fluid Machinery,* ASME, 1965, p. 91.
20. Plesset, M. S. "Temperature Effects in Cavitation Damage." *Trans. ASME, J. Basic Eng.,* Series D, **94:**559, 1972.
21. Hammitt, F. C. "Observations on Cavitation Damage in a Flowing System." *Trans. ASME, J. Basic Eng.,* Series D, **85:**347 (1963).
22. Preece, C. M., ed. *Treatise on Materials Science and Technology.* Vol. 16, *Erosion,* Academic Press, New York, 1979.

LIBERTY EXHIBIT 1017, Page 212

23. Kovats, A. *Design and Performance of Centrifugal and Axial Flow Pumps and Compressors.* Macmillan, New York, 1964.

24. Palgrave, R., and Cooper, P. "Visual Studies of Cavitation in Pumping Machinery." *Proceedings of the Third International Pump Symposium,* Texas A&M University, 1986, pp. 61–68.

25. Cooper, P., Sloteman, D. P., Graf, E., and Vlaming, D. J. "Elimination of Cavitation-Related Instabilities and Damage in High-Energy Pump Impellers." *Proceedings of the Eighth International Pump Users Symposium,* Texas A&M University, 1991, pp. 3–19.

26. Vlaming, D. J. "Optimum Impeller Inlet Geometry for Minimum NPSH Requirements for Centrifugal Pumps." *Pumping Machinery—1989*, ASME, July 1989, pp. 25–29.

27. Hydraulic Institute ANSI/HI 2000 Edition Pump Standards, Hydraulic Institute, Parsippany, NJ www.pumps.org.

28. "Centrifugal Pumps." PTC 8.2-1965, American Society of Mechanical Engineers, New York, 1965.

29. Wislicenus, C. F., Watson, R. M., and Karassik, I. J. "Cavitation Characteristics of Centrifugal Pumps Described by Similarity Considerations." *Trans. ASME* **61:**17, 1939; **62:**155, 1940.

30. Stahl, H. A., and Stepanoff, A. J. "Thermodynamic Aspects of Cavitation in Centrifugal Pumps." *Trans. ASME* **78:**1691, 1956.

31. Salemann, V. "Cavitation and NPSH Requirements of Various Liquids." *Trans. ASME, J. Basic Eng.,* Series D, **81:**167, 1959.

32. Stepanoff, A. J. "Cavitation Properties of Liquids." *Trans. ASME, J. Eng. Power,* Series A, **86:**195, 1964.

33. Cooper, P. "Analysis of Single- and Two-Phase Flows in Turbopump Inducers." *Transactions of the ASME*, Series A, Vol. 89, 1967, pp. 577–588.

34. Lazarkiewicz, S., and Troskolański, A. T. *Impeller Pumps,* Pergamon Press, New York, 1965.

35. Gongwer, C. A. "A Theory of Cavitation Flow in Centrifugal-Pump Impellers." *Trans. ASME,* **63:**29, 1941.

36. Guelich, J. F. *Guidelines for Prevention of Cavitation in Centrifugal Feedpumps.* EPRI CS-6398, 1989.

37. ASTM Standard G-32. *Cavitation Erosion Using Vibratory Apparatus,* American Society for Testing Materials, 1992.

38. Cooper, P., and Antunes, F. F. "Cavitation Damage in Boiler Feed Pumps." *Symposium Proceedings: Power Plant Feed Pumps—The State of the Art*, EPRI CS-3158, July 1983, pp. 2–24 to 2–49.

39. Cooper, P., Sloteman, D. P., and Dussourd, J. L. "Stabilization of the Off-Design Behavior of Centrifugal Pumps and Inducers." *Proceedings of the Second European Congress on Fluid Machinery for the Oil, Petrochemical and Related Industries*, I Mech E Conference Publications, 1984-2, Paper No. C41/84, 1984, pp. 13–20.

40. Stripling, L. B., and Acosta, A. J. "Cavitation in Turbopumps—Part 1." *Transactions of the ASME*, Series D, Vol. 84, 1962, pp. 326–338.

41. Stripling, L. B. "Cavitation in Turbopumps—Part 2." *Transactions of the ASME*, Series D, Vol. 84, 1962, pp. 339–350.

42. Grohmann, M. "Extend Pump Application with Inducers." *Hydrocarbon Processing,* Dec. 1979, p. 121.

43. Doolin, J. H. "Centrifugal Pumps and Entrained Air Problems." *Pump World,* **4**(3), 1978.

44. *Mechanical Engineering.* **93**(6):89, 1971.

LIBERTY EXHIBIT 1017, Page 213

45. Kittredge, C. P. "Hydraulic Transients in Centrifugal Pump Systems." *Trans. ASME,* **78**(6):1807, 1956.

46. Parmakian, J. *Waterhammer Analysis.* Prentice-Hall, Englewood Cliffs, NJ, 1955.

47. Streeter, V. L., and Wylie, E. B. *Hydraulic Transients.* McGraw-Hill, New York, 1967.

48. Bergeron, L. *Waterhammer in Hydraulics and Wave Surges in Electricity.* Wiley, New York, 1961.

49. Addison, H. *Centrifugal and Other Rotodynamic Pumps.* 3rd ed. Chapman & Hall, London, 1966.

50. Richardson, C. A. "Economics of Electric Power Pumping." *Allis-Chalmers Elec. Rev.* **9:**20, 1944.

51. Fraser, W. H. "Flow Recirculation in Centrifugal Pumps." *Tenth Turbomachinery Symposium.* Texas A&M University, College Station, TX, 1981, p. 95.

52. Fraser, W. H. "Recirculation in Centrifugal Pumps." *Materials of Construction of Fluid Machinery and Their Relationship to Design and Performance.* ASME, November 1981, pp. 65–86.

53. Gopalakrishnan, S. "A New Method for Computing Minimum Flow." *Proceedings of the Fifth International Pump Users Symposium.* Texas A&M University, 1988, pp. 41–47.

54. "Code of Practice for Pump Efficiency Testing by the Direct Thermodynamic Method." Report 695/27, The Pump Centre, AEA Technology plc, Birchwood Science Park, Warrington WA3 6AT, UK, June 1995.

55. Agostinelli, A., Nobles, D., and Mockridge, C. R. "An Experimental Investigation of Radial Thrust in Centrifugal Pumps." *Trans. ASME, J. Eng. Power,* Series A, **82:**120, 1960.

56. Biheller, H. J. "Radial Force on the Impeller of Centrifugal Pumps with Volute, Semivolute, and Fully Concentric Casings." *Trans. ASME, J. Eng. Power,* Series A, **87:**319, 1965.

57. Donsky, B. "Complete Pump Characteristics and the Effects of Specific Speeds on Hydraulic Transients." *Trans. ASME, J. Basic Eng.,* Series D, **83:**685, 1961.

58. Swanson, W. M. "Complete Characteristic Circle Diagrams for Turbomachinery." *Trans. ASME* **75:**819, 1953.

59. Knapp, R. T. "Complete Characteristics of Centrifugal Pumps and Their Use in the Prediction of Transient Behavior." *Trans. ASME* **59:**683, 1937; **60:**676, 1938.

60. Kovats, A. "Vibration of Vertical Pumps." *Trans. ASME, J. Eng. Power,* Series A, **84:**195, 1962.

61. Bolleter, U., Leibundgut, E., Sturchler, R., and McCloskey, T. "Hydraulic Interaction and Excitation Forces of High Head Pump Impellers." *Pumping Machinery—1989,* FED-Vol. 81, ASME, 1989, pp. 187–193.

62. Kittredge, C. P. "Estimating the Efficiency of Prototype Pumps from Model Tests." *Trans. ASME, J. Eng. Power,* Series A, **90:**129, 301, 1968.

63. Kittredge, C. P. "Centrifugal Pumps Used as Hydraulic Turbines." *Trans. ASME, J. Eng. Power,* Series A, **83:**74, 1961.

64. Acres American Inc. for U.S. Department of Energy, Idaho National Engineering Laboratory, *Small Hydro Plant Development Program.* Vols. I, II, and III, subcontract No. K-1574, Oct. 1980. Available from National Technical Information Service, U.S. Department of Commerce, Springfield, VA 22161.

65. Lawrence, J. D., and Pereira, L. "Innovative Equipment for Small-Scale Hydro Developments: Waterpower '81." *An International Conference on Hydropower, Proceedings.* Vol. II, Washington, DC, June 22-24, 1981, pp. 1622–1639.

66. Cooper, P., and Nelik, L. "Performance of Multi-Stage Radial-Inflow Hydraulic Power Recovery Turbines." Paper presented at ASME Winter Annual Meeting, New Orleans, December 1984.

LIBERTY EXHIBIT 1017, Page 214

67. Gopalakrishnan, S. "Power Recovery Turbines for the Process Industry." *Proceedings of the Third International Pump Symposium*, Texas A&M University, 1986, pp. 3–11.

68. Hamkins, C. P., Jeske, H. O., Apfelbacher, R. and Schuster, O. "Pumps as Energy Recovery Turbines With Two-Phase Flow." *Pumping Machinery—1989*, FED-Vol. 81, ASME, 1989, pp. 73–81.

69. Kallas, D. H., and Lichtman, J. Z. "Cavitation Erosion." In *Environmental Effects on Polymeric Materials,* D. V. Rosato and R. T. Schwartz, eds., Wiley-Interscience, New York, 1968, pp. 223–280.

FURTHER READING

Anderson, H. H. *Centrifugal Pumps*, Trade and Technical Press, Surrey, England, 1980.

Brennen, C. E. *Hydrodynamics of Pumps*, Concepts ETI, Inc., and Oxford University Press, 1994.

Carter, R. "How Much Torque Is Needed to Start Centrifugal Pumps?" *Power* **94**(1):88, 1950.

Church, A. H. *Centrifugal Pumps and Blowers.* Krieger Publishing, Malabar, FL, 1944.

Heald, C. C. *Cameron Hydraulic Data,* 19th ed., 2002. Flowserve Corporation, Irving, TX, 75039.

Japikse, D., Marscher, W. D., and Furst, R. B. *Centrifugal Pump Design and Performance.* Concepts ETI, Inc., Wilder, VT, 1997.

Moody, L. F., and Zowaki, T. "Hydraulic Machinery." 3rd ed., sec. 26 of *Handbook of Applied Hydraulics.* Davis and Sorenson, eds., McGraw-Hill, New York, 1969.

Spannhake, W. *Centrifugal Pumps, Turbines, and Propellers.* Technology Press, MIT, Cambridge, MA, 1934.

Wislicenus, C. F. *Fluid Mechanics of Turbomachinery.* Dover, New York, 1965.

2.1.4 CENTRIFUGAL PUMP MECHANICAL BEHAVIOR AND VIBRATION

WILLIAM D. MARSCHER
PAUL A. BOYADJIS
RICHARD J. CRONIN
MATTHEW A. GAYDON
WILLIAM J. KELLY
ERIC J. OLSON
MAKI M. ONARI

INTRODUCTION

Vibration is the fundamental measure of the mechanical waste energy within rotating machinery. In this respect it is a major performance phenomenon that is distinct from the hydraulic characteristics that the user demands of a pump, which must be so constructed that it will indeed perform as required. When failures occur in pumps and their associated systems, they generally are either caused by excessive vibration, or can be diagnosed by abnormalities in the vibration characteristics of the pump, which in turn are intimately connected with the design, construction, and application of the machine.

This section deals with the sources of pump mechanical distress and vibration, methods of vibration analysis and testing, and the diagnostic interpretation of pump vibration.

LIBERTY EXHIBIT 1017, Page 216

BASIC PRINCIPLES OF VIBRATION

Vibration consists of the oscillatory motion of one or more locations on a component. This motion can be considered as a function of time (this is how a person intuitively "sees" or "feels" vibration), or as a function of frequency, that is, how many oscillations per second, or hertz (Hz), are occurring. These are two methods of considering the same motion, and are related to each other through the Fourier Transform, often implemented by engineers and their instruments through use of the "Fast Fourier Transform," or FFT. The FFT is able to decompose a complex signal into the various frequency components and phase relationships (timing) between these components that must be present in order for the time signal to have the waveform shape that it exhibits when the vibrational motion is plotted versus time. As will be seen, the FFT vibration versus frequency "spectrum" plot is useful in determining the probable source of vibrations, and whether or not the vibration level is unusual or signifies a problem requiring maintenance attention, or even immediate shutdown of the pump.

The vibrational response of a pump as a mechanical "system" is the result of the excitation forces (internally or externally imposed) imparted to the system, as amplified or attenuated by the inherent mechanical properties of the system itself. The methods discussed in this section allow differentiation between excitation-related and system-related causes. In general, for pump system diagnostic purposes, the most effective manner for evaluating mechanical vibration and pressure pulsation data is in the frequency domain (i.e., an amplitude versus frequency "spectrum"), because a force occurring at a specific frequency typically must be the result of some physical cause at that same frequency, for example, imbalance at 1 × rotational speed (= running speed), and rotating impeller pulsation caused "vane-pass" frequency at the number of impeller vanes (also known as blades when on a rotating member) times running speed. Sometimes, time domain data contain more easily interpreted information, particularly when sporadic impulsive loads are present, such as during cavitation or rub events. A particularly useful form of time domain data is the "orbit," in which the shaft motion versus time in two perpendicular lateral directions are plotted at a given axial location along the shaft, thereby showing the path of the centerline of the shaft during one of its revolutions.

Excitation Frequencies Some basic vibration concepts must be reviewed prior to detailed discussion of excitation forces and frequencies. The rotational speed of a pump is typically discussed in units of "revolutions per minute" or rpm. Vibration frequency data are typically discussed in terms of "cycles per second" or Hertz (Hz). A common means of describing vibration frequency is also in terms of multiples of running speed. For example, a 2× running speed vibration for a pump operating at 3600 rpm would be at a frequency of 120 Hz (3600 rpm × [1 min/60 s] × 2). Pump oscillating excitation forces are characterized not just by their level, but also by the frequencies at which they impart energy to the system, as will be described for the various typical pump excitations in the following paragraphs.

1. **Rotating imbalance** Approximately 40% of all vibration problems in rotating machinery are caused by rotating imbalance, in the authors' experience as well as in studies in various applications.[1] If the rotating components of the pump system are not properly balanced, and operate such that the center of gravity of the shaft or attached components is offset from the axis of rotation, the rotor will experience radial forces at the frequency of the pump operating speed N. This type of excitation would, therefore, be categorized as a $1\times N$ vibration source. The greater the imbalanced mass (m) and associated offset (e) from the rotational axis, the greater the 1× vibration excitation force. Theoretically, the magnitude of the sinusoidal imbalance excitation force would be: $F = me(2\pi f)^2$ where f is the rotational frequency expressed in Hz. The rotating imbalance force will cause an orbiting motion of the shaft, and as the shaft comes into close proximity with its bearings will cause a portion of the imbalance force to be transmitted from the shaft, through the bearings, to the stationary structure where it can be readily measured as a lateral vibration. Some degree of imbalance will always be present. Methods for balancing the rotor system to remove this excitation source are discussed later in this section.

LIBERTY EXHIBIT 1017, Page 217

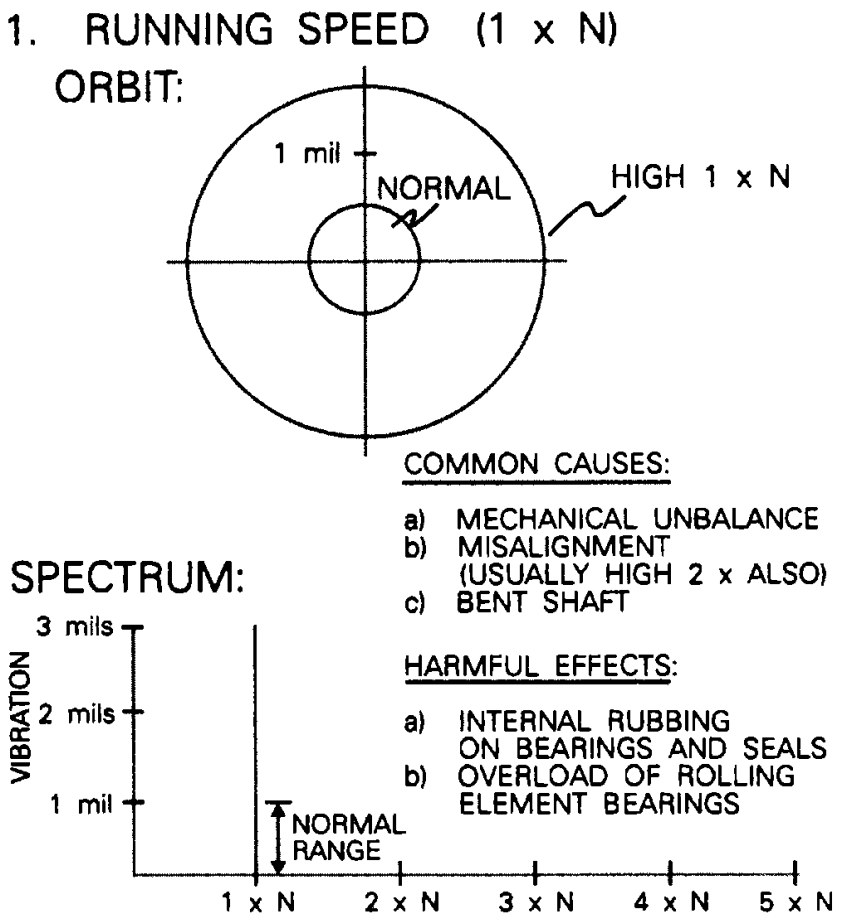


FIGURE 1 Typical orbit and vibration spectrum for a pump with an imbalanced rotor (Mechanical Solutions, Inc.)

Signal processing the vibration data into the frequency domain would reveal a sharp spike at 1× running speed, proportional to the degree of imbalance, while considering it as an orbit in the time domain would result in a large ellipse, more elliptical than circular in shape if the bearing load is significant or if the bearing stiffness is different in the vertical versus horizontal direction, as is often the case. (See Figure 1.)

2. **Misalignment** In the authors' experience as well as in the same studies discussed with regard to balance issues (e.g., Makay[1]), approximately 40% of all vibration problems in rotating machinery are caused by shaft misalignment. Misalignment may be caused by improper installation or extreme differential thermal expansions or pressure-related nozzle loads. The two main types of misalignment are angular and offset. The offset component is the amount that the two centerlines (of the driver and pump) are "offset" from each other (i.e., the distance between the centerlines when extended to be adjacent to each other). The angular component is the differential crossing angle that the two shaft centerlines make when projected into each other, when viewed from first the top, and then in a separate evaluation from the side. In general, misalignment is a combination of both offset and angular misalignment. The vibration data of a misaligned pump system are typically characterized by high 2× lateral vibration. Sometimes the misalignment load can cause higher harmonics (i.e., rotor speed integer multiples, especially 3×), and may even decrease vibration, because it loads the rotor highly eccentrically against its bearing shell, distorting the otherwise perfect 1× sine wave that theoretically is caused by residual imbalance. Alternatively, misalignment may actually cause increased 1× vibration, by lifting the rotor out of its gravity-loaded "bearing pocket," to result in the bearing running relatively unloaded (this can also cause shaft instability, as discussed later). Shown in Figure 2 is a typical orbit and excitation FFT spectrum for misalignment, in which 2× running

LIBERTY EXHIBIT 1017, Page 218

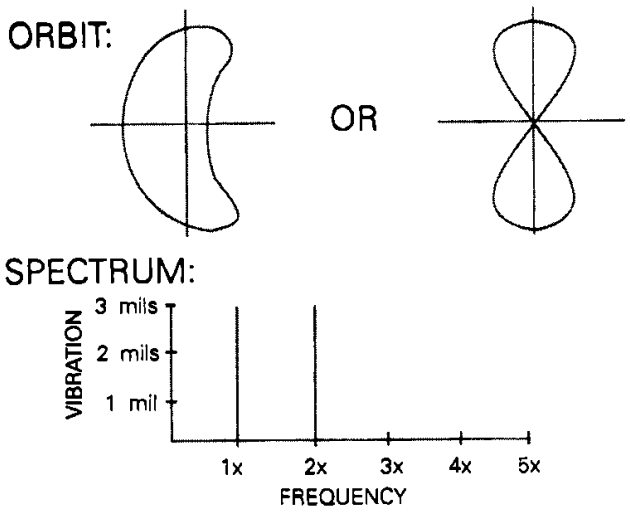


FIGURE 2 Excitation orbit and frequency spectrum for misalignment condition (Mechanical Solutions, Inc.)

speed is the dominant effect. This is often accompanied by relatively large axial motion, also at 2×, because the coupling experiences a nonlinear "crimp" twice per revolution.

3. **Looseness, rubs** A common cause of pump system vibration is looseness in bearing supports or components attached to the shaft. The main symptoms of such a vibration are a number of harmonics at multiples of running speed, a pulsating orbit and potentially a substantial percentage of vibration at exact whole fractions of running speed, such as $\frac{1}{2}$, $\frac{1}{4}$, and so on. Rubs at a bearing, seal or other running clearance have similar symptoms.

4. **Rolling element bearings** Rolling element, or "antifriction," bearings have certain defect frequencies that indicate bearing imperfections. These frequencies are associated with the rate at which flaws in the bearing parts (the inner race, the outer race, the cage, and the rolling element such as ball or needle) interact with each other. Key bearing parameters include the pitch diameter D_p which is the average of the inner and outer race diameters at the ball interface, the shaft rotational speed N, and the ball-to-race contact angle θ measured versus a plane running perpendicular to the shaft axis. The predominant defect frequencies are shown in Figure 3. Note that no bearing is perfect, and these frequencies are always present, to at least a minute degree, even in a healthy bearing, although the defect frequencies may be masked by other phenomena or by the measurement resolution of the probe or signal analyzer used.

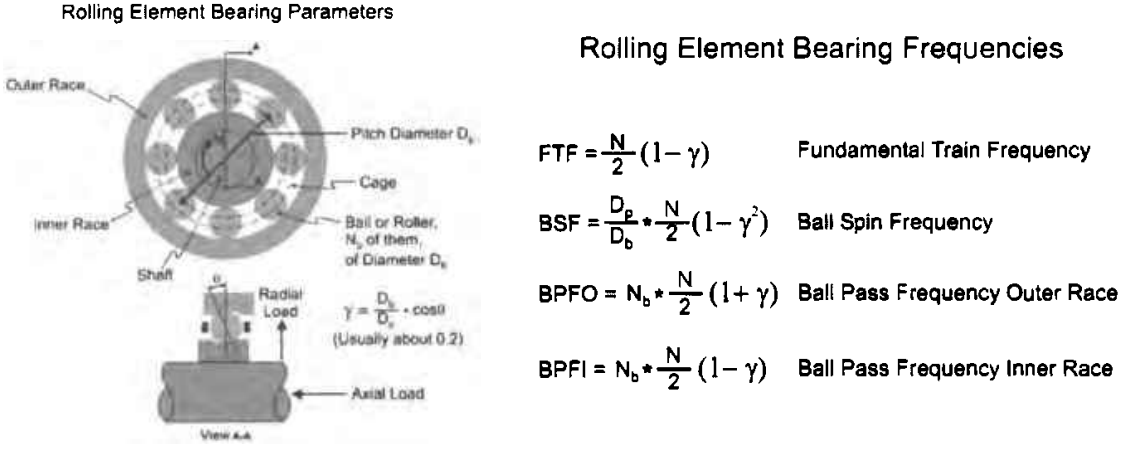


FIGURE 3 Rolling element bearing excitation frequencies (Mechanical Solutions, Inc.)

LIBERTY EXHIBIT 1017, Page 219

Next Page

$$F_{gm} = F_{bull} * T_{bull} = F_{pin} * T_{pin}$$

$$F_{pin} = F_{bull} * \frac{T_{bull}}{T_{pin}}$$

$$F_{app} = \frac{F_{gm}}{N_a}$$

$$F_{tr} = \frac{F_{gm} * N_a}{T_{bull} * T_{pin}} = \frac{F_{bull} * N_a}{T_{pin}} = \frac{F_{pin} * N_a}{T_{bull}}$$

where: F_{gm} = Gear Mesh Frequency (Cycles/Minute)
F_{bull} = Rotational Speed of Bull Gear (Revolutions/Minute)
F_{pin} = Rotational Speed of Pinion (Revolutions/Minute)
T_{bull} = Number of Teeth on Bull Gear
T_{pin} = Number of Teeth on Pinion
F_{app} = Assembly Phase Passage Frequency (Cycles/Minute)
F_{tr} = Tooth Repeat Frequency (Cycles/Minute)
N_a = Number of Assembly Phases (Largest Number that Divides into T_{bull} and T_{pin} without remainder)

FIGURE 4 Gear box excitation frequencies (Mechanical Solutions, Inc.)

5. **Gear boxes** The primary excitation frequency caused by a gear box is the number of gear teeth times the running speed. In the case of a gear box problem, often highly increased vibration at multiples of the gear mesh frequency as well as +/– 1 × *N* sidebands (i.e., modulation) of the gear box harmonics may accompany severe vibration at the gear mesh frequency. A summary of nonmodulated excitation frequencies in gear boxes are shown in Figure 4.
6. **Fluid forces**
   - **i.** *Cavitation.* The phenomenon of cavitation occurs when vapor bubbles form, typically as a result of either insufficient suction pressure ("Net Positive Suction Head Available", $NPSH_A$) or a poor flow pattern at the suction, followed by movement of these bubbles into an area of higher pressure, such that they collapse with great force potentially against impeller or casing surfaces. The collapsing of the bubbles does not occur at a specific frequency, but rather, involves an impulsive load that acts as a broadband excitation to excite a very broad range of frequencies, exciting impeller and casing natural frequencies even into the ultrasonic range. Evidence of cavitation and its strength is therefore typically not evident as a spike on a frequency spectrum (instead it slightly raises the spectrum fairly evenly over a very broad range), but is clearly discernable as powerful random pulses in a pressure or vibration versus time high resolution plot. An example of cavitation pulses in the time domain as evidenced in such plots is given in Figure 5, for a double suction single stage pump in low suction pressure water service.
   - **ii.** *Fluid whirl.* Shaft part-speed (i.e., below running speed, or "subsynchronous") whirl is a forced response at a frequency typically below the first noncritically damped shaft bending natural frequency. It is driven by a moving static pressure field which rotates at some speed below running speed. This fluid rotational speed becomes the whirl speed. The most common cause of whirl is fluid rotation around the impeller front or back shrouds, or in the journal bearing, wear ring, or balance drum clearances. Such fluid rotation is typically about 45% of running speed,

LIBERTY EXHIBIT 1017, Page 220

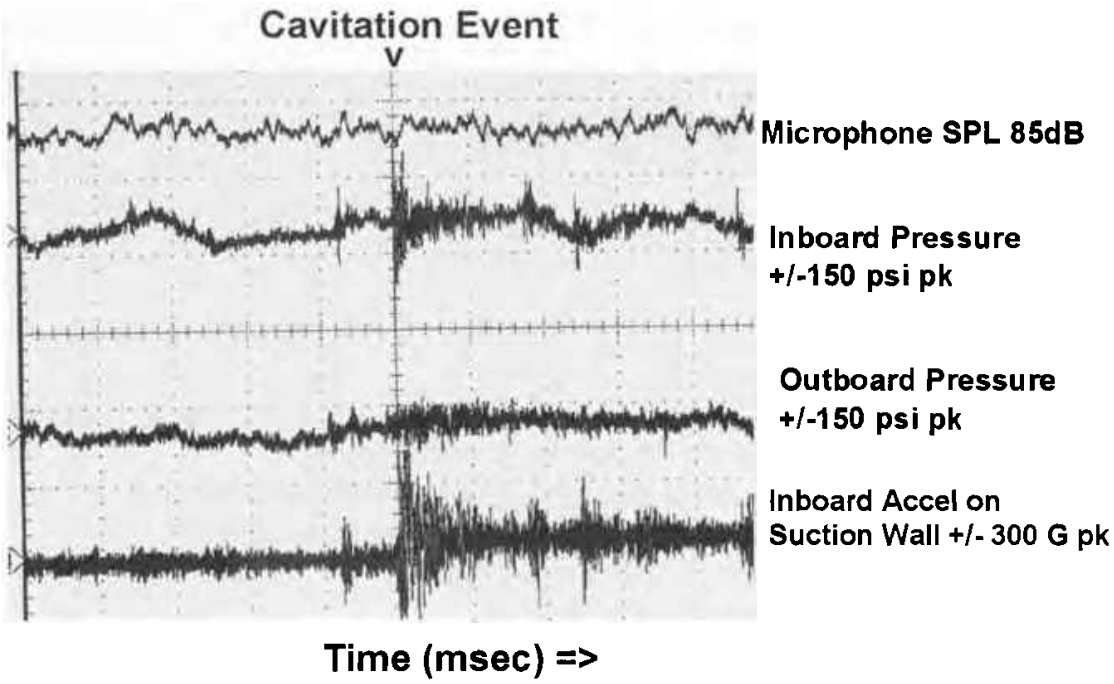


FIGURE 5 Cavitation pulses versus time (0 to 10 msec) in inboard and outboard suction bays of a double suction water pump. The pulse was in the inboard bay in this instance. The microphone, 6 ft away from the inboard suction wall, was not responsive at the high frequency (order of 50 kHz) of the pulse and its ring-down. Note the randomly occurring lower level pulses. In the case where a low pressure zone occurs at one clock position of the inlet, the pulses tend to cluster in groups associated with the impeller vane passing the low pressure zone. According to the authors' analysis, the amplitude and frequency of occurrence of the strongest pulses correlate with erosion damage potential. Bubble collapse in the middle of the passage, away from the walls, causes no damage, and only weak pulse transmission to the walls, as detected by a high frequency accelerometer. (Mechanical Solutions, Inc.)

because the fluid is stationary at the stator wall, and rotating at the rotor velocity at the rotor surface. Thus the bulk of the fluid in the running clearance rotates at roughly half speed.

If this whirl frequency increases to become coincident with a poorly damped natural frequency of the rotor/bearing system, the whirl can transform into a more dangerous motion called "whip." Once shaft whip starts, self-excitation occurs at the natural frequency of the shaft which is coincident with the whirl, such that the vibration response frequency "locks on" to the natural frequency, so that as speed is increased further, the whirling frequency no longer increases in proportion, but remains the same as the shaft natural frequency. During whip, the normally primarily 1× running speed frequency spectrum and roughly circular shaft orbit show a strong pulsing peak at about 45% of the running speed at which whip initiated. In the orbit, whip shows up as a slowly rotating loop reflecting orbit pulsation every other revolution. In rotating machinery, whip is the most common form of "rotordynamic instability," in which dangerously high vibrations occur in spite of how well the machine is balanced, aligned, or otherwise designed. Fortunately, whip is far more common in compressors and turbines than in centrifugal pumps, although it can only be ruled out by either experience with the pump and system in question, or by careful rotordynamic analysis and/or testing.

iii. *Vane pass.* Each time a pump impeller vane (or blade) moves past the volute "cutwater" or diffuser vane, a pressure pulse is imparted to it. The vane pass excitation frequency is therefore at the running speed times the number of impeller vanes, as indicated in Figure 6. This load condition can have a severe effect if any stationary structure or combined rotor and stationary structure natural frequencies happen to coincide with the vane pass frequency.

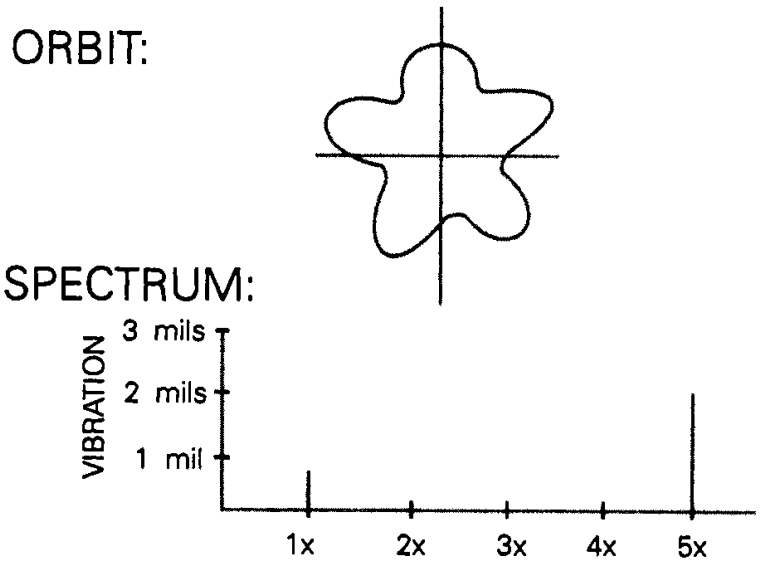


FIGURE 6 Excitation orbit and frequency spectrum for excessive vane pass pulsation (Mechanical Solutions, Inc.)

iv. *Internal suction or discharge recirculation.* If a pump is operated too far away from its best efficiency point (BEP), the angle of attack of incoming flow on the rotating impeller vane is different from that of the optimal design. Vane stalling can occur at either the suction or discharge, leading to portions of the flow reversing direction. The reversing flow is termed internal recirculation (see Section 2.1.1), and can lead to strong vortices, which can develop very low pressure at their tips while they are in the flow passage, causing cavitation, and/or which buffet the pump as they rotate past the impeller vanes. This tends to cause amplitude modulation of the running speed and vane pass frequencies, with a broadband frequency range associated with the statistical average of the vortex rotating speeds (the vortex axes typically slip substantially relative to running speed).

v. *Rotating stall.* Sometimes at the off-BEP flows associated with the internal recirculation condition, and due to the same principle of poor angle-of-attack on the impeller or diffuser vanes, rotating stall may occur, in which a recirculating stall cell (which is generally a recirculation vortex) will propagate circumferentially. This stall cell rotation in an impeller is opposite to the spin of the impeller, by 5 to 35% of rotating speed, resulting in stall cell rotation relative to ground of $0.65\times$ to $0.95\times N$. If the stall cell occurs in the diffuser, it rotates in the same direction as the impeller spin, at a frequency of about 0.05 to $0.35\times$. Although the rotating stall results in a "subsynchronous frequency" (i.e., below running speed), which few phenomena possess other than rotordynamic instability, they are not instabilities but rather forced vibrations, controllable by keeping their rotation frequency at least 10% away from any rotor or structural natural frequency. Typical orbits and spectra for these various types of subsynchronous vibration are shown in Figure 7, and are compared to orbits and spectra for rub or rotordynamic instability.

Natural Frequencies and Mode Shapes The inherent mechanical properties of a system important to its vibrational response include its stiffness, mass, and energy absorption as reflected in the natural frequencies, mode shapes and damping of the rotor and stationary structural system. If a cyclic load is applied to a structure, the response of that structure is dependent on the frequency at which it is excited. At specific frequencies, termed the natural frequencies, the response is dramatically increased, a phenomenon termed resonance. When designing and installing pumps and their systems it is important to ensure that the natural frequencies of the system do not coincide with anticipated excitation frequencies, such as those described above. If an appropriate separation margin

LIBERTY EXHIBIT 1017, Page 222

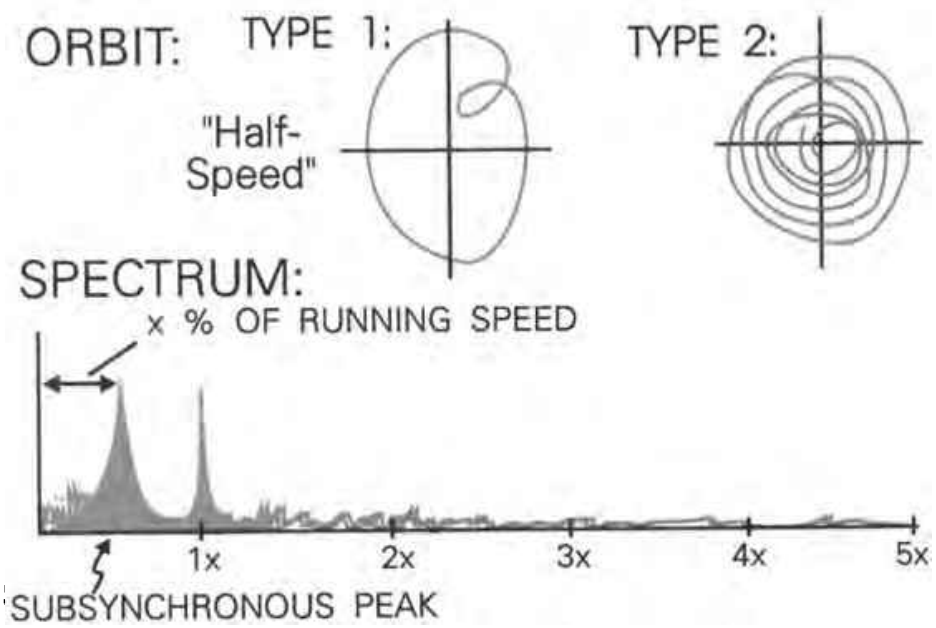


FIGURE 7 Excitation orbit and frequency spectrum for: (Type 1) Rub if x = 0.5×, (Type 1) rotordynamic instability if x = 0.40 to 0.49×, or (Type 2) rotating stall in the diffuser if x = 0.05 to 0.35× or in the impeller if x = 0.65 to 0.95× (Mechanical Solutions, Inc.)

does not exist, excessive vibration can result, even for relatively low energy excitations. A resonance near running speed can result in a pump being chronically "balance sensitive" or "alignment sensitive."

Each natural frequency has a deflection shape, or mode shape, associated with it. This is the shape that the structure takes on during vibration at that frequency. The mode shape also plays a role in the vibration response level. If the applied excitation forces occur at points in the structure which exhibit much movement, then a greater response is expected. Analytical methods for determining system natural frequencies and mode shapes are discussed later in this section.

Natural frequencies of rotating systems are termed critical speeds if their amplification factor is high enough (over 2.5, per API-610[2]). When a rotor's revolution is at a critical speed, the 1× excitation that is always present to some degree will excite the corresponding natural frequency and can cause severe vibration even for normally acceptable levels of imbalance. The natural frequencies and mode shapes can be calculated using the principles of rotordynamics, which are discussed later in this section. Note that the natural frequencies of the rotating system will have dependence on the running speed. For example, at higher speeds, gyroscopic effects become significant and can stiffen lateral modes. Additionally, hydrodynamic effects caused by fluid passing through annular spaces around the shaft also vary with running speed and affect the natural frequencies through the Lomakin effect.[3] Rotor critical speeds should be determined in the design stage of a pump system so that such conditions can be avoided.

As an example, consider the lateral vibration of an impeller-between-bearings multistage pump rotor system. One such typical rotor exhibited the natural frequencies and mode shapes shown in Figure 8.

Resonance, Damping, and Phase Angle When cyclic forces are applied to a system at a frequency equal to its natural frequency a resonant vibration occurs. Damping provides energy absorption and reduces the response. In a centrifugal pump, damping is provided from several sources such as viscous effects of hydrodynamic bearings, hydrostatic effects at annular seals, and structural damping inherent in the materials of construction. Figure 9 depicts the effects of damping on the frequency response function of a system.

LIBERTY EXHIBIT 1017, Page 223

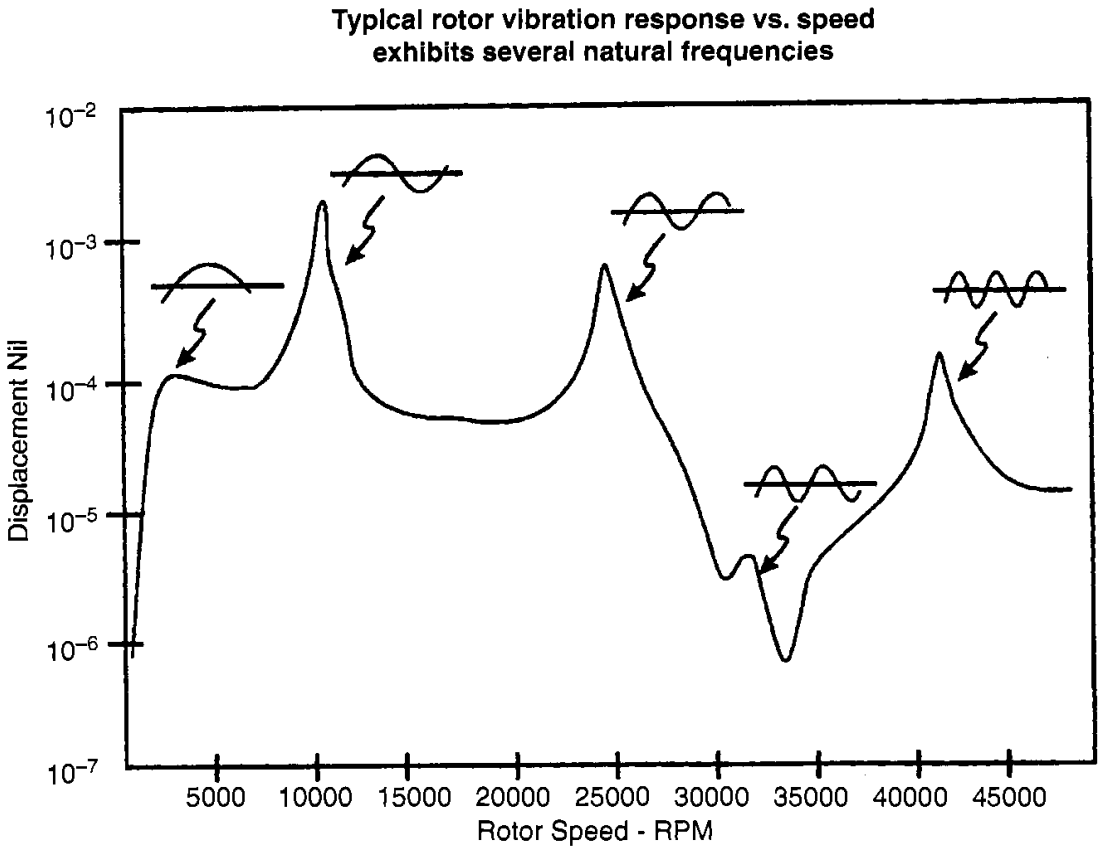


FIGURE 8 Typical mode shapes for a multistage centrifugal pump (Mechanical Solutions, Inc.)

In resonance, the vibration energy from the last peak of the force has come full cycle, and is reinforced when the next peak takes place. The vibration in the next cycle will then include movement due to both peaks, and will be higher than it would be for a single application of the force. The vibration motion keeps being amplified in this way until its large motion uses up more energy than the amount of energy that is being supplied by each additional peak. Unfortunately, the motion at that point is generally quite large, and damaging. To avoid resonance, the natural frequencies of the pump rotor and structure must be well separated from the frequencies at which such repetitive "dribbling" type forces will occur, which tend to be 1× running speed (typical of imbalance), 2× running speed (typical of misalignment), or at the number of impeller vanes time running speed (so-called "vane pass").

In pumps, the vibration amplification (often termed "Q" as shown in Figure 9) due to resonance is usually between a factor of 2 and 25 times what it would be if the force causing the vibration were steady instead of oscillating. Q depends on the amount of energy absorption, called "damping," which takes place due to oscillation. In an automobile suspension, this damping is provided by the shock absorbers. In a pump, it is provided primarily by the bearings and the liquid flowing axially between the rotor and stator in the "annular seals," like the balance piston.

Another important concept in vibration is the "phase angle," which measures the time lag between the application of a force and the vibrating motion which occurs in response to it. A phase angle of zero degrees means that the force and the vibration due to it act in the same direction, moving in step with one another. This occurs at very low frequencies, well below the natural frequency. An example of this is a force being slowly applied to a spring. Alternately, a phase angle of 180 degrees means that the force and the vibration due to it act in exactly opposite directions, so that they are perfectly out of step with each other. This occurs at very high frequencies, well above the natural frequency. At the point of resonance (frequency = natural frequency), phase angle is theoretically 90 degrees.

LIBERTY EXHIBIT 1017, Page 224

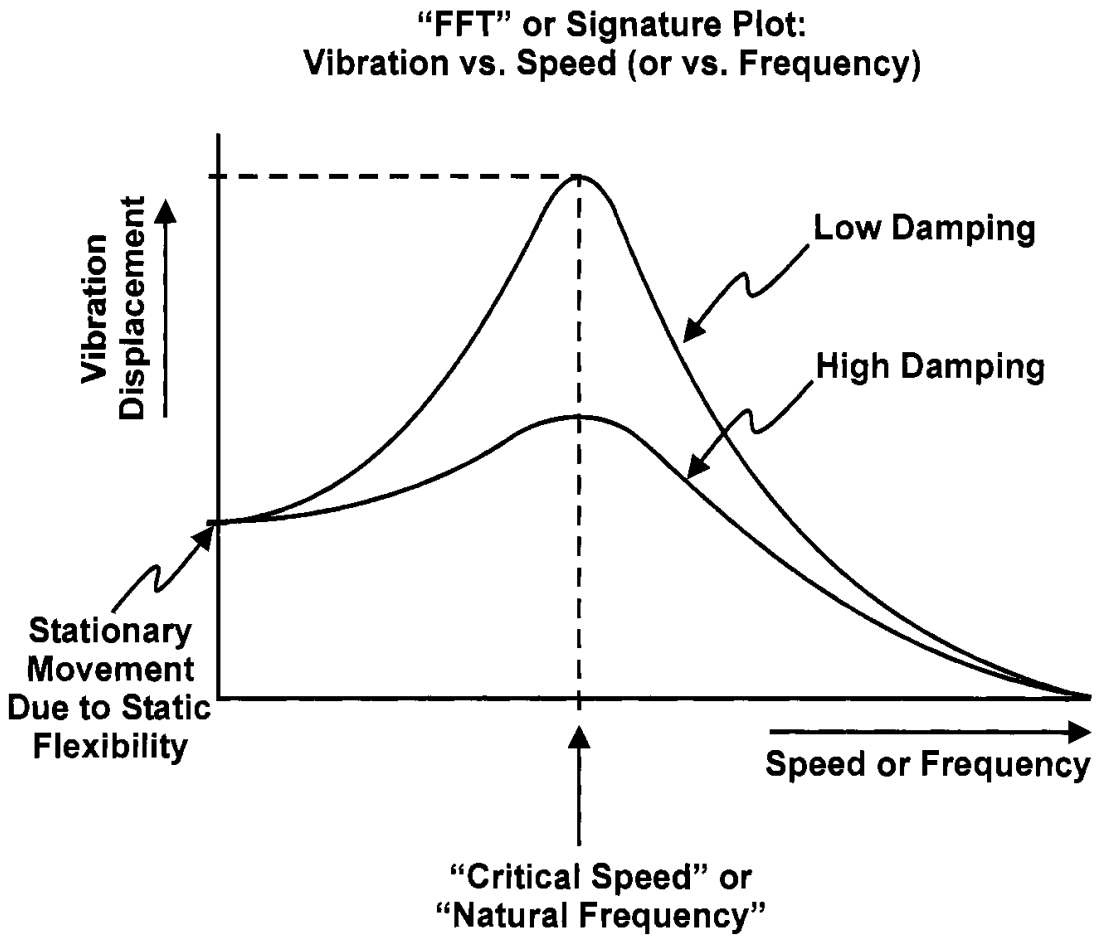


FIGURE 9 Vibration resonance spectrum, displacement x versus frequency f (Mechanical Solutions, Inc.)

Phase angle ϕ is important because it can be used together with peaks in vibration frequency field data to positively identify natural frequencies as opposed to excessive excitation forces. Such identification is useful in order to determine what steps should be taken to solve a vibration problem. The role of phase angle is also important in recognizing and solving rotordynamic instability problems, which typically require different solutions than resonance or excessive oscillating force problems.

These concepts can be described mathematically for simplified vibration systems. For example, consider the mechanical system displayed in Figure 10. The system is comprised of mass m, stiffness k, damping c, and is operated on by a sinusoidal force F as a function of time t: $F(t) = F_o\sin(\omega_f t)$. The dynamic displacement response of such a system would be $x(t)=X\sin(\omega_f t+\phi)$.

For this so-called single degree of freedom (DOF) system, the natural frequency is $\omega_n = (k/m)^{0.5}$ rad/sec, which can be divided by 2π to be put in terms of cycles per second (Hz), and can be further multiplied by 60 to be put in terms of f_n with units of cycles per minute, the same units as pump rpm. Note that k is the effective stiffness of the system, and m is the effective mass of the system, which in USCS units must be divided by the gravitational constant g_o to get consistent units. (See the definition of g_o in the nomenclature of Section 2.1.1.)

For a static loading force equal to F_o, the static displacement S of the mass is equal to F_o/k as shown in Figure 8. For a cyclic force, the amplitude of vibration of the mass, designated by X, is equal to $F_o/((k\text{-}m\omega_f^2)^2 + (c\omega_f)^2))^{0.5}$, where ω_f is the forcing frequency in rad/sec, and c is the damping constant. The maximum amplitude of vibration P occurs when the forcing function frequency ω_f is near the natural frequency. It can be shown that for small values of damping, the magnification factor $P/S = 1/(2\zeta)$, where the damping factor

LIBERTY EXHIBIT 1017, Page 225

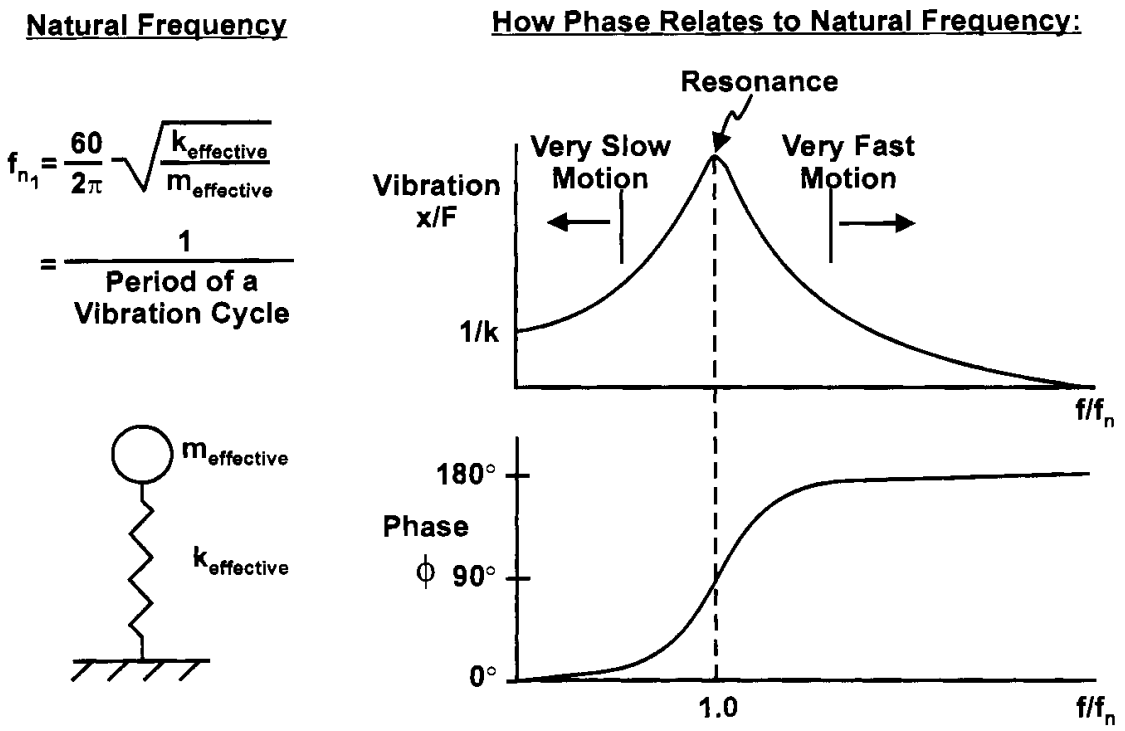


FIGURE 10 Single degree of freedom system (Mechanical Solutions, Inc.)

ζ is defined as the ratio of the damping c to the critical level of damping c_c. A critically damped system will not oscillate if perturbed momentarily from an at rest position. The critical damping level in terms of pump mechanical properties is $c = 2(km)^{0.5}$. Typical pumps have damping significantly less than critical (typically $\zeta = 0.02$ to 0.1).

Often mechanical aspects of a pump system can be reasonably simplified into a single DOF system such as the one described, and approximate natural frequencies and response levels can be estimated. For example, the behavior of the motor of a typical vertical turbine pump resting upon the discharge head of the pump may be very similar to a single DOF system in its first "above ground" dominated bending mode. Similarly, the effective mass and stiffness the rotor of an overhung impeller pump may be estimated to allow for a critical speed prediction. Even mechanical systems that are significantly more complicated than single degree of freedom systems can have their vibratory behavior described as a combination of natural frequencies, each with an effective mass (perhaps distributed in several locations), stiffness, and damping.

THE ROLE OF VARIOUS PUMP COMPONENTS

Impeller Effects on Vibration Impellers are typically the heaviest components and have the largest mass moments of inertia in the pump rotor system. The transverse moment of inertia of an impeller is sometimes neglected in lateral analyses, and this can result in significant errors, particularly for overhung impeller or multistage pumps, or in high-speed applications. With the advent of modern solid modeling software, not only weight, but also the polar and transverse moments of inertia, can be accurately determined from solids models of impellers.

Shafts: Lateral, Torsional, and Axial Stiffness and Motion In general, the lateral stiffness of shafts is directly proportional to the fourth power of the diameter and inversely proportional to the cube of the length. Typically the lengths that govern the lateral stiffness or flexibility of the shafts are the spans between bearings rather than the entire shaft

LIBERTY EXHIBIT 1017, Page 226

length. In the case of overhung pumps, the distance between the impeller(s) and the closest bearing can be more important than the distance between bearings. The torsional stiffness of shafts is directly proportional to the fourth power of the diameter and inversely proportional to the length of the shaft. The axial stiffness of the shaft is directly proportional to the square of the diameter and inversely proportional to the length of the shaft. Both the lateral stiffness and the axial stiffness of shafts are directly proportional to the modulus of elasticity, E, of the material, whereas the torsional stiffness is directly proportional to the modulus of rigidity, G. The selection of bearing span and shaft diameter will dictate the overall stiffness of the shaft and whether the pump will run above or below its first critical speed.

Bearings The purpose of bearings is to provide the primary support to position the rotor and maintain concentricity of the running clearances within reasonable limits. There are several types of pump bearings. The most common type is the plain journal bearing, in which a smooth, ground shaft surface rotates within a smooth surfaced circular cylinder. In this bearing, the load "bearing" effect is provided by a hydrodynamic wedge which builds between the rotating and stationary parts as rotating fluid flows through the narrow part of the eccentric gap between the shaft journal and the cylindrical bearing insert. The eccentricity of the shaft within the journal is caused by the net radial load on the rotor forcing it to displace within the fluid gap. The hydrodynamic wedge provides a reaction force which gets larger as the eccentricity of the shaft journal increases, similar to the buildup of force in a spring as it is compressed. The plain journal bearing has moderately high stiffness, and is relatively inexpensive, with good damping properties, but has high cross-coupled stiffness. The concept of how cross-coupled stiffness is created in a journal bearing or annular sealing cavity is shown in Figure 11. Cross-coupled stiffness can negate the damping, leading to rotordynamic instability. Putting axial grooves in the journal bearing significantly diminishes the cross-coupling. Other types of pump bearings include the rolling element ("antifriction") bearing (inexpensive and stiff, but with little damping), the tilting pad bearing (moderate stiffness and damping, low cross-coupling, but expensive), the magnetic

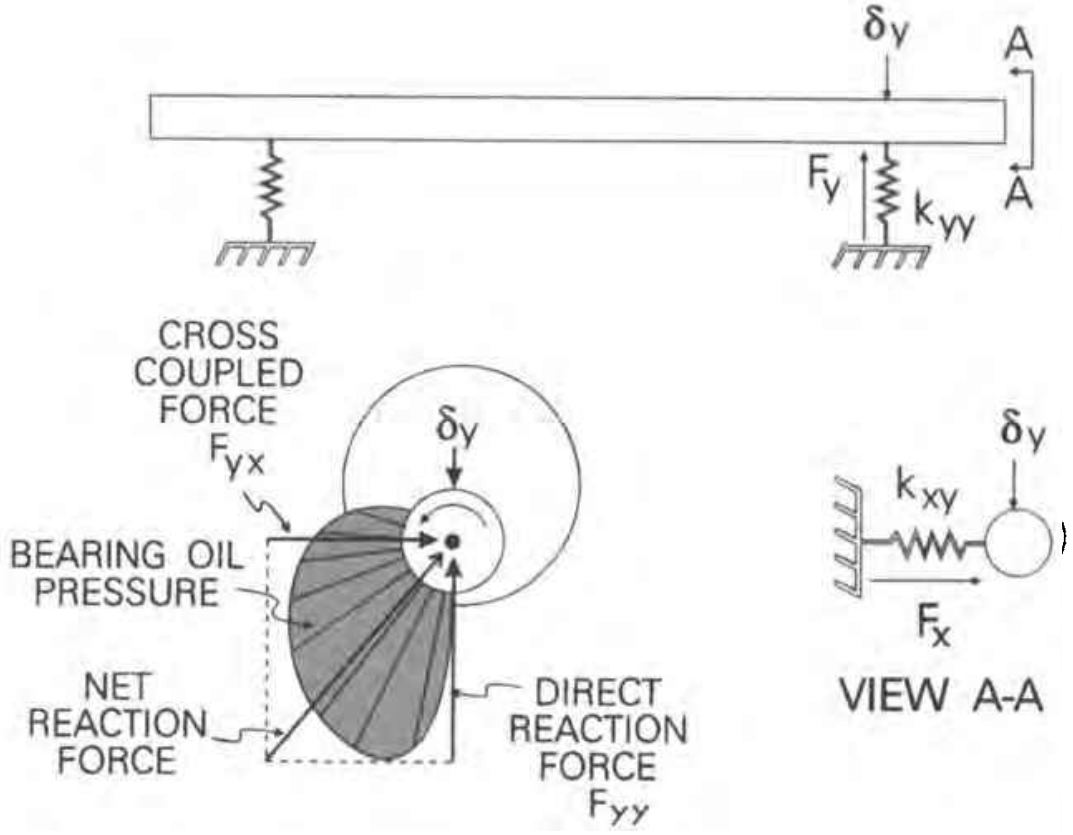


FIGURE 11 The concept of cross-coupled stiffness (Mechanical Solutions, Inc.)

LIBERTY EXHIBIT 1017, Page 227

bearing (low stiffness and expensive, but zero cross-coupling), and the hydrostatic bearing (high stiffness and damping, low cross-coupling, but expensive to install and operate).

Annular Seals and the Lomakin Effect One of the most common types of flow-path seals is the annular seal, with either smooth cylindrical surfaces (plain seals), stepped cylindrical surfaces of several different adjacent diameters (stepped seals), or multiple grooves or channels perpendicular to the direction of flow (serrated, grooved, or labyrinth seals). These areas include the impeller front wear ring, the rear wear ring or diffuser interstage bush rings, and the thrust balancing device leak-off annuli.

Annular seals can dramatically affect pump rotor dynamics, especially multistage pump rotor dynamics, in two ways :

1. By changing the rotor support stiffness and therefore the rotor natural frequencies, thereby either avoiding or inducing possible resonance between strong forcing frequencies at one and two times the running speed and one of the lower natural frequencies.
2. By increasing the rotor support cross-coupled stiffness or, as the seals wear, decreasing the rotor damping, allowing greater magnification factors during resonance, and in the extreme allowing destabilizing forces on the rotor to dominate those associated with stabilizing energy absorption.

These effects are particularly strong in multistage pumps, because multistage rotors are relatively long and flexible. Since the annular seals are primarily in the central portion of the rotor, where they exercise considerable leverage on the first bending mode of the rotor, the contribution of seal stiffness to the rotor support can be comparable to the rotor stiffness itself.

The stiffness and damping of an annular seal is provided in small part by the squeeze-film and hydrodynamic wedge effects well known to journal bearing designers. However, because of the high ratio of axial to circumferential flow rates in annular liquid seals relative to bearings, large forces can develop in the annular clearance space due to the circumferentially varying Bernoulli pressure drop induced as rotor eccentricity develops, as shown in Figure 12. This is known as the Lomakin effect and is the largest stiffness and damping force-generating mechanism within pump annular seals.[3] The primary action of the Lomakin effect is beneficial, through increased system direct stiffness and damping which tend to increase the rotor natural frequency and decrease the rotor vibration response at that natural frequency.

The Lomakin effect depends directly on the pressure drop across the seal, which for constant system flow resistance results in a variation of the Lomakin support stiffness with roughly the square of the running speed. However, in cases of high static head compared to head rise at BEP, there is only a small variation of the Lomakin effect with pump speed. The other important parameters are a diminishing increase in stiffness with increasing annular sealing cavity length, stiffness increase in proportion to diameter, and stiffness decrease in inverse proportion to clearance. Fluid properties are of secondary importance unless very high viscosity liquids are involved.

The Lomakin effect can be calculated with reasonable accuracy through use of bulk flow computer programs. An approximate method for predicting Lomakin effect stiffness is though the following equation, applicable to short L/D sealing gaps in liquid water of any temperature:

$$K_L = k^*\Delta P^*R^*L/C_R$$

Where K_L = Lomakin Stiffness in lbf/in USCS or kN/mm in SI units

k is a unitless constant equal to about 0.4

ΔP is pressure drop in psi in USCS or MN/m^2 in SI units

R is radius in inches in USCS and mm in SI units

L is length in inches in USCS and mm in SI units

C_R is average radial clearance in inches in USCS and mm in SI units

LIBERTY EXHIBIT 1017, Page 228

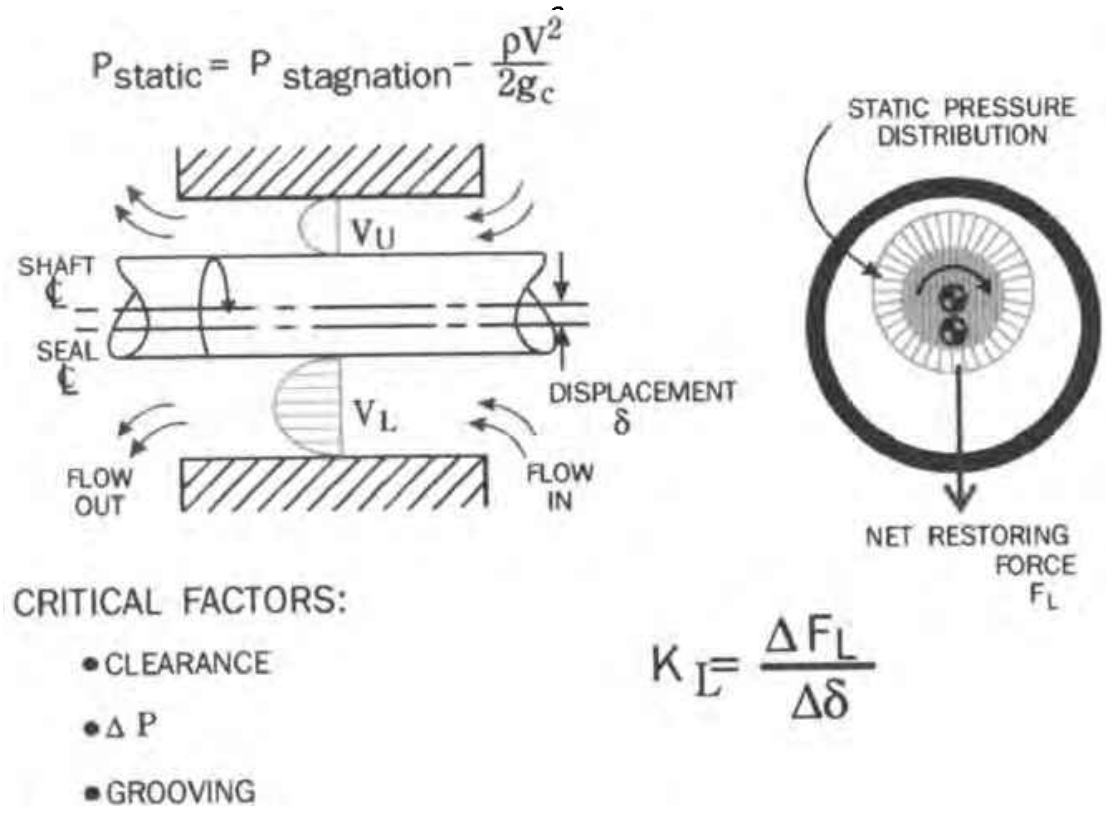


FIGURE 12 The concept of Lomakin effect stiffness K_L (Mechanical Solutions, Inc.)

The physical reason for the strong loss of the Lomakin effect with increased clearance is that increased clearance or circumferential grooving gives the opportunity for equalization of circumferential pressure distribution, which is behind the Lomakin effect. It is important that modern rotors be designed with sufficiently stiff shafts so that any natural frequency that starts above running speed with new clearances remains above running speed with clearances worn to the point that they must be replaced from a performance standpoint.

Mechanical Seals and Packing Mechanical seals do not affect vibration, or specifically pump rotordynamics, significantly. They do not add excitation forces, and unlike most wear rings provide negligible support stiffness and damping. Packing likewise usually has negligible stiffness, but can add considerable damping. When pump designs get changed from packing to mechanical seals, often rotor critical speed problems begin to surface that went unnoticed previously.

Sleeve Effects on Vibration Sleeve effects on vibration depend on the fit-up of sleeves to the shaft and the type of analysis being performed. For a lateral analysis, if the sleeves are press fit to the shaft with tight class of fit, then the added stiffness of the entire length of the sleeve should be included, in the authors' experience; (although, API-684 suggests taking no credit for sleeve stiffness in any circumstance.[4]) If the sleeve is lightly pressed or loose fit to the shaft then no added stiffness is included in the model, but the mass and transverse moment of inertia is to be included at the center of gravity of the sleeve. In a torsional analysis if the sleeve is press fit to the shaft, then it is treated in the same manner as in the lateral analysis, but if the sleeve is loose fit and keyed to the shaft, $\frac{1}{3}$ the diameter of the shaft where the sleeve is located is subtracted from each side of the sleeve and what is left is used as added stiffness to the shaft. When modeling coupling hubs, if the hub is press fit to the shaft then the entire length of the hub is included as added stiffness. If the hub is keyed on with a loose fit, then a $\frac{1}{3}$ penetration of the shaft into the hub is used to limit added stiffness. In both cases, the full mass and moment of inertia are to be included in the analysis.

LIBERTY EXHIBIT 1017, Page 229

Horizontal Pump Casings and Bearing Housings Horizontal pump casings are relatively massive compared to steam turbines and compressors, and historically have not played a strong role in pump rotordynamics, other than to act as a rigid reaction point for the bearings and annular seals. However, pressure on designers to save on material costs occasionally results in excessive flexibility in the bearing housings, which are cantilevered from the casing. The approximate stiffness of a bearing housing can be calculated from beam formulas given in Roark, such as $3EI/L^3$, where L is the cantilevered length of the bearing center from the casing end wall, E is the modulus of elasticity, and I can be determined from the cross section of the bearing housing. The bearing housing stiffness must be combined as a series spring with the bearing film stiffness to determine a total direct "bearing" stiffness for use in rotordynamics calculations. The following series spring formula may be used:

$$\frac{1}{k}_{\text{total}} = \frac{1}{k}_{\text{housing}} + \frac{1}{k}_{\text{bearing}}$$

If resources are available, an accurate determination of the bearing stiffness can be obtained through 3D finite element analysis of the bearing housing. A unit load can be applied to the bearing at the location of the internal journal or ball bearing race, and the applied load divided by the deflection at the load provides the stiffness of the bearing housing.

Vertical Turbine Pumps A vertical turbine pump (VTP) can be described as a vertically mounted pump where the impeller is located in a cylindrical casing mounted in-line to an attached vertical column pipe. The impeller takes fluid directly from the well through a suction bell and bowl assembly, and discharges coaxially into a multivane diffuser and then into the attached column pipe. The column pipe in turn is attached to a discharge head which in turn mounts the pump driver. The discharge head and pump casing may be separated by as little as a few inches (order of 100 mm) or as much as a few thousand feet (order of 1000 m). The pump impeller and driver are connected through intermediate "lineshafting" running down the center of the column pipe and supported by lineshaft bearings spaced according to shaft diameter. If the pumped fluid is corrosive, abrasive, or contains hard particulate, the bearings and intermediate shafting may be enclosed within a pipe ("shaft tube") run concentrically with the column pipe to protect them from damage. In such a case, this enclosing tube is tensioned between the discharge head and the pump casing.

VTPs generally have much more flexible motor and pump casings than comparable horizontal pumps, and more flexible attachment of these casings to the foundation. Due to the flexibility of the discharge heads used to support motors, many structural natural frequencies of vertical pumps tend to fall very close to the 1× running speed of the pumps, and can cause very high vibrations to occur. In addition, the foundation that the pump is mounted on can play a significant role. Finally, the below-ground column piping and pump casing or "bowl assembly" as well as the water added-mass effect need to be assessed to determine if the below-ground components will have a vibration issue, or will combine with the above-ground components and foundation (and possibly piping) to cause a system-related problem. To adequately include discharge head, baseplate, piping, column/bowl assembly, and foundation effects in such pumps, a finite element analysis (FEA) model is required.

If a manual model of a VTP is attempted, the baseplate and foundation may be modeled as torsional springs in series. The spring constants can be based on force versus deflection formulas provided for plates with central moments (see Timoshenko) and for separate "half space" foundations.[5] These hand calculations may produce large errors and should be verified using detailed finite element analysis or field "bump" test results.

The natural frequencies of concern in a VTP are the first several structural bending natural frequencies of the entire assembly, and the enclosing tube if one is used. Lineshaft natural frequencies are occasionally a problem, but generally present a "moving target" to excitations, in terms of their frequency value, because the lineshaft bearings provide very inconsistent support, and so the shaft natural frequencies shift from instant to instant like a guitar string as finger pressure is placed in different locations. The main source of excitation

LIBERTY EXHIBIT 1017, Page 230

for both the structure and the rotor occurs at 1× running speed due to imbalance or shaft bow, and to a lesser extent misalignment. In particular, driver coupling misalignment can influence discharge head vibration at both 1× and 2× running speed. Vane pass excitation is normally not of concern since most VTP casings are designed with multivane diffusers as well as greater impeller vane/diffuser vane spacing, and this minimizes the effect of vane pass frequency in exciting natural frequencies.

The nominal lineshaft (or "intermediate shaft") bearings are normally spaced to place the first lineshaft natural frequencies above running speed, as per recommendations in API-610.[2] These nominal natural frequencies can be estimated if the shaft diameter and bearing spacing is known by using continuous beam equations, where the bearings act as simple supports. Axial loads on the shaft tend to straighten the shaft and raise the natural frequencies above that calculated particularly if the load is high or the shaft bearing spacing is long. In this case the axial stiffening of the shaft must be taken into account using equations developed to account for axial loading.[6] The pump shaft bearings are typically spaced close together such that the pump shaft natural frequencies are well above 2× running speed.

Water both internal and external to the pipe must be taken into account (e.g., the methods of Blevins[7]) or the calculations will be substantially in error. Column pipes are normally set so that a portion is above the water level and a portion below. The column pipe natural frequency calculation should account for the transition from water added mass being internal only to being both internal and external. Similar to the shafting, the enclosing tube natural frequency calculation needs to be adjusted due to axial stiffening of the tube if it is tensioned between the discharge head and the pump casing.

Natural frequencies for VTP discharge heads should be placed to avoid excitation by running speed and to a lesser extent 2× running speed. Prior to the introduction of finite element analysis many manual calculation and simple spreadsheet methods were used to calculate the discharge head natural frequencies, for example using beam equations from Roark,[8] or plate/shell calculations such as Timoshenko.[6] These methods proved to be approximate and still may be suitable for low horsepower (less than 200 bhp or 150 kW) constant speed applications where a single running speed is to be avoided and calculation error can be absorbed. The horsepower limit is given to acknowledge that as the power goes up the overall stiffness of the structure may not increase as quickly as the imbalance force. Running at a natural frequency may produce acceptable vibration in a 10-bhp (7.5-kW) unit but most certainly will produce high vibration in a 100-bhp (75-kW) or more unit. Additionally, shifting the natural frequency of a 10-bhp (7.5-kW) unit to a more suitable location in the field is more easily accomplished if excessive vibrations are encountered. Outside these limits FEA has proven to be a highly accurate (within 5 to 10%) method when employed by personnel familiar with the characteristics of both VTPs and FEA.

Vertical Sewage Pumps Vertically mounted sewage pumps, while typically much more stiff than vertical turbine pumps, are also susceptible to natural frequencies that fall within the operating range of the pump. Like VTPs, vertical sewage pumps have a large potential for exciting a structural natural frequency at 1× or 2× running speed, or vane pass frequency. In addition these units are tall, which in itself makes them susceptible to higher vibration levels since the point of rotation for the unit center of gravity is about the base and allows a small force to create a larger moment. In general a structural lateral natural frequency analysis of the motor/pump assembly should be performed on all new designs and on all variable speed units larger than 100 bhp (75 kW). Up-front analysis work on units less than 100 bhp (75 kW) may be more expensive than field fixes and therefore may not make economic sense for all applications.

If the motor is directly mounted to the volute casing, there is much higher likelihood that a cantilever bending mode of the motor could coincide with the 1× running speed of the pump. If the pump is driven by a long drive shaft with the motor well above the pump, there is less chance of a bending mode of the cantilevered motor, but the drive shaft natural frequencies need to be evaluated. In addition, the bearing towers used to support bearings on sewage pumps are often mistakenly considered as rigid, when in reality they contribute quite a bit of flexibility to the rotor system, and can lead to combined rotor/structural modes.

LIBERTY EXHIBIT 1017, Page 231

Typical nonclog pumps are a single-volute design utilizing an overhung impeller with 1 to 5 vanes, operating at synchronous speeds between 300 and 1800 rpm. Historically, in all but the largest stations, nonclog pumps have been operated start/stop at full and load speed as incoming flow demanded. However, recent trends in station design have shown an increased use of variable speed drives to match incoming and outgoing flows. Variable speed operation is now the norm in all but the smallest stations. With the advent of variable frequency drives (VFDs), in addition to the great operating cost savings provided by eliminating the need to throttle the pump discharge, the possibilities of exciting rotor and structural natural frequencies have increased dramatically, and the need to analyze these pumps has grown along with it.

The three key excitation frequencies of 1×, 2×, and vane pass appear in the vibration spectra even for properly designed nonclog pumps. 1× occurs due to residual imbalance and coupling misalignment produces both 1× and 2×. In 1- to 3-vane impellers, vane pass occurs as a strong excitation, greater than the imbalance force due to the low number of vanes used. In addition, the impellers are designed to pass solids and therefore have wide discharge passages, susceptible to excitation by pressure pulsations. Additionally the majority, by a large margin, of nonclog pumps are a single-volute casing design which produces an unbalanced impeller radial load; (see the work of Agostinelli et al in Section 2.1.3.[9]) Combining the vane pass frequency with 1× and 2× excitation produces a range of excitation sources which are difficult to avoid, and the possibility of exciting a natural frequency is very high if the unit has variable speed.

Most nonclog pump shafts use an overhung impeller design with bearings specified for a life in excess of 50,000 L-10 h and a shaft deflection at the stuffing box held to less than 0.002 in. The long bearing life and maximum shaft size (beyond that necessary for strength, in order to minimize shaft deflection) make it unusual to find a nonclog pump shaft that runs with a first mode lateral natural frequency below the operating rpm. At least 20% margin is recommended.

The operating rpm/power and impeller solid size capabilities combine to produce relatively large polar inertia for the impeller and motor rotor in nonclog pumps. It is not uncommon to find the first torsional natural frequency within the range of 1×, 2×, or vane pass frequency especially when the pump is operated at variable speed. Therefore, a torsional natural frequency analysis should be performed for all nonclog pump applications.

In addition to the pump rotor/bearing tower housing, the motor/discharge volute attachment stiffness, and the stiffness of the pump pedestal "milk stool" (preferably cross-braced in a truss fashion), installation specific characteristics for the foundation and attachment of the piping play a large role in determining the installed natural frequency, as does the effect of entrained water.

Motor stand design heavily influences the installed structural natural frequencies and can be used to shift them to more suitable locations. Changes in wall thickness, rib design, opening size, and mounting plate thicknesses have all been used to shift natural frequencies. In extreme cases running short struts from the foundation to the top of the motor stand can be used to significantly raise natural frequencies.

Natural frequencies for the vertical shafting for these units should be placed to avoid excitations by running speed and other sources by at least 20%. Excitations vary with the coupling used and the shaft location. Universal joint couplings produce 2× and disc-pack couplings produce an excitation at a frequency equal to half the number of disc-pack bolts times rpm. Vane pass excitation can be transferred up the shafting and is a source of excitation for at least the first section of shafting attached to pump and may influence sections above this. It may not be possible to avoid excitation of all natural frequencies, in which case a forced response analysis may be required to ensure that shaft stresses and bearing loads are acceptable.

Motors A structural analysis requires the motor mass, center of gravity, and first reed critical frequency along with the motor mounting characteristics consisting of bolt circle diameter, number of bolts, bolt location, and OD, ID, and thickness of the motor mounting plate. A rotor torsional analysis requires the motor rotor polar inertia and torsional stiffness from rotor center of gravity to the coupling end of the shaft. A rotor lateral analysis (seldom required since motors are designed with their first critical speed at least 25%

LIBERTY EXHIBIT 1017, Page 232

above running speed) requires a motor shaft drawing noting diameters and lengths, bearing locations, bearing types, and mass amounts and locations, and polar inertias.

The authors have tracked motor data over the years and present typical data for evaluating motor data validity and for use in feasibility studies. As can be seen in Figure 13, motor data vary with frame and manufacturer, and actual motor data provided by the original equipment manufacturer (OEM) should always be used to minimize calculation error. The plots were developed from data for 72 motors used mostly in vertical applications. Eleven different vendors are represented with motors ranging from 15 to 6000 bhp (11 to 4500 kW) and 390 to 1200 rpm. Two synchronous motors, five horizontal motors, and three hollow shaft motors are represented. The remaining motors are vertical solid shaft induction motors. The data are plotted against torque recognizing that motors are torque producing machines and their data are best presented in this fashion.

The motor structural "reed" critical frequency data plot shows that the motors when mounted to a rigid structure have structural natural frequencies between 80 to 550% of running speed. The wide range in natural frequencies is mainly due to different construction techniques among vendors and the availability of different motor frame sizes. The plot shows that the average natural frequency decreases as a percent of running speed with increasing motor torque and corresponding motor size increase. It must be remembered that the data supplied by the motor vendor are almost always referenced to mounting the motor to a rigid structure. VTP discharge heads and frame mounted pumps cannot be considered "rigid" and therefore the data presented by the motor vendor should be considered the maximum theoretical natural frequency possible for that motor. Experience has shown that mounting the motor on top of a pump structure, whether it be a VTP or frame mounted unit, produces a motor/pump/pedestal system natural frequency approximately 50 to 80% of the motor/rigid-structure natural frequency. Therefore, the average motor mounted to the average pump produces an installed system natural frequency within +/– a factor of 2 of running speed, easily excitable by 1×, 2×, or vane pass frequency in VFD applications.

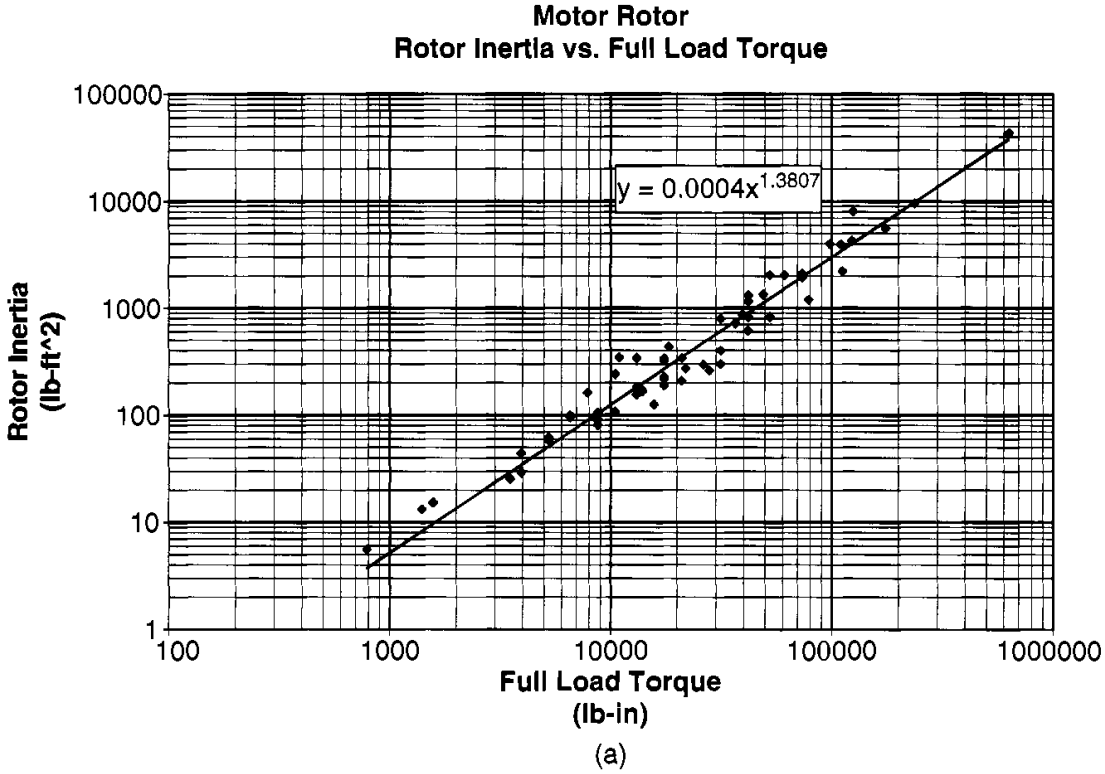
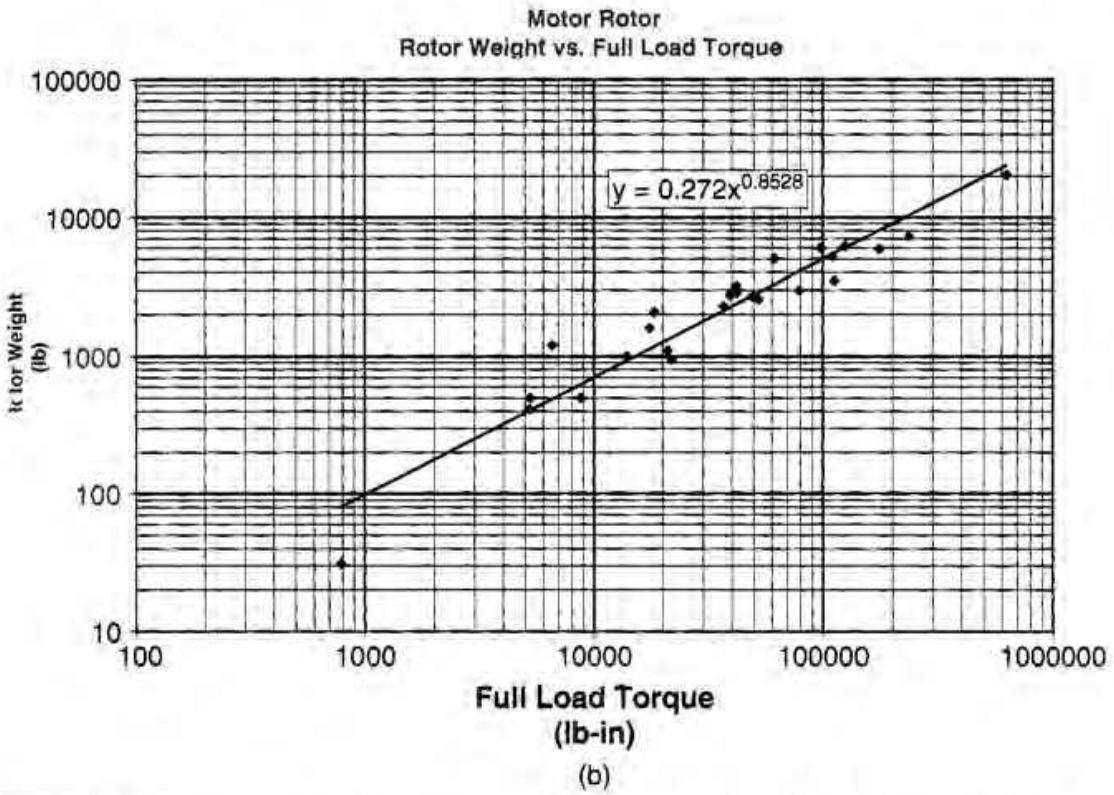


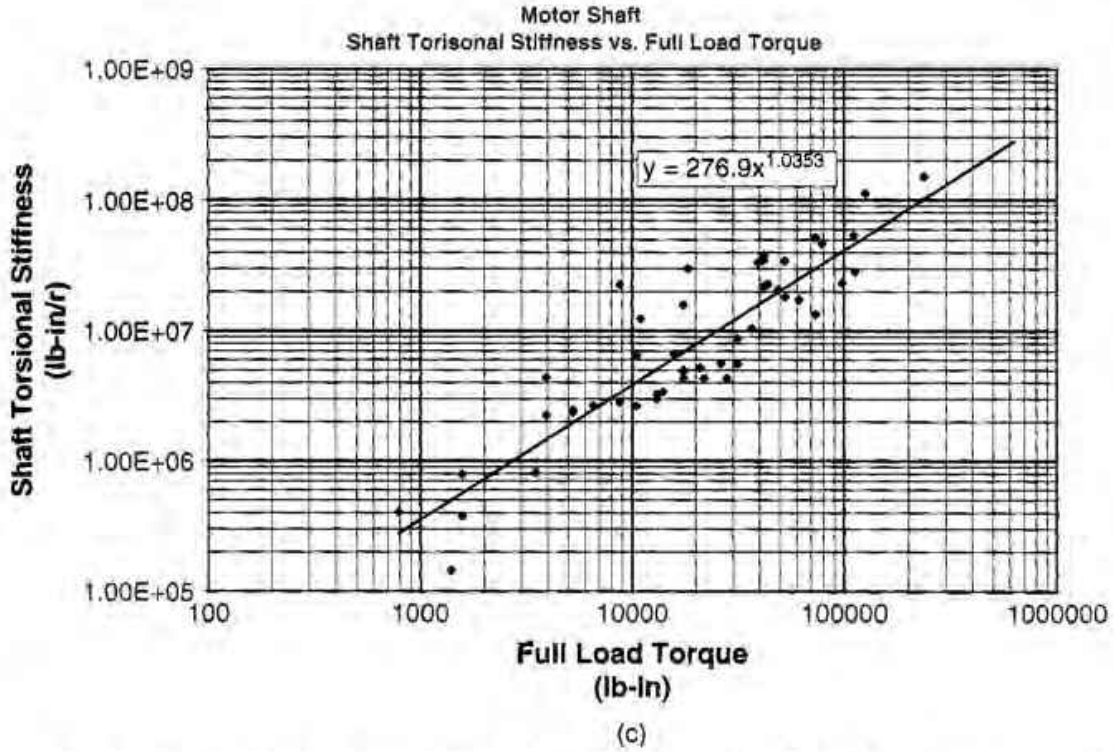
FIGURE 13A Typical motor inertia characteristics (kg-m² = lb-ft²/23.73; N-m = lb-in/8.851) (Mechanical Solutions, Inc.)

LIBERTY EXHIBIT 1017, Page 233



(b)

FIGURE 13B Typical motor weight characteristics (kg = lb/2.205; N-m = lb-in/8.851) (Mechanical Solutions, Inc



(c)

FIGURE 13C Typical motor shaft torsional stiffness characteristics (N-m = lb-in/8.851) (Mechanical Solutions, Inc.)

VFDs In variable speed installations it may not be possible to avoid exciting a natural frequency within the operating range. In this case the designer must place the natural frequency in a location (within the frequency domain) that will do the least harm recognizing the accuracy limitation of the natural frequency calculation method used. For example, assume a pump can be excited by 1× (imbalance), 2× (misalignment), and 3× (vane pass) and the operating range is from 540 to 900 rpm; 60 to 100% speed @ 900 rpm typical for a VFD. Further assume that the specification has called for avoiding natural frequencies by ± 25%. The following results:

		Excitation Frequencies, cpm					
Speed Range rpm		Nmin − 25%	Nmax + 25%	2 × Nmin − 25%	2 × Nmax + 25%	3 × Nmin− 25%	3 × Nmax + 25%
540	900	432	1125	864	2250	1296	3375

In this representative example, no safe haven for natural frequencies exists between 432 and 3375 cpm and the designer must choose a location to place the natural frequencies where they will do the least harm. The question becomes where does least harm exist, based on the nature of each excitation force. In this case all three excitation forces are proportional to the square of the speed. A potentially dangerous excitation force at full speed may have insufficient energy to excite excessive motion at reduced speed. Additionally, in this example 2× misalignment most likely will produce the least force and the unit can be field aligned to minimize this harmonic. In this case the best location for natural frequencies is in the lower 2× excitation range.

THE ROLE OF THE FLUID SYSTEM

Vibration versus Operating Point Ideally, a pump should operate close to its best efficiency point (BEP). Contrary to intuition, centrifugal pumps do not undergo less nozzle loading and vibration as they are throttled back, unless the throttling is accomplished by variable speed operation. Operation well below the BEP at any given speed, just like operation well above that point, causes a mismatch in flow incidence angles in the impeller vanes or in the diffuser vanes or volute tongues of the various stages. This loads up the vanes, and may even lead to "airfoil stalling," with associated formation of strong vortices (miniature tornadoes) that can severely shake the entire rotor system, and can even lead to fatigue of impeller shrouds or diffuser plates or "strong-backs." Such internal flow recirculation can cause cavitation on the *pressure side* of vanes, as opposed to cavitation on the nonpressure side which is caused by lack of sufficient NPSHR. The rotor impeller steady side-loads and shaking that occurs at flows below the onset of suction or discharge recirculation (see Sections 2.1.1 and 2.1.3) leads to the strong possibility of rubs, and excessive rotor loads that can damage bearings. Many plants buy equipment that has more capacity than is needed, to allow for future production expansion, but in doing so may ensure years of unreliable performance of potentially reliable machinery.

The typical effect on vibration of this practice is shown in Figure 14. Never run a pump for extended periods at flow rates below the "minimum continuous flow" provided by the manufacturer. Also, if this flow was specified prior to about 1985, it may be based only on avoidance of flashing and not on recirculation onset, and should be rechecked with the manufacturer.

A strong sign that recirculation is occurring is a "throbbing" vibration at part load, and strong vibration peaks showing up subsynchronously (i.e., below running speed), but not in the range of 0.4 to 0.5× running speed. The 0.4 to 0.5× range implies rotordynamic instability problems sourced in the bearings and annular seals (wear rings or balancing device), as discussed later.

LIBERTY EXHIBIT 1017, Page 235

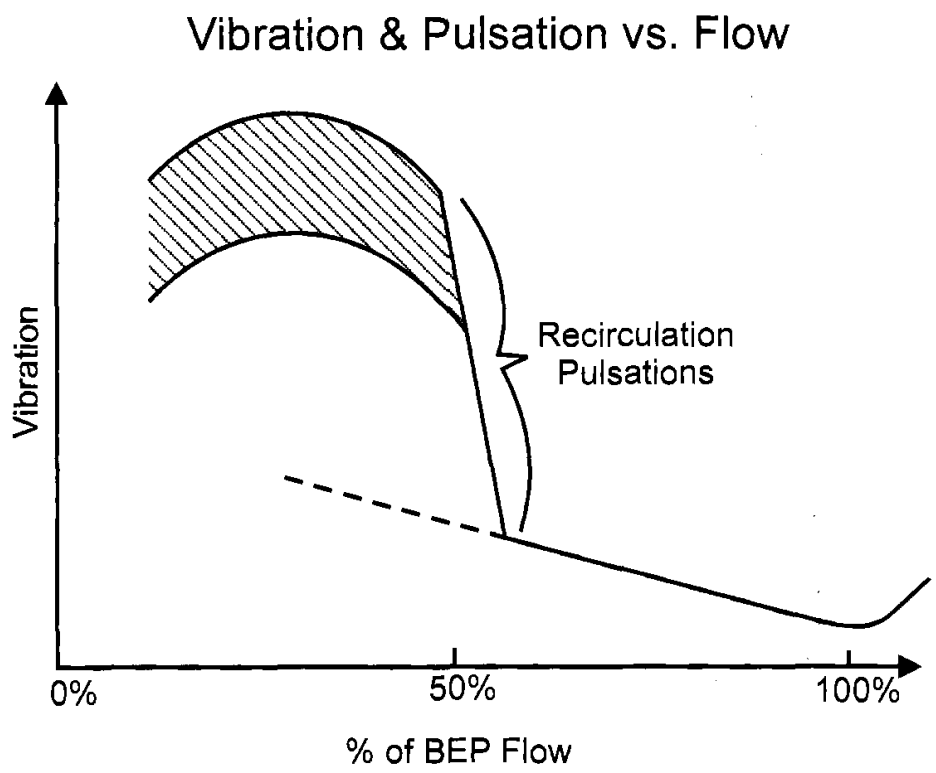


FIGURE 14 Effect on vibration of off-BEP operation (Mechanical Solutions, Inc.)

When stall vortices form, they often spit out the inlet to the impeller, and can cause "rotating stall" where the vortex formation is regular, and proceeds backward through the impeller as it spins forward. This leads to a net forward spin at some percentage of the rotational speed, typically 65 to 95% of rotational speed. This kind of stalling can also happen in a pump diffuser, but in that case typically rotates forward in the diffuser, at a rate of 5 to 35% of rotor speed. When these unexpected frequencies show up in the vibration spectrum, recirculation and rotating stall are often the cause. If such frequencies become equal to a critical speed, excessive vibrations at that frequency could result.

Cavitation Effects on Vibration The main issue of hydraulic concern is that sufficient suction static pressure be present to avoid cavitation. Today, it is understood that this means more than merely having sufficient net positive suction head available (NPSHA) to satisfy the 3% head drop NPSHR (NPSH Required) published by the manufacturer. (See Sections 2.1.1 and 2.1.3.) At NPSHA as much as 3× the NPSHR, high frequency cavitation (sometimes inaudible) can cause serious erosion of the suction side of impeller vanes or wear ring exits. Most cavitation vibration and noise energy is in the 10 to 50 kHz range, and some energy all the way up to 120 kHz. Because cavitation excites a broad range of frequencies at once, as do other phenomena like bearing faults or flow passage turbulence, its presence and its damage potential are best determined with high speed oscilloscopes rather than with FFT analyzers. When significant cavitation is taking place, the shock wave of the bubble collapse shows up strongly (about 100 psi or more p-p) in the signal spike from a high frequency pressure transducer directly exposed to the flow, preferably with line-of-sight to the impeller. If the cavitation is damaging, bubble collapse is at a vane or wall, and the spike shows up as very strong acceleration (typically greater than 100 g's p-p) on an accelerometer on the suction sidewall, and even (to a lesser degree) in other metal components such as bearing housings. The effect is hard to distinguish in the frequency spectrum, but shows up as spikes tens of microseconds long (with subsequent ringdowns) in an oscilloscope trace. g-levels in nondamaging cavitation situations are at least a factor of 10 less in spike strength.

LIBERTY EXHIBIT 1017, Page 236

A-Gap, B-Gap, and Overlap Dr. Elemer Makay introduced these famous concepts, relevant particularly to double suction pumps and high energy pumps such as boiler feed pumps and illustrated in Section 2.1.1. A-Gap is the radial annular width of the passage between the impeller OD and the volute or diffuser sidewall, and "Overlap" is the width (in the direction of leakage flow) of this close clearance area. Small A-Gaps and large overlaps decrease the communication between discharge pulsations and the impeller side passages, limiting the sensitivity of vibration to discharge recirculation, or discharge piping acoustic resonances. B-Gap is the radial distance from the impeller vane tip at the OD to start of the volute tongue or diffuser vane tip. If B-Gap is smaller than 3 to 5% of the impeller radius in diffuser pumps, or 5 to 8% of the impeller radius in volute pumps, then vane pass pulsations are often (not always) much stronger, possibly enough to cause vibration problems or even impeller hub or shroud fatigue cracking.

Hydraulic Instabilities Caused by Flat Pump Curves and Parallel Operation If the pump curve is flat an has a more positive slope than the system resistance curve, particularly when two or more pumps are run in parallel, the opportunity exists for the pump to get "confused" about what flow rate the system requires for a given head. This can lead to large, unstable flow surges. In a different but associated situation, if one of a pair of pumps deteriorates more than its mate when run in parallel, the stronger pump will set the head, and the weaker pump with a flat or positive head curve could be forced to run below minimum continuous flow or even at shutoff, although overall system flow remains high enough to satisfy the end user. This may lead to excessive vibration, and likely reliability problems in the weaker pump.

Thrust Reversals—Reasons and Ramifications Thrust reversals can occur in vertical pumps during start-up. If such upthrusting is greater than the weight of the motor and pump rotor system; uplift can occur, possibly damaging the mechanical seal or thrust bearing components not designed for upthrust. In multistage horizontal pumps, thrust reversal can happen if the flow rate becomes low enough so that flashing occurs, if the pump is run partially air-bound, or if the flow rate is outside the expected flow range so that the balance device overcompensates toward the suction.

Sources and Cures for Vane Pass Vibration Insufficient B-Gap can cause excessive vane pass vibration, in which case B-Gap should be increased under the supervision of a hydraulic designer. Suction or discharge recirculation can also lead to increased vane pass vibration, but usually this is less of a practical problem than the associated cavitation damage. Viable remedies are not to run at such low flows, to modify the impeller design to accommodate a lower flow rate (usually at some expense in efficiency), to put inlet guide vanes in front of the impeller to induce negative swirl, or to put "bulkhead rings" (sometimes called "choke rings," which resemble large washers with ID a little less than the impeller inlet eye diameter) in front of the impeller to reduce the tendency for fluid to recirculate or flow upstream out of the impeller and to increase flow velocity and thereby improve incidence angle.

Piping and Acoustics

1. **Check valve transients** The sudden closure of a check valve can cause a "thermal-hydraulic fluid transient," or waterhammer (see Section 11.3). Large pressure pulsations can result, and can travel upstream through the pump, as well as through the column piping in a VTP. The authors have witnessed 300 psi (2 MPa) pressure pulses due to waterhammer.
2. **Piping elbows and sump anomalies** Sump problems can result in unexpected flow swirl, even if air-sucking vortices are not visible. (See Chap. 13.) Sump vortices can form starting on the floor or walls of the sump, and can have cavitation or air (which comes out of solution in the submerged water) at the center, as illustrated in Section 13.2. Whether or not the vapor is at the center, the swirling flow can cause bad incidence angles at the impeller inlet, leading to unexpected suction recirculation, and resulting cavitation noise and excessive vibration. The remedy is to change the sump configuration

LIBERTY EXHIBIT 1017, Page 237

(e.g., simply adding an inlet cone or changing the suction bell setting), or to put straightening vanes and possibly a vapor trap in the inlet piping.

3. **Piping acoustics** Acoustic resonances are familiar in the wind type of musical instruments. Acoustics of pump piping systems can be complex to analyze but for the most part can be broken down into two common situations, the quarter wave and the half wave. Quarter waves occur when the sound wave within a section of pipe is reflective at one end and open at the other. A good example of a quarter wave is a section of pipe coming from a sump, and attached at the other end to the suction inlet of a pump. A half wave occurs when the sound wave is either reflective at both ends or open at both ends, such as in a discharge header. Instances of half waves are less common than quarter waves. To calculate the acoustic natural frequency within a pipe it is necessary to know the speed of sound within the fluid, which is influenced by the wall thickness of the piping in which the fluid is enclosed. For practical purposes the speed of sound in water in steel piping can be estimated at about 4000 ft/sec (1200 m/s). The first fundamental frequency of a quarter wave is calculated as the fluid speed of sound divided by 4 times the length in feet (m) of the pipe section in question, while the half wave is calculated similarly, but the 4 is replaced with a 2.

   It is important that an acoustic natural frequency not coincide with a source of excitation such as vane pass frequency. If this occurs, piping and headers may shake severely; and it is then necessary to detune the resonance, changing either the affected piping length or the impeller vane number. If neither of those is possible, in constant speed systems acoustic resonances can be diminished by installing a side-pipe "Helmholtz resonator" on the problem pipe wherein the pressure wave becomes strongest, and tuning its quarter wave frequency to the problem acoustic frequency.[7]

4. **Allowable nozzle loads** Pumps are not normally designed to resist the very large force that the piping can impose due to thermal growth or pressurized "bourdon tube" type loading, and this load transfer can overstress the pump or baseplate. The resulting strain can move the pump into misalignment with the motor and can also create rubs in close running clearances. This is why pump manufacturers specify the maximum loading that may be applied to the pump nozzles.

Expansion joints can be used to isolate the pump from the piping, but these create separate concerns since without stiff axial attachment of the piping, the pump nozzle pressure times the nozzle area creates a longitudinal hydraulic thrust that otherwise could easily be dissipated by the piping wall. Therefore the joint should be fastened axially, using an appropriate tie rod system (including mounting plate) capable of carrying the load imposed while not overly constraining the pump to follow any piping movement in the lateral or torsional directions. The potential nozzle longitudinal thrust consists of the pressure force and the fluid momentum at the joint both of which can be substantial for a large pipe; for example, a 42-in (1067-mm) pipe transporting 30,000 gpm (6814 m^3/h) of water at 10 psi (69 kPa) produces 13,854 lbf (61,626 N) due to the pressure and 901 lbf (4008 N) due to momentum. Lack of tie rods or insufficiently sized tie rods will allow transfer of part or all of the load back to the pump and create at the pump flange a pressure pulsation force at vane pass frequency. This pressure pulsation can create unacceptable vibration at vane pass frequency in an otherwise acceptable installation.

ROTORDYNAMICS

Computer Methods Rotordynamic analysis is typically performed by a specialized computer program, able to account for gyroscopics and cross-coupled forces. Older programs use the more computationally efficient Transfer Matrix method, although the massive increase in rapid and inexpensive computational capability has led to conversion to the use of the FEA method, due to its flexibility and its ability to handle more complex models. Traditionally, even using FEA the rotor model is a "stick figure," since greater detail

LIBERTY EXHIBIT 1017, Page 238

is typically not required for sufficient accuracy. In such simplified models, the following assumptions are made:

1. Linear bearing coefficients, which stay constant with deflection. This can result in significant errors for large rotor orbits.
2. Linear, monolithic bearing supports.
3. Perfect impeller and sleeve fits, except as accounted for as a worst-case unbalance.
4. If flexible couplings are used, shaft coupling coefficients are negligible in the radial deflection and shaft bending modes, with finite stiffness only in torsion.
5. It is assumed there is no feedback between vibration and resulting response forces, except during stability analysis.

Gyroscopic Stabilization Gyroscopic forces are important, and can either effectively stiffen or de-stiffen a rotor system. The key factor is the ratio of polar moment of inertia "I_p," the second mass moment taken about the rotor axis, to transverse moment of inertia "I_t," taken about one of the two axes perpendicular to the rotor axis, but passing through the center of mass. This ratio is multiplied by the ratio of the running speed divided by the orbit or "whirl" speed. The whirl speed is the rate of precession of the rotor, which can be "forward" (in the same direction as running speed) or "retrograde" or "backward" (opposite in direction to running speed). The whirl or precessional speed absolute value is generally less than the running speed. It is very difficult to excite backward whirl in turbomachinery, so evaluation is limited to the forward whirl modes. If the product of the inertia and speed ratio is less than 1.0, then the gyroscopic moment is de-stiffening relative to forward whirl, while if it is greater than 1.0, it tends to enhance the rotor spinning about its center axis (i.e., the principle of a gyroscope) and thus contributes apparent stiffness to the rotor system, raising its forward whirl natural frequencies.

Couplings Couplings may provide either a rigid or a pivoting ball-in-joint type connection between the pump and its driver. These are known as "rigid" and "flexible" couplings, respectively. Rigid couplings firmly bolt the driver and driven shafts together, so that the only flexibility between the two is in the metal bending flexure of the coupling shank, acting as a beam. This type of coupling is common in vertical and in small end-suction horizontal pumps. In larger horizontal pumps, especially multistage or high-speed pumps, flexible couplings are essential because they prevent the occurrence of strong moments at the coupling due to angular misalignment. Common types of flexible couplings include gear couplings and disc-pack couplings. Both gear and disc couplings allow the connected shafts to kink, but allow torsional transmission similar to rigid couplings.

In performing a rotordynamics analysis of a rigidly coupled pump and driver, the entire rotor—pump, coupling, and driver—must be analyzed together as a system. In such a model, the coupling is just one more segment of the rotor, with a certain beam stiffness and mass. In a flexibly coupled pump and driver, however, the entire rotor train usually does not need to be analyzed. Instead, the coupling mass can be divided in half, with half added to the pump shaft model, and the other half and the driver shaft ignored in the analysis.

Fluid "Added Mass" The fluid surrounding the rotor adds inertia to the rotor in three ways: the fluid trapped in the impeller passages adds mass directly, the fluid displaced by the presence of the impellers and shaft material adds its mass directly due to the rotor system, since as the rotor vibrates within the fluid it must displace this mass, and the fluid in close clearances must accelerate much faster than the rotor vibration acceleration to preserve continuity, and hence potentially adds mass many times its displaced mass (the so-called Stokes effect).

Impeller Forces As an impeller moves within the surrounding diffuser or volute, reaction forces are set up because of the resulting nonsymmetrical static pressure distribution around the periphery of the impeller. These forces are normally represented by coefficients which are linear with displacement. The primary reaction forces are a negative direct stiffness, and a relatively large cross-coupling stiffness. Both of these forces

LIBERTY EXHIBIT 1017, Page 239

tend to be destabilizing in situations where stability is an issue. Along with reactive forces, there are also active forces which exist independently of the impeller motion and are not affected substantially by it. These forces are primary "excitation forces" for the vibration.

Annular Seal Lomakin Effect Annular seals in pumps can greatly affect dynamics by changing the rotor support stiffness and therefore the rotor natural frequencies.[3] The stiffness and damping of an annular seal is provided in small part by the squeeze-film and hydrodynamic wedge effects well known to journal bearing designers. However, because of the high ratio of axial to circumferential flow rates in annular liquid seals relative to bearings, large forces can develop in the annular clearance space due to the circumferentially varying Bernoulli pressure drop induced as rotor eccentricity develops. This is known as the Lomakin effect as discussed earlier, and is the largest stiffness and damping force generating mechanism within pump annular seals.

The primary action of the Lomakin effect is beneficial, through increased system direct stiffness and damping which tend to increase the rotor natural frequency and decrease the rotor vibration response at that natural frequency. However, overreliance on the Lomakin effect can put the rotor design in the position of being too sensitive to wear of operating clearances, resulting in unexpected rotor failures due to resonance. It is important that modern rotors be designed with sufficiently stiff shafts so that any natural frequency which starts above running speed with new clearances remains above running speed with clearances worn to the point that they must be replaced from a performance standpoint.

Nonlinear Vibration: Parametric Resonance and Fractional Frequencies Certain types of nonlinear vibration response have been found common in turbomachinery. They generally fall into the category of parametric resonance, the details of which are beyond the scope of this section. Typically, parametric resonances are caused by bearing support looseness or a rub at a bearing, seal or other running clearance, allowing a contact/loss-of-contact vibration excitation similar to dribbling of a basketball. The symptoms are a pulsating orbit, with a large amount of vibration at exact whole fractions of running speed, such as $\frac{1}{2}$, $\frac{1}{4}$, and so on.

Cross-Coupling versus Damping and "Log Dec" Cross-coupled stiffness originates from the way fluid films build up hydrodynamically in bearings and other close running clearances, as discussed earlier. The cross-coupling force vector acts in a direction directly opposite to the vector from fluid damping, and many think of it in terms of an effectively negative damping. The action of cross-coupling is very important to stability, in that if the cross-coupling force vector becomes greater than the damping vector, vibration causes reaction forces that lead to ever more vibration, in a feedback fashion.

Subsynchronous Whirl, Whip, and Rotordynamic Stability Rotordynamic stability refers to phenomena whereby the rotor and its system of reactive support forces are able to become self-excited, leading to potentially catastrophic vibration levels even if the active, stable excitation forces are quite low. The most common form of rotordynamic instability is known as shaft "whip," which at lower speeds begins as a more benign phenomenon known as shaft "part-speed whirl." Shaft part-speed whirl is a forced response at a frequency below the first shaft bending natural frequency. It is driven by a fluid excitation force, such that the static pressure field which causes the force is rotating at some speed below running speed. The fluid rotational speed becomes the whirl speed. The most common cause of whirl is fluid rotation around the impeller front or back shrouds, in the wear rings, or in journal bearing clearances. Such fluid rotation is typically about 45% of running speed, because the fluid is stationary at the stator wall, and rotating at the rotor velocity at the rotor surface, such that the bulk of the fluid rotates at roughly half speed in the running clearance. The pressure distribution which drives this whirl is generally skewed such that the cross-coupled component is potentially strong and positive in sign, able to "pump" energy into the rotor whirling motion. If somehow clearance is decreased on one side of the gap, due to eccentricity for example, the resulting cross-coupled force increases further.

LIBERTY EXHIBIT 1017, Page 240

The cross-coupled force acts perpendicular to any clearance closure. In other words, the cross-coupling force acts in the direction that the whirling shaft minimum clearance will be in another 90 degrees of rotation. If the roughly half speed frequency at which the cross-coupled force and minimum clearance are whirling becomes equal to a natural frequency, a 90 degree phase lag shift occurs, which is typical when force frequency equals natural frequency. This phase shift means that the motion in response to the cross-coupling force is delayed from acting for 90 degrees worth of rotation. By the time it acts, therefore, the gap which caused the force has rotated 90 degrees such that the cross-coupled force tends to act in a direction to further close this minimum gap. As the gap closes in response, the cross-coupled force which is inversely proportional to this gap increases further. The cycle continues until all gap is used up, and the rotor is severely rubbing. This final process is shaft whip, and is a dynamic instability in the sense that the process is self-excited once it begins.

The characteristics of shaft whip are that once it starts, all self-excitation occurs at the bending natural frequency of the shaft, so the vibration response frequency "locks on" to the natural frequency. Since whip begins when whirl is close to half the running speed, and is equal to the shaft natural frequency, the normal 1× running speed frequency spectrum and roughly circular shaft orbit now show a strong component at about 45% of running speed, which in the orbit shows up as a loop reflecting orbit pulsation every other revolution. The "lock on" of vibration to the natural frequency means that vibration at speeds above whip initiation will no longer track the whirl's previous constant percentage of running speed.

One method of overcoming rotordynamic instability is to reduce the cross-coupling force which drives it. A complementary solution is to increase system damping to the point that the damping vector, which acts exactly opposite to the direction of the cross-coupling vector, overcomes the cross-coupling. The amount of damping required to do this is commonly measured in terms of "log dec," roughly $2 \times \pi \times$ damping ratio. For centrifugal pumps, it has been found that if the log dec is calculated to be greater than about 0.15 then it is likely to overcome any cross-coupling forces which are present, avoiding instability.

Typical design modifications which reduce the tendency to rotor dynamic instability involve bearing changes, to reduce cross-coupling and hopefully simultaneously increase damping. The most unfavorable type of bearing in this regard is the plain journal bearing, which has very high cross-coupling. Other bearing concepts, with elliptical or offset bores, fixed pads, or tilting pads, tend to reduce cross-coupling, dramatically so in terms of the axially grooved and tilting pad style bearings. Even more effective and controllable, but much more expensive, are the hydrostatic bearing and the actively controlled magnetic bearing. Another bearing effective in reducing cross-coupling relative to damping is the pressure dam bearing.

Shaft Press Fits API publishes a rotor dynamic guideline standard designated API-684.[4] This guideline discusses the standard practices which API uses in establishing the vibration standards for its various machinery specifications such as API-610 for centrifugal pumps.[2] In API-684, the effects are discussed coming from shaft fits, such as occur in slip-fit or press-fit impellers and sleeves. API's opinion is that the effect of such fits is uncertain and generally not large, since asperities and ovality allow slight shaft bending within even a heavily press-fit sleeve or other component. Therefore, for consistency of analysis, API recommends that such fits be ignored, and that any slip or press-fit components be accounted for only in terms of their added mass, not in terms of any stiffness contributions they make to the rotor system. It is the authors' experience that press-fits do increase shaft critical speeds, as determined by test, but generally by less than half the amount of increase expected if the full added stiffness of the press-fit component were added to the rotor model.

Forced Response and Typical Excitation Levels A forced response analysis may be used to predict the vibrational displacement and stress at specific points in a model due to individual excitations. The analysis can be used to demonstrate compliance with vibration requirements when it is not possible to avoid the occurrence of natural frequencies

LIBERTY EXHIBIT 1017, Page 241

within the range of excitation. FEA is the preferred calculation method and the analysis proceeds by first calculating the natural frequencies and mode shapes, and selecting a representative modal damping value. The forced response analysis is then performed. The analyst must enter modal damping ratios, force inputs, and calculation output locations. Modal damping ratios and excitation forces can be difficult to quantify. If modal test data are available, the damping can be estimated from existing vibration spectra by measuring the width of the peaks at half power, such as discussed in API-541.[10] Alternatively, for most pump structures modal damping of 1 to 3% critical damping has proven to be representative. Forces are input at specific locations and response to the individual force is measured at specific locations across the frequency range. The result is a plot of amplitude versus frequency for a specific force at a specific location. Since most loading varies with speed, output from the forced response analysis is often calculated using unit loads, and is post processed to determine amplitude. In this way not only can force be varied with speed, but responses to individual forces at a specific point can be combined using the square root of the sum of the squares (SRSS).

Effects of Bearing Housings and Casings The output in the example presented in Figure 15 shows the response at the top of the bearing housing for a vertically mounted sewage pump, due to a 100-lbf (445-N) unit load excitation at the impeller as well as at the line shaft couplings. Figure 16 shows the expected response at the top of the bearing housing due to 1×, 2×, 3×, and vane pass excitations determined by post processing the data used in Figure 15. The response for each excitation represents the SRSS combination of individual forces at a particular frequency, and considers how those forces vary in magnitude with speed. For 1× the vibration frequency and running frequency coincide. For all other responses the vibration frequency is a multiple of the running frequency; for example, for 2× the response amplitude when running at 10 Hz occurs at 20 Hz. For this example, imbalance force was estimated using the individual component ISO balance criteria limit, and misalignment was assumed equal to imbalance. Vane pass force was estimated by reviewing field vibration response spectra and, based on this, was set at 40% of the impeller radial load divided by the number of vanes.

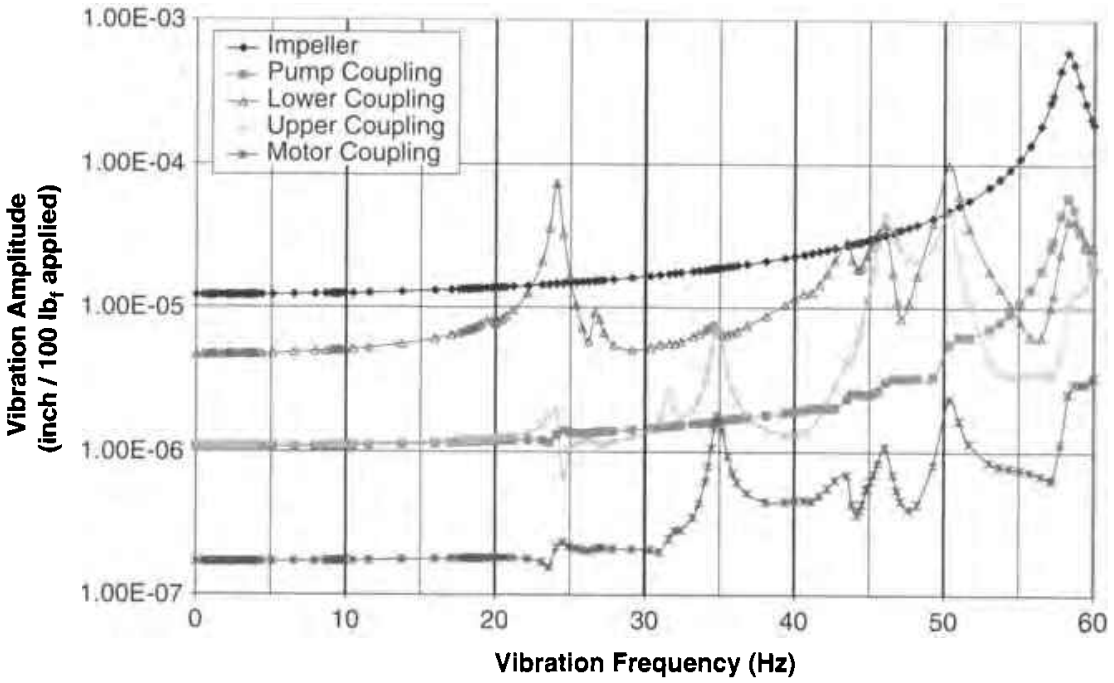


FIGURE 15 Horizontal vibration vs. frequency on pump upper bearing housing due to 100 lbf (445 N) applied separately at five excitation locations (mm = inch × 25.4) (Mechanical Solutions, Inc.)

LIBERTY EXHIBIT 1017, Page 242

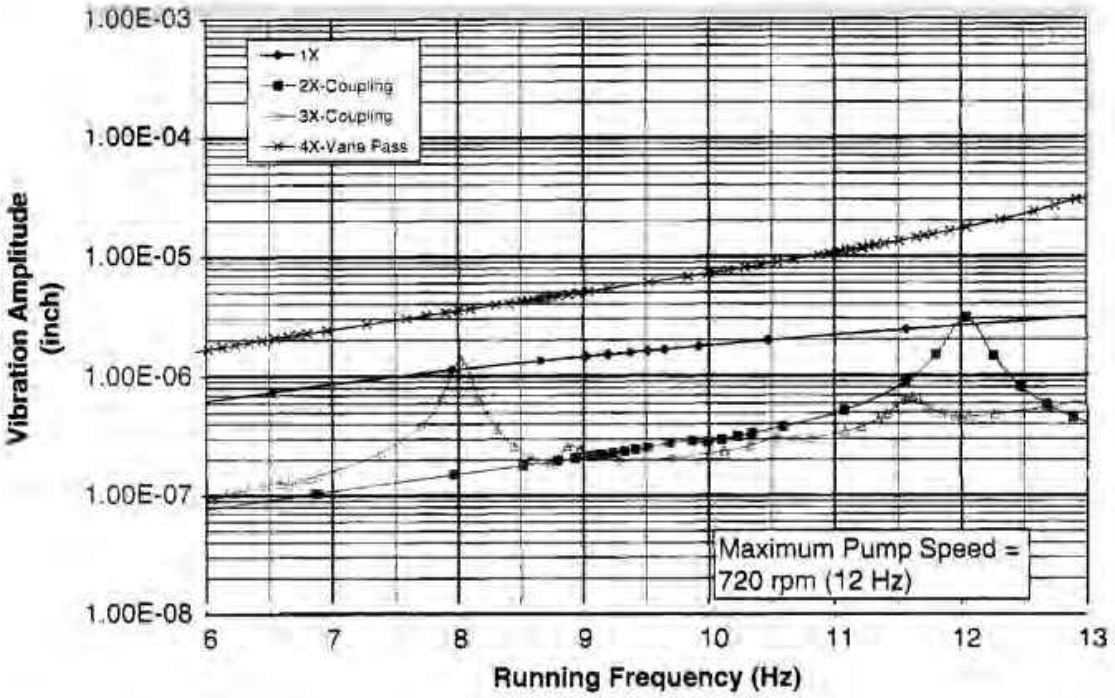


FIGURE 16 Horizontal vibration vs. speed (pump rpm) on pump upper bearing housing due to the combined effect of all excitations (mm = inch × 25.4) (Mechanical Solutions, Inc.)

TORSIONAL VIBRATION

It is important to predict torsional natural frequencies near the running speed of a drive train or at other important excitation frequency sources such as vane pass frequency, 1× and 2× electric motor line frequency, and motor rotating speed times number of poles. Although torsional vibration problems are not common in pump systems, they occur enough to require calculation. In this kind of vibration, the shaft rotates at different instantaneous speed and different phase (superimposed on the steady running speed), creating a torque oscillation along the shaft and creating twisting motion that can generate high destructive stresses. Accelerometers or proximitor probes commonly used to measure lateral vibration will not usually detect this vibration. A severe torsional vibration can exhibit gear noise and tooth distress, coupling wear, keyway fatigue, or motor winding loosening.

Lateral rotor dynamics of pumps can typically be analyzed without including other rotor system components such as the driver or gear box. However, torsional vibration of the pump shaft and all types of vibration of the pump stationary structure are system-dependent, because the vibration natural frequencies and mode shapes will change depending on the mass, stiffness, and damping of rotor components other than those included within the pump itself. The pump assembly must be modeled in terms of at least three bodies: the pump rotor, the coupling hubs (including any spacer), and the driver rotor. If a flexible coupling (e.g., a disc coupling) is used, the coupling stiffness must be included in the analysis. Good estimates of coupling torsional stiffness, often as a function of speed and torque, are listed in the coupling catalog data. Often a range of stiffness for a given size is available, if needed to tune a torsional critical speed to a new value. If a gear box is involved, each gear must be separately accounted for in terms of both inertia and gear ratio. If the pump or driver rotor is not at least ten times as stiff torsionally than the shaft connecting the rotor to the coupling, then the individual shaft lengths and internal impellers should be included in the model. If resonances cannot be avoided, a coupling selection can be optimized based on shaft torsional stress calculations. When the coupling

LIBERTY EXHIBIT 1017, Page 243

is changed usually it results in different weights as well, affecting the lateral critical speed, and rotordynamic reevaluation is recommended. A heavier coupling will reduce the lateral critical speed.

1. **Mass elastic diagrams** For the first step in calculating torsional natural frequencies, the rotor system is divided into stations, and a mass-elastic diagram is used to indicate geometric information about each station of the pump/driver rotor system, in terms of rotary inertia and torsional stiffness distribution. All of this information is used as input for the computer model of the rotary system, as illustrated in Figure 17.
2. **Calculation techniques** Methods for calculating the first several torsional natural frequencies manually are given in Blevins for simple models.[7] Numerical torsional analysis can be performed by using general purpose FEA programs, or specialty programs based on the Holzer method or transfer matrix method (TMM). In all of the computer-based methods, the system of differential matrix equations including damping is:

$$[J]\ddot{\theta} + [C]\dot{\theta} + [K]\theta = 0$$

where

J = diagonal rotary inertia matrix

C = rotary damping matrix

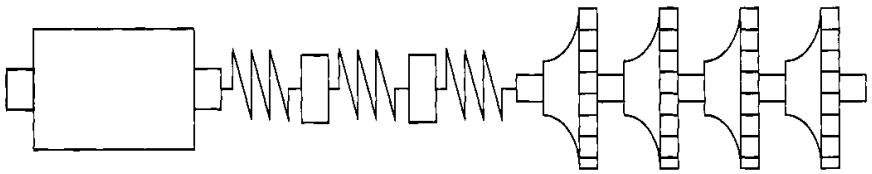
K = torsional stiffness matrix

$\ddot{\theta}$ = angular acceleration vector, rad/sec^2

$\dot{\theta}$ = angular velocity vector, rad/sec

θ = angular displacement vector, rad

3. **Penetration factors** Many rotating machinery components are not integrally machined on the shaft. Thrust collars, sleeves, disks, impellers, and coupling hubs are assembled using shrink fits on the shaft. Depending on the component length, the amount of shrink fit, and the size, such components may or may not contribute significantly to the torsional stiffness. However, API-684 applies the following principles:[4]
   - If the fit of the shrunk-on component is relieved over most of its length, then the torsional stiffening effect is negligible.
   - If a key is used to transfer torque (i.e., in a coupling hub), and has an axial length equal to $\frac{1}{3}$ of the shaft diameter, measured where the key starts, this will not be



Rotary inertia	Driver rotor		Coup. Hub		Coup. Hub	Driven rotor (Pump)
Torsional Stiffness		Drive shaft		Coupling	Driven shaft	
Torsional Damping	Driver loss		Elastomer coupling elem.			Driven loss

FIGURE 17 Torsional model example

LIBERTY EXHIBIT 1017, Page 244

considered an addition of torsional stiffness. If $\frac{1}{3}$ the shaft diameter is greater than the key length the hub is considered loose fit and does not add torsional stiffness.

- If the fit of a shrunk-on component is not relieved over a significant part of its length, made of the same material as the shaft and manufactured with a diametral shrink fit equal or greater than 1 mil/in (μm/mm) of shaft diameter, then the effective torsional stiffness should be assumed identical with the OD of the sleeve or component.
- If the shrunk-on component has a large rotational inertia such that centrifugal loading diminishes the effect of the shrink fit to less than 1 mil/in (μm/mm) remaining press, then the torsional stiffening effect is considered negligible.
- If a shrunk-on component has a nominal fit length with L/D greater or equal to 1, the shaft is assumed to be unrestrained by the hub over an axial length that is $\frac{1}{3}$ of the total length of shrunk surface. This $\frac{1}{3}$ penetration is typically used by coupling vendors when specifying coupling torsional stiffness from hub-to-hub.

4. **Effects of the driver and gear train** For an electric motor, the most important torsional excitation source is the motor rotating speed times the number of poles. If a gear box is involved, each gear must be separately accounted for in terms of inertia, flexibility, backlash, and gear ratio. The gear stiffness can only be approximated, since there are several parameters varying during rotation. These include:
   - Instantaneous point of contact
   - Direction of applied force
   - Number of teeth in contact

   The gear mesh frequency (number of teeth times rotational speed for a given gear) is usually a strong torsional excitation frequency with a typical p.u. (per unit, i.e., oscillation amplitude peak-to-peak fraction of steady torque) factor of about 0.02.
5. **Effects of the bearing, casing and foundation** Typically, the bearing, casing, and foundation of the pump and remainder of the drive train play a negligible role in the torsional dynamics of a pump rotor system.
6. **VFD operation** The use of variable frequency drive (VFD) motors has resulted in significant efficiency improvement in plant operation, because the motor speed can be adjusted to optimize efficiency in the system. For pump systems that involve VFDs, however, special attention should be taken because they provide significant new excitations called "control pulse" frequencies at higher multiples of the simulated line frequency (2 × motor running speed/no. of motor poles), often at 6×, 12×, 18×, and so on. The manufacturer of the controller can predict these excitation frequencies and their associated per unit factors. The p.u. factors of VFDs are reduced considerably in pulse-width-modulation (PWM) based VFDs.
7. **API-684** The API Standard 684, Rotordynamics and Balancing, includes recommendations for torsional analysis, and explains the importance of such analysis for new or modified designs in rotating systems that include untried combinations of impellers, coupling gears, shaft dimensions, and drivers. The API requirements are:[4]
   - Performance of an undamped train torsional natural frequency analysis.
   - Inclusion of the complete drive train.
   - Verification of adequate separation margin between the torsional natural frequencies and significant excitation harmonics (minimum separation margin of +/– 10%), where excitation frequencies include 1× N, 1× and 2× electrical line frequency excitation in motors/generators, VFD control pulse frequencies at 6× multiples of electrical line frequency excitation, and gear mesh.
   - If any torsional interference can not be shifted, a stress and fatigue analysis should be performed to ensure that the interference will not adversely affect the integrity of the machine components.
   - A transient torsional vibration analysis is usually required if a synchronous motor driver is used.

LIBERTY EXHIBIT 1017, Page 245

Transient torsional response of the system should be calculated with respect to excitations during start-up, trip, and motor control changes. Both steady state as well as transient forced response should be in terms of the simultaneous stationary plus oscillating shear stress in the most highly stressed element of the drive train, usually the minimum shaft diameter. Judgment on the acceptability of the assembly's torsional vibration characteristics should be based on whether the forced response shaft stresses are below the fatigue limit by a sufficient factor of safety, at all operating conditions. The minimum recommended factor of safety is 2, for a carefully analyzed rotor system. To determine system stresses quantitatively, a good worst case estimate of the system damping and of the frequencies and magnitudes of all of the significant excitation forces is required. The primary torsional damping is from energy expended by the pump impellers when they operate at slightly higher and lower instantaneous rotating speeds due to the vibratory torsional motion. For acceptability of the torsional rotor system assembly, stress at any condition should be below the fatigue limit with at least safety factor of 2.0 including all stress concentration factors.

8. **Damping and typical excitation levels (p.u. factors)** A reasonable estimate of the amount of torsional damping is expressed in the following equation:

$$C = k\frac{\tau}{N^2}f$$

where

C = damping, in · lbf · s/rad (N · m · s/rad)

k = constant value 19.1

τ = rated torque in · lbf (N · m)

N = rated speed, cycles/min

f = evaluated frequency, cycles/min

To determine the frequencies at which large values of vibratory excitation torque are expected, and the value of the torque occurring at each of these frequencies, the pump torque at any given speed and capacity can be multiplied by "per unit" factor "p.u." The p.u. factor at important frequencies can be obtained from pump, motor, and control manufacturers for a specific system, and it is typically in the range of 0.01 to 0.05 peak-to-peak for important excitations. Unsteady hydraulic torque from the pump is present at a frequency equal to the running speed times 1 as well as times the number of impeller vanes, with the higher values (0.05) being more typical of worst case off-BEP operation and/or impellers with less than four vanes. The most important torsional excitation frequencies from the motor are the number of poles times the motor slip frequency (for induction motors), rotating speed times the number of motor poles, and also the rotating speed itself. The gear mesh frequency is usually an important torsional excitation frequency with a typical p.u. factor of about 0.02.

FINITE ELEMENT ANALYSIS OF PUMP STRUCTURAL VIBRATION

The most common form of vertical pump is the vertical turbine pump, or VTP, which is very different from other pumps, because of its less stringent balancing, shaft straightness, and motor shaft alignment tolerances, and because of its long flexible casing and the casing's flexible attachment to ground, and because of the peculiar spaghetti-like lineshafting which connects the motor to the below-ground liquid-end "bowl assembly" of the pump. However, like other pumps, the bearing loads and the bearing and wear ring clearances are where problems are likely to occur.

Structural Vibration Analysis: Various Levels of Model Fidelity In general, for VTPs and vertically mounted sewage pumps, determination of the vibrations of the stationary

structure, the lineshafting, and the pump and motor rotors should be done simultaneously, using FEA. The goal of such analysis is to determine the vibration mode shapes and natural frequencies of the first roughly 10 vibration modes which involve significant motion of any of the following: any nonrotating portion of the pump, the frame of the closely coupled motor or housing of the variable speed drive (if so equipped), the pump baseplate, the pedestal, or the foundation within the geometrical limits of the model (as defined below). The components in such a model should be represented mathematically in considerable detail, as follows:

- Include foundation mass and stiffness within a radial distance (measured from the center of the pump base) at least equal to the height of the top of the motor relative to the level of attachment of the baseplate to the floor.
- Include piping details important to modal mass and stiffness, such as hangers, bulkheads, and expansion joints, and all the piping and its enclosed fluid within a spherical zone of radius (relative to the centerline) equal to twice the height of the top of the motor relative to the level of attachment of the baseplate to the floor.
- Include the effective flange-to-flange pump casing/bowl assembly stiffness, mass, and location of center-of-mass, of the close-coupled motor and variable speed drive (if so equipped), and of the discharge head or motor stand.
- Include any pedestal, discharge housing, and motor stand stiffness variations between the piping in-line and perpendicular directions, taking particularly into account the effects of coupling access or stuffing box access windows.
- Include the below-ground column piping and bowl assembly (in pump designs such as can pumps which incorporate these components), the fluid in and immediately around the column piping and bowl assembly,[7] any column piping stiffeners or supports, and any shaft enclosure tubing.
- Include the mass of all pump impellers, and either include their nearby bowl bearings or assume they behave as if they are rigidly attached to the pump casing at their center of mass.

It should be noted that when analyzing VTPs or vertically mounted sewage pumps, the best policy is to model the entire pump, motor, and base as a system, and not only model the above-ground components. Important resonances have occurred in pumps involving below-ground activity in concert with above-ground motion. In general, there is no such thing as a strictly "above-ground mode" or "below-ground mode." Although modes may be dominated primarily by above-ground motion, this cannot be counted on.

Combining Structural and Rotor Dynamic Preinstallation Analysis The flexibility of the VTP structure and shafting result in many closely spaced modes within the range of frequencies for which strong exciting forces are expected. An average of one mode per 100 cycles per minute (cpm) is not unusual for deepwell VTPs. VTP pumps also exhibit nonlinear shaft dynamics because of the large shaft excursions which occur in the lightly loaded long length/diameter ratio bearings, as will be explained below. Time-averaging modal methods can be used to experimentally determine the rotor nonlinear response.

An important element of VTP shaft vibrations is the strong effect of axial thrust on the impellers, causing a roughly 10% increase in shaft natural frequencies, as discussed by Kovats, and providing a restoring moment which tends to suppress lateral vibrations in a nonlinear fashion, as explained by Blevins.[7] Another important factor is the statistical character of the support provided by any given lineshaft bearing. If the bearings behaved consistently and linearly, FEA could be used to accurately predict the lineshaft modes. However, the normally lightly loaded lineshaft bearings exhibit a rapid, nonlinear increase in bearing stiffness as the lineshaft gets close to the bearing wall. Given the flexibility of the lineshaft and the weak support provided by the pump column piping, and given the relatively large assembly tolerances and misalignments in the multiple lineshaft bearings

LIBERTY EXHIBIT 1017, Page 247

Next Page

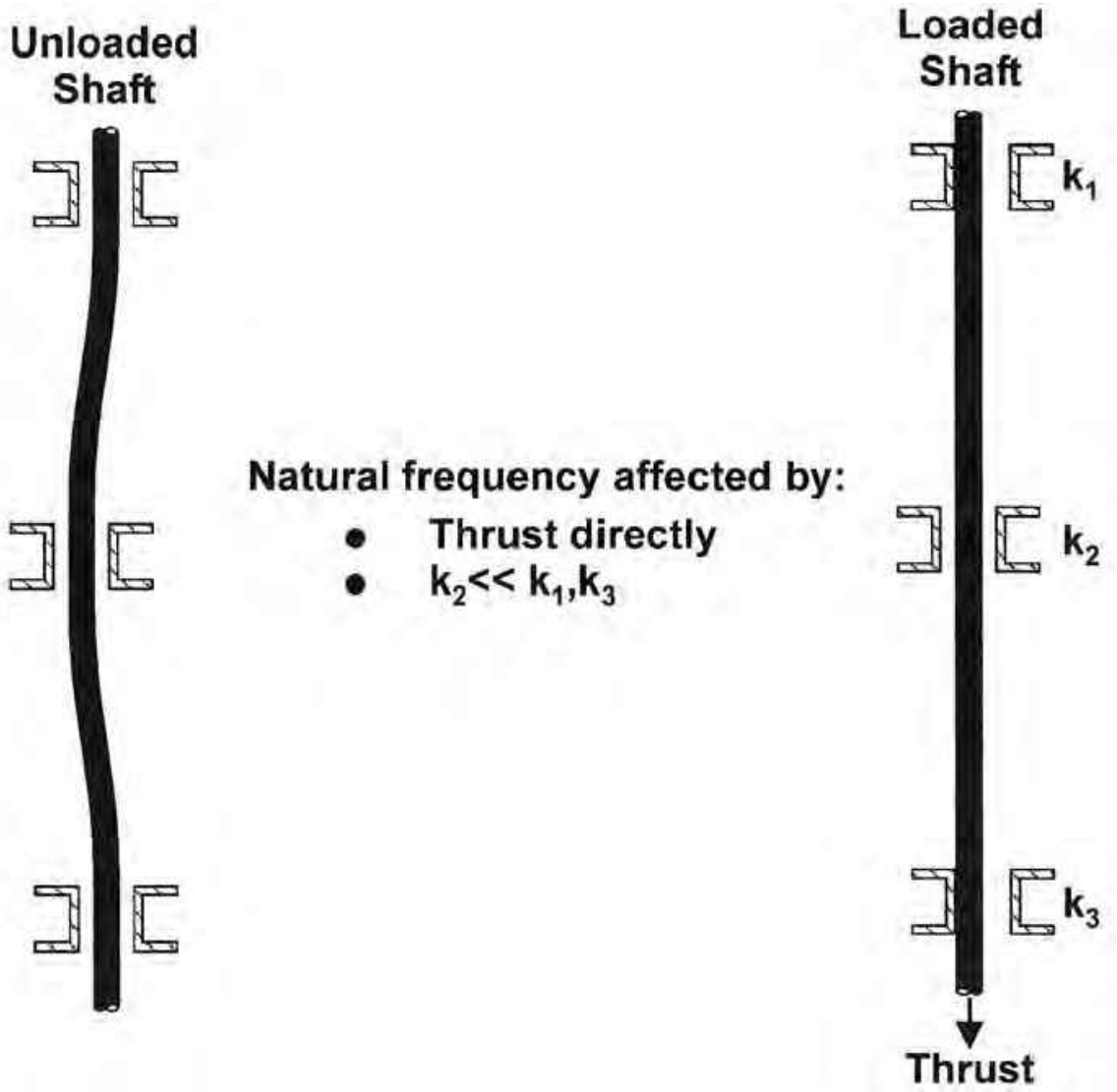


FIGURE 18 "Violin String" effects, influenced by axial thrust and bearing eccentricities (Mechanical Solutions, Inc.)

of these machines, the contribution of each bearing to the net rotordynamic stiffness is a nearly random and constantly changing situation, as explained conceptually in Figure 18. The result is that in practice there is no single value for each of the various theoretically predicted natural frequencies, but rather the natural frequencies of the lineshafting and shaft in the bowl assembly must be considered on a time-averaged and location-averaged basis.

If rotordynamic analysis is performed on VTPs, it should be performed using a validated computer program based on FEA, and the following issues need to be addressed:

- Include all rotating component masses and effective assembled flexibility for the entire pump rotor, the lineshafting, the motor coupling or drive, and the motor rotor. Also include effective added mass for fluid inside and around the impellers and lineshafting.
- Include the stiffness, both direct and cross-coupled, and damping of all bowl, lineshaft, drive, and motor bearings, and of all impeller annular seals (Lomakin effect). It is not generally possible to determine a precise value for these parameters, but a range of values can be identified, with maximum and minimum values established at representative operating points. Separate calculations for shaft natural frequencies and vibration

LIBERTY EXHIBIT 1017, Page 248

Previous Page

amplitudes should be performed for at least three situations: minimum stiffness at all bearings and seals, most probable stiffness at all bearings and seals, and maximum stiffness at all bearings and seals.

- Include the cantilevered stiffness of the motor bearing supports relative to the foundation, and of the bowl and lineshaft bearing supports as influenced primarily by the column piping flexibility.
- Include a forced response analysis and a transient stability analysis using as minimum input calculated mode shapes and natural frequencies for the first 10 rotor modes, and predictions of bearing and annular seal stiffness and damping which bracket expectations, as discussed above. In calculating forced response, include as minimum forces worst-case unbalance in each impeller and in the motor rotor and drive rotors or motor coupling halves, worst case misalignment across the drive or motor coupling, and worst case unsteady or rotating hydraulic forces on each impeller.
- Include torsional as well as lateral, axial, and mixed vibration modes in all analyses. If flexible couplings are used, a reasonable estimate must be made of the coupling torsional, lateral, and axial stiffnesses, which are usually listed as catalog data. It should be assumed that the thrust and radial bearings and annular seals provide no torsional constraint or stiffness.

If a pump is low in power, often analysis will be bypassed. This always entails some degree of risk, since small pumps can resonate just as easily as large pumps. It is the authors' experience that it is cost-effective in the long-run to analyze all pumps of 100 hp (75 kW) or greater in the manner described, prior to installation. In addition, the following should be considered "danger flags," increasing the need for detailed analysis:

- Vibration specifications requiring less than 0.20 ips peak.
- Particularly tall units (L/D greater than 4).
- Variable speed units.
- Pumps that tie into headers that look like flutes, because they may acoustically act like flutes.
- Flexibly supported pillow block bearings on U-joint drive shafting.
- All equipment mounted to a particularly flexible or loss inertia foundation (foundation mass less than 5× the weight of the total weight of the supported equipment).
- Insufficient tie rods, based on calculation of excessive deflection (more than 3 mm or 0.125 in) due to length versus cross-sectional area and worst-case applied load.
- Insufficient length of suction piping.
- Lack of pipe supports close to the pump, when piping is hard-coupled to the pump.

A useful simplified method of predicting lineshaft reliability with a worst-case model known as the "jump rope" model has been reported by Marscher.[11] The concept is to model the lineshaft vibratory motion and loads in the worst-case limit by the deflection and end support forces associated with a whirling jump rope, with the addition of axial thrust and bending stiffness effects. The deflection of such a jump rope may be calculated by a quasi-static analysis, based on D'Alembert's principle with the end conditions set equal to the radius of the circular path of the "hands" (bearing radial clearance) controlling the rope, and the load per unit length at each point along the rope equal to the local displacement, times the mass per unit length, times the square of the rotational frequency. The deflections predicted by this model are worst case, regardless of the value of or linearity of the bearing stiffness, if the circular orbit of the end conditions is set equal to the diametral clearance of the lineshaft bearings, and if the rotor deflection slope within each bearing is set equal to the bearing diametral clearance divided by the bearing length. The latter condition is the so-called "encastre" condition, studied by Downham, and Yamamoto.[12, 13] It is the encastre condition which ultimately limits the shaft deflection and stresses, and the bearing loads; both by limiting the slope of the shaft, and by changing the end support

condition of a shaft length in the analysis from "simple" (i.e., knife edge) to fixed. Compared to the load caused by the whirling shaft mass in this condition, minimal bearing forces are caused by initial unbalance, misalignment, or bends in the shaft; which is why liberal tolerances on these pumps are commercially acceptable. For relatively stiff lineshafting such as in most reactor coolant pumps, the jump rope model gives answers which are too conservative to be useful, but for the majority of VTPs with shafting under 2.5 in diameter and bearing L/D ratios of 2.5 or more it gives a quick method of confirming that shaft stresses and bearing loads are acceptable.

FUNDAMENTALS OF PUMP VIBRATION TESTING

Predictive maintenance and troubleshooting of potential or suspected mechanical problems in pumps begins with the gathering of information which is used to determine the condition of the machine. The analysis of these data is commonly done through trending over time, which is a useful indicator of health. Supplementing such an approach, detailed instantaneous evaluation can diagnose specific problems through analysis of the spectral components of the vibration and, at the highest level, the creation of detailed animations which show the operating deflection shape (ODS) of the machinery during normal operation, and/or during start-up and shutdown transients. In addition to such operational testing and evaluation, experimental modal analysis is a specialized type of vibration testing in which the response of the machinery is measured in response to a known input excitation force (typically either through a broadband-exiting impact or a narrowband shaker scanned though a broad frequency range).

An experienced technician or engineer will couple knowledge of the hydraulic performance and mechanical behavior of the pump with the operational history and details of the pump design to determine probable causes of the problematic vibration. It is advisable to perform vibration testing during commissioning of critical equipment such that a record of the "newly installed" performance of the pump can be kept in the maintenance file for the pump. The vibration behavior of a pump on the manufacturer's test stand can indicate problems with a pump, but will not necessarily be consistent with the pump's behavior when mounted on a rigid foundation and connected to the process piping. In addition to the manufacturer's "birth certificate" testing, it is also important to maintain detailed maintenance and operational records so that changes in vibration can be correlated to physical or operational changes in the system.

Instrumentation choices Critical machinery often has instrumentation permanently installed to measure the bearing housing and/or shaft vibrations. Typical modern instrumentation choices for pump applications are piezoelectric accelerometers (for housing vibration) and eddy current proximity probes (for shaft vibration relative to the housing). While both of these instruments measure vibration, they are quite different. Accelerometers measure the absolute acceleration of the surface on which they are mounted. Proximity probes measure the distance between the probe tip and the shaft. Changes in this distance are a result of vibration of the shaft relative to the housing, but does not include an absolute measurement of the housing on which the probe is mounted (such as with an accelerometer); and therefore from such a measurement, the absolute shaft vibration cannot be known. Older and noncritical machinery often does not have permanently installed instrumentation but is monitored periodically by predictive maintenance personnel using a portable analyzer and an accelerometer held in place by hand pressure or a magnet. The handheld instrumentation can be effective, but the user must beware of "bouncing" or "rocking" of the accelerometer base on the machine contact surface, which is seldom flat or totally clean. A spear point on the accelerometer contact, or a thin layer of wax on a flat accelerometer base, can result in very accurate handheld readings, to frequencies of thousands of kHz.

If a problem is suspected in a pump or its driver, a more detailed investigation can be effective in determining the root cause of the problem and in assessing the risk of an

LIBERTY EXHIBIT 1017, Page 250

unplanned shutdown. Instrumentation which is available for such an investigation includes the following:

1. Portable or permanently installed accelerometers
2. Temporarily or permanently installed proximity probes
3. Dynamic pressure transducers
4. Microphones or their liquid-measuring counterparts, hydrophones
5. Temperature probes and/or infrared photography
6. Strain gages, sometimes monitored on a rotor, through FM telemetry

Each of these instruments can be very useful, but care must be taken to insure their proper application. Common problems which are encountered are loose attachment of accelerometers to the pump; electromagnetic interference, which is particularly problematic when unshielded cables are used; and inaccurate temperature measurement with infrared radiation detection devices due to differences in the emissivity of the surfaces. Consideration must also be given to the resonant frequency of the sensor which will produce a systematic error in frequency measurements close to it. Modern accelerometers have resonant frequencies which are 40 kHz or higher and have a usable frequency range of 10 kHz or higher.

Special instrumentation is available for measurements which must be made in extreme environments. High temperature instrumentation can be used to gather vibration data on boiler feedwater pumps and on steam turbine drivers. This instrumentation often has the signal conditioning electronics removed from the sensor such that it is not exposed to the high temperatures. It is also possible to cool the instrumentation by circulating cooling water through the sensor or its connection to the machine. Integral or intrinsically sealed cable connections allow for underwater use of sensors.

Vibrations can be measured in terms of acceleration (g's), velocity (in/s or mm/s), or displacement (mils or mm). Accelerometers measure the acceleration of the surface on which they are mounted, but it is very common for internal circuitry in either the sensor or the analyzer to convert the signal into velocity. Velocity-based vibration sensors have largely been replaced by accelerometers due to the excellent high frequency response of accelerometers, and the improvements in accelerometer robustness and low frequency performance. Exceptions are in noncontact measurements which cannot use surface mounted accelerometers. These measurements commonly employ eddy current or fiber optic proximity probes (displacement measurement) or lasers (displacement or velocity).

Past perception has been that acceleration sensors were best used to measure high frequency vibrations and displacement sensors were best used to measure low frequency vibrations, while velocity sensors were more universal than either in their application. Modern accelerometers are capable of accurately measuring vibrations at very low frequencies and have been successfully used below 1 Hz, making them universal for most pump applications. However, care must be taken if low frequency acceleration data are integrated to determine the vibration in terms of velocity or displacement. Division by frequency is required, and results in division by zero or at least a very small number at low frequencies, causing significant error. On the other side of the spectrum, proximity probes are capable of accurately measuring vibrations in the kilohertz range which is sufficient for pump applications which require noncontact measurements, and differentiation of displacement to determine velocity, for example, does not lead to significant error.

Vibration Analyzers Vibration analyzers are used to perform operations such as Fast Fourier Transforms (FFTs) on the raw data (vibration versus time) to determine the key vibration frequencies. Handheld portable analyzers are used by maintenance personnel to analyze and store vibration data from machines which do not have permanently installed and monitored instrumentation at key locations. Analyzers used for this type of vibration analysis should have at least two channels such that one channel can serve as a phase reference. Multichannel analyzers which are used by technicians or engineers for troubleshooting problems commonly have 4 to 32 channels of simultaneous data acquisition, and in principle can have hundreds of channels. Multichannel analyzers also have

LIBERTY EXHIBIT 1017, Page 251

digital "tape" recording capabilities, which allow the raw data to be saved for future playbacks, and alternative analysis. This feature is particularly useful for monitoring transient events such as equipment start-ups, speed changes, and load changes. These systems are more complicated and more expensive which makes them more useful to specialists in vibration analysis than to routine data acquisition for predictive maintenance. Regardless of the number of channels, the bookkeeping of measurement locations and directions of the vibrational motion is vital.

The FFT frequency spectrum analysis is critical in the understanding of the physics of most problems in that it breaks down a complex vibration waveform into its discrete frequency components. Analysis of which discrete (also called "filtered") frequency components are dominant in the vibration spectrum provides valuable information which an experienced engineer or technician can use to identify potential root causes for the vibration problem. This information is used to determine the strong excitation frequencies and the vibration level at those frequencies versus tolerable levels, and with proper test procedures can be also used to determine any structural or rotor natural frequencies which are too close to the excitation frequencies, thereby increasing the vibration.

Analysis of vibration data through other more specialized instrumentation and analyzers, such as "shock-pulse-signal" or "stress-energy-signal" analysis, can be used for specific purposes such as identifying faults in rolling element bearings. Such analysis measures and evaluates the high frequency section of the frequency band and is not concerned with measuring narrowband vibrations. Techniques for identifying specific problems in pumps such as bearing faults and cavitation exist and/or are currently under development.

1. **Recommended measurement locations** Locations for vibration measurements on pumps are recommended in the various specifications. The specification must be satisfied at each of these locations in order for the pump to be accepted. In general, it is best to measure the structural vibration at the bearings since these locations are close to the points at which the rotor and structure interact. It is recommended that vibrations be measured in three orthogonal directions at each bearing location, although sometimes the axial direction is bypassed at the nonthrust end of the machine. On critical-service pumps, shaft vibration measurements should be taken in two orthogonal directions at each bearing location for pumps with hydrodynamic journal bearings. Specifications such as API-610 and the HI/ANSI centrifugal pump standards, provide illustrations of typical recommended measurement locations for pumps with overhung rotors, between bearing pumps, and vertically suspended pumps (e.g., vertical turbine pumps).[2,14]

2. **Vibration acceptance testing and specifications**

Specification Limits The vibrations measured on a pump and/or motor typically must remain below some specification limit. These limits have been developed by pump designers and users to set guidelines which indicate when vibrations reach a level which can cause damage to the pump. The goal of these organizations is to provide guidelines which reasonably define acceptable performance without either the manufacturer incurring unnecessary design and manufacturing costs or the end user risking avoidable maintenance costs throughout the life of the pump. The cost of achieving unnecessarily low vibration levels will be passed eventually from the manufacturer to the end user, so appropriate vibration specifications must be carefully considered when purchasing a pump.

Several organizations which have specifications that are commonly applied to pumps are the Hydraulic Institute (HI), American Petroleum Institute (API), and International Standards Organization (ISO). Each of these organizations is preferred by manufacturers and end users in various market segments and/or geographic areas. It is common for purchasers to modify these specifications to satisfy their particular application. Both purchasers and manufacturers should consider the probability of accepting a bad pump due to a vibration specification which is too lenient versus the rejection of a good pump due to a specification which is unnecessarily tight. In both cases additional time and costs are incurred by both the manufacturer and the end user.

When analyzing vibration data and comparing it to a standard, the most important thing to determine is whether the vibration level will result in premature damage to the

LIBERTY EXHIBIT 1017, Page 252

pump or are there indications that the vibration is trending in a way that indicates unacceptable wear in the pump. For pumps which have rolling element bearings, the oscillating forces acting on those bearings can be estimated and used to consider whether the bearings are likely to deteriorate. Rotor vibration on pumps with hydrodynamic journal bearings can lead to the shaft rubbing on the bearings which will result in premature wear. It is typical for a certain percentage of the bearing clearance (normally about 50%) to be used as the maximum allowable peak-to-peak vibration level. Other considerations are fatigue of stationary structural components, fatigue of rotor components, and coupling failure. Equally as important as simply determining whether it is safe to continue to operate is to identify the root cause of any abnormal vibration such that future failures can be eliminated or at least predicted.

The goal of specifications should be to protect all parties—manufacturers, consultants, contractors, and owners—by clearly defining and assigning responsibilities for the avoidance of unacceptable vibration in newly installed pumping systems. The effectiveness of any measures taken to minimize the likelihood of vibration problems, and to quickly solve them if they occur, will depend upon the level of technology used. The inclination or ability of low-bid equipment suppliers to provide an appropriate level of technology should not be assumed, but should be specifically required by the bid and contract.

Injury to rotating and reciprocating machinery due to excessive rotor vibration takes the form of wear or fatigue of the internal components, such as bearings, seals, and shafting. In general, wear rate and fatigue tendency for a specific machine is proportional to the oscillating displacement associated with vibration. However, testing by various sources over the last 70 years has indicated that for *classes* of machines (e.g., centrifugal pumps), operating at perhaps a range of different speeds and loads, vibration velocity rather than displacement, correlates best with likelihood of wear (tribological) or fatigue (metallurgical) failure. The reason for this is not made clear in most references concerning acceptable vibration levels and machinery vibration acceptance standards. Early references on this subject were Rathbone (insurance company data),[15] Blake (the so-called "Haystack Chart"),[16] Baxter and Bernhard (the so-called "IRD Chart"),[17] and Hancock (petrochemical plant experience with vibration level versus failure rate for a large population of industrial pumps).[18]

Each of the classical references concluded that for large groups of machinery of various sizes and speeds, vibration velocity (i.e., the first derivative with respect to time of the vibration displacement) correlated better than displacement with machinery deterioration rate and current state of health. However, for a given machine that vibrates primarily at a constant running speed, as the great majority do (because variable speed machines are still the exception), and when residual imbalance is the main forcing function (as it indeed is for most in-service machinery), it was accepted that either displacement or velocity level could be used for trending purposes. This is because velocity was merely displacement times speed times a units constant, as shown in Figure 19.

BALANCE AND ALIGNMENT

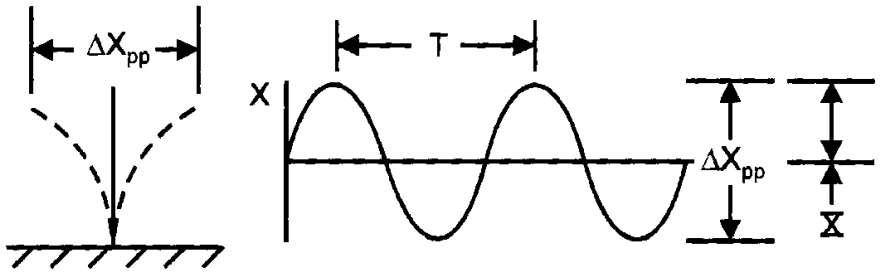
In industry, imbalance and misalignment represent about 80 to 90% of the vibration problems in rotating equipment, and these are relatively easy to fix or minimize most of the time. Balancing means a process to restore the imbalanced rotor to a balanced condition by adjusting the mass distribution of the rotor. Depending on the type of imbalance, rotors can be balanced using either a single plane or a multiplane method, as described below.

Single Plane Balancing Static imbalance is a term used when the central principal axis is displaced parallel to the rotational axis in a rigid rotor. The residual imbalance in such a case requires only a single mass located in a single plane (through the center of mass of the rotor) to balance the rotor, as shown in Figure 20.

Multiplane Balancing The two-plane balancing method is used for rotors with couple unbalance or dynamic unbalance. The couple unbalance or "dynamic imbalance" means a

LIBERTY EXHIBIT 1017, Page 253

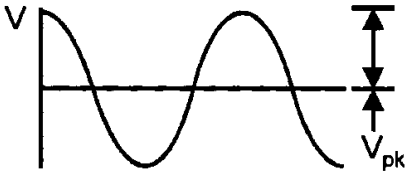
1. Displacement Δx_{pp} (mils or μm)



$f = 1/T$ $\quad X = \bar{X}\sin(2\pi ft)$

2. Velocity V_{pk} (ips or mm/sec) = $\frac{dx}{dt}$

$V_{pk} = \text{constant} * \Delta X_{pp} * f$

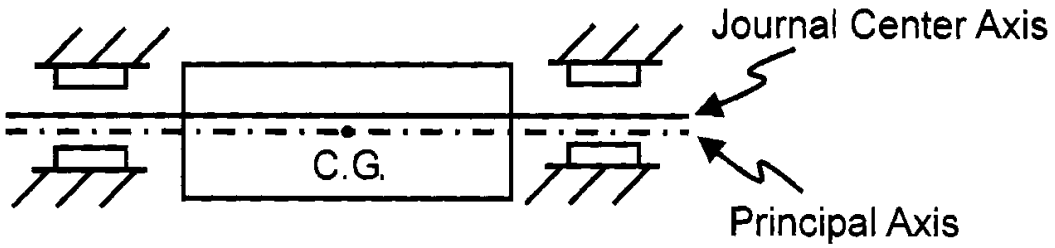


3. Acceleration a_{pk} (g's) = $\frac{dv}{dt} = \frac{d^2x}{dt^2}$

$a_{pk} = \text{constant} * X_{pp} * f^2$

NOTE: $V_{RMS} = 0.707\ V_{pk}$ & $a_{RMS} = 0.707\ a_{pk}$ at any single frequency

FIGURE 19 Relationship of vibration displacement, velocity, and acceleration



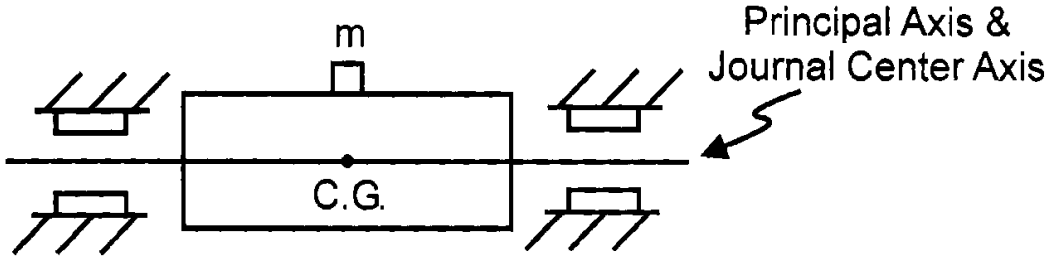


FIGURE 20 Single plane balancing

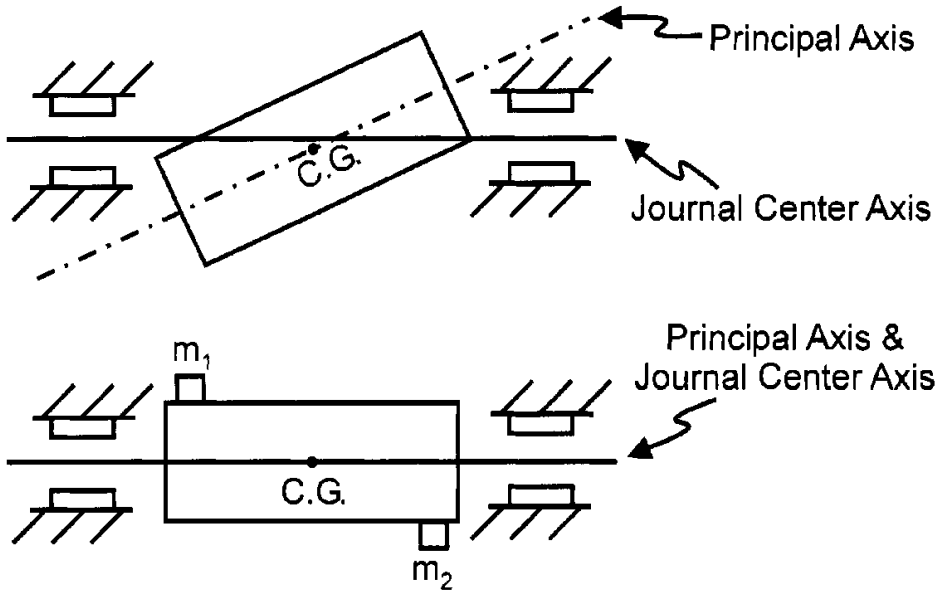


FIGURE 21 Two plane balancing

state of unbalance in a rigid rotor where the central principal axis and the rotation axis are not parallel with each other. In this case, mass is required on each end to balance the rotor. In such a case, at least two planes are required to balance the rotor, as shown in Figure 21.

Balance Specifications In the real life, is impossible to obtain a perfectly balanced rotor. Several standards have been developed over the years to specify the maximum residual unbalance allowable according to the equipment application and operating speed. The ISO 1940 imbalance tolerance standard specifies different grades of imbalance tolerance as a function of speed. Other standards include American Petroleum Institute (API) 610, which has recently been modified and adopted as an ISO standard, as has the HI/ANSI pump standard.[2, 14, 19] For tight fitting components on pump shafts, the recommended balance limit is somewhat tighter than the "precision" ISO Grade G-2. A typical pump balance specification is:

For USCS units, $U = \dfrac{4W}{N}$ in oz-in

For SI units, $U = \dfrac{6350W}{N}$ in gr-mm

where

U = maximum allowable residual unbalance for each plane based on the static weight supported at each end of the rotor

W = portion of static rotor weight supported by each bearing journal (lbm for USCS units and kg for SI units)

N = maximum continuous operating speed of the rotor in revolutions per minute (rpm)

For axially short components (e.g., a thrust washer) the difference between these two can be neglected, and only single plane static balancing is required. For components greater in length than $\frac{1}{6}$ their diameter, dynamic imbalance should be assumed (and in fact is required by API-610 in this case), and at least two plane balancing is required. For rotors operating above their second critical speed (unusual for pumps), even two plane balance may not be enough, and some form of at-speed modal balancing (i.e., balancing

LIBERTY EXHIBIT 1017, Page 255

material removal that takes into account the closest natural frequency mode shape) may be required.

When imbalance occurs, including imbalance caused by shaft bow, it shows up with a frequency of exactly 1× running speed. This is because the heavy side of the rotor is rotating at exactly rotating speed, and so forces vibration movement at exactly this frequency. Typically, this also results in a circular shaft orbit, although the orbit may be oval if the rotor is highly loaded within a journal bearing.

Alignment Measurement Techniques and Guidelines Next to unbalance, in industry misalignment is the primary reason for high vibration in rotating equipment and can cause severe damage on coupling elements through fatigue of dry element coupling diaphragms or shim packs, lubricated gear coupling tooth wear, overheating, bearing preloading, and—in the case of severe misalignment—shaft fatigue.

Over the years, several techniques have been developed for measuring misalignment:

- Straightedge method
- Face and rim method
- Reverse dial indicator
- Continuous alignment monitoring, for example with "Dodd bars" or "Essinger bars"

STRAIGHTEDGE METHOD This is the least accurate method of alignment (0.10 mm or 5 mils), and typically should only used for a quick, rough preliminary alignment by using a straight ruler between coupling hubs with the same outside diameter.

FACE AND RIM METHOD This method uses a dial indicator, and offers more accurate readings (0.010 mm or 0.5 mils). Is typically used in industry for cold readings, where the offset misalignment is measured by placing the dial indicator on one of the hubs, and then measuring the other hub in the radial direction, by rotating both shafts together and taking measurements in each quadrant (every 90 degrees). In this case, the sum of horizontal readings must be equal to the sum of the vertical readings. Usually, the pump manufacturer recommends the misalignment requirement at cold condition in order to reach the desired alignment condition during operation once the thermal growth is reached on both shafts. Offset misalignment is most of the time combined with the angular misalignment. In this case, the reading is taken in the axial direction on the coupling hub (face reading). The disadvantages of this method are that the diameter of the hub surfaces must be circular without imperfections or irregularities on this surface, as well as concentric with the face surfaces, unless the readings are taken by rotating both shafts together. The other disadvantage is that either the pump shaft or the driver should not float axially; otherwise, an axial stop should be used to reduce the face reading errors.

REVERSE DIAL INDICATOR This method is similar to rim method, but in this case, two dial indicators are used, reading on each hub (pump and driver). This method is commonly used in order to verify the alignment once the temperature in the equipment has stabilized, by bringing the equipment to a stop, and then quickly setting up and operating the reverse dial system, as a "hot alignment check." Laser optical alignment is also used, assisted by a computer program to facilitate and reduce the time of the alignment process for the user. This method offers high precision. The principle is simple, and employs a laser beam transmitter, which is clamped to one shaft. A reflecting prism is mounted on the second shaft, with the assembly acting as in the reverse dial indicator method, but typically without shaft sag. The beam passes from transmitter to prism, the angled faces of which then reflect it directly back toward the origin but along a different path. The returning beam strikes a target that electronically senses shift from a zero position. Electronic circuitry translates that shift into the type and amount of misalignment. The necessary adjustments are displayed in the computer program graphics.

DODD BARS Dodd bars can be used to monitor the alignment between two units (driver and driven) during the transient condition until the final thermal growth is reached.[20]

LIBERTY EXHIBIT 1017, Page 256

TABLE 1 Guidelines for proper alignment

Think in terms of offset in combination with parallel misalignment
Reverse Dial Indicator is most foolproof method
Check foot bolt tightness before starting, ensure gage assembly is tight and stiff
Set all gages to mid-travel
Rotate gage assembly several times to "shake-out" hysteresis
Do repeatability readings several times: Readings should repeat within 1 mil, 3:00 + 9:00 = 6:00 + 12:00
Take final readings in 4 positions: 3:00, 6:00, 9:00, 12:00
Quantify sag in indicator measurement arm, on straight rigid shaft
Subtract sag from 12:00 reading, add sag to 6:00 reading
Misalignment should be (this is a general guideline only): Offset: less than 2 mils * (3600/RPM) Parallel: less than $\frac{1}{2}$ mil × (3600/RPM) per axial inch
Remember: Alignment when machine is cold and non-pressurized will be different than when machine is hot and pressurized. May need non-zero "cold offsets" for best COS alignment, and may need compromise alignment for variable COS.
Beware of "soft foot" (e.g., "teetering" pump, or delaminated foundation)

These bars are made of titanium, with low thermal coefficient which reduces the distortion of the readings by reducing the thermal deformation of the bars. Four proximitor probes are mounted on one of the bars on the driver machine bearing bracket monitoring both the horizontal and vertical directions at two axially offset locations on the other bar, which is mounted through a bracket to the driven machine bearing housing.

Sometimes a rotor must be offset when cold and not running in order to be aligned when running and hot. For example, thermal growth of the pump or its pedestal versus the driver could change alignment "hot" versus "cold." This situation can be checked with various continuous monitoring tools, such as Dodd bars or Essinger bars, that monitor the offset and angular movement of the pump and driver bearing housings relative to either each other (Dodd bars) or relative to the foundation as a reference (Essinger bars).

Misalignment is best checked by some form of the reverse dial indicator method (or its laser alignment tool equivalent). Guidelines for a proper alignment process are provide in Table 1.

FIELD VIBRATION TROUBLESHOOTING PROCEDURES

Typically, vibration monitoring programs are designed to determine if there is a serious vibration problem, but more sophisticated analysis is required to determine the root cause of the problem and to identify suitable fixes. A good starting point for troubleshooting of vibration problems is to identify particular operating conditions (speeds, flow rates, and so on) which result in high vibrations. The next step is to measure high resolution vibration spectra at the conditions which result in high vibrations to identify the frequencies at which the highest components of vibration are present and the locations on the machinery where the highest vibration occurs. This basic information can be used to sort through potential causes of the vibration using a vibration troubleshooting list, as shown in Table 2. In some cases, additional data such as pressure pulsation measurements may be required to

LIBERTY EXHIBIT 1017, Page 257

TABLE 2 Pump vibration troubleshooting list

Multiples of Rotational Speed	Other Symptoms	Probable Causes
0.05 to 0.35x	Vibration response is broad in frequency	Diffuser or return channel stall
Exactly $\frac{1}{2}\times$, $\frac{1}{3}\times$, $\frac{1}{4}\times$ etc.	Vibration may increase dramatically shortly after this appears, except in vertical pumps with four or more lineshaft bearings, where it is common and not harmful	Light rub, possibly combined with low shaft or bearing support natural frequency
0.40 X (Approx)	Shaft has rolling element bearings	Bearing Cage Defect
0.42 to 0.48 X	Near rotor lateral natural frequency and the orbit has a secondary loop.	Rotordynamic instability due to fluid whirl in close clearances, e.g., bearing "oil whip"
	Onset is sudden at a speed roughly 2 times the excited natural frequency, and "locks" onto the natural frequency in spite of further speed increase	
0.65 to 0.95×	Smaller peaks at (1-f) X, and at sidebands of ±(1-f) X of the first several multiples of running speed.	Internal flow recirculation probably at suction
	Often accompanied by rumbling noise and beating.	
	Occurs at part-load capacities, but disappears at very low capacity.	
	Independently depends on speed and flow	
Less than 1×	Increased broadband vibration and noise level below running speed as NPSH decreases, especially at high flows.	Cavitation without recirculation
	Often accompanied by decreased vibration and noise above 1×.	

(*Continued*)

LIBERTY EXHIBIT 1017, Page 258

TABLE 2 Pump vibration troubleshooting list (*Continued*)

Multiples of Rotational Speed	Other Symptoms	Probable Causes
1×	Stronger on shaft than on housing.	Imbalance in Rotating Assembly or bent rotor
	Hydraulic performance and/or suction pressure normal	
	Axial vibrations within normal limits	
	Vibrations increase with roughly speed squared	
1×	Vibration highest on drive end housing	Pump coupling imbalance
1×	Vibration high on driver IB or OB housing, low on pump	Driver rotor imbalance
1×	Natural frequency near 1×	Resonance
1×	Axial vibrations are over $\frac{1}{2}$ of Horizontal or Vertical vibrations.	Pump/driver misalignment at the coupling
	Vibrations increase much slower than the square of the speed	
	Bearing oil temperature is high.	
1×	Discharge pressure pulsations are strong at 1×	Clogged or damaged impeller passage
	Discharge pressure pulsations are not strong at impeller vane pass (single volute pump)	
1×	Discharge pressure pulsations are strong at 1× Discharge pressure pulsations are strong at impeller vane pass, especially for flows far above or below BEP	Volute tongue designed too close to impeller OD (B-gap), or excessive impeller/volute eccentricity
2×	Both shaft and housing vibrations are strong	Clogged or damaged impeller passage
	Discharge pressure pulsations are strong.	
	Impeller vane pass vibrations are low (twin volute pump)	

LIBERTY EXHIBIT 1017, Page 259

2×	Both shaft and housing vibrations are strong	Volute vanes designed too close to impeller OD (B-gap), or clogged or damaged volute, or excessive impeller eccentricity
	Discharge pressure pulsations are strong	
	Unusually high vane pass vibrations and discharge pressure pulsations	
2×	Shaft vibrations much stronger than housing vibrations, and approach or exceed bearing clearance	Volute eccentricity, Looseness in bearing support or cracked shaft
	Decrease in shaft first bending natural frequency	
	Other multiples of running speed may be stronger than usual	
2×	Shaft vibrations stronger than housing	Torsional excitation
	Strong torque pulsations	
2×	Axial vibrations are more that $\frac{1}{2}$ of Horizontal or Vertical	Pump/driver misalignment at the coupling
	1x vibrations are also high	
	Bearing oil temperature is high	
Number of Impeller Vanes Times Running Speed (m*X)	Both shaft and housing vibrations high	Volute too close to impeller OD due to design (B-gap) or excessive rotor eccentricity
	Reasonably low discharge pressure pulsations	
m*X	Housing vibrations much higher than shaft vibrations	Piping mechanical resonance at vanepass
m*X	Discharge pressure pulsations high at vane pass frequency high	Acoustic resonance in discharge pipe
	Suction pressure pulsations reasonably low	

(*Continued*)

LIBERTY EXHIBIT 1017, Page 260

TABLE 2 Pump vibration troubleshooting list (*Continued*)

Multiples of Rotational Speed	Other Symptoms	Probable Causes
m*X	Suction pressure pulsations also high	Acoustic resonance in suction pipe
m*X	Pump rotor or casing natural frequency close to vane pass	Resonance
Several multiples of running speed (1×, 2×, etc.)	Orbit shows sharp angles or shows evidence of "ringing"	Internal rub or poorly lubricated gear coupling
	Spectrum shows evidence of exactly $\frac{1}{2}$ or $\frac{1}{3}\times$ response	
	Grinding noises and speed changes may be evident	
Several multiples of running speed (1×, 2×, etc.)	Orbit is "fuzzy" but does not pulse or "ring"	Jammed, clogged, or damaged seal
	Seal coolant flow is unexpectedly high or low, and may exhibit high temperature	
	Spectrum may also exhibit $\frac{1}{3}$ or $\frac{1}{2}$ running speed	
Several multiples of running speed (1×, 2×, etc.)	Orbit pulses, usually in one direction much more than the other	Shaft support looseness, especially in bearing insert or cap retention.
	Shaft vibrates more than housing	
Several multiples of running speed (1×, 2×, etc.)	Shaft orbit fairly steady	Looseness in pump casing, pedestal, or foundation.
	housing vibrates more than shaft	
	Often combined with vibration response over a broad range of frequencies below running speed	

LIBERTY EXHIBIT 1017, Page 261

Number of Bearing Rolling Elements (Nb) times about $\frac{1}{2}$ Rotor Speed N	freq f = 0.4 Nb*N/2 approx	Defect Bearing Outer Race
	freq f = 0.5 Nb*N/2 approx	Defect in Ball or Roller
	freq f = 0.6 Nb*N/2 approx	Defect in Inner Race
2 times line frequency	Very directional	Motor Stator Eccentricity
2 times line frequency	Very directional	Shorted stator lamination (induces thermal eccentricity)
	Increases as motor operates (warms up)	
2 times line frequency	Pulsing vibration 2× LF and closest harmonic of running speed	Motor Rotor Eccentricity
	Also pole pass sidebands around running speed, pole pass frequency = slip frequency * number of poles	
2 times line frequency	Sidebands at $\frac{1}{3}$× LF	Loose or broken phase connection
Rotor bar pass frequency	2× LF sidebands around rotor bar pass frequency (RBPF)	Loose or Open Rotor Bars
	Often higher 2× RBPF than 1× RBPF	

LIBERTY EXHIBIT 1017, Page 262

narrow down potential causes. This list can serve as a guide for additional measurements or in some circumstances may even lead directly to the root cause and solution.

Vibration testing to determine pump mechanical health is similar in nature to the "chest rapping" and "heart and lung listening" tests that a physician performs during a physical. Comparing to established norms the amplitude and frequency resulting from chest impacts and from your naturally occurring pulse and aspiration, the doctor diagnoses your condition. When vibration field problems occur, analogous testing can be performed, for example, signature analysis can determine the frequencies which are most strongly excited, suggesting possible root causes to someone familiar with the vibration characteristics of the pump internal components and the systems to which the pump is attached. Following signature analysis, experimental modal analysis (EMA) has proven its ability to separately determine the excitation forces and the natural frequencies of the pump system.

Troubleshooting Techniques The following measurements are suggested as a minimum for predictive maintenance or vibration troubleshooting of any style pump :

1. What the vibration level is on both bearing housings on pump, and on the pump-side (i.e., "inboard") bearing housing on driver in the vertical, horizontal, and axial directions.
2. How hydraulic performance compares to design. In other words, for a given speed and capacity (i.e., flow rate), how close is the head of the pump to the curve supplied by the manufacturer, especially near the design or best efficiency point (BEP)? Are the head and capacity steady when the operator tries to hold the pump at a constant speed? Is the motor or steam turbine driver required to provide more power than expected?
3. What the bearing shell or lubricant exit or sump temperatures are.
4. Whether the suction pressure is steady at a given operating point, and well above NPSH requirements.
5. Whether unusual noises are present at certain operating conditions, and if so, what their main frequencies are.

For high energy multistage pumps, particularly, the following measurements are also recommended:

1. Vibration of the shaft relative to the housing near each bearing, using proximity probes permanently installed in each bearing housing to monitor vertical, horizontal, and axial displacement and vibration.
2. What the monitored leakage rates and exit temperatures are in the thrust balancing device (if any) leak-off line and seal coolant feed or lubrication lines (if any).
3. Whether any unexpected wear particles or pumpage contamination are detectable in samples taken of the lubricant on a regular basis.
4. What the pump shaft and casing natural frequencies are, and what the vibration response to a unit load near the bearings is at these frequencies, as determined by experimental modal analysis.

Recognizing and Solving Vibration Problems Probably 90% of all pump vibration problems can be solved by careful balancing of the rotor assembly, alignment of the coupling when the system is at its rated conditions (especially if it is hot), for example, per Dodd, and running the pump within the bounds of its specified head versus capacity curve.[20] Remaining pump vibration problems are generally due to a resonance of a system natural frequency with one of the excitation forces common to all pumps, such as residual unbalance. During resonance, the rotor vibrations can exceed clearances, or excessive bearing loads can occur, even if unbalance, misalignment, and hydraulic loads are within normally acceptable limits.

In the case of resonance, simple trial-and-error field fixes, such as addition of clamped weights or brace-stiffening of the apparently offending portions of the structure, can often

LIBERTY EXHIBIT 1017, Page 263

be effective. However, if such "fixes" only shift the problem to a slightly different frequency, and cannot be made effective within a reasonable period of time, it is important to stop cut-and-try and answer the following questions :

1. Are the excitation forces within normally acceptable limits?
2. What are the natural frequencies of the rotating and stationary parts of the pump and attached structures when they are assembled as a system, and have they changed?
3. What are the excitation force frequencies in the actual installation, and do they coincide with the any of the assembled system natural frequencies?
4. If there is a vibration problem due to excessive excitation force or a resonance, how can the pump or system be changed most easily to solve the problem? In testing for resonance, typical vibration test locations include the bearing housings, the casing, the pedestal or baseplate near the pump attachment bolts, the baseplate near the foundation bolts, the nearby foundation and piping, and any already instrumented or exposed portion of the pump shaft including the driver coupling.

In performing vibration troubleshooting, generalized charts matching symptoms to possible causes can be useful for many typical or simple problems. However, do not rely too heavily on such lists, especially if their initial application does not lead to immediate resolution of the problem. Persistent pump vibration problems are usually due to an unexpected combination of factors, some of which are specific to the particular pumping system, like mechanical or acoustical piping resonances, or hot running misalignment of the pump/driver due to thermal distortions of the piping or baseplate. With this warning, a list of some of the more common pump vibration symptoms and their causes is given in Table 2. The list is *not* meant to be all inclusive, and is in the order of the frequency value observed, not in order of likelihood or importance to reliability. Definitions useful in reading this list are:

Runout: False vibrations picked up by a proximity probe, actually reflecting shaft scratches, gouges, undulations, and so on, or static shaft bends or misalignment ("mechanical runout"), or eddy current sensitivity variations along the shaft surface or instrumentation noise ("electrical runout"). This can be determined by observing the apparent shaft orbit when the shaft is slowly turned.

Inboard: The coupling side of the pump or driver.

Outboard: The "nondriven" end of the pump or driver opposite to the coupling.

Narrowband: Vibration response which is at a single frequency.

Broadband: Vibration response which covers a band of frequencies on a spectrum plot.

Puzzle Approach It is often not possible to measure the behavior of the entire pump from measurements on the accessible portions of the pump. In such cases, knowledge of the pump and system can be used in conjunction with the available vibration data to "puzzle through" likely causes of the vibration problem. For instance, it is difficult to measure the rotor deflections at the many locations along the span of the rotor in a multistage pump. However, the deflected shape of the rotor at key frequencies can be deduced from measurements at the bearing locations (to identify natural frequencies of lateral rotor modes) when combined with rotordynamic calculations for the rotor system.

A time-proven technique for identifying and solving many problems is to determine the offending excitation sources and the natural frequencies of the structure and rotor. Knowledge of both helps an engineer or technician to determine if the vibration problem is a result of an abnormally high excitation force as would be expected from rotor imbalance, or a result of a normal excitation force which is being amplified by a nearby natural frequency. The symptom is the same in either case, but the means of fixing the problem (not just alleviating the symptom and allowing it to return later) is significantly different. In the case of an abnormally high 1× excitation force, correcting the balance of the rotor may be a suitable solution. In the case of amplification from a natural frequency, balance of the rotor will be a short-lived solution which will permit the vibrations

LIBERTY EXHIBIT 1017, Page 264

to increase to unacceptable levels as the rotor wears or deposits accumulate and the imbalance returns.

Complementary Measurements Many problems manifest themselves as mechanical vibration in pumps, but effectively troubleshooting them often requires measurements in addition to the external structural vibration. Measurements which help to define the cause of the vibration are dynamic pressure measurements in the suction and discharge piping, acoustic measurements, thermography, static and dynamic torque measurement, oil or grease analysis, and electric current spectral analysis. These complementary measurements can identify abnormally high pressure pulsations in the suction or discharge, acoustic resonance in the piping, high torque pulsations resulting from electrical problems, and other unexpected difficulties.

Oil Monitoring Analysis A new technology has reached maturity recently known as oil monitoring analysis.[21] This involves monitoring the condition of the bearing lubricant, both to determine whether the lubricant needs replacing, as well as to use the lubricant as a "telltale" of whether there are problems in the pump or its driver. Typical methods include chemical analysis and the observance of the amount of particulates in the flow. Chemical analysis can consist of determining the oil's total acid number TAN or total base number TBN (determines if the antioxidation capability of the oil has degraded, implying excessive temperature in the bearing), running a spectroscopic analysis in which the atomic spectra of the small particles and other constituents in the oil are examined (determines if bearing metal is flaking off, or if dirt or contaminants are entering the oil), or running a water-detection test such as a Karl Fischer test. Particulate analysis can take the form of observing the degree to which light is blocked by a lubricant sample (implies how many particles are in the oil), or can consist of "ferrography" in which metal particles are collected from the flowing oil by a magnetic strip, and examined under a microscope for shape, size, and color. Other specialty tests are possible, from the intuitive (smell and color) to the very sophisticated (electron microscope examination of wear particles).

Oil analysis is better than vibration for picking up the early stages of lubrication or wear problems in rolling element bearings or gears, or for detecting severe misalignment where each rotor is "pinned" against its bearing housing by the misalignment forces.

Thermography Thermography involves mapping out the surface temperatures on a machine or system component, looking for lack of symmetry where symmetry should exist, for example, around the periphery of a bearing housing.[22] It can be a very sensitive method of discovering particular problems. In the case of the bearing housing, for example, if a heavy misalignment were present, a hot spot would be observed on one side of the pump bearing housing, and a hot spot would be also observed on the opposite side of the driver bearing housing. Thermography is most easily implemented using thermally sensitive video equipment, but infrared cameras are still very expensive, particularly if temperatures are shown in color rather than as shades of gray. Although it takes a little more time, exactly the same information is available for a much smaller budget by plotting on paper the readings from a surface thermometer, surface thermocouple, or an inexpensive infrared gun. In the case of either a $40,000 infrared camera or a $200 infrared gun, be careful that what is being detected is emitted radiation, which depends not only on the true temperature, but also on the emissivity of the surface, typically about 1.0, but which can decrease up to about a factor of 2 depending upon amount dirt, roughness of the surface, and whether the surface has been freshly painted. If readings are taken off a piece of material (e.g., fresh duct tape) firmly pasted on the surface rather than from the surface itself, problems with this issue can be avoided.

Electric Current Spectrum Monitoring Oak Ridge National Laboratory (ORNL) and the U.S. Navy pioneered this method. It involves observing output from an oscilloscope or FFT analyzer at the output from an inductive "clamp-on" electric current probe, that is attached in an encircling manner around a motor phase lead.[22] The evaluation is like

interpreting a vibration spectrum, such that whatever frequencies show up strongly in the current are assessed relative to whether they are too high in current, and if so what would physically cause this. The most common problem frequencies are induction motor 2× slip frequencies (including 1× speed +/– 2× slip "sidebands"), of course the line frequency, twice the line frequency, the rotor bar passing frequency, and the stator slot passing frequency. Broken rotor bars, for example, lead to increased slip sidebands and stronger levels of slotpass. Theoretically, faults in the pump that affect the motor torque and therefore current should also be evident in the spectrum, but generally vibration is more sensitive for pump problem detection.

Operating Deflection Shapes A very useful modern troubleshooting method is called operating deflection shape (ODS) analysis. In this method, vibration is detected by probe signals fed into an FFT analyzer, where the data are taken in three orthogonal directions at all representative locations on a pump and its relevant system (baseplate, nearby piping, driver, exposed shafting). The data are taken such that, as probes are "roved" over the pump and system during different portions of the test, one reference probe is always left at the same location and direction, to allow "phasing" (timing) of when the motion peaks in one group of test points versus another. The resulting database is plotted as an animation that exaggerates the scale of the motion, so that it is easy to make physical interpretations of causes for high vibration at a certain frequency. For example, a high pump versus motor out-of-phase oval motion may be observed at a frequency of 2× running speed, indicating misalignment.

Experimental Modal Analysis or "Bump" Testing It is possible that, in spite of competent preinstallation vibration analysis, complicated vibration problems may still occur in the final installation due to, for instance, idiosyncrasies in foundation material properties or in bolted joint behavior, inaccurate mass information supplied by motor or drive manufacturers, or an accidental defect in materials or workmanship. If the standard field service troubleshooting procedures of the pump manufacturer are not effective within a reasonable period of time, then modal analysis testing can be used to understand such problems quickly, particularly when combined with ODS. In addition, some form of modal analysis, using known exciting forces, such as from a calibrated impact hammer, should be used at the time that the pump and piping installation is completed to verify that the frequency versus excitation force frequency margins of structural vibration modes closest to 1×, 2×, and vane pass frequencies meet acceptance standards. If problems exist, modal analysis software can be used to extend the experimentally based model with "what-if" proposed bracing or other modifications (called structural dynamics modification) should be used to determine practical solutions. However, exercise care:

- Modal analysis testing requires skill and experience to be applied usefully to pumps and pumping systems. Proof of such capability should be supplied by the agent who will perform the test.
- The modal analysis test should include at least 50 locations (usually with three orthogonal directions at each location) of the response probes, including the corners of the baseplates, the foundation floor and pedestal, key segments of the pump stationary structure (e.g., vertical pump discharge head flanges, horizontal pump bearing housings and casing ends, driver housing ends), and the nearby attached piping and other important structural details.
- The test should include a means for discriminating between apparent modal response caused by undocumented pump operational forces and environmental background vibrations, and the actual modal response due to the documented artificial excitation forces of the modal test.

In experimental modal analysis (EMA), a known force (constant at all frequencies within the test range) is put into a pump, and the pump's vibration response exclusively due to this force is observed and analyzed. EMA can determine the vibration characteristics

of pumps either on the test stand or in the field. The actual natural frequencies of combined casing, piping, and supporting structure can be obtained, and if time-averaging data collection procedures are used, EMA can also determine the rotor natural frequencies at the pump operating conditions. Separately, the frequencies of strong excitation forces within the pump can be estimated by comparing the vibration versus frequency spectrum of the pump's EMA artificial force response to the signature analysis spectrum of the pump's response to the naturally occurring forces from within the pump and from its attached system and environment. Figure 22 shows how the broadband "terrain" or peaks and valleys from an EMA impact test, when amplitude is plotted logarithmically to accentuate low level response and put it on the same footing as the largest response frequencies, can be used to better understand whether the high vibrations are caused by the amplifying effect of a natural frequency, or are just due to an excessive oscillating force. Knowing this allows a troubleshooter to focus on the root cause, and provide a fundamental fix.

The main tools required to do EMA are a multichannel FFT frequency analyzer, a computer with specialty software, a set of vibration response probes such as accelerometers

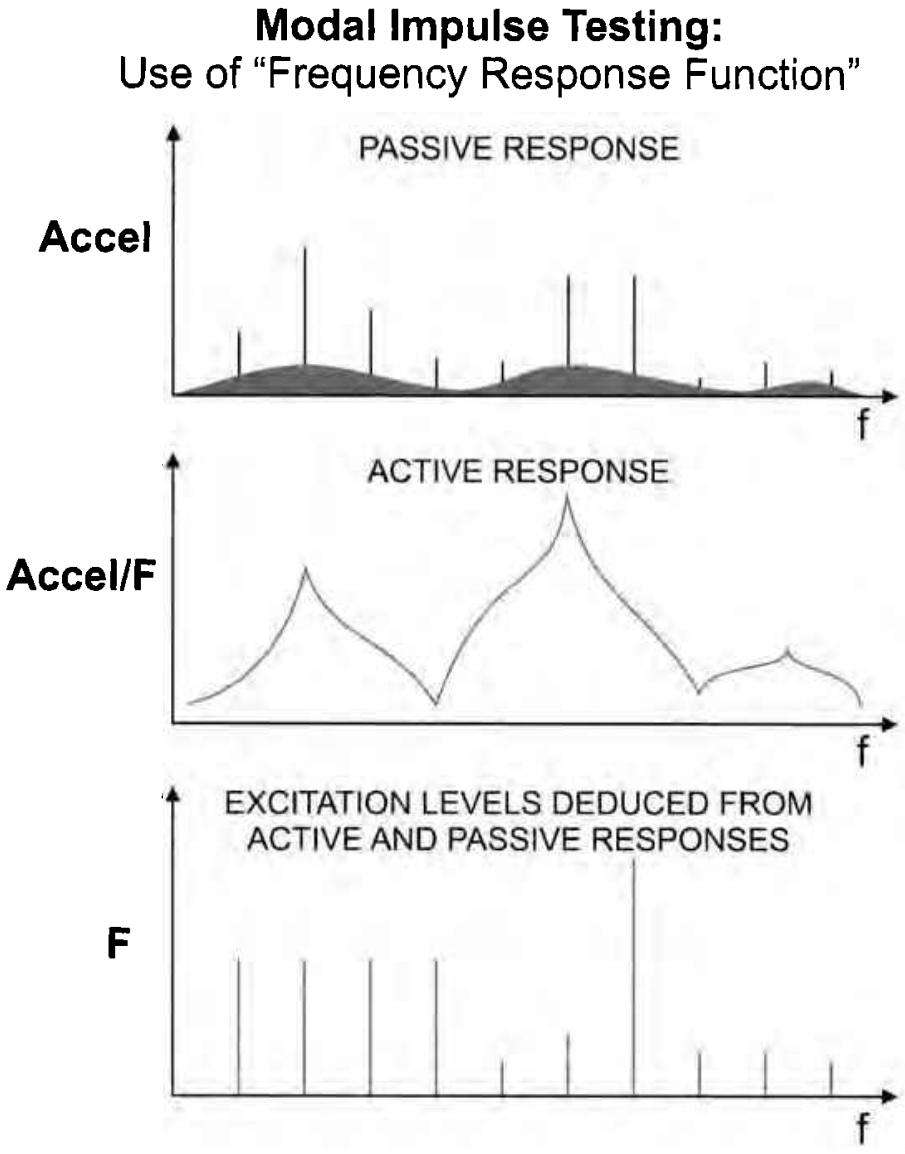


FIGURE 22 Vibration frequency spectrum dependence of natural frequencies and forces F (Mechanical Solutions, Inc.)

LIBERTY EXHIBIT 1017, Page 267

or proximity probes, and a load-cell-instrumented impact hammer designed to spread its force over a frequency range which covers the test range, as if the results of a number of shaker tests were combined.

The impact hammer should have an accelerometer load cell in its head which is calibrated to indicate the force being applied. During an EMA test, the signal from the hammer input force accelerometer is sent to one channel of the spectrum analyzer, and the signals from the vibration response probes are sent to the other channels. Dividing, at each frequency, the response channels by the impulse force channel gives the "frequency response function" (FRF) of the pump and its attached system. The peaks of the FRF are the noncritically damped natural frequencies, and the width and height of the peaks indicate the damping of each natural frequency, and how sensitive vibration at the test location is to forces which occur in the vicinity of the hammer impact at frequencies near a given natural frequency. The details of classical modal analysis and its application are given by Ewins.[23]

A variation of EMA has been developed by Marscher to achieve useful results within the time and operational constraints of actual field tests. This technique is known as time averaged pulse (TAP™). The method statistically reorganizes the data obtained from modal analysis in order to reliably determine structural natural frequencies and mode shapes, resonating force locations and frequencies, and rotor critical speeds, with all testing performed while the pump remains operating at the problem running condition. The method then uses classical modal analysis processing techniques to produce an animated model of each natural frequency's vibration pattern, and to make predictions about the effectiveness of proposed design changes, such as stiffer bearings, new piping supports, or a thicker baseplate. The TAP™ method may be applied to machines at any operating speed and load.[24,25,26]

Determining the critical speeds of a pump rotor by impacting while the pump is operating at the condition of interest provides an alternative to the current practice of basing critical speeds on the peaks of "waterfall plots" of spectra obtained during pump start-ups or shutdowns. Waterfall plots can poorly represent pump rotor dynamic performance during steady state operation due to the strong sensitivity of annular seal stiffness and damping to operating conditions. The primary reason that pump natural frequencies are sensitive to operating condition is the Lomakin effect, which can significantly change the rotor support stiffness and damping, depending upon the pump's speed and load. The strong dependence on speed of a large fraction of the rotor support stiffness leads to differences between the frequencies of peaks in the transient waterfall plot and actual natural frequencies at steady state operating conditions of interest. This error is greater in pumps than in compressors and gas turbines, where circumferential variation in the seal static pressure does not get as high and therefore waterfall plotting has enjoyed success.

The analytical counterpart of the waterfall plot is the Campbell diagram, which plots vibration excitation frequency versus running speed. Since the strongest vibration excitations in pumps usually occur at integer multiples of the running speed, these are plotted on the diagram as diagonal lines emanating from the plot origin. Likewise, roughly horizontal lines are plotted for the first several calculated rotor natural frequencies. Intersections of excitation and natural frequency curves are marked by circles of radius equal to 10% of the frequency at which the intersection occurs. If any part of any circle lies between two vertical lines which represent the minimum and maximum running speeds, then a resonance is predicted, requiring steps to shift the problem natural frequency, increase its damping until it is critically damped, or eliminate the exciting force.

PROGNOSIS: DETERMINING PROBLEM SEVERITY

Physical Relationship between Vibration and Damage Figures 23 and 24 show typical failure modes and associated frequencies in a representative pump style. The point of these figures is not to be all inclusive of pump problems, but to show major issues, and how the problem relates to the resulting vibration.

LIBERTY EXHIBIT 1017, Page 268

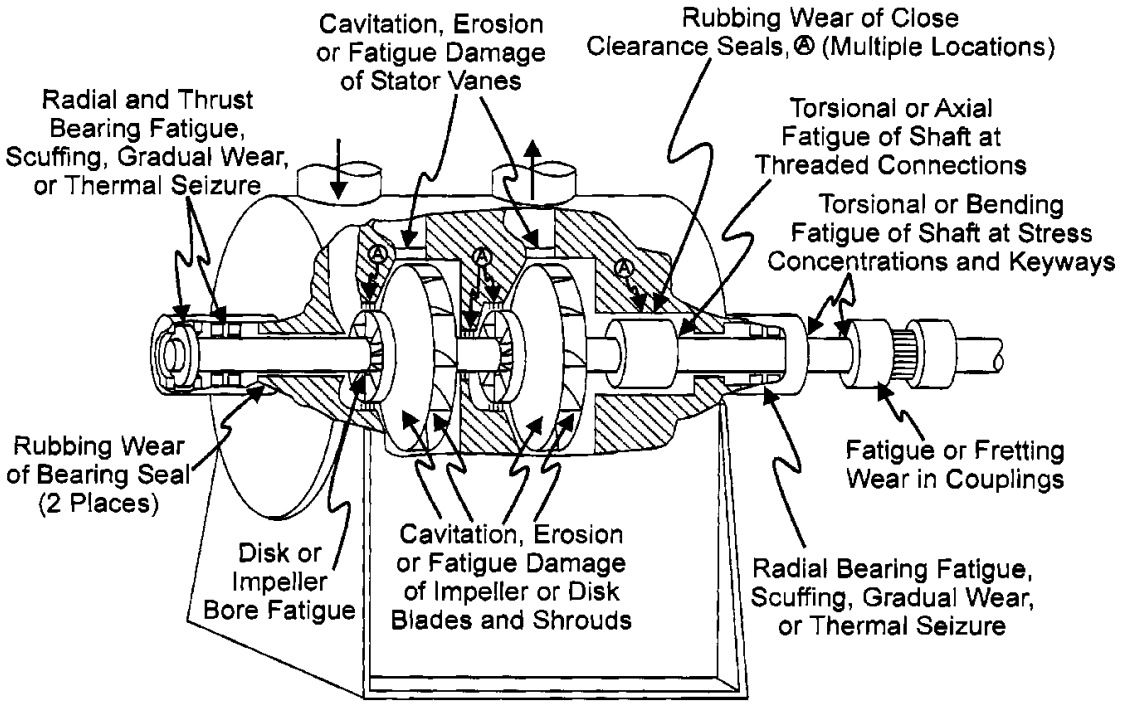


FIGURE 23 Horizontal pump symptoms of typical hydraulic or mechanical problems (Mechanical Solutions, Inc.)

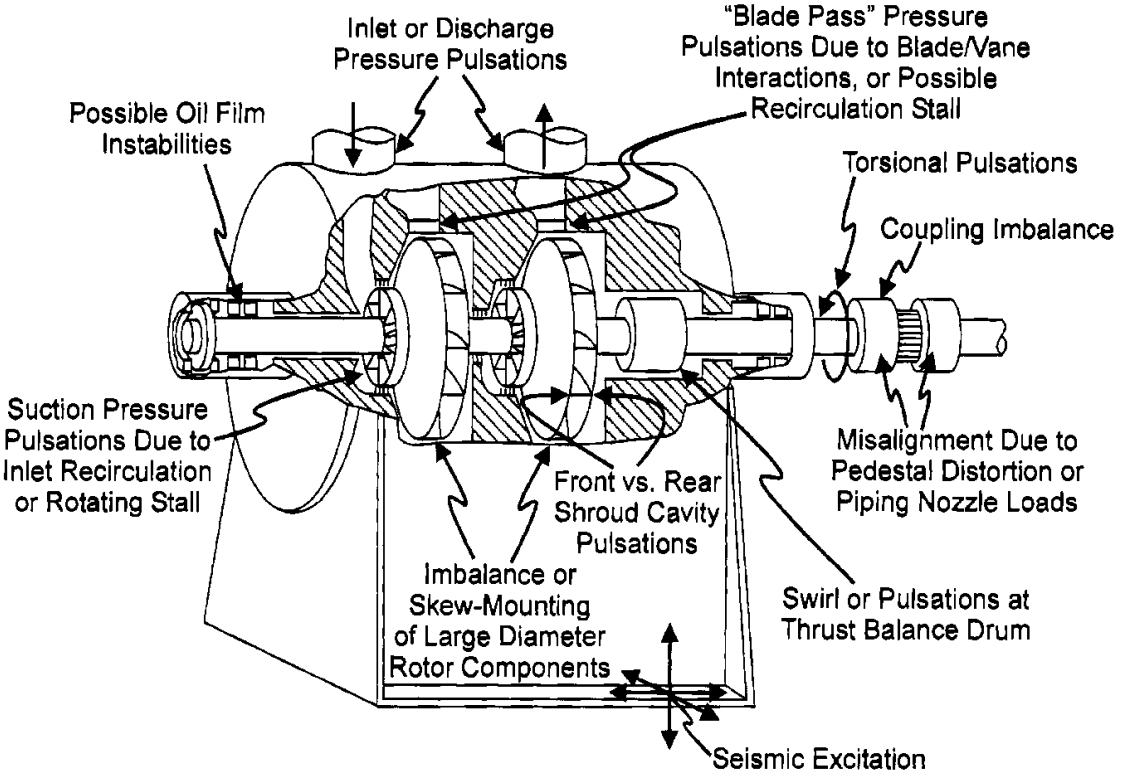


FIGURE 24 Typical frequencies associated with pump failure modes (Mechanical Solutions, Inc.)

CONCLUSION

Machinery issues such as the effects of nozzle loads and procedures for checking acceptability of vibration can seem deceptively simple. In reality, it takes education and experience to reach the correct conclusion relative to the many interrelated issues associated with choosing and operating a centrifugal pump.

ACKNOWLEDGMENTS

The authors would like to that their company, Mechanical Solutions, Inc., for use of the figures and tables presented in this section. Thanks also to Michael Marscher who crafted most of the figures and helped with document formatting, and to the company technical staff for many of the analysis methods, test procedures, and examples provided. Thanks also to the group of companies the authors have been employed by in various positions, pursuing the work of the type discussed, and to the end-user customers on whose equipment much of the experience reflected in this section was gained.

REFERENCES

1. Makay, E., Szamody, O. *Recommended Design Guidelines for Feedwater Pumps in Large Power Generating Units*. EPRI Rpt CS-1512, Sept 1980.
2. API 610, 10th ed., Amer. Pet. Instit., Washington, DC, c. 2004.
3. Lomakin, A. A. "Calculation of the critical speed and the conditions to ensure dynamic stability of the rotors in high pressure hydraulic machines, taking account of the forces in the seals" (in Russian). *Energomashinostroenie*, Vol. 14, No. 4, 1958, pp. 1–5.
4. API 684, 1st ed., Tutorial on the API Standard Paragraphs Covering Rotor Dynamics and Balancing: An Introduction to Lateral Critical Speed and Train Torsional Analysis and Rotor Balancing, c. 1996.
5. Reichert, Hall, Woods. *Vibrations of Soils and Foundations*. Prentice-Hall, c. 1970.
6. Timoshenko, S., Woinowsky-Krieger, S. *Theory of Plates and Shells*, 2nd ed. McGraw-Hill, New York, c. 1959.
7. Blevins, R. D. *Formulas for Natural Frequency and Mode Shape*. Robert Krieger Publishing Co., Malabar, FL, c. 1984.
8. Roark, R. J., and Young, W. C. *Formulas for Stress and Strain*, 5th ed. McGraw-Hill, New York, c. 1975.
9. Agostinelli, A., Nobles, D., and Mockridge, C. R. "An Experimental Investigation of Radial Thrust in Centrifugal Pumps," *J. Engrg. for Power, Trans ASME*. Vol. 82, 1960.
10. API 541, 4th ed., Form-Wound Squirrel-Cage Induction Motors—500 HP and Larger, c. 2004.
11. Marscher, W. D. "The Effect of Fluid Forces at Various Operation Conditions on the Vibrations of Vertical Turbine Pumps." *Proceedings of the IMechE, Radial Loads and Axial Thrusts on Pumps*, Feb. 5, 1986.
12. Downham, E. "Theory of Shaft Whirling, No. 5—The Influence of Plain Bearings on Shaft Whirling." *The Engineer*. Nov. 8, 1957.
13. Yamamoto, T. "On the Critical Speeds of a Shaft." *Memoirs of the Faculty of Engineering*, Vol. 6. Nagoya University, Japan, Oct. 1954.
14. HI/ANSI Standards, 2000 Edition, The Hydraulic Institute, Parsippany, NJ, c. 2000.
15. Rathbone, T. "Vibration Tolerance." *Power Plant Engineering*, Vol. 43, Nov. 1939.

LIBERTY EXHIBIT 1017, Page 270

16. Blake, M. "New Vibration Standards for Maintenance." *Hydrocarbon Processing and Petroleum Refining.* January 1964.
17. Baxter, R. L., and Bernhard, D. L. "Vibration Tolerances for Industry." ASME 67-PET-14, 1967.
18. Hancock, W. P. *How to Control Pump Vibration. Hydrocarbon Processing.* March 1974.
19. ISO 1940, "Mechanical Vibration—Balance Quality Requirements for Rotors in a Constant (Rigid) Shape, Rev. 2." International Standards Organization, c. 2002.
20. Dodd, V. R. *Total Alignment.* The Petroleum Publishing Co., Tulsa, OK, c. 1974.
21. STLE. "Suggested Reading Material for the Oil Monitoring Analyst Exam." 2007. www.stle.org/oma/read.cfm.
22. Marscher, W. D. "Vibration Chapter and Predictive Maintenance Chapter." *STLE Tribology & Lubrication Handbook.* STLE Park Ridge, IL, 1997.
23. Ewins, D. J. *Modal Testing: Theory and Practice.* Research Studies Press, Wiley, New York, c. 1984.
24. Marscher, W. D. "Determination of Pump Rotor Critical Speeds During Operation through Use of Modal Analysis." *Proceedings of the ASME 1986 WAM Symposium on Troubleshooting Methods and Technology.* Anaheim, CA, Dec. 1986.
25. Marscher, W. D. "How to Use Impact Testing to Solve Pump Vibration Problems." *Proceedings of the EPRI Power Plant Pumps Symposium.* Tampa, FL, June 1991.
26. Marscher, W. D. "The Determination of Rotor Critical Speeds While Machinery Remains Operating through Use of Impact Testing." *IMAC Conf.* Orlando, FL, SEM, Feb. 1999.

FURTHER READING

Allaire, P. E. et al. "Dynamics of Short Eccentric Plain Seals with High Axial Reynolds Number." *J. Spacecraft AIAA.* Vol. 15, No. 6, c. 1978.

API 686, 1st ed., Recommended Practices for Machinery Installation and Installation Design, c. 1996.

Arndt, N., Acosta, A. J., Brennen, C. E., and Caughey, T. K., "Rotor-Stator Interaction in a Diffuser Pump." NASA Tech Briefs, MFS-26092, March 1979. (Presented at the Gas Turbine and Aero Exposition, June 5–9, 1988, Amsterdam, The Netherlands).

Black, H. F. "Effects of Fluid-Filled Clearance Spaces on Centrifugal Pump Vibrations." *Eighth Turbomachinery Symposium.* Texas A&M University, c. 1979.

Bolleter, U. *Blade Passage Tones of Centrifugal Pumps, Vibrations.* Vol. 4, No. 3, Sept 1988, pp. 8–13.

Bowman, D., Marscher, W., and Reid, S. "Pump Rotor Critical Speeds: Diagnosis and Solutions." *Proceedings of the International Pump Symposium,* Texas A&M University, April 1990.

Chen, Y. N. "Rotating Stall in Radial Compressors and Pumps as Rossby Waves Associated with Transient Vortices." *Sulzer Technical Review,* Jan. 1990, pp. 51–56.

Childs, D. "Finite Length Solutions for Rotordynamic Coefficients of Turbulent Annular Seals." *ASME/ASLE Lubrication Conf.,* ASME Paper 82-LUB-42, Oct. 1982.

Childs, D., and Moyer, D. "Vibration Characteristics of the HPO Turbopump of the SSME." *ASME J. of Engineering for Gas Turbines and Power,* Vol. 107, Jan. 1985, pp. 152–159.

Corely, J. E. "Vibrational Problems of Large Vertical Pumps and Motors." *Proceedings of the Ninth Turbomachinery Symposium.* Texas A&M University, 1980.

Crease, A. B. *Design Principles and Lube of Gear Couplings, Int'l Conf on Flexible Couplings.* IMechE, July 1977.

LIBERTY EXHIBIT 1017, Page 271

Eshelman, R. L. "The Role of Sum and Difference Frequencies in Rotating Machinery Fault Diagnosis." The Institution of Mechanical Engineers, C272/80, Second International Conference, Vibrations in Rotating Machinery, 1980.

Franz, R., Acosta, A. J., Brennen, C. E., and Caughey, T. K. "The Rotordynamic Forces on a Centrifugal Pump Impeller in the Presence of Cavitation." *Transactions of the ASME J. of Fluids Engineering*, Vol. 112, Sept. 1990, pp. 264–271.

France, D. "Rotordynamics Considerations in the Design of High Speed Centrifugal Pumps." *Proceedings of the Indian Pump Mfrs. Assn.*, March 1987.

Gopalakrishnan. *Critical Speed in Centrifugal Pumps.* ASME 82-GT-277, c. 1982.

Guelich, J. F., Bolleter, U. "Pressure Pulsations in Centrifugal Pumps." *Transactions of the ASME J. of Vibration and Acoustics*, Vol. 114, April 1992, pp. 272–279.

Gunter, E. J., and Li, D. F. *Unbalance Response Analysis of Dual Rotor Systems.* University of Virginia Report No. UVA/643092/MAE81/138, Charlottesville, VA, March 1978.

Harris, C. M., and Crede, C. E. *Shock and Vibration Handbook*, 4th ed. McGraw-Hill, New York, c. 1995.

Hergt, P., Krieger, P. "Radial Forces in Centrifugal Pumps with Guide Vanes." *Proceedings of the IMechE*, Vol. 184, Pt. 3N, 1970.

Japikse, D. J., Marscher, W. D., et al. *Centrifugal Pump Design and Performance.* Publ. Concepts NREC,Wilder, VT, c. 1997.

Jen, C.-W., and Marscher, W. "Experimental Modal Analysis of Turbomachinery Rotors Using Time—Averaging." *Proceedings of the International Modal Analysis Conference.* Orlando, FL, Jan. 26, 1990.

Jery, B., Acosta, A., Brennan, C., Caughey, T. "Hydrodynamic Impeller Stiffness, Damping, and Inertia in the Rotordynamics of Centrifugal Flow Pumps." *Proceedings of the Rotordynamic Instability Problems in High Speed Turbomachinery.* Texas A&M University, 1984.

Jones, R. M. "Rolling Element Bearing Status Using Frequency Analysis." *Tutorial in Proceedings of the TAMU International Pump Symposium.* Houston, TX, Mar. 2000.

Kovats, A. "Vibration of Vertical Pumps." *ASME Journal of Engineering for Power,* April 1962.

Marscher, W. D. "Structural Design and Analysis of Modern Turbomachinery Systems, Chap. 7." *Sawyer's Gas Turbine Engineering Handbook*, 3rd ed., Vol. I. Turbomachinery Publications, Norwalk Ct, c. 1985.

Marscher, W. D. "The Relationship Between Pump Rotor System Tribology and Appropriate Vibration Specifications for Centrifugal Pumps." *Proceedings of the IMechE Third European Congress on Fluid Machinery for the Oil and Petrochemical Industries.* The Hague, Netherlands, May 1987.

Marscher, W. D. Subsynchronous Vibration in Boiler Feed Pumps Due to Stable Response to Hydraulic Forces at Part Load." *Proceedings of the IMechE Conference on Part Load Pumping Control and Behavior.* Edinburgh, Scotland, Sept. 1988.

Marscher, W. D. "Analysis and Test of Multistage Pump Wet Critical Speeds." *ASLE/ASME Joint Tribology Conference.* Ft. Lauderdale, FL, Oct. 1989.

Marscher, W. D., "The Effect of Variable Frequency Drives on Vibration Problems in Vertical Pumps." *Proceedings of the Water & Wastewater Conference.* Barcelona, Spain, April 1990.

Marscher, W. D. "Vibration Test and Analysis of a Barrel Boiler Feed Pump Exhibiting Non-Synchronous Vibration." *Proceedings of the IMechE Seminar on Vibrations in Pumps.* London, Dec. 1990.

Marscher, W. D. "Bearing Application and Lubrication Chapter." *Modern Marine Engineer's Manual*, 3rd ed. Cornell Maritime Press, Centreville, MD, 1999.

Marscher, W. D. "Avoiding Failures in Centrifugal Pumps." *Tutorial in Proceedings of the TAMU International Pump Symposium.* Houston, TX, Feb. 2002.

Marscher, W. D. "Centrifugal Pump Rotordynamics." *Tutorial in Proceedings of the TAMU International Pump Symposium.* Houston, TX, March 2007.

LIBERTY EXHIBIT 1017, Page 272

Massey, I. "Subsynchronous Vibration Problems in High Speed Multistage Centrifugal Pumps." *Proceedings of the 14th Turbomachinery Symposium*. Turbomachinery Laboratories, Texas A&M University, 1985.

Meyer, R. J. *Solve Vertical Pump Vibration Problems, Hydrocarbon Processing*, Vol. 56, 1977.

Ohashi, H., Sakurai, A., Nishihama, J. *Influence of Impeller and Diffuser Geometries on the Fluid Forces of Whirling Impeller*. N89-22907, 1988 TAMU Instability. Conf., pp. 285–305.

Pace, S. E., Florjancic, S., Bolleter, U. "Rotordynamic Developments for High Speed Multistage Pumps." *Proceedings of the Third Pump Symposium*. Texas A&M University, 1986.

Pottie, K., Bayon, A., De Lope, M. R., Mota, M. "2003, Seismic Analysis on Modified Service Water Pumps." *Proceedings of the TAMU International Pump Symposium*. Houston, TX, March 2003.

Sanks, R. L. *Pumping Station Design*, 2nd ed., Chapter 22 "Vibration and Noise" by J. G. Lilly and W. D. Marscher, Butterworth-Heinemann, Boston, c. 1998.

Sembler, W. J. *Fluid Transfer Devices / Pumps Chapter, Modern Marine Engineer's Manual*, 3rd ed. Cornell Maritime Press, Centreville, MD, 1999.

Smith, J. D. *Gears and their Vibration*. Marcel Dekker, c. 1983.

Thomson, W. T. *Theory of Vibration with Applications*. Prentice-Hall, c. 1981.

Tsujimoto, Y., and Acosta, A. "Theoretical Study of Impeller and/or Vaneless Diffuser Attributed Rotating Stalls and Their Effects on Whirling Instability of a Centrifugal Impeller." *Work Group on the Behaviour of Hydraulic Machinery under Steady Oscillatory Conditions*. Lille, France, Sept. 9–11, 1987.

SECTION 2.2
CENTRIFUGAL PUMP CONSTRUCTION

2.2.1
CENTRIFUGAL PUMPS: MAJOR COMPONENTS

IGOR J. KARASSIK
C. C. HEALD

CLASSIFICATION AND NOMENCLATURE

A centrifugal pump, stripped of all its refinements, has two main parts: (1) a rotating element, including an impeller and a shaft, and (2) a stationary element made up of a casing, casing cover, and bearings.

In a centrifugal pump, the liquid is forced by atmospheric or other pressure into a set of rotating vanes. These vanes constitute an impeller that discharges the liquid at its periphery at a higher velocity. This velocity is converted to pressure energy by means of a volute (see Figure 1) or by a set of stationary diffusion vanes (see Figure 2) surrounding the impeller periphery. Pumps with volute casings are generally called *volute pumps*, while those with diffusion vanes are called *diffuser pumps*. Diffuser pumps were once quite commonly called *turbine pumps*, but this term has become more selectively applied to the vertical deep-well centrifugal diffuser pumps usually referred to as *vertical turbine pumps*. Figure 1 shows the path of the liquid passing through an end-suction volute pump operating at rated capacity (the capacity at which best efficiency is obtained).

Impellers are classified according to the major direction of flow in reference to the axis of rotation. Thus, centrifugal pumps may have the following:

- Radial-flow impellers (see Figures 22, 30, 31, 32, and 33)
- Axial-flow impellers (see Figure 26)
- Mixed-flow impellers, which combine radial- and axial-flow principles (see Figures 24 and 25)

LIBERTY EXHIBIT 1017, Page 274

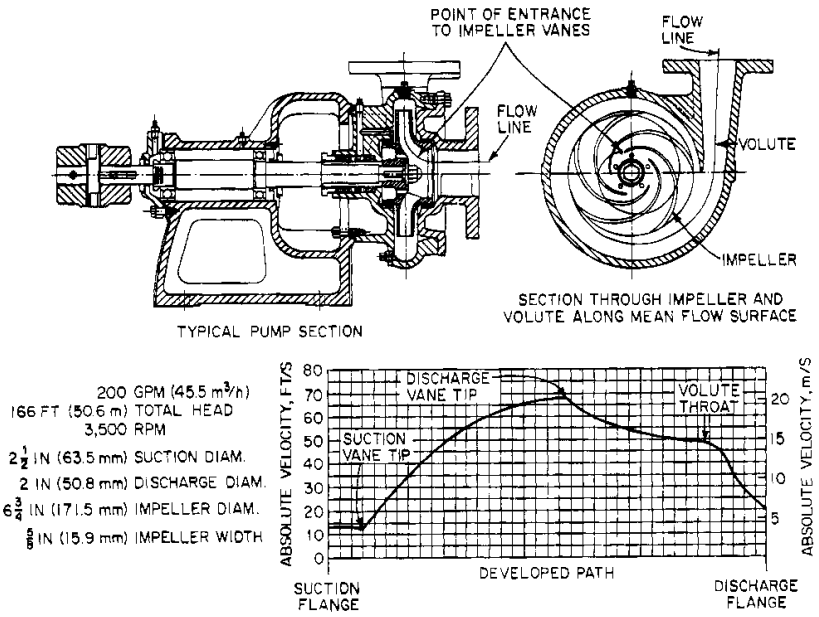


FIGURE 1 A typical single-stage, end-suction volute pump (Flowserve Corporation)

Impellers are further classified in one of two categories:

- Single-suction, with a single inlet on one side (see Figures 22 and 33)
- Double-suction, with liquid flowing to the impeller symmetrically from both sides (see Figures 23, 24, and 34)

The mechanical construction of the impellers gives a still further subdivision into

- Enclosed, with shrouds or side walls enclosing the waterways (see Figures 22, 23, and 24)
- Open, with no shrouds (see Figures 26 and 30)
- Semiopen or semienclosed (see Figure 32)

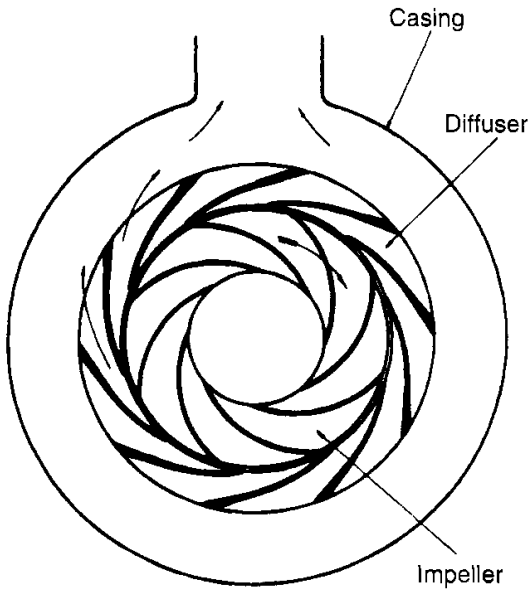


FIGURE 2 A typical diffuser-type pump

A pump in which the head is developed by a single impeller is called a *single-stage pump*. Often the total head to be developed requires the use of two or more impellers operating in a series, each taking its suction from the discharge of the preceding impeller. For this purpose, two or more single-stage pumps can be connected in a series or all the impellers can be incorporated in a single casing. The unit is then called a *multistage pump*.

The mechanical design of the casing provides the added pump classification of *axially split* or *radially split*, and the axis of rotation determines whether the pump is a horizontal or vertical unit.

Horizontal-shaft centrifugal pumps are classified still further according to the location of the suction nozzle:

- End-suction (see Figures 1, 8, 11, and 12)
- Side-suction (see Figures 7 and 10)
- Bottom-suction (see Figure 14)
- Top-suction (see Figure 21)

Some pumps operate in air with the liquid coming to and being conducted away from the pumps by piping. Other pumps, most often vertical types, are submerged in their suction supply. Vertical-shaft pumps are therefore called either *dry-pit* or *wet-pit* types. If the wet-pit pumps are axial-flow, mixed-flow, or vertical-turbine types, the liquid is discharged up through the supporting drop or column pipe to a discharge point above or below the supporting floor. These pumps are consequently designated as *aboveground discharge* or *belowground discharge units*.

Figures 3, 4, and 8 show typical constructions of a horizontal double-suction volute pump, the bowl section of a single-stage axial-flow propeller pump, and a vertical dry-pit single-suction volute pump, respectively. The names recommended by the Hydraulic Institute for various pump parts are given in Table 1.

CASINGS AND DIFFUSERS

The Volute Casing Pump This pump (refer to Figure 1) derives its name from the spiral-shaped casing surrounding the impeller. This casing section collects the liquid discharged by the impeller and converts velocity energy to pressure energy.

A centrifugal pump volute increases in area from its initial point until it encompasses the full 360° around the impeller and then flares out to the final discharge opening. The

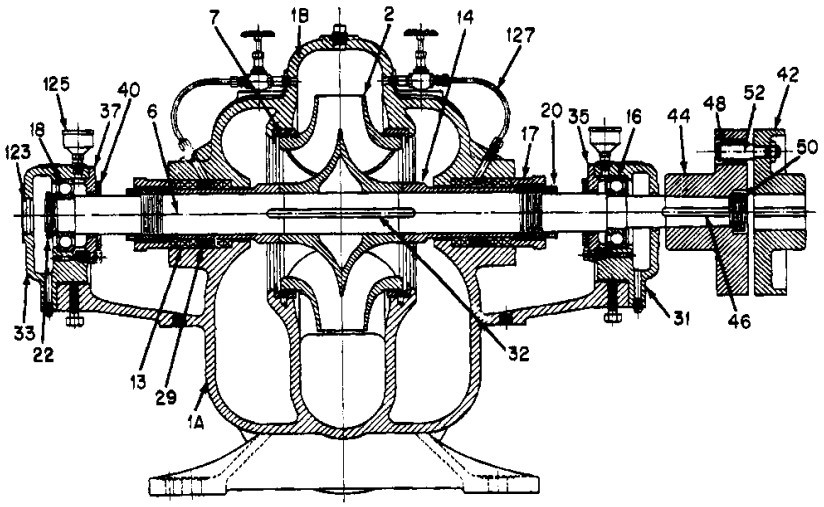


FIGURE 3 Horizontal, single-stage, double-suction volute pump (the numbers refer to parts listed in Table 1) (Flowserve Corporation)

TABLE 1 Recommended names of centrifugal pump parts[a]

Item no.	Name of part	Item no.	Name of part
1	Gasing	33	Bearing housing (outboard)
1A	Gasing (lower half)	35	Bearing cover (inboard)
1B	Gasing (upper half)	36	Propeller key
2	Impeller	37	Bearing cover (outboard)
4	Propeller	39	Bearing bushing
6	Pump shaft	40	Deflector
7	Gasing ring	42	Coupling (driver half)
8	Impeller ring	44	Coupling (pump half)
9	Suction cover	46	Coupling key
11	Stuffing box cover	48	Coupling bushing
13	Packing	50	Coupling lock nut
14	Shaft sleeve	52	Coupling pin
15	Discharge bowl	59	Handhole cover
16	Bearing (inboard)	68	Shaft collar
17	Gland	72	Thrust collar
18	Bearing (outboard)	78	Bearing spacer
19	Frame	85	Shaft enclosing tube
20	Shaft sleeve nut	89	Seal
22	Bearing lock nut	91	Suction bowl
24	Impeller nut	101	Column pipe
25	Suction head ring	103	Connector bearing
27	Stuffing box cover ring	123	Bearing end cover
29	Lantern ring (seal cage)	125	Grease (oil) cup
31	Bearing housing (inboard)	127	Seal pipe (tubing)
32	Impeller key		

[a]These parts are called out in Figures 3, 4, and 8.

wall dividing the initial section and the discharge nozzle portion of the casing is called the tongue of the volute or the "cutwater." The diffusion vanes and concentric casing of a diffuser pump fulfill the same function as the volute casing in energy conversion.

In propeller and other pumps in which axial-flow impellers are used, it is not practical to use a volute casing. Instead, the impeller is enclosed in a pipe-like casing. Generally, diffusion vanes are used following the impeller proper, but in certain extremely low-head units these vanes may be omitted.

A diffuser is seldom applied to a single-stage, radial-flow pump, except in special instances where volute passages become so small that machined or precision-cast volute or diffuser-like pieces are utilized for precise flow control. Conventional diffusers are often applied to multistage pump designs in conjunction with guide vanes to direct the flow efficiently from one impeller (stage) to another in a minimum radial and axial space. Diffuser vanes are used as the primary construction method for vertical turbine pumps and single-stage, low-head propeller pumps (see Figure 4).

Radial Thrust In a *single-volute pump casing* design (see Figure 5), uniform or near uniform pressures act on the impeller when the pump operates at design capacity (which coincides with the best efficiency). At other capacities, the pressures around the impeller are not uniform (see Figure 6) and there is a resultant radial reaction (F). A detailed discussion of the radial thrust and of its magnitude is presented in Section 2.1.3. Note that the unbalanced radial thrust increases as capacity decreases from that at the design flow.

For any percentage of capacity, this radial reaction is a function of total head and of the width and diameter of the impeller. Thus, a high-head pump with a large impeller diameter will have a much greater radial reaction force at partial capacities than a low-head

LIBERTY EXHIBIT 1017, Page 277

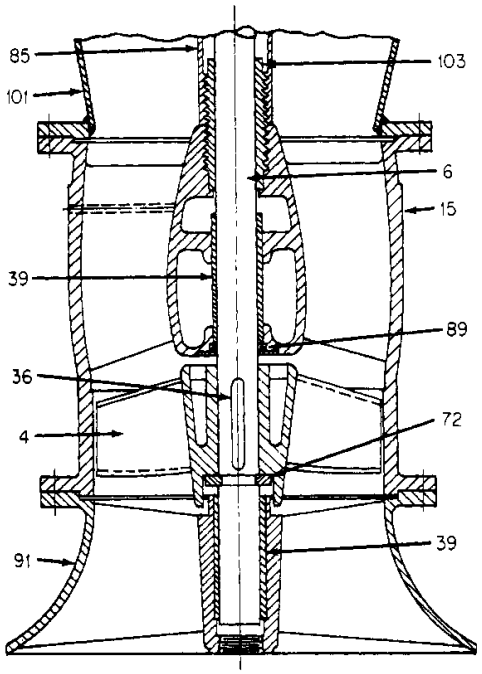


FIGURE 4 Vertical wet-pit diffuser pump bowl (the number refers to parts listed in Table 1) (Flowserve Corporation)

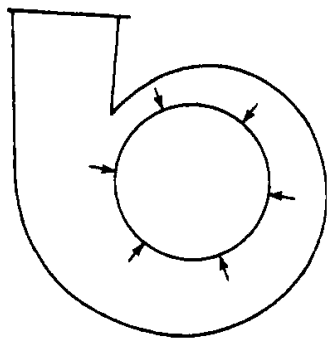


FIGURE 5 Uniform casing pressures exist at design capacity, resulting in zero radial reaction

pump with a small impeller diameter. A zero radial reaction is not often realized; the minimum reaction occurs at design capacity.

Although the same tendency for unbalance exists in the diffuser-type pump, the reaction is limited to a small arc repeated all around the impeller. As a result, the individual reactions cancel each other out as long as flow is constantly removed from around the periphery of the diffuser discharge. If flow is not removed uniformly around its periphery, a pressure imbalance may occur around the diffuser discharge that will be transmitted back through the diffuser to the impeller, resulting in a radial reaction on the shaft and bearing system.

In a centrifugal pump design, shaft diameter as well as bearing size can be affected by the allowable deflection as determined by the shaft span, impeller weight, radial reaction forces, and torque to be transmitted.

Formerly, standard designs compensated for radial reaction forces encountered at capacities in excess of 50% of the design capacity for the maximum-diameter impeller of the pump. For sustained operations at lower capacities, the pump manufacturer, if properly advised, would supply a heavier shaft, usually at a much higher cost. Sustained operations at extremely low flows without the manufacturer being informed at the time of purchase are a much more common practice today. This can result in broken shafts, especially older designs, on high-head units.

Because of the increasing application of pumps that must operate at reduced capacities, it has become desirable to design standard units to accommodate such conditions. One solution is to use heavier shafts and bearings. Except for low-head pumps in which only a small additional load is involved, this solution is not economical. The only practical answer is a casing design that develops a much smaller radial reaction force at partial capacities. One of these is the *double-volute* casing design, also called the *twin-volute* or *dual-volute* design.

The application of the double-volute design principle to neutralize radial reaction forces at reduced capacity is illustrated in Figure 7. Basically, this design consists of two 180° volutes, and a passage external to the second joins the two into a common discharge. Although a pressure unbalance exists at partial capacity through each 180° arc, the two

LIBERTY EXHIBIT 1017, Page 278

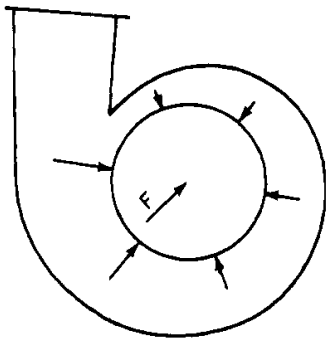


FIGURE 6 At reduced capacities, uniform pressures do not exist in a single-volute casing, resulting in a radial reaction F

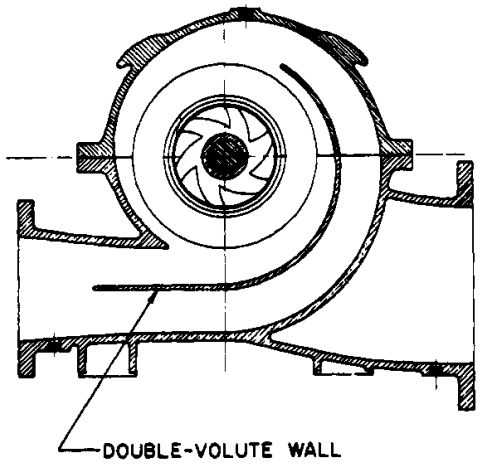


FIGURE 7 Transverse view of a double-volute casing pump

forces are approximately equal and opposite. Thus, little if any radial force acts on the shaft and bearings. Section 2.1.3 also covers this topic.

The double-volute design has many hidden advantages. For example, in large-capacity medium- and high-head single-stage vertical pumps, the rib forming the second volute that separates it from the discharge waterway of the first volute strengthens the casing (see Figure 8).

The individual stages of a multistage pump can be made double volute, as illustrated in Figure 9. The kinetic energy of the pumped liquid discharged from the impeller must be transformed into pressure energy and then must be turned 180° to enter the impeller of the next stage. The double volute therefore also acts as a return channel. The back view in Figure 9 shows this as well as the guide vanes used to straighten the flow into the next stage. An alternative to the volute design for multistage pumps is the diffuser and its return vanes that channel the flow from the discharge of the diffuser vanes back into the impeller of the next stage.

Solid and Split Casings *Solid casing* implies a design in which the discharge waterways leading to the discharge nozzle are all contained in one casting or fabricated piece. The casing must have one side open so that the impeller can be introduced into it. Because the sidewalls surrounding the impeller are actually part of the casing, a solid casing, strictly speaking, cannot be used, and designs normally called solid casing are really radially split (refer to Figure 1 and see Figures 11 and 12).

A *split casing* is made of two or more parts fastened together. The term *horizontally split* had regularly been used to describe pumps with a casing divided by a horizontal plane through the shaft centerline or axis (see Figure 10). The term *axially split* is now preferred. Because both the suction and discharge nozzles are usually in the same half of the casing, the other half may be removed for inspection of the interior without disturbing the bearings or the piping. Like its counterpart horizontally split, the term *vertically split* is poor terminology. It refers to a casing split in a plane perpendicular to the axis of rotation. The term *radially split* is now preferred.

End-Suction Pumps Most end-suction, single-stage pumps are made of one-piece solid casings. At least one side of the casing must be open so that the impeller can be assembled in the pump. Thus, a cover is required for that side. If the cover is on the suction side, it becomes the casing sidewall and contains the suction opening (refer to Figure 1). This is called the *suction cover* or *casing suction head*. Other designs are made with casing covers (see Figure 11) and still others have both casing suction covers and casing covers (refer to Figure 8 and see Figure 12).

LIBERTY EXHIBIT 1017, Page 279

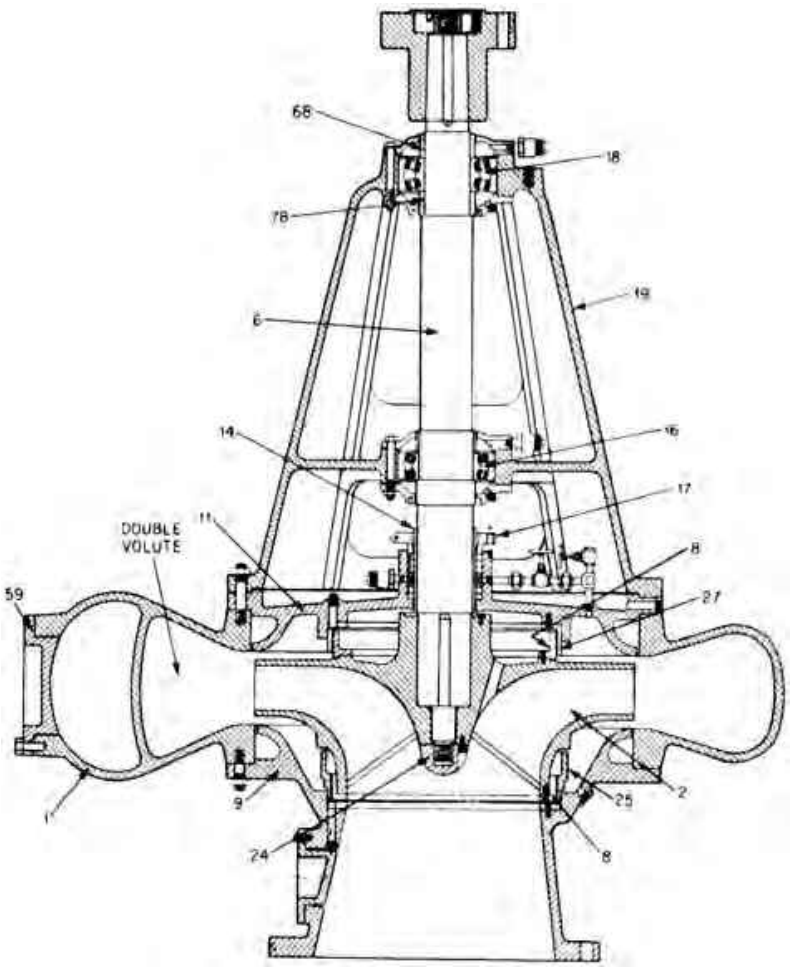


FIGURE 8 The sectional view of a vertical-shaft, end-suction pump with a double-volute casing (the numbers refer to parts listed in Table 1) (Flowserve Corporation)

For general service, the end-suction, single-stage pump design is extensively used for small pumps with a 4- or 6-in (102- or 152-mm) discharge size for both motor-mounted and coupled types. In these pumps, the small size makes it feasible to cast the volute and one side integrally. Whether or not the seal chamber side or the suction side is made integrally with the casing is usually determined by the most economical pump design.

For larger pumps, especially those for special services such as sewage handling, there is a demand for pumps of both rotations. A design with separate suction and seal chamber heads permits the use of the same casing for either rotation if the flanges on the two sides



FIGURE 9 The double volute of a multistage pump, front view (left) and back view (right) (Flowserve Corporation)

LIBERTY EXHIBIT 1017, Page 280



FIGURE 10 An axially split casing, horizontal-shaft, double-suction volute pump (Flowserve Corporation)

are made identical. There is also a demand for vertical pumps that can be disassembled by removing the rotor and bearing assembly from the top of the casing. Many horizontal applications of the pumps of the same line, however, require partial dismantling from the suction side. Such lines are most adaptable when they have separate suction and casing covers.

Casing Construction for Open- and Semiopen-Impeller Pumps In the open- or semiopen impeller pump, the impeller rotates within close clearance of the pump casing or suction cover (refer to Figure 11). If the intended service is abrasive, a side plate is mounted within the casing to provide a renewable close-clearance guide to the liquid



FIGURE 11 End-suction pump with semiopen impeller (Flowserve Corporation)

LIBERTY EXHIBIT 1017, Page 281

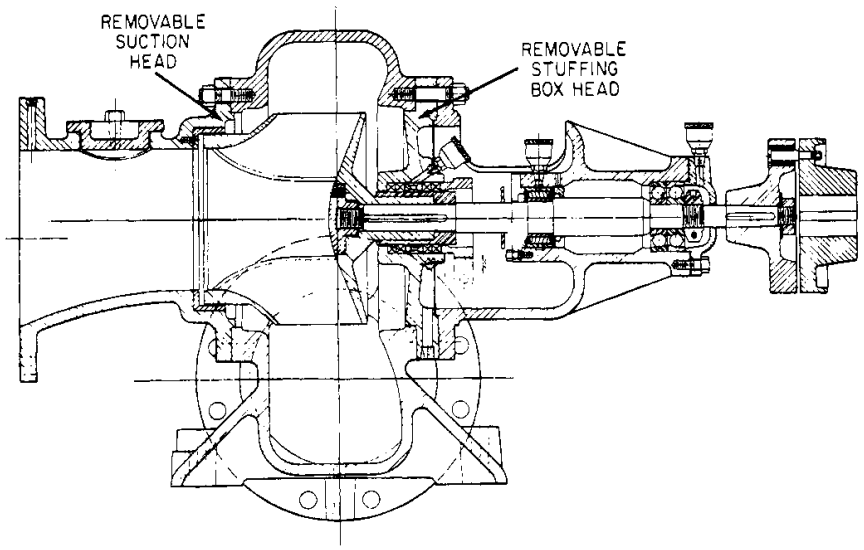


FIGURE 12 End-suction pump with removable suction and stuffing box heads (Flowserve Corporation)

flowing through the impeller. One of the advantages of using side plates is that abrasion-resistant material, such as stainless steel, can be used for the impeller and side plate, while the casing itself may be of a less costly material. Although double-suction, semiopen-impeller pumps are seldom used today, they were common in the past and were generally made with side plates.

In order to maintain pump efficiency, a close running clearance is required between the front unshrouded face of the open or semiopen impeller and the casing, suction cover, or side plate. Pump designs provide either jackscrews or shims to adjust the position of the thrust bearing housing (and, as a result, the axial position of the shaft and impeller) relative to the bearing frame.

Pre-rotation and Stop Pieces Improper entrance conditions and inadequate suction approach shapes may cause the liquid column in the suction pipe to spiral for some distance ahead of the impeller entrance. This phenomenon is called *pre-rotation*, and it is attributed to various operational and design factors in both vertical and horizontal pumps.

Pre-rotation is usually harmful to pump operation because the liquid enters between the impeller vanes at an angle other than that allowed in the design. This frequently lowers the net effective suction head and the pump efficiency. Various means are used to avoid pre-rotation both in the construction of the pump and in the design of the suction approaches.

Practically all horizontal, single-stage, double-suction pumps and most multistage pumps have a suction volute that guides the liquid in a streamline flow to the impeller eye. The flow comes to the eye at right angles to the shaft and separates unequally on the two sides of the shaft. Moving from the suction nozzle to the impeller eye, the suction waterways are reduced in area, meeting in a projecting section of the sidewall dividing the two sections. This dividing projection is called a *stop piece*. To minimize pre-rotation in end-suction pumps, a radial-fin stop piece projecting toward the center is sometimes cast into the suction nozzle wall.

Nozzle Locations The discharge nozzle of end-suction, single-stage horizontal pumps is usually in a top-vertical position (refer to Figures 1 and 11). However, other nozzle positions can be obtained, such as top-horizontal, bottom-horizontal, or bottom-vertical. Figure 13 illustrates the flexibility available in discharge nozzle locations. Sometimes the pump frame, bearing bracket, or baseplate may interfere with the discharge flange, prohibiting a bottom-horizontal or bottom-vertical discharge nozzle position. In other instances, solid casings cannot be rotated for various nozzle positions because the seal chamber connection would become inaccessible.

LIBERTY EXHIBIT 1017, Page 282

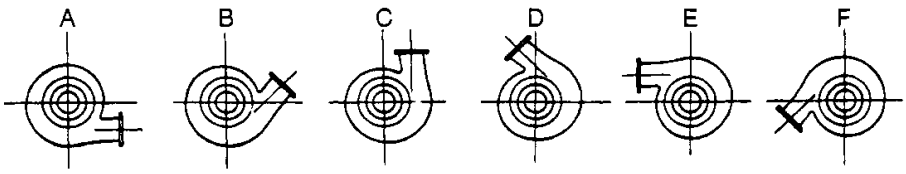


FIGURE 13 Possible positions of discharge nozzles for a specific design of an end-suction, solid-casing, horizontal-shaft pump. The rotation illustrated is counterclockwise from suction end.

Practically all double-suction, axially split casing pumps have a side discharge nozzle and either a side- or a bottom-suction nozzle. If the suction nozzle is placed on the side of the pump casing with its axial centerline (refer to Figure 10), the pump is classified as a *side-suction pump*. If its suction nozzle points vertically downward (see Figure 14), the pump is called a *bottom-suction pump*. Single-stage, bottom-suction pumps are rarely made in sizes below a 10-in (254-mm) discharge nozzle diameter.

Special nozzle positions can sometimes be provided for double-suction, axially split casing pumps to meet special piping arrangements, such as a radically split casing with bottom suction and top discharge in the same half of the casing. Such special designs are generally costly and should be avoided.

Centrifugal Pump Rotation Because suction and discharge nozzle locations are affected by pump rotation, it is important to understand how the direction of rotation is defined. According to Hydraulic Institute standards, rotation is defined as clockwise or counterclockwise by looking at the driven end of a horizontal pump or looking down on a vertical pump. To avoid misunderstanding, clockwise or counterclockwise rotation should always be qualified by including the direction from which one looks at the pump.

The terms *inboard end* or *drive end* (the end of the pump closest to the driver) and *outboard end* or *nondrive end* (the end of the pump farthest from the driver) are used only with horizontal pumps. The terms lose their significance with dual-driven pumps. Any centrifugal pump casing pattern can be arranged for either clockwise or counterclockwise rotation, except for end-suction pumps, which have integral heads on one side. These require separate directional patterns.



FIGURE 14 A bottom-suction, axially split casing single-stage pump (Flowserve Corporation)

Previous Page

Casing Handholes Casing handholes are furnished primarily on pumps handling sewage and stringy materials that may become lodged on the impeller suction vane edges or on the tongue of the volute. The holes permit removal of this material without completely dismantling the pump. End-suction pumps used primarily for liquids of this type are provided with handholes or access to the suction side of the impellers. These access points are located on the suction head or in the suction elbow. Handholes are also provided in drainage, irrigation, circulating, and supply pumps if foreign matter may become lodged in the waterways. On very large pumps, manholes provide access to the interior for both cleaning and inspection.

Mechanical Features of Casings Most single-stage centrifugal pumps are intended for service at moderate pressures and temperatures. As a result, pump manufacturers usually design a special line of pumps for high operating pressures and temperatures rather than make their standard line unduly expensive by making it suitable for too wide a range of operating conditions.

If axially split casings are subject to high pressure, they tend to "breathe" at the split joint, leading to misalignment of the rotor and, even worse, leakage. For such conditions, internal and external ribbing is applied to casings at the points subject to the greatest stress. In addition, whereas most pumps are supported by feet at the bottom of the casing, high temperatures require centerline support so that, as the pump becomes heated, expansion will not cause misalignment.

Series Units For large-capacity medium-high-head conditions, two single-stage, double-suction pumps can be connected in a series on one baseplate with a single driver. Such an arrangement was at one time very common in waterworks applications for heads of 250 to 400 ft (76 to 122 m). One series arrangement uses a double-extended shaft motor in the middle, driving two pumps connected in a series by external piping. In a second type, a standard motor is used with one pump having a double-extended shaft. This latter arrangement may have limited applications because the shaft of the pump next to the motor must be strong enough to transmit the total pumping horsepower. If the total pressure generated by such a series unit is relatively high, the casing of the second pump could require ribbing. Higher heads per stage are becoming more and more common, and series units are generally used in only very high ranges of total head.

MULTISTAGE PUMP CASINGS

Although the majority of single-stage pumps are of the volute-casing type, both volute and diffuser casings are used in multistage pump construction. Because a volute casing gives rise to radial thrust, axially split multistage casings generally have staggered volutes so that the resultant of the individual radial thrusts is balanced out (see Figures 15 and 16). Both axially and radially split casings are used for multistage pumps. The choice between the two designs is dictated by the design pressure, with 2000 lb/in^2 (138 bar)* being typical for 3600-rpm axially split casing pumps.

Axially Split Casings Regardless of the arrangement of the stages in the casing, it is necessary to connect the successive stages of a multistage pump. In the low and medium pressure and capacity ranges, these interstage passages are cast integrally with the casing proper (see Figures 17 and 18). As the pressures and capacities increase, the desire to maintain as small a casing diameter as possible, coupled with the necessity of avoiding sudden changes in the velocity or the direction of the flow, leads to the use of external interstage passages cast separately from the pump casing. They are formed in the shape of a loop, bolted or welded to the casing proper (see Figure 19).

Interstage Construction for Axially Split Casing Pumps A multistage pump inherently has adjoining chambers subjected to different pressures, and means must be made

*1 bar = 10^5 Pa

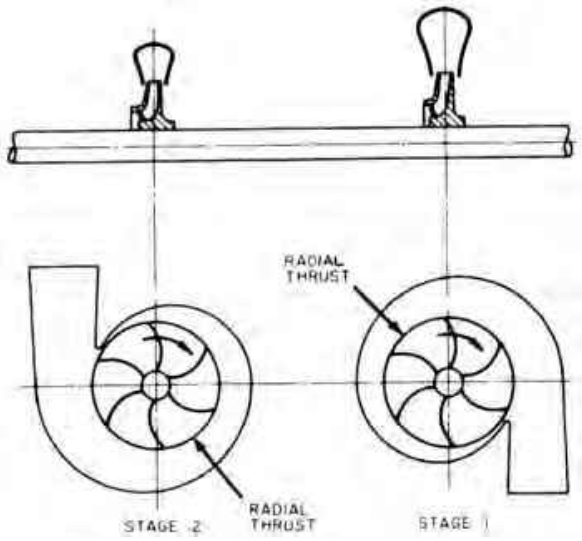


FIGURE 15 An arrangement of a multistage volute pump for radial-thrust balance

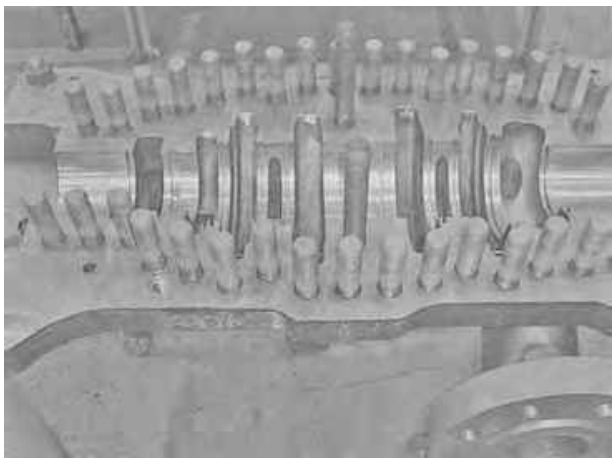


FIGURE 16 The horizontal flange of an axially split casing pump (Flowserve Corporation)

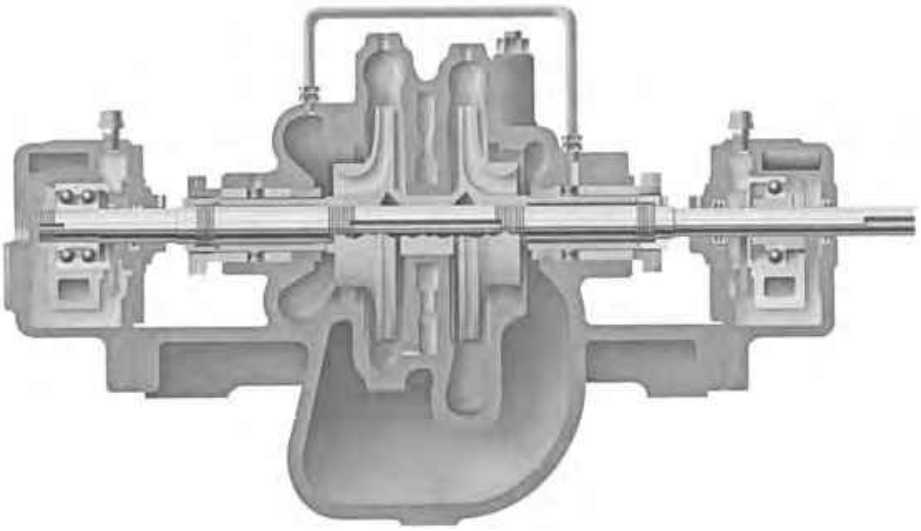


FIGURE 17 Two-stage axially split casing volute pump for small capacities and pressures up to 450 lb/in^2 (31 bar) (Flowserve Corporation)



FIGURE 18 Two-stage axially split casing volute pump for pressures up to 500 lb/in² (34 bar) (Flowserve Corporation)

available to isolate these chambers from one another so that the leakage from high to low pressure will take place only at the clearance joints formed between the stationary and rotating elements of the pump. Thus, the leakage will be kept to a minimum. The isolating wall used to separate two adjacent chambers of a multistage pump is called a *stage piece*, *diaphragm*, or *interstage diaphragm*. The stage piece may be formed of a single piece, or it may be fitted with a renewable stage piece bushing at the clearance joint between the stationary stage piece and the part of the rotor immediately inside the former. The stage pieces, which are usually solid, are assembled on the rotor along with impellers, sleeves, bearings, and similar components. To prevent the stage pieces from rotating, a locked tongue-and-groove joint is provided in the lower half of the casing. Clamping the upper casing half to the lower half securely holds the stage piece and prevents rotation.

The problem of seating a solid stage piece against an axially split casing is one that has given designers much trouble. First, there is a three-way joint and, second, this seating must make the joint tight and leakproof under a pressure differential without resorting to bolting the stage piece directly to the casing.

To overcome this problem, it is wise to make a pump that has a small-diameter casing so that when the casing bolting is pulled tight, there is a seal fitting of the two casing halves adjacent to the stage piece. The small diameter likewise helps to eliminate the possibility of a stage piece cocking and thereby leaving a clearance on the upper-half casing when it is pulled down. No matter how rigidly the stage piece is located in the lower-half casing, there must be a sliding fit between the seat face of the stage piece and that in the upper-half casing so that the upper-half casing can be pulled down. Each stage piece,



FIGURE 19 A two-stage double-suction, axially split volute pump with an external interstage passsage bolted to the casing (Flowserve Corporation)

LIBERTY EXHIBIT 1017, Page 286

furthermore, must be arranged so that the pressure differential developed by the pump will tend to seat the piece tightly against the casing rather than open up the joint.

We have said that axially split casing pumps are typically used for working pressures of up to 2000 lb/in^2 (138 bar). High-pressure piping systems, of which these pumps form a part, are inevitably made of steel because this material has the valuable property of yielding without breaking. Considerable piping strains are unavoidable, and these strains, or at least a part thereof, are transmitted to the pump casing. The latter consists essentially of a barrel that is split axially, flanged at the split, and fitted with two necks that serve as inlet and discharge openings. When piping stresses exist, these necks, being the weakest part of the casing, are in danger of breaking off if they cannot yield. Steel is therefore the safest material for pump casings whenever the working pressures in the pump are in excess of 1000 lb/in^2 (70 bar).

This brings up an important feature in the design of the suction and discharge flanges. Although raised-face flanges are perfectly satisfactory for steel-casing pumps, their use is extremely dangerous with cast-iron pumps. This danger arises from the lack of elasticity in cast iron, which leads to flange breakage when the bolts are being tightened, the fulcrum of the bending moment being located inward from the bolt circle. As a result, it is essential to avoid raised-face flanges with cast-iron casings as well as the use of a raised-face flange pipe directly against a flat-face cast-iron pump flange. Suction flanges should obviously be suitable for whatever hydrostatic test pressure is applied to the pump casing.

The location of the pump casing feet is not critical in smaller pumps operating at discharge pressures below 275 lb/in^2 (19 bar) and at moderate temperatures of up to 300°F (150°C). Since the unit is relatively small, very little distortion is likely to occur. However, for larger units operating at higher pressures and temperatures, it is important that the casing be supported at the horizontal centerline or immediately below the bearings (refer to Figure 19).

Radially Split Double-Casing Pumps The oldest form of radially split casing multistage pump is commonly called the *ring-section*, *ring-casing*, or the *doughnut type*. When more than one stage was found necessary to generate higher pressures, two or more single-stage units of the prevalent radially split casing type were assembled and bolted together.

In later designs, the individual stage sections and separate suction and discharge heads were held together with large throughbolts. These pumps, still an assembly of bolted-up sections, can present serious dismantling and reassembly problems because suction and discharge connections have to be broken each time the pump is serviced. The double-casing pump retains the advantages of the radially split casing design and minimizes the dismantling problem.

The basic principle consists of enclosing the working parts of a multistage centrifugal pump in an inner casing and building a second casing around this inner casing. The space between the two casings is maintained at the discharge pressure of the last pump stage. The construction of the inner casing follows one of two basic principles: (1) axial splitting (see Figure 20) or (2) radial splitting (see Figure 21).

The double-casing pump with radially split inner casing is an evolution of the ring-casing pump with added provisions to ease dismantling. The inner unit is generally constructed exactly as a ring-casing pump. After assembly, it is inserted and bolted inside a cylindrical casing that supports it and leaves it free to expand under temperature changes. The suction and discharge nozzles form an integral part of the outer casing, and the internal assembly of the pump can be withdrawn without disturbing the piping connections.

Hydrostatic Pressure Tests It is standard practice for the manufacturer to conduct hydrostatic tests for the parts of a pump that contain fluid under pressure. This means that the pump casing and, where applicable, parts like suction or casing covers are assembled with the internal parts, removed, and are then subjected to a hydrostatic test,

LIBERTY EXHIBIT 1017, Page 287

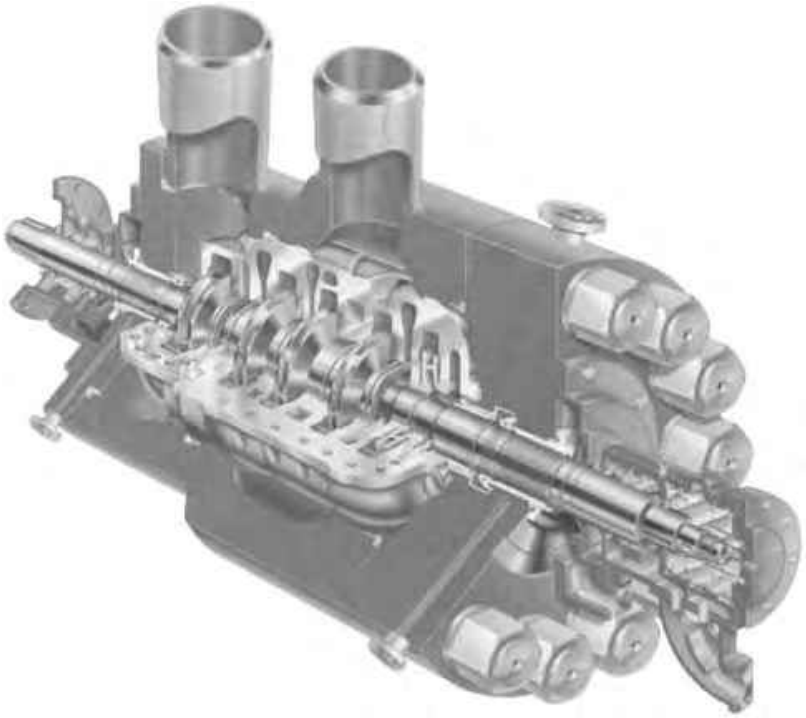


FIGURE 20 Double-casing multistage pump with axially split inner casing (Flowserve Corporation)

generally for a minimum of 30 min. Such a test demonstrates that the casing containment is sound and that there is no leakage of fluid to the exterior.

Additional tests may be conducted by the pump manufacturer to determine the soundness of internal partitions separating areas of the pump operating under different pressures.

The definition of the applicable hydrostatic pressure for these tests varies. The most generally accepted definition is that given by the Hydraulic Institute Standards. Each part

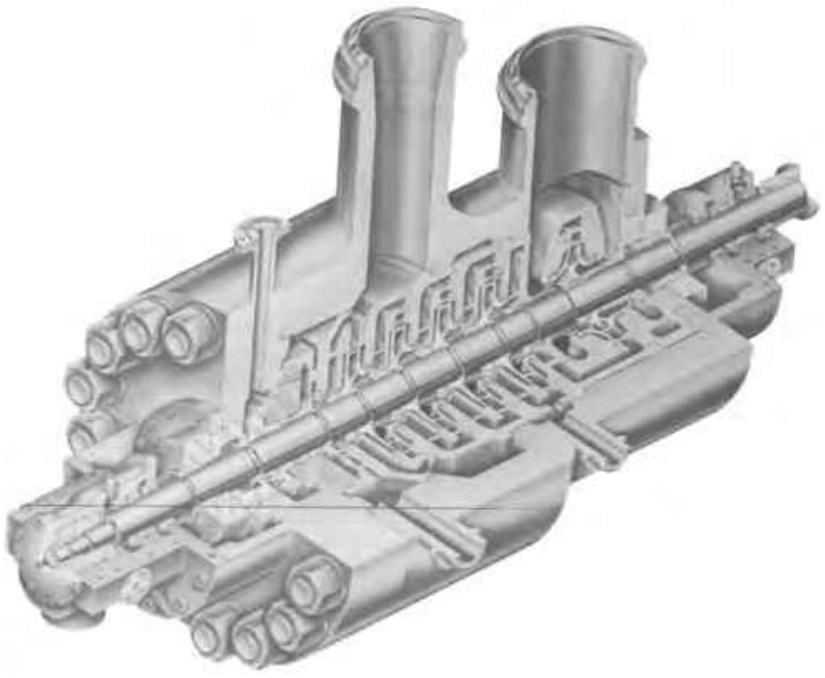


FIGURE 21 Double-casing multistage pump with radially split inner casing (Flowserve Corporation)

of the pump that contains fluid under pressure shall be capable of withstanding a hydrostatic test at not less than the greatest of the following:

- 150% of the pressure that will occur in that part when the pump is operated at rated conditions for the given application of the pump, except thermoset parts
- 125% of the pressure that would occur in that part when the pump is operating at rated speed for a given application, but with the pump discharge valve closed

IMPELLERS

In a single-suction impeller, the liquid enters the suction eye on one side only. A double-suction impeller is, in effect, two single-suction impellers arranged back to back in a single casing. The liquid enters the impeller simultaneously from both sides, while the two casing suction passageways are connected to a common suction passage and a single suction nozzle.

For the general service single-stage, axially split casing design, a double-suction impeller is favored because it is theoretically in an axial hydraulic balance and because the greater suction area of a double-suction impeller permits the pump to operate with less net absolute suction head. For small units, the single-suction impeller is more practical for manufacturing reasons, as the waterways are not divided into two very narrow passages. It is also sometimes preferred for structural reasons. End-suction pumps with single-suction overhung impellers have both first-cost and maintenance advantages unobtainable with double-suction impellers. Most radially split casing pumps therefore use single-suction impellers. Because an overhung impeller does not require the extension of a shaft into the impeller suction eye, single-suction impellers are preferred for pumps handling suspended matter, such as sewage. In multistage pumps, single-suction impellers are almost universally used because of the design and first-cost complexity that double-suction staging introduces.

Impellers are called radial vane or radial flow when the liquid pumped is made to discharge radially to the periphery. Impellers of this type usually have a specific speed below 4200 (2600) if single-suction and below 6000 (3700) if double-suction. Specific speed is discussed in detail in Section 2.1.3. The units for specific speed used here are in USCS rpm, gallons per minute, and feet. In SI, they are rpm, liters per second, and meters. Impellers can also be classified by the shape and form of their vanes:

- The straight-vane impeller (see Figures 22, 30, 31, 32, and 33)
- The Francis-vane or screw-vane impeller (see Figures 23 and 24)
- The mixed-flow impeller (see Figure 25)
- The propeller or axial-flow impeller (see Figure 26)

In a *straight-vane radial impeller*, the vane surfaces are generated by straight lines parallel to the axis of rotation. These are also called *single-curvature vanes*. The vane surfaces of a *Francis-vane radial impeller* have a double curvature. An impeller design that has both a radial-flow and an axial-flow component is called a *mixed-flow impeller*. It is generally restricted to single-suction designs with a specific speed above 4200 (2600). Types with lower specific speeds are called *Francis-vane impellers*. Mixed-flow impellers with a small radial-flow component are usually referred to as propellers. In a true propeller, or *axial-flow impeller*, the flow strictly parallels the axis of rotation. In other words, it moves only axially.

An inducer is a low-head, axial-flow impeller with few blades that is placed in front of a conventional impeller. The hydraulic characteristics of an inducer are such that it requires considerably less NPSH than a conventional impeller. Both inducer and impeller are mounted on the same shaft and rotate at the same speed (see Figure 27). The main purpose of the inducer is not to generate an appreciable portion of the total pump head, but to increase the suction pressure to a conventional impeller. Inducers are therefore used

LIBERTY EXHIBIT 1017, Page 289



FIGURE 22 Straight-vane, radial, single-suction closed impeller (Flowserve Corporation)



FIGURE 23 Francis vane, radial, closed impeller (Flowserve Corporation)



FIGURE 24 Medium specific speed, Francis vane radial impeller (Flowserve Corporation)



FIGURE 25 Open mixed-flow impeller (Flowserve Corporation)



FIGURE 26 Axial-flow impeller (Flowserve Corporation)

LIBERTY EXHIBIT 1017, Page 290



FIGURE 27 A centrifugal pump with a conventional impeller preceded by an inducer (Flowserve Corporation)

to reduce the NPSH requirements of a given pump or to permit the pump to operate at higher speeds with a given available NPSH. For a further discussion of inducers, see Section 2.1 and Section 2.1.3.

The relation of single-suction impeller profiles to specific speed is shown in Figure 28. The classification of impellers according to their vane shape is naturally arbitrary inasmuch as there is much overlapping in the types of impellers used in the different types of pumps. For example, impellers in single- and double-suction pumps of low specific speeds have vanes extending across the suction eye. This provides a mixed flow at the impeller entrance for low pickup losses at high rotative speeds but enables the discharge portion of the impeller to use the straight-vane principle. In pumps of higher specific speed operating against low beads, impellers have double-curvature vanes extending over the full vane surface. They are therefore full Francis-type impellers. The mixed-flow impeller, usually a single-suction type, is essentially one-half of a double-suction, high-specific-speed, Francis-vane impeller.

In addition, many impellers are designed for specific applications. For instance, the conventional impeller design with sharp vane edges and restricted areas is not suitable for handling liquids containing rags, stringy materials, and solids like sewage because it will become clogged. Special nonclogging impellers with blunt edges and large waterways have been developed for such services (see Figure 29). For pumps up to the 12- to 16-in (305- to 406-mm) discharge size, these impellers have only two vanes. Larger pumps normally use three or four vanes.

Impeller Mechanical Types Mechanical design also determines impeller classification. Accordingly, impellers may be completely open, semiopen, or closed.

Strictly speaking, an *open impeller* (see Figure 28) consists of nothing but vanes attached to a central hub for mounting on the shaft without any form of sidewall or shroud. The disadvantage of this impeller is structural weakness. If the vanes are long, they must be strengthened by ribs or a partial shroud. Generally, open impellers are used in small, low-energy pumps. One advantage of open impellers is that they are better suited for handling liquids containing stringy materials. It is also sometimes claimed that they are better suited for handling liquids containing suspended matter because the solids in such matter are more likely to be clogged in the space between the rotating shrouds of a closed impeller and the stationary casing walls. It has been demonstrated, however, that closed impellers do not clog easily, thus disproving the claim for the superiority of the open-impeller design. In addition, the open impeller is much more sensitive to wear than the closed impeller and therefore its efficiency may deteriorate rather rapidly.

The open impeller rotates between two side plates, between the casing walls of the volute, or between the casing cover and the suction head. The clearance between the

LIBERTY EXHIBIT 1017, Page 291

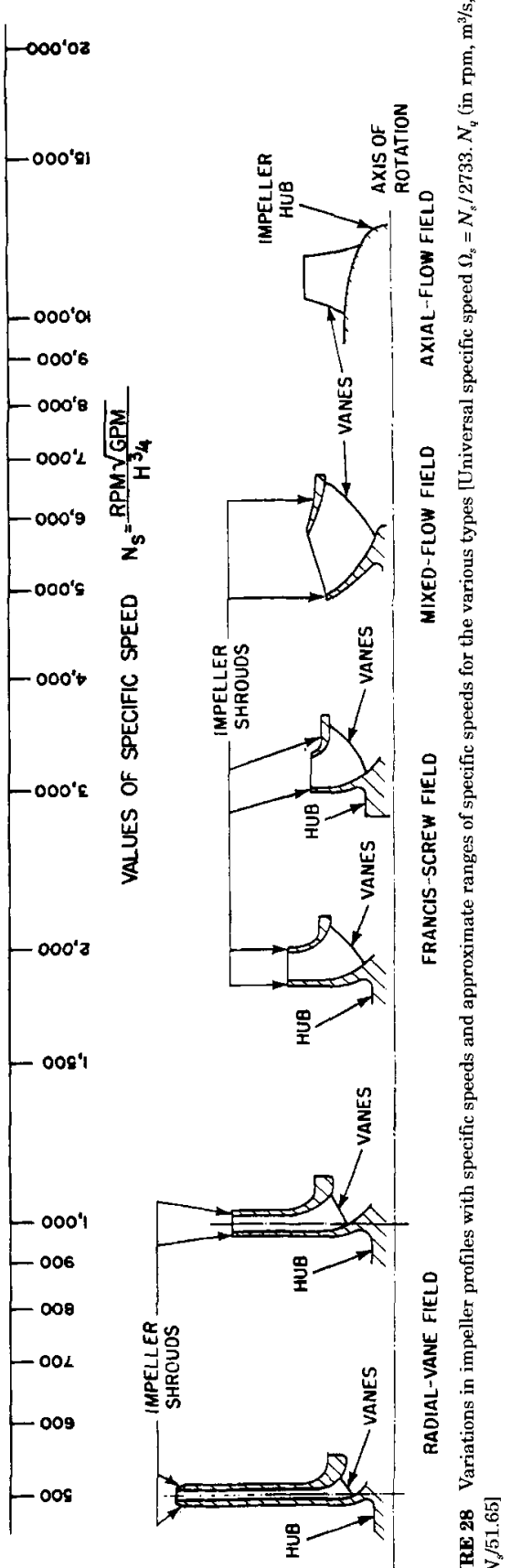


FIGURE 28 Variations in impeller profiles with specific speeds and approximate ranges of specific speeds for the various types [Universal specific speed $\Omega_s = N_s/2733$. N_q (in rpm, m^3/s, m) $= N_s/51.65$]

LIBERTY EXHIBIT 1017, Page 292

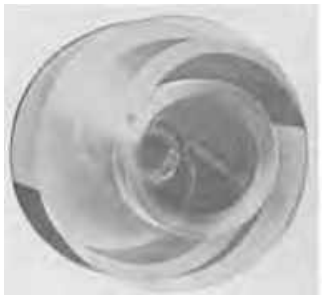


FIGURE 29 Phantom view of a radial-vane nonclogging impeller (Flowserve Corporation)



FIGURE 30 Barske-type radial multiple-vane open impeller with multiple balance holes to reduce axial pressure unbalance (axial thrust) (Flowserve Corporation)

impeller vanes and the sidewalls enables a certain amount of water slippage. This slippage increases as wear increases. To restore the original efficiency, both the impeller and the side plate(s) must be replaced. This, incidentally, involves a much larger expense than would be entailed in closed impeller pumps where simple rings form the leakage joint.

The *semiopen impeller* (see Figures 30 through 33) incorporates a single shroud, usually at the back of the impeller. This shroud may or may not have *pump-out vanes*, which are vanes located at the back of the impeller shroud. This function reduces the pressure at the back hub of the impeller and prevents foreign matter from lodging in back of the impeller that would interfere with the proper operation of the pump and the seal chamber. The back shrouds may also be scalloped or relieved with balance holes through them (see Figure 33) to reduce axial unbalance.

The *closed impeller* (refer to Figures 22 through 24), which is almost universally used in centrifugal pumps handling clear liquids, incorporates shrouds or sidewalls that totally enclose the impeller waterways from the suction eye to the periphery. Although this design prevents the liquid slippage that occurs between an open or semiopen impeller and its side plates, a running joint must be provided between the impeller and the casing to separate the discharge and suction chambers of the pump. This running joint is usually formed by a relatively short cylindrical surface on the impeller shroud that rotates within a slightly larger stationary cylindrical surface. If one or both surfaces are made renewable, the leakage joint can be repaired when wear causes excessive leakage.

If the pump shaft terminates at the impeller so that the latter is supported by bearings on one side, the impeller is called an *overhung impeller*. This type of construction is the best for end-suction pumps with single-suction impellers.

Impeller Nomenclature The inlet of an impeller just before the section where the vanes begin is called the suction eye (see Figure 34). In a closed-impeller pump, the suction eye



FIGURE 31 Radial vane open impeller (Flowserve Corporation)



FIGURE 32 Open impeller with scalloped back shroud walls to reduce axial pressure unbalance (Flowserve Corporation)



FIGURE 33 Semiopen reversed vane impeller with partially scalloped shroud - (a) back side has close running clearance to wear plate; (b) front side, showing entrance to back side, vane inlet edges and balance holes (Flowserve Corporation)

diameter is taken as the smallest inside diameter of the shroud. In determining the area of the suction eye, the area occupied by the impeller shaft hub is deducted.

The *hub* is the central part of the impeller that is bored out to receive the pump shaft. The term, however, is also frequently used for the part of the impeller that rotates in the casing fit or in the casing wearing ring. It is then referred to as the *outer impeller hub* or the *wearing-ring hub* of the shroud.

WEARING RINGS

Wearing rings provide an easily and economically renewable leakage joint between the impeller and the casing. A leakage joint without renewable parts is illustrated in Figure 39. To restore the original clearances of such a joint after wear occurs, the user must either (1) build up the worn surfaces by welding or metal spraying, or (2) buy new parts.

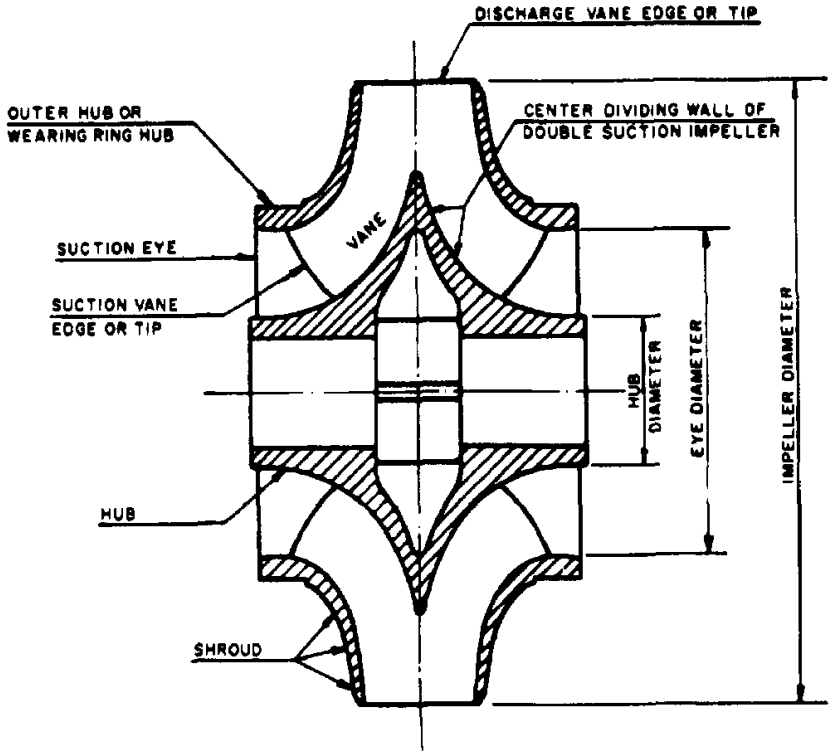


FIGURE 34 Parts of a double-suction impeller

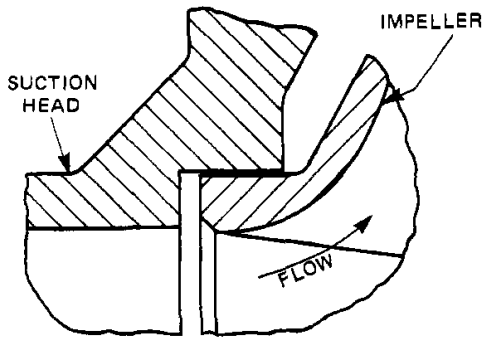


FIGURE 35 A plain flat leakage joint with no rings

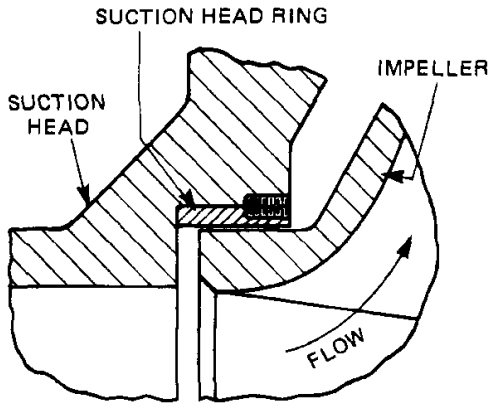


FIGURE 36 A single flat casing ring construction

The new parts are not very costly in small pumps, especially if the stationary casing element is a simple suction cover. This is not true for larger pumps or where the stationary element of the leakage joint is part of a complicated casting. If the first cost of a pump is of prime importance, it is more economical to provide for remachining both the stationary parts and the impeller. Renewable casing and impeller rings can then be installed (see Figures 36, 37, and 38). The nomenclature for the casing or stationary part forming the leakage joint surface is as follows: (1) *casing ring* (if mounted in the casing), (2) *casing ring* or *suction head ring* (if mounted in a suction cover or head), and (3) *casing cover ring* or *head ring* (if mounted in the casing cover or head). Some engineers like to identify the part further by adding the word *wearing*, such as *casing wearing ring*. A renewable part for the impeller wearing surface is called the *impeller ring*. Pumps with both stationary and rotating rings are said to have *double-ring construction*.

Wearing Ring Types Various types of wearing-ring designs, and the selection of the most desirable type depends on the liquid being handled, the pressure differential across the leakage joint, the rubbing speed, and the particular pump design. In general, centrifugal pump designers use the ring construction that they have found to be most suitable for each particular pump service.

The most common ring constructions are the flat type (see Figures 36 and 37) and the L type. The leakage joint in the former is a straight, annular clearance. In the L-type ring (see Figure 39), the axial clearance between the impeller and the casing ring is large, so the velocity of the liquid flowing into the stream entering the suction eye of the impeller is low. The L-type casing rings shown in Figures 39 and 40 have the additional function of guiding the liquid into the impeller eye; they are called *nozzle rings*. Impeller rings of the L type shown in Figure 40 also furnish protection for the face of the impeller wearing-ring hub.

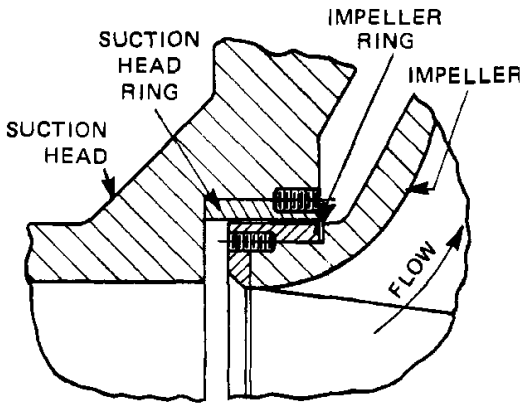


FIGURE 37 A double flat ring construction

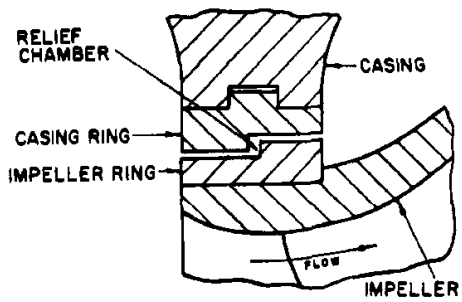


FIGURE 38 A step-type leakage joint with double rings

LIBERTY EXHIBIT 1017, Page 295

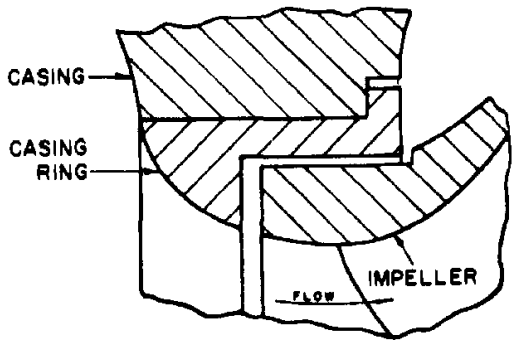


FIGURE 39 An L-type nozzle casing ring

Some designers favor labyrinth-type rings (see Figures 41 and 42) that have two or more annular leakage joints connected by relief chambers. In leakage joints involving a single unbroken path, the flow is a function of both the area and the length of the joint as well as of the pressure differential across the joint. If the path is broken by relief chambers (Figures 38, 41, and 42), the velocity energy in the jet is dissipated in each relief chamber, increasing the resistance. As a result, with several relief chambers and several leakage joints for the same actual flow through the joint, the area and hence the clearance between the rings can be greater than for an unbroken, shorter leakage joint.

The single labyrinth ring with only one relief chamber (refer to Figure 41) is often called an *intermeshing ring*. The *step-ring type* (refer to Figure 38) utilizes two flat-ring elements of slightly different diameters over the total leakage joint width with a relief chamber between the two elements. Other ring designs also use some form of relief chamber. For example, one commonly used in small pumps has a flat joint similar to that in Figure 40, but with one surface broken by a number of grooves. These act as relief chambers to dissipate the jet velocity head, thereby increasing the resistance through the joint and decreasing the leakage.

For raw water pumps in waterworks service and for larger pumps in sewage services in which the liquid contains sand and grit, *water-flushed rings* have been used (see Figure 43). Clear water under a pressure greater than that on the discharge side of the rings is piped to the inlet and distributed by the cored passage, the holes through the stationary ring, and the groove to the leakage joint. Ideally, the clear water should fill the leakage joint with some flow to the suction and discharge sides to prevent any sand or grit from getting into the clearance space. Wearing-ring flush is also employed in some process pumps when pumping solids or abrasives to minimize ring wear by injecting a compatible clean liquid between the rings.

In large pumps (with roughly a 36-in [900-mm] or larger discharge size), particularly vertical, end-suction, single-stage volute pumps, size alone permits some refinements not found in smaller pumps. One example is the inclusion of inspection ports for measuring ring clearance (see Figure 44). These ports can be used to check the impeller centering after the original installation as well as to observe ring wear without dismantling the pump.

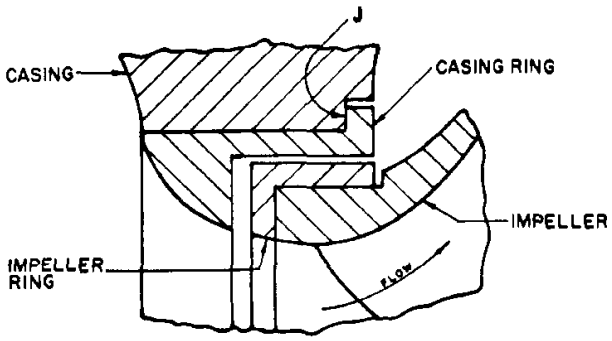


FIGURE 40 Double rings, both of L type

LIBERTY EXHIBIT 1017, Page 296

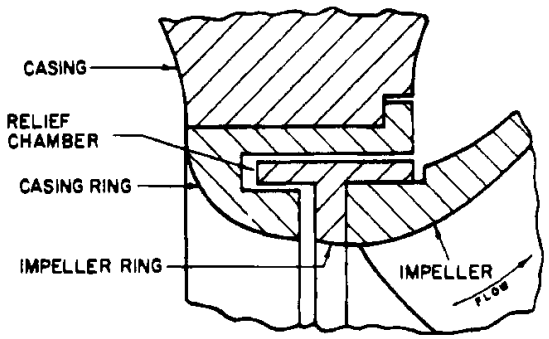


FIGURE 41 A single-labyrinth, intermeshing type. It is a double-ring construction with a nozzle-type casing ring.

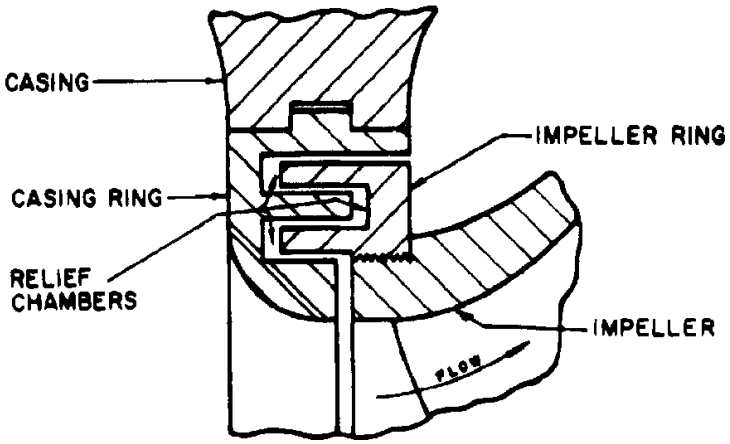


FIGURE 42 Labyrinth-type rings in a double-ring construction

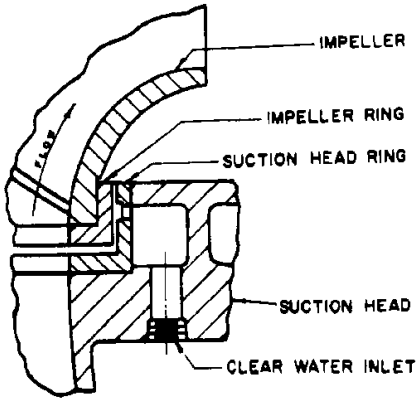


FIGURE 43 Water-flushed wearing ring

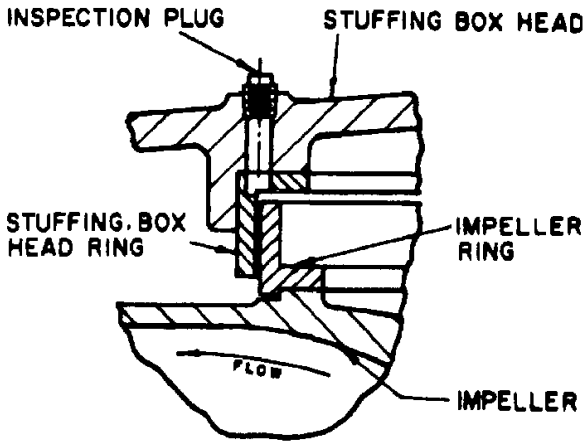


FIGURE 44 Wearing ring with an inspection port for checking clearance

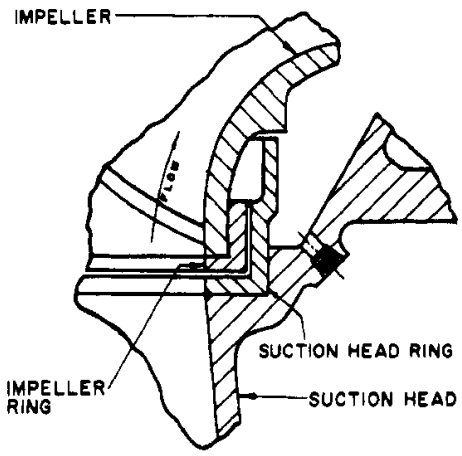


FIGURE 45 Dam-type ring construction

The lower rings of large vertical pumps handling liquids containing sand and grit in intermittent services are highly susceptible to wear. During shutdown periods, the grit and sand settle out and naturally accumulate in the region where these rings are installed, as it is the lowest point on the discharge side of the pump. When the pump is started again, this foreign matter is washed into the joint all at once and causes wear. To prevent this action in medium and large pumps, a dam-type ring is often used (see Figure 49). Periodically, the pocket on the discharge side of the dam can be flushed out.

One problem with the simple water-flushed ring is the failure to get uniform pressure in the stationary ring groove. If pump size and design permit, two sets of wearing rings arranged in tandem and separated by a large water space (see Figure 46) provide the best solution. The large water space enables a uniform distribution of the flushing water to the full 360° of each leakage joint. Because ring 2 is shorter and because a greater clearance is used there than at ring 1, equal flow can take place to the discharge pressure side and to the suction pressure side. This design also makes it easier to harden or coat the surfaces.

For pumps handling gritty or sandy water, the ring construction should provide an apron on which the stream leaving the leakage joint can impinge, as sand or grit in the jet will erode any surface it hits. Thus, a form of L-type casing ring similar to that shown in Figure 45 should be used.

Wearing-Ring Location In some designs, leakage is controlled by an axial clearance (see Figure 47). Generally, this design requires a means of adjusting the shaft position for

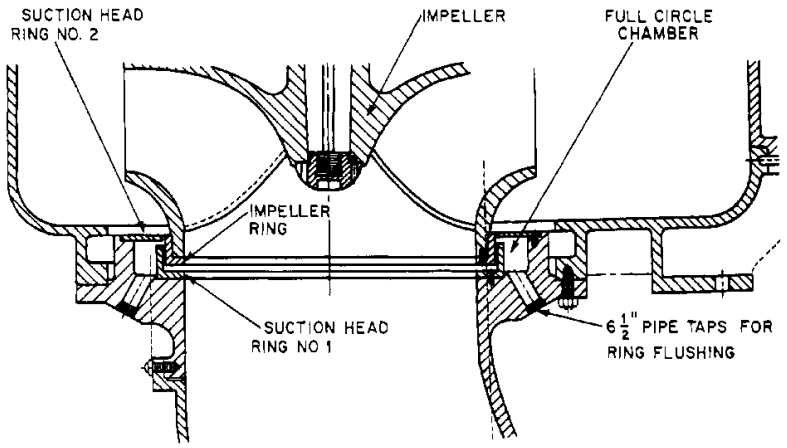


FIGURE 46 Two sets of rings with space between for flushing water (Flowserve Corporation)

LIBERTY EXHIBIT 1017, Page 298

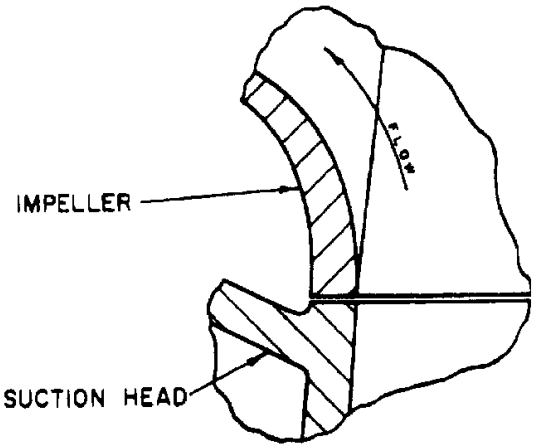


FIGURE 47 A leakage joint with axial clearance

proper clearance. Then, if uniform wear occurs over the two surfaces, the original clearance can be restored by adjusting the position of the impeller. A limit exists to the amount of wear that can be compensated, because the impeller must be nearly central in the casing waterways.

Leakage joints with axial clearance are not popular for double-suction pumps because a very close tolerance is required in machining the fit of the rings in reference to the centerline of the volute waterways. Joints with radial clearances, however, enable some shifting of the impeller for centering. The only adverse effect is a slight inequality in the lengths of the leakage paths on the two sides.

So far, this discussion has treated only those leakage joints located adjacent to the impeller eye or at the smallest outside shroud diameter. Designs have been made where the leakage joint is at the periphery of the impeller. In a vertical pump, this design is advantageous because the space between the joint and the suction waterways is open and so sand or grit cannot collect. Because of rubbing speed and because the impeller diameters used in the same casing vary over a wide range, the design is impractical in regular pump lines.

Mounting Stationary Wearing Rings In small single-suction pumps with suction heads, a stationary wearing ring is usually pressed into a bore in the head and may or may not be further locked by several set screws located half in the head and half in the ring (refer to Figure 37). Larger pumps often use an L-type ring with the flange held against a face on the head. In axially split casing pumps, the cylindrical casing bore (in which the casing ring will be mounted) should be slightly larger than the outside diameter of the ring. Unless some clearance is provided, distortion of the ring may occur when the two casing halves are assembled. However, the joint between the casing ring and the casing must be tight enough to prevent leakage. This is usually provided by a radial metal-to-metal joint (refer to Figure 39) arranged so that the discharge pressure presses the ring against the casing surface.

As it is not desirable for the casing ring of an axially split casing pump to be pinched by the casing, the ring will not be held tightly enough to prevent its rotation unless special provisions are made to keep it in place. One means of accomplishing this is to place a pin in the casing that will project into a hole bored in the ring or, conversely, to provide a pin in the ring that will fit into a hole bored in the casing or into a recess at the casing split joint.

Another method is to have a tongue on the casing ring that extends around 180° and engages a corresponding groove in one-half of the casing. This method can be used with casing rings having a central flange by making the diameter of the flange larger for 180° and cutting a deeper groove in that half of the casing.

Many methods are used for holding impeller rings on the impeller. Probably the simplest is to rely on a press fit of the ring on the impeller or, if the ring is of proper material,

LIBERTY EXHIBIT 1017, Page 299

on a shrink fit. Designers do not usually feel that a press fit is sufficient and often add several machine screws or set screws located half in the ring and half in the impeller, as in Figure 37.

An alternative to axial machine screws being located half in the ring and half in the impeller is the radial pin, which goes through the center of the ring into the impeller (or from the inside of the impeller eye outward into the ring). This pinning method avoids having to drill and tap holes half in a hardened wearing ring and half in a softer impeller hub. For higher speeds, installing the radial pins from the inside of the impeller eye outward into the wearing ring captures the pins and protects against pin loss, especially at higher operating speeds. Generally, some additional locking method is used rather than relying solely on friction between the ring and the impeller.

In the design of impeller rings, consideration has to be given to the stretch of the ring caused by centrifugal force, especially if the pump is of a high-speed design for the capacity involved. For example, some pumps operate at speeds that would cause the rings to become loose if only a press fit is used. For such pumps, shrink fits should be used or, preferably, impeller rings should be eliminated.

Wearing-Ring Clearances Typical clearance and tolerance standards for nongalling wearing-joint metals in general service pumps are shown in Figure 48. They apply to the following combinations: (1) bronze with a dissimilar bronze, (2) cast-iron with bronze, (3) steel with bronze, (4) Monel metal with bronze, and (5) cast-iron with cast iron. If the metals gall easily (like the chrome steels), the values given should be increased by 0.002 to 0.004 in.

The tolerance indicated is positive for the casing ring and negative for the impeller hub or impeller ring.

In a single-stage pump with a joint of nongalling components, the correct machining dimension for a casing-ring diameter of 9.000 in would be 9.000 plus 0.003 and minus 0.000 in. For the impeller hub or ring, the values would be 9.000 minus 0.018 (or 8.982) plus 0.000 and minus 0.003 in. Diametral clearances would be between 0.018 and 0.024 in. Obviously, clearances and tolerances are not translated into SI units by merely using conversion multipliers; they are rounded off as they are in the USCS system. The SI values for the previous USCS examples given are outlined here.

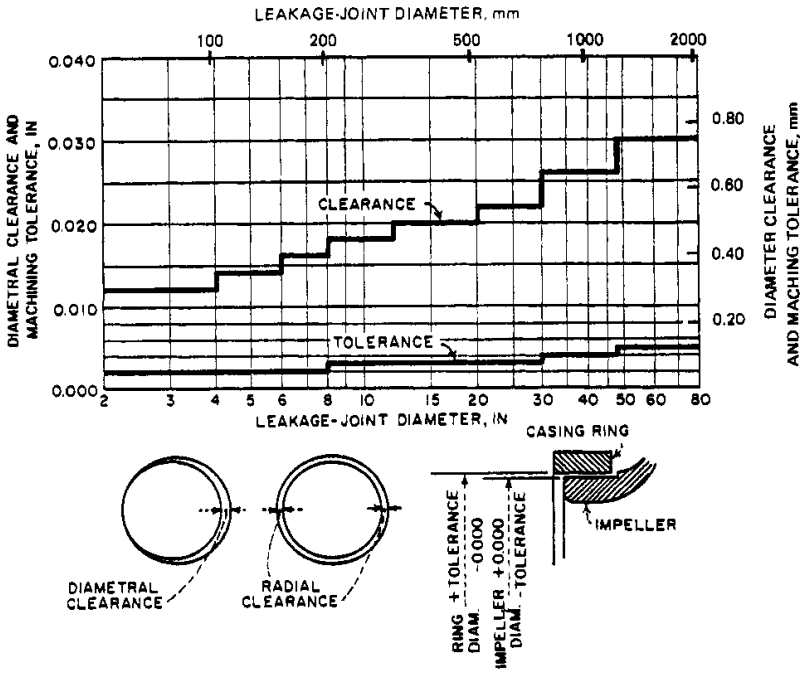


FIGURE 48 Wearing-ring clearances for single-stage pumps using nongalling materials

LIBERTY EXHIBIT 1017, Page 300

For a single-stage pump with a casing ring diameter of 230 mm, the machining dimensions would be as follows:

Casing ring	230 plus 0.08 and minus 0.00 mm
Impeller hub	230 minus 0.50 (229.5) plus 0.00 and minus 0.08 mm
Diametral clearances	Between 0.50 and 0.66 mm

Naturally, the manufacturer's recommendation for ring clearances and tolerances should be followed.

AXIAL THRUST

Axial Thrust in Single-Stage Pumps with Closed Impellers The pressures generated by a centrifugal pump exert forces on both stationary and rotating parts. The design of these parts balances some of these forces, but separate means may be required to counterbalance others.

An axial hydraulic thrust on an impeller is the sum of the unbalanced forces acting in the axial direction. Because reliable, large-capacity thrust bearings are readily available, an axial thrust in single-stage pumps remains a problem only in larger, higher speed units. Theoretically, a double-suction impeller is in hydraulic axial balance, with the pressures on one side equal to and counterbalancing the pressures on the other (see Figure 49). In practice, this balance may not be achieved for the following reasons:

1. The suction passages to the two suction eyes may not provide equal or uniform flows to the two sides.
2. External conditions, such as an elbow located too close to the pump suction nozzle, may cause unequal flow to the two suction eyes.
3. The two sides of the discharge casing waterways may not be symmetrical, or the impeller may be located off-center. These conditions will alter the flow characteristics between the impeller shrouds and the casing, causing unequal pressures on the shrouds.
4. Unequal leakage through the two leakage joints can upset the balance.

Combined, these factors can create an axial unbalance. To compensate for this, all centrifugal pumps, even those with double-suction impellers, incorporate thrust bearings.

The ordinary single-suction, closed, radial-flow impeller with the shaft passing through the impeller eye (refer to Figure 49) is subject to an axial thrust because a portion of the front wall is exposed to suction pressure and thus relatively more backwall

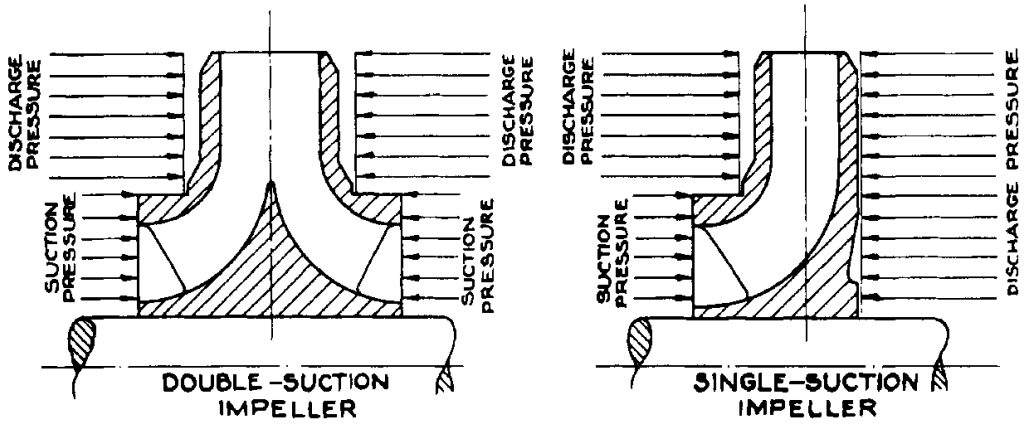


FIGURE 49 The origin of pressures acting on impeller shrouds to produce an axial thrust

LIBERTY EXHIBIT 1017, Page 301

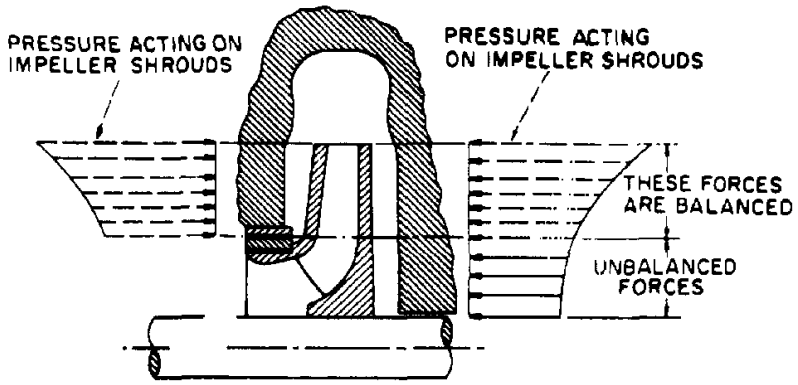


FIGURE 50 Pressure distribution on the front and back shrouds of the single-suction impeller with a shaft through the impeller eye

surface is exposed to discharge pressure. If the discharge chamber pressure is uniform over the entire impeller surface, the axial force acting toward the suction would be equal to the product of the net pressure generated by the impeller and the unbalanced annular area.

Actually, pressure on the two single-suction, closed impeller walls is not uniform. The liquid trapped between the impeller shrouds and casing walls is in rotation, and the pressure at the impeller periphery is appreciably higher than the impeller hub. Although we need not be concerned with the theoretical calculations for this pressure variation, Figure 50 describes it qualitatively. Generally speaking, the axial thrust toward the impeller suction may be about 20 to 30% less than the product of the net pressure and the unbalanced area.

To eliminate the axial thrust of a single-suction impeller, a pump can be provided with both front and back wearing rings. To equalize the thrust areas, the inner diameter of both rings is made the same (see Figure 51). Pressure approximately equal to the suction pressure is maintained in a chamber located on the impeller side of the back wearing ring by drilling balancing holes through the impeller. Leakage past the back wearing ring is returned to the suction area through these holes. However, with large single-stage, single-suction pumps, balancing holes are considered undesirable because leakage back to the impeller suction opposes the main flow, creating disturbances. In such pumps, a piped connection to the pump suction replaces the balancing holes.

Another way to eliminate or reduce an axial thrust in single-suction impellers is to use pump-out vanes on the back shroud. The effect of these vanes is to reduce the pressure

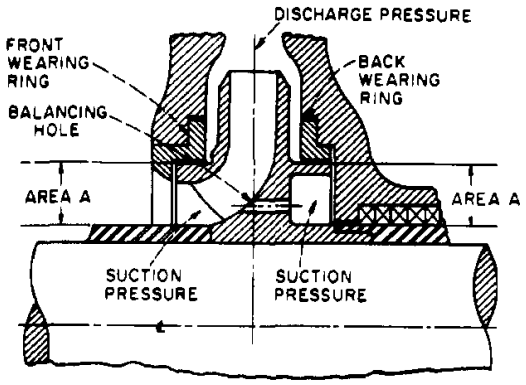


FIGURE 51 Balancing the axial thrust of a single-suction impeller by means of wearing rings on the back side and balancing holes

LIBERTY EXHIBIT 1017, Page 302

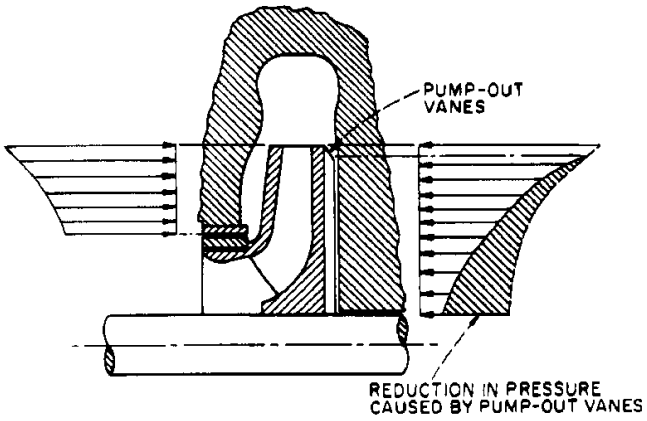


FIGURE 52 Pump-out vanes used in a single-suction impeller to reduce axial thrust

acting on the back shroud of the impeller (see Figure 52). This design, however, is generally used only in pumps handling dirty liquids where it keeps the clearance space between the impeller back shroud and the casing free of foreign matter.

So far, our discussion of axial thrust has been limited to single-suction, closed impellers with a shaft passing through the impeller eye that are located in pumps with two seal chambers, one on either side of the impeller. In these pumps, suction-pressure magnitude does not affect the resulting axial thrust.

On the other hand, axial forces acting on an overhung impeller with a single seal chamber (see Figure 53) are definitely affected by suction pressure. In addition to the unbalanced force found in a single-suction, two-seal chamber design (refer to Figure 50), there is an axial force equivalent to the product of the shaft area through the seal chamber and the difference between suction and atmospheric pressure. This force acts toward the impeller suction when the suction pressure is less than atmospheric or in the opposite direction when it is higher than atmospheric.

When an overhung impeller pump handles a suction lift, the additional axial force is very low. For example, if the shaft diameter through the stuffing box is 2 in (50.8 mm) (area = 3.14 in^2 or 20.26 cm^2), and if the suction lift is 20 ft (6.1 m) of water equivalent to an absolute pressure of 6.06 lb/in^2 (0.42 bar abs), the axial force caused by the overhung impeller and acting toward the suction will be only 27 lb (121 N). On the other hand, if the suction pressure is 100 lb/in^2 (6.89 bar), the force will be 314 lb (1405 N) and will act in the opposite direction. Therefore, because the same pump may be used under many conditions

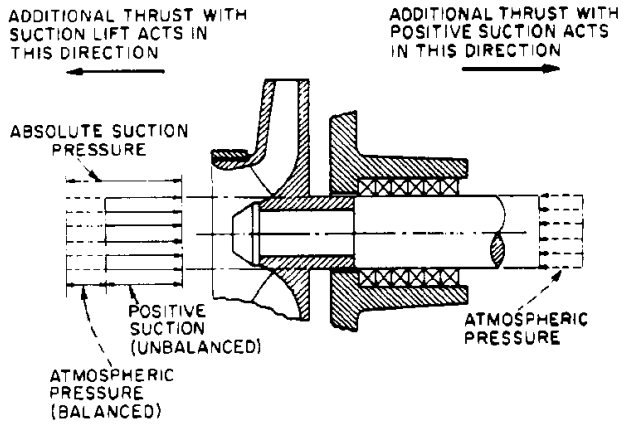


FIGURE 53 An axial thrust problem with a single-suction, overhung impeller and a single stuffing box or seal chamber

over a wide range of suction pressures, the thrust bearing of pumps with single-suction, overhung impellers must be arranged to take the thrust in either direction. They must also be selected with a sufficient thrust capacity to counteract forces set up under the maximum suction pressure established for that particular pump.

This extra thrust capacity can become quite significant in certain special cases, such as with boiler circulating pumps. These are usually of the single-suction, single-stage, overhung impeller type and may be exposed to suction pressures as high as 2800 lb/in^2 gage (193 bar). This is approximately the vapor pressure of 685°F (363°C) boiler water. If such a pump has a shaft diameter of 6 in (15.24 cm), the unbalanced thrust would be as much as 77,500 lb (346,770 N), and the thrust bearing has to be capable of counteracting this.

Axial Thrust of Single-Suction Semiopen Radial-Flow Impellers The axial thrust generated in semiopen impellers is higher than that in closed impellers. This is illustrated in Figure 58, which shows that the pressure on the open side of the impeller varies from essentially the discharge pressure at the periphery (at diameter D_2) to the suction pressure at the impeller eye (at diameter D_1). The pressure distribution on the back shroud is essentially the same as that illustrated in Figure 50, varying from discharge pressure at the periphery to some portion of this pressure at the impeller hub. This latter pressure is, of course, substantially higher than the suction pressure. The unbalanced portion of the axial thrust on the impeller is represented by the cross-hatched area in Figure 54.

One of the means available for partially balancing this increased axial thrust is to provide the back shroud with pump-out vanes, as in Figure 52.

Fully open impellers or semiopen impellers with a portion of the back shroud removed produce an axial thrust somewhat higher than closed impellers and somewhat lower than semiopen impellers.

Axial Thrust of Mixed-Flow and Axial-Flow Impellers The axial thrust in radial impellers is produced by the static pressures on the impeller shrouds. Axial-flow impellers have no shrouds, and the axial thrust is created strictly by the difference in pressure on the two faces of the impeller vanes. In addition, a difference may exist in pressure acting on the two shaft hub ends, one generally subject to discharge pressure and the other to suction pressure.

With mixed-flow impellers, axial thrust is a combination of forces caused by the action of the vanes on the liquid and those arising from the difference in the pressures acting on the various surfaces. Wearing rings are often provided on the back of mixed-flow impellers, with either balancing holes through the impeller hub or an external balancing pipe leading back to the suction.

Except for very large units and in certain special applications, the axial thrust developed by mixed-flow and axial-flow impellers is carried by thrust bearings with the necessary load capacity.

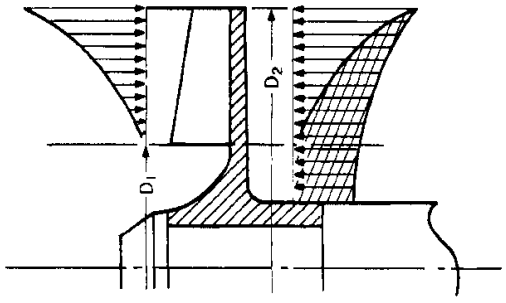


FIGURE 54 Axial thrust in a semiopen single-suction impeller

LIBERTY EXHIBIT 1017, Page 304

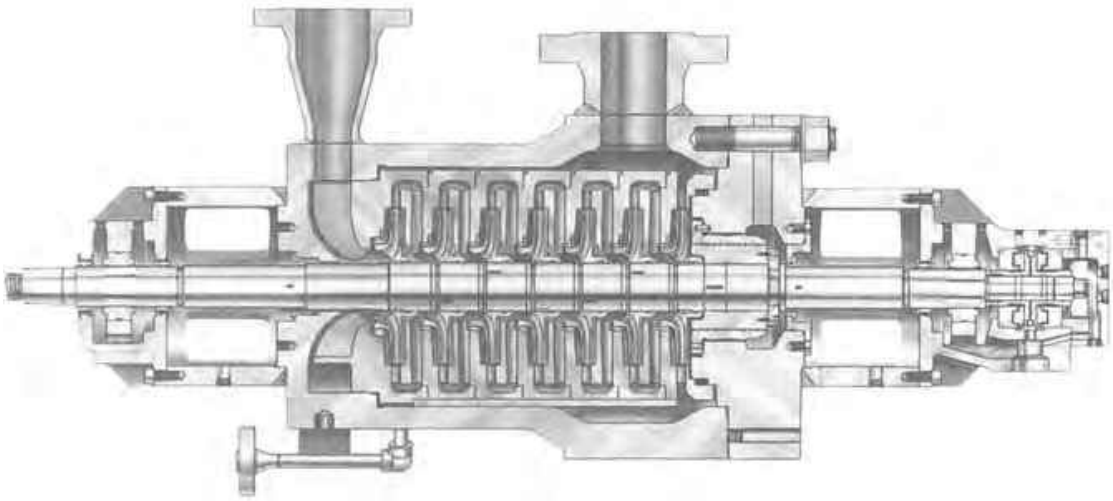


FIGURE 55 Multistage pump with single-suction impellers facing in one direction and hydraulic balancing device (Flowserve Corporation)

Axial-Thrust in Multistage Pumps Most multistage pumps are built with single-suction impellers in order to simplify the design of the interstage connections. Two obvious arrangements are possible for the single-suction impellers:

1. Several single-suction impellers can be mounted on one shaft, each having its suction inlet facing in the same direction and its stages following one another in ascending order of pressure (see Figure 55). The axial thrust is then balanced by a hydraulic balancing device.
2. An even number of single-suction impellers can be used, one-half facing in one direction and the other half facing in the opposite direction. With this arrangement, an axial thrust on the first half is compensated by the thrust in the opposite direction on the other half (see Figure 56). This mounting of single-suction impellers back to back is frequently called *opposed impellers.*

An uneven number of single-suction impellers can be used with this arrangement, provided the correct shaft and interstage bushing diameters are used to give the effect of a hydraulic balancing device that will compensate for the hydraulic thrust on one of the stages.

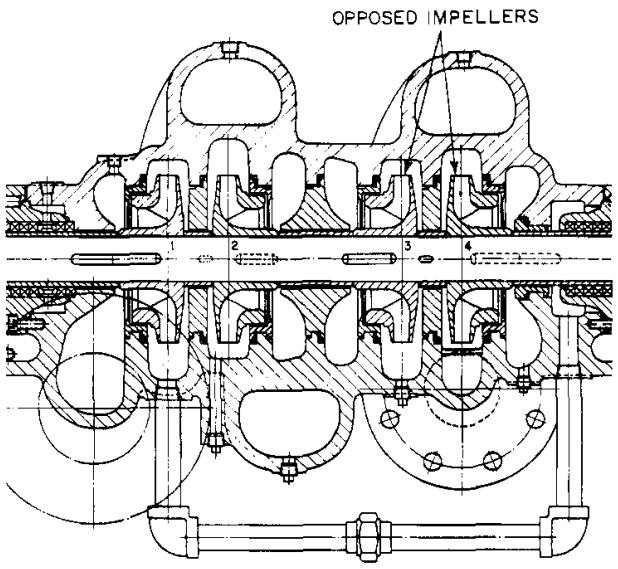


FIGURE 56 A four-stage pump with opposed impellers (Flowserve Corporation)

LIBERTY EXHIBIT 1017, Page 305

It is important to note that the opposed impeller arrangement completely balances an axial thrust only under the following conditions:

- The pump must be provided with two seal chambers.
- The shaft must have a constant diameter.
- The impeller hubs must not extend through the interstage portion of the casing separating adjacent stages.

Except for some special pumps that have an internal and enclosed bearing at one end, and therefore only one seal chamber, most multistage pumps fulfill the first condition. Because of structural requirements, however, the last two conditions are not practical. A slight residual thrust is usually present in multistage opposed impeller pumps and is carried on the thrust bearing.

HYDRAULIC BALANCING DEVICES

If all the single-suction impellers of a multistage pump face the same direction, the total theoretical hydraulic axial thrust acting toward the suction end of the pump will be the sum of the individual impeller thrusts. The thrust magnitude will be approximately equal to the product of the net pump pressure and the annular unbalanced area. Actually, the axial thrust turns out to be about 70 to 80% of this theoretical value.

Some form of hydraulic balancing device must be used to balance this axial thrust and to reduce the pressure on the seal chamber adjacent to the last-stage impeller. This hydraulic balancing device may be a balancing drum, a balancing disk, or a combination of the two.

Balancing Drums The balancing drum is illustrated in Figure 57. The balancing chamber at the back of the last-stage impeller is separated from the pump interior by a drum that is usually keyed to the shaft and rotates with it. The drum is separated by a small radial clearance from the stationary portion of the balancing device, called the *balancing-drum head*, or balancing sleeve, which is fixed to the pump casing.

The balancing chamber is connected either to the pump suction or to the vessel from which the pump takes its suction. Thus, the back pressure in the balancing chamber is only slightly higher than the suction pressure, the difference between the two being equal to the friction losses between this chamber and the point of return. The leakage between

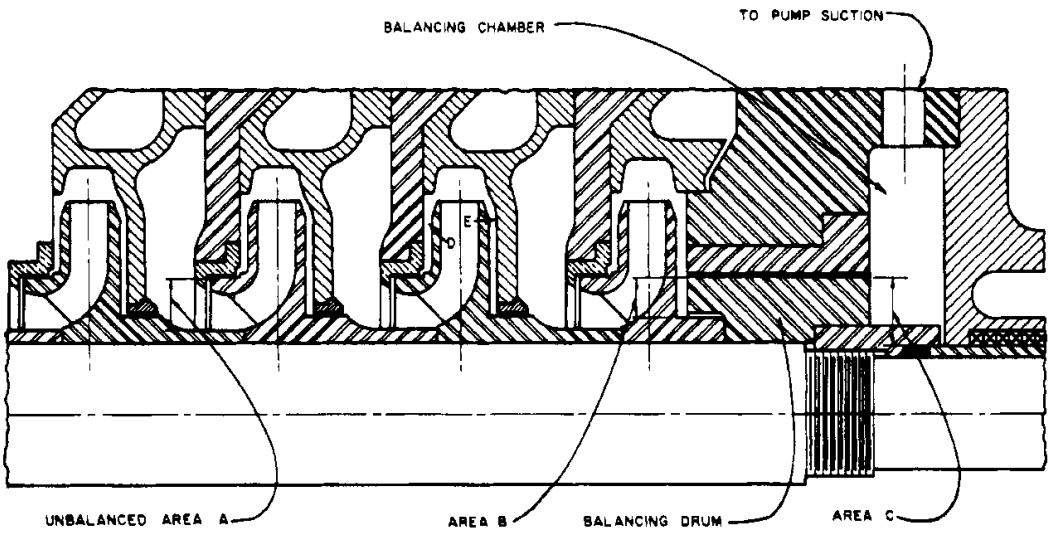


FIGURE 57 Balancing drum

the drum and the drum head is, of course, a function of the differential pressure across the drum and of the clearance area.

The forces acting on the balancing drum in Figure 57 are the following:

- *Toward the discharge end*: the discharge pressure multiplied by the front balancing area (area *B)* of the drum
- *Toward the suction end*: the back pressure in the balancing chamber multiplied by the back balancing area (area *C)* of the drum

The first force is greater than the second, thereby counterbalancing the axial thrust exerted upon the single-suction impellers. The drum diameter can be selected to balance the axial thrust completely or within 90 to 95%, depending on the desirability of carrying any thrust-bearing loads.

It has been assumed in the preceding simplified description that the pressure acting on the impeller walls is constant over their entire surface and that the axial thrust is equal to the product of the total net pressure generated and the unbalanced area. Actually, this pressure varies somewhat in the radial direction because of the centrifugal force exerted upon the liquid by the outer impeller shroud (refer to Figure 50). Furthermore, the pressures at two corresponding points on the opposite impeller faces *(D* and *E* in Figure 57) may not be equal because of a variation in clearance between the impeller wall and the casing section separating successive stages. Finally, a pressure distribution over the impeller wall surface may vary with head and capacity operating conditions.

This pressure distribution and design data can be determined quite accurately for any one fixed operating condition, and an effective balancing drum could be designed on the basis of the forces resulting from this pressure distribution. Unfortunately, varying head and capacity conditions change the pressure distribution, and as the area of the balancing drum is necessarily fixed, the equilibrium of the axial forces can be destroyed.

The objection to this is not primarily the amount of the thrust, but rather that the direction of the thrust cannot be predetermined because of the uncertainty about internal pressures. Still it is advisable to predetermine normal thrust direction, as this can influence external mechanical thrust-bearing design. Because 100% balance is unattainable in practice and because the slight but predictable unbalance can be carried on a thrust bearing, the balancing drum is often designed to balance only 90 to 95% of the total impeller thrust.

The balancing drum satisfactorily balances the axial thrust of single-suction impellers and reduces pressure on the discharge-side stuffing box. It lacks, however, the virtue of automatic compensation for any changes in axial thrust caused by varying impeller reaction characteristics. In effect, if the axial thrust and balancing drum forces become unequal, the rotating element will tend to move in the direction of the greater force. The thrust bearing must then prevent excessive movement of the rotating element. The balancing drum performs no restoring function until such time as the drum force again equals the axial thrust. This automatic compensation is the major feature that differentiates the balancing disk from the balancing drum.

Balancing Disks The operation of the simple balancing disk is illustrated in Figure 58. The disk is fixed to and rotates with the shaft. It is separated by a small axial clearance from the balancing disk head, or balancing sleeve, which is fixed to the casing. The leakage through this clearance flows into the balancing chamber and from there either to the pump suction or to the vessel from which the pump takes its suction. The back of the balancing disk is subject to the balancing chamber back pressure, whereas the disk face experiences a range of pressures. These vary from discharge pressure at its smallest diameter to back pressure at its periphery. The inner and outer disk diameters are chosen so that the difference between the total force acting on the disk face and that acting on its back will balance the impeller axial thrust.

If the axial thrust of the impellers should exceed the thrust acting on the disk during operation, the latter is moved toward the disk head, reducing the axial clearance between

LIBERTY EXHIBIT 1017, Page 307

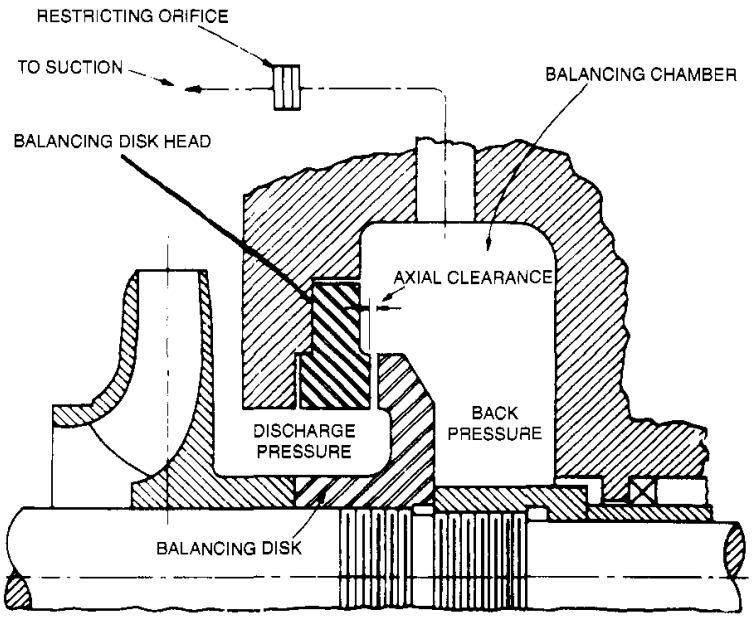


FIGURE 58 A simple balancing disk

the disk and the disk head. The amount of leakage through the clearance is reduced so that the friction losses in the leakage return line are also reduced, lowering the back pressure in the balancing chamber. This lowering of pressure automatically increases the pressure difference acting on the disk and moves it away from the disk head, increasing the clearance. Now the pressure builds up in the balancing chamber, and the disk is again moved toward the disk head until an equilibrium is reached.

To assure proper balancing in disk operation, the change in back pressure in the balancing chamber must be of an appreciable magnitude. Thus, with the balancing disk wide open with respect to the disk head, the back pressure must be substantially higher than the suction pressure to give a resultant force that restores the normal disk position. This can be accomplished by introducing a restricting orifice in the leakage return line that increases back pressure when leakage past the disk increases beyond normal. The disadvantage of this arrangement is that the pressure on the seal chamber is variable, a condition that may be injurious to the life of the seal and therefore should avoided.

Combination Balancing Disk and Drum For the reasons just described, the simple balancing disk is seldom used. The combination balancing disk and drum (see Figure 59) was developed to obviate the shortcomings of the disk while retaining the advantage of automatic compensation for axial thrust changes.

The rotating portion of this balancing device consists of a long cylindrical body that turns within a drum portion of the disk head. This rotating part incorporates a disk similar to the one previously described. In this design, radial clearance remains constant regardless of disk position, whereas the axial clearance varies with the pump rotor position. The following forces act on this device:

- *Toward the discharge end*: the sum of the discharge pressure multiplied by area A, plus the average intermediate pressure multiplied by area B
- *Toward the suction end*: the back pressure multiplied by area C

Whereas the position-restoring feature of the simple balancing disk required an undesirably wide variation of the back pressure, it is now possible to depend upon a variation of the intermediate pressure to achieve the same effect. Here is how it works: When the pump rotor moves toward the suction end (to the left in Figure 59) because of increased axial thrust, the axial clearance is reduced and pressure builds up in the intermediate

LIBERTY EXHIBIT 1017, Page 308

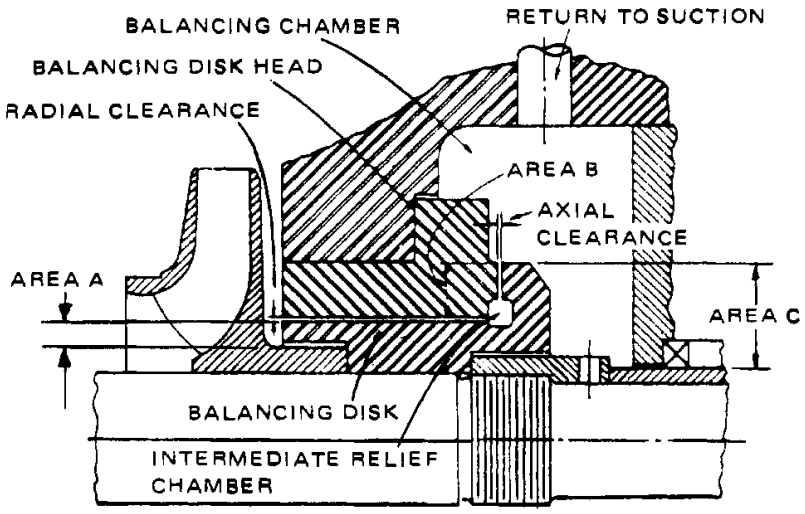


FIGURE 59 A combination balancing disk and drum

relief chamber, increasing the average value of the intermediate pressure acting on area *B*. In other words, with reduced leakage, the pressure drop across the radial clearance decreases, increasing the pressure drop across the axial clearance. The increase in intermediate pressure forces the balancing disk toward the discharge end until equilibrium is reached. Movement of the pump rotor toward the discharge end would have the opposite effect, increasing the axial clearance and the leakage and decreasing the intermediate pressure acting on area *B*.

Now numerous hydraulic balancing device modifications are in use. One typical design separates the drum portion of a combination device into two halves, one preceding and the second following the disk (see Figure 60). The virtue of this arrangement is a definite cushioning effect at the intermediate relief chamber, thus avoiding too positive a restoring action, which might result in the contacting and scoring of the disk faces.

SHAFTS AND SHAFT SLEEVES

The basic function of a centrifugal pump shaft is to transmit the torques encountered when starting and during operation while supporting the impeller and other rotating parts. It must do this job with a deflection less than the minimum clearance between rotating and stationary parts. The loads involved are (1) the torques, (2) the weight of the parts, and (3) both radial and axial hydraulic forces. In designing a shaft, the maximum allowable deflection, the span or overhang, and the location of the loads all have to be considered, as does the critical speed of the resulting design.

Shafts are usually proportioned to withstand the stress set up when a pump is started quickly, such as when the driving motor is energized directly across the line. If the pump handles hot liquids, the shaft is designed to withstand the stress set up when the unit is started cold without any preliminary warm-up.

Critical Speeds Any object made of an elastic material has a natural period of vibration. When a pump rotor or shaft rotates at any speed corresponding to its natural frequency, minor unbalances will be magnified. These speeds are called the *critical speeds*.

In conventional pump designs, the rotating assembly is theoretically uniform around the shaft axis and the center of mass should coincide with the axis of rotation. This theory does not hold for two reasons. First, minor machining or casting irregularities always occur. Second, variations exist in the metal density of each part. Thus, even in vertical-shaft machines having no radial deflection caused by the weight of the parts, this eccentricity of the center of mass produces a centrifugal force and therefore a deflection when

LIBERTY EXHIBIT 1017, Page 309

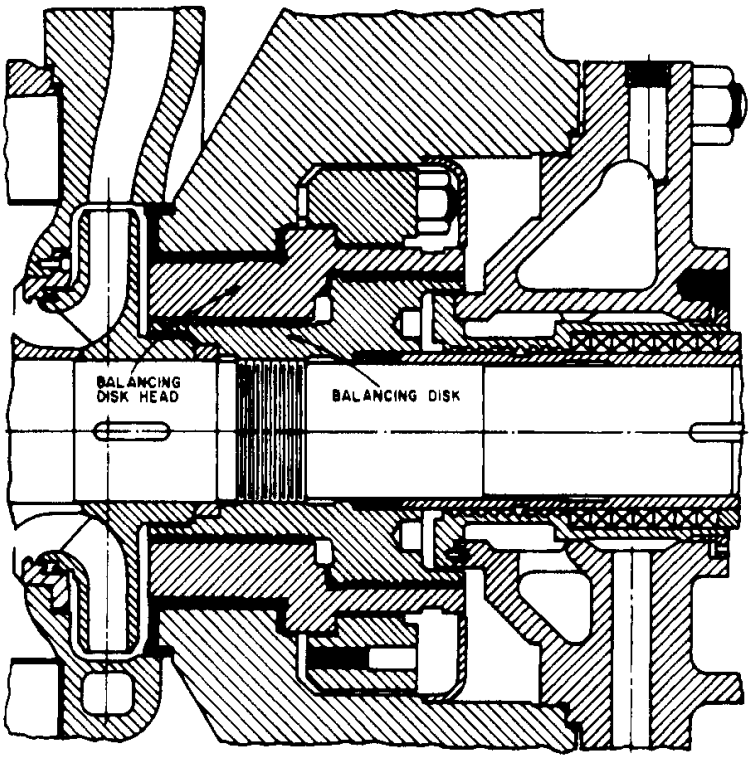


FIGURE 60 A combination balancing disk and drum with a disk located in the center portion of the drum (Flowserve Corporation)

the assembly rotates. At the speed where the centrifugal force exceeds the elastic restoring force, the rotor will vibrate as though it were seriously unbalanced. If it is run at that speed without restraining forces, the deflection will increase until the shaft fails.

Rigid and Flexible Shaft Designs The lowest critical speed is called the first critical speed, the next highest is called the second, and so forth. In centrifugal pump nomenclature, a *rigid shaft* means one with an operating speed lower than its first critical speed. A *flexible shaft* is one with an operating speed higher than its first critical speed. Once an operating speed has been selected, relative shaft dimensions must still be determined. In other words, it must be decided whether the pump will operate above or below the first critical speed.

Actually, the shaft critical speed can be reached and passed without danger because frictional forces tend to restrain the deflection. These forces are exerted by the surrounding liquid, and the various internal leakage joints acting as internal liquid-lubricated bearings. Once the critical speed is passed, the pump will run smoothly again up to the second speed corresponding to the natural rotor frequency, and so on to the third, fourth, and all higher critical speeds.

Designs rated for 1800 rpm (or lower) are usually of the rigid-shaft type. On the other band, high-head 3600 rpm (or higher) multistage pumps, are frequently of the flexible-shaft type. It is possible to operate centrifugal pumps above their critical speeds for the following two reasons: (1) very little time is required to attain full speed from rest (the time required to pass through the critical speed must therefore be extremely short) and (2) the pumped liquid in the internal leakage joints acts as a restraining force on the vibration.

Shaft Sizing Shaft diameters are usually larger than what is actually needed to transmit the torque. Two factors that assure this conservative design are a) shaft deflection limit requirements at the impellers and mechanical seal faces, and b) requirements for ease of rotor assembly.

LIBERTY EXHIBIT 1017, Page 310

For between bearings pumps (single-stage double-suction, multistage), the maximum shaft diameter is at the impeller mounting surface. From there, the shaft is stepped down in diameter toward the bearing mounting surfaces and the coupling mounting surface. The shaft size at the coupling must consider torsional strength; the remainder of the shaft size is based on other considerations, including the steps in diameter required for shaft nuts or other axial location devices for the impeller and sealing members (mechanical seal components or shaft sleeves for packing. When these considerations have been decided, the rotor must be analyzed for conformance to the dynamic requirements or deflection and critical speed. These topics are covered in Section 2.3.

Shaft Sleeves Pump shafts are usually protected from erosion, corrosion, and wear at seal chambers, leakage joints, internal bearings, and in the waterways by renewable sleeves. Years ago, the most common shaft sleeve function was to protect the pump shaft from wear at stuffing box packing. However, most pumps today use mechanical seals, not packing. Furthermore, most mechanical seals today are cartridge mechanical seals, and the sleeve is part of the seal package. Packing and mechanical seal topics are covered in Section 5.

Shaft sleeves serving other functions are given specific names to indicate their purpose. For example, a shaft sleeve used between two multistage pump impellers in conjunction with the interstage bushing to form an interstage leakage joint is called an *interstage* or *distance sleeve*.

For between bearings pumps, a favored shaft sleeve construction for pumps equipped with packing uses an external shaft nut to hold the sleeve in an axial position against the impeller hub. Sleeve rotation is prevented by a key, usually an extension of the impeller key (see Figure 61). The axial thrust of the impeller(s) is transmitted through the sleeve to the external shaft nut.

For pumps using cartridge mechanical seals, the preferred design is shown in Figure 63. An internal impeller nut locates the impeller axially on both sides, leaving a large open seal chamber for installing the seal cartridges and locking them to both the seal chamber and the shaft. When shaft nuts are used to retain the sleeves and impellers axially, they are usually manufactured with right- and left-hand threads. The friction of the pumpage and inadvertent contact with stationary parts or bushings will tend to tighten the nuts against the sleeve and impeller hub (rather than loosen them). Usually, the shaft sleeves utilize extended impeller keys to prevent rotation.

In pumps with overhung impellers, various types of sleeves are used. Most pumps use mechanical seals, and the shaft sleeve is usually a part of the mechanical seal package supplied by the seal manufacturer. Many mechanical seals are of the cartridge design, which is set and may be bench-tested for leakage prior to installation in the pump. (For a further discussion of mechanical seals, see Section 5.2.)

For overhung impeller pumps that utilize packing for sealing, the packing sleeves generally extend from the impeller hub through the seal chambers (or stuffing boxes) to protect

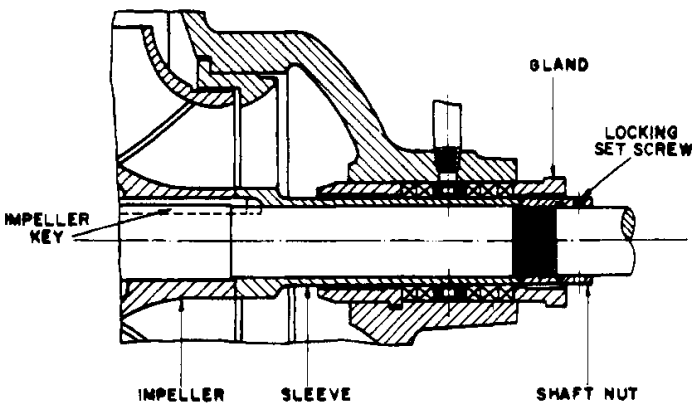


FIGURE 61 A sleeve with external locknut and impeller key extending into the sleeve to prevent rotation

LIBERTY EXHIBIT 1017, Page 311

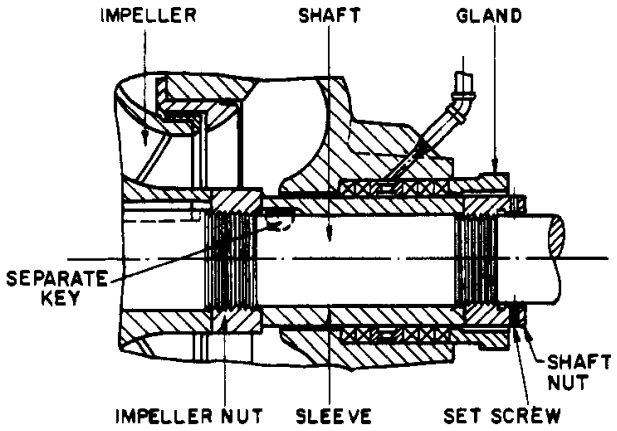


FIGURE 62 A sleeve with an internal impeller nut, external shaft-sleeve nut, and a separate key for the sleeve

the pump shaft from wear (see Figure 63). The sleeves are usually keyed to the shaft to prevent rotation. If a hook-type sleeve is used, the hook part of the sleeve is clamped between the impeller and a shaft shoulder to maintain the axial position of the sleeve. A hook-type sleeve used to be popular for overhung impeller pumps that operate at high temperatures because it is clamped at the impeller end and the rest of the sleeve is free to expand axially with temperature changes. But with the increased use of cartridge-type seals, the use of hook-type sleeves is minimal today.

In designs with a metal-to-metal joint between the sleeve and the impeller hub or shaft nut, a sealing device is required between the sleeve and the shaft to prevent leakage. Pumped liquid can leak into the clearance between the shaft and the sleeve when operating under a positive suction head and air can leak into the pump when operating under a negative suction head. This seal can be accomplished by means of an *O-ring*, as shown in Figure 64, or a flat gasket. For high temperature services, the sealing device must be either acceptable for the temperature to which it will be exposed, or it must be located outside the high temperature liquid environment. An alternative design used for some high-temperature process pumps is shown in Figure 65. In this arrangement, the contact surface of the hook-type sleeve and the shaft is ground at a 45° angle to form a metal-to-metal seal. That end of the sleeve is locked, but the other is *free* to expand with temperature changes.

When O-rings are used, any sealing surfaces must be properly finished to ensure a positive seal is achieved. All bores and changes in diameter over which O-rings must be passed should be properly radiused and chamfered to protect against damage during assembly. Guidelines for assembly dimensions and surface finish criteria are listed in O-ring manufacturers' catalogs.

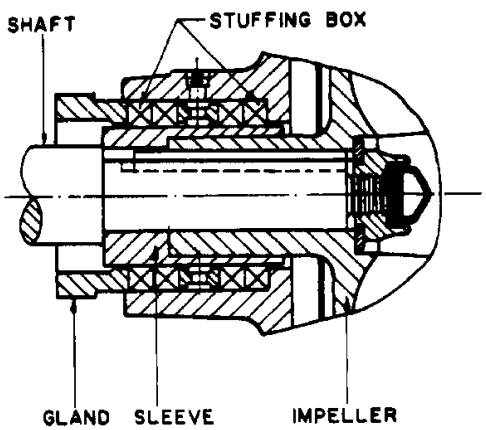


FIGURE 63 A sleeve for pumps with an overhung impeller

LIBERTY EXHIBIT 1017, Page 312

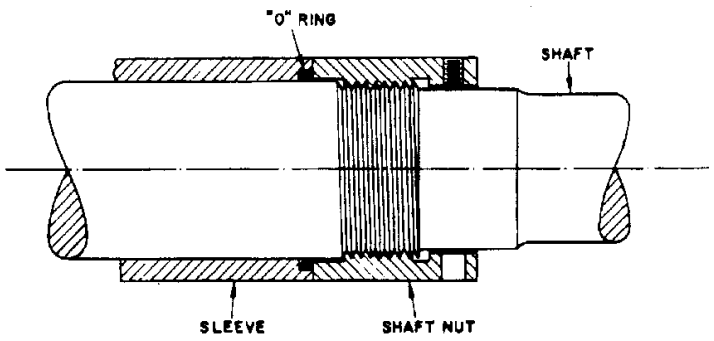


FIGURE 64 A seal arrangement for the shaft sleeve to prevent leakage along the shaft

Material for Packing Sleeves Packing sleeves are surrounded in the stuffing box by packing. The sleeve must be smooth so that it can turn without generating too much friction and heat. Thus, the sleeve materials must be capable of taking a very fine finish, preferably a polish. Cast-iron is therefore not suitable. A hard bronze is generally used for pumps handling clear water, but chrome or other stainless steels are sometimes preferred. For pumps subject to abrasives, hardened chrome or other stainless steels give good results. In most applications, a hardened chromium steel sleeve will be technically adequate, and the most economical choice. For severe or unusual conditions, coated sleeves are used. Ceramic coatings, applied using a plasma spray process, have also been used. Chromium oxide and aluminum oxide are the most common ceramic coatings. Both are extremely hard and resist abrasive wear well.

Ceramic coatings have been replaced in some applications by tungsten carbide coatings applied using a *high-velocity oxyfuel* (HVOF) process. The superior impact resistance and bond strength of these coatings is well documented. Another coating that is widely used on pump sleeves is a nickel-chromium-silicon-boron self-fluxing coating. This coating has a good resistance to galling and moderate resistance to abrasive wear.

Sleeves intended for coating should be machined with an undercut, so that the coating does not extend to the edge of the sleeve. This will prevent chipping at the edge, especially with the more brittle ceramic coatings.

SEAL CHAMBERS AND STUFFING BOXES

Seal chambers have the primary function of protecting the pump against leakage at the point where the shaft passes out through the pump pressure casing. If the pump handles a suction lift and the pressure at the bottom of the seal chamber (the point closest to the

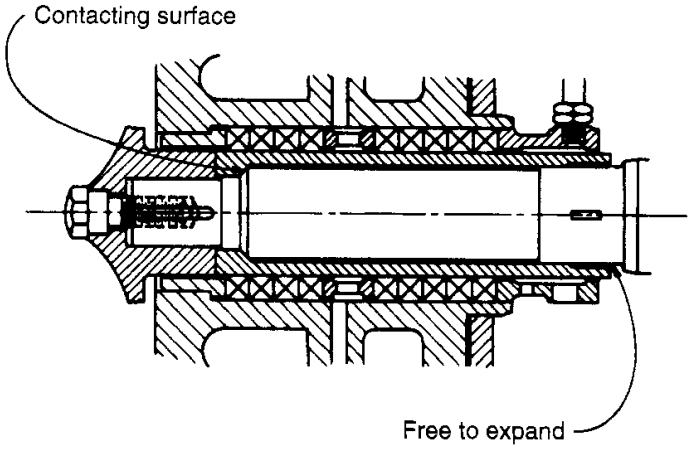


FIGURE 65 A sleeve with a 45° bevel contacting surface

LIBERTY EXHIBIT 1017, Page 313

inside of the pump) is below atmospheric, the seal chamber function is to prevent air leakage into the pump. If this pressure is above atmospheric, the function is to prevent liquid leakage out of the pump.

When sealing is accomplished by means of a mechanical seal, the seals are installed in a *seal chamber*. When sealing is accomplished by means of packing, the seal chamber is commonly referred to as a *stuffing box*. Packing and mechanical seal topics are covered in Section 5.

Sealing Liquid Arrangements When a pump handles clean, cool water, sealing liquid connections are usually to the pump discharge or, in multistage pumps, to an intermediate stage. An independent supply of sealing water should be provided if any of the following conditions exist:

- A suction lift in excess of 15 ft (4.5 m)
- A discharge pressure under 10 lb/in^2 (0.7 bar)
- Hot water (over 250°F or 120°C) being handled without adequate cooling (except for boiler-feed pumps, in which lantern rings are not used)
- Muddy, sandy, or gritty water being handled
- The pump is a hot-well pump.
- The liquid being handled is other than water, such as acid, juice, molasses, or sticky liquids, without special provision in the stuffing box design for the nature of the liquid

If the suction lift exceeds 15 ft (4.5 m), excessive air infiltration through the stuffing boxes may make priming difficult unless an independent seal is provided. A discharge pressure under 10 lb/in^2 (0.7 bar) may not provide sufficient sealing pressure. Hot-well (or condensate) pumps operate with as much as a 28-in Hg (710 mm Hg) vacuum, and air infiltration would take place when the pumps are standing idle in standby service.

When sealing water is taken from the pump discharge, an external connection may be made through small-diameter piping (see Figure 66) or internal passages. In some pumps, these connections are arranged so that a sealing liquid can be introduced into the packing or mechanical seal space through an internal drilled passage either from the pump casing or from an external source. When the liquid pumped is used for sealing, the external connection is plugged. If an external sealing liquid source is required, it is connected to the external pipe tap with a socket-head pipe plug inserted at the internal pipe tap.

For packing, it is sometimes desirable to locate the lantern ring with more packing on one side than on the other. For example, in gritty-water services, a lantern ring location closer to the inner portion of the pump would divert a greater proportion of sealing liquid into the pump, thereby keeping grit from working into the box. An arrangement with most of the packing rings between the lantern ring and the inner end of the stuffing box would be applied to reduce dilution of the pumped liquid.

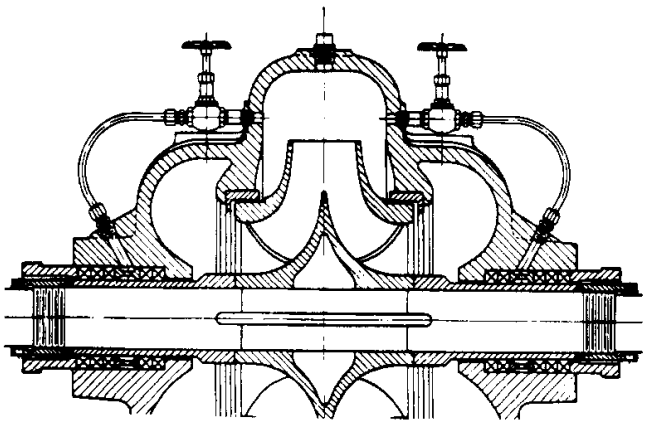


FIGURE 66 Piping connections from the pump discharge to seal cages

LIBERTY EXHIBIT 1017, Page 314

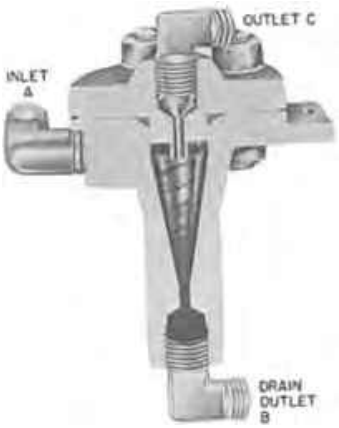


FIGURE 67 An illustration of the priniciple of cyclone separators (Flowserve Corp.)

Some pumps handle water in which there are small, even microscopic, solids. Using water of this kind as a sealing liquid introduces the solids into the leakage path, shortening the life of the packing and sleeves. It is sometimes possible to remove these solids by installing small pressure filters in the sealing water piping from the casing to the stuffing box.

Filters ultimately get clogged, though, unless they are frequently backwashed or otherwise cleaned out. This disadvantage can be overcome by using a cyclone (or centrifugal) separator. The operating principle of the cyclone separator is based on the fact that if a liquid under pressure is introduced tangentially into a vortexing chamber, a centrifugal force will make it rotate in the chamber, creating a vortex. Particles heavier than the liquid in which they are carried will hug the outside wall of the vortexing chamber and the liquid in the center of the chamber will be relatively free of foreign matter. The action of such a separator is illustrated in Figure 67. Liquid piped from the pump discharge or from an intermediate stage of a multistage pump is piped to inlet tap A, which is drilled tangentially to the cyclone bore. The liquid containing solids is directed downward to the apex of the cone at outlet tap B and is piped to the suction or to a low-pressure point in the system. The cleaned liquid is taken off at the center of the cyclone at outlet tap C and is piped to the stuffing box.

Sand that will pass through a No. 40 sieve will be completely eliminated in a cyclone separator with supply pressures as low as 20 lb/in^2 (1.4 bar). With 100 lb/in^2 (7-bar) supply pressure, 95% of the particles of 5-micron size will be eliminated.

Most city ordinances require that some form of backflow preventer be interposed between city water supply lines and connections to equipment where backflow or siphoning could contaminate a drinking water supply.

This is the case, for instance, with an independent sealing supply used for stuffing boxes of sewage pumps. Quite a variety of backflow preventers are available. In most cases, the device consists of two spring-loaded check valves in a series and a spring-loaded, diaphragm-actuated, differential-pressure relief valve located in the zone between the check valves (see Figure 68).

Stuffing Box Packing See Section 5.1.

MECHANICAL SEALS VERSUS PACKING

Sealing with a packed stuffing box is impractical for many conditions of service. In an ordinary packed stuffing box, the sealing between the rotating shaft or shaft sleeve and the stationary portion of the stuffing box (or seal chamber) is accomplished by means of rings of packing forced between the two surfaces and held tightly in place by a packing gland. The leakage around the shaft is controlled by merely tightening or loosening the packing

LIBERTY EXHIBIT 1017, Page 315

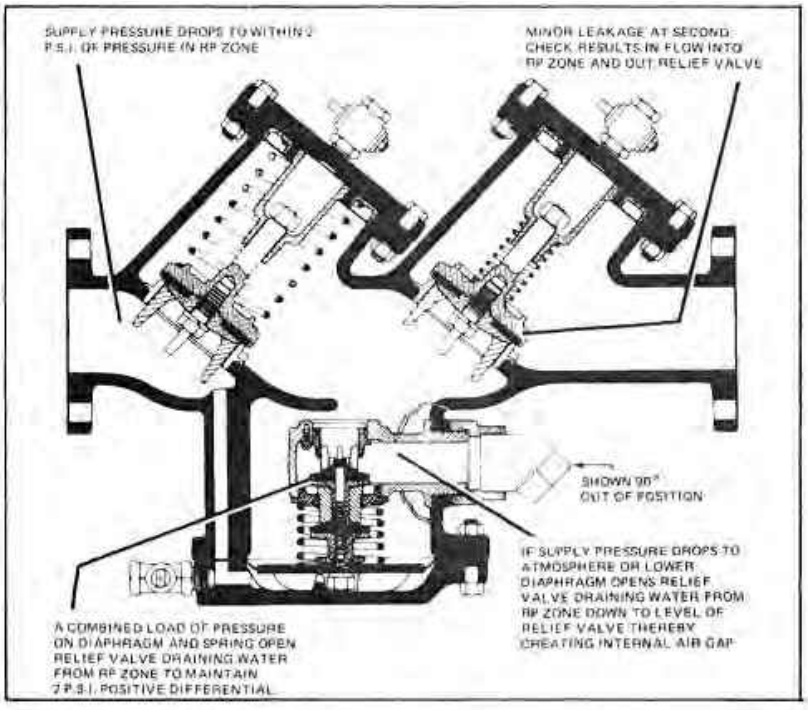


FIGURE 68 Backflow preventer (Hersey Products)

gland nuts (or bolts). The actual sealing surfaces consist of the axial rotating surface of the shaft or shaft sleeve and the stationary packing. Attempts to reduce or eliminate all leakage from a conventional packed stuffing box increase the compressive load of the packing gland on the packing. The packing, being semiplastic, forms more closely to the shaft or shaft sleeve and tends to reduce the leakage. After a certain point, however, the leakage between the packing and the rotating shaft or shaft sleeve becomes inadequate to carry away the heat generated by the packing rubbing on the rotating surface, and the packing fails to function. This failure can result in burned packing, packing "blow out," and severely damaged shaft or shaft sleeve surfaces. If the sealing surface is coated, this coating may be destroyed. Even before this condition is reached, the shaft or shaft sleeve may be severely worn and scored by the packing, so that it becomes impossible to pack the stuffing box satisfactorily.

These undesirable characteristics prohibit the use of packing as a sealing method if some leakage of the pumpage to the atmosphere is not acceptable. Packing is limited in its application pressure and temperature range (see Section 5.1), and it is usually not acceptable for any flammable or hazardous pumping services. To address these limitations, the mechanical seal was developed (see Section 5.2). The mechanical seal has found general acceptance in nearly all pumping applications. Packing is still used in certain low-pressure, low-temperature applications where leakage of the pumpage is not a problem and a history of satisfactory, economical service exists.

Mechanical seals are not always the solution to every sealing situation. Seals are still subject to failure, and their failure may be more rapid and abrupt than that of packing. If packing fails, the pump can many times be kept running by temporary adjustments until it is convenient to shut it down. If a mechanical seal fails, most often the pump must be shut down immediately. As both packed stuffing boxes and conventional mechanical face seals are subject to wear, both are subject to failure. Whether one or the other should be used depends on the specific application and the experience of the user. In some cases, both give good service and the choice becomes a matter of personal preference or cost. Table 2 adds other comments and summarizes some advantages and disadvantages of packing and mechanical seals.

Centrifugal Pump Mechanical Seals See Section 5.2.

Previous Page

TABLE 2 Comparison of packing and mechanical seals

Advantages	Disadvantages
Packing	
1. Lower initial cost 2. Easily installed as rings and glands are split 3. Good reliability to medium pressures and shaft speeds 4 Can handle large axial movements (thermal expansion of stuffing box versus shaft) 5. Can be used in rotating or reciprocating applications 6. Leakage tends to increase gradually, giving warning of impending breakdown	1. Relatively high leakage 2. Requires regular maintenance 3. Wear of shaft of shaft sleeve can be relatively high 4. Power losses may be high
Mechanical seals	
1. Very low leakage/no leakage 2. Require no maintenance 3. Eliminate sleeve wear/shaft wear 4. Very good reliability 5. Can handle higher pressures and speeds 6. Easily applied to carcinogenic, toxic, flammable, or radioactive liquids 7. Low power loss	1. Higher initial cost 2. Easily installed but may require some disassembly of pump (couplings and so on)

Source: John Crane Inc.

Injection-Type Shaft Seals See Section 5.3.

BEARINGS

See Section 6.

Oil Film or Sleeve Bearings See Section 6.1.

COUPLINGS

Centrifugal pumps are connected to their drivers through couplings of one sort or another, except for close-coupled units, in which the impeller is mounted on an extension of the shaft of the driver.

Because couplings can be used with both centrifugal and positive displacement pumps, they are discussed separately in Section 9.3.

BEDPLATE AND OTHER PUMP SUPPORTS

For very obvious reasons, it is desirable that pumps and their drivers be removable from their mountings. Consequently, they are usually bolted and doweled to machined surfaces

that in turn are firmly connected to a foundation. To simplify the installation of horizontal-shaft units, these machined surfaces are usually part of a common bedplate on which either the pump or the pump and its driver have been prealigned.

Bedplates The primary function of a pump bedplate is to furnish mounting surfaces for the pump feet that can be rigidly attached to the foundation. Mounting surfaces are also necessary for the feet of the pump driver or drivers and for the feet of any independently mounted power transmission device. Although such surfaces could be provided by separate bedplates or by individually planned surfaces, it would be necessary to align these separate surfaces and fasten them to the foundation with the utmost care. Usually, this method requires in-place mounting in the field as well as drilling and tapping for the bolts after all the parts have been aligned. To minimize such field work, coupled horizontal-shaft pumps are usually purchased with a continuous base extending under the pump and its driver. Ordinarily, both these units are mounted and aligned at the place of manufacture.

Although such bases are designed to be quite rigid, they deflect if improperly supported. It is therefore necessary to support them on a foundation that can supply the required rigidity. Furthermore, as the base can be sprung out of shape by improper handling during transit, it is imperative that the alignment be carefully rechecked during erection and prior to starting the unit.

As the unit size increases, so does the size, weight, and cost of the base required. The cost of a prealigned base for most large units exceeds the cost of the field work necessary to align individual bedplates or soleplates and to mount the component parts. Such bases are therefore used only if appearances require them or if their function as a drip collector justifies the additional cost. Even in fairly small units, the height at which the feet of the pump and the other elements are located may differ considerably. A more rigid and nice-looking installation can frequently be obtained by using individual bases or soleplates and building up the foundation to various heights under the separate portions of equipment.

Baseplates are usually provided with a raised edge or raised lip around the base to prevent dripping or draining onto the floor (see Figure 69). The base itself is sloped toward one end to collect the drainage for further disposal. A drain pocket is provided near the bottom of the slope, sometimes with a mesh screen. A tapped connection in the pocket permits piping the drainage to a convenient point.

Bedplates are usually fabricated from steel plate and structural steel shapes (see Figures 70 and 71). Even though most of these fabrications have a drain capability, because of the popular use of mechanical seals and the containment of stuffing box leakage for pumps that continue to use shaft packing (leakage is usually collected in the bearing

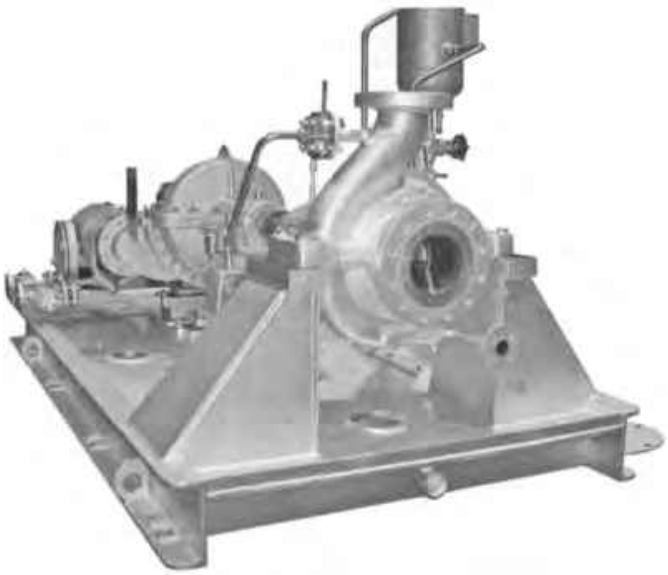


FIGURE 69 Horizontal shaft overhung pump and driver on a structural steel bedplate with a raised edge around the base and a tapped drainage connection (Flowserve Corporation)

LIBERTY EXHIBIT 1017, Page 318

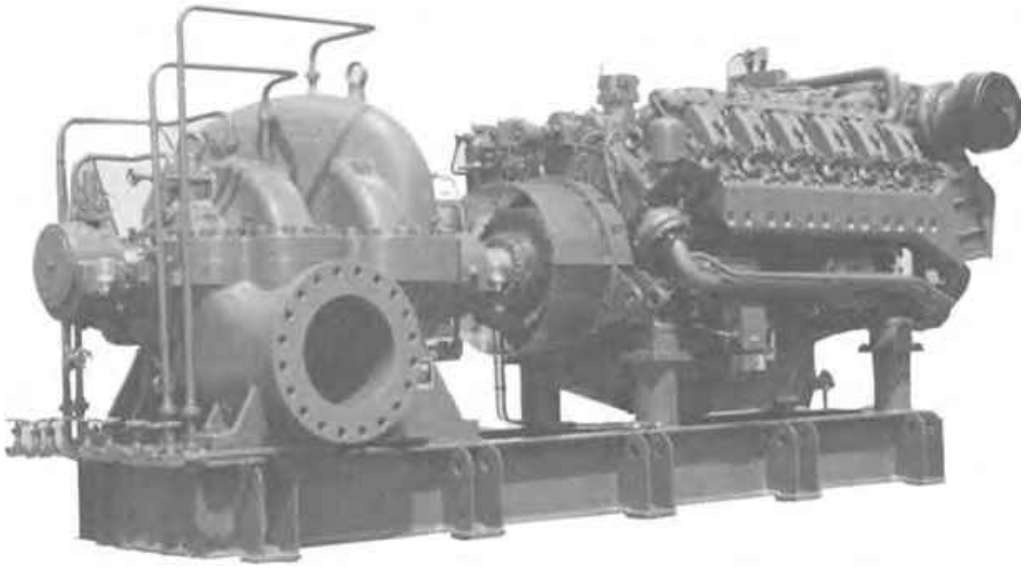


FIGURE 70 Horizontal shaft centrifugal pump and internal combustion engine mounted on a structural steel bedplate (Flowserve Corporation)

bracket and piped to a common collecting point), the bedplate surfaces actually are seldom used to collect leakage from the pumping equipment during operation. Bedplate drain surfaces are usually employed to contain the leakage of pumpage and other liquids during pump maintenance and removal or in the event of a seal or packing failure.

Soleplates Soleplates are cast-iron or steel pads located under the feet of the pump or its driver and are embedded in the foundation. The pump or its driver is doweled and bolted to them. Soleplates are customarily used for vertical dry-pit pumps and also for some of the larger horizontal units to save the cost of the large bedplates otherwise required.

Centerline Support For operation at high temperatures, the pump casing must be supported as near to its horizontal centerline as possible in order to prevent excessive strains caused by temperature differences. Such strains might seriously disturb the alignment of the unit and eventually damage it. Centerline construction is usually employed in boiler-feed, refinery, and hot-water circulating pumps (see Figure 72). The exact temperature at which centerline support construction becomes mandatory varies from 250°F to 350°F (121°C to 177°C).

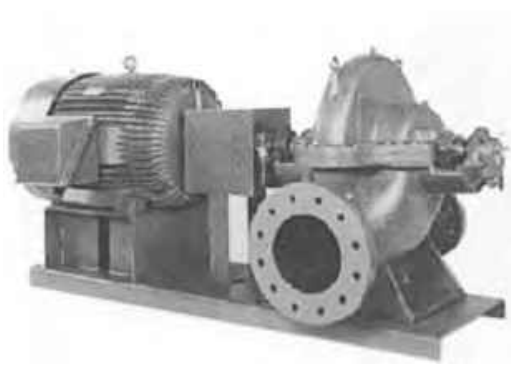


FIGURE 71 Horizontal shaft centrifugal pump and driver on a structural steel bedplate made of a simple channel shape (Flowserve Corporation)



FIGURE 72 Single-stage, double-suction pump with centerline support (Flowserve Corporation)

LIBERTY EXHIBIT 1017, Page 319

Horizontal Units Using Flexible Pipe Connections The previous discussion of bedplates and supports for horizontal-shaft units assumed their application would be to pumps with piping setups that do not impose hydraulic thrusts on the pumps. If flexible pipe connections or expansion joints are desirable in the suction or discharge piping of a pump (or in both), the pump manufacturer should be so advised for several reasons. First, the pump casing will be required to withstand various stresses caused by the resultant hydraulic thrust load. Although this is rarely a limiting or dangerous factor, it is best that the manufacturer have the opportunity to check the strength of the pump casing. Second, the resulting hydraulic thrust has to be transmitted from the pump casing through the casing feet to the bedplate or soleplate and then to the foundation. Usually, horizontal-shaft pumps are merely bolted to their bases or soleplates, and so any tendency to displacement is resisted only by the frictional grip of the casing feet on the base and by relatively small dowels. If flexible pipe joints are used, this attachment may not be sufficient to withstand the hydraulic thrust. If high hydraulic thrust loads are to be encountered, therefore the pump feet must be keyed to the base or supports. Similarly, the bedplate or supporting soleplates must be of a design that will permit transmission of the load to the foundation. Each of these design elements must be checked to confirm their capability to withstand hyraulic thrust loads from flexible pipe connections. Preferably expansion joints will be restrained to avoid transmitting loads to the pump nozzles.

VERTICAL PUMPS

Vertical-shaft pumps fall into two classifications: dry-pit and wet-pit. Dry-pit pumps are surrounded by air, and the wet-pit types are either fully or partially submerged in the liquid handled.

Vertical Dry-Pit Pumps Dry-pit pumps with external bearings include most small, medium, and large vertical sewage pumps, most medium and large drainage and irrigation pumps for medium and high heads, many large condenser circulating and water supply pumps, and many marine pumps. Sometimes the vertical design is preferred (especially for marine pumps) because it saves floor space. At other times, it is desirable to mount a pump at a low elevation because of suction conditions, and it is then also preferable or necessary to have the pump driver at a high elevation. The vertical pump is normally used for large capacity applications because it is more economical than the horizontal type, all factors considered.

Many vertical dry-pit pumps are basically horizontal designs with minor modifications (usually in the bearings) to adapt them for vertical-shaft drive. This is not true of small- and medium-sized sewage pumps, however. In these units, a purely vertical design is the most popular. Most of these sewage pumps have elbow suction nozzles (see Figures 73 and 74) because their suction supply is usually taken from a wet well adjacent to the pit in which the pump is installed. The suction elbow usually contains a handhole with a removable cover to provide easy access to the impeller.

To dismantle one of these pumps, the stuffing box head must be unbolted from the casing after the intermediate shaft or the motor and motor stand have been removed. The rotor assembly is drawn out upward, complete with the stuffing box head, the bearing housing, and the like. This rotor assembly can then be completely dismantled at a convenient location.

Vertical-shaft installations of single-suction pumps with a suction elbow are commonly furnished with either a pedestal or a base elbow (refer to Figure 73), both of which can be bolted to soleplates or even grouted in. The grouting arrangement is not desirable unless there is full assurance that the pedestal or elbow will never be disturbed or that the grouted space is reasonably regular and the grout will separate from the pump without excessive difficulty.

Vertical single-suction pumps with bottom suction are commonly used for larger sewage, water supply, or condenser circulating applications. Such pumps are provided with wing feet that are bolted to soleplates grouted in concrete pedestals or piers (see Figure 75).

LIBERTY EXHIBIT 1017, Page 320

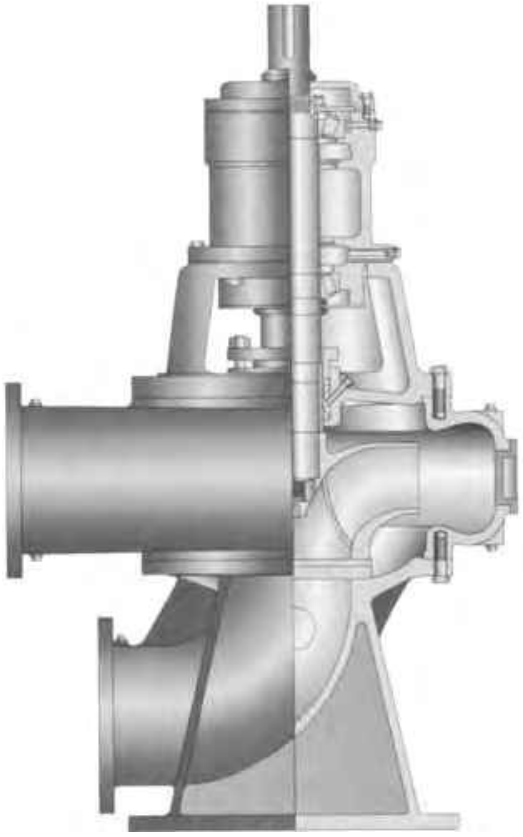


FIGURE 73 Section of a vertical sewage pump with end-suction (elbow) and side discharge (Flowserve Corporation)

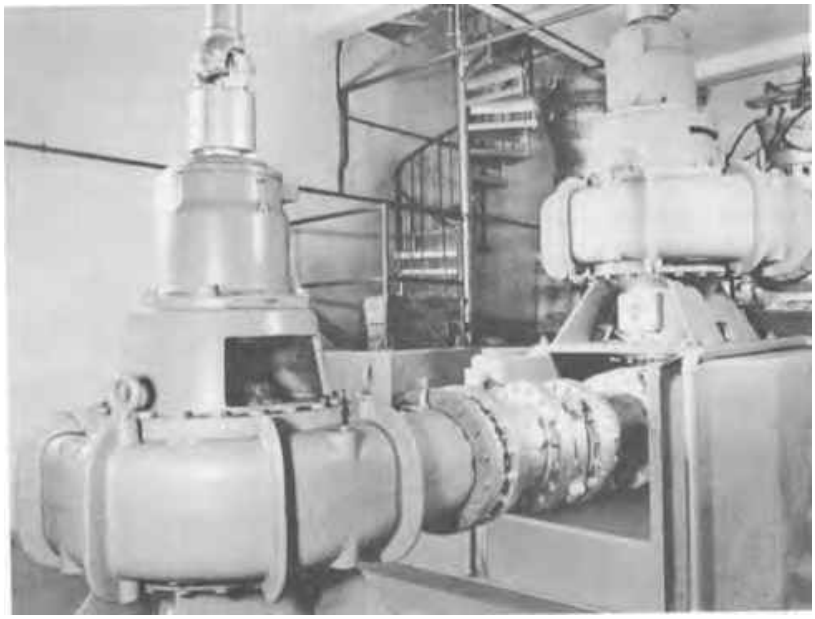


FIGURE 74 An installed vertical sewage pump similar to that shown in Figure 102 (Flowserve Corporation)

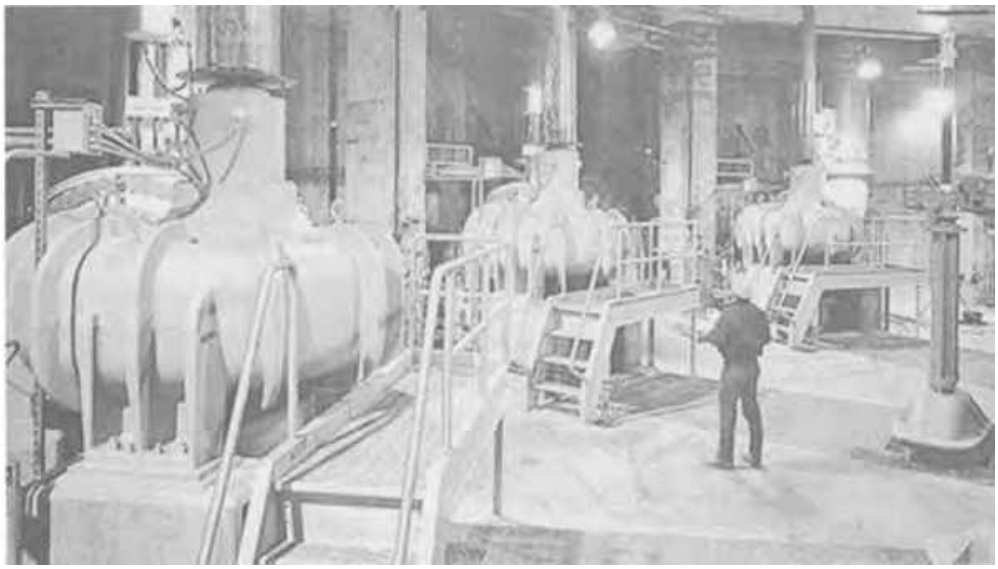


FIGURE 75 Vertical bottom-suction volute pumps installed in a sewage pumping station (Flowserve Corporation)

Sometimes the wing feet may be grouted right in the pedestals. These must be suitably arranged to provide proper access to any handholes in the pump and to allow clearance for the elbow suction nozzles if these are used.

If a vertical pump is applied to a condensate service or some other service for which the eye of the impeller must be vented to prevent vapor binding, a pump with a bottom single-inlet impeller is not desirable because it does not permit effective venting. Neither does a vertical pump employing a double-suction impeller (see Figure 76 The most suitable design for such applications incorporates a top single-inlet impeller (see Figure 77).



FIGURE 76 A vertical double-suction volute pump with a direct-mounted motor (Flowserve Corporation)

LIBERTY EXHIBIT 1017, Page 322

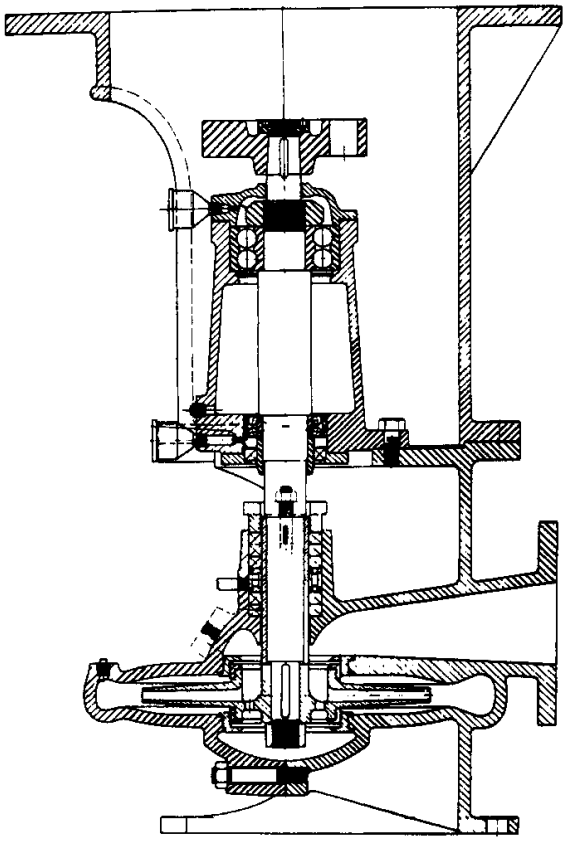


FIGURE 77 A section of a vertical pump with a top-suction inlet impeller (Flowserve Corporation)

If the driver of a vertical dry-pit pump can be located immediately above the pump, it is often supported on the pump itself. The shafts of the pump and driver may be connected by a flexible coupling, which requires that each have its own thrust bearing. If the pump shaft is rigidly coupled to the driver shaft or is an extension of the driver shaft, a common thrust bearing is used, normally in the driver.

Although the driving motors are frequently mounted on top of the pump casing, one important reason for the use of the vertical shaft design is the possibility of locating the motors at an elevation sufficiently above the pumps to prevent the accidental flooding of the motors. The pump and its driver may be separated by an appreciable length of shafting, which may require steady bearings between the two units. Section 9.3.1 discusses the construction and arrangement of the shafting used to connect vertical pumps to drivers located some distance above the pump elevation.

Bearings for vertical dry-pit pumps and for intermediate guide bearings are usually antifriction grease-lubricated types to simplify the problem of retaining a lubricant in a housing with a shaft projecting vertically through it. Larger units, for which antifriction bearings are not available or desirable, use self-oiling, babbitt steady bearings with spiral oil grooves (see Figures 78 and 79). Figure 79 illustrates a vertical dry-pit pump design with a single-sleeve line bearing. The pump is connected by a rigid coupling to its motor (not shown), which is provided with a line and a thrust bearing.

Vertical dry-pit centrifugal pumps are structurally similar to horizontal-shaft pumps. It is to be noted, however, that many of the large, vertical, single-stage, single-suction (usually bottom) volute pumps that are preferred for large storm water pumpage, drainage, irrigation, sewage, and water supply projects have no comparable counterpart among horizontal-shaft units. The basic U-section casing of these pumps, which is structurally weak, often requires the use of heavy ribbing to provide sufficient rigidity. In the comparable water turbine practice, a set of vanes (called a *speed ring*) is employed between the casing and the runner to act as a strut. Although the speed ring does not adversely affect the operation of a water turbine, it would function basically as a diffuser in a pump because of the inherent hydraulic

LIBERTY EXHIBIT 1017, Page 323

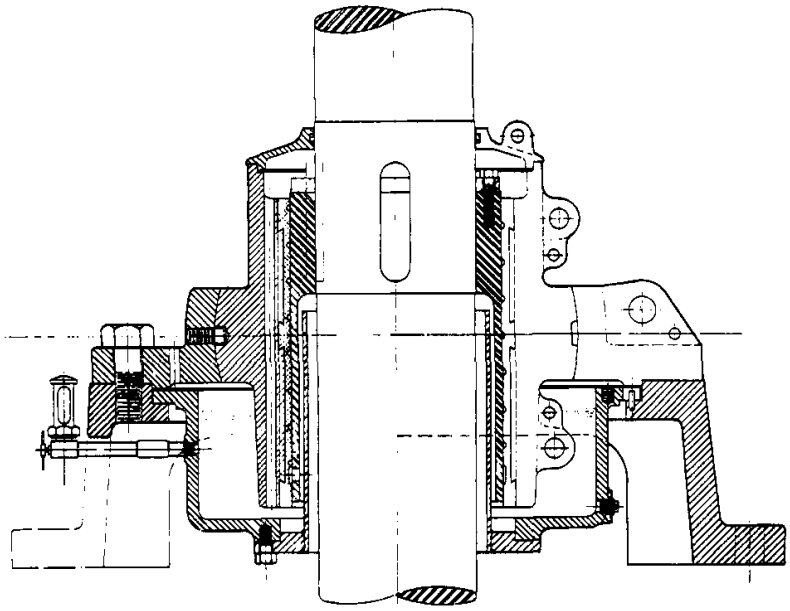


FIGURE 78 A self-oiling, babbitt steady bearing for large vertical shafting (Flowserve Corporation)

limitations of that construction. Some high-head pumps of this type have been made in the twin-volute design. The wall separating the two volutes acts as a stengthening rib for the casing, thus making it easier to design a casting strong enough for the pressure involved.

Bases and Supports for Vertical Pumping Equipment Vertical-shaft pumps, like horizontal-shaft units, must be firmly supported. Depending upon the installation, the unit can be supported at one or several elevations. Vertical units are seldom supported from walls, but even that type of support is sometimes encountered.

Occasionally, a nominal horizontal-shaft pump design is arranged with a vertical shaft and a wall used as the supporting foundation. Regular horizontal-shaft units can be used for this purpose without modification, except that the bedplate is attached to a wall. Careful

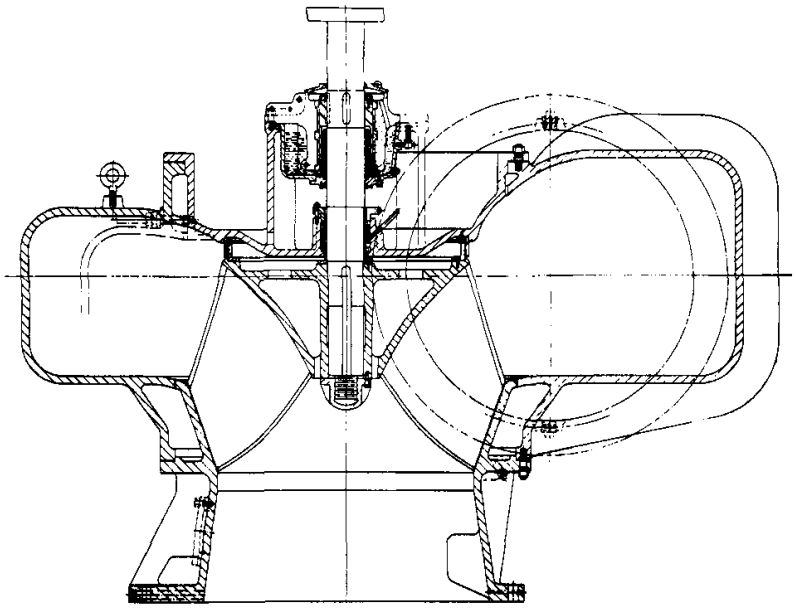


FIGURE 79 A section of a large, vertical, bottom-suction volute pump with a single sleeve bearing (Flowserve Corporation)

LIBERTY EXHIBIT 1017, Page 324

attention must be given to the arrangement of the pump bearings to prevent the escape of the lubricant. Installations of double-suction, single-stage pumps with the shaft in the vertical position are relatively rare, except in some marine or navy applications. Hence, manufacturers have few standard pumps of this kind arranged so that a portion of the casing forms the support (to be mounted on soleplates). Figure 76 shows such a pump, which also has a casing extension to support the driving motor.

Vertical Wet-Pit Pumps Vertical pumps intended for submerged operations are manufactured in a great number of designs, depending mainly upon the service for which they are intended. Small pumps of this type are often referred to as *sump pumps*. Wet-pit centrifugal pumps can be classified in the following manner:

- Vertical turbine pumps
- Propeller or modified propeller pumps
- Volute pumps

Vertical Turbine Pumps Vertical turbine pumps were originally developed for pumping water from wells and have been called *deep-well pumps, turbine well pumps,* and *borehole pumps.* As their application to other fields has increased, the name *vertical turbine pumps* has been generally adopted by manufacturers. This is not too specific a designation because the term *turbine pump* has been applied in the past to any pump employing a diffuser. There is now a tendency to designate pumps using diffusion vanes as *diffuser pumps* to distinguish them from *volute pumps.* As that designation becomes more universal, applying the term *vertical turbine pumps* to the construction formerly called *turbine well pumps* will become more specific.

The largest fields of application for the vertical turbine pump are pumping from wells for irrigation and other agricultural purposes, for a municipal water supply, and for industrial water supplies, as well as for processing, circulating, refrigerating, and air conditioning. This type of pump has also been utilized for brine pumping, mine dewatering, oil field repressuring, and other purposes.

These pumps have been made for capacities as low as 10 or 15 gpm (2 or 3 m^3/h) and as high as 25,000 gpm (5700 m^3/h) or more and for heads up to 1000 feet (300 m). Most applications naturally involve the smaller capacities. The capacity of the pumps used for bored wells is naturally limited by the size of the well as well as by the rate at which water can be drawn without lowering its level to a point of insufficient pump submergence.

Vertical turbine pumps should be designed with a shaft that can be readily raised or lowered from the top to permit proper positioning of the impeller in the bowl. An adequate thrust bearing is also necessary to support the vertical shafting, the impeller, and the hydraulic thrust developed when the pump is in service. As the driving mechanism must also have a thrust bearing to support its vertical shaft, it is usually provided with one large enough to carry the pump parts as well. For these two reasons, the hollow-shaft motor or gear is most commonly used for vertical turbine pump drives. In addition, these pumps are sometimes made with their own thrust bearings to allow for a belt drive or for a drive through a flexible coupling by a solid-shaft motor, gear, or turbine. Dual-driven pumps usually employ an angle gear with a vertical motor mounted on its top.

The design of vertical pumps illustrates how a centrifugal pump can be specialized to meet a specific application. Figure 80 illustrates a turbine design with closed impellers and enclosed-line shafting and another turbine design with closed impellers and open-line shafting.

The bowl assembly, or section, consists of the suction case (also called *suction head* or *inlet vane*), the impeller or impellers, the discharge bowl, the intermediate bowl or bowls (if more than one stage is involved), the discharge case, the various bearings, the shaft, and the miscellaneous parts, such as keys, impeller-locking devices, and the like. The column pipe assembly consists of the column pipe, the shafting above the bowl assembly, the shaft bearings, and the cover pipe or bearing retainers. The pump is suspended from the driving head, which consists of the discharge elbow (for above ground discharge), the motor or driver and support, and either the stuffing box (in an open-shaft construction) or the assembly

LIBERTY EXHIBIT 1017, Page 325

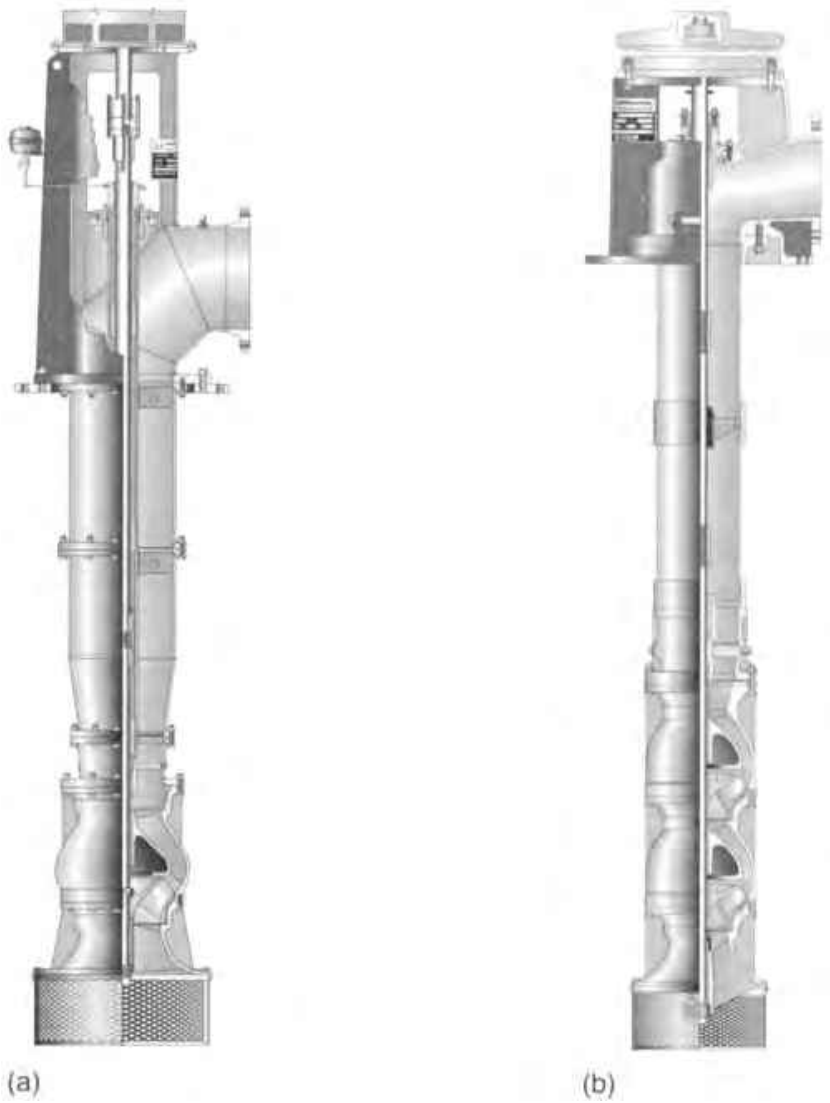


FIGURE 80 A vertical turbine pump design with enclosed impellers and: (a) enclosed line shafting and (b) open-line shafting (Flowserve Corporation)

for providing tension on the cover pipe and introducing a lubricant into it. Below ground discharge is taken from a tee in the column pipe, and the driving head functions principally as a stand for the driver and a support for the column pipe.

Liquid in a vertical turbine pump is guided into the impeller by the suction case or head. This may be a tapered section for the attachment of a conical strainer or suction pipe, or it may be a bell mouth.

Semiopen and enclosed impellers are both commonly used. For proper clearances in the various stages, the semiopen impeller requires more care in assembly on the impeller shaft and more accurate field adjustments of the vertical shaft position in order to obtain the best efficiency. Enclosed impellers are favored over semiopen ones because wear on the latter reduces capacity, which cannot be restored unless new impellers are installed. Normal wear on enclosed impellers does not affect impeller vanes, and worn clearances may be restored by replacing wearing rings. The thrust produced by semiopen impellers may be as much as 150% of that by enclosed impellers.

Occasionally, in power plants, the maximum water level that can be carried in the condenser's hot well will not give adequate NPSH for a conventional horizontal condensate pump mounted on the basement floor, especially if the unit has been installed in a space originally allotted for a smaller pump. Building a pit for a conventional horizontal condensate

LIBERTY EXHIBIT 1017, Page 326



FIGURE 81 Vertical turbine can pump for condesate service (Flowserve Corporation)

pump or a vertical dry-pit pump that will provide sufficient submergence involves considerable expense. Pumps of the design shown in Figure 81 have become quite popular in such applications. This is basically a vertical turbine pump mounted in a tank (often called a can) that is sunk into the floor. The length of the pump has to be such that sufficient NPSH will be available for the first-stage impeller design, and the diameter and length of the tank have to allow for proper flow through the space between the pump and tank and then for a turn and flow into the bell mouth. Installing this design in an existing plant is naturally much less expensive than making a pit because the size of the hole necessary to install the tank is much smaller. The same basic design has also been applied to pumps handling volatile liquids that are mounted on the operating floor and not provided with sufficient NPSH.

Propeller Pumps Originally, the term *vertical propeller pump* was applied to vertical wet-pit diffuser or turbine pumps with a propeller or axial-flow impellers, usually for installation in an open sump with a relatively short setting (see Figures 82 and 83). Operating heads exceeding the capacity of a single-stage axial-flow impeller might call for a pump of two or more stages or a single-stage pump with a lower specific speed and a mixed-flow impeller. High enough operating heads might demand a pump with mixed-flow impellers and two or more stages. For lack of a more suitable name, such high-head designs have usually been classified as propeller pumps also.

LIBERTY EXHIBIT 1017, Page 327

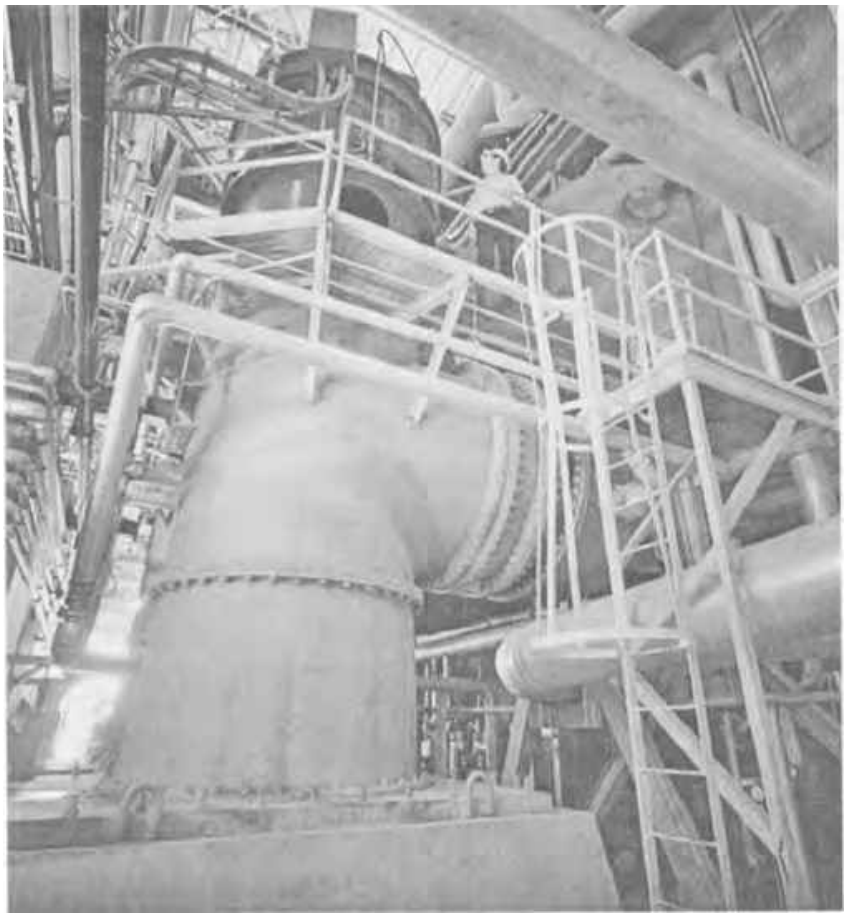


FIGURE 82 Vertical propeller pump installed (Flowserve Corporation)

Although vertical turbine pumps and vertical modified propeller pumps are basically the same mechanically and could even be of the same specific speed hydraulically, a basic turbine pump design is suitable for a large number of stages. A modified propeller pump design, however, is basically intended for a maximum of two or three stages.

Most wet-pit drainage, low-head irrigation, and storm water installations employ conventional propeller or modified propeller pumps. These pumps have also been used for condenser circulating services, but a specialized design dominates this field. As large power plants are usually located in heavily populated areas, they frequently have to use badly contaminated water (both fresh and salt) as a cooling medium. Such water quickly shortens the life of fabricated steel. Cast iron, bronze, or an even more corrosion-resistant cast metal must therefore be used for the column pipe assembly. This requirement means a very heavy pump if large capacities are involved. To avoid the necessity of lifting this large mass for maintenance of the rotating parts, some designs (one of which is illustrated in Figure 84) are built so that the impeller, diffuser, and shaft assembly can be removed from the top without disturbing the column pipe assembly. These designs are commonly designated as *pullout* designs.

Like vertical turbine pumps, propeller and modified propeller pumps have been made with both open- and enclosed-line shafting. Except for condenser circulating services, enclosed shafting, using oil as a lubricant but with a grease-lubricated tail bearing below the impeller, seems to be favored. Some pumps handling condenser circulating water use enclosed shafting but with water (often from another source) as the lubricant, thus eliminating any possibility of oil getting into the circulating water and coating the condenser tubes.

Propeller pumps have open propellers. Modified propeller pumps with mixed-flow impellers are made with both open and closed impellers.

LIBERTY EXHIBIT 1017, Page 328

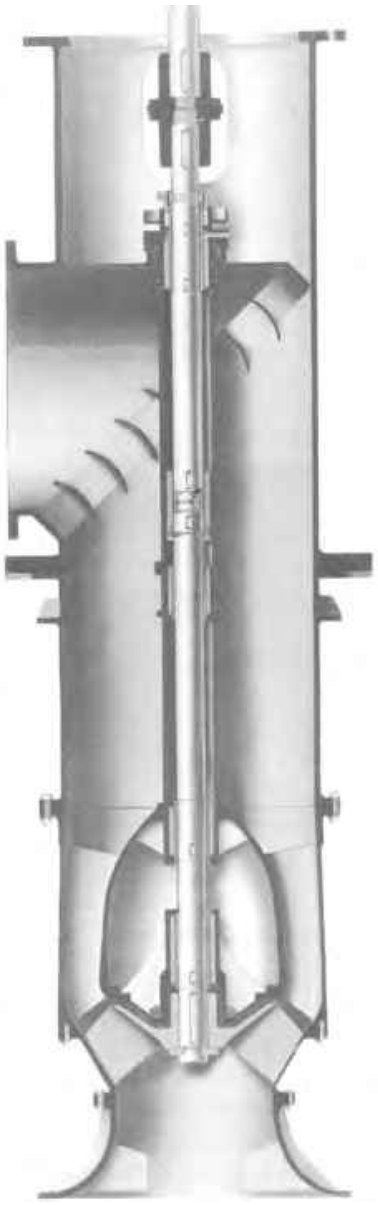


FIGURE 83 Vertical propeller pump with above ground discharge (Flowserve Corporation)



FIGURE 84 Vertical pull-out design allows the rotating element and critical non-rotating wear components to be removed for inspection and replacement without removing the complete pump (Flowserve Corporation)

Volute Pumps A variety of wet-pit pumps are available. The liquid pumped, be it clean water, sewage, abrasive liquids or slurries, dictates whether a semiopen or an enclosed impeller will be used, whether the shafting will be open or closed to the liquid pumped, and whether the bearings will be submerged or located above the liquid.

Figure 85 illustrates a single-volute pump with a single-suction enclosed nonclog impeller, no pump-out vanes or wearing-ring joints on the hack side of the impeller, and enclosed shafting. The pump is designed to be suspended from an upper floor by means of a drop pipe and for pumping sewage or other solid-laden liquids. To seal against leakage along the shaft at the point where it passes through the casing, a seal chamber or a stuffing box is provided. The design of a stuffing box can be either like the one shown in Figure 86, which uses rings of packing and a spring-loaded gland, or the one shown in Figure 87, which uses U-cup packing requiring no gland. The pump shown in Figure 85 uses two

LIBERTY EXHIBIT 1017, Page 329

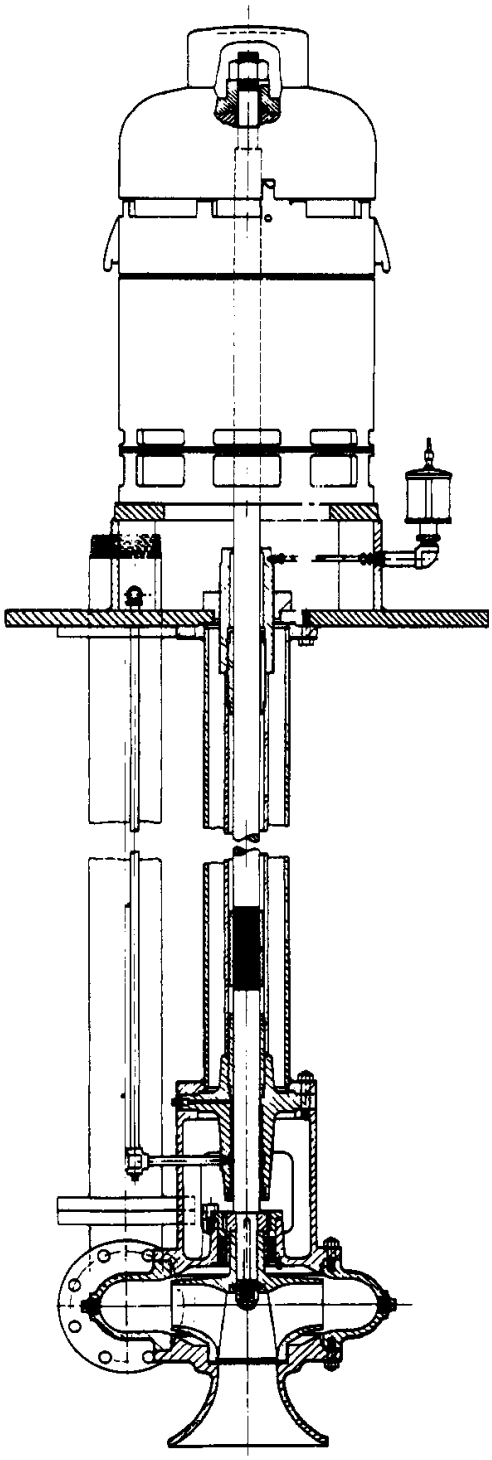


FIGURE 85 A section of a vertical wet-pit, nonclogging pump (Flowserve Corporation)

sleeve bearings above the impeller. The bottom bearing is grease-lubricated, and a seal is provided to prevent grease leakage as well as to keep out any grit. The upper bearing connects the shaft cover pipe to the pump-bearing bracket and the upper end of the cover pipe to the floorplate. This bearing is gravity-feed oil-lubricated. If intermediate bearings are required, they are also supported by the cover pipe and are oil-lubricated. The pump thrust is carried by the motor, which can be either a hollow-shaft or a solid-shaft construction. The latter type requires the use of a rigid coupling between the pump and motor shafts.

LIBERTY EXHIBIT 1017, Page 330

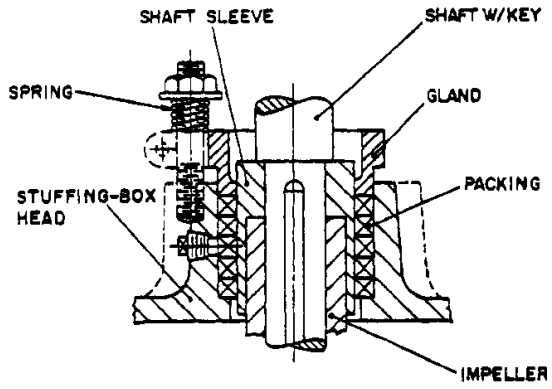
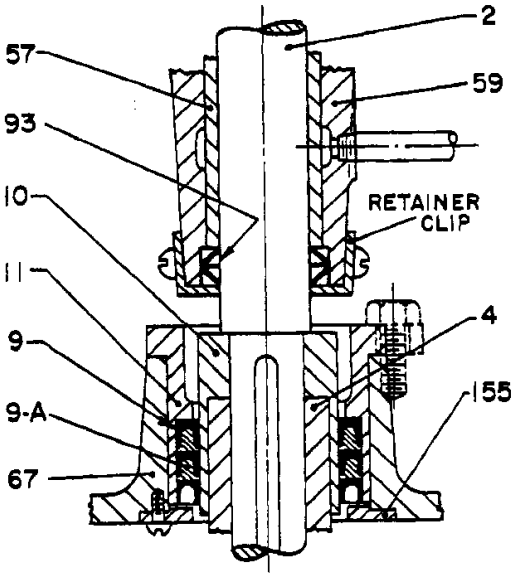


FIGURE 86 A typical stuffing box arrangement

In most applications, these volute-type pumps have been replaced with vertical wet-pit pumps with the stuffing box/seal chamber in the discharge head.

A design that uses open shafting and no seal chamber or stuffing box at the pump casing, incorporating its own thrust bearing, is shown in Figure 88. It may also offer a recessed impeller option, suitable for pumping heavy concentrations of solid material (such as sludges or slurries) or in certain food-processing applications. Pumped liquid leakage from the casing is relieved back to the suction through holes in the support pipe. The seal chamber or stuffing box at the driver floor elevation is used only when gas tight construction is desired. The lower and any intermediate sleeve bearings are grease-lubricated as shown, but gravity-feed oil lubrication is also available in other designs. The upper antifriction thrust bearing is grease-lubricated. A solid shaft motor and a flexible shaft are used.

Figure 89 illustrates what is called a *cantilever-shaft pump*, which has the unique feature of having no bearings below the liquid surface. The shaft is exposed to the liquid pumped. External antifriction grease-lubricated bearings are provided above the floor and are properly spaced to support the rigid shaft. They carry both the thrust and the radial load. A flexible coupling is used between the pump and the solid-shaft motor. The stuffing box at the floorplate may be eliminated if holes are provided in the drop pipe to maintain the liquid level in the pipe even with the sump liquid level. Either semiopen or enclosed impellers may be used.



STATIONARY PARTS

REF. NO.	NO. OF PCS.	NAME OF PARTS
9	3	U-CUP SEAL RING
9-A	2	SPACERS
11	1	SEAL RING ADAPTER
57	1	LOWER PUMP BEARING
59	1	BEARING BRACKET
67	1	STUFFING-BOX HEAD
93	2	OIL SEAL
155	1	SEAL-RING RETAINER

ROTATING PARTS

REF. NO.	NO. OF PCS.	NAME OF PARTS
2	1	SHAFT W/KEY
4	1	IMPELLER
10	1	SHAFT SLEEVE

FIGURE 87 A stuffing box arrangement with U-cup packing (Flowserve Corporation)

LIBERTY EXHIBIT 1017, Page 331



FIGURE 88 A vertical wet-pit volute pump with open shafting, no seal chamber (stuffing box), and its own thrust bearing (Flowserve Corporation)

An interesting design of the wet-pit pump is shown in Figure 90. It uses a single-stage, double-suction impeller in a twin-volute casing. Because the axial thrust is balanced, the thrust bearing need carry only the weight of the rotating element. The pump requires no stuffing box or mechanical seal. The shaft is entirely enclosed, and the bearings are externally lubricated, either with oil or with water. The lower bearing receives its lubrication from an external pipe connection.

The term sump pump ordinarily conveys the idea of a vertical wet-pit pump that is suspended from a floorplate or sump cover. It could be supported by a foot on the bottom of a well, be motor-driven and automatically controlled by a float switch, and be used to remove drainage collected in a sump. The term does not indicate a specific construction, for both diffuser and volute designs are used. These may be single-stage or multistage and have open or closed impellers of a wide range of specific speeds.

For small capacities driven by fractional-horsepower motors, *cellar drainers* can be used. These are small and usually single-stage volute pumps with single-suction impellers (either top or bottom suction) supported by a foot on the casing. The motor is supported well above the impeller by some form of column enclosing the shaft. These drainers are made as complete units, including float, float switch, motor, and strainers.

The larger sump pumps are usually standardized but obtainable in any length, with covers of various sizes (on which a float switch may be mounted) and the like. Duplex units, that is, two pumps on a common sump cover (sometimes with a hole for access to the sump), are often used. Such units may operate their pumps in a fixed order, or a mechanical or electric alternator may be used to equalize their operation.

The Application of Vertical Wet-Pit Pumps Like all pumps, the vertical wet-pit pump has advantages and disadvantages. One advantage is that installation does not require a separate dry pit to collect the pumped liquid. If the impeller (first-stage impeller in multistage pumps) is submerged, no priming problem exists and the pump can be automatically controlled without fear of its ever running dry. Moreover, the available NPSH is greater (except in closed tanks) and often permits a higher rotative speed for the same

LIBERTY EXHIBIT 1017, Page 332

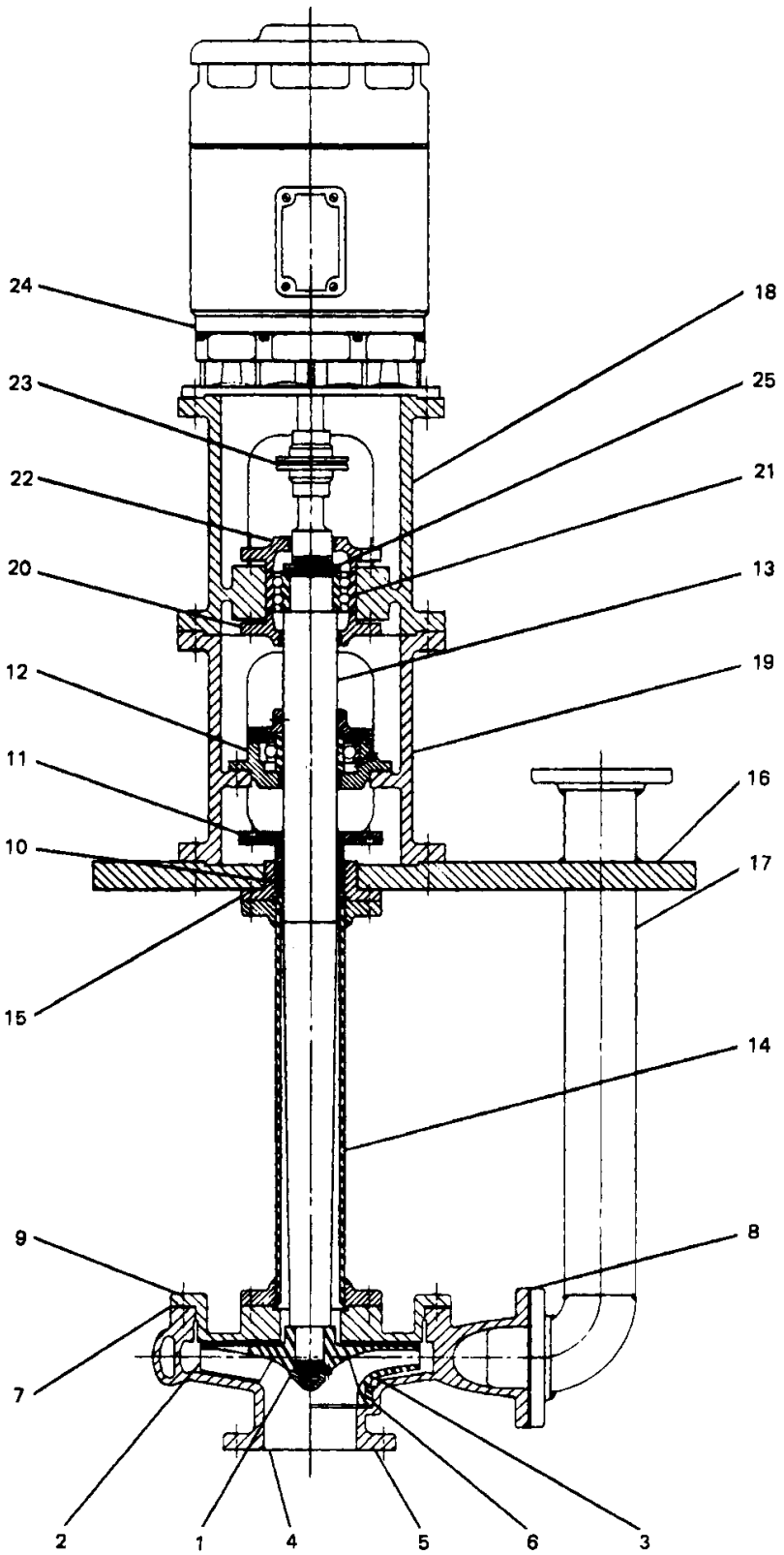


FIGURE 89 Vertical wet-pit cantilever-type volute pump: (1) impeller nut, (2) open impeller, (3) closed impeller, (4) open casing, (5) closed casing, (6) casing wearing ring, (7) casing gasket, (8) discharge flange gasket, (9) back cover, (10) packing or mechanical seal, (11) packing or seal gland, (12) radial bearing, (13) shaft, (14) supporting pipe, (15) separate stuffing box, (16) sump cover, (17) discharge pipe, (18) upper motor pedestal, (19) lower motor pedestal, (20) lower thrust bearing cover, (21) thrust bearing, (22) upper thrust bearing cover, (23) coupling, (24) motor, (25) bearing locknut and washer (Laurence Pump)

LIBERTY EXHIBIT 1017, Page 333



FIGURE 90 Double-suction, wet-pit pump (Flowserve Corporation)

service conditions. A second advantage is that the motor or driver can be located at any desired height above any flood level.

It has the following mechanical disadvantages: (1) the possibility of freezing when idle, (2) the possibility of damage by floating objects if the unit is installed in an open ditch or similar installation, (3) the inconvenience of lifting out and dismantling for inspection and repairs, no matter how small, and (4) the pump bearings have a relative short life unless the water and bearing design are ideal. In summary, the vertical wet-pit pump is the best pump available for some applications. It's not ideal but can be the most economical for certain installations, a poor choice for some, and the least desirable for still others.

Axial Thrust in Vertical Pumps with Single Suction Impellers The subject of axial thrust in horizontal pumps has already been discussed in this section. When pumps are installed in a vertical position, additional factors need be taken into account when determining the amount and direction of the thrust to be absorbed in the thrust bearings.

The first and most significant of these factors is the weight of the rotating parts, which is a constant downward force for any given pump, completely independent of the pump operating capacity or total head. Since in most cases the single-suction impellers of vertical pumps are mounted with the suction eye facing downward, the normal hydraulic axial thrust is exerted downward and the weight of the rotating parts is additive to this axial thrust.

The second factor involves the dynamic force (or change in momentum) caused by the change in the direction of flow, from vertical to either horizontal or partly horizontal, as the pumped liquid flows through the impeller. This force acts upward and balances a small portion of the hydraulic downthrust and of the rotor weight. The magnitude of this force for water having a specific weight (force) of 62.34 lb/ft^3 (9.79 kN/m^3) is

in USCS units
$$F_u = \frac{KV_e^2A_e}{2g(2.31)}$$

in SI units
$$F_u = \frac{KV_e^2A_e}{2g(1.02)}$$

where F_u = upthrust, lb (N)
K = constant related to the impeller type
V_e = velocity in the impeller eye ft/s (m/s)
A_e = net eye area, in^2 (cm^2)
g = 32.2 ft/s^2 (9.81 m/s^2)

The constant K is 1.0 for a fully radial-flow impeller, less than 1.0 for a mixed-flow impeller, and essentially 0 for a fully axial-flow impeller.

Under normal operating conditions, the upward thrust caused by the change of momentum is hardly significant in comparison with the downward thrust caused by the

LIBERTY EXHIBIT 1017, Page 334

unbalanced pressures acting on the single-suction impeller. Consider the example of an impeller with the following characteristics:

Capacity	2500 gpm (568 m^3/h)
Total head	231 ft (70.4 m)
Net pressure	100 lb/in^2 (6.89 bar)
Unbalanced eye area	40 in^2 (258 cm^2)

If we neglect the effect of the pressure distribution on the shrouds of the impeller, the downward thrust is

in USCS units $$100 \times 40 = 4000 \text{ lb}$$

in SI units $$6.89 \times 10^5 \times \frac{258}{10{,}000} = 17{,}800 \text{ N}$$

The upward force caused by the change of momentum is

in USCS units $$\frac{1.0 \times \left(\frac{2500 \times 0.32}{40}\right)^2 \times 40}{64.4 \times 2.31} = 107.5 \text{ lb}$$

in SI units $$\frac{1 \times \left(\frac{568 \times 10{,}000}{258 \times 3600}\right)^2 \times 258}{2 \times 9.81 \times 1.02} = 481 \text{ N}$$

This is certainly negligible relative to the downward hydraulic axial thrust.

The situation is quite different, however, during the startup of a vertical pump. Although the motor may get up to full speed in just a few seconds, it takes a certain amount of time for the total head to increase from zero that corresponding to the normal operating capacity. Consequently, the pump will be operating in a very high capacity range. Since the upward force caused by the change of momentum varies as the square of the capacity while the downward axial thrust caused by pressure differences is very low, there can be a momentary net upward force, or upthrust. This means that thrust bearings intended to accommodate the axial thrust of vertical pumps must be capable of accommodating some thrust in the upward direction in addition to the normal downward thrust. This is particularly true for pumps with relatively low heads per stage and with short settings because in these units the rotor weight does not at all times compensate for the upthrust from the change in momentum.

Particular care must be exercised in defining the range of vertical movement allowed for the thrust bearings because any such movement must remain within the displacement limits of any mechanical seal used in the pump.

In rather rare cases, a close-coupled vertical pump is operated at such a high capacity that a continuous net upthrust is generated. Such operations can damage the pump because the line shaft is operated in compression and may buckle, causing vibration and bearing wear. The manufacturer's comments should be invited if such an operation is contemplated.

Shaft Elongation in Vertical Pumps The elongation of a vertical pump shaft is caused by three separate phenomena: (1) the tensile stress caused by the weight of the rotor, (2) the tensile stress caused by the axial thrust, and (3) the thermal expansion of the shaft.

In most cases, the tensile stress created by the axial thrust is several times greater than that created by the weight. In a typical example of a 16,000-gpm (3636-m^3/h) pump designed for a 175-ft (53.3-m) head and 50 ft (15.25 m) long, the elongation caused by the weight of a 1600-lb (726-kg) impeller will be of the order of 0.0033 in (0.084 mm). The elongation caused by the axial thrust will be approximately 0.0315 in (0.8 mm).

The elongation caused by thermal expansion has to be considered from two angles. First, if the shaft and the stationary parts are built of materials that have essentially

LIBERTY EXHIBIT 1017, Page 335

the same coefficient of expansion, both will expand equally and no significant relative elongation will take place. Second, if the pumps are operated in essentially the same range of temperatures in which they were assembled, no significant relative expansion will take place, even if dissimilar coefficients of expansion are involved. Whatever the case, the pump manufacturers take these factors into consideration by providing the necessary vertical end-play between the stationary and rotating pump components.

Loads on Foundations of Vertical Pumps If the motor support is integral with the pump discharge column, as in Figures 80, 82, and 83, and if the hydraulic thrust is carried by the motor thrust bearing, this thrust is not additive to the deadweight of the pump and of its motor plus the weight of the water contained in the pump, insofar as the load on the foundations is concerned. This is because the pump and motor mounted in this fashion form a self-contained entity and all internal forces and stresses are balanced within this entity. If the pump and motor are supported separately, however, as in Figure 91, and are joined by a rigid coupling that transmits the pump hydraulic

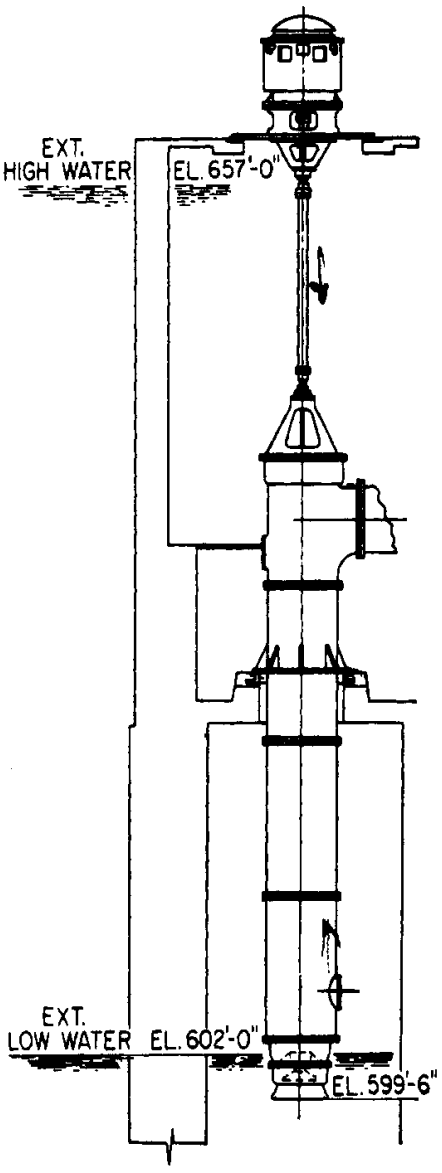


FIGURE 91 The vertical pump and driving motor supported separately (Flowserve Corporation)

LIBERTY EXHIBIT 1017, Page 336

thrust to the motor thrust bearing, the foundations will carry the following loads when the pump is running:

- *The foundation supporting the motor*: the weight of the motor plus the weight of the pump rotor plus the axial hydraulic thrust developed by the pump
- *The foundation supporting the pump*: the weight of the pump stationary parts plus the weight of the water in the pump, including the water in the discharge pipe supported by the foundation, less the axial hydraulic thrust developed by the pump

Since when the pump is idle the foundation supporting the pump is not benefited by the reduction in load equivalent to the axial hydraulic thrust, both running and idle operating conditions must be considered in this case.

Typical Arrangements of Vertical Pumps A pump is only part of a pumping system. The hydraulic design of the system external to the pump will affect the overall economy of the installation and can easily have an adverse effect upon the performance of the pump itself. Vertical pumps are particularly susceptible because the small floor space occupied by each unit offers the temptation to reduce the size of the station by placing the units closer together. If the size is reduced, the suction arrangement may not permit the proper flow of water to the pump suction intake. Recommended arrangements for vertical pumps are discussed in Section 13.1.

SPECIAL PURPOSE PUMPS

In addition to the more or less general purpose pumps described on the preceding pages, literally hundreds of centrifugal pumps are intended for very specific applications. Although it is impossible to describe every one of these special purpose designs, many of them are discussed and illustrated in Section 12, covering a variety of pump services. However, several specific designs are seeing rapidly increasing usage and so are discussed in greater detail here.

Submersible Motor-Driven Wet-Pit Pumps The installation of conventional vertical wet-pit pumps with the motor located above the liquid level may require a considerable length of drive shafting, particularly in the case of deep settings. The addition of this shafting, of the many line bearings, and possibly of an external lubrication system may represent a major portion of the total installed cost of the pumping unit. Furthermore, shaft alignment becomes more critical, and shaft elongation and power losses increase rapidly as the setting is increased, especially for deep-well pumps.

A great variety of submersible motors have been developed to obviate these shortcomings. They are described in Section 9.1.1, and a classification of the various types of such motors is presented in that section. Submersible wet-pit pumps eliminate the need for extended shafting, shaft couplings, a mechanical seal or stuffing box, a subsurface motor stand, and, in some cases, an expensive pump house. Both vertical turbine and volute-type wet-pit pumps may be so driven.

Figures 92 and 93 illustrate, respectively, the external appearance and a cross section of a vertical turbine pump driven by a submersible motor located at the bottom of the pump. The pump suction is through a perforated strainer located between the motor and the first-stage impeller bowl. There is, of course, no shafting above the pump and the pump-and-motor unit is supported by the discharge pipe only. No external lubrication is required. The motor is completely enclosed and oil-filled and is provided with a thrust bearing to carry the pump downthrust. A mechanical seal is provided at the motor shaft extension, which is connected to the pump shaft with a rigid coupling. Only a discharge elbow and the electric cable connection are seen above the surface support plate. On occasion, this type of pump is used horizontally as a booster pump in a pipeline, and in such cases the elbow at the discharge is eliminated.

Vertical wet-pit volute-type sump pumps can also be obtained with close-coupled submersible motors (see Figure 94) for drainage, sewage, process, and slurry services.

LIBERTY EXHIBIT 1017, Page 337

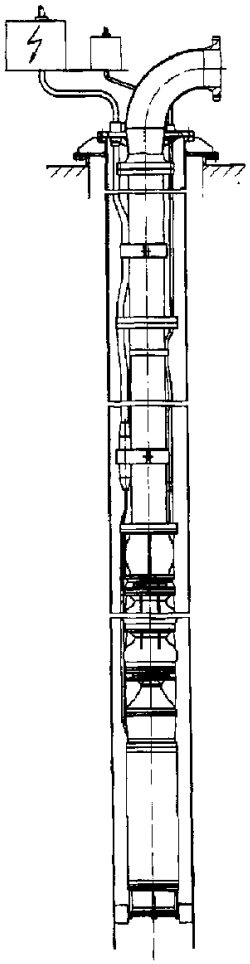


FIGURE 92 Vertical turbine pump driven by a submersible motor (Flowserve Corporation)

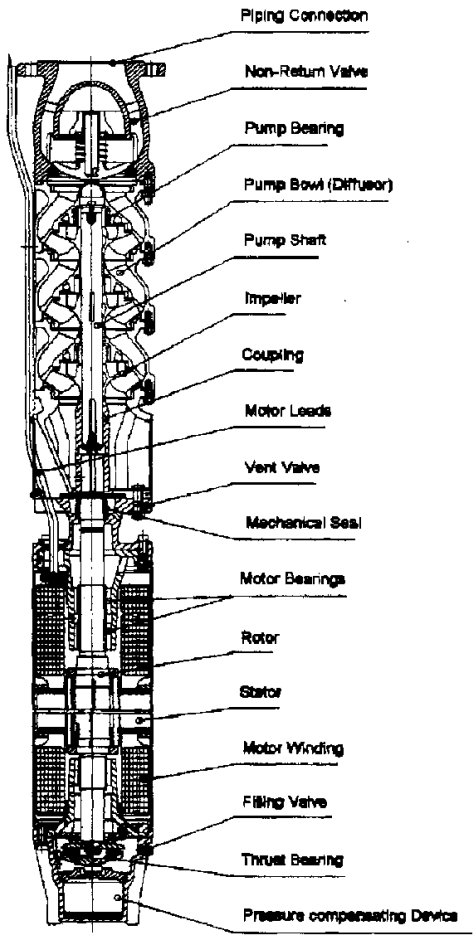


FIGURE 93 Cross-sectional view of a submersible pump (Flowserve Corporation)

Small portable pumps are available with flexible discharge hoses and built-in water-level motor control switches activated by trapped air pressure. Motors for these pumps are usually oil-filled and have a single mechanical shaft seal but are also available in a hermetically sealed design. The submersible motors are cooled by the liquid in which they are immersed and therefore should not be run dewatered, although some motors can operate for short periods (10 to 15 min) this way.

In a pump-motor combination (see Figure 95), the motor is cooled by the pumped liquid as it moves through a passage around the sides of the motor. This design also uses a pressurized oil-seal chamber to assure positive sealing.

Sealless Pumps Sealless pumps are available for pumping corrosive, volatile, radioactive, and otherwise hazardous liquids. Canned motor pumps are an assembly of a standard centrifugal pump and a squirrel-cage induction motor in a hermetically sealed unit. Modifying a recirculating flow system in a canned motor pump can allow it to be used in applications at up to 1000°F (538°C).

Magnetic drive pumps are an assembly of a rotor, an impeller, product lubricated bearings, and a magnetic carrier inside an isolation shell or diaphragm. This rotor is driven by magnets outside the shell or diaphragm. No mechanical connection exists between the driven magnets and the driving magnets. No seals exist and thus we have the term "sealless." Sealless pumps are described in detail in Section 2.2.3.

Straight-Radial-Vane High-Speed Pumps For handling volatile liquids at low flow rates and high heads, the straight-radial-vane impeller in a diffuser casing offers several

LIBERTY EXHIBIT 1017, Page 338

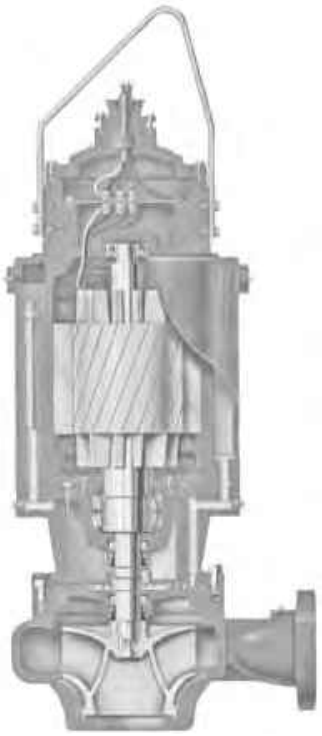


FIGURE 94 A section of a submersible, solids handling pump (Flowserve Corporation)

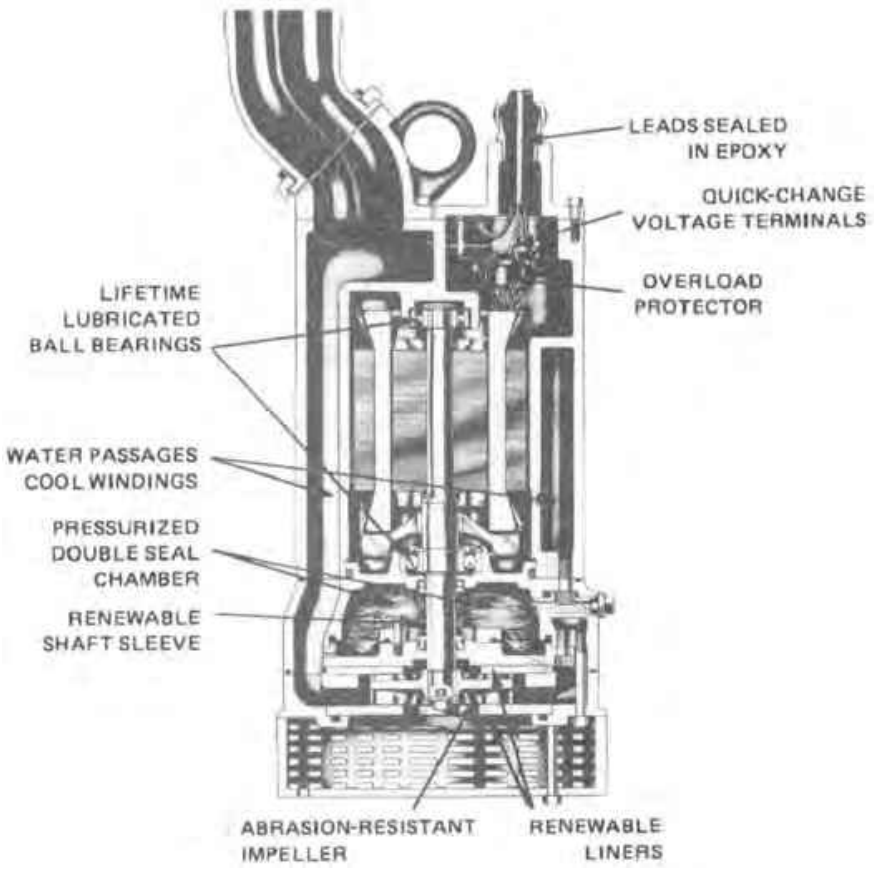


FIGURE 95 A portable submersible pump (Peabody Barnes)

LIBERTY EXHIBIT 1017, Page 339

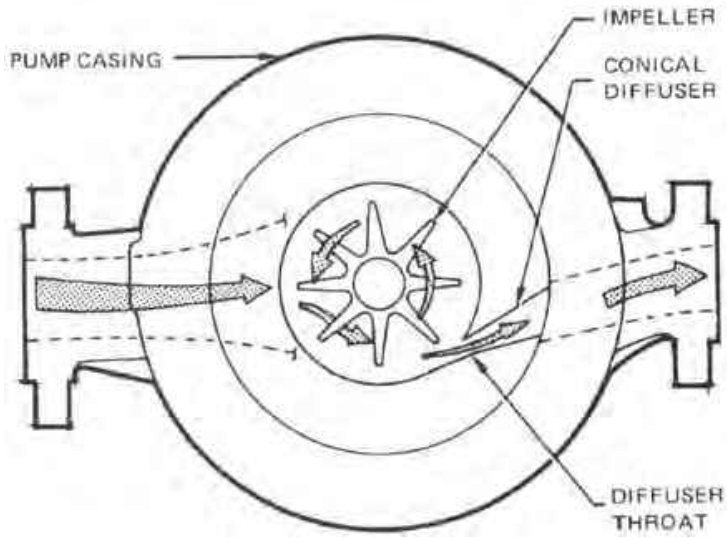


FIGURE 96 A straight-radial-vane impeller in a single emission-point, conical-diffuser circular casing (Sundyne Corporation)

advantages. Volatile, low-specific-gravity, poor-lubricity liquids require larger running clearances, which is not possible with conventional high-head multistage centrifugal or positive displacement pumps. High-head pumping of these liquids can be handled by operating this completely open impeller at very high speeds through an integral gear increaser and with very large impeller-to-casing clearance, typically 0.030 to 0.070 in (0.76 to 1.8 mm). Tests of one manufacturer's design have shown this clearance can increase to 0.125 in (3.2 mm) with virtually no change in performance, and consequently there is no need to provide adjustment for impeller axial clearance. A pump of this design can also run "dry," as liquid lubricity is not required to lubricate the bearings, which can be separately lubricated (providing the mechanical seal is lubricated).

Figure 96 illustrates one manufacturer's design of a radial-vane high-speed pump. The impeller rotates in a circular casing that has a single emission point leading to a conical diffusion section. The advantage of this type of casing is that the conversion to pressure occurs outside the circular housing, thus eliminating any recirculation forces that would require a close clearance between the impeller and casing. For higher flow ranges, a double emission point design, as shown in Figure 97, is used. This additional emission acts like a double-volute casing in conventional centrifugal pumps.

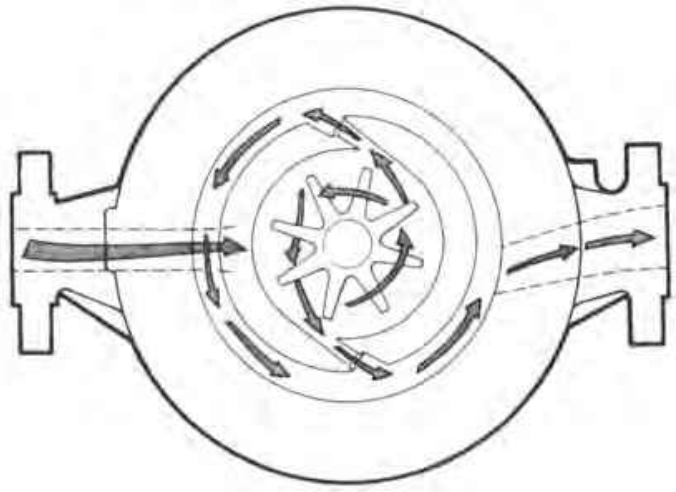


FIGURE 97 A straight-radial-vane impeller in a double-emission-point, conical-diffuser circular casing (Sundyne Corporation)

LIBERTY EXHIBIT 1017, Page 340

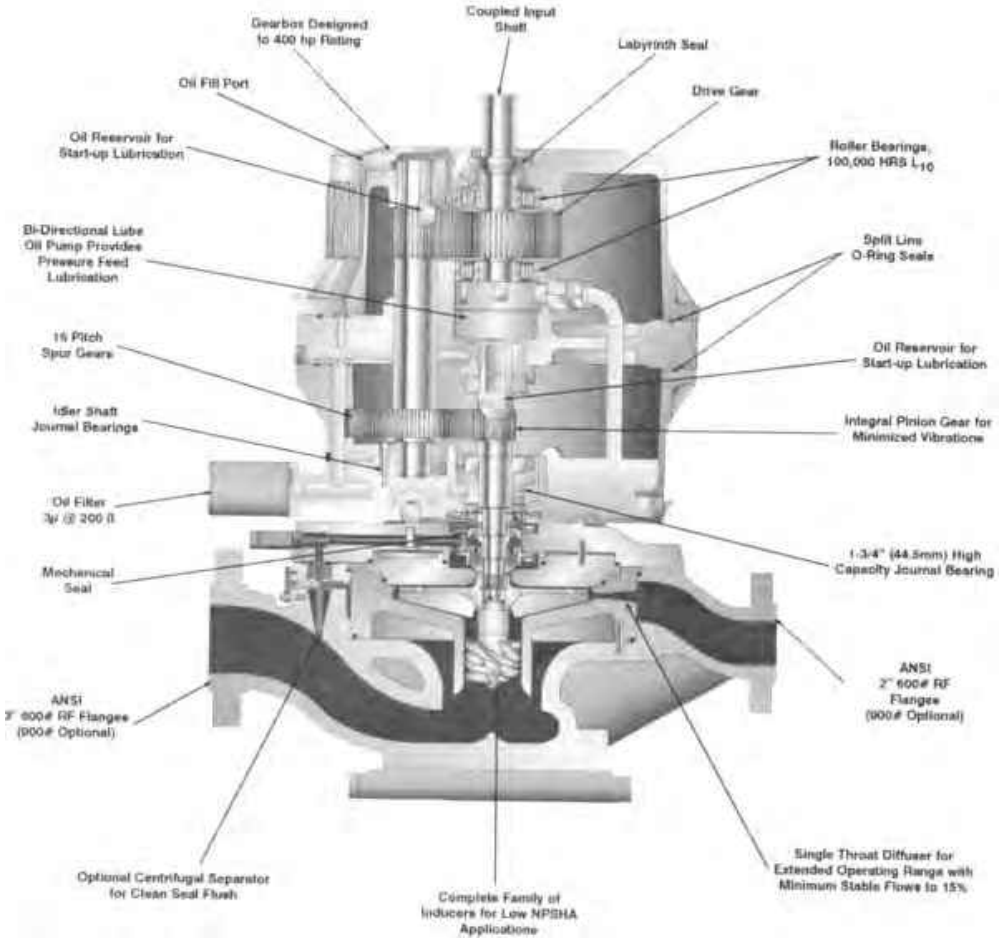


FIGURE 98 A section of a straight-radial-vane impeller and inducer in a conical-diffuser circular casing with an integral gear increaser with the following: (1) pump casing, (2) impeller, (3) impeller bolt, (4) impeller tab washer, (5) inducer, (6) diffuser, (7) diffuser cover, (8) upper throttle bushing, (9) seal housing, (10) single shaft sleeve, (11) pump seal rotating face, (12) gearbox seal rotating face, (11) pump mechanical seal, (14) gearbox mechanical seal, (15) separator orifice, (16) separator fitting, (17) gearbox output housing, (18) gearbox input housing, (19) bearing plate, (20) interconnecting shaft, (21) low-speed shaft, (22) input gear, (23) lower idler gear, (24) high-speed shaft, (25) pinion gear, (26) idler shaft, (27) O-ring packings (Sundyne Corporation).

Figure 98 is a sectional view of this pump with an integral speed increaser. Because of the high rotative speed, a single-stage pump can achieve the head normally associated with multistage centrifugal or positive displacement pumps. With this smaller liquid end and an integral gear box, cost and space savings can be appreciable.

2.2.2
CENTRIFUGAL PUMP PRIMING

IGOR J. KARASSIK
C. J. TULLO
F. W. BUSE

When a pump is first put into service, its passageways are filled with air. If the suction supply is above atmospheric pressure, this air will be trapped in the pump and compressed somewhat when the suction valve is opened. Priming is accomplished by venting the entrapped air out of the pump through a valve provided for this purpose. A centrifugal pump is primed when the passageways of the pump are filled with the liquid to be pumped. The liquid replaces the air, gas, or vapor in the passageways. This may be done manually or automatically.

Unlike a positive displacement pump, a centrifugal pump that takes its suction from a supply located below the pump, which is under atmospheric pressure, cannot start and prime itself (unless designed to be self-priming, as described later in this section). At its rated capacity, a positive displacement pump will develop the necessary pressure to exhaust air from its chambers and from the suction piping. Centrifugal pumps can also pump air at their rated capacity, but only at a pressure equivalent to the rated head of the pump. Because the specific weight of air is approximately $\frac{1}{800}$ that of water, a centrifugal pump can produce only $\frac{1}{800}$ of its rated liquid pressure. For every 1 ft (1 m) water has to be raised to prime a pump, the pump must produce a discharge head of air of approximately 800 ft (m). It is therefore apparent that the head required for a conventional centrifugal pump to be self-priming and to lift a large column of liquid (and in some cases to discharge against an additional static liquid head) when pumping air is considerably greater than the rating of the pump. Centrifugal pumps that operate with a suction lift can be primed by providing: (1) a foot valve in the suction line, (2) a single-chamber priming tank in the suction line or a two-chamber priming tank in the suction and discharge lines, (3) a priming inductor at the inlet of the suction line, or (4) some form of vacuum-producing device.

FOOT VALVES

A foot valve is a form of check valve installed at the bottom, or foot, of a suction line. When the pump stops and the ports of the foot valve close, the liquid cannot drain back to the

LIBERTY EXHIBIT 1017, Page 342

suction well if the valve seats tightly. A foot valve does not always seat tightly, and the pump occasionally loses its prime. However, the rate of leakage is generally small, and it is possible to restore the pump to service by filling and starting it promptly. This tendency to malfunction is increased if the liquid contains small particles of foreign matter, such as sand, and foot valves should not be used for such service. Another disadvantage of foot valves is their unusually high frictional loss.

The pump can be filled through a funnel attached to the priming connection or from an overhead tank or any other source of liquid. If a check valve is used on the pump and the discharge line remains full of liquid, a small bypass around the valve permits the liquid in the discharge line to be used for repriming the pump when the foot valve has leaked. Provision must be made for filling all the passageways and for venting out the air.

PRIMING CHAMBERS

The Single-Chamber Tank A single-chamber primer is a tank with a bottom outlet that is level with the pump suction nozzle and directly connected to it. An inlet at the top of the tank connects with the suction line (Figure 1). The size of the tank must be such that the volume contained between the top of the outlet and the bottom of the inlet is approximately three times the volume of the suction pipe. When the pump is shut down, the liquid in the suction line may leak out, but the liquid in the tank below the suction inlet cannot run back to the supply. When the pump is started, it will pump this entrapped liquid out of the priming chamber, creating a vacuum in the tank. The atmospheric pressure on the supply will force the liquid up the suction line into the priming chamber.

Each time the pump is stopped and restarted, a quantity of liquid in the priming tank must be removed to create the required vacuum. Because of possible back siphoning, the liquid volume in the tank is reduced. Unless the priming tank is refilled, it has limited use. Automatic refilling of the priming tank cannot occur if the pump has a discharge check valve unless there is sufficient backflow from the discharge system before the check valve seats.

Because of their size, the use of single-chamber priming tanks is restricted to installations of relatively small pumps, usually to a 12-in (305-mm) suction line (approximately 2000 gpm [450 m^3/h]).

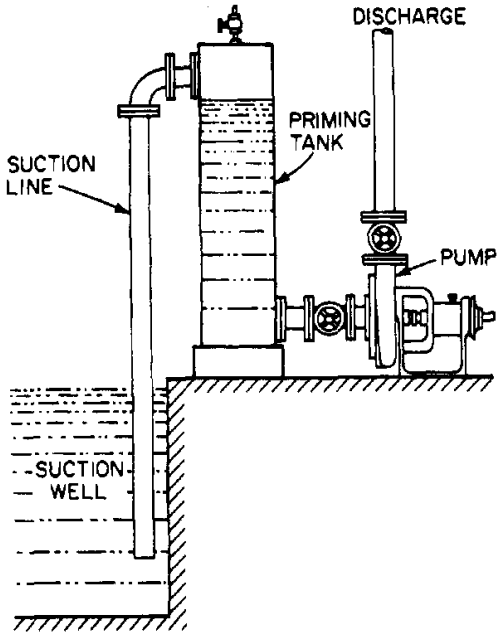


FIGURE 1 Single-chamber priming tank

LIBERTY EXHIBIT 1017, Page 343

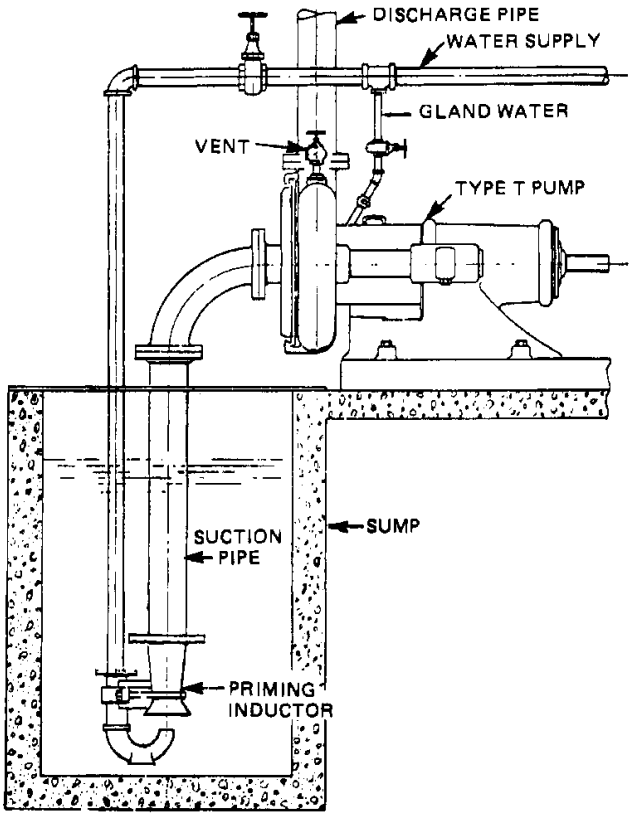


FIGURE 2 Priming inductor (Nagle Pumps)

PRIMING INDUCTORS

If a separate source of liquid of sufficient capacity and pressure is available, it can be used to fill the suction line of the pump to be primed through the use of an inductor, as shown in Figure 2. For water, the pressure must be equal to about 4 lb/in^2 for each foot (90 kPa for each meter) of head necessary to prime the pump, measured from the lowest liquid level in the sump from which priming must be accomplished to the top of the pump. The amount of liquid necessary depends on the pressure.

Because the inductor is a positive-pressure device, leaks in the suction line or at the pump seal or stuffing box are not critical. The service liquid can be left on or turned off after pumping is initiated. If left on, the head developed by the pump (therefore the flow also) will be increased.

An additional feature of the priming inductor is that operation is possible even when the suction line is covered with sediment. When the pump and suction line are filled, backflow results, mixing the solids and the liquid.

TYPES OF VACUUM DEVICES

Almost every commercially made vacuum-producing device can be used with systems in which pumps are primed by evacuation of air. Formerly water-jet, steam-jet, or air-jet primers had wide application, but with the increase in the use of electricity as a power source, motor-driven vacuum pumps have become more popular.

Ejectors Priming ejectors work on the jet principle, typically using steam, compressed air, or water as the operating medium. A typical installation for priming with an ejector

LIBERTY EXHIBIT 1017, Page 344

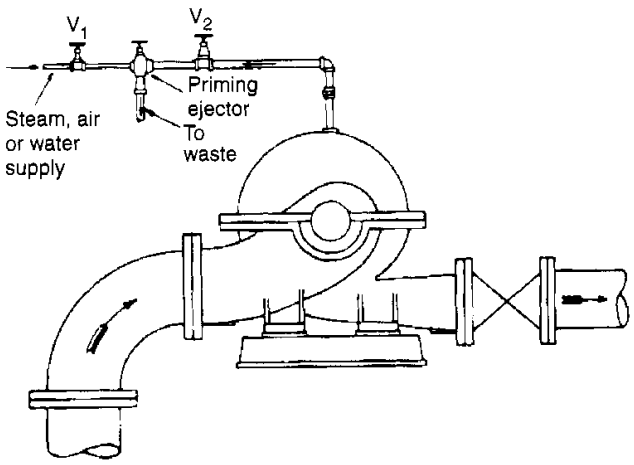


FIGURE 3 Arrangement of priming with an ejector

is shown in Figure 3. Valve V_1 is opened to start the ejector, and then valve V_2 is opened. When all the air has been exhausted from the pump, liquid will be drawn into and discharged from the ejector. When this occurs, the pump is primed and valves V_2, and V_1 are closed, in that order.

An ejector can be used to prime a number of pumps if it is connected to a header through which the individual pumps are vented through isolating valves.

Dry Vacuum Pumps Dry vacuum pumps, which may be of either the reciprocating or the rotary oil-seal type, cannot accommodate mixtures of air and liquid. When they are used in priming systems, some protective device must be interposed between the centrifugal pump and the dry vacuum pump to prevent liquid from entering the vacuum pump. The dry vacuum pump is used extensively for central priming systems.

Wet Vacuum Pumps Any rotary, rotative, or reciprocating pump that can handle air or a mixture of air and liquid is classified as a wet vacuum pump.

The most common type of wet vacuum pump is a centrifugal displacement type of pump consisting of a round, multiblade rotor revolving freely in an elliptical casing partially filled with liquid. The curved rotor blades project radially from the hub and, with the side shrouds, form a series of pockets and buckets around the periphery.

The rotor revolves at a speed high enough to throw the liquid out from the center by centrifugal force. This forms a solid ring of liquid revolving in the casing at the same speed as the rotor, but following the elliptical shape of the casing. It will be readily seen that this forces the liquid to alternately enter and recede from the buckets as the rotor at high velocity.

If a solid stream of liquid circulates in this pump in place of air or of an air and liquid mixture, the pump will not be damaged but it will require more power. For this reason, in automatic priming systems using this type of vacuum pump, a separating chamber or trap is provided so liquid will not reach the pump.

Liquid needed for sealing a wet vacuum pump can be supplied from a source under pressure, with the shutoff valve operated manually or through a solenoid connected with the motor control. It is, however, preferable to provide an independent sealing liquid supply by mounting the vacuum pump on a base containing a reservoir. This is particularly desirable in locations where freezing *may* occur, as a solution of antifreeze can be used in the reservoir.

CENTRAL PRIMING SYSTEMS

If there is more than one centrifugal pump to be primed in an installation, one priming device can be made to serve all the pumps. Such an arrangement is called a central priming

LIBERTY EXHIBIT 1017, Page 345

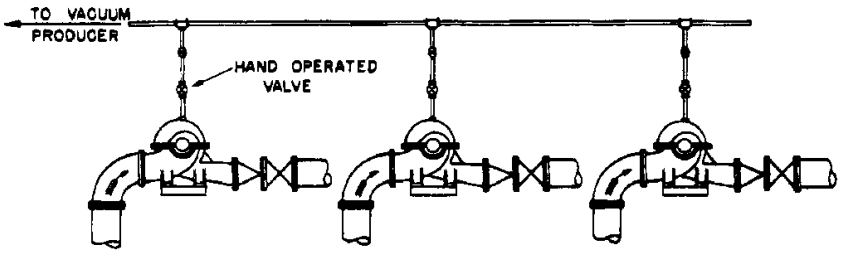


FIGURE 4 Connections for a central priming system

system (Figure 4). If the priming device and the venting of the pumps are automatically controlled, the system is called a central automatic priming system.

Vacuum-Controlled Automatic Priming System A vacuum-controlled automatic priming system consists of a vacuum pump exhausting a tank. The pump is controlled by a vacuum switch and maintains a vacuum in the tank of 2 to 6 in Hg (50 to 150 mm Hg) above the amount needed to prime the pumps with the greatest suction lift. The priming connections on each pump served by the system are connected to the vacuum tank by automatic vent valves and piping (Figure 5). The vacuum tank is provided with a gage glass and a drain. If liquid is detected in the vacuum tank as the result of leakage in a vent valve, the tank can be drained. Automatic vent valves consist of a body containing a float that actuates a valve located in the upper part. The bottom of the body is connected to the space being vented. As air is vented out of the valve, water rises in the body until the float is lifted, and the valve is closed.

A typical vent valve designed basically for vacuum priming systems is illustrated in Figure 6. The valve is provided with auxiliary tapped openings on the lower part of the body for connection to any auxiliary vent points on the system—for instance, when air is to be exhausted simultaneously from the high point of the discharge volute and the high point of the suction passageways. When one or more of these vent points are points of higher pressure, such as the top of the volute of the pump, an orifice is used in the vent line to limit the flow of liquid. Otherwise, a relatively high constant flow of liquid from the discharge back to the suction would take place, causing a constant loss. Where a unit is used more or less constantly, a separate valve should be used for each venting point.

The system shown in Figure 5 is the most commonly used central automatic priming system. It can use either wet or dry motor-driven vacuum pumps. Most central priming systems are provided with two vacuum pumps. The usual practice is to have the control of one vacuum pump switched on at some predetermined vacuum and the control of the second switched on at a slightly lower vacuum.

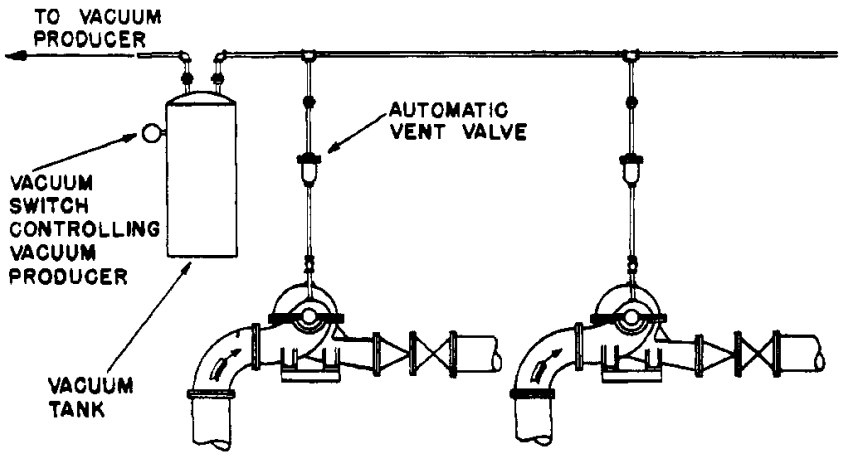


FIGURE 5 Vacuum-controlled central automatic priming

LIBERTY EXHIBIT 1017, Page 346

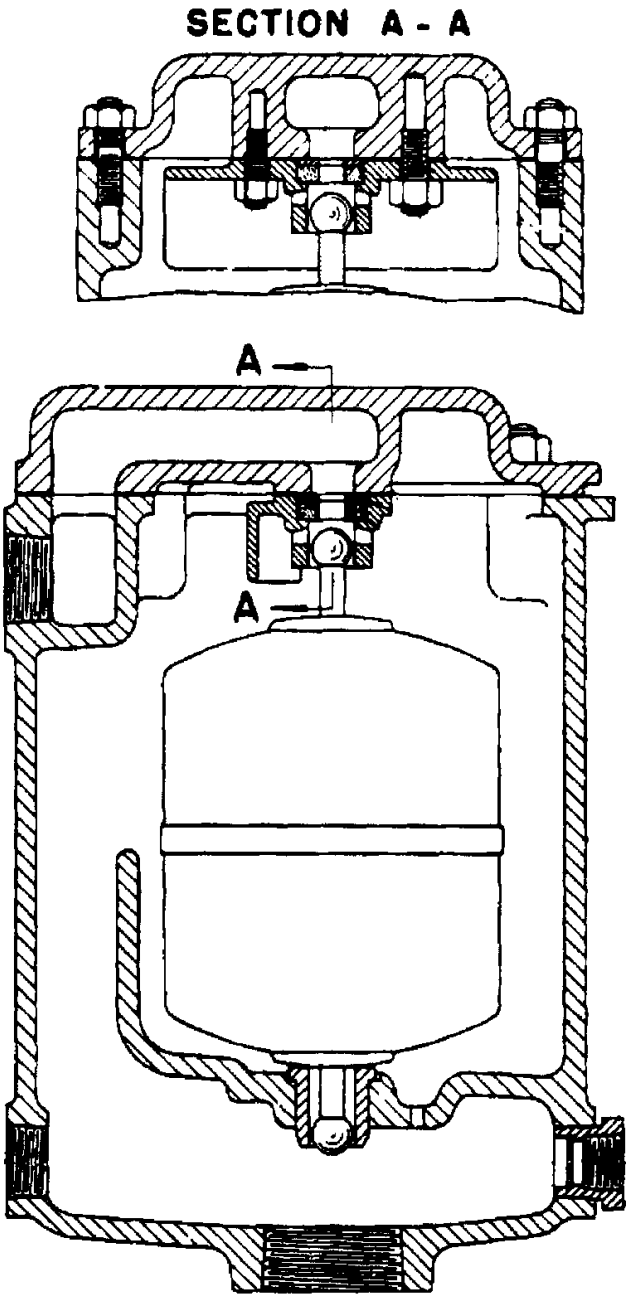


FIGURE 6 Automatic vent valve (Nash Engineering)

Combination dry reciprocating-type vacuum pump and vacuum tank units are commercially available in various sizes. The operation of a typical unit can be explained as follows, referring to Figure 7.

The primer automatically stops and starts itself to maintain a minimum vacuum in its tank at all times, regardless of whether the centrifugal pumps it serves are operating or not.

A vacuum header is run from the primer to the centrifugal pumps, and connection is made to the priming valve mounted on each pump. The vacuum in the primer tank removes the air from the pump and suction line via the vacuum header and priming valve. Liquid rises up the suction line and fills the pump. The liquid cannot enter the vacuum header because the float mechanism in the priming valve closes when the liquid reaches it.

If, for any reason, the liquid level in the pump drops, the priming valve immediately opens and the vacuum restores the liquid level. The pumps are thus kept permanently primed.

LIBERTY EXHIBIT 1017, Page 347

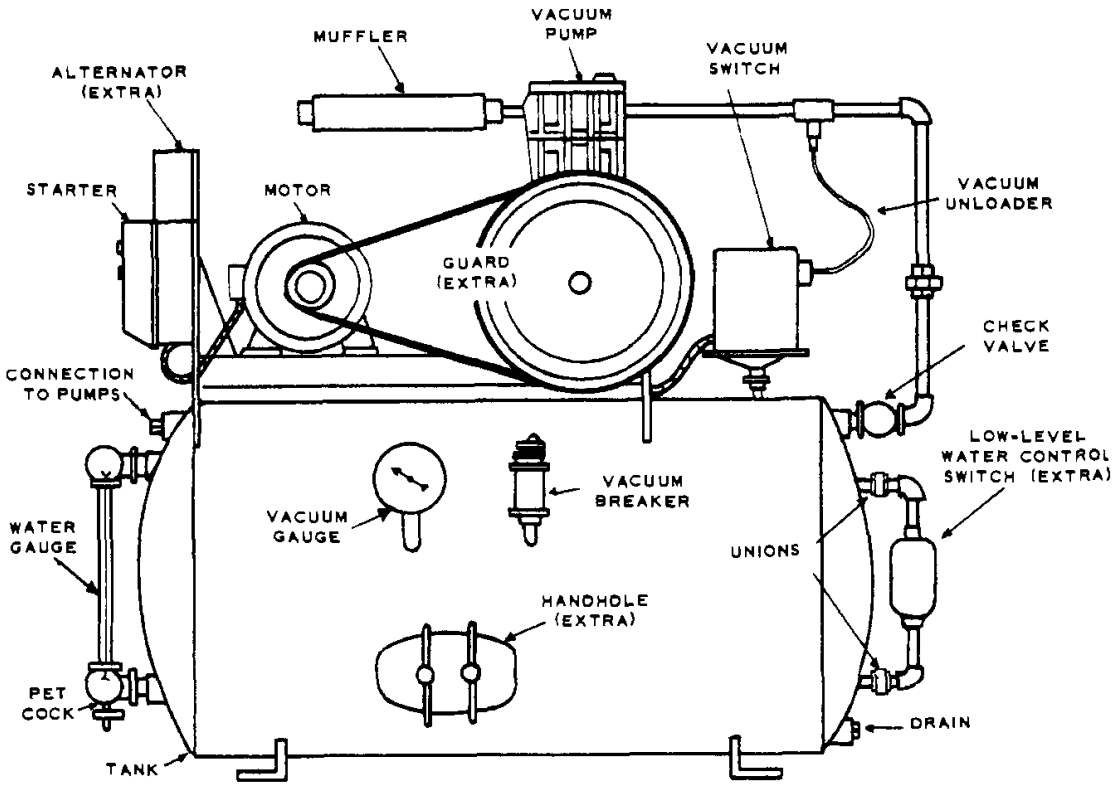


FIGURE 7 Combination dry reciprocating-type vacuum pump and vacuum tank (Apco/Valve and Primer)

Automatic priming systems using ejectors are also feasible, and several such systems are commercially available.

SELF-PRIMING PUMPS

The basic requirement for a self-priming centrifugal pump is that the pumped liquid must be able to entrain air in the form of bubbles so the air will be removed from the suction side of the pump. This air must be allowed to separate from the liquid after the mixture of the two has been discharged by the impeller, and the separated air must be allowed to escape or to be swept out through the pump discharge. Such a self-priming pump therefore requires, on its discharge side, an air-separator, which is a relatively large stilling chamber, or reservoir, either attached to or built into the pump casing. Alternatively, a small air bleed line can be installed from the discharge pipe between the pump and the discharge check valve back to the suction source.

There are two basic variations of the manner in which the liquid from the discharge reservoir makes the pump self-priming: (1) recirculation from the reservoir back to the suction and (2) recirculation within the discharge and the impeller itself.

Recirculation at Discharge This form of priming is distinguished from the preceding method by the fact that the priming liquid is not returned to the suction of the pump but mixes with the air either in the impeller or at its periphery. The principal advantage of this method, therefore, is that it eliminates the complexity of internal valve mechanisms.

One such self-priming pump is illustrated in Figure 8. An open impeller (A) rotates in a volute casing (B), discharging the pumped liquid through passage C into the reservoir (D). When the pump starts, the trapped liquid carries entrained air bubbles from the suction to the discharge chamber. There, the air separates from the liquid and escapes, whereas the liquid in the reservoir returns to the impeller through the recirculation port

LIBERTY EXHIBIT 1017, Page 348

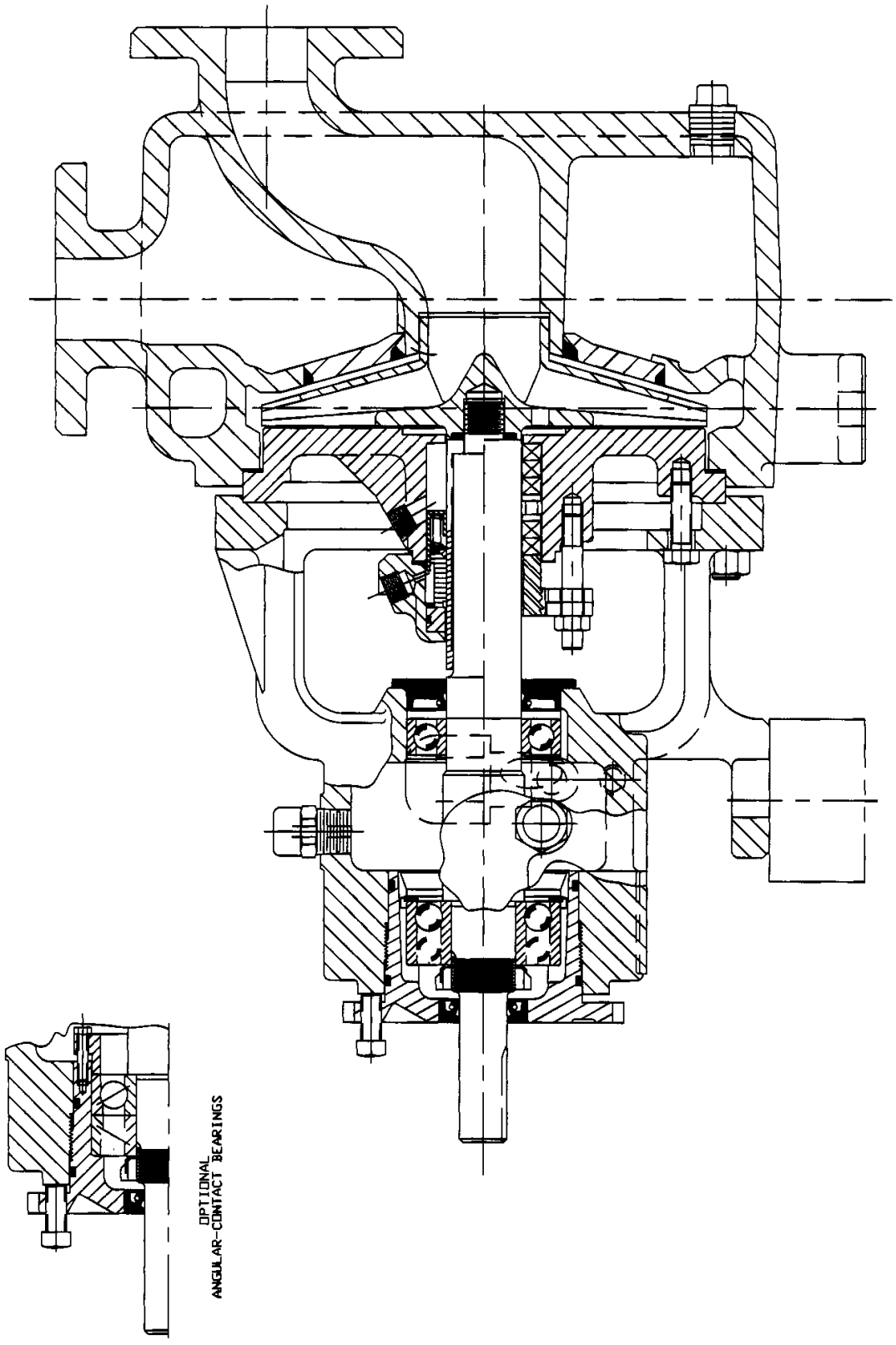


FIGURE 8 Self-priming pump with recirculation at discharge (Flowserve Corporation)

LIBERTY EXHIBIT 1017, Page 349

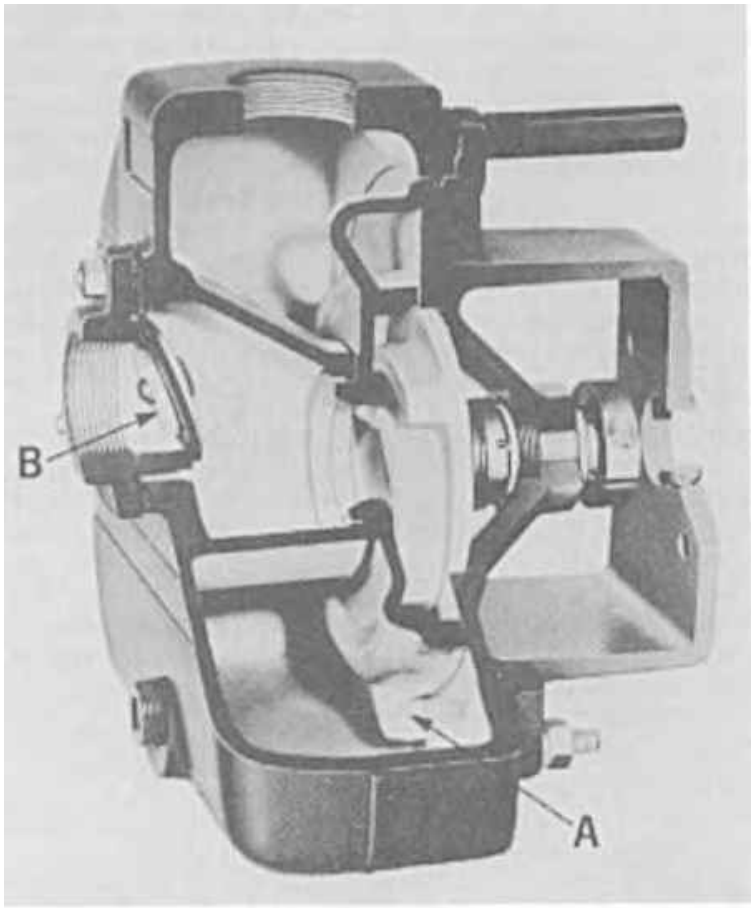


FIGURE 9 Self-priming pump with recirculation at discharge (Peabody Barnes)

(F), reenters the impeller and, after mixing once more with air bubbles, is discharged through passage C. This operation is repeated continuously until all the air in the suction line has been expelled. After the pump is primed, a uniform pressure distribution is established around the impeller, preventing further recirculation. From this moment on, the liquid is discharged into the reservoir bath at C and at F.

Figure 9 illustrates another form of self-priming pump with recirculation at the discharge. In this arrangement, the return of the liquid to the impeller periphery takes place through a communicating passage (A) located at the bottom of the pump casing. After the pump is primed, liquid is delivered into the reservoir at the discharge both through its normal volute discharge and through port A. In the pump illustrated in Figure 9, a check valve at the pump suction (B) acts to prevent the draining of the pump after it has been stopped.

Regenerative Turbine Pumps Because these pumps can handle relatively large amounts of gas, they are inherently self-priming as long as sufficient liquid remains in the pump to seal the clearance between the suction and discharge passages. This condition is usually met by building a trap in the pump suction.

SPECIAL APPLICATIONS

Systems for Sewage Pumps A pump handling sewage or similar liquids containing stringy material can be equipped with automatic priming, but special precautions must be used to prevent carry-over of the liquid into the vacuum-producing device.

LIBERTY EXHIBIT 1017, Page 350

One approach is to use a tee on the suction line immediately adjacent to the pump suction nozzle, with a vertical riser mounted on the top outlet of the tee. This riser is blanked at the top, thus forming a small tank. The top of the tank is vented to a vacuum system through a solenoid valve. The solenoid valve in turn is controlled electrically through electrodes located at different levels in the tank. The solenoid valve closes if the liquid reaches the top electrode and opens if the liquid level falls below the level of the lower electrode.

Another solution permits the use of an automatic priming system with a separate motor-driven vacuum pump controlled by a discharge-pressure-actuated pressure switch. An inverted vertical loop is incorporated in the vacuum pump suction line to the pump being primed. This prevents the sewage from being carried over into the vacuum pump because this pump shuts down before the liquid reaches the top of the loop.

Systems for Air-Charged Liquids Some types of liquid have considerable dissolved gas that is liberated when the pump handles a suction lift. In such installations, an air-separating tank (also called a *priming tank* or an air *eliminator)* should be used in the suction line. One type (Figure 10) uses a float-operated vent valve to permit the withdrawal of air or other gas. Another common arrangement uses a float valve mounted on the side of the tank to directly control the starting and stopping of the vacuum pump. Unless the air-separating tank is relatively large and the vacuum pump is not oversized, there is danger of frequent starting and stopping of the vacuum pump in such a system. When sand is present as an impurity in the liquid, the air-separating tank can be made to also function as a sand trap.

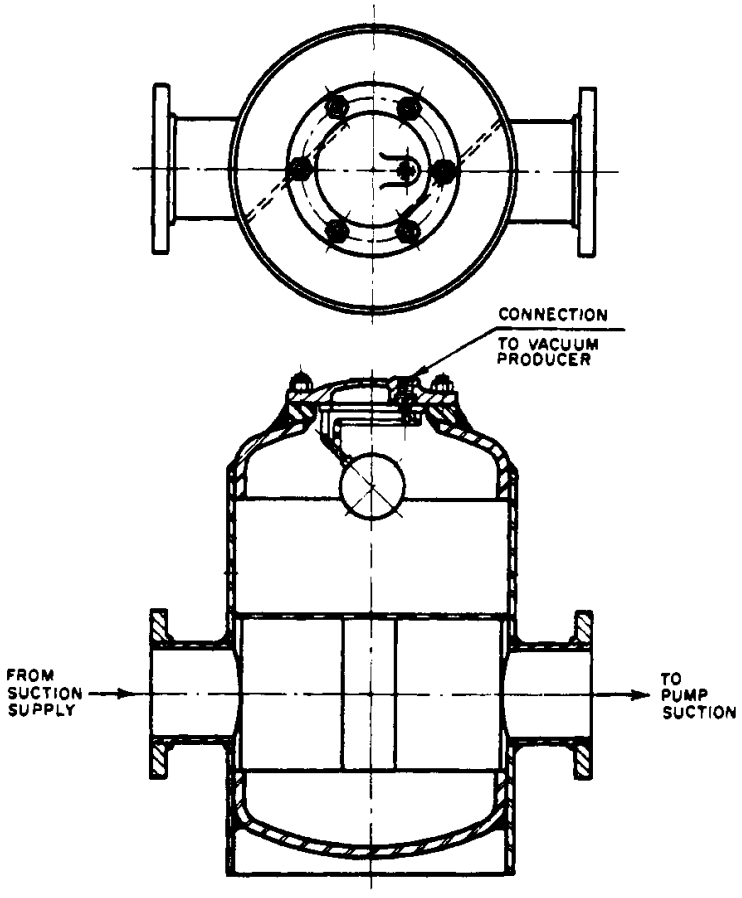


FIGURE 10 Air separating chamber

Previous Page

Systems for Units Driven by Gasoline or Diesel Engines An automatic priming system using motor-driven vacuum pumps can be used for centrifugal pumps driven by diesel engines if a reliable source of electric power is available in the station. An auxiliary vacuum pump driven by a gasoline engine might be desirable for emergency use in case of electric power failure. Alternatively, a direct-connected wet vacuum pump with controls similar to those used in motor-driven automatically primed units is very satisfactory.

The choice of the priming device for a gasoline-engine centrifugal pump depends on the size of the pump, the required frequency of priming, and the portability of the unit. Most portable units are used for relatively low heads and small capacities, for use in pumping out excavations and ditches, for example. Self-priming pumps of various types are most satisfactory for this service and are preferable to regular centrifugal pumps.

It is possible to utilize the vacuum in the intake manifold of a gasoline engine as a means of priming or keeping the pump primed. The rate at which the air can be drawn from the pump in this manner is relatively low, so many of these units use foot valves. They are initially primed by filling the pump manually. Provision must be made to prevent liquid from being drawn over into the manifold.

TIME REQUIRED FOR PRIMING

The time required to prime a pump with a vacuum-producing device depends on: (1) the total volume to be exhausted, (2) the initial and final vacuums, and (3) the capacity of the vacuum-producing device over the range of vacuums that will exist during the priming cycle. The calculations for determining the time necessary to prime a pump are complicated. To permit close approximations, jet primers are usually rated in net capacity for various lifts. It is necessary to divide the volume to be exhausted by the rating to obtain the approximate priming time. Unless such a simplified method is available, the selection of the size of a primer is best left to the vendor of the equipment.

Central automatic priming systems are usually rated for the total volume to be kept primed. The time initially required to prime each unit served by the central system is not usually considered, as the basic function of the system is to keep the pumps primed and in operating condition at all times.

PREVENTION OF UNPRIMED OPERATION

Various controls may be used to prevent the operation of a pump when it is unprimed. These controls depend upon the type of priming system used. For many installations, a form of float switch in a chamber connected with the suction line is used. If the level in the chamber is above the impeller eye of the pump, the float switch control allows the pump to operate. If the liquid falls below a safe level, the float switch acts through the control to stop the pump, to prevent its being started, to sound an alarm, or to light a warning lamp. Such a valve and switch are illustrated in Figure 11.

GENERAL

Because a great number of automatic priming devices and systems are available, care should be taken to use the type or variation best suited to the application. The discussion of priming in this section does not, of course, cover all makes and modifications available for every specific application.

An automatic priming system will often allow units to be operated with excessive air leakage into the suction lines. This is poor practice because it requires the operation of the vacuum producer for greater periods of time than normally necessary.

LIBERTY EXHIBIT 1017, Page 352

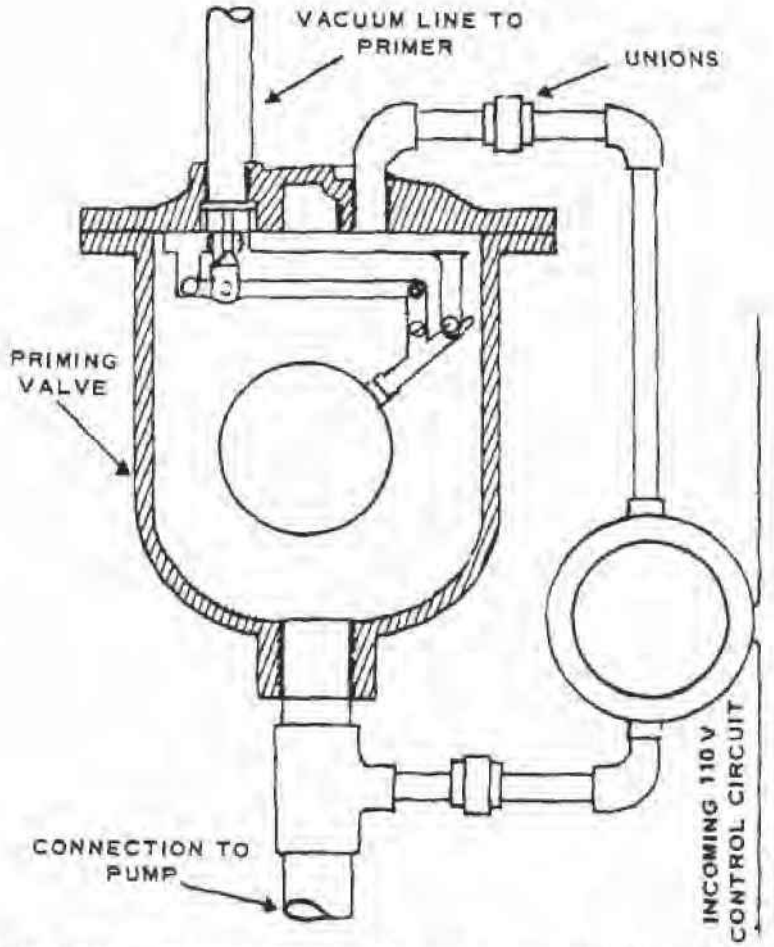


FIGURE 11 Priming valve with liquid level control switch (Apco/Valve and Primer)

FURTHER READING

Apco/Valve and Primer Corp. *Automatic Pump Primers,* Technical Bulletin 721, Schaumburg, IL, 1978.

Hrivnak, S. J. "Why Doesn't Your Self-Priming Pump Work?" *Pumps and Systems Magazine*, June, 1999.

Karassik, I. J., and Carter, R. Chap. 21 in *Centrifugal Pumps: Selection, Operation, and Maintenance.* McGraw-Hill: New York, 1960.

LIBERTY EXHIBIT 1017, Page 353

2.2.3
SEALLESS PUMPS

FREDERIC W. BUSE
STEPHEN A. JASKIEWICZ

Sealless pumps are developed to eliminate the liquid leakage to the atmosphere that occurs from pumps that employ packing or mechanical seals. This leakage is usually toxic or dangerous to the environment; sometimes the leakage is valuable. Eighty percent of the applications are for pressures below 200 lb/in^2 (13.8 bar) and below 250°F (120°C).

Sealless pumps are divided into two categories: magnetic drive pumps and canned motor pumps. The two categories compete against themselves in certain applications, but for the most part they each have their own market niche into which they are applied. Both have encapsulated inner driven mechanisms. On a magnetic drive pump (see Figure 5 in Section 2.2.3.1), the impeller is mounted to an inner magnet carrier. The inner and outer magnetic carriers are sealed by what is called a shell, which contains pump internal pressure. On a canned motor pump (see Figure 1 in Section 2.2.3.2), the impeller is mounted directly to the motor rotor. The atmospheric sealing element between the motor stator and rotor is called a liner or "can." Both magnetic drive and canned motor pumps use product lubricated bearings of compatible design and materials. These bearings are usually cooled and lubricated by the pump liquid.

The following sections describe both magnetic drive and canned motor pumps.

LIBERTY EXHIBIT 1017, Page 354

SECTION 2.2.3.1
MAGNETIC DRIVE PUMPS

FREDERIC W. BUSE
GREGORY M. DENAULT

The principle of a magnetic drive pump is the elimination of the seal or packing in an overhung pump (Figure 1) and cutting the shaft in two at the seal location (Figure 2a). On the inner or wet end half of the shaft (Figure 2b), an inner magnet assembly (a) is placed on a shaft (b) supported by product lubricated bearings (c). On the other cut portion of the shaft, an outer magnet assembly (d) is placed on the power shaft (e). Between the inner and outer magnet assemblies, a static seal (f) isolates the shell (g) or diaphragm and the pumped liquid from the atmosphere. The magnetic flux from the outer magnet assembly drives the inner magnet assembly and impeller(s). The outer assembly is mounted directly to either its own bearing assembly in a frame housing (Figure 3) or motor shaft (Figure 4). Figure 5 shows a cross section of a magnetic drive frame mounted pump.

Magnetics A magnetic circuit usually consists of two sets of permanent magnets and inner and outer conducting rings (Figure 6). The conducting rings can be cast iron, ductile iron, carbon steel, or a 400 series stainless steel.

Magnet Materials The first permanent magnets, developed in the 1940s, were made of aluminum-nickel-cobalt (AlNiCo) and used in small chemical pumps. Development of rare earth magnets in the 1980s made it possible to have a small power package that could drive larger pumps. The two types of rare earth materials commonly used are neodymium iron boron (NdFeB) and samarium cobalt (SmCo). The SmCo is four times stronger than AlNiCo. NdFeB, at 70°F (21°C), is 20% stronger than SmCo. The advantage of SmCo is the maximum service temperature of 550°F (288°C), almost twice that of NdFeB, which is 300°F (149°C). Figure 7 shows the strength versus temperature characteristics of the two materials. The cost of SmCo, however, is about twice that of NdFeB.

The magnets have a maximum temperature at which they lose all magnetism in an irreversible process; the magnets do not regain magnetism as they cool. This temperature is the Curie temperature and is shown for each magnet material in Table 1.

Conduction Ring The amount of transmittal torque depends on the overall gap (Figure 8) between the poles of the magnets and the thickness of the conducting ring (Figure 9). If

LIBERTY EXHIBIT 1017, Page 355

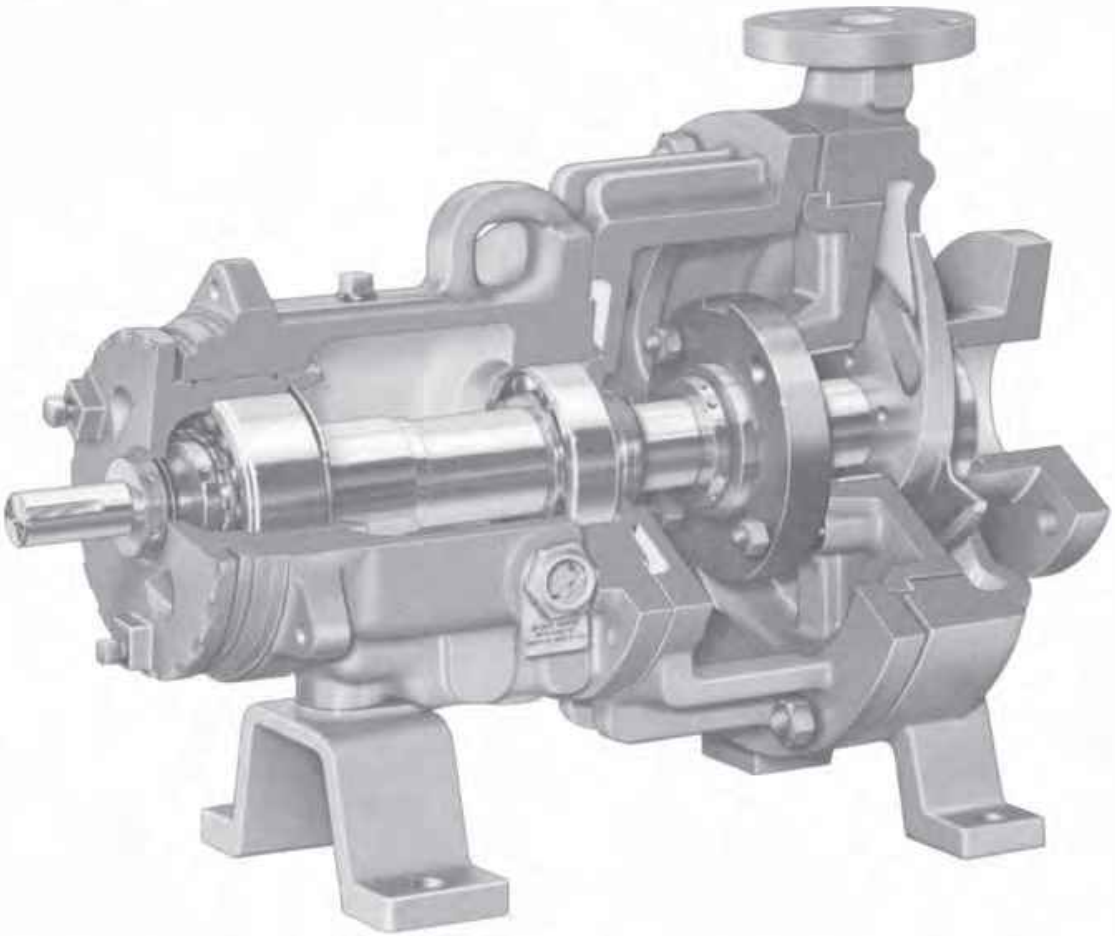


FIGURE 1 Pump with conventional bearing housing and mechanical seal (Flowserve Corporation)

the thickness of the conducting ring is too small, it will become saturated with flux and the torque capability will be reduced.

Gap The "overall gap" (Figure 8) is made up of the air gap, containment shell thickness, liquid gap, and encapsulation. Gap dimensions are based on the pressure requirement for the shell, the number of magnets (single or dual), and the material of the shell (metallic or nonmetallic) in the gap.

EXAMPLE Dimensions shown as in (mm)

Mean diameter (on radius dimensions)	4.6 (117)	6.0 (152.4)
Air gap minimum	.030 (0.762)	.045 (1.143)
Containment shell thickness: Hastelloy C	.040 (1.016)	.060 (1.524)
Polymer	.120 (3.048)	.150 (3.810)
Liquid gap	.035 (0.889)	.035 (0.889)
Encapsulation	.030 (0.762)	.030 (0.762)
Overall gap (basis Hastelloy C)	.135 (3.429)	.170 (4.318)
Overall gap (basis polymer)	.215 (5.461)	.260 (6.604)

In the previous example, the same overall gap was maintained for polymer and Hastelloy C shells. This allows for interchangeability of the magnetic assemblies independent of shell material.

LIBERTY EXHIBIT 1017, Page 356

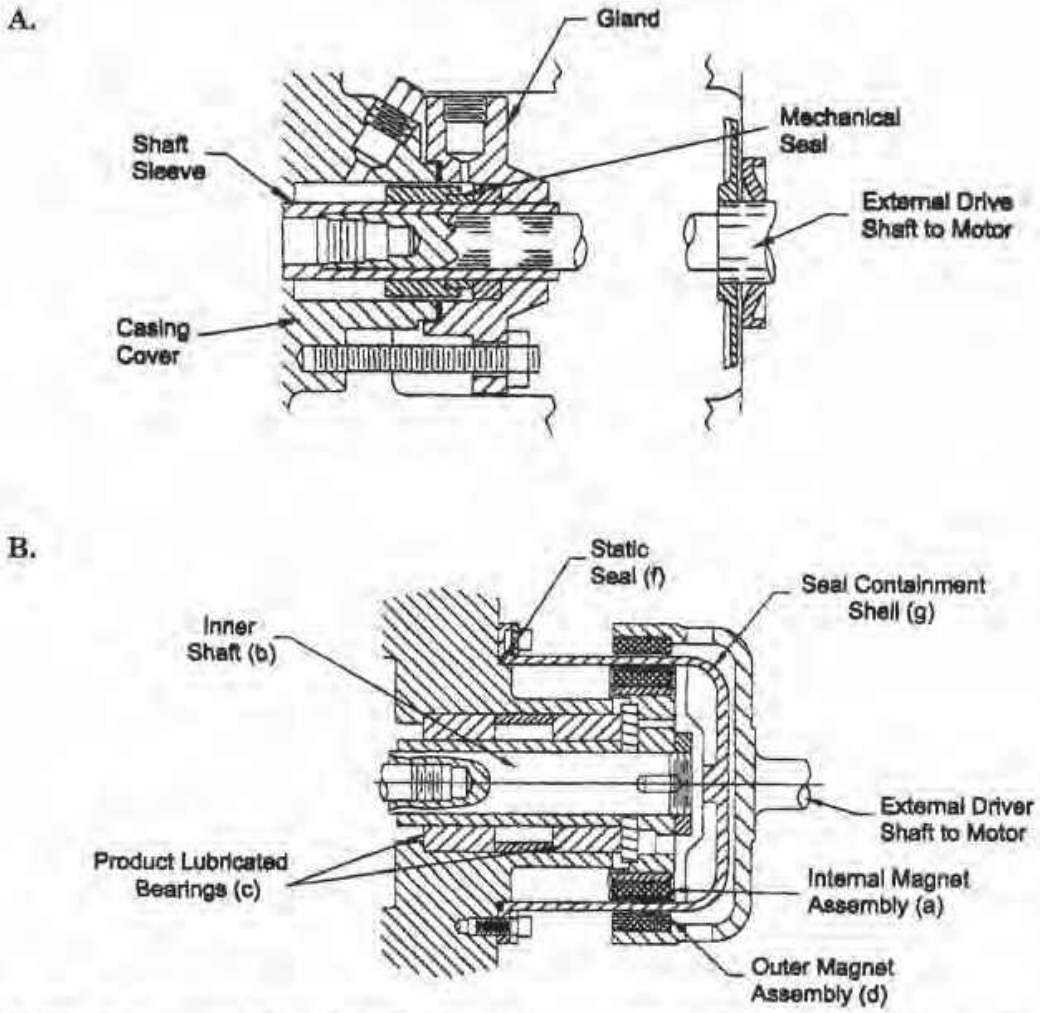


FIGURE 2 Comparison of typical mechanical seal arrangement and sealless pump drive configuration: (a) arrangement for typical mechanical through casing cover, (b) sealless drive configuration

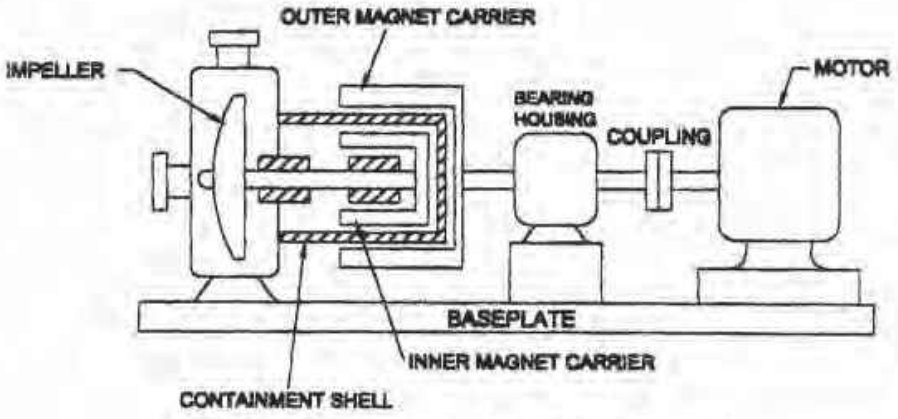


FIGURE 3 Frame-mounted magnet drive arrangement

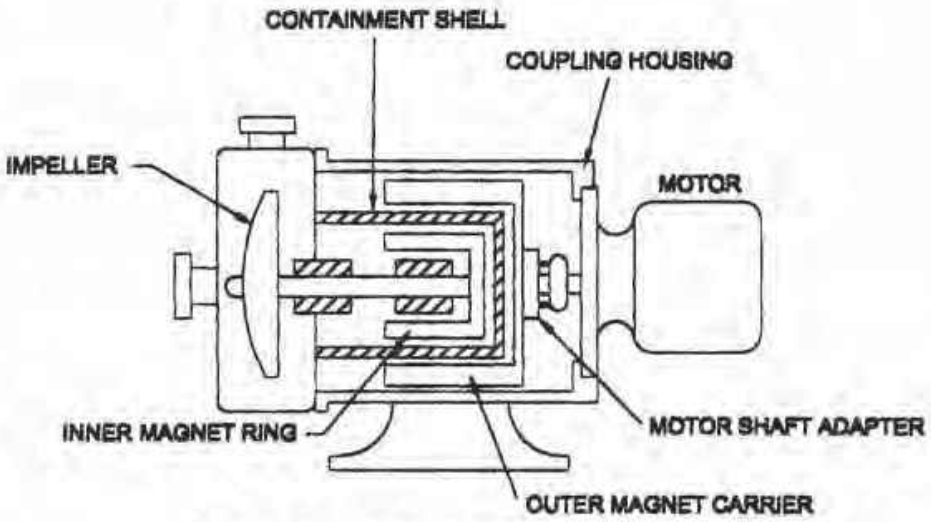


FIGURE 4 Close-coupled magnet drive arrangement

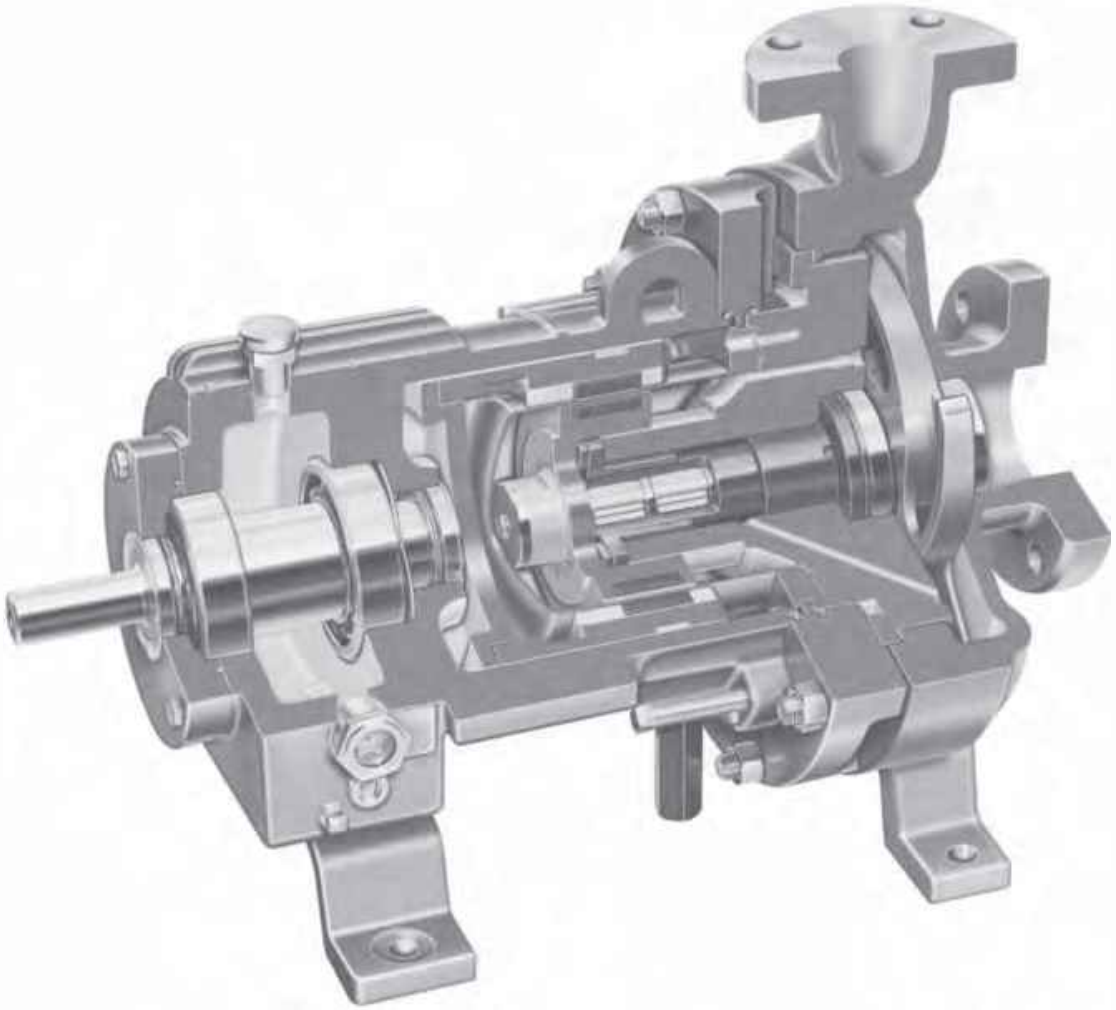


FIGURE 5 Cross-section of a frame-mounted magnet-driven pump (Flowserve Corporation)

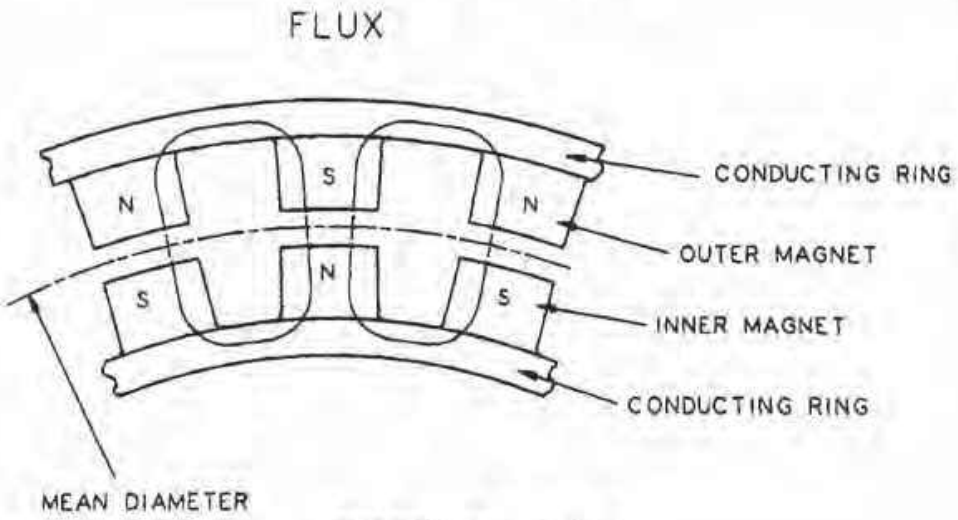


FIGURE 6 Magnetic circuit

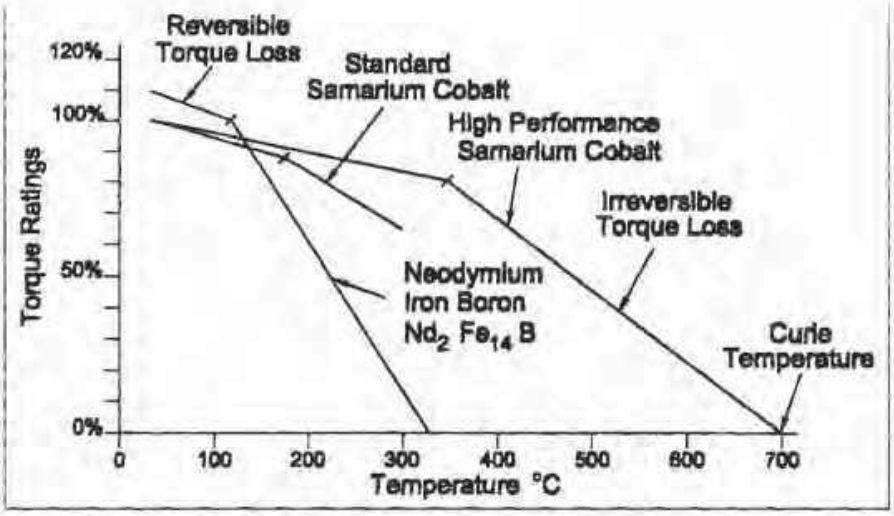


FIGURE 7 Magnet strength versus temperature

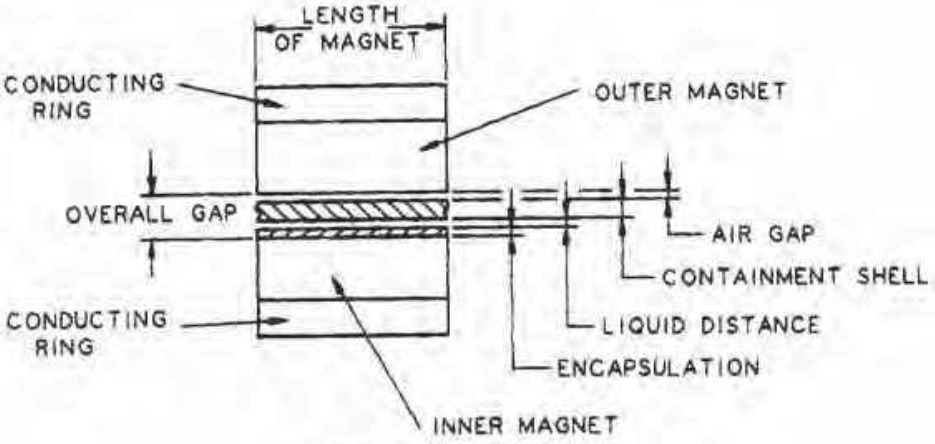


FIGURE 8 Magnet configuration

TABLE 1 Operating and Curie temperatures for magnet materials

Type of Magnet Material	Operating Temperature (°F/°C)	Curie Temperature (°F/°C)
AlNiCo	660/305	800/425
NdFeB	250–300/120–137 (Depending on grade)	600/310
SmCo	500–660/260–350 (Depending on grade)	1300/700

Transmittal Torque The torque transmitted by the magnets depends on the following:

- Flux density of the magnets, B_g
- Operating temperature of the magnets (which will change B_g)
- Length of the magnet poles, L
- Number of magnets per ring, M
- Mean ratios between the ID of the outer assembly magnets and OD of the inner assembly magnets, r
- Overall gap between the ID and OD of the magnets in the assembly, g
- A constant, K, which changes as a function of the specific design

Torque is determined from the following relationship, with appropriate units:

$$T = \frac{K \times B_g^2 \times L \times M \times r}{g}$$

For a given design type and configuration, the torque varies inversely as the square of the overall gap. Depending on costs and specific design construction, an assembly ring of magnets can have either one continuous length of magnets of a series of 1, 2, 3, or more rows of individual magnets.

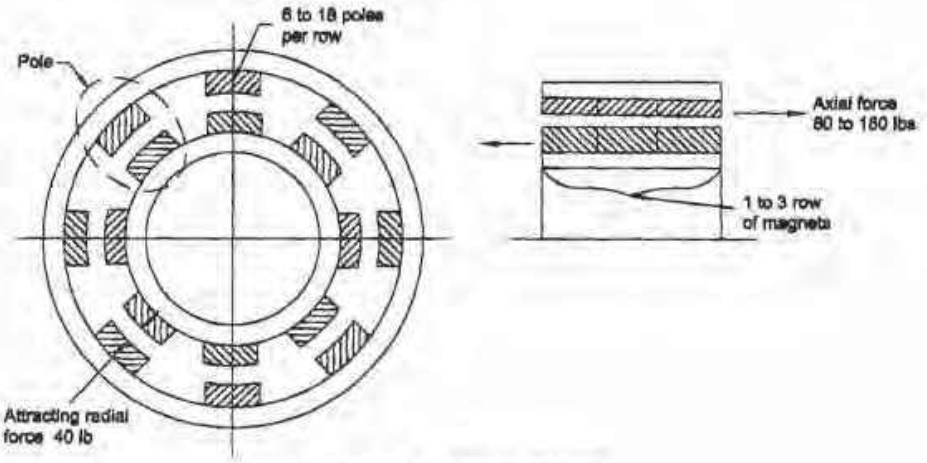


FIGURE 9 Rows of magnets

TORQUE CAPABILITY

The ultimate torque is the static "breakaway torque." To determine this, the magnet carriers are assembled so the inner carrier is locked in position. Then a torque is applied by bar and weights or by a torque wrench to the outer carrier. The torque value at which the two carrier assemblies break loose from each other radially—or "decouple"—is called the "breakaway torque." The designer has to account for the driver start-up acceleration time, start-up torque, and an appropriate safety factor to apply to the breakaway torque to determine the allowable applied torque.

Table 2 gives examples of the torque capability of assemblies composed of NdFeB blocks of magnet 0.75 in wide × 0.38 in high × 1.125 in long (19 mm × 9.65 mm × 28.6 mm) with a 0.180-in (4.6-mm)-thick conducting ring.

Basic Dimensioning of Magnet Blocks The magnet blocks can be made too long or too short, resulting in handling, magnet molding, or flux density problems. The ratio of the dimensions for magnet blocks for successful designs is as follows:

- Block width is two to three times the thickness.
- Block length is three to five times the thickness.
- Doubling the block thickness will increase the strength by approximately 20%.

For reference: 1.0 in^3 (16.387 cm^3) of NdFeB per assembly at a mean diameter of 4.0 in (101.6 mm) with a 0.25 in (6.35 mm) overall gap produces approximately 7 ft · lb (9.5 N • m) of torque. A 3% reduction in flux density is equal to a 6% reduction in torque.

Characteristics of magnet material:

Density: 0.273 lb/in^3 (7.56 g/cm^3)

Tensile: 12×10^3 lb/in^2 (844 kg/cm^2)

Compression: 110×10^3 lb/in^2 (7.7×10^3 kg/cm^2)

Flex stress: 36×10^3 lb/in^2 (2.53×10^3 kg/cm^2)

Coefficients of thermal expansion are shown in Table 3.

Radial and Axial Magnet Forces The inner and outer carriers have to be restrained radially by bearings from contacting each other. In the example of "Torque Capability," a single row of 18 magnets with a 6 in (152 mm) mean diameter, the radial force with magnets concentric is 40 lb (18 kgf). When the magnets are offset by 0.005 in (0.127 mm), the radial force is 55 lb (25 kgf) (Figure 9). When the magnets are against each other (no gap), the radial force is 80 lb (36 kgf).

In the previous example, it takes 60 lb (27 kgf) in an axial direction to separate a single row of concentric magnets and 180 lb (82 kgf) for three rows. It is strongly advisable that provisions be made for personnel to address these loads during assembly and disassembly of the carriers.

Encapsulation of Inner Carrier Magnetics Encapsulation can be accomplished with either metallic or polymer materials. The encapsulation of the inner magnet and conducting ring is probably the most expensive and extensive process in a magnetic drive sealless

TABLE 2 Torque capability of magnet assemblies

Mean Diameter in (mm)	Magnets/Row	Overall Gap in (mm)	Breakaway Torque ft-lb (N • m)
4.3 (109)	12	0.240 (6.10)	30 (40)
6.0 (152)	18	0.260 (6.60)	60 (80)

LIBERTY EXHIBIT 1017, Page 361

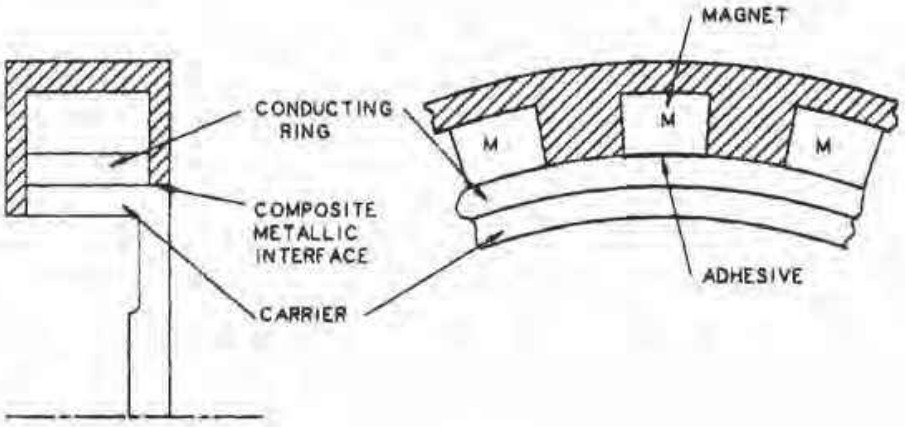
TABLE 3 Coefficients of thermal expansion (in/in/°F × 10^{-6})/(cm/cm/°C × 10^{-6})

Magnet material	Parallel to Axis	Perpendicular to Axis
NdFeB	5 (9)	9 (16.2)
SmCo	20 (36)	16 (28.8)

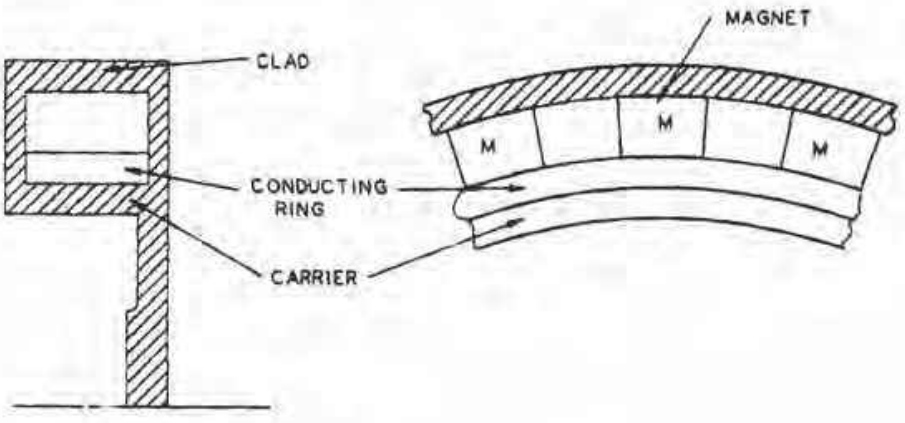
pump. After encapsulation, the carrier should be nondestructively tested to confirm 100% effectiveness.

The pros and cons of polymer encapsulation (Figure 10a) are as follows:

1. Limited to 250 to 300°F (120 to 150°C)
2. The overall gap is increased because of the required thickness of the polymer.
3. Magnets must be restrained mechanically on the conducting ring by adhesives or high-strength polymers around the magnets.
4. Polymers like PFA/PTFE or PEEK are more corrosive-resistant than most metals.
5. Production polymer construction is much less expensive than metallic construction.
6. Polymer tooling is expensive.



(A) NONMETALLIC COMPOSITE



(B) METALLIC

FIGURE 10 Encapsulation of magnets using (A) nonmetallic composition and (B) metallic clad

LIBERTY EXHIBIT 1017, Page 362

The pros and cons of metallic encapsulation (Figure 10b) are as follows:

1. Temperature rating can be 550°F (288°C).
2. Thickness of the encapsulation material over the magnets can be as little as 0.030 in (0.76 mm).
3. Welding of the components can be conventional, electron beam, or laser. However, care must be taken with conventional welding to prevent the arc from jumping toward the magnet flux.
4. If castings are used for the inner carrier, porosity can be a problem.
5. Gassing of polymers from welding heat coming out of the seams can be a problem.
6. Adhesives are not required to keep the magnets in place at 3600 rpm with metallic encapsulation; the outer shield performs this function.

Encapsulation of Outer Carrier Magnets The magnets for the outer carriers do not have to be encapsulated (Figure 11). However, material like NdFeB has an affinity for water absorption that results in rusting and swelling. The magnets can then break loose and move in position relative to one another. It is highly recommended that they be encapsulated with an epoxy or metal sheathing for atmospheric protection and handling.

Construction The outer carrier can be a casting or fabrication. The carrier is attached to the power end shaft in the bearing housing (Figure 3) or directly to a motor shaft, which is then called *close coupled construction*. When attached to the bearing housing shaft, there is very little axial or radial load applied to the bearings. This lightly loaded condition can result in internal skidding of the rolling element bearings within their races, resulting in premature bearing failure. Therefore, it is best to preload the bearings with a spring to prevent skidding. This can be accomplished outside of the bearing by a spring-loading feature (Figure 11).

Containment Shell The containment shell shape and thickness depends on working pressure, material, and temperature. The shell thickness is usually uniform. To keep the length of the shell to a minimum, a square-ended shell can be used. However, unless the end of the shell is made extra thick, it would have a relatively low pressure capability. Therefore, an end shape which is elliptical or spherical is used to obtain higher pressure capability (Figure 12).

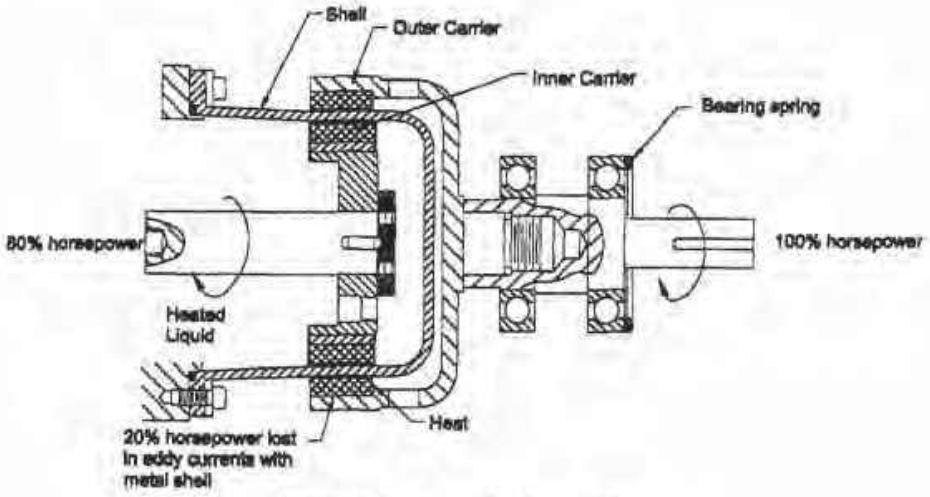


FIGURE 11 Inner and outer carrier

LIBERTY EXHIBIT 1017, Page 363

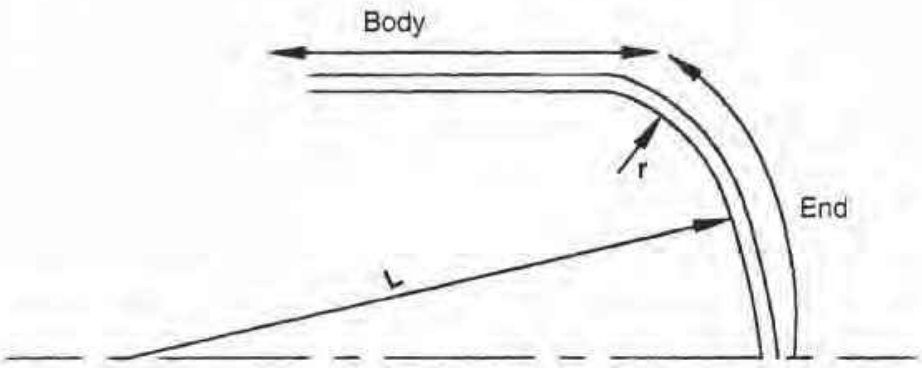


FIGURE 12 Shell ratio L/r for pressure

Examples of how allowable shell pressure varies with the shape of the end plate are shown in Table 4.

The classes of materials used for containment shells (Figure 11) include metals, polymers, and ceramics. The characteristics of containment shells of various materials are shown in Table 5. The main advantage of polymer or ceramic shells is that there are no eddy current losses. Therefore, cooling of the magnets is not required.

Eddy Currents Metallic or metallic-lined shells will produce eddy currents. Depending on the thickness of the shell, the eddy current losses (P_L) can amount to as much as 20% of the total power.

$$P_L = \frac{K \times T \times L \times N^2 B_g{}^2 D^3 M}{R}$$

where K = a constant, depending on the design
T = thickness of the shell
L = length of magnets (times the core of magnets) N = speed, rpm
B_g = flux density of the magnets
D = mean diameter
M = number of sets of magnets
R = electrical resistivity, microhms per cm³ (electrical resistivity for various shell materials is given in Table 6)

The effect of material selection on heat buildup is shown in Table 7. The tabulation shows the temperature rise of the air space inside a shell with only the outer carrier spinning

TABLE 4 Pressure capabilities of shells with various end shapes for the same thickness and material

Shape	L/r	Allowable pressure—lb/in² (kPa)	Ratio of allowable pressure to that for a flat plate
Flat	533	9 (62)	1.0
Flat	267	23 (158)	2.55
Elliptical	28	113 (779)	12.6
Elliptical	8	209 (1440)	23.2
Spherical	1	815 (5620)	90.5

LIBERTY EXHIBIT 1017, Page 364

TABLE 5 Characteristics of containment shells of various materials

Material	Metal	Reinforced Polymer	Ceramic	Metal with PTFE
Construction	Welded or hydroformed	Injection molded	Set and fired	Spray coated
Temperature limit—°F (°C)	−300 to + 750 (−150 to +400)	−40 to +250 (−4 to + 120)	32 to 2000+ (0 to 1100+)	32 to 350 (0 to 175)
Thickness—in (mm)	0.030 to 0.040 (0.76 to 1.0)	0.170 (4.3)	0.250 to 0.380 (6.35 to 9.6)	0.050 (1.27)
Heat conductivity*	Hastelloy C = 71 AISI 316 = 7.5	3	6	Higher than metal alone
Creep	None	None	None	Some
Thermal shock	1000+ (537+)	375 (190)	500 (260)	—
Eddy currents	316 is twice Hastelloy C	None	None	Same as metal

*Approximate thermal conductivity in Btu/h/ft²/°F. Multiply by 0.488 to get calories/h/cm²/°C

TABLE 6 Electrical resistivity of various shell materials

Shell Material	Electrical Resistivity (R), microhms per cm³
Hastelloy C	130
AISI 316L	74
Inconel 625	129
Nimonic 90	115
Titanium	53
K-Monel	58
Alloy 20	75

TABLE 7 Effect of material selection on heat build-up

Material of Shell	Thickness in (mm)	Time min	kW	°F (°C)	°F/min (°C/min)
AISI 316	0.43 (10.9)	Start	0.40	80 (27)	—
AISI 316	0.43 (10.9)	5.0	0.30	500 (260)	100 (38)
Hastelloy C	0.43 (10.9)	0.5	0.24	170 (77)	340 (171)
Hastelloy C	0.43 (10.9)	5.0	0.21	370 (188)	74 (23)

around a metallic shell (no inner carrier in place) at 3550 rpm. The carrier has 12 magnets, 1.25 in (3.175 cm) long, with a mean diameter of 4.25 in (11.43 cm).

This illustrates the difference between AISI 316 and Hastelloy C shells at 3550 rpm. At 1750 rpm, the power loss for AISI 316 would be one-fourth that at 3550 rpm, which may not result in excess power consumption.

There are also axially laminated metal shells available that substantially reduce eddy current (I^2R) losses. These laminations work on the principle that when a shell length is cut in half, the eddy current losses are reduced to one-fourth their original value. If the one-half shell length is cut in half again, the resulting pieces have eddy current losses one-sixteenth that of the original shell. A shell design made of segments sealed together to make a full-length shell will thus reduce total eddy current losses.

Dual Containment As a precaution against leakage due to a breech in the primary containment shell, a dual or double-containment arrangement can be used. This double layering of shells (Figure 13) usually consists of a combination of a nonmetallic and metallic shell. The pressure rating of the secondary shell is equal to that of the primary shell. It is designed to operate at least 48 to 120 h after a breach in the primary shell occurs. A pressure monitor is inserted in the flange of the secondary shell to detect pressure buildup from primary shell leakage.

Bearings The internal shaft system of the pump is supported by one or more bearings. Some designs use a rotating shaft; others use a mandrel on which the bearings rotate. The bearing, which consists of a journal and bushing, is made of various materials, depending on the loads and pumpage (used for product lubrication). The bearing loads are from the weight of the components and hydraulic forces from the impeller and inner carrier. The impeller forces are both radial and axial.

Most magnetic drive sealless pumps are single-stage volute pumps that have the same radial bearing loads as comparable conventionally sealed pumps. The main difference with the sealless pump is that there is almost no overhang from the impeller to the first bearing. The load on the bearing, therefore, is almost equal to that of the impeller. In a conventionally sealed pump, the load on the radial bearing is almost twice that of the impeller. This can be seen by comparing Figures 1 and 5.

The axial load will depend on whether the impeller is enclosed or semiopen (Figure 14). Enclosed impellers usually have horizontal front rings and may also have a back ring or pump-out vanes. Semiopen impellers have no rings, but they usually employ scallops in the shroud to reduce the effective pressure area (Figure 15). Axial thrust force is further reduced by employing pump-out vanes (POV) or pump-out slots (POS) on the back shroud of the impeller to reduce the amount of pressure on the impeller back shroud.

The enclosed impeller can have less radial and axial load than a semiopen impeller. This is usually accomplished by employing back rings (Figure 14b). To ensure positive

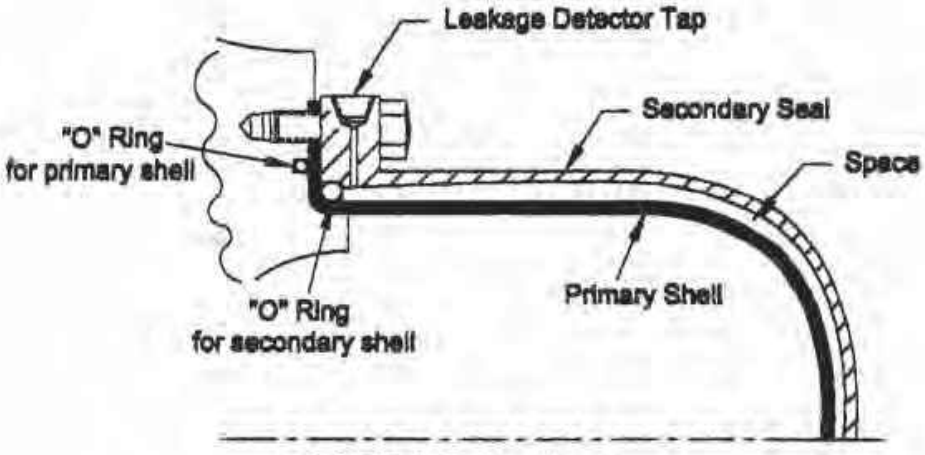


FIGURE 13 Dual containment

LIBERTY EXHIBIT 1017, Page 366

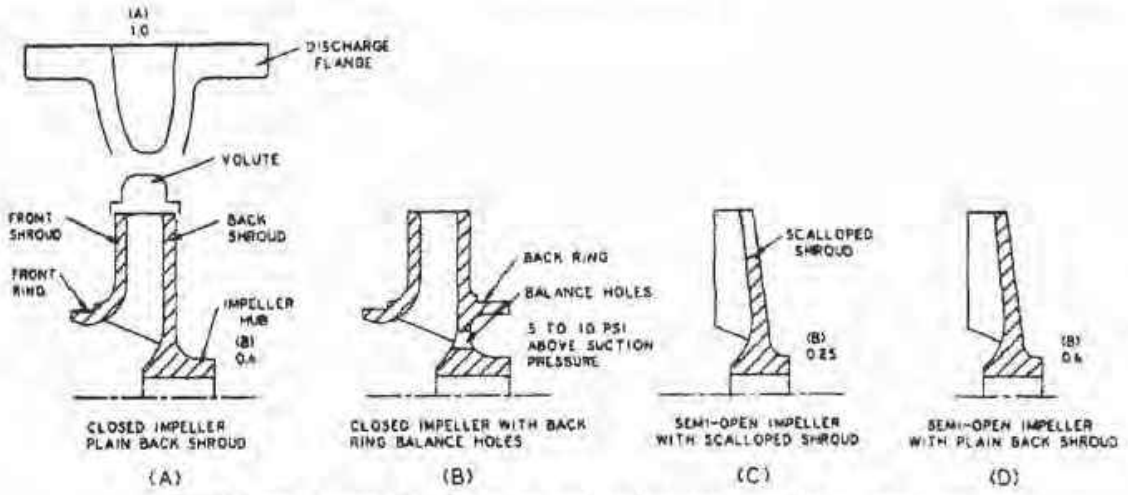


FIGURE 14A through D Various enclosed and semiopen impeller configurations

pumping in the lubrication flow path in magnetic drive pumps, POV-POS on an enclosed or semiopen impeller are recommended.

Liquids pumped in chemical or petroleum plants may have low viscosity, low specific gravity, or low specific heat. These characteristics can result in boundary lubrication rather than hydrodynamic lubrication of the product lubricated bearings. Therefore, bearings are selected using pressure-velocity (PV) values. Some limiting PV values for various bearing material combinations are shown in the following section on bearing materials.

Bearing Materials Table 8 shows PV values for various bearing journal and thrust face materials. When loads exceed a PV value of 150,000, the bearing should have an alignment compensator built in to correct for inaccuracies in perpendicularity, concentricity, and parallelism of parts.

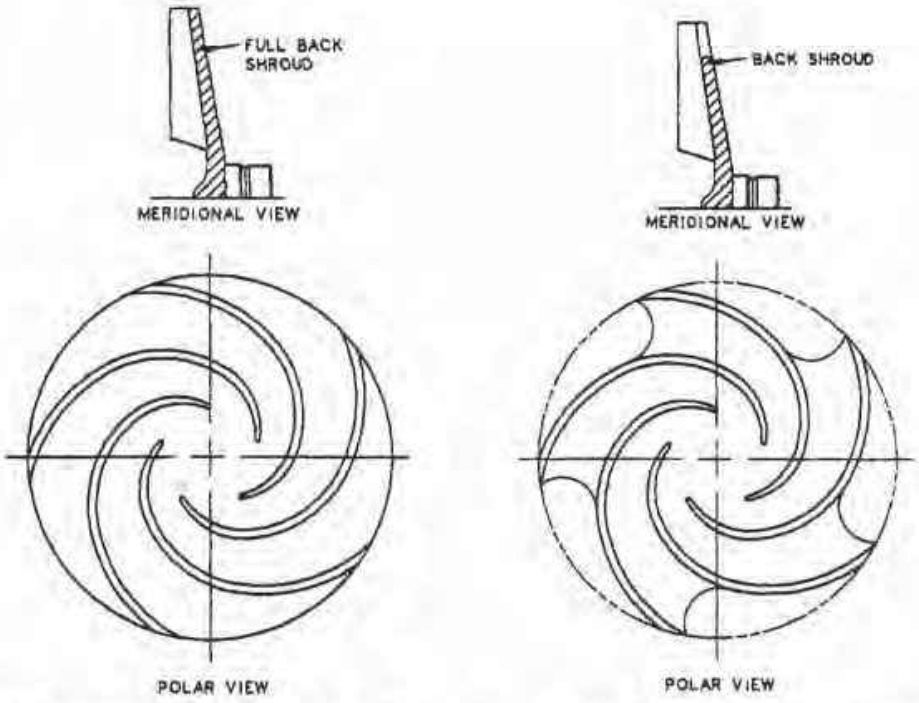


FIGURE 15A and B Semiopen impellers with a full back shroud and with a partially scalloped back shroud

LIBERTY EXHIBIT 1017, Page 367

TABLE 8 PV values for various bearing journal and thrust face materials

Bushing Materials	Journal/Thrust Face PV ($\times 10^3$)*
Carbon graphite vs. AISI 316	150
Carbon graphite vs. chrome oxide hardened coating	250
Silicon carbide vs. hardened coating	250
Silicon carbide vs. carbon graphite	300
Silicon carbide vs. silicon carbide	500
PEEK—carbon-filled vs. hardened coating	150
Polyimide-carbon filled vs. hard coating	150

P = Net load/projected area (minus area for slots), psi

V = Velocity at the shaft diameter or mean diameter of the thrust face in ft/min

*Note: Multiplying the PV values in the table by 2.1 will give values equal to P in kPa and V in m/min.

When designing the bearing, thermal expansion and heat conductivity properties must be considered. Some designs have a temperature range of −300 to +750°F (−150 to +400°C). Table 9 lists bearing material characteristics to facilitate selection of the proper material for the intended application.

Particles For the softer bearing materials, the maximum particle size should be no more than 10% of the diametral clearance for a bearing with no grooves and no more than 20% for a bearing with grooves. Polymers and graphites are much softer than silicon carbides or hard coatings, and they are not recommended for liquids with hard particles. Silicon carbide versus silicon carbide will grind up most particles. For particle concentrations of 50 parts per million (ppm) or less, particle hardness is generally not a factor in bearing performance.

Strainers of 100 mesh are recommended to reduce the amount and size of particles going through the flow path. These strainers are installed for internal or external injection. Remember: Particles that will pass through a 100 mesh screen may be as large as 0.006 in (0.15 mm), whereas nominal diametral bearing clearances of 0.002 in (0.05 mm) are common.

TABLE 9 Bearing material characteristics

Material	Thermal Expansion (note 1)	Heat Conductivity (note 2)	Hardness (note 3)
AISI 316	9.6	7.5	160 BHN
Hastelloy C	6.7	71	170 BHN
Carbon graphite	2.6	5	95 Vickers
Silicon carbide—self-sintered	2.2	85	2400 Vickers
Silicon carbide with carbon	2.0	75	2400 Vickers
PEEK—Carbon-filled	8.0	6	
Polyimide—Carbon-filled	5.0		100 to 150 BHN
Aluminum oxide			1800 Vickers
Chrome oxide			1800 Vickers

Note 1: in/in/°F $\times 10^{-6}$ (multiplied by 1.411 to get cm/cm/°C)

Note 2: BTU/h/ft²/°F (multiply by 0.488 to get calories/h/cm²/°C)

Note 3: $R_C \times 25$ = Vickers; BHN $\times 10 = R_C$

LIBERTY EXHIBIT 1017, Page 368

Note also that the bearing material combination of silicon carbide against silicon carbide or against carbon is electrically conductive.

Running Dry Most sealless pump failures occur because the pump system is not monitored and the pump is allowed to run dry. When this happens, the bearings will run dry. When the bearings run dry, hard, brittle bearing materials such as self-sintered silicon carbide will fail within minutes. Graphite silicon carbide may run dry for as many as 10 to 20 min with no damage. The polymers, which are poor heat conductors, expand inwardly and seize against the mating surface. The graphites will also move inwardly, but they tend to wear rather than seize, which results in excessive clearances when the pump is stopped and cooled. One optional design uses Teflon strips that expand inwardly when the unit runs dry so the shaft runs on the Teflon rather than on the silicon carbide, thus helping to avoid bearing failure.

Another option is to employ an external circulating tank, with no external running parts, that will provide the bearings with external lubricating liquid should dry operation occur. This type of external tank system has allowed pumps to operate for two hours or more without incurring damage to the bearings.

Flow Path The amount and direction of flow for cooling of the magnets and lubrication of the bearings is critical to the operation of a sealless pump (Figure 16). It is preferable for the liquid to lubricate the bearings before being heated by the magnets. This reduces the possibility of vaporization of the liquid occurring at the thrust-bearing faces. The amount of liquid circulated through the system is usually between 1 and 8 gpm (4 and 30 L/min). It is usually channeled to the front and back bearings, the thrust bearing face, across the magnets, and to the impeller hub. Some manufacturers have computer programs that calculate the flow, pressure, and temperature of the cooling/lubricating flow at various critical locations along the flow path. These programs can also account for the effects of the liquid specific gravity, specific heat, and viscosity. The local pressure and temperature is used to determine the vapor pressure at that point to ensure that the liquid is not flashing. The programs can also calculate axial thrust and determine if the lubrication

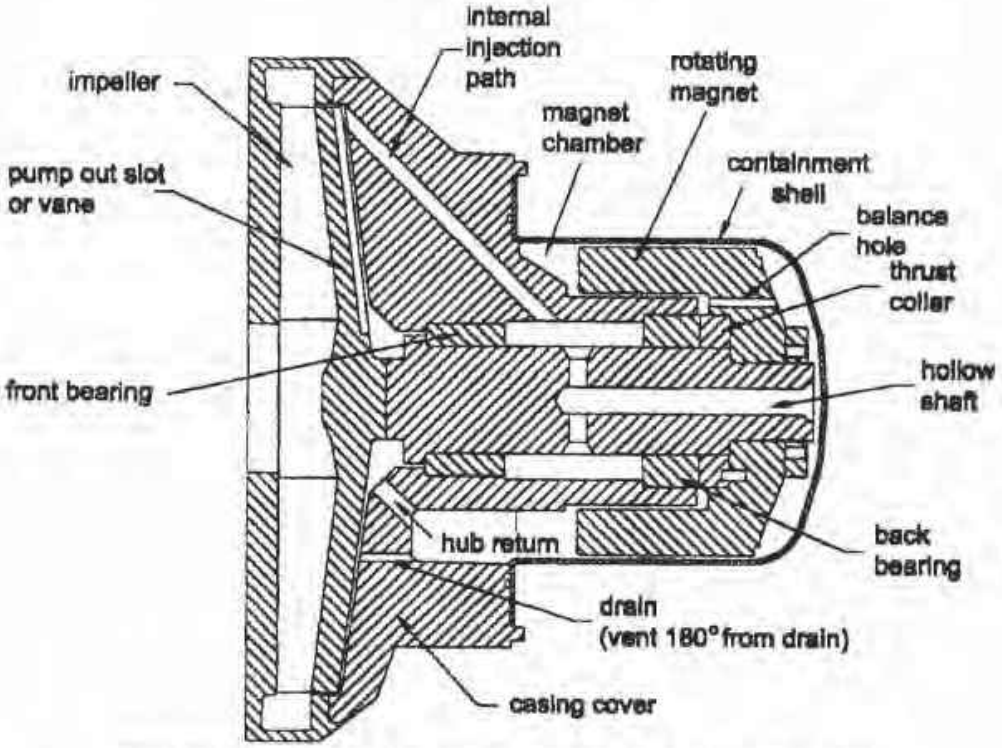


FIGURE 16 Magnetic sealless pump components for the internal flow system.

LIBERTY EXHIBIT 1017, Page 369

at the thrust bearing face is hydrodynamic or boundary. This is done at various flow rates, impeller diameters, and pump speeds.

The temperature rise of the liquid as it travels through the cooling-lubricating flow path depends to a great extent on the liquid's characteristics, such as specific gravity, specific heat, vapor pressure, and viscosity. With a nonmetallic shell on ambient water service, a typical temperature rise might be 1 to 2°F (0.5 to 1°C). For a metallic shell, with its much higher eddy current losses, the temperature rise could be as much as 8 to 12°F (4 to 7°C).

Performance The head capacity curve of a typical two-pole speed sealless pump matches that of a conventionally sealed pump; however, the overall efficiency is lower. With a nonmetallic shell, the efficiency may be only about two points less at the best efficiency point flow rate, but as much as six points less at one-half the best efficiency point flow rate. When a metallic shell is used, the efficiency at best efficiency point flow rate may be as much as 8 to 12 points lower than a comparable pump with a mechanical seal (Figure 17).

APPLICATION ADVANTAGES OF SEALLESS PUMPS:

- No leakage to the environment
- No loss of valuable liquids
- Lower noise levels
- High suction pressure does not affect the axial thrust
- Can handle liquids from 0 to 4 toxicity rating
- Because of no leakage, there is much less chance of a fire
- Easier to obtain construction permits and permits for continued operation
- Less external piping required

APPLICATIONS THAT SHOULD BE REVIEWED BEFORE SEALLESS PUMPS ARE APPLIED:

- Dirty liquids
- High temperature

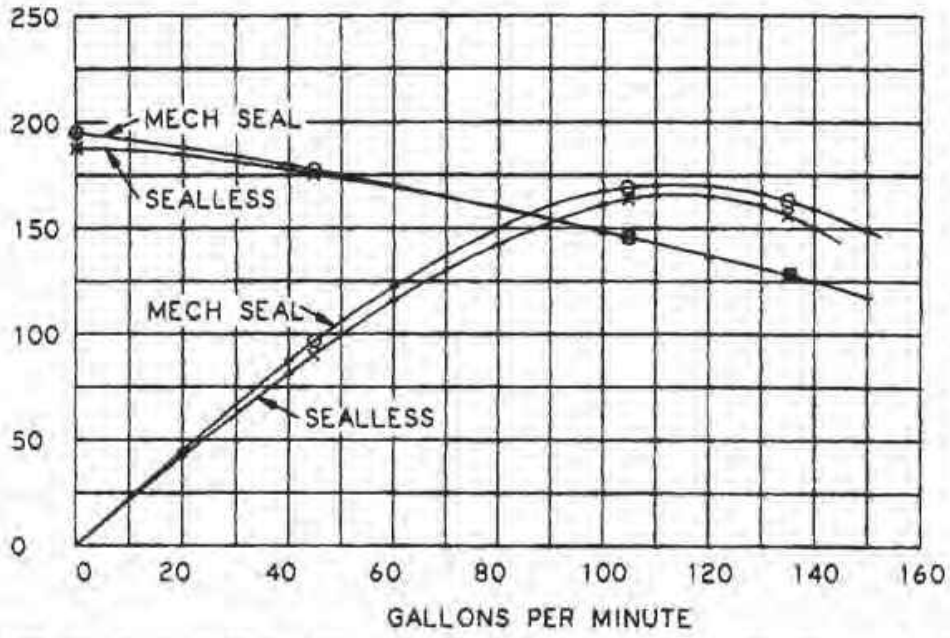


FIGURE 17 Typical performance for a 1.5 × 1.0 × 6 pump at 3550 rpm, comparing characteristics for sealless versus mechanical seal construction

LIBERTY EXHIBIT 1017, Page 370

- Liquids that solidify
- Viscous liquids above 200 centipoise
- Oversize drivers that can cause decoupling during acceleration
- Cavitation of liquid in the impeller eye that can result in excess thrust
- Excessive entrained gas

FURTHER READING

American National Standard for Sealless Centrifugal Pumps, ANSI/HI 5.1-5.6-2000, Hydraulic Institute, Parsippany, NJ www.pumps.org.

Hydraulic Institute ANSI/HI 2000 Edition Pumps Standards, Hydraulic Institute, Parsippany, NJ www.pumps.org.

Sealless Pumps for Petroleum, Heavy Duty Chemical, and Gas Industry Services, API Standard 685, 2000, The American Petroleum Institute, 1220 L Street, Northwest, Washington, D.C. www.api.org.

Specification for Sealless Horizontal End Suction Centrifugal Pumps for Chemical Process, ANSI/ASME B73.3M-1997, The American Society of Mechanical Engineers, 345 East 7th Street, New York, NY www.ASME.org.

Eierman, R. "A User's View of Sealless Pumps—Their Economics, Reliability, and the Environment." *Proceedings of the Seventh International Pump Users Symposium*. Texas A&M University, College Station, TX, March 1990, pp. 127–133.

Hernandez, T. "A User's Engineering Review of Sealless Pump Design Limitations and Features." *Proceedings of the Eighth International Pump Users Symposium*. Texas A&M University, College Station, TX, March 1991, pp. 129–145.

Littlefield, D. "Sealless Centrifugal Pumps." *Proceedings of the Eleventh International Pump Users Symposium*. Texas A&M University, College Station, TX, March 1994, pp. 115–119.

Guinzburg, A., and Buse, F. "Computer Simulation of the Flowpath in Magnetic Seal-less Pumps." *Proceedings of the Fifteenth International Pump Users Symposium*. Texas A&M University, College Station, TX, March 1998, pp. 1–9.

LIBERTY EXHIBIT 1017, Page 371

SECTION 2.2.3.2
CANNED MOTOR PUMPS

STEPHEN A. JASKIEWICZ

A canned motor pump (CMP) is a combination pump and induction motor built together into a single hermetically sealed unit (see Figure 1). For single stage, centrifugal, canned motor pumps (see Figure 2) the impeller (A) is normally of the closed type, and is mounted on one end of the rotor shaft, which extends from the motor section into the pump casing. The rotor (B) is submerged in the fluid being pumped and is, therefore, "canned" to isolate the motor components from contact with the process fluid. The stator (C) is also "canned" to isolate the motor windings from the fluid being pumped. Bearings (D) are submerged in the system fluid and are continually lubricated. The outer stator band assembly (G) in conjunction with a sealed electrical connection (F) provides a positive secondary containment in the event of the primary containment, stator liner (E), failure.

The canned motor pump has only one moving part, a combined rotor-impeller assembly that is driven by the magnetic field of an induction motor. A portion of the pumped fluid is channeled to flow through the rotor cavity to cool the motor and lubricate the bearings. For an external circulated pump a self-cleaning filter can be provided to remove any solids from the recirculation fluid before it enters the bearing section of the motor. The stator windings and rotor armature are protected from contact with the recirculating fluid by a corrosion resistant, nonmagnetic, alloy liner (E) which completely seals or "cans" the stator winding.

Canned motor pumps can be modified for pumping hot fluids, up to 1000°F (538°C), volatile liquids, fluids with high melting points, liquids with solids, slurries and high pressure system pressures. To be used in these types of applications the recirculation flow must be conditioned to prevent any solids or vapors from entering or forming in the motor section of the pump.

Because there is only one rotating assembly, canned motor pumps do not require shaft or coupling alignments that are necessary for other types of pumps. Centerline supported pump casings are also not required for pumping liquids at elevated temperatures since the entire pump will "move" with the piping. Pumps can be installed in either the horizontal

LIBERTY EXHIBIT 1017, Page 372



FIGURE 1 Typical canned motor pump (Teikoku Electrical Manufacturing Corp.)

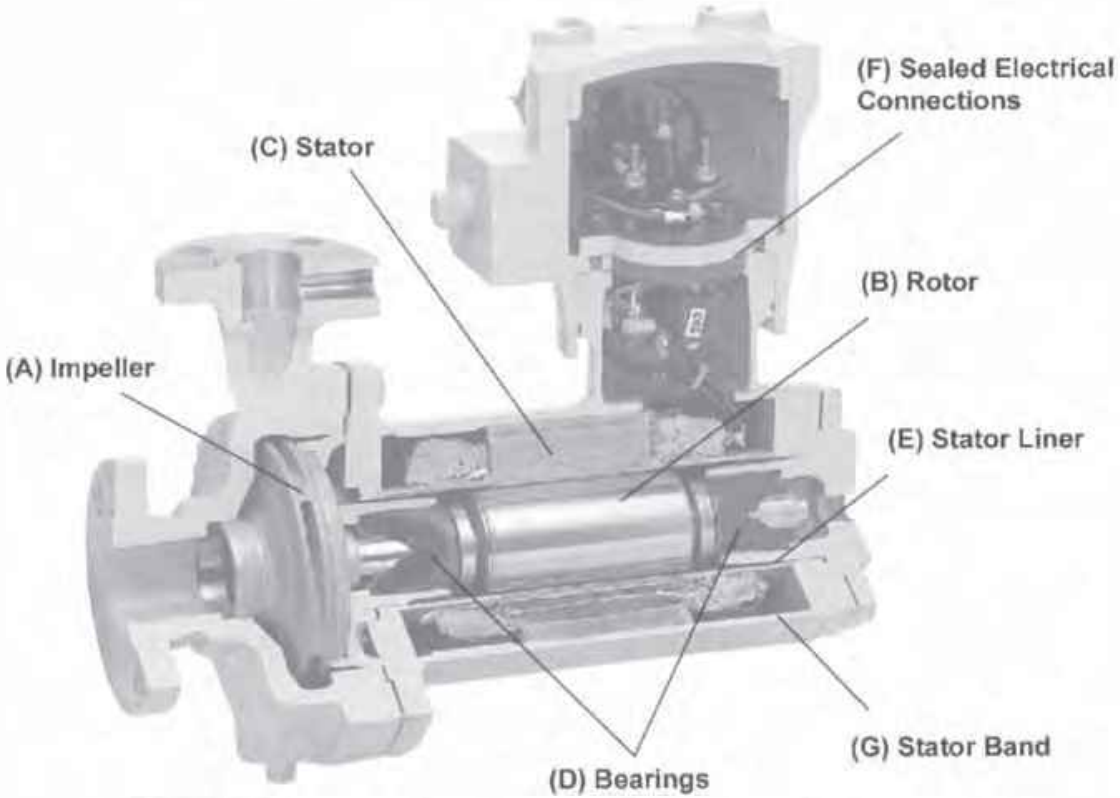


FIGURE 2 Components of a canned motor pump (Teikoku Electrical Manufacturing Corp.)

or vertical position, pump casing up or down. Mounting in the vertical position offers the advantage of greatly reducing the radial loads on the bearings. This feature is very significant with high horsepower motors or when pumping liquids with very low viscosities.

BASIC DESIGN

Stator Assembly The stator assembly of canned motor pumps (see Figure 3) consists of a set of one- or three-phase windings (A). Stator laminations (B) are constructed of low-silicon grade steel. Laminations and windings are mounted inside the cylindrical stator band (C). End bells (D and E), welded to the stator band, close off the ends of the stator assembly. The stator liner (F) is supported on the outside diameter by the steel lamination of the motor. Backup sleeves (G) are provided to strengthen those areas of the stator liner not supported by the stator laminations. The stator liner is, in effect, a cylindrical "can" placed in the stator bore and welded to the rear end bell and front end bell shroud to hermetically seal off the windings from contact with the liquid being pumped. Terminal leads (H) from the windings are brought out through a pressure tight lead connector (I) mounted on the stator band and terminated in an electrical connection box.

Motors are designed and manufactured specifically for use in canned motor pumps or components of conventional motors are modified. A wide variety of motor insulations are available ranging from temperature limits of 266°F (130°C) to above 700°F (371°C).

Canned motor pumps can be documented and labeled for use in explosion proof locations. Because the pump and motor are one unit, the complete assembly must be tested and approved for explosion proof applications. Explosion proof pumps are rated either as Class 1, Group D, Division 1 or Class 1, Group C and D, Division 1.

Canned motor pumps perform very well when used with variable speed drives (VSDs). Unless the motor windings and bearing support systems are specifically designed for high speeds the speed range is usually limited to 1000 to 4200 revolutions per minute (rpm).

Rotor Assembly The rotor assembly is a squirrel cage induction rotor constructed and machined for use in canned motor pumps (see Figure 4). It consists of a machined corrosion

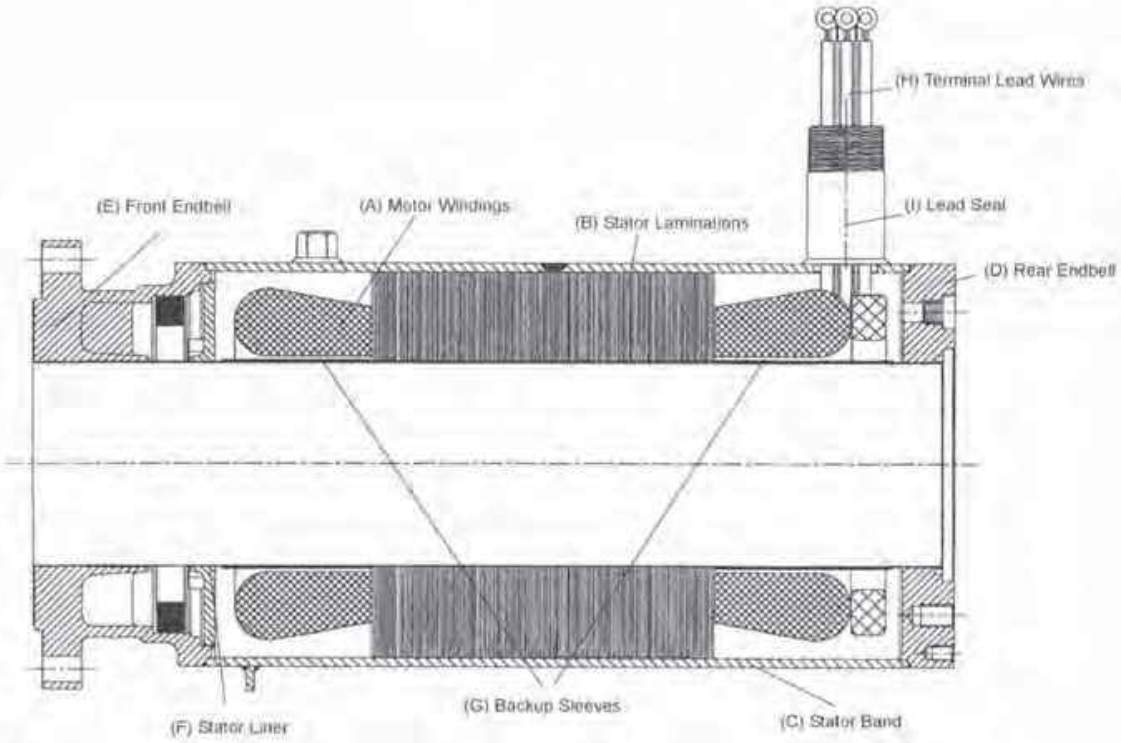


FIGURE 3 Stator assembly (Chempump, a Division of Teikoku USA Inc.)

LIBERTY EXHIBIT 1017, Page 374

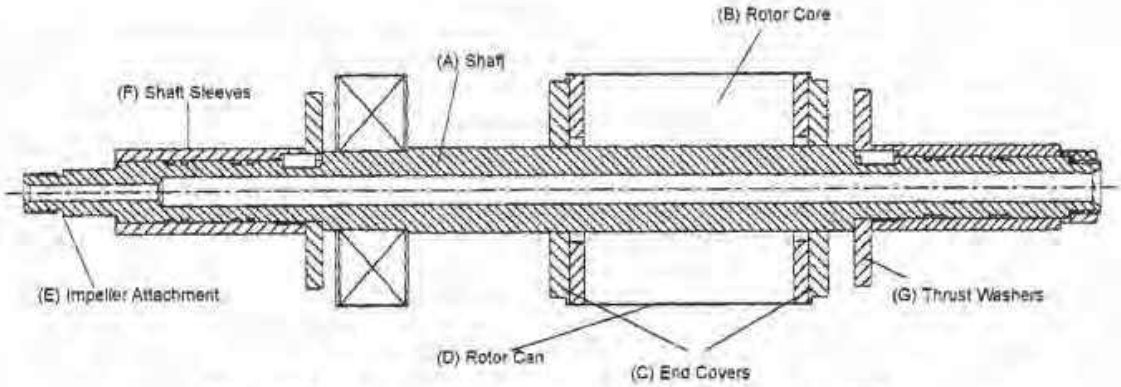


FIGURE 4 Rotor assembly (Chempump, a Division of Teikoku USA Inc.)

resistant shaft (A), laminated core (B) with copper or aluminum bars and end rings, corrosion resistant end covers (C), and a corrosion resistant sleeve (D). Various methods are used to attach the impeller to the motor shaft (E).

The rotor end covers are welded to the shaft and rotor sleeve, which surrounds the outside of the rotor, thus hermetically sealing off the rotor core from contact with the liquid being pumped.

Some manufacturers offer replaceable shaft sleeves (F) and axial thrust surfaces (G) for longer service life and ease of maintenance. Shaft sleeves can be constructed entirely of a hardened material such as silicon carbide and stellite or just the journal area can be coated with a hardened material such as tungsten carbide or chrome oxide.

Bearings Only two bearings are required for most canned motor pumps. These bearings are normally cooled and lubricated by the pumped fluid; therefore, the bearing material must be compatible with the process fluid. A multitude of materials are available, such as various grades of carbon graphite, antimony, silicon carbide, aluminum oxide and a variety of polymers. Bearing selection is dependent on the compatibility with the process fluid, the amount of solids present, and the pumping temperature.

A hydrodynamic bearing is the most common type of bearing used. The components of the bearings are both stationary (connected to the stator) and rotating with the rotor assembly. The fluid pumped fluid passes between the stationary bearing and shaft journal bearing causing the rotating assembly to run on a thin film of liquid; this should prevent contact between the journal and bearing. Most (stationary) bearings are grooved, either helical or straight grooves, on the inside diameter to increase the flow of process fluid through the journal area, thereby increasing the thickness of the fluid film and decreasing the temperature of the bearings.

Internal Clearances The overall gap between the stator windings and the rotor armature is critical to the design and operation of the canned motor pump. Increasing the gap between the iron of the motor windings and the rotor armature decreases the efficiency of the motor. Materials of construction of the stator liner also have an effect on motor efficiency. Stainless steels and Hastelloy are the most common materials used for stator liners and rotor sleeves. While stainless steel is less expensive, Hastelloy has higher corrosion resistance, is a stronger material and has lower electrical losses. Motor efficiency in canned motor pumps is not only important for energy cost considerations but also in the amount of heat input to the recirculation fluid.

The stator liner is a wetted, pressure boundary component; typically ranges in thickness from 0.010 to 0.040 in (0.254 to 1.016 mm), depending on the design pressure of the pump and other construction factors. For higher-pressure applications, the liner may remain at the same thickness, but its outside diameter is supported by the motor laminations and by backup sleeves located on both sides of the motor. By doing this, canned motor pumps have been designed to withstand working pressures up to 8000 lb/in^2 with 0.015-in (0.381-mm) stator liners, heavy walled backup sleeves, and reinforced stator cores.

LIBERTY EXHIBIT 1017, Page 375

The rotor armature, also a wetted component, is protected from the process fluid by a sleeve and two end covers. The thickness of the rotor sleeve typically ranges from 0.010 to 0.25 in (0.254 to 6.35 mm). The running clearance between the rotating motor armature and the stationary stator liner is usually about 0.020 in (0.508 mm) diametrically.

The total diametrical clearance between the journal and bearings ranges from 0.0025 to 0.067 in (0.0635 to 1.702 mm), and sometimes higher, depending on the specific manufacturer's design, bearing materials and power of the motor.

Secondary Containment Canned motor pumps offer a level of safety and process fluid containment unavailable with any other type of pump. Positive secondary containment of the process fluid is a built-in feature with canned motor pumps when the motor lead wires are housed in a pressure-retaining lead seal. In the event of a failure of the primary containment shell (stator liner) the outer stator band becomes a secondary containment vessel preventing the process fluid from entering the environment.

The outer stator band is far removed from the rotation element, making it impossible for the rotating element to make contact. The secondary containment system should be designed and tested to same pressure and temperature rating as the pump. Materials of construction of the stator band assembly should also be considered when pumping a highly corrosive fluid. When pumping dangerous fluids that require secondary containment, many users will install a device to detect the loss of the primary containment liner to shut the pump down. The most common device specified is a pressure switch mounted to the stator band assembly.

PRINCIPLE OF OPERATION

Flow Path Most canned pumps, when pumping relatively clean, nonvolatile fluids, will channel a small portion of the process fluid through the motor section. This fluid cools and lubricates the bearings and also removes heat generated by the motor. The circulation path can be either external or internal to the pump. With external circulation (see Figure 5), the recirculation fluid is piped outside of the pump, through a filter, then into the motor section of the unit. The filter assembly (see Figure 6) is self-cleaning and located in the discharge flange of the pump. Pumps having internal circulation have the recirculation

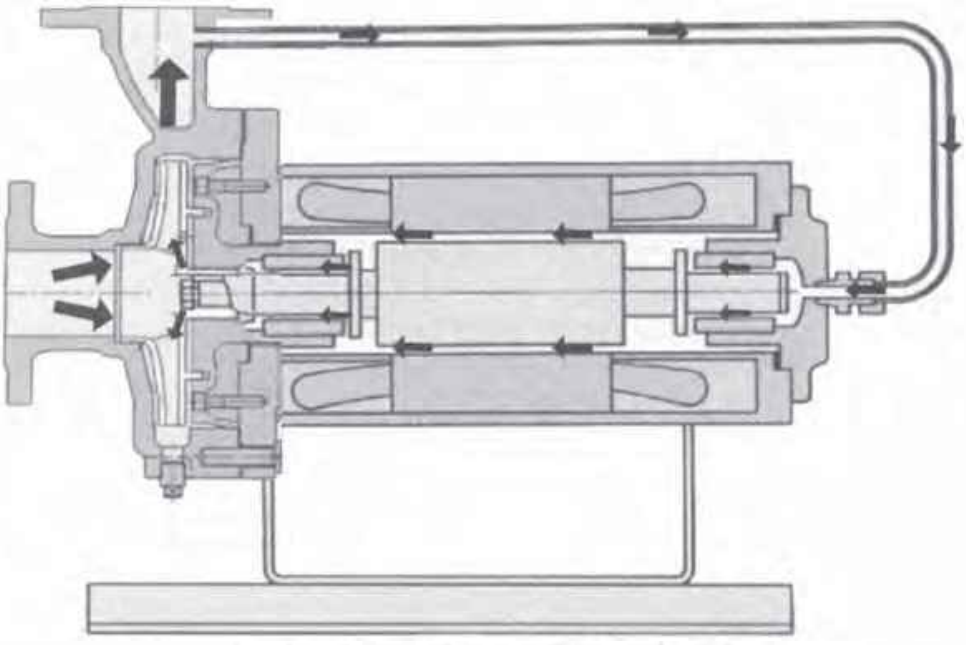


FIGURE 5 External circulation (Teikoku USA Inc.)

LIBERTY EXHIBIT 1017, Page 376

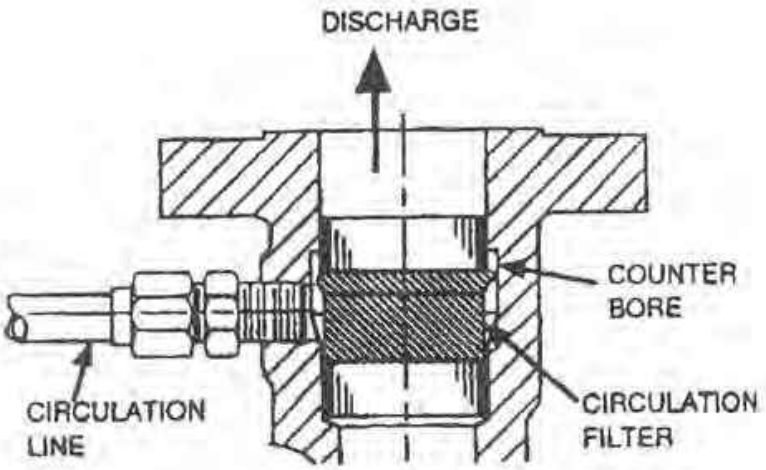


FIGURE 6 Filter assembly (Chempump, a Division of Teikoku USA Inc.)

contained within the pump. Filtering the recirculation liquid is not available with internal circulation.

In either external or internal circulation, the flow path is from the high-pressure area of the pump (pump discharge or pump chamber at the tip of the impeller) returning to the low-pressure area (eye of the impeller). The amount of liquid recirculated through the motor section ranges from 1 to 16 gpm (4 to 60 L/m) depending on the size of the pump and the pressure developed by the liquid end.

Thrust Balance The most common type of bearings used in canned motor pumps are product lubricated hydrodynamic bearings. With these types of bearings, the rotating assembly is allowed to float axially. This movement is know as "end play" and is defined as the movement of the rotor, in the axial direction, between the forward and rear contact points (normally the thrust bearings). A principle of hydraulic thrust balance is commonly used to position the rotation assembly between the forward and rear mechanical contact points. Based on hydraulic forces generated by the rotating impeller, automatic thrust balance is accomplished by the pressure of the pumped fluid. Pressure chambers are designed either within the pump chamber using the movement of the impeller or rear of the pump controlling the rate of return of the process fluid.

Figure 7 illustrates hydraulic thrust balance within the pump casing. Balance chambers are located on the front and rear of the impeller. When a change in axial load changes the position of the impeller, either forward or rear, there is an equalizing change of hydraulic pressure in the balance chambers, which immediately returns the rotation assembly into a balance position.

With the use of hydrodynamic bearings and hydraulic thrust balance, the rotating assembly is "floating" in the pumped fluid with no mechanical contact. For this reason it is best to operate canned motor pumps continuously or with a minimum of start-stops.

Applications Canned motor pumps can be used for every pumping application from clean, nonvolatile fluids to highly volatile, high-temperature, high-pressure, and slurry services. Numerous bearing and shaft materials are available along with various modifications to the internal bearing lubrication system to prevent vapors and solids from entering or forming in the bearing system.

When pumping volatile fluids, the motor section can be pressurized by an auxiliary impeller located on the rotor. The recirculation fluid, which normally returns to the eye of the impeller, is channeled to the pressurized section of the liquid end increasing the pressure in motor section (see Figure 8). This design allows a volatile fluid to remain liquid inside the motor cavity even with a temperature increase caused by motor heat. Another method to handle fluids near their boiling point is to reverse the recirculation flow path. Instead of returning the heated liquid back to the eye of the impeller the recirculation liquid

LIBERTY EXHIBIT 1017, Page 377

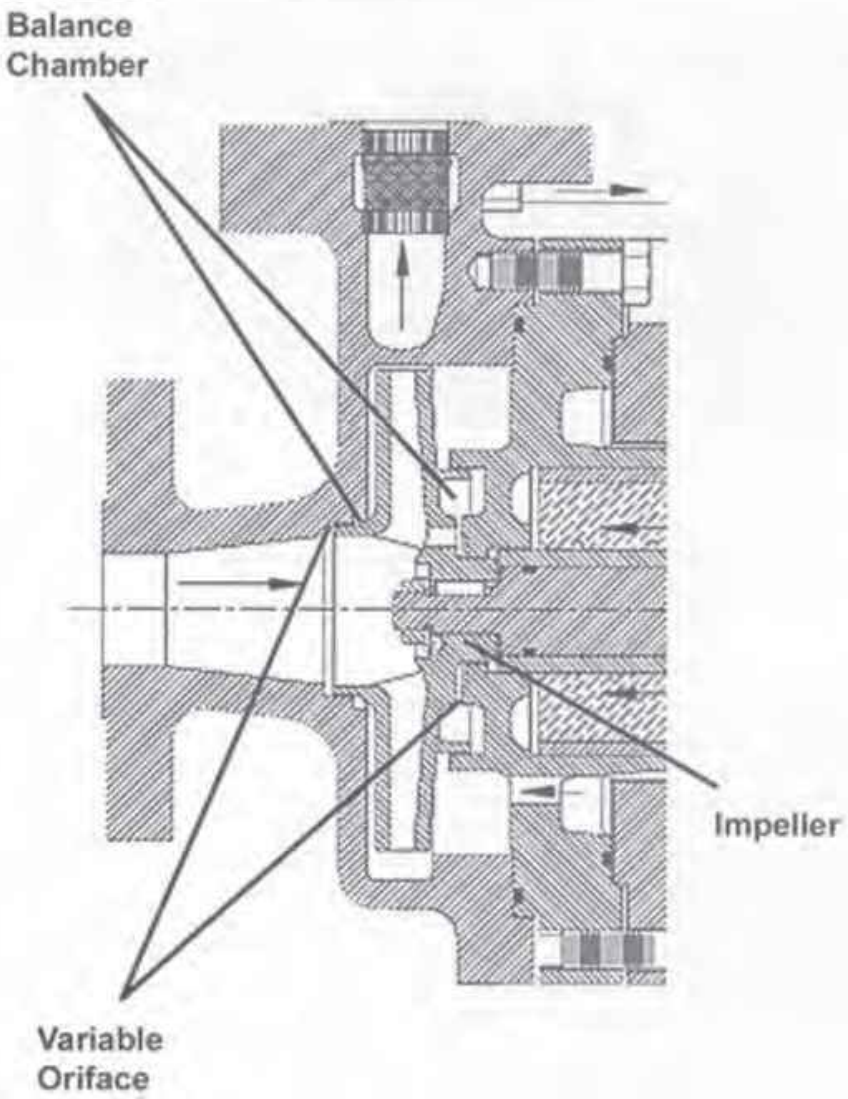


FIGURE 7 Hydraulic thrust balance (Chempump, a Division of Teikoku USA Inc.)

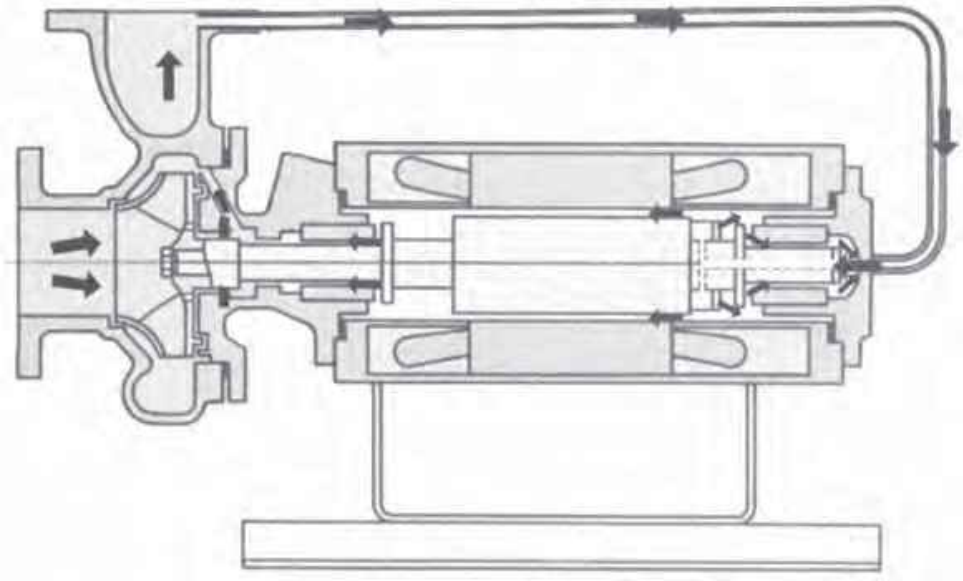


FIGURE 8 Pressurized circulation (Teikoku USA Inc.)

LIBERTY EXHIBIT 1017, Page 378

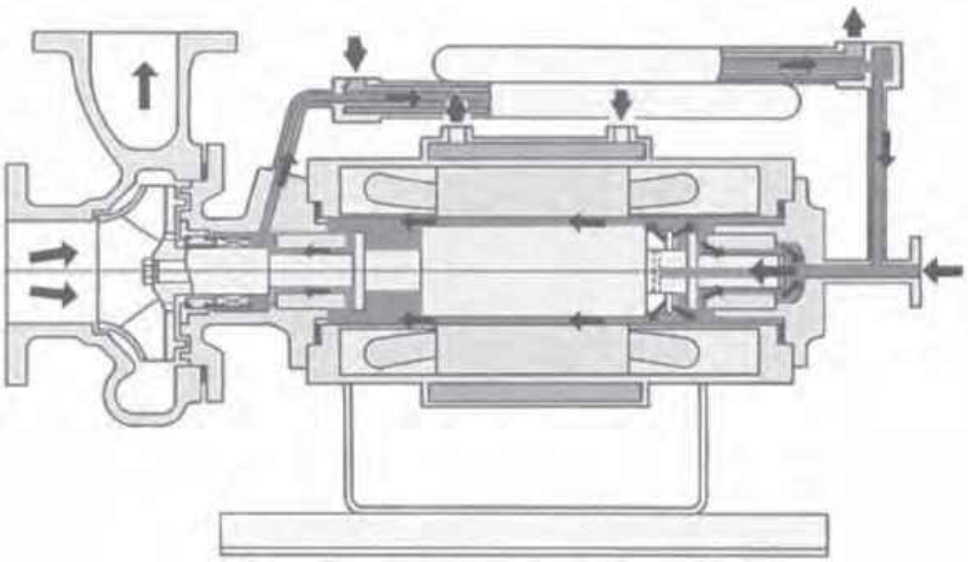


FIGURE 9 Externally cooled motor (Teikoku USA Inc.)

exits the pump and is returned to the suction vessel. The reverse circulation option provides a continuous vent of the motor chamber.

For pumping fluids at temperatures above 400°F (200°C) water-cooled and non-water-cooled designs are available. The water-cooled design isolates the motor and bearings from the pumped fluid (see Figure 9). The circulating fluid in the motor section is used for lubrication of the bearings and cooling of the motor. This fluid remains in the motor section and is circulated through the rotor cavity by an auxiliary impeller, which is an integral part of the rotor assembly. The fluid in the motor section is forced across the rotor and through the bearings then through an auxiliary heat exchanger. The heat exchanger is cooled by water or a suitable heat transfer fluid. The non-water-cooled design has a motor insulation system constructed of materials designed to operate at high temperatures. The material of the bearings must also be designed for temperatures in excess of 650°F (350°C). The power lead connection is extended away from the motor so the electrical connection box is at ambient temperatures (see Figure 10).



FIGURE 10 High temperature non-water-cooled motor (Teikoku Electrical Manufacturing Corp.)

LIBERTY EXHIBIT 1017, Page 379

The slurry design has the same modifications as the high-temperature, water-cooled design with the addition of a closure seal between the motor and the pump to prevent any solids from entering the motor chamber. This design completely isolates the slurry in the pump casing from the liquid in the motor. A clean fluid is back flushed through the motor to lubricate the bearings and cool the motor. A small portion of the flush fluid flows, passes through the closure seal into the process fluid. The amount of liquid mixing with the process fluid varies depending on the type of closure seal, but is usually much less than 1 gpm (4 L/m).

Pressure-Temperature Profile The single most important consideration in the application and successful operation of canned motor pumps is bearing environment control. The process fluid cools and lubricates the bearings and removes the heat generated by the motor. The fluid cooling the bearings must remain in a liquid state to provide adequate bearing lubrication.

A number of variables must be considered when considering the condition of the recirculation fluid. These variables include: vapor pressure, specific heat, specific gravity, viscosity, pump efficiency, motor efficiency, motor load, recirculation flow rate, and the recirculation flow pressure. The physical properties of the fluid should be provided as a function of temperature. Figure 11 illustrates the heat rise calculations for a specific application. Figure 12 is an example of a typical pressure-temperature profile of a sealless pump. If the flow rate varies, a profile should be calculated for each design condition.

A pressure-temperature profile should be calculated for any application where there is any doubt concerning the condition of the recirculation fluid. As a minimum it is recommended to have a pressure-temperature profile for maximum, minimum, and design flow and temperature conditions.

Installation Installation of a canned motor pump is much less costly than other pumps because canned motor pumps do not require any special base plates or mounting pads. In fact, many canned motor pumps are stilt mounted or bolted directly into the system piping. There is only one shaft in a canned motor pump, therefore, alignment is not necessary nor is pump orientation. The unit can be mounted either horizontally or vertically, with the pump casing up or down. The sleeved bearings are located in the bearing housing. Alignment of the bearings is accomplished by a registered fit between the bearing housings and the stator assembly so all internal alignment is accomplished at final assembly.

Diagnostics Diagnostic systems are available to monitor and display the condition of the internal wear components of the pump. More advanced diagnostic systems will continuously indicate both axial and radial wear by monitoring the position of the rotating assembly. Continuous wear indication allows the pump user to trend the wear of the pump and schedule standard wear parts replacement long before a major failure would occur. Remote outputs are also available on these diagnostic systems for the user to link the pump wear data to a data control system (DCS). These outputs include a digital, RS-485 signal, an analog 4-20 mA, or a relay designed to shut down the pump or signal an alarm when a certain amount of bearing wear has occurred.

These diagnostic tools are the single most important advancement in the technology of pumping equipment. Having access to data on the condition of the pump provides the user with the opportunity to perform predictive and preventative maintenance on equipment and systems. Figure 13 illustrates the type of information available when using an RS-485 output linked to a data collection system.

Industrial Standards Due to the unique design of canned motor pumps (pump and motor combined into a single unit), they are designed to conform to many international standards. Motors can be supplied to meet many international standards as well. Third party testing and certification are available from:

- Underwriter Laboratories (UL)
- Factor Mutual (FM)

LIBERTY EXHIBIT 1017, Page 380

Heat Rise Calculations

PUMP MODEL NC-A60-10-N5
FLUID TRICHLOROSILANES
Bypass, GPM 0

CIRCULATION PATH	STANDARD	REVERSE	PRESSURIZED
Desired Flow (GPM	300	300	300
TDH (FT)	240	240	240
Temperature, inlet (F)	150	150	150
Specific Heat, (btu/lb F)	0.26	0.26	0.26
Specific Gravity	1.24	1.24	1.24
Hydraulic Horsepower	22.5	22.5	22.5
Total Pump Flow (GPM)	300	300	300
Pump Efficiency - Note 1.	58	58	58
Motor Output (HP)	38.9	38.9	38.9
Delivered Pump Head, (FT)	240	240	240
Motor Efficiency - Note 3.	80		80
Motor Input (KW)	36.2		36.2
Overall Efficiency	46.4		46.4
Impeller Diameter (IN)	8.5		8.5
Motor Circulation Flow (GPM)	7		6
Process Wire-Water Eff.	46.4	46.4	46.4
Total Circ rate (GPM) - Note 2.	9	6	6
Suction Pressure PSIA at NPSH= 61 FT	77.3	77.3	77.3
TEMPERATURE RISE			
Standard circ (pump)	1.4	0.8	1.4
temp. pump exit	151.4	150.8	151.4
circ flow (motor)	23.2	25.6	25.6
total temperature rise	24.6	26.4	26.9
max temp. circ. flow	174.6	176.4	176.9
Est. P vap, psia	63	64.6	
Percent max circ flow		0.9	
Min. Motor pressure, psig		112.1	
Circ press/ differential		0.27	

Note 1. Efficiency at "Total pump flow"
Note 2. Total Circ Flow includes front bearing flow (does not affect temp rise).
Note 3. Motor efficiency includes windage loss (correct for specific gravity)
Note 4. System heat added with reverse circulation is "total heat" less "motor heat".

HEAT BALANCE			
Total heat input (btu/min)	1104.7	1104.7	1104.7
Standard circ (pump)	1105.9	645.5	1105.9

FIGURE 11 Heat rise (Chempump, a Division of Teikoku USA Inc.)

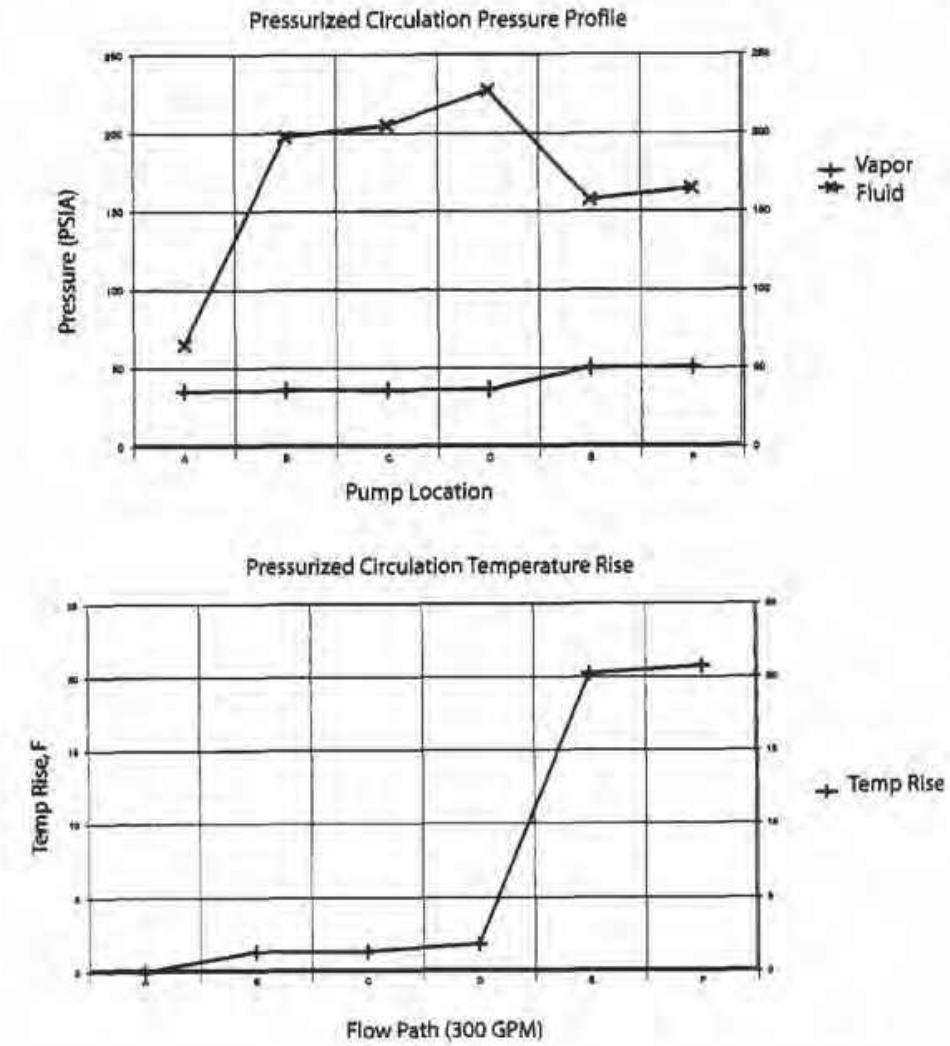


FIGURE 12 Pressure-temperature profile (Chempump, a Division of Teikoku USA Inc.)

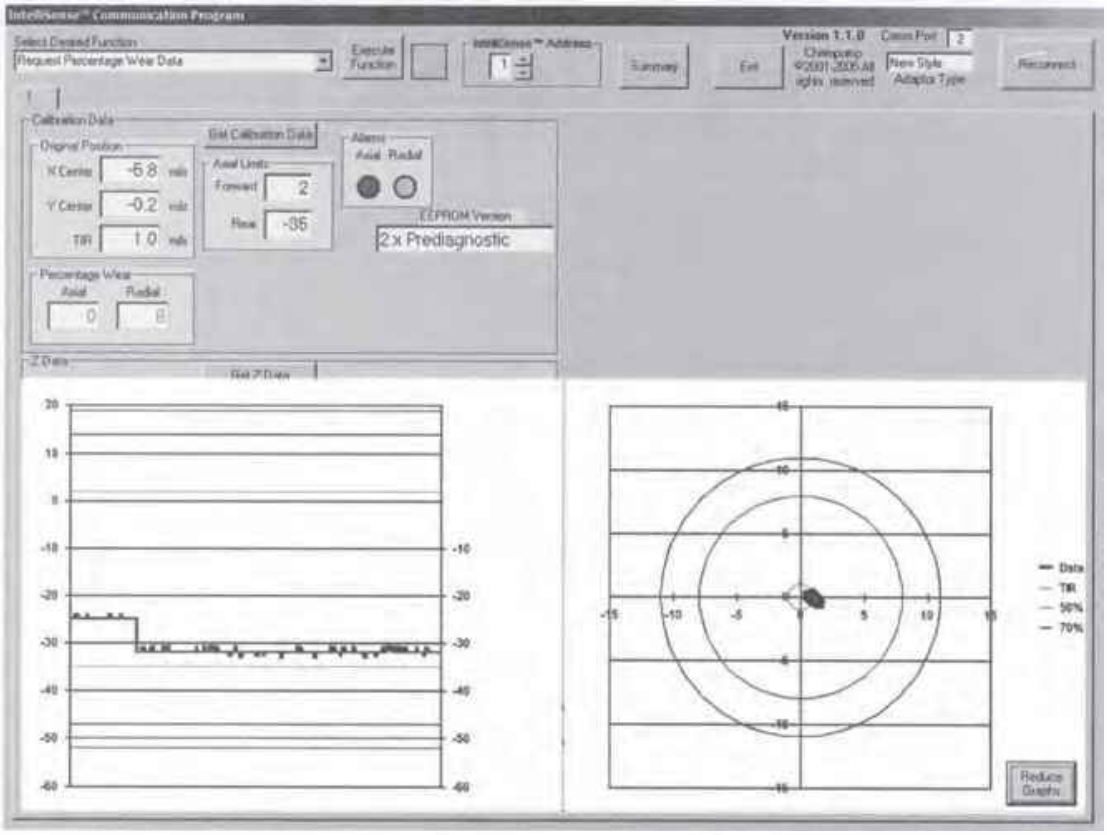


FIGURE 13 Rotor position output data

- Canadian Standards Association (CSA)
- Japanese Industrial Standards (JIS)
- ATEX
- CE
- Institute of Electrical and Electronics Engineers (IEEE)

Materials can be purchased to meet the standards of the American Society of Testing and Materials (ASTM). Certified Material Test Reports (CMTR) can also be supplied.

Designs can conform to:

- American Society of Mechanical Engineers (ASME NCA-4000)
- Canadian Standards Association (CSA-Z299.3)
- Military Standard (MIL-I-45208)

Complete pumps can meet the requirements of:

- ANSI/HI 5.1-5.6-2000, "American National Standard for Sealless Centrifugal Pumps"
- ASME-B73.3-3M-2003, "Specification for Sealless Horizontal End Suction Centrifugal Pumps for Chemical Process"
- API Standard 685, "Sealless Centrifugal Pumps for Petroleum, Heavy Duty Chemical and Gas Industry Services"
- ISO 15783-2002, "Sealless Rotodynamic Pumps-Class II"
- ISO 13709-2003, "Centrifugal pumps for petroleum, petrochemical and natural gas industries"

LIBERTY EXHIBIT 1017, Page 383

FURTHER READING

American National Standard for Sealless Centrifugal Pumps, ANSI/HI 5.1-5.6-2000, Hydraulic Institute, Parsippany, NJ. www.pumps.org.

Hydraulic Institute ANSI/HI 2000 Edition Pump Standards, Hydraulic Institute, Parsippany, NJ. www.pumps.org.

Sealless Pumps for Petroleum, Heavy Duty Chemical, and Gas Industry Services, API Standard 685, 2000, American Petroleum Institute, 1220 L Street, Northwest, Washington, D.C. www.api.org.

International Organization of Standards, ISO 15783:2002 and 13709:2003. 1 rue de Varembe, Case postale 56, CH-1211 Geneve 20, Switzerland. www.iso.org.

Jaskiewicz, S., and Rosenbaum, M. "Intelligent Sealless Pumps—A Unique Evolution." *World Pumps*, Vol. 2003, Number 442, July 2003, pp. 16–21.

Littlefield, D. "Sealless Centrifugal Pumps." *Proceedings of the Eleventh International Pump Users Symposium*. Texas A&M University, College Station, TX, March 1994, pp. 115—119.

Le Blue, J., Jr., and Lobach J. "Continuous Monitoring of Sealless Pumps." *Proceedings of the Fifteenth International Pump Users Symposium*. Texas A&M University, College Station, TX, March 1998, pp. 125–131.

Sealless Rotodynamic Pumps—Class II, ISO 15783:2002. International Organization for Standardization (ISO), Geneva, Switzerland. www.iso.ch

C • H • A • P • T • E • R • 3

DISPLACEMENT PUMPS

SECTION 3.1
POWER PUMP THEORY

WILLIAM K. CHAPLIS
FREDERIC W. BUSE

A power pump is a positive displacement machine consisting of one or more cylinders, each containing a piston or plunger. The pistons or plungers are driven through slider-crank mechanisms and a crankshaft from an external source. The capacity of a given pump is governed by the rotational speed of the crankshaft.

Unlike a centrifugal pump, a power pump does not develop pressure; it only produces a flow of fluid. The downstream process or piping system produces a resistance to this flow, thereby generating pressure in the piping system and discharge portion of the pump. The flow fluctuates at a rate proportional to the pump speed and number of cylinders. The amplitude of the fluctuations is a function of the number of cylinders. In general, the greater the number of cylinders, the lower the amplitude of the flow variations at a specific rpm.

All power pumps are capable of operating over a wide range of speeds, thereby making it possible to produce a variable capacity when coupled to a variable speed drive. Each pump has maximum suction and discharge pressure limits that, when combined with its maximum speed, determine the pump's power rating. The pump can be applied to power conditions that are less than its maximum rating but at a slight decrease in mechanical efficiency.

The power pump is a positive displacement device. When operating, it will continue to deliver flow independent of the pressure in the discharge piping system. Unlike a centrifugal pump, a power pump will not "deadhead" or "go back on its curve" in response to increasing discharge pressure. When this pressure exceeds the design limits of the pump, mechanical failure—often catastrophic—will result. For this reason, all piping systems incorporating power pumps must have discharge pressure relief devices to limit the pressure in the piping system and avoid pump failure. These devices must be located between the discharge connection on the pump and the first isolation valve in the piping system.

This section has been organized to provide sufficient power pump theory to properly select a pump for most applications. It is recognized that the proper pump metallurgy for the pumped fluid must be used, but due to the vast number of possible fluids, selection of pump metallurgy is outside the scope of this section.

LIBERTY EXHIBIT 1017, Page 386

The subject of Net Positive Suction Head (NPSH) is mentioned in several places in this section and is covered in more detail in Section 3.4, "Displacement Pump Performance, Instrumentation, and Diagnostics." For basic power pump selection, it is only necessary to understand that the NPSH available from the suction system must be sufficiently above the NPSH required by the pump to operate properly.

SELECTION THEORY

Power Brake horsepower (bhp) is a function of a pump's capacity (flow rate), differential pressure, and overall efficiency. It is an essential criterion for selecting the drive components but is not valuable for pump selection. A large pump operating well below its design rating can meet the same horsepower requirements as a smaller pump running at a higher speed. Unless the application requires a derated pump, it is usually more economical to select a pump at the upper end of its design rating.

The brake horsepower for the pump is

In USCS units $$bhp = (Q \times Ptd \times 100)/(1714 \times OE)$$

In SI units $$kW = (Q \times Ptd \times 100)/(36 \times OE)$$

where Q = delivered capacity (flow rate), gpm (m^3/h)
Ptd = differential pressure (discharge − suction), lb/in^2 (bar)
OE = overall efficiency, %

NOTE: One bar equals 10^5 Pa.

Capacity The capacity Q is the total volume of fluid delivered per unit of time. This fluid includes liquid, entrained gases, and solids at the specified conditions.

Displacement Displacement D, gpm (m^3/h), is the calculated capacity (volume flow rate) of the pump with no slip losses. For single-acting plunger or piston pumps, this is

In USCS units $$D = A \times m \times n \times s/231$$

In SI units $$D = A \times m \times n \times s \times 6 \times 10^{-5}$$

where A = cross-sectional area of plunger or piston, in^2 (mm^2)
m = number of plungers or pistons
n = rpm of pump
s = stroke of pump, in (mm) (half the linear distance the plunger moves in one revolution)
231 = in^3/gal

For double-acting plunger or piston pumps, this is

In USCS units $$D = (2A - a)m \times n \times s/231$$

In SI units $$D = (2A - a)m \times n \times s \times 6 \times 10^{-5}$$

where a is the cross-sectional area of the piston rod, in^2 (mm^2).

Pressure The pressure Ptd used to determine brake horsepower is the differential pressure or discharge pressure minus the suction pressure. In most applications, the suction pressure is small relative to the discharge pressure. However, when pumping some compressible liquids, such as methane and propane, the suction pressure may be 20 to 30% of the discharge pressure. For accurate brake horsepower calculations, always include the suction pressure. Figure 1 shows a typical performance curve for a power pump.

LIBERTY EXHIBIT 1017, Page 387

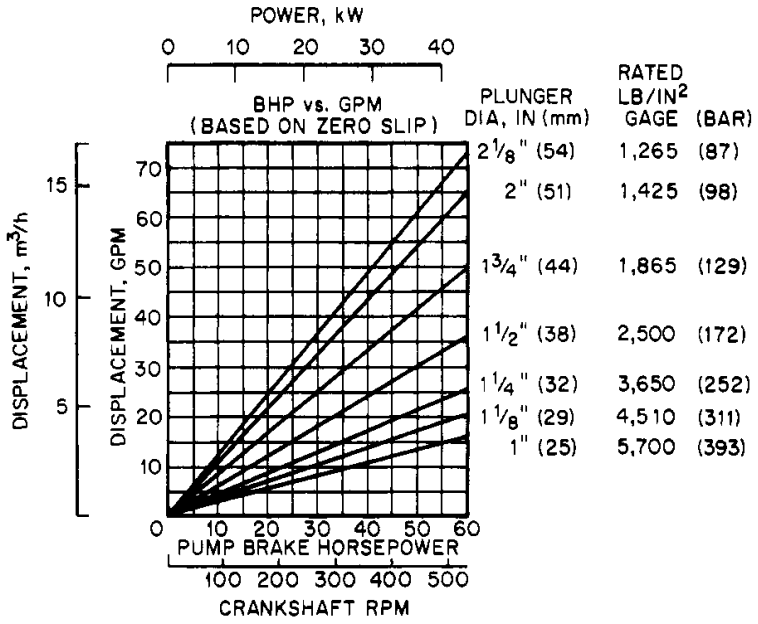


FIGURE 1 Typical power pump performance: brake horsepower versus gallons per minute (kilowatts versus m^3h) based on zero slip (Flowserve Corporation)

Slip Slip (S) is the loss of capacity due to internal and external pump leakage. External leakage occurs primarily through the stuffing box via the packing. Internal leakage is primarily the backflow past the suction and discharge valves. Backflow occurs when a valve remains open for a fraction of a second as the plunger or piston reverses direction. A small amount of leakage may occur across the piston in a double acting pump from the high pressure side to the low pressure side. Slip is expressed as a percentage loss of the displacement flow rate and is typically 1 to 4%:

$$S = 100 \times (B + V + L)/D$$

where S = Slip, %
B = Leakage through the stuffing box
V = Backflow across the valves
L = Internal leakages

Fluid viscosity, pump speed, and discharge pressure can all have an effect on slip, which is shown in Tables 1 and 2.

Mechanical Efficiency The mechanical efficiency of a power pump is

In USCS units ME = displacement power/power in = $P_{displ}/P_{in} = D \times Pdt/1714 \times P_{in}$

In SI units ME = displacement power/power in = $P_{displ}/P_{in} = D \times Pdt/36 \times P_{in}$

where P_{in} is the input power from the driver, bhp (kW).

The mechanical efficiency of a power pump is the sum of all the frictional losses in the fluid and power ends. These include the plungers and packing, the crossheads, the rod seals, and the bearings. The efficiency of a single acting pump often exceeds 90%, while a

TABLE 1 Slip in a pump with a plate valve

Centistokes	100	1,000	2,000	6,000	10,000	12,000
Slip, %	8	8.5	9.5	20	41	61

LIBERTY EXHIBIT 1017, Page 388

TABLE 2 Slip as a function of pump speed and pressure

	Slip, %		
Pressure, lb/in² (bar)	At 440 rpm	At 390 rpm	At 365 rpm
4000 (275)	11	22	34
3000 (207)	9	20	31
2000 (138)	7	18	30
1000 (69)	7	15	27.5

double-acting piston pump will be 88% due to the additional piston and rod seals. If the pump is equipped with internal gearing, an additional 2% loss is common.

Most power pumps are designed to accept a range of plunger or piston sizes. When the larger plungers are used, the increased diameter of the packing/seals and plunger/liners will result in higher frictional losses than with smaller components. As a rule, doubling the plunger/piston diameter will decrease the mechanical efficiency by 8%. Mechanical efficiency is also affected by speed and, to a lesser extent, by developed pressure, as indicated in Tables 3 and 4.

Speed Pump speed, or, more correctly, stroke rate, is one of the most critical selection criteria for power pumps. The rotating and reciprocating parts of the power end, as designated, are often capable of speeds twice that of the actual pump rating. The maximum pump speed is determined by the design of the fluid end, the hydraulic capability of the anticipated suction system, and the required life of the plungers, packing, and valves. Most power pump standards limit the plunger speed from 140 to 280 ft/min (0.71 to 1.42 m/s). The plunger speed is

In USCS units $Sp = s \times n/6$

In SI units $Sp = s \times n/30{,}000$

where Sp = plunger or piston speed, ft/min (m/s).

s = stroke of the pump, in (mm) (half of the linear distance the plunger or piston moves in one revolution)

n = rpm of pump

All pumps have a minimum speed limit, usually determined by a decrease in the adequate lubrication to the bearings in the power end.

Volumetric Efficiency Volumetric efficiency (VE) is the ratio of the discharge volume to the suction volume, expressed as a percentage, plus the slip. It is proportional to the ratio r and the developed pressure where r is the ratio of the internal volume of fluid between valves when the plunger or piston is at the top of the peak of its back stroke (C + D) to the plunger or piston displacement (D) (see Figure 2).

Since the discharge volume cannot be readily measured at discharge pressure, it is taken at suction pressure. Taking the discharge volume at the suction pressure results in a higher volumetric efficiency than using the calculated discharge volume at discharge

TABLE 3 The effect of speed on mechanical efficiency at a constant developed pressure

% of full speed	44	50	73	100
***ME*, %**	93.3	92.5	92.5	92.5

LIBERTY EXHIBIT 1017, Page 389

TABLE 4 The effect of pressure on mechanical efficiency at constant speed

% of full-load developed pressure	20	40	60	80	100
ME, %	82	88	90.5	92	92.5

pressure because of fluid compressibility. Compressibility becomes important when pumping water or other liquids over 6000 lb/in^2 (414 bar), and it should be taken into consideration when determining the actual delivered capacity into the discharge system.

Figure 3 shows the approximate volumetric efficiency for water (not including slip).

Based on the expansion back to suction capacity,

$$VE = 100 \times (1 - Ptd \times \beta \times r)/(1 - Ptd \times \beta) - S$$

Based on discharge capacity,

$$VE = 100 \times (1 - Ptd \times \beta \times r) - S$$

where β is the compressibility factor of the liquid being pumped. Figure 4 shows approximate values of β for various liquids.

When the compressibility factor is not known, but the suction and discharge density can be determined in pounds per cubic foot, the following equations can be used for calculating *VE*:

Based on suction capacity,

$$VE = 100 \times [r - (p_d/p_s)(r - 1)] - S$$

Based on discharge capacity,

$$VE = 100 \times [1 - r(1 - p_s/p_d)] - S$$

where p_s = suction density
p_d = discharge density
S = slip

Torque The average torque required by a power pump is independent of the pump speed, assuming the suction and discharge pressures are held constant. This means that the pump is a "constant torque" device and, unlike a centrifugal pump, will have a flat speed-torque curve. The torque required at the input shaft is as follows:

In USCS units $M = p \times 5250/n$

In SI units $M = p \times 9.549/n$

where M = pump torque, lb-ft (N · m)
n = speed, rpm
p = power, bhp (kW)

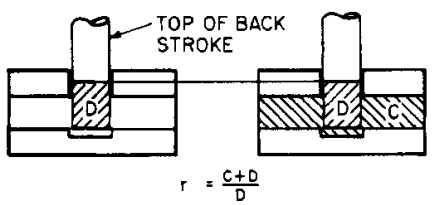


FIGURE 2 The ratio *r* (Flowserve Corporation)

LIBERTY EXHIBIT 1017, Page 390

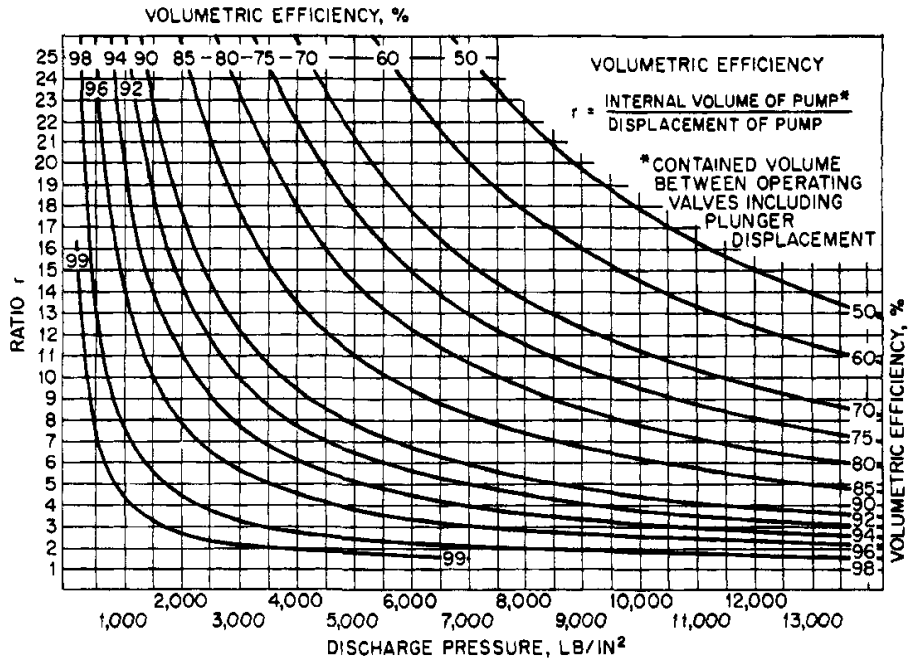


FIGURE 3 Volumetric efficiency (Flowserve Corporation) (lb/in² × 0.69 = bar)

Break-away torque, or start-up torque, is the torque required to initiate the motion of the pump to enable it to accelerate to a constant speed. If the pump is started against an open bypass to pump suction, the torque requirement is 25% of the running torque. If the pump is started against full discharge pressure, the torque requirement is 125% of the running torque. When selecting a drive system, the break-away torque of the pump must

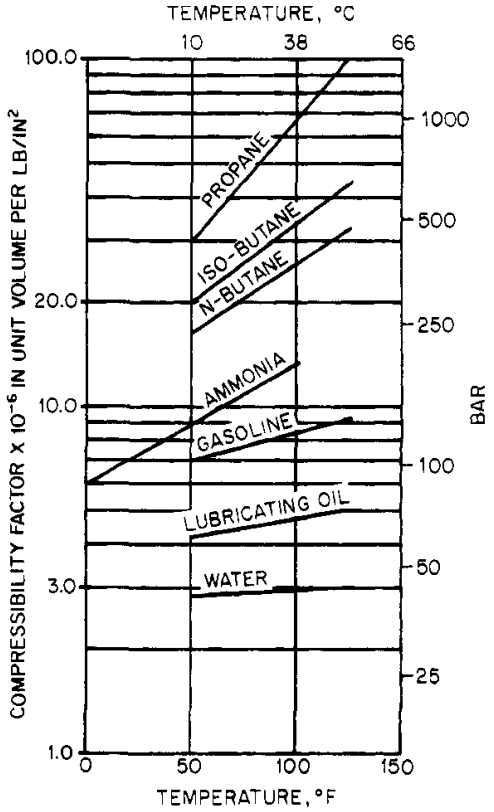


FIGURE 4 Compressibility factor (Flowserve Corporation) (bar × 14.5 = lb/in²)

LIBERTY EXHIBIT 1017, Page 391

TABLE 5 The pulses per revolution and pulse amplitude for various pump types

Pump Type	No. of Cylinders	Pulses per Rev.	Pulse Amplitude
Duplex, double-acting	4	8	+24% − 22%
Triplex, single-acting	3	6	+ 6% − 17%
Quintuplex, single-acting	5	10	+ 2% − 5%
Septuplex, single-acting	7	14	+1.2% − 2.6%
Nonoplex, single-acting	9	18	+0.6% − 1.5%

be considered. Special "high torque" motors are often required if the pump is to be started under the load.

If a variable frequency drive (VFD) is used for pump speed/capacity control, torque fluctuations or pulsations may require the drive manufacturer to provide special electronic dampening circuits. The normal pulsating flow of the pump causes the input power to fluctuate at approximately the same magnitude as the flow pulses. The frequency of these pulses per revolution of the crankshaft is twice the number of cylinders (see Table 5).

If the pump has internal gearing, or if the pump is being driven by an external gear reducer, the torque pulsation values listed should be divided by the gear ratio.

Derating Power pumps can be derated in order to achieve acceptable performance or part life in a variety of special applications. The most common derating is pump speed. Experience has shown that the life of fluid-end expendable parts, such as plungers, packing, and valves, can be extended if the pump speed/plunger velocity is reduced when pumping certain fluids. Some guidelines for acceptable plunger speeds are shown in Table 6.

Pumping high-viscosity fluids may also require the speed of a power pump to be derated. Some attempts have been made to establish standards for speed derating as a function of the fluid viscosity. Unfortunately, these methods have been based on power pump designs that were established for water or similar low-viscosity services. If a pump has been designed specifically for a high-viscosity service, only moderate speed derating may be required. Generally, pumps designed with large internal fluid passages, low-valve velocities, and larger plungers or pistons will need less derating.

Power pumps should be derated for a rod load if system or process "upsets" cannot be avoided. These are usually applications where the gas content of the pumped fluid can lead to abnormal pressure pulsations or cavitations in the fluid cylinder.

TABLE 6 Guidelines for acceptable plunger speeds

Fluid	Plunger Speed, ft/min (m/s)
Cold water	315–354 (1.6–1.8)
Hot water 140–194°F (60–90°C)	217–256 (1.1–1.3)
Hot water over 194°F (90°C)	157–217 (0.8–1.1)
Salt water	236–276 (1.2–1.4)
Cold oil	315–354 (1.6–1.8)
Hot oil	256–295 (1.3–1.5)
Crude oil	217–276 (1.3–1.5)
Liquid ammonia	197–236 (1.0–1.2)
Carbamate	138–158 (0.7–0.8)
Slurry	158–197 (0.8–1.0)
Fatty acid	236–295 (1.2–1.5)
Light hydrocarbons	177–236 (0.9–1.2)
Glycol	256–295 (1.3–1.5)
High-viscosity liquids	138–197 (0.7–1.0)

LIBERTY EXHIBIT 1017, Page 392

FLUID END THEORY

Pumping Cycle Unlike the relatively smooth, continuous flow of fluid through a centrifugal pump, the flow of fluid through a power pump occurs in a transitory dynamic condition called a *pumping cycle*. The event that initiates this cycle is the linear movement of the plunger or piston. In Figure 5, r is the radius of the crank in feet (meters), L is the length of the connecting rod in feet (meters), C equals L / r, and ω equals $(2\pi / 60) \times$ rpm. Thus, X, the linear movement of the piston or plunger is

$$X = r\left[1 - \cos\theta + L\left(1 - \sqrt{1 - \frac{r^2}{L^2}(\sin\theta)^2}\right)\right]$$

As the plunger (or piston) withdraws from the fluid cylinder or pumping chamber, the volume of the cylinder increases. The pressure in the cylinder decreases in response to the increased volume. Since most of the fluids handled by power pumps are relatively incompressible, very little plunger movement is required to cause a pressure drop. When the cylinder pressure drops sufficiently below suction pressure, the differential pressure begins to open the suction valve. The valve opens gradually and smoothly at the start of the suction stroke because the velocity and acceleration of the plunger are small.

Fluid flows through the suction valve assembly, following the plunger and filling the cylinder. As the plunger decelerates at the end of the suction stroke, the suction valve gradually returns to its seat. Ideally, the suction valve is completely closed as the plunger comes to a stop.

The motion of the slider-crank mechanism causes the plunger to reverse direction and start its discharge stroke. The fluid trapped in the fluid cylinder is compressed until the cylinder pressure exceeds the discharge pressure by an amount sufficient to begin to open the discharge valve. As with the suction valve, the discharge valve continues to open until it reaches its travel limit or until the velocity of fluid through the valve becomes constant. As the plunger decelerates, the valve moves back toward its seat. Again, ideally, the discharge valve closes when the motion of the plunger stops.

The number of pumping cycles in a single revolution of the crankshaft is the same as the number of cylinders in the pump. Every cylinder will "pump" in a sequence determined by the "firing order" of the crankshaft. The cylinders are arranged in parallel, with each one discharging into a common discharge manifold. In industry terms, the pump is usually identified by the number of plungers or pistons on the crankshaft. They are the same for single- or double-acting pumps (see Table 7).

Pulsations The pulsating characteristics of the fluid flowing into and out of power pumps are significantly influenced by the number of plungers or pistons. Discharge flow pulsations are the most critical because of the high energy potential generated when the system resistance reacts with the flow to create pressure. Since the magnitude of the discharge pulsation is mostly affected by the number of cylinders, increasing the number of cylinders will reduce the flow pulsations.

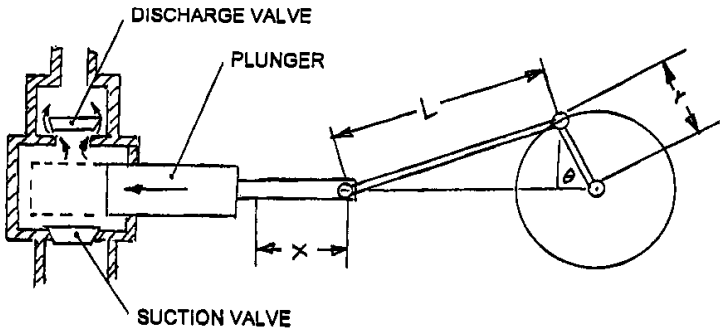


FIGURE 5 Slider-crank mechanism

TABLE 7 Industry terms for the number of plungers or pistons

Number	Term
1	Simplex
2	Duplex
3	Triplex
4	Quadruplex
5	Quintuplex
6	Sextuplex
7	Septuplex
9	Nonuplex

The acceleration and velocity of the plunger or piston will determine the rate that the fluid is discharged from the cylinder. The approximate velocity of the plunger or piston is

$$S = \frac{dx}{dt} = r\left(\sin\theta + \frac{\sin 2\theta}{2C}\right)\omega$$

The approximate acceleration of the plunger or piston is

$$Cp = \frac{d^2x}{dt^2} = r\left(\cos\theta + \frac{\cos 2\theta}{C}\right)\omega^2$$

The momentary rate of discharge capacity is the cross-sectional area A of the plunger or piston times velocity:

For single-acting plunger or piston $A = 0.785 \times D^2$

For double-acting piston $A - a = 0.785\,(D^2 - d^2)$

The total discharge Q is equal to ALS', where S' is the number of effective strokes in a given time. The quantity Q is the area of the curve, the mean height of which is

$$Total\ Q/t = ALS'/t = ALS''$$

where S'' is the number of strokes per second and t is time in seconds.

Figures 6 and 7 show discharge rates for two types of pumps. Tables 8 and 9 show how variations from the mean are related to the change in the number of plungers with a C of approximately 6:1. This shows that pumps with an even number of cylinders have a higher flow variation than pumps with an odd number of cylinders. Table 9 shows the variations in a triplex with changes in C = L/R.

Valves A pump valve in its simplest form is a free-moving plug that is opened when the force of the liquid below the valve exceeds the force of the liquid above it. When the force above the valve becomes greater than the lower, the plug closes and forms an effective seal to fluid "backflow" and pressure loss. If the valve does not perform this function efficiently, the performance of the pump can be degraded to the point where no flow is produced.

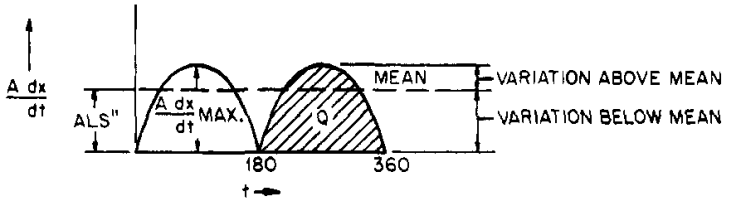


FIGURE 6 The discharge rate for a single double-acting pump (Flowserve Corporation)

LIBERTY EXHIBIT 1017, Page 394

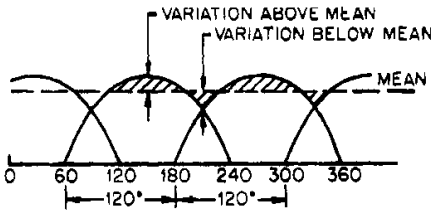


FIGURE 7 The discharge rate for a triplex single acting pump (Flowserve Corporation)

A valve will be in equilibrium when the forces above and below the valve are balanced (see Figure 8):

$$\text{Equilibrium} = P_1 \times A_1 = P_2 \times A_2 + S_f + M$$

where P = the pressure below the valve
A = the area below the valve exposed to P
P = the pressure above the valve
A = the area above the valve exposed to P
S_f = the force of the valve spring (if any)
M = the mass of the valve and half the mass of the spring

The significance of this simple equation becomes apparent when you remember that the valve is operating in a dynamic environment of constantly changing pressures in a time frame that is measured in tenths of a second. Add to that the requirement that the valve must pass a volume of fluid in each opening cycle with minimal pressure drop, and it becomes clear that the pump valve is the most critical component in the fluid end in terms of pump operability.

The pump designer will size the valves to provide a flow area, called the *spill area*, that prevents preestablished velocity limits from being exceeded. The spill area of various valve types is given in Table 10. The velocity of the fluid flowing through the spill area is called the spill velocity, V, shown in Table 11:

In USCS units V (ft/sec) = gpm through the valve × 0.642/spill area of the valve, in^2

In SI units V (m/s) = m^3/h through valve × 555.6/spill area of the valve, mm^2

The quantity 0.642 (555.6) is used because all the liquid passes through the valve in half the stroke.

Valve Dynamics Valve dynamics is the mechanical response of the valve to the changes of pressure across the valve. Using a suction valve as an example, the valve starts its cycle

TABLE 8 The effect of the number of plungers on variations in capacity from the mean (C is approx. 6:1)

Type	Number of Plungers	% Above Mean	% Below Mean	Total %	Plunger Phase
Duplex	2	24	22	46	180 deg.
Triplex	3	6	17	23	120 deg.
Quadruplex	4	11	22	33	90 deg.
Quintaplex	5	2	5	7	72 deg.
Sextuplex	6	5	9	14	60 deg.
Septuplex	7	1	3	4	51.5 deg.
Nonuplex	9	1	2	3	40 deg.

LIBERTY EXHIBIT 1017, Page 395

TABLE 9 The effect of change in C on variations in capacity from the mean for a triplex pump

C	% Above Mean	% Below Mean	Total %
4:1	8.2	20.0	28.2
5:1	7.6	17.6	25.2
6:1	6.9	16.1	23.0
7:1	6.4	15.2	21.6

when the valve is closed and the plunger is at the start of its suction stroke (maximum insertion into the cylinder). As the plunger starts withdrawing from the cylinder, the internal volume in the cylinder starts to increase. This increasing volume results in decreasing cylinder pressure that, in turn, hydraulically unbalances the valve and the valve begins to open. There is usually a slight lag in the valve opening versus the start of the plunger motion of about 5 to 20° of crankshaft rotation. Traditionally, the opening valve lag is attributed solely to the inertia required to set the valve in motion and the preload of the valve spring. In the last few years, the theory of *valve stiction* has been proposed as an additional cause of valve opening lag.

Valve stiction, as the name implies, can be an additional force to overcome when the valve is trying to lift off its seat. One version of the theory is that a cohesive force exists between the fluid molecules and the sealing surfaces of the valve and seat. This can be demonstrated by trying to separate two wet, highly machined plates. The second stiction theory focuses on possible fluid dynamic conditions that may occur as fluid starts to flow across the valve seat. Valve seats do not have "knife edge" sealing surfaces; they have a width that distributes the stresses in the valve and seat. The stiction theory postulates that the flow of fluid from the smaller area at the center of the seat to the larger area around the seat causes a pressure drop across the seat. The pressure drop is the result of the radial divergence of the fluid and is strong enough to momentarily prevent the valve from opening. Extreme cases have even resulted in a circumferential ring of cavitation located at the center of the sealing areas of the seat and valve.

Field testing valves with special grooves and radial slots in the sealing face has proven successful in reducing stiction and opening valve lag in some cases. Narrowing the sealing faces may also prove effective, although part life may decrease due to increased stress and decreased wear area. Additional computer modeling and testing is required before the stiction theory can be completely validated.

As the valve continues to open, the spill area increases proportionally. It must be remembered that fluid is now flowing through the valve at an increasing rate while trying to fill the expanding cylinder volume created by the plunger withdrawal. Ideally, the motion of the valve will exactly correspond to the flow rate of the fluid through the valve, and the valve follows a smooth trajectory to a full open position (see Figure 9).

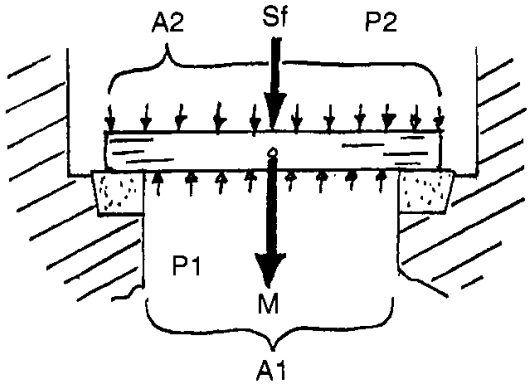
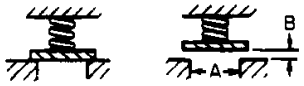
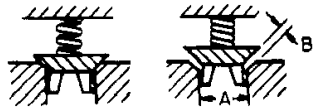
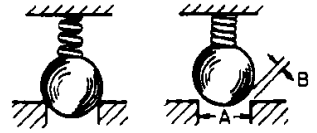
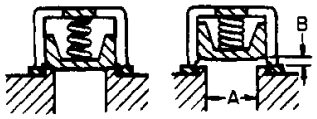
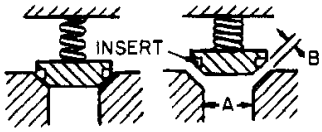


FIGURE 8 Force balance of a typical valve

LIBERTY EXHIBIT 1017, Page 396

TABLE 10 Types of valves and their applications (Flowserve Corporation)

TYPE	SKETCH A = SEAT AREA B = SPILL AREA	PRESSURE, PSI (BAR)	APPLICATION
PLATE		5,000 (345)	CLEAN FLUID. PLATE IS METAL OR PLASTIC
WING		10,000 (690)	CLEAN FLUIDS. CHEMICALS
BALL		30,000 (2,069)	FLUIDS WITH PARTICLES. CLEAR, CLEAN FLUID AT HIGH PRESSURE. BALL IS CHROME PLATED
PLUG		6,000 (414)	CHEMICALS
SLURRY		2,500 (172)	MUD, SLURRY. POT DIMENSIONS TO API-12. POLYURETHANE OR BUNA-N INSERT

This idyllic situation only occurs in very slow running pumps that are fitted with oversized valves. In modern higher speed pumps, the valve often accelerates at a rate fast enough to create a spill area greater than that required to maintain a constant flow velocity. At this point, the valve motion momentarily stops, and the valve may even start to close before the fluid flow once again matches the spill area. The valve then returns to the smooth trajectory until the maximum valve lift occurs.

After the plunger passes the mid point of its stroke, it starts decelerating. The flow of fluid through the valve is high enough to start to build pressure in the cylinder and unbalance the valve and start the valve closing. The valve spring has reached its maximum compression and, if properly designed, will help accelerate the valve back toward the seat. When the plunger reaches the end of the suction stroke, the valve should also be closing. The amount of crankshaft rotation that occurs between the time when the plunger reaches the end of its stroke and when the valve is completely closed is called the *delayed valve closing* and is normally 2 to 12° of crank rotation. Although a delayed valve opening may have little effect on overall pump performance, a delayed valve closing certainly will. A valve that is partially open when the plunger reverses direction will result in backflow. Backflow, as the name implies, is the reverse flow of fluid back across the valve and results in lower pump volumetric efficiency.

TABLE 11 Valve spill velocities

Valve	Spill velocity, ft/s (m/s)
Clean liquid suction valve	3–8 (0.9–2.4)
Clean liquid discharge valve	6–20 (1.8–6)
Slurry suction and discharge valve	6–12 (1.8–3.7)

LIBERTY EXHIBIT 1017, Page 397

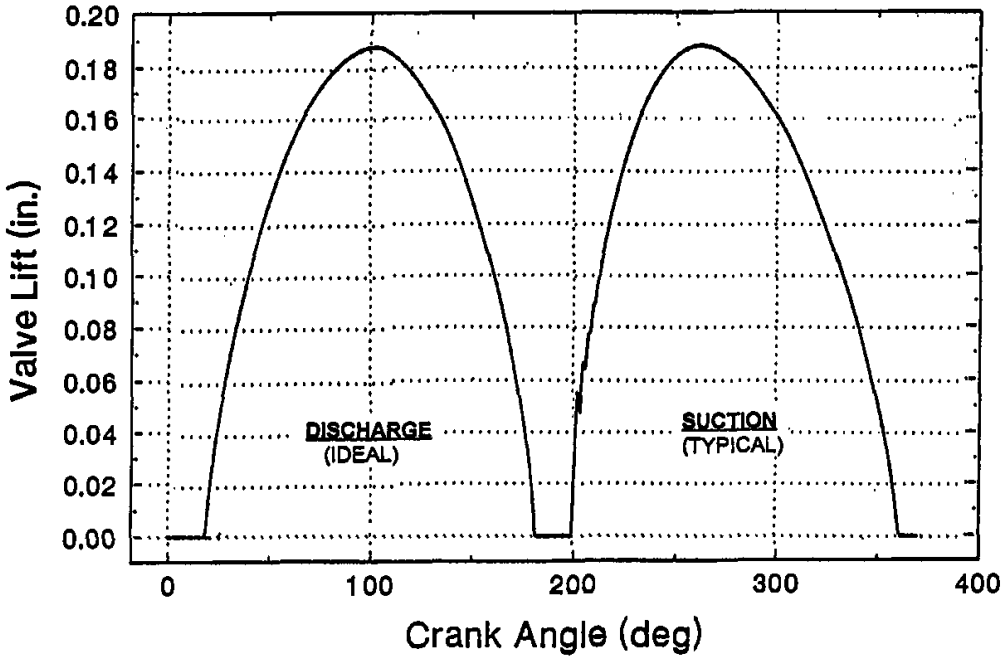


FIGURE 9 Valve lift versus crank angle (in × 2.54 = cm)

Many pump valves are designed with mechanical limits to the distance that the valve is allowed to open or lift. This is normally done to avoid overstressing the valve spring and to minimize the overall height of the valve assembly. Valve motion for a valve designed with a mechanical stop is shown in Figure 10. Another advantage of this design is that the valve does not have to travel as far during its closing cycle, compared to valves with no mechanical limits. The disadvantage is the potential for impact damage to the valve if it strikes the stop with excessive force.

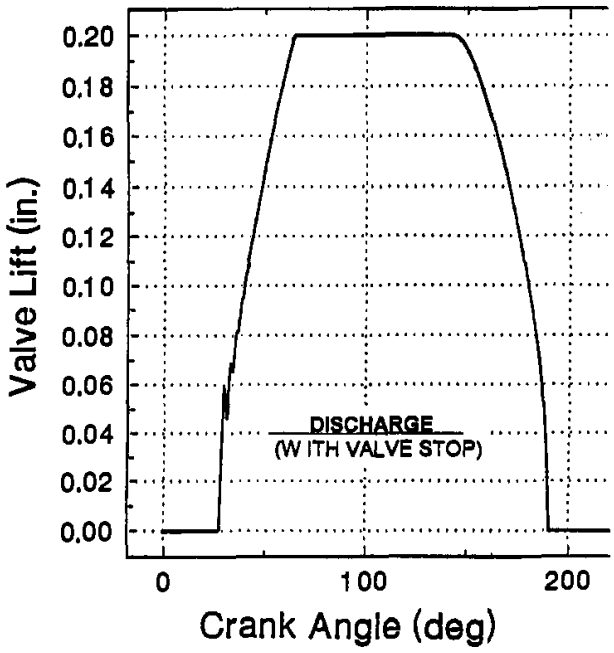


FIGURE 10 Valve lift versus crank angle for a valve with a mechanical stop (in × 2.54 = cm)

LIBERTY EXHIBIT 1017, Page 398

The importance of valve mass to overall valve dynamics has been the subject of much debate among pump designers over the years. There is no question that the mass of the valve must be overcome in order to open the valve. Test data are also available that shows no appreciable difference in the performance of pumps fitted with hollow ball valves versus identical pumps with solid ball valves. This apparent contradiction can be explained by studying valve acceleration at various parts of the valve cycle using advanced computer modeling.

It has already been explained above why a valve can hesitate, or stop opening, during the opening portion of its cycle. It's also been stated that when the valve spill area is large enough to establish a hydraulic balance, the valve will stop opening. What actually occurs is the valve starts decelerating as it comes closer to hydraulic equilibrium. If the valve is properly designed, it will contact its mechanical stop just as its acceleration/deceleration is very low. In that case, the valve mass has little significance on the impact force of the valve on the stop. The same holds true of the impact force of the valve on the seat as it closes. If the valve is properly designed, a 62-lb (28-kg) solid ball valve operating at 100 cycles per minute can strike the seat with less than 20 lb (9 kg) of force.

Although pump valves operate in a liquid medium, the shape of the valve is not an important design consideration for most applications. The relatively small distance that a valve travels is not sufficient for the fluid dynamics of a shape to have a measurable effect on valve dynamics. The only exception to this is valves in pumps handling high-viscosity liquids. For these applications, the ball valve, often spring-loaded, has proven to reduce closing valve lag and increase volumetric efficiency better than any other type of valve.

The most critical component in the optimization of valve dynamics is the valve spring. The pump designer normally selects a valve spring that will exert a certain amount of "pre-load" on the valve when it is closed. This pre-load helps the valve to close smoothly on the seat and avoid rebound (and possible backflow). Too high a preload in the suction valve may result in higher net positive suction head required (NPSHR). In the discharge valve, excessive preload can cause abnormally high pressure spikes in the fluid cylinder just before the valve opens.

The other valve spring design criterion is the spring rate. Every compression spring develops a predetermined resistance per unit length. This value is expressed in pounds per inch (kg per cm). As the valve is opening, the increasing spring force helps the valve obtain hydraulic balance faster. It also helps to limit the impact force of the valve on the stop. At the start of the closing cycle, the stored energy in the compressed spring helps the valve respond faster to the pressure changes in the fluid cylinder as the plunger starts to decelerate. Again, if the spring is properly designed, the closing valve lag will be minimized.

No published guidelines exist for the proper amount of valve spring pre-load or spring rate. Most pump designers use proprietary values, generated through a combination of in-house and field testing. However, although these values produce low NPSHR and high volumetric efficiency in most cases, the valve dynamics may not be close to being optimized. It should also come as no surprise that pumps fitted with "off-the-shelf" commercially available valves do not operate as well as pumps having optimized valve dynamics.

With the recent advent of advanced computer modeling of pump valves, it is now possible to optimize valve dynamics for a specific set of pump operating parameters. We may also see valve designs in the near future having variable rate valve springs, hydraulic dampening, and mechanisms that induce rotation as the valve opens and closes.

POWER END THEORY

The power end or drive end of a power pump consists of a crankshaft, connecting rods, crossheads, and bearings, all housed in a rigid structure referred to as the frame. Details of the design and construction of these components are covered in Section 3.2, "Power Pump Design and Construction." The slider-crank mechanism that converts rotational driving energy to the reciprocating motion that actuates the pistons or plungers can be found in reciprocating gas compressors, automotive engines, and stationary and marine engines. However, the stress loading pattern of power pump components is unique to this type of mechanism.

LIBERTY EXHIBIT 1017, Page 399

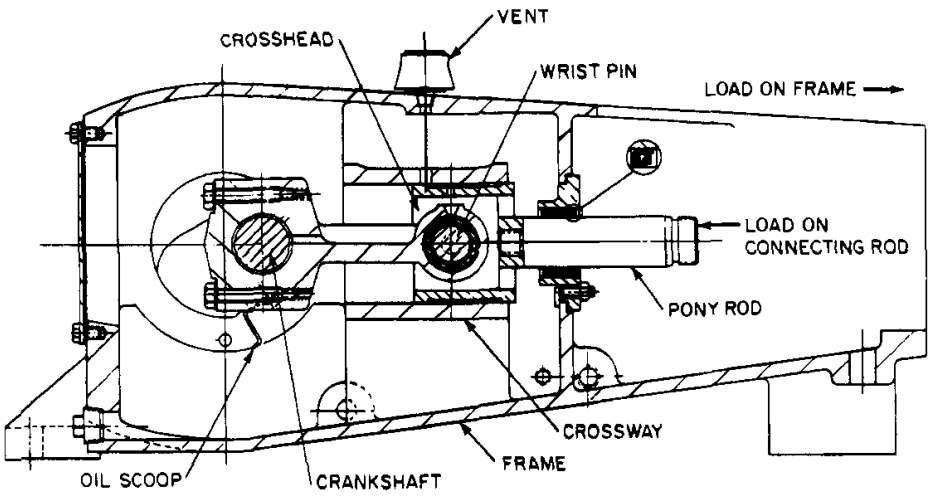


FIGURE 11 Power end, horizontal pump (Flowserve Corporation)

Applying Rod Load to the Power End As stated earlier, the loading on the power end is called the rod load and is the product of the area of the plunger multiplied by the maximum discharge pressure. In a gas compressor or engine, this loading increases over 90 to 180° of crank rotation before maximum loading is reached. In a power pump, the maximum loading is reached in less than 30° of crank rotation due to the relative incompressibility of the pumpage. Since this loading cycle is repeated with each plunger stroke, the actual loading resembles a shock load more than a simple cyclic fatigue load. The design criteria for the stressed components of the power end must therefore include the material's capability to absorb shock loads and overall safety factors greater than 3:1.

Another critical factor in the capability of the power-end components to handle the rod load is how the load is applied. Figures 11 and 12 show the direction of the load on the

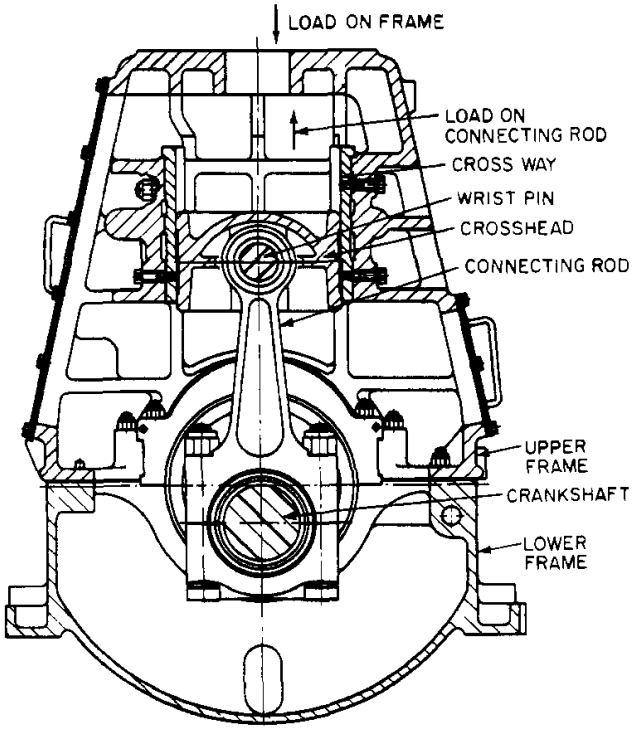


FIGURE 12 Power end, vertical pump (Flowserve Corporation)

frame and connecting rod for two different power end configurations. On vertical pumps with outboard packed stuffing boxes, the frame is in compression and the crosshead and connection rod are in tension. With horizontal, single-acting pumps, the frame is in tension, and the crosshead and connecting rod are in compression. The material selection and factors of safety must be altered accordingly.

Liquid Separation from the Plunger It has already been explained that fluid flows through the suction valve (and suction manifold and related piping) to fill the increasing cylinder volume caused by the withdrawal of the plunger. If the plunger accelerates faster than the flow of incoming liquid, the liquid will lose contact or separate from the plunger. The void that forms will be at a pressure lower than anywhere else in the cylinder. If the pumpage contains entrained gas, the gas may come out of a solution in this low-pressure area. The gas bubbles, when recompressed later in the plunger stroke, can cause cavitation damage to the plunger and surrounding cylinder.

The geometry of the slider-crank mechanism affects the point at which liquid separation occurs. As the ratio of the connecting rod length to the crank radius increases, the pump speed at which liquid separation occurs will decrease. Since liquid separation can be the determining factor in a pump's NPSHR, the pump designer must carefully evaluate the slider-crank geometry in order to optimize the pump's hydraulic performance. The pump speed at which water will separate from the end of the plunger can be calculated from the following:

In USCS units:
$$\text{rpm} = 54.5\sqrt{\frac{(34 - h_s - h_f)A_s}{LR[l - (l/LR)]A_p}}$$

In SI units:
$$\text{rpm} = 16.6\sqrt{\frac{(10.36 - h_s - h_f)A_s}{LR[l - (l/LR)]A_p}}$$

where h_s = suction head, ft (m)
h_f = piping frictional loss, ft (m)
A_s = area of suction pipe, in^2 (mm^2)
L = length of connecting rod, centerline to centerline, ft (m)
R = crank radius, ft (m)
l = length of pipe where resistance to flow is to be measured, ft (m)
A_p = area of plunger, in^2 (mm^2)

Unbalanced Forces Due to the relatively slow speed of a power pump, the inertia loads of the rotating/reciprocating parts are low enough to avoid the vibration problems associated with centrifugal pumps. For that reason, power pump crankshafts are not normally balanced. However, when the power pump is coupled to a drive containing a high-speed motor and gear reducer, a torsional analysis of the pump/drive unit may be required. For this analysis, the unbalanced forces of the rotating and reciprocating pump components can be calculated as follows:

Unbalanced Reciprocating Parts Force (F_{rec}) Parts are typically about one-third of the connecting rod weight (the crosshead, the crosshead bearing, the wrist pin, the pony rod, and the plunger). Additional parts on vertical pumps include the pull rods, yoke, and plunger nut.

$$F_{rec} = \frac{W}{g}\omega^2 R\left(\cos\theta + \frac{R}{L}\cos\theta\right)$$

where F_{rec} = reciprocating parts force, lb (N)
W = weight of all reciprocating or rotating parts, lb (N)

g = 32.2 ft/s^2 (9.81 m/s^2)

ω = $(2\pi/60) \times n$ (n = pump rpm)

R = one-half of stroke, ft (m)

L = length of connecting rod, centerline to centerline, ft (m)

θ = crank angle; usually maximum force is at $\theta = 0°$, $\cos\theta = 1$

Unbalanced Rotating Parts Force (F_{rot}) Parts are typically about two-thirds of the connecting rod weight, crank end bearing, and crankpin, where the variables are as above.

$$F_{rot} = \frac{W}{g}\omega^2 R$$

Mechanical Efficiency The mechanical efficiency of a single-acting power pump without internal gears is typically 90 to 92%. Over half of the mechanical losses are due to the frictional drag of the plungers through the packing. The remaining losses are from the bearings, the crosshead-to-crosshead guide friction, and the extension rod-to-gland seal friction. If these components are properly lubricated, very few power-end design options are available that will produce a measurable increase in mechanical efficiency. Decreasing the diameter of the plungers and minimizing the number of packing rings will result in a small efficiency increase.

FURTHER READING

American National Standard for Reciprocating Power Pumps for Nomenclature, Definitions, Application and Operation, ANSI/HI 6.1-6.5-2000, Hydraulic Institute, Parsippany, NJ. www.pumps/org

Positive Displacement Pumps—Reciprocating, API Standard 674. 2nd Edition, 1994, The American Petroleum Institute, Washington, D.C. www.api.org

Henshaw, T. L. *Reciprocating Pumps*. Van Norstrand Reinhold Company, Inc., New York, 1987.

Miller, J. E. *The Reciprocating Pump—Theory, Design and Use*. John Wiley & Sons, Inc., New York, 1987.

SECTION 3.2
POWER PUMP DESIGN AND CONSTRUCTION

WILLIAM K. CHAPLIS
FREDERIC W. BUSE

The power pump, as a piece of rotating equipment, would seem to have a great deal in common with a reciprocating gas compressor or diesel or gas engine. All have crankshafts, bearings, connecting rods, and lubricating oil systems that use the pump frame as an oil reservoir. All have a fluid or gas end that contains relatively high pressure and includes some type of valving that enables the equipment to perform its required task.

Due to the unique operating characteristics of the power pump, very little design criteria or construction details can be directly transferred from these other mechanisms. Because of the high compressibility of most gases, the resulting cyclic loadings are applied to the various rotating, reciprocating, and pressure-retaining components in a smoother manner. Therefore, gas-driven or gas-pumping mechanisms can operate at speeds three or four times higher than a reciprocating pump with good reliability and low vibration levels.

It has been said that a power pump has more in common with a jackhammer because of the constant high-cycle shock loading that it must be designed to withstand. Therefore, very conservative material selections, stress limits, and factors of safety have been established by the pump designers for all continuous duty applications. Intermittent duty applications can be met using less stringent design criteria.

Seldom is a power pump designed for one specific application having one specific set of operating conditions. Consequently, few pump designs are truly optimized. The best economical approach has been to design a power end capable of accepting a number of fluid ends, which in turn allows the pump to operate over a wide range of hydraulic conditions. By using different plunger diameters for a specific operating pressure, the designer tries to "load up" the power to its maximum continuous rod load rating while maintaining the pump speed at a level just sufficient to provide the required flow rate.

A power pump has its cylinders operating in parallel with interconnecting suction and discharge manifolds. Additional cylinders are sometimes added to a basic power-end design in order to obtain higher flow rates. The most common examples of this approach are the quintuplex pumps that have an 80% component interchangeability with triplex

LIBERTY EXHIBIT 1017, Page 403

pumps. Triplex (three cylinder), quintuplex (five cylinder), septuplex (seven cylinder), and nonoplex (nine cylinder) pumps have been designed that have over a 90% interchangeability of parts. Only the power frame and crankshaft are unique to a specific pump size.

Factors of safety are used in power pump design and application. A connecting rod assembly, for instance, normally has a safety factor in excess of a 3:1 ratio because if a connecting rod fails in operation, it normally destroys many other power-end parts. A nodular iron frame will have a high safety factor also, primarily due to the requirement for thick wall sections to mount interfacing parts and to reduce operating noise levels. Some fluid-end expandable parts in the stuffing box and valves have safety factors below a 1.5:1 ratio because these parts are normally replaced before they would fail due to fatigue.

There has been a trend in past years in most industries to purchase power pumps that operate at higher and higher speeds. This has been driven by the economics of buying smaller, higher speed equipment versus the older, large, slower speed pumps. This trend seems to be loosing some momentum, especially in critical applications. It remains for the pump purchaser and pump supplier to jointly evaluate each application and try to arrive at a pump selection that will provide the most reliable performance for the lowest installed cost and operating cost.

LIQUID END

The liquid end consists of the cylinder, the plunger or piston, the valves, the stuffing box, the manifolds, and the access covers. Figure 1 shows the liquid end of a horizontal pump, and Figure 2 shows the same for a vertical pump.

Cylinder (Working Barrel) The cylinder is the body where the pump pressure to overcome discharge pressure is developed. It is continuously under fatigue. Cylinders on many horizontal pumps have suction and discharge manifolds integral with the cylinder. Vertical pumps have separate manifolds.

A cylinder containing the passages for more than one plunger is referred to as a *single cylinder*. When the cylinder is used for one plunger, it is called an *individual cylinder*. Individual cylinders are used where developed stresses or replacement costs are high.

Cast cylinders are usually limited to the developed pressures listed in Table 1. Forged cylinders are made from 1020 and 4140 carbon steel; 304L, 316L, 17-4 PH, and 15-5 PH stainless steels; and nickel aluminum bronze. In recent years, duplex stainless steels have seen an increase in usage when higher strength and corrosion resistance is required.

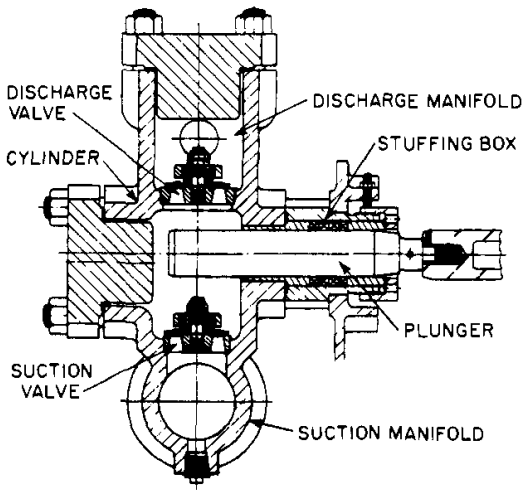


FIGURE 1 A liquid-end horizontal pump (Flowserve Corporation)

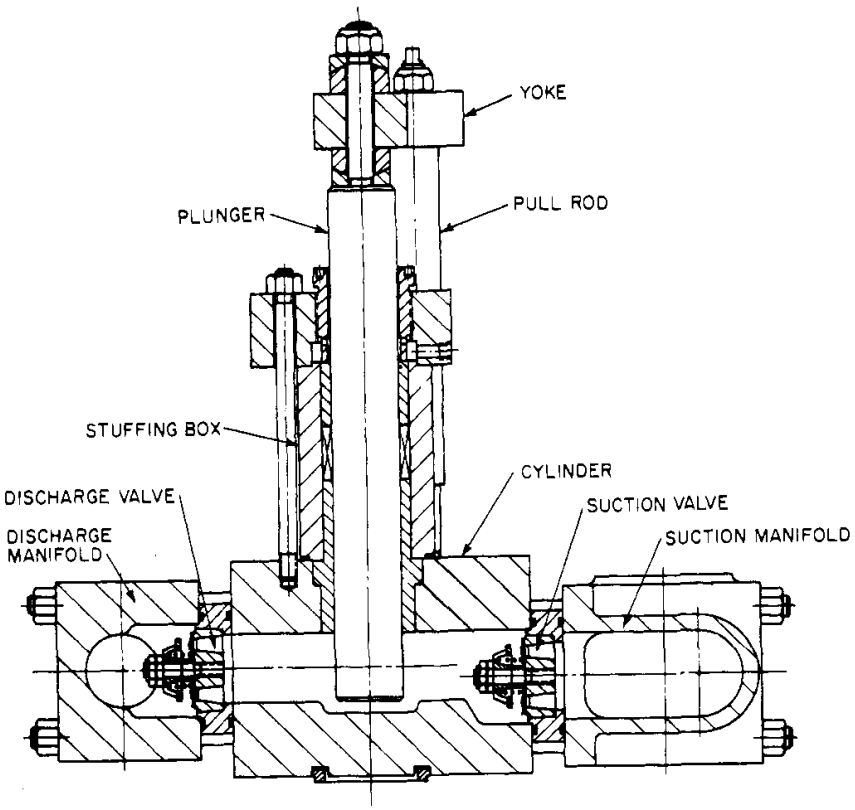


FIGURE 2 A liquid-end vertical pump (Flowserve Corporation)

Forged cylinders have a 4:1 to 6:1 forging reduction on all sides of the cylinder to obtain a homogeneous internal structure. This type of cylinder requires heat treatment after forging to eliminate the stresses that occur during the forming operation. The pump designer must minimize the section thickness of the cylinder or residual stresses may remain after machining the internal bores.

The highest stresses occur at the intersection of the horizontal and vertical internal bores. Unlike a simple cylinder where the internal stresses are analyzed as a single hoop stress, the stress at the intersecting bores of a power pump cylinder are based on a double hoop stress. In Figures 3 and 4, the distances b and d are the internal diameters, a and c are the diameters to the nearest obstruction of the solid material of the cylinder, P is the developed pressure, and S is the resulting stress. Stress concentration factors at the intersecting bores can be omitted if the radius is not less than 0.25 in (1.5 mm). Above 3000 lb/in^2 (207 bar), the internal bores should have a surface finish of 63 rms minimum.

During each plunger cycle, the developed pressure goes from suction pressure to discharge pressure and back to suction. For a pump operating at 360 strokes per minute, over six million fatigue cycles will occur in less than 12 days. For this reason, very conservative allowable stress limits are used. Normally, these limits range from 10,000 to 25,000 lb/in^2 (69 to 172 Mpa), depending on the material of the cylinder, duty cycle, and liquid being

TABLE 1 Maximum pressure in cast cylinders

Material	lb/in^2 (bar)
Cast iron	2000 (137)
Aluminum bronze	2500 to 3000 (172 to 207)
Steel	3000 (207)
Ductile iron	3000 (207)

LIBERTY EXHIBIT 1017, Page 405

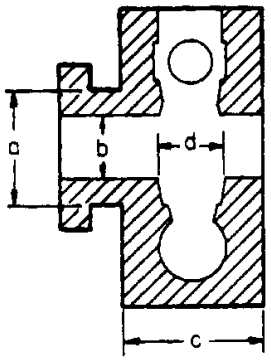


FIGURE 3 Stress dimensions for a horizontal liquid end (Flowserve Corporation)

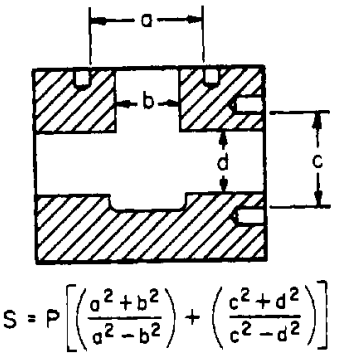


FIGURE 4 Stress dimensions for a vertical liquid end (Flowserve Corporation)

pumped. The allowable stress is a function of the fatigue stress of the material for the liquid being pumped and the life cycles required.

Due to improper suction system design, misapplications, or process upsets, instantaneous pressure in the cylinder may be much higher than design pressure. When the liquid contains entrained gas that can be released because of inadequate suction pressure, the resulting cavitation can cause instantaneous pressure four to five times the design pressure. This results in reducing the life of the cylinder and other liquid-end components, as well as damaging pressure pulsations in the suction and discharge piping systems.

For continuous duty pumps operating above 10,000 lb/in^2 (690 bar) of discharge pressure, special liquid-end designs have been developed. In Figure 5, the intersecting bores have been eliminated by arranging the suction and discharge valves on the same axis as the plunger. This means the stresses in the cylinder will be only half of those in a comparable T-block design.

Plungers The plunger transmits the force that develops the pressure. It is normally a solid construction of up to 5 in (127 mm) in diameter. Above that dimension, it may be made hollow to reduce its weight. Small-diameter plungers used for 6000 psi (414 bar) and above should be reviewed for possible buckling. Plunger speeds range from 150 to 350 fpm (46 to 107 m/s). The surface finish normally is between 14 and 20 rms. A finish below 8 rms should be avoided because excessive packing leakage may occur due to the inability of the packing to seal properly on the smooth surface.

Although some plungers are made of heat-treated or case-hardened steel, the most common are the hard-coated or solid ceramic. The hard coatings are normally flame sprayed powders of Colmonoy or tungsten carbide, or ceramic oxides. These can be applied over base materials of 1020 carbon steel or 316L stainless steel. Ceramic oxide is normally limited to 200°F (93°C) and is used for soft water, crude oil, mild acids, and mild alkalis.

The porosity and bond strength of coatings must be carefully evaluated for use with higher operating pressures. Under those conditions, the liquid may penetrate the pores of the coating and lift the coating off the base material. Ceramic plungers also have special requirements and limitations. This type of plunger is often constructed as a solid bar, closed-end tube of ceramic, bonded to a metal end cap or plug. A vent must be provided to allow the pressure inside the plunger to equal the atmospheric pressure or the ceramic-to-metal bond may fail or the plunger may explode. In addition to the normally fragile nature of any ceramic plunger, the solid ceramic plunger is susceptible to failure due to thermal shock.

Pistons Pistons are used for water pressures up to 2000 lb/in^2 (138 bar). For higher pressures, a plunger is usually used. Pistons are cast iron, bronze, or steel with reinforced elastomer sealing rings (see Figure 6). They are most frequently used in duplex, double-acting pumps. The latest trend is to use pistons in single-acting triplex pumps.

LIBERTY EXHIBIT 1017, Page 406

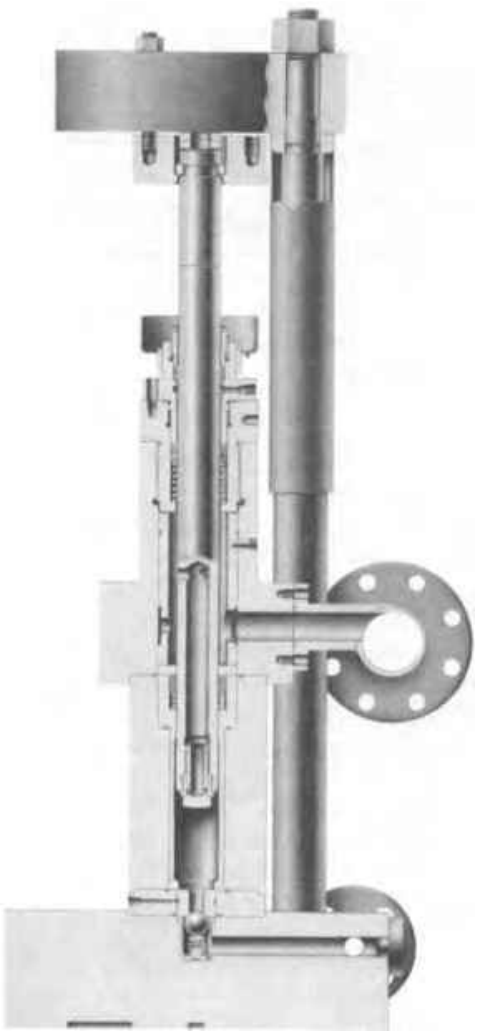


FIGURE 5 Special high-pressure liquid-end designs arrange the suction and discharge valves on the same axis as the plunger, thus eliminating intersecting bores (Flowserve Corporation).

Stuffing Box The stuffing box assembly consists of a stuffing box, upper and lower bushings, packing, and a gland. For ease of maintenance, the stuffing box assembly is usually removable (see Figure 7).

The stuffing box bore is machined to a 63 rms finish to ensure packing sealing and life. A single hoop stress equation is used to determine the wall thickness with an allowable stress limit of 10,000 to 20,000 lb/in^2 (69 to 138 MPa).

The bushings that guide the plunger have a 63 rms finish with approximately 0.001 to 0.002 in (0.02 to 0.05 mm) of diametrical clearance per inch of the plunger diameter. The

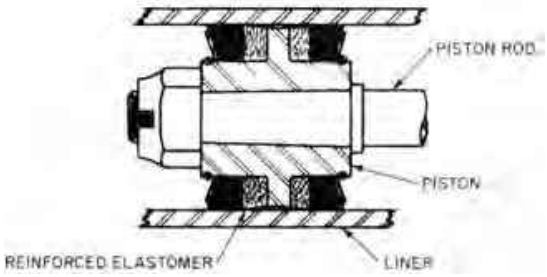


FIGURE 6 Elastomer face piston (FWI)

LIBERTY EXHIBIT 1017, Page 407

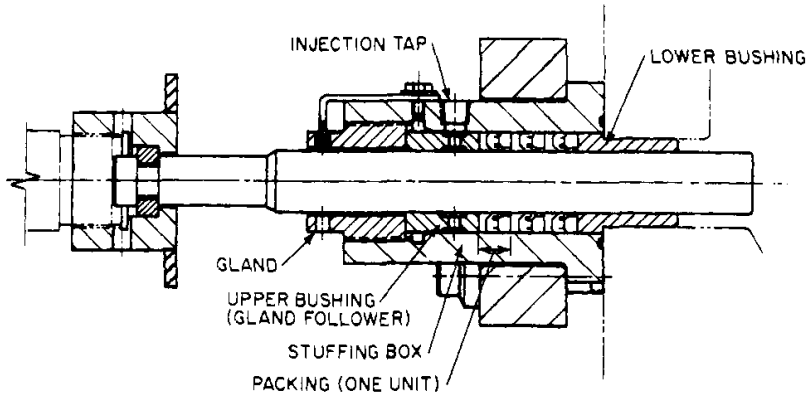


FIGURE 7 A stuffing box (Flowserve Corporation)

lower bushing is sometimes secured in an axial position to prevent movement of the packing. Bushings are made of bearing bronze, Ni-resist, or cast iron. Stainless steel can be used if its antigalling properties with the plunger coating can be verified.

Packing is either square cross-section, woven construction, or molded V or chevron-shaped (see Figure 8). Some types use metal backup adapters. A packing set consists of top and bottom adapters and one or more packing sealing rings. A stuffing box can use two to five rings of packing, depending on the pressure and the fluid being pumped. Packing rings are usually made up of a number of composite materials selected for their strength, wear resistance, and lubricity, including neoprene, Teflon, cotton duct, and Kevlar.

Packing can be made self-adjusting by installing a spring between the bottom of the packing set and the lower bushing or bottom of the stuffing box. This arrangement eliminates overtightening the packing and enables a more uniform break-in. Packing can be lubricated through a grease fitting or by an auxiliary lubricator driven through a take-off on the crankshaft.

For chemical or slurry service, a lower injection ring is used for flushing. This prevents concentrated pumped fluid from impinging directly on the packing. This injection can be continuous or synchronized to inject only on the suction stroke. Flush glands at the outboard end of the stuffing box are employed when a toxic vapor is present or when the leakage may flash.

The stuffing box for the piston rod of a double-acting pump is similar in construction to that of a stuffing box for a plunger. The primary difference is that it must seal against pressure being developed while the rod moves back through the packing. Single-acting pistons do not employ a stuffing box. Leakage past the piston-sealing rings goes into the frame extension to mix with the continuously circulating lubricant.

Cylinder Liner The cylinder wear liner (refer to Figure 6 and see Figure 9) is usually of Ni-resist material. Its length is slightly longer than the stroke of the pump to enable an assembly entrance taper of the piston into the liner. In double-acting pumps, the liner has packing to prevent leakage from the high-pressure side to the low pressure side of the

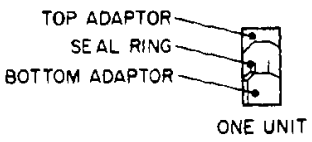


FIGURE 8 Chevron packing (Flowserve Corporation)

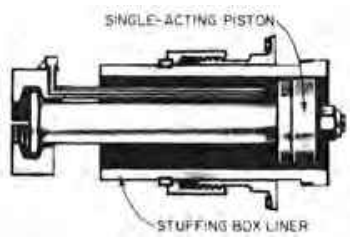


FIGURE 9 Single-acting piston stuffing box (Flowserve Corporation)

LIBERTY EXHIBIT 1017, Page 408

cylinder. Because of the brittleness of the liner, the construction should be such that the liner is not compressed. The finish of the bore of the liner is approximately 16 rms.

Valves Many types of valve designs exist. Which type is used depends on the application. The main parts of a valve assembly are the seat and sealing member, usually a disc, ball, or plate. The plate movement is controlled by a spring or retainer. The seat usually uses a taper where it fits into the cylinder or manifold. The taper not only gives a positive fit but permits easy replacement of the seat.

Some pumps use the same size suction and discharge valve for interchangeability (refer to Figure 2). Some use larger suction valves than discharge valves for improved NPSH reasons. Others use larger discharge valves than suction valves because the cylinder configuration requires the suction valve to be removed through the location of the discharge valve (refer to Figure 1). Because of space considerations, valves are sometimes used in clusters on each side of the plunger to obtain the required total valve area that reduces valve velocity.

Table 2 shows seat and plate hardness for some valve materials. Seats and plates made of 316 stainless steel material are usually chrome-plated or flame-sprayed to give them the desired surface hardness.

The flow area of the valve must be large enough to prevent significant pressure drop or restriction to flow. Normally, suction valves are sized for 6 to 8 ft/s velocity, and the discharge valves and sized for 8 to 12 ft/s.

The valve springs must be made of corrosion-resistant material and designed to withstand high-cycle fatigue stresses. Under no situation should the valve operation enable the spring to go to a solid stack height or wire-to-wire condition. The ends of the spring must be ground flat and square with a maximum perpendicularity of 3 degrees.

Manifolds These are the chambers where the liquid is disbursed or collected for distribution before or after passing through the cylinder. In horizontal pumps and some vertical pumps, the manifolds are cast or machined integral with the fluid cylinder. Most vertical pumps have the suction and discharge manifolds separate from the cylinder (refer to Figure 2).

Suction manifolds are designed to eliminate air pockets from the flange to the valve entrance (see Figure 10). Separate suction manifolds are cast iron, cast bronze, or fabricated steel. Discharge manifolds are steel forgings or fabricated steel. The manifolds have a minimum deflection to prevent gasket shifts when subjected to maximum operating pressures.

The velocity through the manifolds of a clean liquid is 3 to 5 ft/s (0.9 to 1.5 m/s) at the suction and 6 to 16 ft/s (1.8 to 4.9 m/s) at the discharge. Suction and discharge manifold velocities in a slurry service are 6 to 10 ft/s (1.8 to 3 m/s). Slurry services have a minimum velocity of 6 ft/s (1.8 m/s) to prevent the heavier slurry particles from falling out of solution.

In USCS units, V (ft/s) = pump gpm $\times$ 0.321/cross-sectional area of the manifold, in^2

In SI units, V (m/s) = pump m^3/h $\times$ 277.8/cross-sectional area of the manifold, mm^2

TABLE 2 Recommended material hardness for valve plate and seat

Material	Plate	Seat
	Rockwell C hardness	
329	30 to 35	38 to 43
440	44 to 48	52 to 56
17-4 PH	35 to 40	40 to 45
15-5 PH	35 to 40	40 to 45
	Brinell hardness	
316	150 to 180	150 to 180

LIBERTY EXHIBIT 1017, Page 409

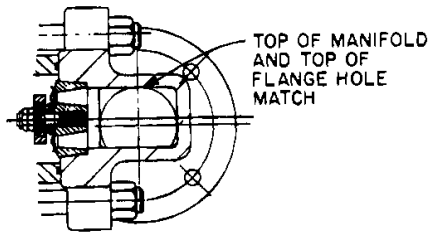


FIGURE 10 A suction manifold construction to eliminate air pockets (Flowserve Corporation)

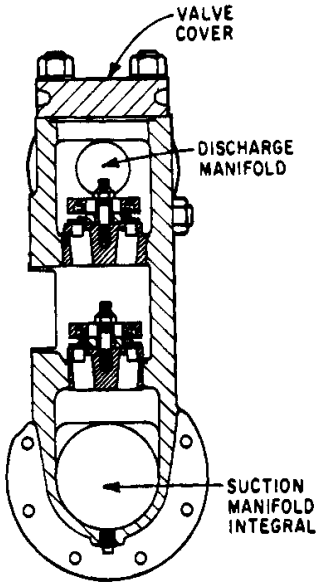


FIGURE 11 An integral suction and discharge manifold (Gardner-Denver)

A water hammer creates an additional pressure (which is added to the rated pump pressure), as does hydraulic shock loading. The discharge manifold rating is then made equal to or greater than the sum of these pressures.

Valve Covers Valve covers are used to provide accessibility to the valves without disturbing the cylinder, manifold, or related piping (see Figures 11 and 12).

Plunger Covers and/or Cylinder Heads These are used on horizontal pumps to provide accessibility to the plunger, piston, and cylinder liner (refer to Figures 11 and 12 and see Figure 13).

POWER END

The power end contains the crankshaft, connecting rods, crossheads, pony rod, bearings, and frame (see Figures 14 and 15). Basic designs are horizontal and vertical with sleeve or antifriction bearings. Some have integral drive gears.

Frame The frame absorbs the plunger load and torque. Vertical pumps with outboard packed stuffing boxes (refer to Figure 2) have the frame in compression (refer to Figure 14). With horizontal single-acting pumps, the frame is in tension (refer to Figure 15). Frames are usually close-grain cast iron with relatively thick cross-sections. This combination provides superior dampening for the normal low-frequency cyclic loading. Some intermittent duty pumps, specifically designed for mobile services, are constructed of lighter weight, fabricated steel plate.

The frame is usually vented to the atmosphere. However, when the atmosphere is detrimental to the working parts of the frame, such as an ammonia attack on bronze bearings, the frame can be purged continuously with nitrogen gas.

Crankshaft The crankshaft (see Figures 16, 17, and 18) varies in construction, depending on the design and power output of the pump. In horizontal pumps, the crankshafts are usually of nodular iron or cast steel. Vertical pumps use forged steel or machined billet crankshafts. Because the crankshafts have a low mass and operate at relatively low

LIBERTY EXHIBIT 1017, Page 410